

Handbook of
Ferroalloys
Theory and Technology



Edited by
Michael Gasik



Introduction

Michael M. Gasik Editor

Aalto University Foundation, Espoo, Finland

Chapter Outline

1.1 Introduction to Ferroalloys	3	Acknowledgments	7
1.2 The Scope and Structure of the Book	5	References	7

1.1 INTRODUCTION TO FERROALLOYS

Ferroalloys (and master alloys in general) have been developed to improve the properties of steels and alloys by introducing specific alloying elements in desirable quantities in the most feasible technical and economic way. Ferroalloys are namely alloys of one or more alloying elements with iron, employed to add chemical elements into molten metal. Not a single steel grade is produced without ferroalloys (Wood and Owen, 2005). Ferroalloys production is an important part of the manufacturing chain between the mining and steel and alloys metallurgy: the main task of the ferroalloys industry is the primary recovery (reduction) of needed metals from natural minerals. As ores also include nonmetallic minerals (gangue), they have to be dressed (beneficiated, enriched) by one or several successive methods (gravitational, magnetic, electric, and flotation separation, or in some cases by chemical means) to produce useful mineral concentrates in which the leading content of the metal is much higher in comparison with the original ore (Gasik and Lyakishev, 2005). This allows the production of higher-grade ferroalloys with a higher content of leading elements and a lower content of impurity elements (usually phosphorus, sulfur, and nonferrous metals), and it significantly reduces specific energy consumption and production costs.

There are several reasons why ferroalloys are used to add necessary elements. The alloying element might be difficult to obtain in pure form and it makes less sense to purify it (also from iron) if the purpose is to add it

back to iron-based steel melt. It just may not be stable in a condensed form at steelmaking temperatures. The alloying element alone might have too much affinity to oxygen or nitrogen, which would lead to its premature oxidation before it would be utilized. Eventually, the costs of 1 kg of alloying element in its ferroalloy form are many times lower than the costs for its pure form.

Ferroalloys are usually classified in two groups: bulk (major) ferroalloys (produced in large quantities) and minor ferroalloys (produced in smaller quantities, but of a high importance). Bulk ferroalloys are used in steelmaking and steel or iron foundries exclusively, whereas the use of special ferroalloys is far more varied. About 85% to 90% of all ferroalloys are used in steelmaking; the remaining ferroalloys are used for nonferrous alloys (e.g., those that are nickel or titanium based) and by the chemicals industry ([Gasik and Lyakishev, 2005](#)).

Historically, the ferroalloys production technology used in the 19th century was developed for blast furnaces (high-carbon ferromanganese, low-grade ferrosilicon), as at those times it was the main route for cast iron processing. However, in a blast furnace it is not possible to produce ferroalloys with elements that have a higher affinity for oxygen or with low carbon content. This led to the development of ferroalloys to be manufactured (smelted) in electric furnaces at the beginning of the 20th century.

Today, almost all ferroalloys are produced in submerged arc furnaces ([Fig. 1.1](#)), where raw materials (ores), reductants (coke, silicon-based ferroalloys, aluminum), iron additions (iron ore or steel scrap), and fluxes (lime, magnesia, dolomite, limestone, fluorspar, etc.) are loaded and smelted, followed by the tapping of slag and metal.

With the first experience of ferroalloys smelting, it became evident that more research was needed to improve our understanding of the thermodynamics of liquid melts; ferroalloy and slag formation ([Holappa and Xiao, 2004](#)); the kinetics of reduction and phase transformation; the structure, properties, and stability of solid ferroalloys, mineral raw materials, and reducing agents applied; and the electric and thermal properties of all charge components. Later, the issues of better energy and resource utilization, lower emissions requirements ([Tanaka, 2008](#)), and increasing demands to improve the purity and costs of ferroalloys set new challenges for improving the quality and price competitiveness of ferroalloys and their production processes.

It is now well understood that the main technical and economic performance indicators of ferroalloys production and application (i.e., their competitiveness) could be substantially improved with systematic fundamental and applied research, allowing for the development and implementation of better energy-saving smelting processes, the creation of more sophisticated electric furnace equipment with automated control systems, and enhancements to process management.

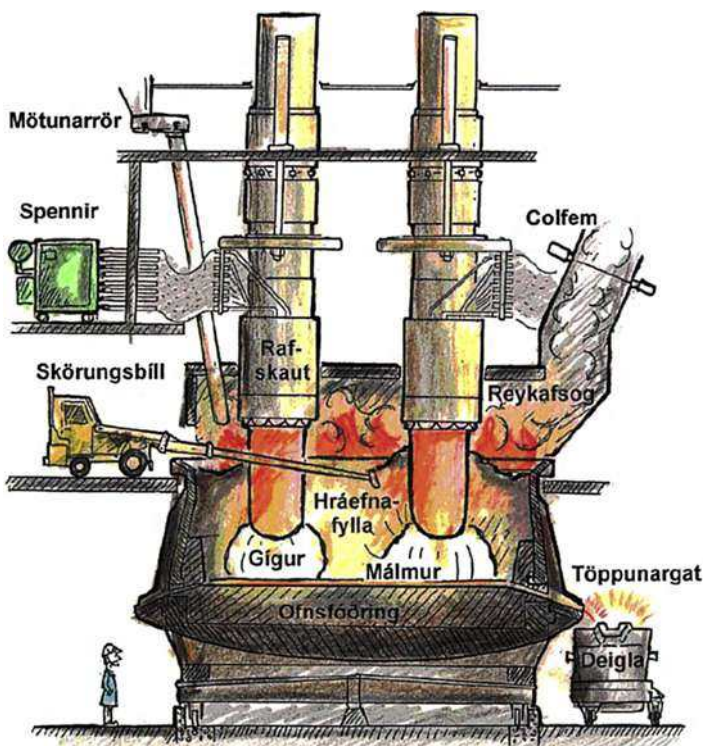


FIGURE 1.1 The general artistic impression of the modern submerged arc furnace process.
(Courtesy of Dr. Þorsteinn Hannesson, Elkem Iceland.)

1.2 THE SCOPE AND STRUCTURE OF THE BOOK

In the 20th century, several books were published and numerous conferences were held concerning the domain of ferroalloys. However, whereas several editions and new titles have been published in the Commonwealth of Independent States (CIS) (previously Union of Soviet Socialist Republics [USSR]) and China, in the Western world possibly the last specifically dedicated book by Durrer and Volkert was released in German as its next edition (Durrer and Volkert, 1972). This book has been translated into several languages and remains one of the basic books on this topic.

Contemporary publications in ferroalloys are widely spread among different journals, reports, and conference proceedings, and it is not an easy task to present a coherent picture to a reader. Taking into account the developments in ferroalloys processing theory and technology, a need has been identified to collect and unite modern knowledge in a consistent way, suitable for students and professionals. The current text was originally formulated as

a comprehensive collection of theory and technology outlooks in ferroalloys, but later it was tailored to a handbook-like style.

The goal of this book is to provide a unified, combined overview of ferroalloys technology, which is reasonably formulated to answer questions concerning specific ferroalloys, their processing peculiarities, and used equipment and its operation, as well as relevant environmental issues.

The book is divided in three sections: a general section (I), a section on major (bulk) ferroalloys (II), and a section on minor ferroalloys (III). The general section deals with ferroalloy basics, thermodynamics, the kinetics of reduction and general processing issues, electric furnace operations, environmental issues, and so on. The second section describes the theory and technology of ferroalloys with silicon, manganese, and chromium. The last section explores all other industrially relevant ferroalloys, as well as the peculiarities of their processing and applications. For every specific ferroalloy (i.e., its leading element), there is a chapter that includes brief information about the element and its properties, reactions, and equilibria with other major relevant elements (iron, oxygen, carbon, silicon, aluminum, nitrogen, etc.). Raw materials (minerals, ores) for this element and methods of their preparation are described, and the ferroalloy's smelting techniques are presented, along with the practical details and peculiarities one needs to know to ensure successful processing.

The authors have decided not to spend too much time discussing, for example, specific reactions between different substances and their thermodynamic parameters, as recently all thermodynamic data are retrieved from databases using more complex Gibbs minimization methods for equilibrium assessment, and thus the numerical values of the parameters do not need to be explicitly known. The same concerns phase equilibria diagrams, which in this book have been mostly recalculated using the latest available software programs (FactSage 6.2 and ThermoCalc R) with their own proprietary databases. Some thermodynamic analyses and diagrams were also calculated with HSC Chemistry 7.1 (Outotec Corp., Finland).

It is not possible to gather and present the most complete information about specific ferroalloys or details about their processing: many such features are plant or mine specific and might not be valuable for general use. Therefore, the book's philosophy is to present knowledge about general ferroalloys worldwide, along with sufficient details for practical use, rather than focusing on the thermodynamics for reducing specific oxides or the like (this information can be easily found in other metallurgy books and conference proceedings).

The materials in this book are also intended to help students, plant engineers, managers, and researchers in the fields of electrometallurgy, mining, and steelmaking to obtain a basic knowledge of the theory and technology of smelting different ferroalloys in accordance with the modern world practice and scientific level of development.

ACKNOWLEDGMENTS

As the editor of this book, I would like to acknowledge the enormous support received from all contributors and my colleagues at Aalto University, especially Dr. Y. Bilotksy, Dr. A. Lokki-Luoto, Lic. Tech., and M. Malinina, and to thank them for their valuable assistance in materials gathering and preparation. Special thanks also to Outotec Corp. (Finland) and the Foundation of Helsinki University of Technology, which provided the financial support that made this book possible.

Michael M. Gasik
Espoo, December 2012

REFERENCES

- Durrer, R., Volkert, G., 1972. Metallurgie der Ferrolegierungen. 2. Auflage. Metallurgy of Ferroalloys, second edition. Springer-Verlag, 700 pp.
- Gasik, M.I., Lyakishev, N.P., 2005. Physical chemistry and technology of electro-ferroalloys, Systemnye tekhnologii. Dnepropetrovsk, Ukraine, 448 pp.
- Holappa, L., Xiao, Y., 2004. Slags in ferroalloys production – review of present knowledge. Journal of the South African Institute of Mining and Metallurgy 104, 429–437.
- Tanaka, K., 2008. Assessment of energy efficiency performance measures in industry and their application for policy. Energy Policy 36, 2887–2902.
- Wood, E., Owen, M., 2005. Ferro-alloy directory. Metal Bulletin plc, 13–97.

Basics of Ferroalloys

Lauri Holappa

Aalto University, Espoo, Finland

Chapter Outline

2.1 Introduction: Background for Ferroalloys Development and Production	9	2.5 Energy and Emissions Issues of the Ferroalloys Industry	22
2.2 Ferroalloys in the Development of Steels	12	2.5.1 Energy Demand for Ferroalloys Making	22
2.3 A Case: Ferroalloys for Stainless Steels	14	2.5.2 CO ₂ Emissions from Ferroalloys Production	23
2.4 Recent Ferroalloys Production and Markets Development	17	2.6 Future Outlook for the Ferroalloys Industry	26
		References	27

2.1 INTRODUCTION: BACKGROUND FOR FERROALLOYS DEVELOPMENT AND PRODUCTION

The history of ferroalloys is relatively short compared to bronze or iron development. Ancient iron artifacts investigated are mostly fairly pure iron, containing carbon as the only alloying element. Carbon control by carburizing/decarburizing treatments was traditionally understood by blacksmiths and was used throughout the “Iron Age” to adjust steel properties. Steel produced via the direct reduction route in bloomeries remained naturally unalloyed because iron oxide was reduced at such low temperatures that iron was formed in the solid state. Other components like manganese and silicon, which are typical in modern steels, were found only as natural impurities, yet mainly in slag inclusions in steel. When higher shaft furnaces were developed from bloomeries, stronger air blasting through tuyeres was needed. Temperature in the combustion zones was increased, and the iron formed dissolved more carbon and melted: thus, a blast furnace process was discovered. This development happened in the late Medieval Age in Central Europe. The product was carbon-saturated cast iron

that typically contained a small percentage of silicon and eventually also some manganese, depending on the ore composition. Pig iron from blast furnaces was used as foundry iron for castings or converted to steel by difficult and time-consuming refining process. These processes were gradually developed, but steel from bloomeries kept its dominance until the 19th century. In the early 19th century, two main methods were used to refine hot metal from blast furnaces to steel. They were puddling with an oxidizing flame in a reverberatory furnace and the crucible process in which iron oxide (ore, scale) was added into hot metal to react with carbon and to get low-carbon steel (Flemings and Ragone, 2009; Tylecote, 1984). Principally some alloying would have been possible, but several prerequisites had to be met before rational alloying could be carried out. First, the breakthrough inventions in chemistry during the end of the 18th and early 19th centuries with the discovery of elements (like nickel, oxygen, manganese, chromium, molybdenum, and silicon from 1751 to 1824) and the understanding of chemical reactions like combustion/oxidation and reduction made it possible to recognize essential events of contemporary iron and steel-making processes and to start developing new processes (Engels and Nowak, 1983). Second, there should be some evidence of beneficial influences of additions on steel properties, which requires an understanding of steel microstructure and the influencing mechanisms of alloying elements. Third, it should be possible to produce potential alloying materials at a reasonable price. During the last half of the 1800s, these prerequisites gradually began to be fulfilled.

In steelmaking the decisive breakthrough was the invention of the converter process by Henry Bessemer in 1855. He realized that oxygen from air blown inside the carbon-rich hot metal burned the carbon dissolved in iron melt. He also succeeded in developing a proper reactor and technology for the Bessemer process. Bessemer's steel converter was, however, lined with acid silica refractory. Even if it could operate at temperatures up to 1600°C, the lining life was short. Because of the acid environment, the low-basicity slag was unsuitable for phosphorus removal. This was a big problem at that time in Great Britain, where plenty of P-bearing iron ores were available. The problem was solved when S.G. Thomas and P.C. Gilchrist succeeded in developing basic doloma lining, introduced in 1878–1879 (Barracough, 1990). Doloma is a calcia-magnesia mixture obtained by burning natural dolomite ($(\text{Ca}, \text{Mg})\text{CO}_3$) mineral. Basic Thomas converters gradually replaced acid Bessemer converters. Also the open-hearth process (involving a reverberatory furnace heated by flame), developed by the Siemens and Martin brothers in 1860–1870, which started with acid lining, adopted basic lining and the new steelmaking practice as well. Thus, basic lining was available for electric furnaces when they started to be used for steelmaking in the beginning of the 1900s and for the production of ferroalloys too.

In parallel with Bessemer's process development, Scottish metallurgist Robert Mushet discovered a way to add manganese-containing *spiegeleisen* in liquid steel to “kill” it. The term *killing* stemmed from the prevention of steel

melt “boiling” (actually carbon-oxygen reaction and formation and removal of CO gas, which appears as boiling). Certain additions like spiegeleisen were observed to eliminate this “wild” state and to “kill” the steel. Manganese was thus first used for steel deoxidation. Its beneficial effect to avoid hot shortness by binding excess sulfur was soon recognized (Tylecote, 1984). Spiegeleisen was already produced in the 18th century in blast furnaces, containing 8% to 15% Mn and ~5% C. Mushet was also one of those who developed the first “tool steels” with 1% to 2% Mn and high tungsten content in the 1860s. Robert Hadfield invented the first high-manganese steel in the 1880s by introducing a work hardening steel with 11% to 14% Mn and 1% C (Tylecote, 1984). This steel grade has remained principally unchanged and still has a firm position in impact- and wear-resistance type working applications (e.g., in railway crossings). At this time, it also became evident that alloying or modifying steel with pure elements is not economical. Further, it might be technically challenging or impossible (e.g., dissolution of metallic tungsten in a steel melt would take an enormously long time).

At that time metallurgists started to consider the addition of alloying elements to steel in the form of a ferroalloy—an alloy of iron with at least one other element (except carbon, which is as cementite, Fe_3C , or graphite in cast irons). Small-scale production of ferroalloys began in the 1860s with the use of the crucible process. Chromium or manganese ore was reduced by coal in graphite crucibles, which were heated to high temperatures to get liquid high-carbon ferroalloy (~25% Cr). High-Mn ferromanganese production was also started in a blast furnace by the French Terre Noire Co in 1877 with 80% Mn and 6% to 7% C. It was also demonstrated that FeSi could be produced in a blast furnace, as could low-content FeTi and FeV ferroalloys. On the other hand, production of FeCr in the same way was found difficult because of the high melting point of the slag formed during smelting (Volkert and Frank, 1972). When electric furnace technology was introduced at the end of the 1800s, electric smelting of ferroalloys gradually progressed in the early 1900s, and today all ferroalloys that require furnace technology are produced exclusively in electric furnaces.

The occurrence of silicon in iron has its historical origin in blast furnace iron making. Advisedly or by accident, relatively high Si contents (several percents) were obtained in pig iron depending on the blasting practice, blast furnace burden material, charcoal, and other factors. Generally, high silicon in cast iron promotes graphite formation and thus improves ductility. In the early 1900s, however, the exact explanation was not known, and the knowledge of how to produce good-quality castings was more art than science. In the early 1800s, Swedish chemist Jacob Berzelius produced a kind of ferrosilicon by crucible reduction. He also succeeded in separating elemental silicon, which he called “silicium,” in 1824 (Engels and Nowak, 1983). Berzelius observed that silicon burned in air and formed silica (silicon oxide). The production of elemental silicon turned out to be very difficult, so ferrosilicon was produced

instead. It was possible to produce Si-containing hot metal in blast furnaces up to 20% Si in the late 19th century. The product was used for steel deoxidation and alloying. When the electric furnace was developed at the turn of the century, the production technology for FeSi was also developed.

Smelting in an electric furnace and reduction with carbon (coke, charcoal, coal) thus constitute the method on which production of most ferroalloys was founded and special furnace constructions and technologies were developed. In ferroalloys production furnaces are designed to operate in submerged arc mode (submerged arc furnace [SAF]), in which the high resistivity of the charge is utilized for smelting.

The processes described so far are based on carbothermic reduction operating at high temperatures. Sinter or pellets prepared from concentrates and eventually lumpy ore are reduced by coke to form the ferroalloy. The heat for the reactions is generated by electric arcs (with plasma temperatures \sim 18 000° to 20 000°C) formed between the tips of the electrodes in the furnace. The temperatures of materials near the arc zone may reach \sim 2800° to 3000°C, whereas the temperatures in the main reaction zone are typically around 1600° to 1800°C. Because of the strongly endothermic reduction reactions in the smelting process of a ferroalloy, huge amounts of electricity are consumed. In modern FeCr and FeMn processes, typical electricity consumptions are 3000 to 3500 kWh/t ferroalloy, and in the FeSi process typical electricity consumption can reach up to 7000 or 8000 kWh/t FeSi for a high-silicon (75% Si) ferroalloy.

2.2 FERROALLOYS IN THE DEVELOPMENT OF STEELS

As mentioned, old historical iron artifacts were made of almost pure iron containing only carbon as the alloying element. Properties like hardness, strength, and toughness were controlled by changing carbon content with the use of carburizing or decarburizing treatments, skills that had been mastered by blacksmiths. Historical “super steels” like “Damascus” steel and “Bulat” steel, which used Indian “Wootz” iron as a raw material, had amazing properties that are difficult to attain with modern technologies. Rather, in these steels the properties were based on complicated and sophisticated processing with a combination of high and low carbon source materials, which form a composite layered structure via forging-folding-welding tens and maybe hundreds of times (Reibold et al., 2006; Smith, 1988). Famous Japanese *katana* swords were made of Tatara iron, which contained some titanium within iron sand (ilmenite $\text{FeO}\cdot\text{TiO}_2$) and was typically used as an iron source. Also, traditional Japanese sword masters used a folding/forging technique.

Generalized steel alloying was not possible until the 19th century. When understanding of basic chemistry, including analytical chemistry, progressed, it became possible to measure steel composition. At the same time, great advancements were attained in materials investigations and characterization. An important tool in materials research was optical microscopy, which could

reveal the microstructure of steel and find relations between steel composition, microstructure, and properties. A contemporary of Bessemer, H.C. Sorby in Sheffield, was one pioneer who examined steel microstructure (Tylecote, 1984). The value of metallography was appreciated in Europe by 1885. At that time a French research group at Creusot-Loire investigated relations between the microstructure and heat treatment of steels. The polymorphic forms of iron and different microstructures were identified (austenite, ferrite, cementite, pearlite, martensite, and, somewhat later, bainite in the 1920s). The invention of electron microscopy in the 1930s and its development as a common tool for materials scientists further improved knowledge about steel structure and phenomena influencing its structure and properties.

In most steels, carbon is the base element influencing the structure, but by adding different alloying elements, the formation of microstructures and their properties could be controlled. Further, new precipitated phases could be obtained, like carbides (with Cr, Mo, Nb, Ti, V, W, etc.), nitrides, or carbonitrides (Al, Nb, Ti, V). Edgar C. Bain, who in the early 1920s discovered the structure named bainite, and H.W. Paxton, gave a comprehensive summary of the behavior of different alloying elements in steels and their influences on microstructure and properties in the book *Alloying Elements in Steel* (Bain and Paxton, 1966). In the following 50 years, enormous progress was made in the development of new steels with improved performance properties. Improved knowledge of thermodynamics, kinetics, and mechanisms of precipitates formation and phase transformations in different steels has been the basis for creating new steel grades and manufacturing methods. The processes and science of heat treatments have strongly evolved. One example is the thermo-mechanical controlled rolling process, which can produce better mechanical properties in steels with less alloying but a cheaper and faster process route (DeArdo et al., 1990). Figure 2.1 summarizes the most important properties of steels and the process stages where these properties are mainly determined.

Because of great innovations in steelmaking processes, steels can be produced with high “purity” (a low content of impurities like S, P), a low content of interstitial atoms (N, H, and C in ultra-low-carbon grades), and ultimate cleanliness (low oxygen content, strict inclusion control, and the absence of harmful precipitates). Technological developments in processes also have given means to new evolutions in microalloyed and high-alloyed steels. The requirements for the alloying materials depend not only on the need of alloying to attain the desired analysis limits, but depending on the process stage and circumstances, sometimes quite strict requirements can be set regarding the chemistry and physical state of the alloys. Consequently, a wide variety of alloy materials have become available with various compositions specified to certain purposes and in different forms (e.g., lumps, grains, powder, wire, cored wire). Except for different carbon grades, the ferroalloys can be categorized—for example, according to Al-, Ti-, Ca-, Mg-, P-, or S-contents as well as metallic impurities (Cr, Ni, Cu, Sn, As, Sb, etc.).

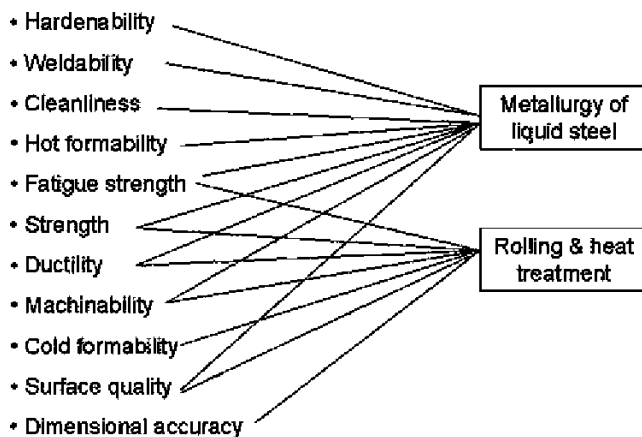


FIGURE 2.1 Relations of steel properties to metallurgical treatments of steel in liquid and solid states.

2.3 A CASE: FERROALLOYS FOR STAINLESS STEELS

Among high-alloyed steels, stainless steels are a special case because of their large production amount and central position as users of ferrochromium. Furthermore, other ferroalloys are also used extensively for stainless steel production. The history of stainless steel is quite short, as the effect of chromium on the improved corrosion resistance of iron was only recognized in the early 1800s. However, at that time it was not yet possible to produce chromium or chromium ferroalloy had to be produced industrially. Reducing chromium from chromite ore ($\text{FeO}\cdot\text{Cr}_2\text{O}_3$) is difficult and needs high temperatures $\sim 1700^\circ\text{C}$ for efficient reduction and liquid slag formation during the process. High temperature also sets strict requirements for a furnace and its lining material.

The first trials to produce “stainless steels” were performed soon after 1900. The “stainless era” is usually said to have begun in 1912 when austenitic Cr-Ni stainless steel was patented by the company Krupp, followed by ferritic and martensitic stainless steels created by other inventors (Tylecote, 1984). Acid-resistant Mo-containing stainless steels were introduced later in the 1920s. In the following decade, fundamentals of main types of stainless steels and their properties were duly examined, but production grew slowly because of the obstacle of a too-high carbon content. Today it is evident that in most stainless steels, carbon content should be very low (typically below 0.05%) to avoid the formation of carbides, which impair corrosion resistance and cause the “sensitization” phenomenon (a type of grain boundary corrosion). In the steelmaking process, the carbon problem is linked to chromium: when carbon is oxidized for removal, Cr also starts to oxidize. This meant that high-carbon FeCr could not be used for stainless steel without drastic chromium losses

during steelmaking. A lot of chromium should be added after decarburization by using low-carbon FeCr, which is more expensive than a high-carbon grade. Low-carbon FeCr should also have a higher Cr:Fe ratio to minimize the amount of alloying required, but so-called charge FeCr typically had rather low Cr:Fe (containing only 50% to 55% Cr). Therefore, to produce low-carbon FeCr, ores with a high chromium content are preferred. Special processes were developed to decarburize FeCr—for example, single or double treatment with slag to make “affine” (<4% C) and “sur-affine” (<0.5% C) FeCr grades. The stainless steel production exceeded 1 Mt/year in 1950. Stainless steel production received a boost with the invention of the argon-oxygen decarburization (AOD) process, taken into operation in the 1960s. It made possible the use of high-carbon FeCr and to decarburize the melt by diluting oxygen by Ar gas and thus lowering the partial pressure of CO, which is formed (Krivsky, 1973). In 1976, the world production of stainless steels exceeded 5 Mt, reaching 10 Mt in 1988, 20 Mt in 2002, and 30 Mt in 2010 (based on data from www.worldstainless.org, 2012), as shown in Figure 2.2.

Stainless steels can be divided in several groups depending on their alloying and structure. Austenitic stainless steels (ASTM classification 300 series) form the biggest group, accounting for 55% to 60% of all stainless (Fig. 2.3). A classic example is 18/8 steel with 18% Cr and 8% Ni. If better corrosion resistance, especially against pit corrosion, is required, the nickel content is raised to 11% to 14% and molybdenum is added (2% to 4%). The carbon

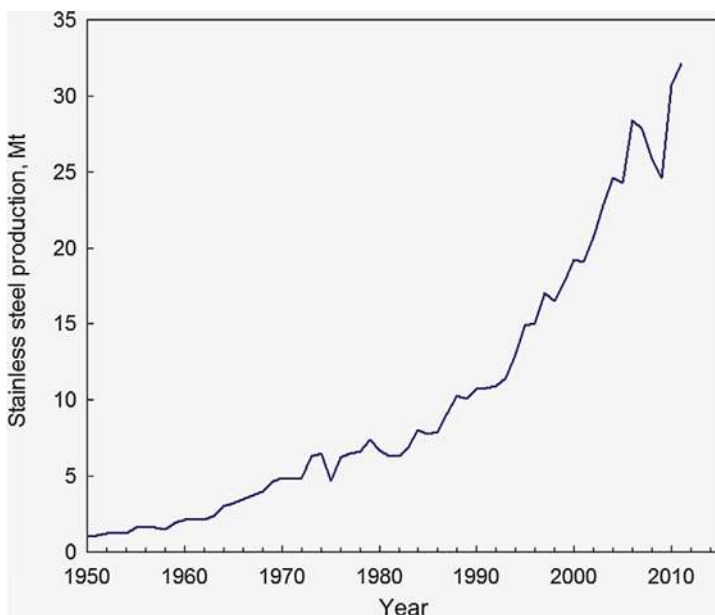


FIGURE 2.2 Growth dynamics of the worldwide production of stainless steel.

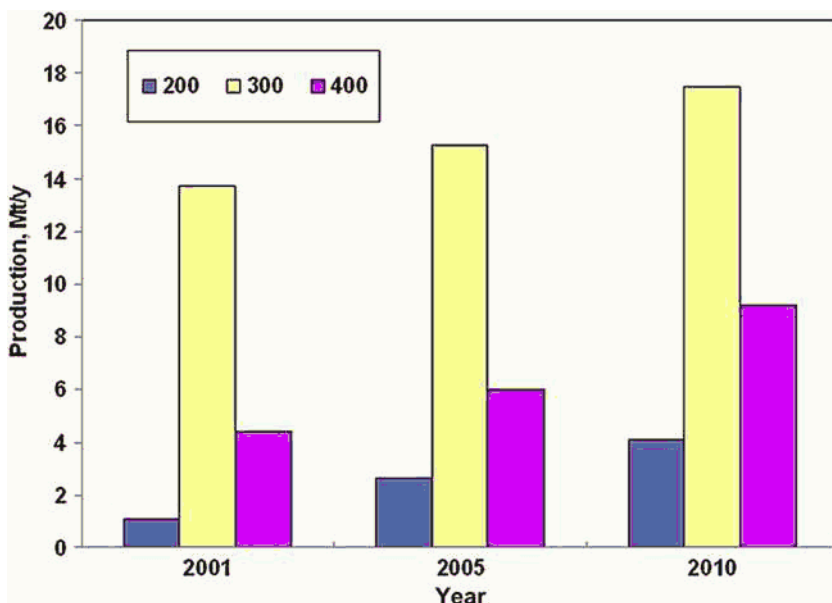


FIGURE 2.3 Share of stainless steel grades by category (200, 300, and 400 series).

maximum is normally 0.03% C (“L” grades), but in high temperature grades may be typically up to 0.08% C (“H” grades).

The second major group is represented by ferritic stainless steels, some 30% of all the stainless (400 series) (see Fig. 2.3). Here, chromium content is from 10.5% to 30%, and it can contain some Mo and even Ni. Carbon content is limited, like in austenitic steels. A relatively new group of stainless steels is “duplex stainless steels,” which have approximately same fraction of austenite and ferrite in their structure. An example analysis is 21% to 23% Cr, 4.5% to 6.5% Ni, 2.5% to 3.5% Mo, 2% Mn, and C_{max} 0.03%. Duplex steels have better mechanical properties because of their structure.

Martensitic stainless steels belong to ferritic steels but have a higher carbon content (0.1 to 1% C), which makes them hardenable when quenching after heat treatment. Corrosion resistance is not as good as it is in corresponding low-carbon grades but good mechanical properties make these steels applicable in different tools, dental and surgical instruments, cutlery, and so on. A typical martensitic stainless steel has 12% to 14% Cr, <2% Ni, 0.2% to 1% Mo, 1% Mn, 1% Si, and 0.3% C.

Because of the high contents of alloying elements in stainless steels, their price is sensitive to changes in alloying costs. When nickel prices climbed up, increased attention was paid to finding substitutes for nickel in austenitic 300 series stainless steels. A common austenite stabilizer is manganese. In the 200 series stainless steels, Cr content is kept to 16% to 19%, but Ni content is

decreased to around 5% (in some grades only 1% to 2% Ni) and Mn content is raised to 5% or 10% Mn. Also copper (Cu) and nitrogen (N) can partly substitute for nickel. Significant production of these Cr-Mn-Ni stainless steels, known since the 1930s, began in the United States in the 1950s ([ASM Handbook, 1990](#)). After the year 2000, production of the 200 series steels increased, especially in China and India, and exceeded 10% of the total stainless steel production in 2005; it is currently on the level of 12% to 14% (see [Fig. 2.3](#)).

2.4 RECENT FERROALLOYS PRODUCTION AND MARKETS DEVELOPMENT

As the ferroalloys are primarily used in steelmaking, different grades of alloys have been developed to fulfill the varying requirements of the steel industry. As discussed earlier, most of the chromium is added in the form of high-carbon charge FeCr (50% to 55% Cr, 2% to 5% Si, 6% to 8% C, and the balance is Fe). Also, for different alloying purposes, different Cr-alloys are produced with higher Cr and lower carbon contents than in Charge HC (high-carbon) FeCr. Typical composition is 60% to 70% Cr, 2% to 3% Si, and in different carbon categories: high-carbon (HC) grades with 5% to 8% C, medium-carbon (MC) grades with 1% to 4% C, and low-carbon (LC) grades with 0.1% to 0.5% C. Even lower carbon contents are available. The world leader in ferrochrome production is South Africa with 3.6 Mt in 2008; China is second with 2.2 Mt, followed by India and Kazakhstan with about 1 Mt/year. Kazakhstan, South Africa, and India have the largest chromite resources known. Russia and Finland are the next big producers with productions of about 0.25 Mt/year. [Figure 2.4](#) shows the progression of the world's ferrochromium production. Over 80% of all FeCr goes into stainless steel and high-alloyed steels. The rest is used in low-alloyed steels (typically 0.3% to 2.0% Cr) to improve hardenability and strength. Concerning the need of FeCr for stainless steels, it is noteworthy that a significant share of the all Cr units (on average 30% to 40%) comes from recycled stainless scrap and the rest (60% to 70%) comes from "virgin" ferrochrome alloy.

Ferroalloys production is firmly coupled with steel production, and the time-dependent production rates follow each other. The total world steel production is presented in [Figure 2.5a](#) and the total ferroalloys production in [Figure 2.5b](#), except for ferrochrome even ferromanganese, silicomanganese, and ferrosilicon. In 2008–2010 about 5.7 Mt of ferromanganese, 8.5 to 9.5 Mt of silicomanganese, and 7.5 to 8 Mt of ferrosilicon were produced annually.

A comparison of the production of the mentioned "bulk" ferroalloys since the 1980s reveals some interesting features. Concerning manganese alloys, there has been a clear transition from FeMn to SiMn ([Fig. 2.6](#)): in the beginning of the 1980s FeMn was produced much more than SiMn, in the beginning of 2000 the produced amounts were equal, but in 2010 the FeMn/SiMn ratio was ~0.6 ([Brown, 1984](#); [Corathers et al., 2012](#); [Fenton, 1996](#)).

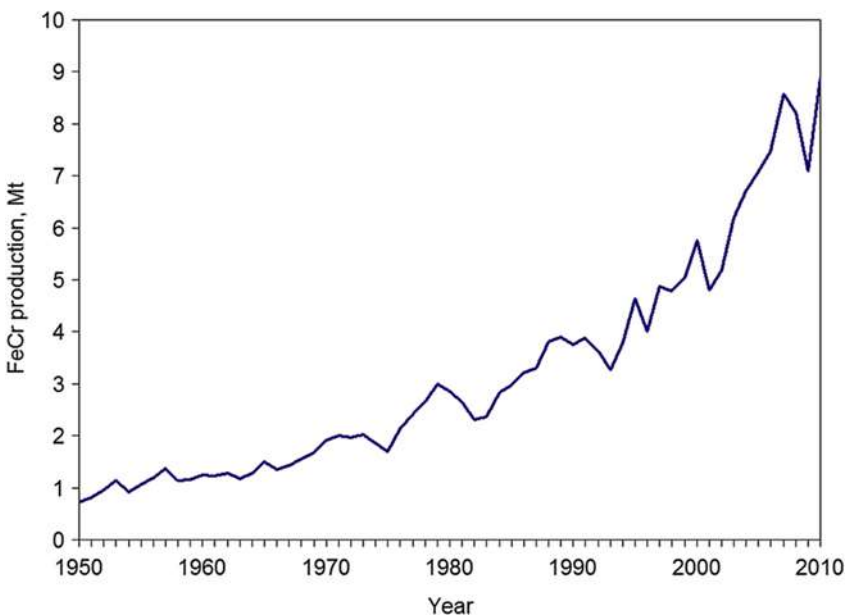


FIGURE 2.4 World production of ferrochromium.

There have been some changes in production technology: ferromanganese production in blast furnaces has reduced from 30% to about 10%, and most FeMn production now occurs via submerged arc furnaces (SAF). All silicomanganese is produced in SAFs. Silicomanganese is a suitable addition to be used for the deoxidation of most steels, whereas ferromanganese and ferrosilicon are used mainly for alloying purposes. Nevertheless, the growing trends shown in Figure 2.6 are comparable with the trend of steel production.

By calculating the apparent ferroalloy consumption per all kinds of steels produced, eventual trends in “alloying degree” can be observed (Fig. 2.7). The average consumption of ferroalloys has been 2.2% to 2.4% of the mass of steel, but it has grown to 3% in recent years. However, this does not refer to real growth of “degree of alloying” but describes the fast growth of high-alloyed stainless steels. As most chromium is added as charge FeCr with low Cr content (50% to 55%), the quantity of the ferroalloy addition is still emphasized.

Despite the volatility of metals markets, ferroalloys production is rather steady as it represents one of the major backbones of steelmaking. Besides steels, ferroalloys are used also for special materials production (foundry castings, superalloys, low-iron and nonferrous alloys, welding materials, etc.). Figure 2.8 presents a map of the producing countries. Countries with reported ferroalloys production are marked (data collected from various sources as of 2010). Nevertheless, there is also local ferroalloys production

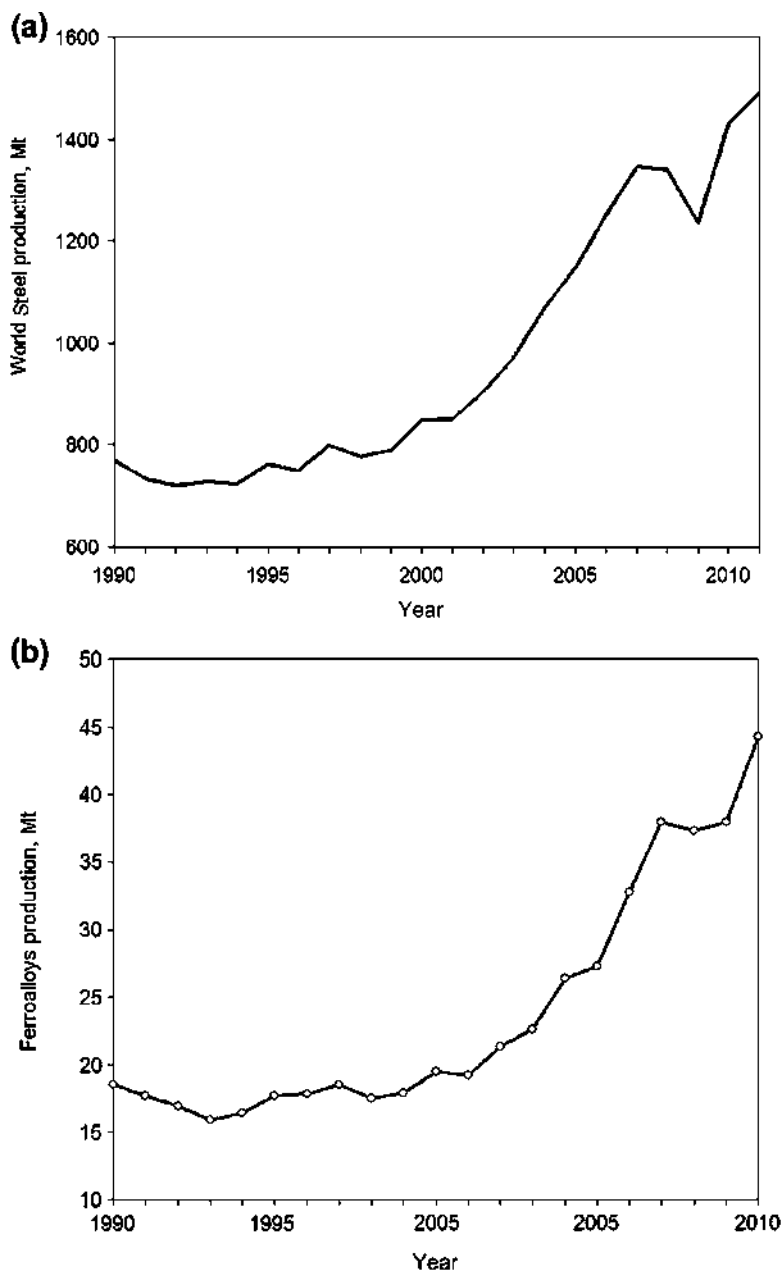


FIGURE 2.5 World production of steel (a) and ferroalloys (b).

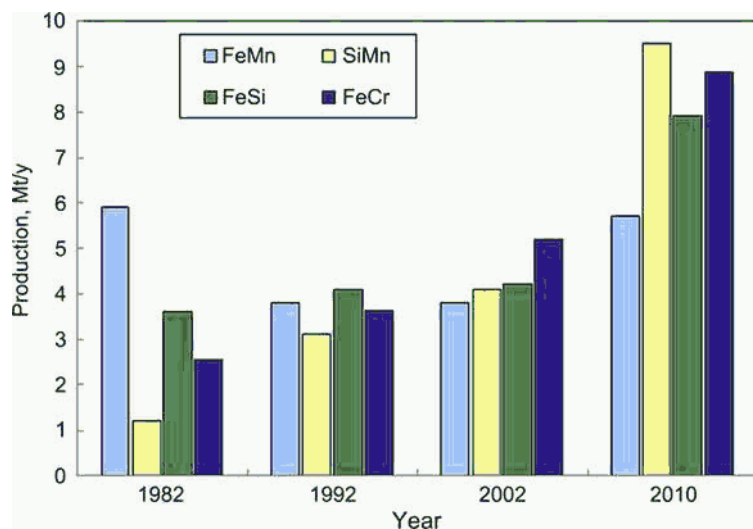


FIGURE 2.6 World production of FeMn, SiMn, FeSi, and FeCr alloys.

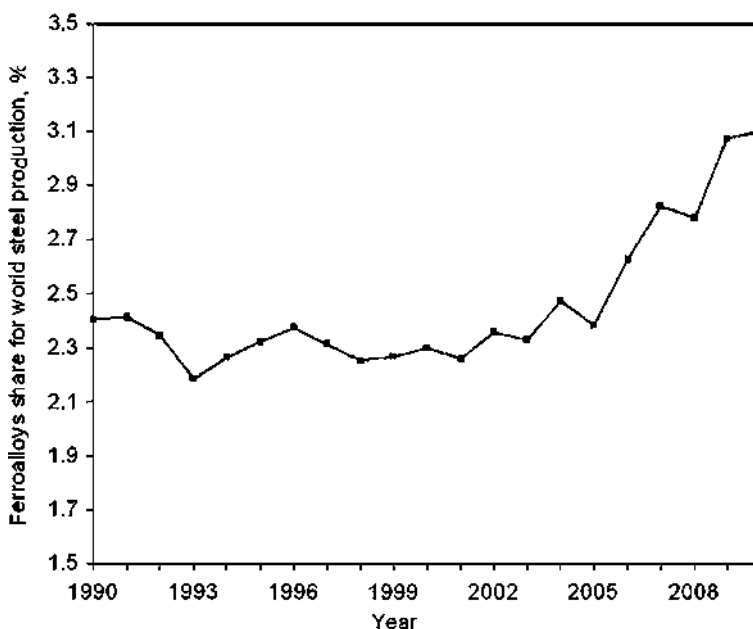


FIGURE 2.7 Average consumption of ferroalloys, percentage to steel.

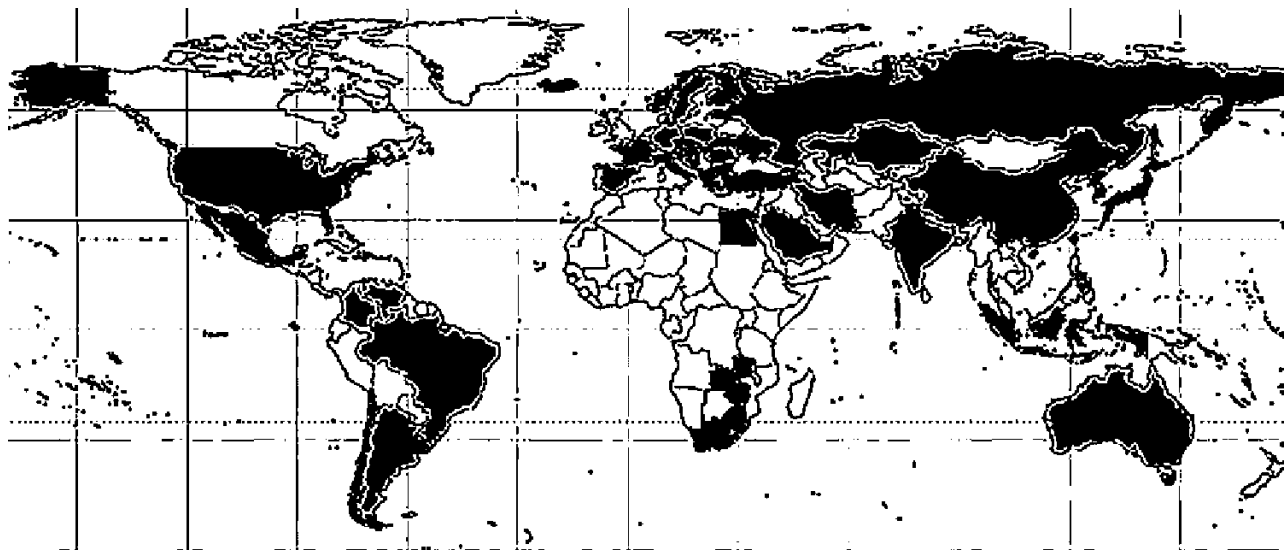


FIGURE 2.8 World map with major ferroalloys producers marked (2010).

FIGURE 2.9 Periodic table showing ferroalloy major leading elements (dark gray) and co-occurring (minor) elements (light gray).

in-house in some metallurgical plants for that company's own use as well as occasional smelting campaigns to satisfy peak demands or to utilize locally available resources.

Finally, the modified periodic table (Fig. 2.9) shows the ferroalloys spectrum. Elements marked in dark gray are so-called leading elements (i.e., ferroalloys with these elements are produced explicitly), and the content of these elements is specified by standards and is monitored. Elements marked in light gray co-occur in ferroalloys but usually are not specifically separated. For example, cobalt often occurs in ferronickel during smelting, but the alloy is still ferronickel as nickel is the leading element in this case.

2.5 ENERGY AND EMISSIONS ISSUES OF THE FERROALLOYS INDUSTRY

2.5.1 Energy Demand for Ferroalloys Making

Today's ferroalloys are almost always produced by smelting in electric submerged arc furnaces (SAFs); only a comparatively small amount of ferromanganese is still produced in blast furnaces. A conventional SAF is an open furnace from which off-gas is mixed and combusted with a large amount of air. A "closed furnace," however, is designed to maintain CO-rich off-gas by collecting, cleaning, and storing it for further utilization. An intermediate type, referred to as a "semiclosed" furnace, is still common for FeSi and special alloys production. It is still possible to recover off-gas from this type of furnace, but it is less calorific. There is a strong trend toward closed furnaces with gas recovery and utilization; for instance, in ferrochrome production closed furnaces have rapidly increased ([Holappa, 2010](#)). As an example, some basic data of FeCr and FeMn ferroalloys making are reviewed in [Table 2.1](#).

TABLE 2.1 Consumption of Raw Materials and Energy When Producing HC FeCr and FeMn: Conversion of Coke to Electricity: 1 kg coke = 7.7 kWh

Ferroalloy Type	HC FeCr		HC FeMn
	Open	Closed	Closed
SAF type			
Feed type	Lumpy/fine, no preheating	Pellets, preheating	No preheating
Ore, kg/t	2400–3000	2300–2400	1900–2400
Reducing agent, kg/t	550–700	500–550	410–500
Fluxes, kg/t	100–400	200–300	—
Electrodes (paste), kg/t	8–25	7–10	8–25
Electricity, kWh/t	3800–4500	3100–3500	2200–3200
Potential coke energy, kWh/t	4200–5400	3900–4200	3100–3500
Total energy input, kWh/t	8000–9900	7000–7700	5300–6700

2.5.2 CO₂ Emissions from Ferroalloys Production

Ferroalloys production is an energy-intensive industry with a high consumption of electricity but only a moderate consumption of coke and minor consumption of other fuels and reductants. This affects direct CO₂ emissions. Table 2.2 has been calculated based on the literature data (Corathers et al., 2012; Lindstad et al., 2007; Sjardin, 2003) of emission factors for different processes and production numbers. For these ferroalloys, different grades (high, medium, low carbon; different silicon content) with different emission factors were integrated. Carbon dissolved in ferroalloys was not included as an emission in ferroalloys production.

As shown, the total emissions from four main ferroalloys with 32 Mt annual production were about 63 Mt, from which an approximate figure about 87 Mt CO₂ for total ferroalloys production (44 Mt) can be given as a rough estimate. However, the emissions data given in Table 2.2 are only for direct emissions from the combustion of carbon when coke and eventually coal are used for reduction as well as from electrodes consumption. One has to add indirect emissions generated in electricity production (see Table 2.1), so, depending on the method of electricity generation, the indirect CO₂ emissions

TABLE 2.2 Emission Factors, Production, and Estimated Global Emissions for Common Ferroalloys

Ferroalloy	Emission Factor, t CO ₂ /t Alloy	Production, Mt	Estimated CO ₂ Emissions, Mt
HC FeCr HC	1.3–1.63	8.9	14
HC FeMn	1.3–1.79	5.7	10
FeSi (45% to 90% Si)	2.5–4.8	7.9	23
SiMn	1.4–1.66	9.5	16
Total		32	63

can be large. **Table 2.3** shows CO₂ emission factors in the biggest ferroalloys-producing countries (see Graus and Worrell, 2011). Countries that have plenty of renewable energy (including nuclear power) naturally have low emission factors when compared with countries that are using coal power. In such conditions the total emission factor can be doubled compared to the value of the direct emission factor. The emission factor should be one decisive criterion when erecting and operating ferroalloys plants.

Although more data of energy and materials consumption in different processes/furnaces can be found in the literature, any direct comparison is impossible because of the use of different raw materials, process conditions, products, definitions of terms, and so on. A new approach for process

TABLE 2.3 CO₂ Emissions in Total Power Generation by Selected Countries in 2007 (g/kWh): The Values Are Heat-Corrected (Graus and Worrell, 2011).

Country	CO ₂ , g/kWh	Country	CO ₂ , g/kWh
Australia	921	Kazakhstan	488
Brasilia	71	Norway	3
China	823	Russia	363
Finland	164	South Africa	862
India	948	Ukraine	413
Japan	451		

evaluation is the best available technology (BAT) procedure. BAT was defined by EC Directive 96/61 Article 2(11) as follows:

The most effective and advanced stage in the development of activities and their methods of operation which indicates the practicable suitability of particular techniques for providing in principle the basis for emission limit values designed to prevent, and where that is not practicable, generally to reduce the emissions and the impact on the environment as a whole.

This definition implies that BAT not only covers the technology used but also the way in which the installation is operated, thereby ensuring a high level of environmental protection as a whole. BAT takes into account the balance between the costs and environmental benefits. The following list summarizes the most effective and advanced technologies for use on the ferroalloy production line (Holappa, 2011; Worrell et al., 2008):

- Concentrate sintering by utilizing CO gas from a smelting furnace.
- Preheat charge material for the smelting furnace by utilizing off-gas from the SAF.
- Prereduce the charge before smelting in the SAF. This is a potential but unestablished subprocess for certain ferroalloys.
- Smelt in closed SAFs with efficient off-gas recovery, filtering, and energy utilization in-plant or in neighbor users.
- Use of a semiclosed furnace (for FeSi) is acceptable if energy can be recovered from CO gas.
- Utilize latent heats of liquid ferroalloy and slag from the smelting furnaces.
- Improve the recovery of metals. Cr yield into FeCr is typically 90% to 95%, and for Mn in FeMn production the yield ranges from less than 80% to more than 90% depending on the slag practice and recycling.
- Integrate ferroalloy production with steel production, with other industries and for use within society. This might give excellent possibilities for energy recovery, electricity production, CO gas utilization, heat recovery, and utilization.
- Apply efficient gas cleaning for dust, heavy metals, and toxic emissions.
- Use a closed water system to remove particulates and harmful components.
- Recycle, reuse, and utilize solid wastes like slags as by-products.

From the viewpoint of energy, the first five aspects are most significant. Today only in one plant is the heat content of liquid FeCr directly utilized in stainless steel making (Holappa, 2010). Improvement of metals yields is a metallurgical problem but is also connected with recycling and process integration. The last three aspects listed are environmental issues and thus extremely important. When operating at high temperatures, a lot of dust is generated via vaporization and other mechanisms. In addition to valuable and harmless components, the dust often contains harmful, even poisonous, components. Therefore, the dust must be carefully collected and prevented from ending up in air, water, or soil.

It is reasonable to expect an energy-saving potential of 20% to 30% on a global level by adopting the best available techniques as widely as possible. With efficient integration, the benefit can be even higher. Another option is to introduce renewable biomaterial (i.e., charcoal) as a substitute reductant for coke and to mitigate greenhouse gas emissions by CO₂ recovery and sequestration. In large production units, this might be economically reasonable and realizable.

2.6 FUTURE OUTLOOK FOR THE FERROALLOYS INDUSTRY

Progress in the ferroalloys industry has closely followed developments in the steel industry, and this course will continue. The rapid growth in stainless steel use has driven a corresponding growth at least for chromium (FeCr) and nickel (Ni, FeNi, NiO): the average annual growth rate in this sector has been more than 5%. The demand for stainless steel has increased, particularly in China and India, the two largest countries by population. Such growth is assumed to continue, at least in India, and to extend to other developing regions in Southeast Asia, Africa, and South America. As the history of high-tonnage production is quite short, the amount of recycled stainless steel is limited, which means there will be a growing demand for primary alloying materials, especially Cr, Ni, and Mo. Concerning the other bulk ferroalloys FeMn, FeSi, and SiMn, the demand is bound more to low-alloyed carbon steels. Growth has been more moderate, 2% per year on average. Future growth is expected to take place almost solely in developing countries. At a 2% growth rate, the annual production of steel worldwide will exceed 2500 Mt by the 2040s, which means there will also be remarkable growth in different sectors of the ferroalloys industry.

What will be the requirements for the grades and quality of ferroalloys in the future? The base compositions of bulk ferroalloys come from the reconciliation of raw materials, production technology, and customers' wishes and requirements. A common meeting point for the seller and buyer is money (i.e., cost, price, and utility value). Especially in high-alloyed steels, the contents of major components (Cr, Mn, Si, etc.) and minor components (generally carbon, in FeCr silicon) have a strong influence on the processing time, slag, temperature control, and other details. These components are difficult to evaluate today but will become more critical in the future. A component regarded as an impurity, such as phosphorus, can be critical in stainless steel making, as its removal is practically impossible, whereas the amount of sulfur is relatively easy to decrease in the later stage of the converter process or even in the ladle stage. Concerning alloying and trimming additions in later process stages, typically in ladles, high contents of the alloy metal are important (e.g., in FeCr, FeMn, FeSi) to minimize the total addition. Depending on the steel grade to be produced, metallic impurities can be critical (e.g., aluminum and titanium) because they influence inclusions in steel and can cause problems in casting. Of course, gaseous components (nitrogen, oxygen, hydrogen) are important; most

often, high contents are harmful, causing problems in different stages of the steelmaking process until the final product is generated.

In 2009, Holappa (2010) surveyed worldwide experts in the field of ferroalloys production to ask about the importance of different factors concerning the sustainable production of ferroalloys. The 17 responses represented almost the same number of enterprises or institutions on six continents that dealt with central ferroalloys (FeCr, FeMn, FeSi). The survey consisted of questions concerning raw materials and pretreatment, energy issues, environmental issues, by-products, and economic aspects. Almost all the issues presented were regarded as important, and respondents believed their value would grow until 2020. Electric energy was ranked first among all factors. Economic issues (investment and operation costs, energy cost) had the next highest ranking, probably partly reflecting the recession that prevailed when the questionnaire was distributed. The next most important issue was energy efficiency, which included CO utilization, raw materials pretreatment (sintering/pelletizing), and emissions in air and water, almost all of which were given the same high weight. Overall, the ferroalloys industry has numerous challenges ahead, and it must undergo technological modernization and in-depth transformation in consideration of environmental issues. On the other hand, it is a rapidly and steadily growing branch, which makes regeneration easier and gives it the most potential.

REFERENCES

- A.S.M. Handbook, 1990. Vol. 1: Properties and Selection: Irons, Steels, and High-Performance Alloys, tenth ed. ASM International, Metals Park, Ohio USA, 1063 pp.
- Bain, E.C., Paxton, H.W., 1966. Alloying elements in steel, second ed. ASM, Metals Park, Ohio, USA, 291 pp.
- Barraclough, K.C., 1990. Steelmaking 1850–1900. The Institute of Metals, London, 320 pp.
- Brown, R.E., 1984. Ferroalloys. Minerals yearbook: Metals and minerals. US Bureau of Mines 1, 353–375.
- Corathers, L.A., Gambogi, J., Kuck, P.H., Papp, J.F., Polyak, D.E., Shedd, K.B., 2012. Ferroalloys (Advance Release). Minerals yearbook. US Bureau of Mines, 1–17.
- DeArdo, A.J., Garcia, C.I., Palmiere, E.J., 1990. Thermomechanical processing of steels. ASM Handbook, vol. 4. Heat Treating. ASM International, USA. 237–55.
- Engels, S., Nowak, A., 1983. Auf der Spur der Elemente (Searching for the Elements). 3. Auflage, third edition. VEB Deutscher Verlag für Grundstoffindustrie, Leipzig, 324 pp.
- Fenton, M., 1996. Ferroalloys. Minerals yearbook: Metals and minerals. US Bureau of Mines 1, 1–10.
- Flemings, M.C., Ragone, D.V., 2009. Puddling: a new look at an old process. ISIJ International 49, 1960–1966.
- Graus, W., Worrell, E., 2011. Methods for calculating CO₂ intensity of power generation and consumption: a global perspective. Energy Policy 39, 613–627.
- Holappa, L., 2010. Towards sustainability in ferroalloy production. Journal of the South African Institute of Mining and Metallurgy 110 (12), 1–8.

- Holappa, L., 2011. Toward sustainability in ferroalloys and steel production. Fray International Symposium: Metals and Materials Processing in a Clean Environment, Cancun, Mexico, 5, 203–217.
- Krivosky, W.A., 1973. The Linde argon-oxygen process for stainless steel: a case study of major innovation in a basic industry. *Metall. Trans.* 4, 1439–1447.
- Lindstad, T., Olsen, S.E., Tranell, G., Færden, T., Lubetsky, J., 2007. Greenhouse gas emissions from ferroalloys production. *Proc. Conf. INFACON-XI* New Delhi, India, 457–66.
- Reibold, M., Paufler, P., Levin, A.A., Kochmann, W., Pätzke, N., Meyer, D.C., 2006. Materials: Carbon nanotubes in an ancient Damascus sabre. *Nature* 444 (7117), 286.
- Sjardin, M., 2003. CO₂ emission factors for non-energy use in the non-ferrous metal, ferroalloys and inorganics industry. Copernicus Institute, Utrecht, 63 pp.
- Smith, C.S., 1988. A history of metallurgy: the development of ideas on the structure of metals before 1890, second edition. MIT Press, Cambridge MA, USA, 297 pp.
- Tylecote, R.F., 1984. History of metallurgy, 3rd impression. The Metals Society, London, 182 pp.
- Volkert, G., Frank, K.-D., 1972. Metallurgie der Ferrolegerungen, Durrer/Volkert 2. Auflage. Springer-Verlag, Berlin, 700 pp.
- Worrell, E., Price, L., Neelis, M., Galitsky, C., Zhou, N., 2008. World best practice energy intensity values for selected industrial sectors. Report of Ernest Orlando Lawrence Berkeley National Laboratory. LBNL-62806 REV 2, 51.

Theory of Ferroalloys Processing

Heikki Jalkanen and Michael Gasik

Aalto University Foundation, Espoo, Finland

Chapter Outline

3.1 General Theory of the Processes of Ferroalloys Production	29	3.1.5 Basics of Heat Transfer in Ferroalloys Processing	65
3.1.1 Introduction to Ferroalloys and their Processing	29	3.1.6 Basics of Mass and Momentum Transfer in Ferroalloys Processing	70
3.1.2 Processes in Materials Production	35		
3.1.3 Thermodynamics of Pyrometallurgical (High-Temperature Chemical) Processes	37	3.2 Ferroalloys Components and Their Properties	72
3.1.4 Kinetics of Pyrometallurgical Processes	58	3.2.1 Metallic Melts	72
		3.2.2 Oxide Melts (Slags and Fluxes)	74
		3.2.3 Carbon Reductants for Ferroalloys Processing	79
		References	81

3.1 GENERAL THEORY OF THE PROCESSES OF FERROALLOYS PRODUCTION

3.1.1 Introduction to Ferroalloys and their Processing

Ferroalloys, by definition, are alloys of two or more metals, of which one is iron. The U.S. Bureau of Mines defines *ferroalloy* as an alloy of iron with at least one other element except carbon. The most conventional elements used in ferroalloys are Mn, Si, Cr, Ca, Al, Ba, Sr, Mg, Ti, V, W, Mo, Nb, REM (including Y, La, and La-group metals), Ta, Zr, Ni, and B. In much smaller quantities, other ferroalloys might be made for specific applications. The

impurities normally considered as harmful (either for the alloy itself or for the steel where this alloy will be applied) are S, P, Cu, Sn, Sb, Bi, As, and so on and gases O, H, and N. The main components of ferroalloys are called leading elements (e.g., manganese is the leading element in ferromanganese). The degree to which the leading element is recovered specifies the technical and economic feasibility and effectiveness of the ferroalloys technology. Analyses and comparisons of the performance of ferroalloys production from raw materials of different composition and method for furnaces in various designs and capacities are usually normalized to basis tons. The *basis ton* of a ferroalloy has a fixed defined content of the leading element. For example, the standard grade ferrosilicon FeSi45 can contain 41% to 47% Si, but the processing parameters and the efficiency are normalized to the 45% Si content. The main classes of commercial ferroalloys are shown in [Table 3.1](#).

The main share of ferroalloys is used in steelmaking for deoxidation and alloying of steels, as well as to modify cast iron, manufacture welding electrodes, and produce compounds as a starting material for the protective coatings for mineral processing. Ferroalloy properties depend largely on the physical and chemical properties of their major elements. Most ferroalloys contain relatively large amounts of iron, which enables the dissolution of the recovered leading element and reduces the activity of the latter, decreases the melting point (or melting range) of many ferroalloys, controls the density, and improves the utilization of the leading elements in steel and alloys deoxidation and alloying. The formation of metallic solutions of a leading element with iron reduces their activity, which favors the change of Gibbs energy for the reduction process.

The quality of ferroalloys includes many parameters besides the variation in chemical composition and size: density, surface conditions, nonmetallic and slag inclusions, and gases (oxygen, hydrogen).

The main indicator of the quality of a ferroalloy is its chemical composition and, above all, the content of the leading element. It is important to have consistency in alloying element amounts in ferroalloys from heat to heat, allowing the manufacture of standard products.

An important feature of the quality of ferroalloys is their size distribution. If the lumps are too large, they might not have time to be dissolved in the liquid steel. If they are too fine, the alloy might oxidize in air or in the slag before acting according to its main function. Also, some fine powders may present a risk of fire or formation of fumes, causing losses of the ferroalloy. Also important are the mechanical properties of ferrous alloys, because they determine the selection of crushing equipment to produce alloys with a predefined grain size.

3.1.1.1 Classification of Ferroalloy Processes by Reductant Type Reduction by Carbon (Carbothermal Processes)

In these processes, carbon is the main reductant of the metal oxides. The overall reaction can be represented as $MeO_x + yC \rightarrow Me + MeC_z + CO$ (carbides may

TABLE 3.1 Common Classes of Commercial Ferroalloy Types

Leading Element(s)		Main Products
“Bulk” Ferroalloys		
FeSi, Si	Si	Ferrosilicon (all grades), crystalline silicon
FeMn, SiMn, Mn	Mn, Mn + Si, Mn + N	High-, medium-, low-carbon ferromanganese, silicon manganese, manganese metal, nitrided manganese, manganese, master alloys
FeCr, FeSiCr	Cr, Cr + Si, Cr + N	High-, medium-, low- and ultralow-carbon ferrochrome, charge chrome, ferrosilicochrome, chromium metal, nitrided ferrochrome, and master alloys
“Minor” Ferroalloys		
FeW	W	Ferrotungsten
FeMo	Mo	Ferromolybdenum
FeV	V	Ferrovanadium
Fe(Si)Ca, FeSi(Ba,Mg,Sr)	(Ca,Ba,Sr,Mg) + Si	Silicocalcium (calcium silicon), silicobarium, silicomagnesium, silicostromium, complex alloys (Fe-Si-Mg-Ca; Si-Ca-Ba-Fe; Si-Ba-Sr and others)
FeNb	Nb, Nb + Ta	Ferroniobium, Ni-Nb, Nb-Ta-Fe; Nb-Ta-Al-Mn-Si-Ti; Nb-Ta-Al
FeTi	Ti	Ferrotitanium, Fe-Si-Ti, Ti-Cr-Al, Ti-Al-Cr-Fe, Ti-Ni
FeB, FeBAl	B, B+Al	Ferroboron, ferroboral and alloys with boron (Ni-B, Cr-V, greynal)
FeAl, FeSiAl	Al, Al + Si	Silico-aluminum, ferro-aluminum, ferrosilicoaluminum, Fe-Al-Mn-Si, Fe-Mn-Al
FeSi-REM	Rare earth metals (sum of REM)	REM-Si; REM-Si-Fe, REM-Al-Si
FeSiZr, FeAlZr	Zr	Ferrosilicon-zirconium, ferroaluminum-zirconium
FeNi, FeCo	Ni, Co, Ni+Co	Ferronickel, ferrocobalt

or may not form depending on the reacting metal and the conditions of the process). One of the major reduction products is carbon monoxide gas, which is removed from the reaction zone, and this provides the irreversibility of the reaction. Carbon can reduce practically all the elements from their oxides at sufficiently high temperatures. The disadvantages of carbon as a reducing agent are mainly the formation of carbides or high-carbon melts and larger required heat input dictating the use of electric arc furnaces of large power.

Reduction by Silicon (Silicothalmic Processes)

Silicon reduction of metals from their oxides occurs with the formation of silicon-rich metal melts $MeO_x + Si \rightarrow [Me, Si] + SiO_2$, and in some cases metal silicides might also form if they are stable at the reaction temperatures. Pure silicon is never used as a reductant for economic reasons. Most commonly, silicon is introduced by the same ferroalloy type as being produced but with high silicon content. Thus, silicon reduction of manganese is used with Fe-Mn-Si alloys, and chromium is used for Fe-Cr-Si alloys. These high-silicon alloys are produced separately and used only for reduction purposes. The main advantages of this method are low carbon content in the resulting alloys and exothermic reaction, thus allowing the use of low-power furnaces (<10 MVA).

Unlike carbon, silicon oxide is not removed from the furnace and forms a high-silica slag, which upon accumulation decreases the reaction rate and finally stops the process because of the very high activity of silica. To avoid this reaction, fluxes must be added as slag formers (most commonly lime CaO, calcined dolomite $[CaO \cdot MgO]$, or maybe some other products with high basicity).

Silicon as the reducing agent can be used to reduce oxides of elements possessing a higher chemical affinity for oxygen than silicon, if there is an excess of silicon in the melt. Silicon as a reducing agent has some disadvantages: additional use of fluxing agents and difficulty of obtaining low-silicon alloys.

Reduction by Aluminum (Aluminothermal Processes)

Reduction by aluminum proceeds with the reaction $MeO_x + (2x/3)Al \rightarrow Me + (x/3)Al_2O_3$, which is accompanied by a significant exothermal effect. This makes it possible to carry out the process without an external heat supply (out of furnace) or with much less heat versus carbon reduction. During exothermic reactions, a very high temperature might be reached (2400 to 2800 K), which ensures the formation of liquid slag and metal and a good separation of the metal and slag phases at a high rate.

Aluminum is able to reduce a wide range of chemical elements (that have a lower affinity for oxygen than aluminum) and to obtain alloys with very low carbon and silicon, which is essential for getting pure metals (e.g., metallic chromium). The process is relatively simple and requires minor capital costs. It

also could be realized in combination with premelting oxides and fluxes in an electric furnace following out-of-furnace reduction, which can significantly intensify the process and reduce the amount of aluminum required. The high-alumina slags find their utilization in the production of synthetic slags for steel treatment and in high-alumina cements for construction.

The disadvantages of aluminum reduction include the high costs of metallic aluminum, too high viscosity of high-alumina slag (it is difficult to separate metal and slag if the temperature is not high enough), and the possibility of lower metal recovery because of the formation of suboxides of leading metal and aluminates $x\text{MeO}\cdot\text{Al}_2\text{O}_3$.

3.1.1.2 Classification of Ferroalloy Processes by Technological Features

Continuous and Batch Processes

Ferroalloy processes are divided into continuous and periodic. Continuous processes are characterized by continuous loading of the charge and periodic (or continuous) slag and ferroalloy tapping. The charge is in the furnace at a certain level throughout the process. The electrodes are immersed in a charge continuously. The furnaces used for these processes usually have high power (>16 MVA) and the reducing agents are carbon materials (coke, char, charcoal, anthracite coal).

Batch processes use a certain amount of charge material for the same heat. The charge loaded into the furnace is completely melt, leading to the reduction of the elements. The products are released periodically (metal and slag tapping), most often at the same time.

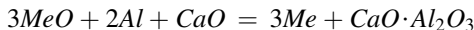
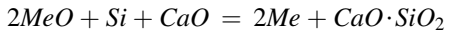
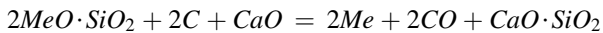
Slag and Slag-Less Processes

For the slag-less process, ferroalloys are smelted when the amount of slag formed is small (3% to 5% by weight of the metal), such as in crystalline silicon smelting, and ferrosilicon (FeSi) and ferrosilicochrome (FeSiCr) processing. This slag forms from small quantities of oxides, ores, and concentrates in the coke ash that were not reduced during the heat.

Slag processes, on the other hand, are accompanied by the formation of a considerable amount of slag. The amount of the slag can be 120% to 150% of metal mass smelting of high-carbon ferromanganese (HC FeMn) and ferrosilicomanganese (SiMn) and 200% to 350% for low-carbon ferrochrome (LC FeCr) and manganese metal.

Flux and Fluxless Processes

Smelting of ferroalloys in a batch (periodic) process most often is made by the flux method, although under certain suitable conditions flux-less smelting is feasible. With the fluxing method, the reduction of metal oxides proceeds with the reactions for every reductant type as follows schematically:



Introduction of the flux decreases the activity of SiO_2 in the slag, which is accompanied by an increase in the output of recovered metal. Common flux materials contain CaO , MgO , and possibly other components that are able to make up the strongest chemical compounds with reaction products or gangue oxides (SiO_2 , Al_2O_3). This also decreases the viscosity of the slag, which leads to a more complete extraction of the leading element and better ferroalloy quality.

In the flux-less method, power consumption is lower and the productivity of the furnace is much higher; however, the degree of recovery of a metal into a ferroalloy decreases. Tapped slag still contains significant amounts of oxides of leading elements and is generally used for the smelting of ferroalloys by carbon reduction—that is, in the second-stage process. The flux-less method can be applied only to high-quality ores and concentrates with low impurities content.

Ferroalloys could also be processed in a secondary metallurgy, using melting of metal and iron scrap or residues from the metallurgical industry, and these processes do not usually involve a substantial reduction part. The raw materials contain oxides, sometimes sulfides or metals (in scrap) of elements other than just the components for a certain ferroalloy to be produced.

The preceding step of any ferroalloy production usually includes sintering, briquetting, or pelletizing raw materials (oxide ores or concentrates) with partial prereduction and partial metallization of iron and some alloying elements prior to the final smelting. The first step of smelting (commonly in a submerged electric arc furnace, electric resistance furnace, or, more seldom, in reverberatory or shaft furnace) is the reduction of the oxides that are still in the solid state before melting. At high temperatures, oxides form liquid slag and, with the progress of the reduction, a metallic phase (melt). The chemical species tend to distribute between the molten ferroalloy melt and the slag in certain proportions. Thus, ferroalloy smelting processes consist of several steps within a wide temperature range, being a combination of step-by-step reduction and formation of molten phases (alloys, slags) and a gas phase (reduction products: carbon monoxide, carbon dioxide, hydrogen, water vapor, gaseous oxides, and other volatile products). The charge being fed into the furnace usually consists of different solid phases (ore lumps or sintered pellets of iron and alloying element, oxide concentrates, slag formers [fluxes], recycled material). Inside the furnace, partially molten charge is placed on the surface of molten slag, which is usually set on the top of molten alloy. There is also a remarkable temperature gradient between the phases present in the furnace and an intensive turbulent mixing of the components, especially near the electrodes.

The basic phenomena of the smelting process are formation and separation of molten ferroalloy and slag. The gangue and the impurities from the ore, which form the slag phase, might be partially reduced and dissolved in the metal alloy. This might be allowable, unless the impurities' concentration exceeds a certain level set by the alloy specification. Impurities could be further removed from the ferroalloy with refinement by special (flux) treatment. The resulting composition of the ferroalloy depends on many thermodynamic and kinetic prerequisites for the formation of molten phases and gas phases by chemical interaction as well as the distribution of raw material constituents between the phases.

All processes in the furnace take place in both macroscopic and atomic-molecular levels. These processes need to have a certain driving force related to the macroscopic and molecular level mechanisms, which control the system inertia (i.e., the rate of the process: rate of chemical reactions, matter and energy transportation). When the equilibrium state is reached, the driving forces of all processes approach zero value and the prerequisites for the advance of processes disappear. The rate of processes depends, on the macroscopic level, on the geometrical and mechanical factors of the process (like the structure and dimensions of the reactor, size and porosity of solid reacting particles like pellets and ore lumps, viscosity, and efficiency of mixing of the liquid and gaseous reacting phases) and in the atomic/molecular level on the resistance of matter transformation processes like chemical reactions and matter transportation processes (diffusion, convection). The driving forces of matter transformation processes are created by affecting the matter *thermally*, conveying heat to the matter (heating) or removing heat (cooling), *mechanically*, increasing or decreasing the pressure, and *chemically*, bringing the matter to be processed in contact with reactive matter leading to a rise of thermodynamic driving forces for chemical transformation and reactions.

3.1.2 Processes in Materials Production

Metals (and materials in general) production, like ferroalloy smelting, is a combination of matter and energy transformation and transportation processes (Table 3.2). A phenomenological classification of major chemical processes at different levels, relevant to ferroalloys production, is shown in Figure 3.1.

From this picture, the major areas of ferroalloys processing theory can be identified as chemical thermodynamics (reduction processes theory, phase formation, phase equilibria), heterogeneous chemical kinetics (the rate of the reactions and phases transformation, different transport processes as regulated by viscosity, electrical conductivity, thermal conductivity, diffusion), and multiphysical phenomena (combined and coupled heat, mass, momentum, and charge transfer in heterogeneous, dynamic media). These areas are briefly described further in this chapter.

TABLE 3.2 Overall Classifications of Generic Processes in Ferroalloys Production

Transformation Phenomena	
Matter	Energy
Chemical reaction and phase transitions	Heat release/absorption in matter (phase) transformations
Phase state change: melting/solidification, evaporation/condensation	Energy conversion in mechanical processes
Dissolution/precipitation	Energy transformation in electromagnetic processes (joule heating, induction heating, reactive losses)
Surface processes: adsorption/desorption	
Transportation Phenomena	
Matter	Energy (Heat)
Fluid flow transport (convection)	Convective transport with fluid flow
Diffusion	Thermal and electrical conduction
Osmotic phenomena	Electromagnetic radiation
Flow in porous media	

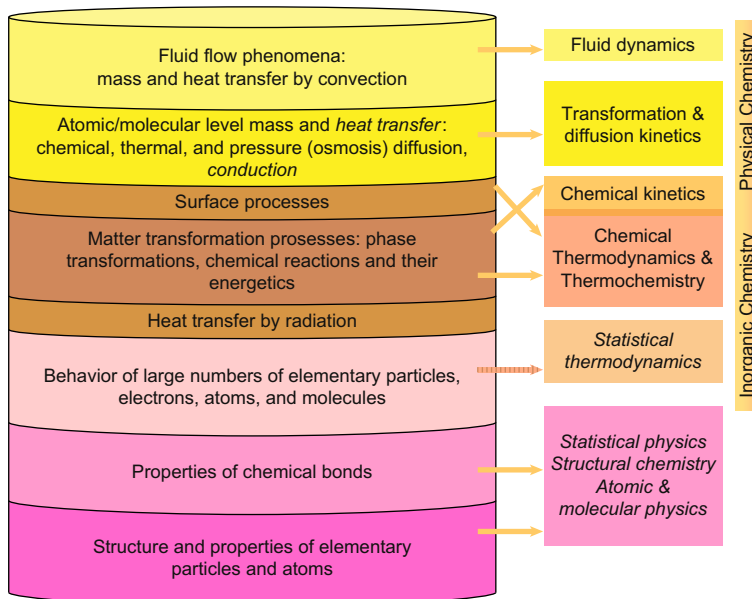


FIGURE 3.1 Schematic presentation of processes from atomic/molecular-level to macroscopic-level phenomena and the theoretical tools used to analyze those phenomena.

3.1.3 Thermodynamics of Pyrometallurgical (High-Temperature Chemical) Processes

3.1.3.1 General Thermodynamic Considerations and Definitions

According to general thermodynamics, the common driving force for any matter and energy transformation process is the tendency to maximize the system entropy S . This means the tendency toward equalization temperature (thermal energy), pressure (mechanical energy), and chemical potentials of all the individual species within the system (reactor, furnace, etc.). Equalization of chemical potentials takes place through matter transformation (reaction within the phase and between the phases) and transportation (diffusion of species from areas of higher chemical potentials to areas of lower chemical potentials). In this context, “chemical potential” should be considered in a more general sense, including purely chemical contributions as well as surface energy, mechanical stress state, and so on if such forces are present.

The equalization of temperature proceeds through conduction, convection, and radiation and equalization of pressure through fluid flow or the deformation of the solid phases. The rate of the total process combination of various matter transformation processes, like in the smelting of ferroalloys, is controlled by the kinetics of chemical transformations (reactions) as well as by the rates of the mentioned matter and energy transportation processes (see Table 3.2 and Fig. 3.1). The rate of chemical reactions, as well as diffusion, normally increases with increasing temperature. The rate of matter transportation by fluid flow depends on the amount of introduced mechanical energy (mixing) and fluidity within the reaction system (viscosity of the liquid/molten phases within the reactor). The rate of matter transportation in solid phases depends on the diffusivity of the species within the phases and the active surface area available (the dispersion degree of the component). The quantitative analysis and modeling of rate phenomena in reaction systems such as ferroalloys smelting processes is a complex and challenging task.

At constant temperature (T) and pressure (P), the general driving force for smelting processes is the tendency to minimize the Gibbs free energy (G) of the system. The Gibbs energy minimization analysis is the normal approach for predicting the tendencies and directions of chemical processes and for defining of the final equilibrium state of the process. Even if the equilibrium state is not reached, it nevertheless reveals to which extent the process might be theoretically implemented.

Thermodynamic and thermal properties of the phases undergoing the transformations are described by the set of principal thermodynamic quantities: entropy (S), enthalpy (H), internal energy (U), Gibbs energy (G), Helmholtz energy (F), and heat capacity (C_p at constant pressure and C_v at constant volume). In spontaneous, uncontrolled processes the entropy tends to increase, and this can be treated as a driving force for matter and energy transformation

and transportation. In controlled processes like most industrial processes where T , P , or volume (V) of the system is kept constant, or stepwise processes along with changing $T/P/V$ with a constant amount of matter, the direction of individual matter transformation processes and equilibrium conditions can be analyzed by Gibbs (free) energy G at constant temperature and pressure or by Helmholtz (free) energy F at constant temperature and volume, respectively. The energy transformations of the system at constant pressure are related to enthalpy H and at constant volume (when the system is not doing external work by increasing volume against external pressure) to internal energy, U . These quantities are linked to system state variables (T , P , V , and S) by fundamental differential equations:

$$U \text{ (internal energy)} : dU = -PdV + TdS \quad (1)$$

$$H \text{ (enthalpy)} : dH = TdS + VdP \quad (2)$$

$$F \text{ (Helmholtz energy)} : dF = -PdV - SdT \quad (3)$$

$$G \text{ (Gibbs energy)} : dG = VdP + SdT \quad (4)$$

The temperature or pressure dependence of the state variables of a single, homogeneous phase (pure element, compound, molten or liquid solution, gas mixture) with constant composition can be obtained from total derivatives of these variables:

$$\begin{aligned} P &= -\frac{\partial U}{\partial V}\Big|_S = -\frac{\partial F}{\partial V}\Big|_T; & T &= \frac{\partial U}{\partial S}\Big|_V = \frac{\partial H}{\partial S}\Big|_P; \\ V &= \frac{\partial H}{\partial P}\Big|_S = \frac{\partial G}{\partial P}\Big|_T; & S &= -\frac{\partial F}{\partial T}\Big|_V = \frac{\partial G}{\partial T}\Big|_P. \end{aligned} \quad (5)$$

As the material (phase) heat capacity is linked to change of its heat value (thermal energy stored) with temperature, for constant pressure (C_p) or volume (C_v) conditions it might be written as follows:

$$C_P = \frac{\partial H}{\partial T}\Big|_P = T \frac{\partial S}{\partial T}\Big|_P; \quad C_V = \frac{\partial U}{\partial T}\Big|_V = T \frac{\partial S}{\partial T}\Big|_V. \quad (6)$$

The heat capacity of any material and phase is commonly expressed in the standard polynomial form as a function of temperature,

$$C_P(T) = A + BT + CT^{-2} + DT^2 + ET^3 + \dots, \quad (7)$$

where coefficients A , B , C , D , E ,... are tabulated or included in all existing thermodynamic databases for a number of substances. Temperature dependences of enthalpy and entropy of homogeneous condensed phases are usually written as the sum of integrals of heat capacities of every stable phase state

temperature range plus the sum of the respective enthalpy or entropy of the phase transformation itself (if present; e.g., melting or structure changes):

$$H(T) = H_{298}^0 + \sum_{phase} \int_{T_{1,phase}}^{T_{2,phase}} C_P^{phase}(T) dT + \sum_{phase} (\Delta H_{phase}) \quad . \quad (8)$$

$$S(T) = S_{298}^0 + \sum_{phase} \int_{T_{1,phase}}^{T_{2,phase}} \frac{C_P^{phase}(T)}{T} dT + \sum_{phase} \left(\frac{\Delta H_{phase}}{T_{phase}} \right)$$

Here the values with index 298 mean values at the standard reference state (298.15 K and 1 bar pressure), T_1 and T_2 are temperatures of the specific phase stability range, and ΔH_{phase} with T_{phase} are, respectively, the change of enthalpy at the phase transformation and the temperature of this phase transformation. For example, for pure chromium in the temperature range 298 to 1000 K, the heat capacity function (7) in J/mol·K is

$$C_P(T)_{Cr} = 26.906 - 3.784 \cdot 10^{-3} \cdot T - 278500 \cdot T^{-2} + 8.86 \cdot 10^{-3} \cdot T^2$$

and for the range 1000 to 2180 K (until the melting point) it is

$$C_P(T)_{Cr} = 26.911 - 3.79 \cdot 10^{-3} \cdot T - 278010 \cdot T^{-2} + 8.863 \cdot 10^{-3} \cdot T^2$$

(the standard values of H°_{298} and S°_{298} are zero for pure elements by default). When chromium melts, the heat capacity of liquid chromium becomes nearly constant (50 J/mol·K) over 2180 K. However, at the melting point chromium enthalpy is increased by $\Delta H_{Cr} = 21004$ J/mol (latent heat of melting) and entropy by 9.635 J/mol·K. The free Gibbs energy of any phase might be calculated with known enthalpy and entropy values as

$$G(T) = H(T) - T \cdot S(T), \quad (9)$$

where $H(T)$ and $S(T)$ are defined by (8). Additionally, the partial Gibbs energy of the component (known as chemical potential μ_i of this component) is defined as the change of the molar Gibbs energy with an increasing number of moles of this component n_i , keeping T , P , and other component amounts (n_j) constant:

$$\mu_i = \overline{G}_i = \left. \frac{\partial G}{\partial n_i} \right|_{n_j, T, P}. \quad (10)$$

The application of chemical potential is an important part of solution thermodynamics and reactions analysis, as shown in the following discussion. Values of standard states of all elements have been evaluated and presented in a functional form (Dinsdale, 1991).

The common approach to the thermodynamic analysis of chemical processes like pyrometallurgical processes involves constant temperature and pressure; accordingly, the functions used in energy analysis and the analysis of

equilibrium conditions and driving forces of matter transformations are usually enthalpy H and Gibbs energy G . The equilibrium state of a material system is related to the minimum Gibbs energy of the whole system.

It is important for any thermodynamic analysis to be based on a clear definition of the system and its properties, temperature, pressure, and volume, as well as the amount and quality (elemental composition) of matter. The thermodynamic analysis of the usual metallurgical processes, including the smelting of ferroalloys, is based on an isothermal-isobaric approach (i.e., matter transformations), and their driving forces and equilibrium state are analyzed at constant temperature and pressure. Although temperature in pyrometallurgy is not equal within the furnace or with time (in batch processes), in the great majority of processes the pressure changes are not significant with the advance of the processes (the obvious exception is the vacuum treatment of alloys). This means that a thermodynamic analysis of the processes when based on Gibbs energy minimization should be spatially and timely divided into stages to correctly evaluate the advance of these processes.

In pyrometallurgical processes like reduction and smelting of oxide raw materials for ferroalloys production, the changes of thermodynamic properties of the phases are accompanied by a combination of chemical reactions between the reductant (carbon, silicon, or aluminum) and oxides, formation of slag and molten metal phases, mutual dissolution of oxides and reduced metallic components, phase transformations (melting of solid phases, precipitation of solids from other molten or solid phases as a result of chemical reactions), evaporation of species, and so on. The direction and extent (the equilibrium state) of these processes can be predicted by the combination of the molar Gibbs energy of each phase and the material balance at each level of temperature and pressure. For a process to be thermodynamically possible, the combination of all matter transformations and reactions taking place should lead to a decrease of the total Gibbs energy of the reacting system. By combining enthalpy analyses of the system (all matter transformation processes and energy flows do exchange with the system environment, constituting the heat balance), one will get a comprehensive picture of the process: in which direction the amount and composition of each of the phases present in the process (ferroalloy, slag, furnace gas composition) tend to progress by the individual matter transformation processes at each particular temperature.

Enthalpy analysis connected with the matter transformation processes explains the need of energy to be added to the system (heating) or removed from the system (cooling) when certain temperatures should be achieved in the process environment. [Table 3.3](#) schematically shows the relations between free energy and some important driving forces.

Next, three of the most important applications of thermodynamics in ferroalloys processing are considered in more detail: change of the Gibbs energy with chemical reactions, with formation of solutions, and for describing phase transformations.

TABLE 3.3 Schematic Relations of Gibbs Free Energy and Other Thermodynamic Parameters with Some Important Driving Forces of Different Processes

Type of Process	Driving Force	Remarks
Chemical reactions, phase transformations	$\partial G/\partial \xi _{T,P} < 0$	Change of Gibbs energy with extent of the reaction or transformation progress (ξ)
Species diffusion (molecular/atomic)	$\nabla(\partial G/\partial n_i)_{n_j,T,P} \neq 0$	Gradient of partial Gibbs energy (chemical potential) in space and time
Species diffusion and migration (ionic/charged)	$Z \nabla E \neq 0$	Electric field gradient acting on Z-charged species
Surface flow of species	$\nabla \sigma \neq 0$	Nonzero surface energy gradient
Fluid mass flow	$\nabla P \neq 0$	Nonzero pressure gradient, causing velocity \mathbf{u}
Heat conduction	$\nabla T \neq 0$	Nonzero temperature gradient
Heat convection	$\mathbf{u} \cdot \rho C_p T \neq 0$	Heat flux with fluid at non-zero velocity
Heat radiation	$\Delta T \neq 0$	Nonzero temperature difference between points

3.1.3.2 Thermodynamics of Solutions

Solutions formed by two or more components generally do not preserve their composition if there is a chemical or phase transformation process (which obviously is the goal of alloy processing). In this case, equations (1) through (4) must be complemented by the sum of chemical potentials (10) of all presenting species, $\sum_i n_i d\mu_i$. In the case of equilibrium, the expected change of Gibbs energy (dG) must be zero, thus

$$dG = 0 \rightarrow VdP + SdT + \sum_i n_i d\mu_i = 0, \quad (11)$$

which is known as the Gibbs-Duhem equation. From (11) it immediately follows that at constant temperature and pressure ($dT = dP = 0$), the equilibrium requires no changes in the chemical potentials of the components in all phases.

Upon formation of any solution, the solution free Gibbs energy is not equal to the sum of the free energies of pure constituents because of the increase of mixing entropy. For solutions having k components with n_i moles of every component i , the molar fraction of every component is

$$X_i = \frac{n_i}{\sum_{j=1}^k n_j}. \quad (12)$$

The Gibbs energy of 1 mol of the solution is the sum of the Gibbs energies of all of the components, proportional to their molar fractions, plus a contribution from ideal mixing and a contribution from nonideality (called “excess free energy”):

$$\begin{aligned} G^m &= \sum_j X_j G_j^0 + RT \sum_j X_j \ln X_j + \Delta G^{xs} \\ \Delta G^m &= RT \sum_j X_j \ln X_j + \Delta G^{xs} = \Delta H^m - T \Delta S^m, \end{aligned} \quad (13)$$

where G°_j is the molar Gibbs energy of pure component j , X_j is molar fraction of the j -component, $R = 8.314 \text{ J/mol}\cdot\text{K}$ is the universal gas constant, and ΔG^{xs} is the excess Gibbs energy of mixing. Changes in the enthalpy and entropy of solution formation are defined in the same way as for Gibbs energy (9). The Gibbs energy of ideal mixing describes the effect of dilution of a substance when mixing into the phase without interaction between the components assuming completely statistical random mixing. Any deviations from random mixing of species or a nonzero thermal effect of solution formation make the system nonideal ($\Delta G^{xs} \neq 0$). The excess Gibbs energy of mixing describes the “chemical” interaction between the species in the ($\Delta H^{xs} \neq 0$) phase and deviation from random mixing ($\Delta S^{xs} \neq 0$).

As with equation (10), the chemical potential of a component in the multicomponent solution, expressed in terms of molar fractions, is

$$\mu_i = \left(\frac{\partial G_m}{\partial n_i} \right)_{n_j} = G_m + (1 - X_i) \left(\frac{\partial G_m}{\partial X_i} \right)_{X_j/X_k} - \sum_{j \neq i}^{K-1} X_j \left(\frac{\partial G_m}{\partial X_j} \right)_{X_j/X_k}, \quad (14)$$

which allows the calculation of chemical potential for any cross-section of the compositional space by derivation of Gibbs energy (13). Special care must be taken when selecting proper concentration paths for free energy and chemical potential calculations, because in a multicomponent system they may depend on the integration path. Chemical potential μ_i is an important thermodynamic variable, as it is directly linked with the activity of this component, a_i :

$$a_i(X_i) = \exp \left(\frac{\mu_i(X_i) - \mu_i^0}{RT} \right); \quad \mu_i(X_i) = \mu_i^0 + RT \ln(a_i(X_i)). \quad (15)$$

Activity, or the “corrected concentration” of a component, is a measure of the effectiveness of the component in the solution in respect to its reactions with other components. Raoult made a classical definition of activity, relating activity to the partial pressure of a dissolved component over a solution versus its reference state:

$$a_i(X_i) = P_i(X_i)/P_i^0, \quad (16)$$

where P_i is the partial pressure of this species in the solution and P^0 is the pressure of this substance in the reference state ($a_i^0 = 1$). In Raoultian formalism,

this state is assumed to be pure substance, and many thermodynamic calculations use that by default. The ratio of activity to the real concentration of the component is called the *activity coefficient* $\gamma_i = a_i/X_i$, which is a measure of solution nonideality (in ideal solutions, $\gamma = 1$ in the whole concentration range).

Note that in both definitions of activity (15) and (16), the absolute values depend on the selection of the reference state. The reference state selection is of paramount importance in chemical thermodynamics, as wrong or incompatible states would make all thermodynamic calculations useless.

When the concentration of one component is low enough (“dilute”), a so-called Henrian reference state is assumed whereby the activity coefficient is taken as a constant. This, however, has a limited application, to “dilute” solutions only ($\gamma^\infty_i = \text{const}$ when $X_i \rightarrow 0$), and in general the degree of dilution cannot be assigned a numerical value. Thus, a solution seen as a “dilute” one from a practical point of view (such as a few ppm of oxygen in solid chromium) might be nondilute in a Henrian sense (Lupis, 1983; Pelton, 2001).

To obtain the chemical potential (14), the free energy function must be a continuous and differentiable function of the amount of the substance in the solution phase, otherwise the derivation in (14) cannot be performed. The chemical potential and thus activity of the reference state have to be measurable and continuous functions in real solutions.

Historically in metallurgy it was not uncommon to take the reference state as 1 wt. % of the substance in the solvent (in steelmaking, 1% oxygen in liquid iron at 1600°C, for instance, even if such a solution cannot exist). However, as mentioned by some researchers (Hillert, 1998; Kubaschewski and Alcock, 1979; Lupis, 1983), such selections are often confusing and should not be used. Although some handbooks state that the selection of the reference state is a matter of taste and usability, any such selection should not violate basic thermodynamic principles. To determine whether the standard state is correctly defined, the following issues should be taken into account. The activity function of any component must fulfill the following three relations:

$$\left(\frac{\partial \ln a_i}{\partial T} \right)_{P, x_i} = - \frac{\bar{H}_i - \bar{H}_i^0}{RT^2} \quad (17a)$$

$$\left(\frac{\partial \ln a_i}{\partial P} \right)_{T, x_i} = \frac{\bar{V}_i - \bar{V}_i^0}{RT} \quad (17b)$$

$$\left(\frac{\partial \ln a_i}{\partial x_i} \right)_{T, P, x_j/x_k (j, k \neq i)} > 0. \quad (17c)$$

Two first equations (17a and 17b) are derived from the Clausius-Clapeyron equation. The third equation (17c) follows from (15) and means the activity of any substance in the solution will always increase when it is added to the

system (Gasik, 2001). Thus, every correct reference state must be achievable within the proper concentration range (the solution phase, where it is being sought, must exist). It should always be a state (1) that is achievable by continuously changing the substance concentration while keeping the same solution (phase) structure type, (2) that always has unity value of the activity, and (3) for which its derivatives by temperature (at constant pressure) and by pressure (at constant temperature) are always zero (if they are nonzero, this is not a thermodynamically correct reference state).

For the solutions that do not cover the whole composition range (e.g., in the case of saturation limit), the standard state cannot be chosen as a pure component, because rule (17c) would be violated, and in equations (17a) and (17b) partial enthalpy and partial molar volume respectively would be unobtainable. In such a case (beyond the saturation limit) adding more moles of the compound to the system will not increase its chemical potential in the solution but will only vary the solution fraction (Fig. 3.2). Here the reference state must be chosen at the substance saturation point, when all three relations (17a–c) hold.

Therefore, “hypothetical” states may not generally satisfy the main thermodynamic rules and thus cannot be recommended, as they only cause additional confusion (Kubaschewski and Alcock, 1979). In earlier thermodynamics of metallurgic processes, Wagner formalism with Taylor’s series expansion was conventionally used (Lupis, 1983) when the standard state was chosen as 1% wt. of the component even if this solution could not exist. This may cause misleading results when attempting to equilibrate such activities with other phases and should not be used, as emphasized by Kubaschewski and Alcock (1979). Taylor’s series expansion is only valid within the vicinity of the differentiation (expansion) point and generally might not be extrapolated over the wider concentration range. Hillert (1998) has also shown that traditional Wagner’s expressions for free energy are invalid in respect to the Gibbs-Duhem equation (11) unless a special correction term is added.

Activity and activity coefficient are always functions of temperature, pressure, and composition of the solution phase. The knowledge of the activity

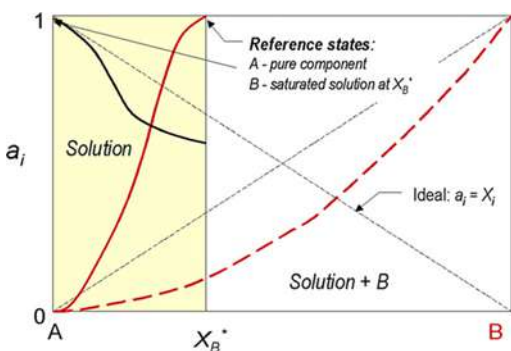


FIGURE 3.2 Activities and reference states in the A-B system with limited solubility.

of a component versus these variables allows one to calculate the resulting mixture and solution composition at some set of environmental variables and to determine favorable process parameters for the smelting or refining processes.

For gaseous mixtures the activity of species is expressed as fugacity, but in most ferroalloys production processes the behavior of gas mixtures is close to ideal (low pressures) and the fugacity is nearly equal to the gas partial pressure. The use of activities is also essential for calculating the system equilibrium when chemical reactions or phase transformations are involved.

3.1.3.3 Thermodynamics of Chemical Reactions

Any chemical reactions between species A_i could be written as

$$v_1A_1 + v_2A_2 + v_3A_3 + \dots = v_nA_n + v_{n+1}A_{n+1} + v_{n+2}A_{n+2} + \dots,$$

where v_i refers to stoichiometric coefficients of species. In the short form, the mathematic expression of the reaction is $\sum_i v_i A_i = 0$, where coefficients for

the reagents are positive and those for products are negative. The driving force for the reaction is the change of the Gibbs free energy (equations 4 and 9), which might also include changes resulting from the formation of solution (13). Written in terms of chemical potentials, this might be expressed as

$$\begin{aligned}\Delta G_{reac} &= \sum_{products} v_i \mu_i - \sum_{reagents} v_j \mu_j \\ &= \left(\sum_{products} v_i \mu_i^\circ - \sum_{reagents} v_j \mu_j^\circ \right) + RT \left(\sum_{products} v_i \ln a_i - \sum_{reagents} v_j \ln a_j \right),\end{aligned}$$

which can be compactly written as

$$\Delta G_{reac} = \Delta G_{reac}^0 + RT \ln \left(\frac{\prod_{products} a_i^{v_i}}{\prod_{reagents} a_j^{v_j}} \right) = \Delta G_{reac}^0 + RT \ln K_P. \quad (18)$$

This equation is known as the acting masses law, connecting free energy change with equilibrium constant K_P , components' activities, and temperature. The reaction proceeds only in the case $\Delta G_{reac} < 0$ and until the ΔG_{reac} reaches zero value. Therefore, in the equilibrium, when no changes are observed in the system, it is experimentally possible to determine components' concentrations and with correct activities calculate the standard Gibbs energy change of the reaction ΔG° . The driving force of all matter transformations—including evaporation, condensation, phase transitions, and precipitation of solids from solution—can be related to Gibbs energies of the phases involved in the process in question.

The standard Gibbs energy of individual formation reaction ΔG° shows the stability of pure compounds, relative tendencies for compound formation, or chemical reactions of species with same reactants. Figure 3.3 presents a diagram

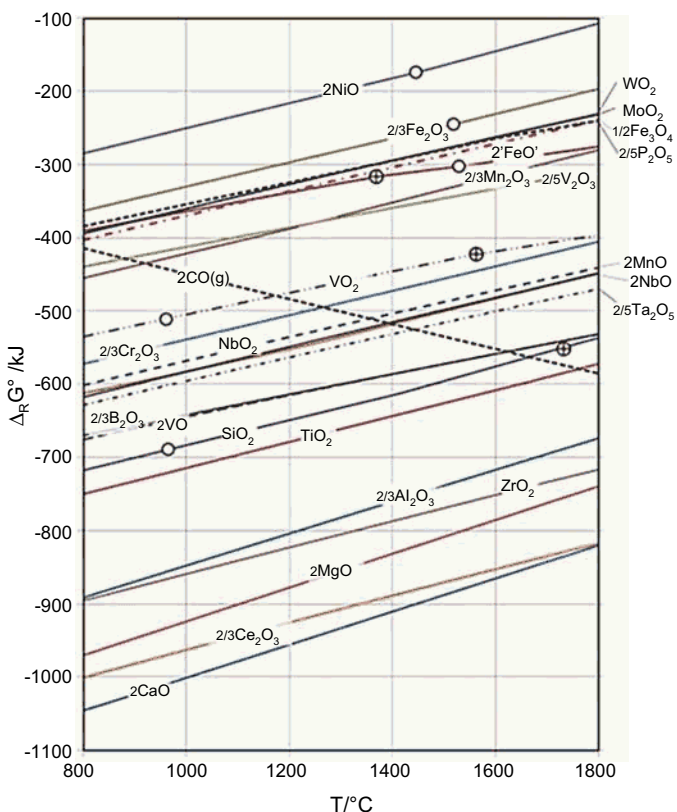


FIGURE 3.3 Ellingham diagram (ΔG°) for some oxides corresponding to the reaction of type $2x/y \text{Me} + O_2(\text{g}) = 2/y \text{Me}_x\text{O}_y$ (i.e., per one mole of oxygen O_2 . (Calculated by HSC Chemistry 7.)

of standard Gibbs energies for the formation of oxides versus temperature (called the Ellingham diagram). The more negative the standard Gibbs energy of reaction is, the stronger the tendency for that reaction and the more stable the formed compound. In general, the element whose oxide has a more negative value of standard Gibbs energy of formation is in principle able to reduce oxides with less negative Gibbs energy of formation.

As Figure 3.3 illustrates, the stability of condensed oxides decreases with increasing temperature with the exception of gaseous carbon monoxide, formed in the carbothermic reduction of oxides, which is the main method used to produce ferroalloys. The increase in the stability of carbon monoxide with temperature means that the efficiency of carbothermic reduction increases with increasing temperature. Carbothermic reduction can be used in principle up to the reduction of titanium if the process is carried out at high temperatures up to 1800°C . The information in Figure 3.3 reveals that the most easily reducible oxide of common ferroalloy elements is nickel oxide and the most stable one is

cerium oxide. However, one has to keep in mind that this diagram (as do similar ones) assumes activities of all components equal to unity (pure phases) and does not take into account possible gaseous suboxides formation (e.g., SiO , Al_2O , AlO) or carbides (TiC , Cr_3C_2 , etc.). When a reducible element forms a solution (e.g., with iron), its activity drops and the theoretical reduction temperature (when $\Delta G^\circ = 0$) decreases. This is one of the reasons why it is possible to produce many metals in the form of ferroalloys, but not as pure elements (Al, Ca, Mg, Zr, Ti, REM, etc.).

For example, let's consider reduction of silicon by carbon:



The analysis shows that the temperature when $\Delta G_{\text{SiO}_2}^\circ$ reaches zero value is 1665°C . It shows when the reduction starts if all silica, carbon, and silicon are pure phases and the gas is only carbon monoxide at 1 bar pressure (i.e., the reaction equilibrium constant $K_P = 1$). To determine what happens if one of these conditions does not hold, let's write a total Gibbs energy (18) for this reaction:

$$\begin{aligned}\Delta G_{\text{SiO}_2} &= \Delta G_{\text{SiO}_2}^0 + RT \ln \left(\frac{P_{\text{CO}}^2 \cdot a_{\text{Si}}}{a_{\text{SiO}_2} \cdot a_{\text{C}}} \right) \\ &= 494711 - 355.26 \cdot T + 8.314 \cdot T \ln \left(\frac{P_{\text{CO}}^2 \cdot a_{\text{Si}}}{a_{\text{SiO}_2} \cdot a_{\text{C}}} \right). \quad (19)\end{aligned}$$

Suppose that the process uses pure carbon reductant ($a_{\text{C}} = 1$) and the gas phase consists of only CO ($P_{\text{CO}} = 1$). In this case, the temperature of the reduction is determined by $\Delta G_{\text{SiO}_2} = 0$, which now depends on the $a_{\text{Si}}/a_{\text{SiO}_2}$ ratio (Table 3.4).

As follows from Table 3.4 and equation (19), it is beneficial to decrease the activity of the reduced element (silicon) by, for example, forming a ferroalloy melt and increasing the activity of the oxide being reduced. This rule of thumb applies to all metallurgical processes, including ferroalloys.

Other common reductants used in the metallothermic reduction of ferroalloys (silicon and aluminum) are more powerful in reducing ferroalloy

TABLE 3.4 Dependence of the Starting Reduction Temperature for Silica Reduction by Carbon (19) from the Activities of Silicon and Silica

Activity of SiO_2	Activity of Si	Ratio $a_{\text{Si}}/a_{\text{SiO}_2}$	Calculated Temperature of Reduction, $^\circ\text{C}$
1	1	1	1665
1	0.5	0.5	1635
1	0.1	0.1	1566
0.5	0.1	0.2	1595

components (Fe, Ni, W, Mo, Mn, Nb, Ta, V, B, Si, Ti, Zr, and Ce) than carbon because they have higher negative Gibbs energy values of the reaction. Figure 3.4 shows the difference in reduction efficiency among carbon, silicon, and aluminum in relation to some oxides of common ferroalloy elements. For the elements forming the most stable oxides (like zirconium and cerium), the more effective reductants are magnesium and calcium, as Figures 3.3 and 3.4 show. Metallothermic reduction is applied also when the low-carbon ferroalloys are required, even when carbothermic reduction is effective enough.

In considering the data shown in Figure 3.4, one has to keep in mind that these Gibbs energy values are standard ones (i.e., for pure phases only). For instance, if the reduction of ZrO_2 by Si has too much positive free energy to proceed, it does not mean that a reduction of zirconium is impossible at low zirconium concentrations and realistic temperatures. At 1600°C , $K_P = 1.265 \cdot 10^{-5}$ for the reaction $\text{ZrO}_2 + \text{Si} = \text{SiO}_2 + \text{Zr}$, so with pure silicon, silica, and zirconia the reaction will be still possible if $a_{\text{Zr}} < K_P$. In the actual process, however, all the elements form solutions, so the effect of changes to activities will be more complex and sometimes not straightforward because there might be competitive reactions.

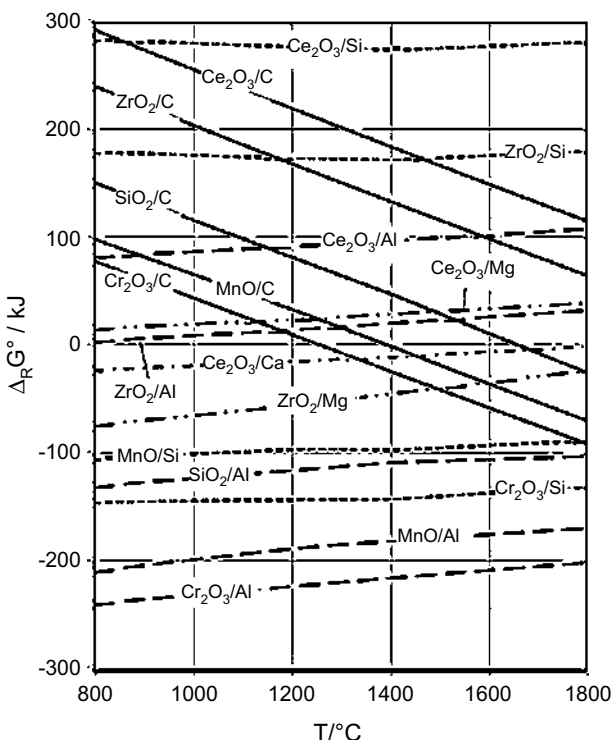


FIGURE 3.4 Comparison of standard Gibbs energies of reduction reactions of some oxides by Al, Si, and C per one mole of reductant. (Calculated by HSC Chemistry 7.)

In the carbothermic smelting of ferroalloys there are some undesired side reactions, like the evaporation of species in the form of volatile oxides and solid carbides. The latter phenomenon is not necessarily harmful if high carbon content in the alloy is permissible. Some standard Gibbs energies for metal carbides formation are presented in Figure 3.5. This Ellingham diagram for the formation of carbides shows that the tendency for the formation (precipitation) of carbides during the carbothermic smelting of ferroalloys increases in the following order: Fe (the least stable), Mn, Al, Si, B, Mo, Ce, V, Cr, Ti, and Ta (the most stable).

Chemical reactions tend to proceed at constant temperature and pressure in a reaction system in so far as they lead to the decrease of the system's Gibbs energy (i.e., when an equilibrium state has been reached). Consider, as another example, the formation of ferronickel by the reduction of wüstite ('FeO') and nickel monoxide (NiO):

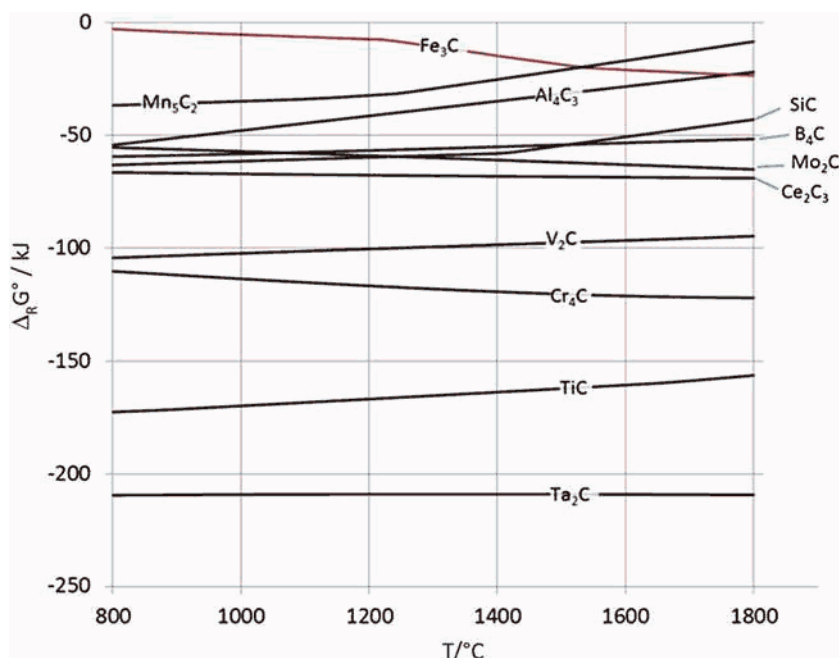


FIGURE 3.5 Standard Gibbs energies of formation of some carbides per one mole of carbon. (Calculated by HSC Chemistry 7.)

Figure 3.6 presents the change of Gibbs energy at 1600°C under atmospheric pressure with the progress of the reactions for the system, which has only iron oxide; Figure 3.7 presents the change for the system with an equimolar 1:1 ratio of ‘FeO’ and NiO. In the second example, the oxides form a molten mixture and the reduction products form a binary alloy (ferronickel). At high temperatures both ‘FeO’-NiO and Fe-Ni binary systems are close to ideal solutions—that is, the activities of these components are close to their mole fractions. The chemical reactions tend to proceed in so far as the derivative of system Gibbs energy in relation to reaction extent ($\partial G/\partial \xi$) is negative until it reaches the zero value where the Gibbs energy minimum has been reached.

Figures 3.6 and 3.7 show that the total Gibbs energy change might be lower than the standard value because of the formation of solutions and changes in the components’ activities. In Figure 3.7 this requires a three-dimensional representation, as there are more degrees of freedom in the system. The minimum of the free energy is reached, resulting in an alloy with 0.78 mol Ni and 0.025 mol

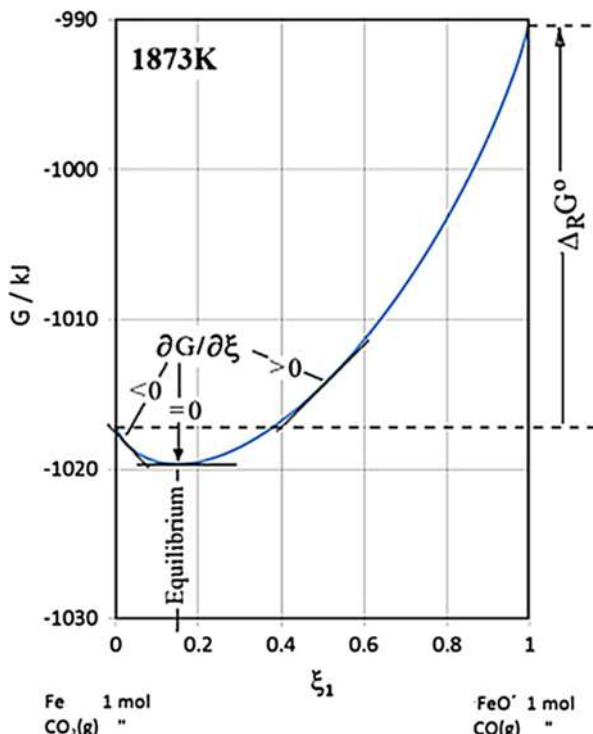


FIGURE 3.6 Gibbs energy of a reaction system ‘FeO’+ CO(g) as a function of the reaction progress (reaction extent ξ) and the driving force of the reduction reaction, the first derivative of Gibbs energy with reaction extent ξ . (Calculated by HSC Chemistry 7.)

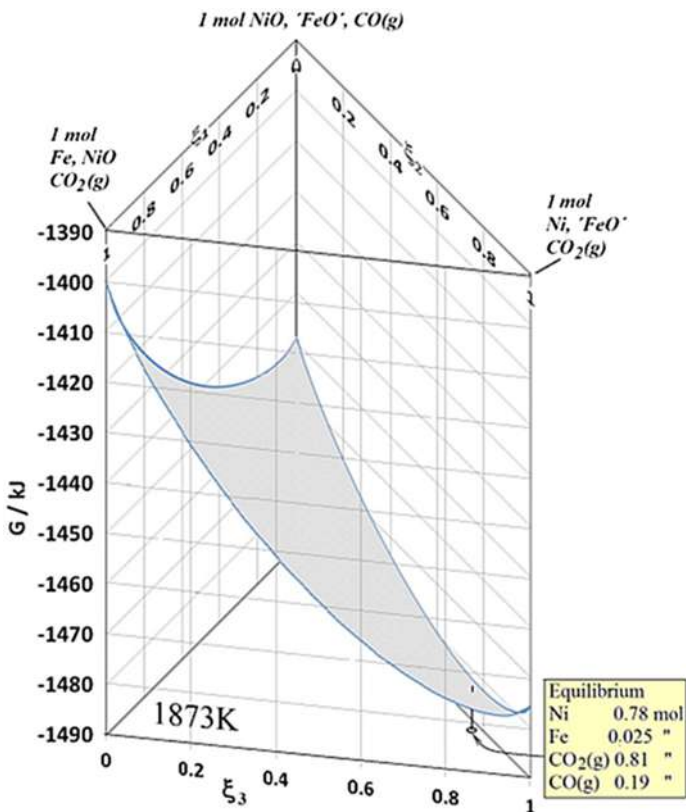


FIGURE 3.7 Gibbs energy surface of a reaction system with initial composition 'FeO' + NiO + CO(g) as a function of the reaction extent of independent reduction reactions 'FeO' + CO(g) = Fe + CO₂(g) and NiO + CO(g) = Ni + CO₂(g). The third reaction, Ni + 'FeO' = Fe + NiO, is not independent but is a sum of 'FeO' reduction and NiO oxidation reactions. $\Delta_R G^\circ(1873\text{K}) = 27.1 \text{ kJ/mol}$ for 'FeO' and -48.1 kJ/mol for NiO reduction. (Calculated by HSC Chemistry 7.)

Fe (~96.8% Ni mol), although the starting nickel concentration was 50% mol. The difference shows that in this case nickel (rather than iron) is preferentially reduced, leading to Ni-rich alloy formation.

The rate of the reactions depends on the kinetics of the chemical interaction and mass transfer in every specific case. If there are several reactions using the same reactants, such as in the system consisting of wüstite ('FeO') and nickel oxide, and the rates of the reactions are different, one reaction can pass the equilibrium state, but with time the system will return to the equilibrium state by opposing reactions with gaseous and condensed reactants. So if the reduction of nickel oxide is faster (in the second example) and its reduction passes the total equilibrium composition, the equilibrium state tends to be approached by a backward reaction (NiO) + [Fe]_{alloy} = [Ni]_{alloy} + ('FeO').

Therefore, besides the standard Gibbs energy of reaction, changes of elements and species activities (the formation of solutions) control the driving force of the process and the equilibrium state of chemical interaction. Figure 3.8 shows the progress of equilibrium reduction of iron chromite FeCr_2O_4 as a function of carbon addition at 1600°C (calculated using FactSage 6.2 databases) with the solution model for liquid iron-based solution. The first reduction reaction is $\text{FeCr}_2\text{O}_4 + \text{C(s)} \rightarrow \text{Fe(l)} + \text{CO} + \text{Cr}_2\text{O}_3$ and the second one (progressing significantly when the first one is practically finished) is $\text{Cr}_2\text{O}_3 + 3\text{C} \rightarrow 2[\text{Cr}]_{\text{FeCr}} + 3\text{CO}$.

So the liquid iron forms first, and then it dissolves reduced chromium lowering its activity and assisting the reduction process. According to information in the database for Fe alloys in FactSage 6.2, the activity coefficient of Cr in the Fe-Cr-C alloy is about 0.8 to 0.95 and that of C is about 0.1 to 0.5, increasing with each increasing degree of reduction. When chromium oxide is completely reduced and oxygen potential in the reaction system is reduced to a certain, sufficiently low level, there is a tendency for chromium carbide to form (the next reaction).

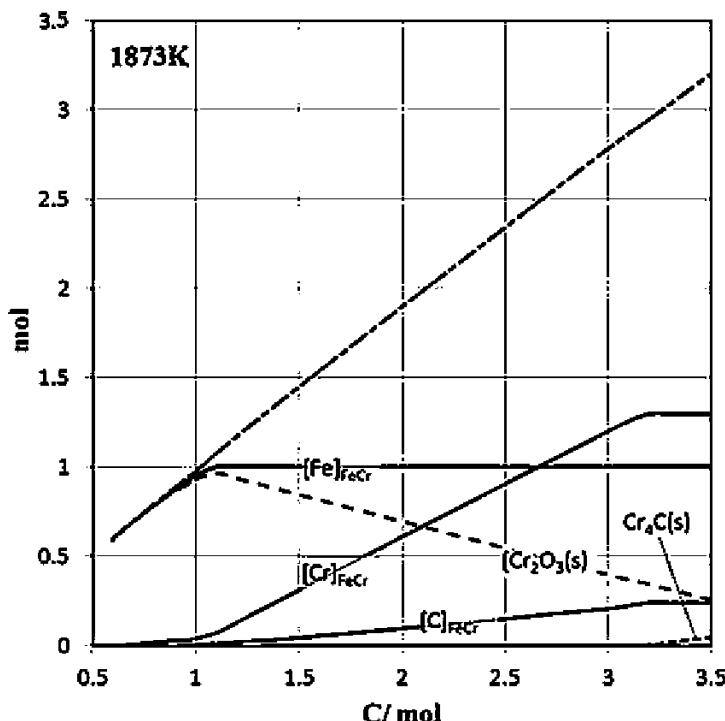


FIGURE 3.8 The progress of equilibrium reduction of one mole of chromite, FeCr_2O_4 , by carbon and the formation of ferrochromium (FeCr) as a function of carbon addition. (Calculated by FactSage 6.2.)

The reduction of oxides by CO formed during primary carbothermic reduction (by carbon) is also possible depending on the stability of oxide and the activity of reduced components in molten ferroalloy, although this process plays a certain role only for metals with less stable oxides (NiO, MoO₂, WO₂, 'FeO'). The role of carbon monoxide in the carbothermic reduction could be important as the secondary reductant, especially as the kinetic prerequisites for gaseous reduction are better because of the higher mobility of reductant than in solid-solid, solid-molten, or molten-molten reduction—carbon does not melt, even at high temperatures, not to mention its evaporation. Even if carbon monoxide is not as such an effective reductant for most ferroalloy component oxides, the back reduction of carbon dioxide $\text{CO}_2 + \text{C(s)} \rightarrow 2\text{CO}$, formed in the secondary reduction by carbon monoxide (chromium oxide reduction, for example) $\text{Cr}_2\text{O}_3 + 3\text{CO} \rightarrow 2[\text{Cr}]_{\text{FeCr}} + 3\text{CO}_2$, will keep the partial pressure of carbon dioxide low in the reaction environment and enables the reduction of even stable oxides by carbon monoxide (Gasik, 2001).

Thermodynamic calculations concerning the advance of individual reactions and final equilibrium state in metallurgical processes such as ferroalloys melting offer important information about the behavior of the reaction environment under various stages of the process, important for ruling and running the process, even when the final equilibrium state in the actual process has not been reached. Calculations of the equilibrium state of complex high-temperature processes like the various stages of ferroalloy smelting are hard to determine because of the complexity of the reaction system—a series of reactants and uneven conditions like temperature and charge composition at various locations in the reactor. In ferroalloys smelting based on lumpy ore or pelletized concentrates and carbon from coal with impurities as reductant, complex solid and molten phases with often remarkable amounts of various components, not only the oxides of iron and desired alloy element in the charge and formed alloy, can contain a number of auxiliary components.

There are a series of commercial programs for thermodynamic calculations, even for complex reaction environments like those in ferroalloy smelting, with a series of models for both metallic and nonmetallic solution phases. Typical examples are HSC Chemistry (www.outotec.com/HSC), FACTSage (www.factsage.com), ThermoCalc (www.thermocalc.se), Pandat (www.computherm.com/pandat.html), and MatCalc (matcalc.tuwien.ac.at). Modern thermodynamic databases are organized for automated data retrieval, so there is less use for tabulating standard Gibbs energy values or activity functions.

3.1.3.4 Equilibrium Phase Diagrams

In the development of new and the improvement of existing technological processes of ferroalloys production, the phase equilibria data in binary, ternary, and more complex metal, oxide, nitride, silicide, and carbide systems are of great importance. Study of the position of the boundary lines, equilibrium

concentration fields of the phases, and their physical transformation ranges is crucial for alloy compositions and for the determination of optimal processing parameters. Many phase equilibria diagrams are calculated with thermodynamic databases and the support of experimental data by thermal analysis. Phase diagrams of elements help to explain why the formation of only certain grade compositions of ferroalloys is beneficial, why the slags formed should have proper composition, and how the process parameters should be adjusted in relation to changes in chemical composition and temperature.

This is a brief outline of only the phase diagram types and their peculiarities; the reader is advised to consult specialist literature related to the theory of phase equilibria and the CALPHAD (CALculation of PHase Diagrams) method in general (Dinsdale, 1991; Hillert, 1998; Kubaschewski and Alcock, 1979; Pelton, 2001). It is a well-known procedure based on the concept of deriving the thermodynamic functions of a system from all available experimental data (Dinsdale, 1991; Saunders and Miodownik, 1998). The thermodynamic functions are expressed as polynomials of temperature, and the numerical values of the polynomial coefficients are obtained using optimization techniques (Pelton, 1988). The Gibbs energies of pure elements with respect to temperature $G_i^0(T)$ are represented by $G_i^0(T) = a + bT + cT\ln T + dT^2 + e/T + fT^3 + iT^4 + jT^7 + k/T^9$, as referred to the constant enthalpy values of the Standard Element Reference (SER) H_i^{SER} at 298.15 K and 1 bar (Dinsdale, 1991). The solution phases (liquid, solid solutions) are described by substitutional or interstitial solution models, where the Gibbs energy of the phase is given by (13) and the excess Gibbs energy G_i^{xs} is expressed in different forms.

For example, in the binary Fe-Cr system, four phases may formally exist. The liquid phase has only one sublattice (no miscibility gap) with Cr and Fe, whereas the BCC phase has two sublattices (1:3 ratio; Fig. 3.9) with chromium and iron in one and vacancies in the other, $(\text{Cr}, \text{Fe})(\text{Va})_3$. The iron-rich FCC phase also has two sublattices, but with the equal ratio $(\text{Cr}, \text{Fe})(\text{Va})$. The most complex structure has sigma-phase CrFe, which thermodynamic description requires three sublattices $(\text{Fe})_8(\text{Cr})_4(\text{Fe}, \text{Cr})_{18}$.

For a simple substitutional solution (only one lattice site with random occupation, e.g., liquid phase) for the excess Gibbs terms, using the Redlich-Kister-Muggianu polynomial, one obtains

$$G_m^{\text{xs}} = \sum_i \sum_{j < i} X_i X_j \sum_{v=0}^{V_{\max}} {}^v L_{ij} (X_i - X_j)^v + \sum_i \sum_{j < i} \sum_{k < j} \frac{X_i X_j X_k}{X_i + X_j + X_k} \left(X_i L_i^{(ijk)} + X_j L_j^{(ijk)} + X_k L_k^{(ijk)} \right), \quad (22)$$

where L_{ij} are respective binary and ternary temperature-dependent interaction parameters. For example, the expression for excess Gibbs energy for the liquid Fe-Cr phase might be written as $G_{LIQ}^{\text{xs}} = X_{\text{Fe}} X_{\text{Cr}} ({}^0 L_{\text{FeCr}} + {}^1 L_{\text{FeCr}} (X_{\text{Fe}} - X_{\text{Cr}}))$.

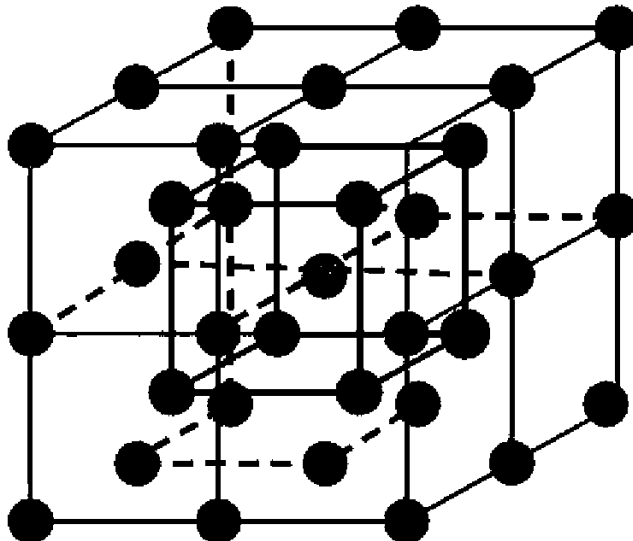


FIGURE 3.9 The model of two sublattices in the BCC Fe-Cr solid solution.

Numerical values of interaction parameters are retrieved from thermodynamic databases during calculations.

As all the ferroalloys systems are rather complex, involving many species and elements, the easiest way to start is to examine the binary phase diagrams of major components, moving further to cross sections of ternary and higher systems and adding more and more components. The hypothetical complex phase equilibrium diagram A-B shown in Figure 3.10 summarizes most possible phase transitions and transformation reactions, explained in Table 3.5 (Gasik et al., 2009).

Some of the phase diagrams are shown schematically in Figures 3.11 through 3.13. The simplest phase diagrams appear when A and B components have full mutual solubility in solid and liquid states (Fig. 3.11). This is typical for isomorphic systems and for components with very close properties. Figure 3.12 shows the eutectic system, where A and B are partially soluble in the solid state but completely soluble in liquid. This leads to a separation of the solid solutions α and β upon cooling, finishing with spontaneous eutectic solidification below eutectic temperature.

The eutectoid system is similar to that described earlier, but here A and B form several solid solutions, where in the high-temperature one (γ -phase) they have complete solubility. Upon cooling, this phase undergoes eutectoid transformation with a mechanism similar to that used for the eutectic one but without the liquid phase. A well-known system is iron-carbon with eutectoid temperature $\sim 738^\circ\text{C}$ at 0.8% C, which is important for the heat treatment of steels. Many systems in ferroalloys production have this kind of transformation.

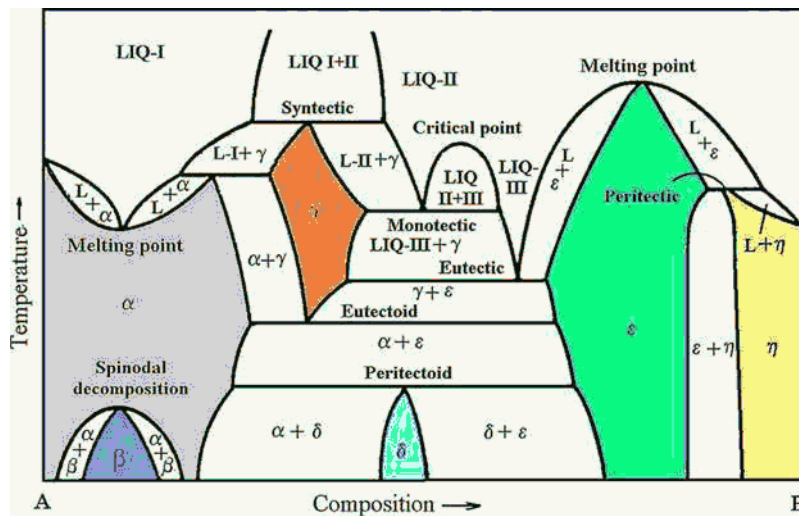


FIGURE 3.10 The hypothetical phase equilibria diagram showing possible phase transformations in a binary system. Areas of stability of homogeneous solid phases are shaded. (From Gasik et al., 2009.)

TABLE 3.5 General Classification of Different Phase Transformations (see Fig. 3.10)

Name	Reaction Type (Examples in Fig. 3.10)
Eutectic Type	
Eutectic	$L_{III} \leftrightarrow \gamma + \varepsilon$
Eutectoid	$\gamma \leftrightarrow \alpha + \varepsilon$
Monotectic	$L_{II} \leftrightarrow \gamma + L_{III}$
Monotectoid	$\gamma \leftrightarrow \gamma_1 + \beta$ (not shown in Fig. 3.10)
Catalectic	$\gamma \leftrightarrow L_I + \beta$ (not shown in Fig. 3.10)
Peritectic Type	
Peritectic	$L_I + \gamma \leftrightarrow \alpha; L + \varepsilon \leftrightarrow \eta$
Peritectoid	$\alpha + \varepsilon \leftrightarrow \delta$
Syntectic	$L_I + L_{II} \leftrightarrow \gamma$
Other	
Spinodal decomposition	$\alpha \leftrightarrow \beta + \alpha_I/\alpha_{II}$
Critical point	$L_I + L_{II} \leftrightarrow L; L_{III} + L_{II} \leftrightarrow L$

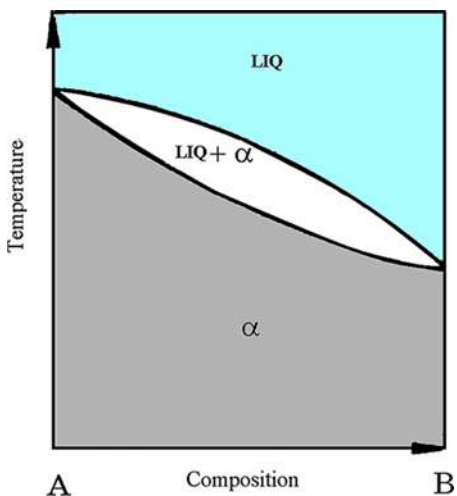


FIGURE 3.11 Equilibrium phase diagram showing complete solubility in solid and liquid states.

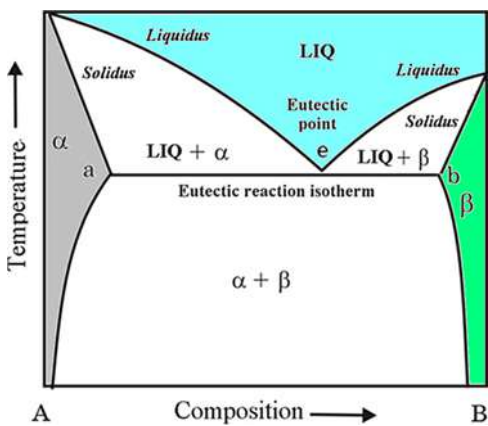


FIGURE 3.12 Eutectic equilibrium phase diagram with two solid solutions (α -rich α , B -rich β). Maximal solubility of B in α - A is observed at eutectic temperature (point "a") and maximal solubility of A in β - B is observed at point "b." Eutectic composition is marked by "e."

The peritectic systems have a transformation that occurs during heating as decomposition turns one of the solid phases into a liquid and a new solid phase—that is, the solid phase melts incongruently (with decay; see Fig. 3.10). In the peritectoid reaction, a similar process includes decomposition of the solid phase into two new solid phases upon heating.

For a system with more than two components, three-dimensional representation is normally needed. The composition coordinates are located in the horizontal plane (a triangle for a ternary system) and temperature is the vertical coordinate. Figure 3.14 shows a schematic of the $\text{FeO}-\text{MnO}-\text{SiO}_2$ system used to describe slags of ferromanganese and ferro-silicon-manganese processing. Here, different zones of the compounds can be seen together with a silica-rich, two-liquids immiscibility region (dashed lines).

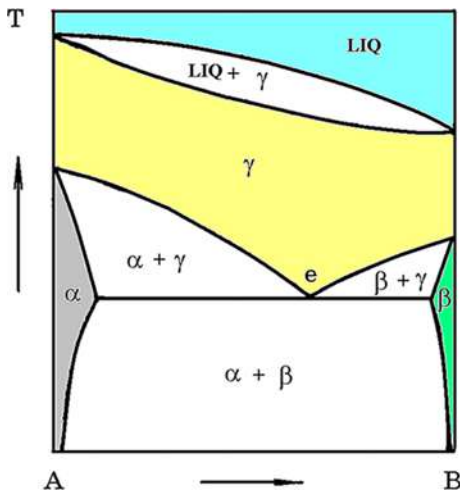


FIGURE 3.13 Eutectoid equilibrium phase diagram with three solid solutions (α , β , γ). The eutectoid point is marked by “e.”

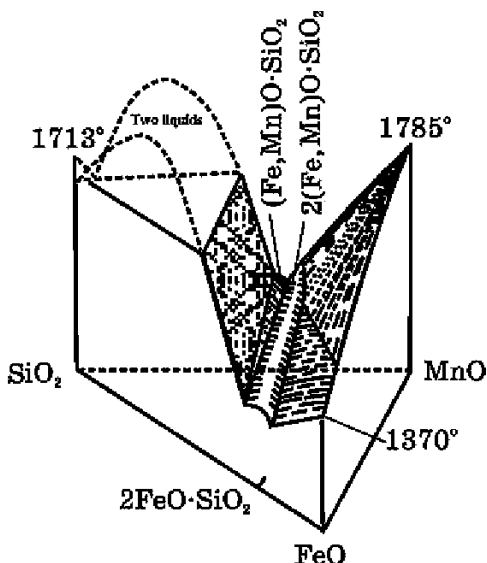


FIGURE 3.14 The schematics of the ternary FeO-MnO-SiO₂ system. (From Gasik et al., 2009.)

Systems with four or more components are difficult to represent in three-dimensional space and usually minor components' compositions are fixed, allowing variation of only compounds of interest.

3.1.4 Kinetics of Pyrometallurgical Processes

The reaction environment for ferroalloys production is complex. At low temperatures, where alloy containing oxide phases are solid, the direct solid-

solid reaction between carbon and oxides is very slow (the reactions with other reductants [Si, Al] proceed under different conditions, mentioned later). The reduction is carried out mostly by CO and H₂ (if there is moisture in the charge). In that case the reduction is a combination of oxide reduction by CO and its regeneration by the reaction of CO₂ with carbon (Fig. 3.15).

At higher temperatures when liquid phases are formed, the reduction is carried out by solid carbon in the carbon/slag interfaces and by carbon monoxide bubbling through the slag (including CO formed by carbon from electrodes). The reaction rate in that case is very complex and depends on many factors such as fluid flow and mixing intensity in slag; slag viscosity; the size of and distribution of carbon particles in the slag; and the amount, size, and distribution of CO and CO₂ bubbles in slag. So it is difficult to analyze and quantitatively describe the kinetics of reduction smelting in ferroalloys production.

There are a variety of reaction mechanisms, often based on different methods of heat and mass transfer. Reaction mechanisms may consist of the diffusion of one reactant through a product layer, external mass transfer (via diffusion, migration, convection, etc.) in the environment, thermal diffusion (heat transfer), adsorption, absorption, and desorption stages. These mechanisms may change if the reactant's state or condition changes. Most reactions in metallurgy are between solids and fluids in which the solid participates as a reactant that undergoes chemical changes. The overall fluid–solid reaction involves a combination of the following individual steps (Flammersheim and Opfermann, 1999):

- Transfer of the fluid reactants and the fluid products between the bulk fluid and the external surface of the solid particle
- Diffusion of the fluid reactants and the fluid products within the pores of the solid, if the solid contains open porosity

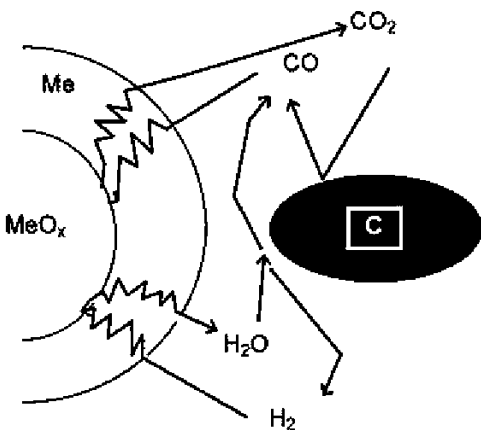


FIGURE 3.15 The schematic of the solid-state reduction of a metal oxide with CO and hydrogen in the presence of solid carbon. (From Gasik, 2001.)

- Chemical reaction between the fluid reactant and the solid at the fluid–solid interface
- Transfer of the reaction heat within the solid
- Transfer of heat between the external surface of the solid and the surroundings by convection and radiation
- Changes in the structure of the solid resulting from chemical reaction and heat.

These stages might be roughly allocated to the generic scheme shown in Figure 3.15, and it is understood that every such stage may have its own kinetics. Nevertheless, it might be possible to apply some principles of formal chemical kinetics to describe the overall reaction rate, even if it cannot possibly show the right reaction mechanism. In some cases, this formal reaction rate gives a hint about the limiting stage of the process (e.g., whether the overall reaction rate is limited by diffusion, surface of the reaction interface, or the transformation kinetics) and therefore possibilities for its improvement.

Reduction of iron-based and nonferrous oxide raw materials plays an important role in chemical metallurgy, because they relate to the production of metals from natural and secondary materials. Most raw materials are used in the form of oxide concentrates (iron ore, manganese ore, chromite, etc.) or pure (enriched) oxides (W, Mo, etc.). Kinetic peculiarities of reduction are also of great interest, and they are the bases for the development of industrially feasible technology and equipment. On the lab scale, kinetics is often studied by thermal analysis, which has been used in many areas of metallurgy to great advantage for explaining metallurgical processes. Its applications are in a range of studies of ores, oxides, scales, semifinished products, ferroalloys, and steels, as well as in studies on the reduction and oxidation of metals.

The application of kinetic analysis to reduction reactions includes two basic aspects. Scientifically, it includes the establishment of individual steps of the entire process as a model, as well as their clarification and interpretation. Technically the kinetic analysis is important as a tool for data extraction from measurements to provide an adequate kinetic model with minimum parameters. This kinetic model could be further applied for the process of prediction and optimization. In formal chemical kinetics, “reaction rate” usually means the rate of formation/destruction of the reagents in a certain period of time. For example, for a reversible reaction of the wüstite reduction by CO, as shown earlier for the thermodynamics of ferro-nickel formation (20): $\text{FeO} + \text{CO} \leftrightarrow \text{Fe} + \text{CO}_2$, the reaction rate is

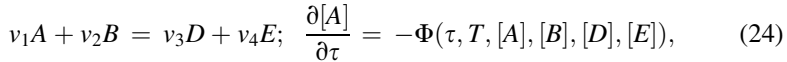
$$v_P = \left\{ -\frac{dN_{\text{FeO}}}{d\tau} \right\}_d - \left\{ \frac{dN_{\text{FeO}}}{d\tau} \right\}_r = \left\{ -\frac{dN_{\text{CO}}}{d\tau} \right\}_d - \left\{ \frac{dN_{\text{CO}}}{d\tau} \right\}_r = \left\{ \frac{dN_{\text{Fe}}}{d\tau} \right\}_d - \left\{ -\frac{dN_{\text{Fe}}}{d\tau} \right\}_r = \left\{ \frac{dN_{\text{CO}_2}}{d\tau} \right\}_d - \left\{ -\frac{dN_{\text{CO}_2}}{d\tau} \right\}_r,$$

where N_i is the instant amount of moles of the component i , τ is the time, and v_P is the reduction rate. Subscript d refers to the direct reaction and r refers to the

reverse reaction. In the equilibrium, the rates of direct reaction (reduction of iron oxide) and the reverse reaction (oxidation of iron) are equal, and the resulting Gibbs energy change (20) is zero. Experimentally it was observed that for reactions the rate depends on the concentration of the starting compounds and temperature (if all other parameters are equal):

$$v_P = k_d [n_{FeO}]^{a1} [n_{CO}]^{b1} - k_r [n_{FeO}]^{a2} [n_{CO}]^{b2}, \quad (23)$$

where k_d and k_r are direct and reverse reaction rate constants, n_i is the concentration of component i , and $a1\dots b2$ refer to the reaction rate exponents. It is important to note that these exponents usually are in no way related to the stoichiometry coefficients of the reaction. To get the reduction rate, the differential equation (23) should be solved as a function of time, temperature, and components' concentration. However, simplified equations like (23) are very rare in real kinetic process analysis. To extend the formal mechanism for other reduction reaction types, let's start with a reaction equation in a general form:



where $[X]$ refers to concentrations of components (A and B are the starting compounds; D and E are the reaction products), τ refers to time, T is the temperature, and Φ is a conversion function (Flammersheim and Opfermann, 1999). With certain limitations, it is possible to apply the Arrhenius theory for (24), although this procedure is not rigorously justified. It is further assumed that the conversion function can be described by two separable functions, k for Arrhenius-type dependence and f for mechanism dependence: $\Phi(\tau, T(\tau), [A], [B], [D], [E]) = k(T(\tau)) \cdot f([A], [B])$. The complete separation of variables in this differential equation is only possible for one-step processes. For the reaction rate function $k(T(\tau))$, several types of the equation have been suggested in the form of

$$k(T(\tau)) = A_r \cdot (T(\tau))^m \exp\left(-\frac{E_r}{RT(\tau)}\right), \quad (25)$$

where A_r is the frequency factor, $1/s$, E_r is the activation energy (J/mol), R is the universal gas constant (8.314 J/mol·K), and T is the time-dependent temperature. The exponent m in (25) depends on the consideration of the mechanism of reaction: the collision theory predicts $m = \frac{1}{2}$, in the theory of the activated state $m = 1$, and in the classical Arrhenius theory $m = 0$. Table 3.6 lists a series of the most typical reaction types along with their f functions. This list contains classic homogeneous reactions and typical solid-state reactions and their definitions (Brown et al., 1980; Flammersheim and Opfermann, 1999). The parameter α here means normalized reaction extent (it is zero if no reaction has yet taken place and unity when the reaction has completed).

Practical analysis of the kinetics of reduction or transformation is commonly made using thermal analysis (TA) methods. These methods and their use are defined in several DIN, CEN, and ASTM standards. Thermal

TABLE 3.6 Reaction Types and Equations for Reaction

$$\text{Rate } \partial\alpha/\partial\tau = -A_r \exp(-E_r/(RT)) \cdot f(\alpha, 1-\alpha)$$

$f(\alpha, 1-\alpha)$	Reaction Type
α	First-order reaction
α^2	Second-order reaction
α^n	n^{th} order reaction
$2 \cdot \alpha^{1/2}$	2-D phase boundary reaction
$3 \cdot \alpha^{2/3}$	3-D phase boundary reaction
$1/(2(1-\alpha))$	1-D diffusion
$-1/\ln(\alpha)$	2-D diffusion
$3 \cdot \alpha^{1/3}(\alpha^{-1/3} - 1)/2$	3-D diffusion (Jander's type)
$3/(\alpha^{-1/3} - 1)/2$	3-D diffusion (the Ginstling-Brounstein type)
$2 \cdot \alpha \cdot (-\ln(\alpha))^{1/2}$	2-D nucleation
$3 \cdot \alpha \cdot (-\ln(\alpha))^{2/3}$	3-D nucleation
$n \cdot \alpha \cdot (-\ln(\alpha))^{(n-1)/n}$	n -D nucleation/nucleus growth (Avrami/Erofeev)
$\alpha \cdot (1 + K_{\text{cat}} \cdot (1 - \alpha))$	First-order reaction with autocatalysis through the reactants

analysis is commonly defined as a group of techniques in which a physical property of a substance is measured as a function of temperature, while the substance is subjected to a controlled temperature program (Brown, 1989). The most used methods are thermogravimetry (TG; monitoring mass changes of the specimen), differential thermal analysis (DTA; monitoring temperature changes of the specimen versus reference), and differential scanning calorimetry (DSC; monitoring the heat flux needed to keep the temperature of the specimen closest to the temperature of the reference). Several methods could be combined into a single measuring device; this is called “simultaneous thermal analysis” (STA). This combination also involves other techniques such as mass spectrometry (MS) or Fourier transform infrared spectrometry (FTIR).

Figure 3.16 shows an example of the kinetic data of the reduction of molybdenum trioxide at four different temperatures in the laboratory thermal balance, where mass change has been recorded in time. It shows that temperature from 700° to 800°C is not enough to reach complete reduction (relative mass change does not approach zero, as would be expected for the reaction $\text{MoO}_3 \rightarrow \text{Mo}$), staying at ~1/3 of the theoretical mass loss. This indicates that only 1 of 3 atoms of oxygen is removed and the final reduction product is MoO_2 . At 900 to 1000°C, almost full reduction takes place, leading to metallic molybdenum.

This example is one of the simplest as there are no solid solutions, liquid phases, carbides, or other compounds formed. Realistic processes such as

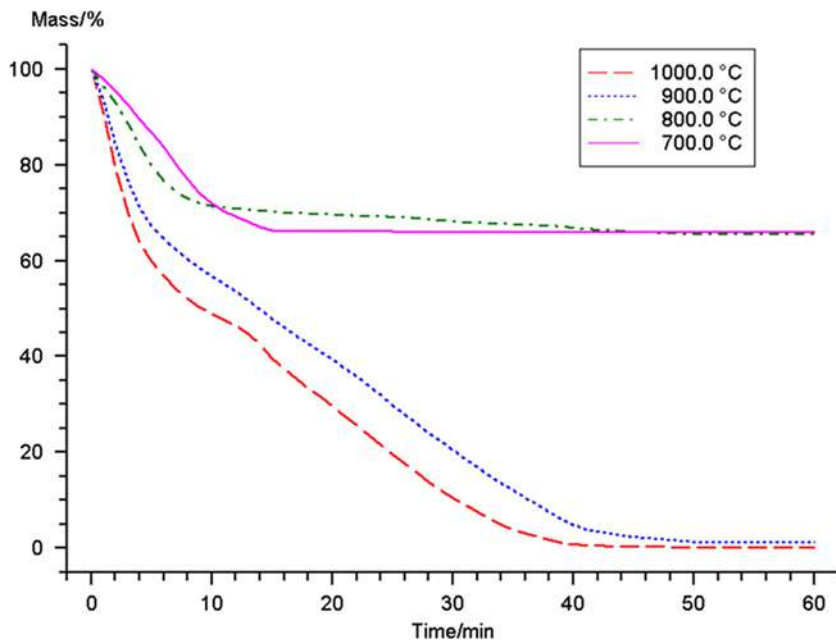


FIGURE 3.16 Kinetics of the reduction of molybdenum trioxide (relative mass, %) at four different temperatures in the laboratory thermal balance. (Uses data presented by Ostrik and Gasik, 1993.)

reduction of chromites or manganese ore by carbon in the presence of iron and slag-forming phases are much more complex, and the identification of the thermal analysis data is far from trivial. Nevertheless such experimental information helps to point out possible process stages and potential side reactions such as evaporation of the material or formation of intermediates. To demonstrate, Figure 3.17 shows data on simultaneous thermal analysis of nickel laterite ore. Here, changes in mass of the specimen (TG, %), thermal effects (exothermic and endothermic, DSC), and the evolution of gases (integral Gram-Schmidt signal) are overlaid.

The figure shows that the mass loss curve has several stages and that some thermal effects are correlated with the release of gases (e.g., the endothermic effect around 100°C accompanied with peak of the gas absorption signal. This is possibly associated with the release of water vapor). The gases coming out of the specimen are identified via Fourier transform infrared (FTIR) spectrometry analysis (Fig. 3.18).

In Figure 3.19, the data from Figure 3.18 are projected onto a spectral map. It shows that a major water release takes place after about 1000 s upon heating (~90° to 120°C), coinciding with a significant mass loss (Fig. 3.17). A major CO₂ peak release—at around 2000 to 3000 s (~400° to 550°C)—is possibly associated with decomposition of carbonates in the ore sample. Using this type

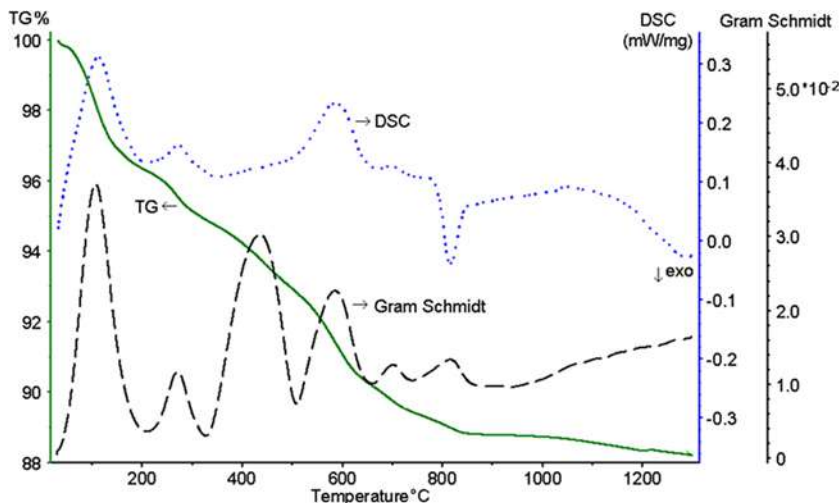


FIGURE 3.17 Kinetics of the transformation of nickel laterite ore at heating. Data are shown for mass loss (TG, %), thermal effects (DSC, mW/mg; exothermic reactions give a negative heat flux signal), and gases release (Gram-Schmidt trace, relative absorbance units; indicates degree of infrared absorption in the gas phase). (Data provided by M. Gasik and M. Friman.)

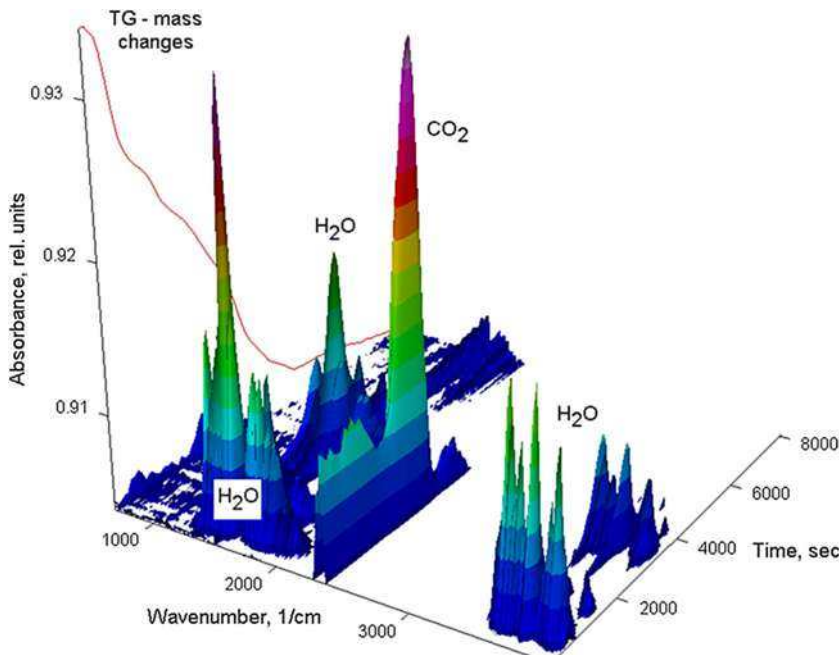


FIGURE 3.18 Example of gas evolution during the heating of nickel laterite ore (Fig. 3.17), where the spectral response of the Gram-Schmidt signal is expanded. Spectral areas of CO_2 and water are marked. The trace line on the left is the mass change (TG signal) from Figure 3.17.

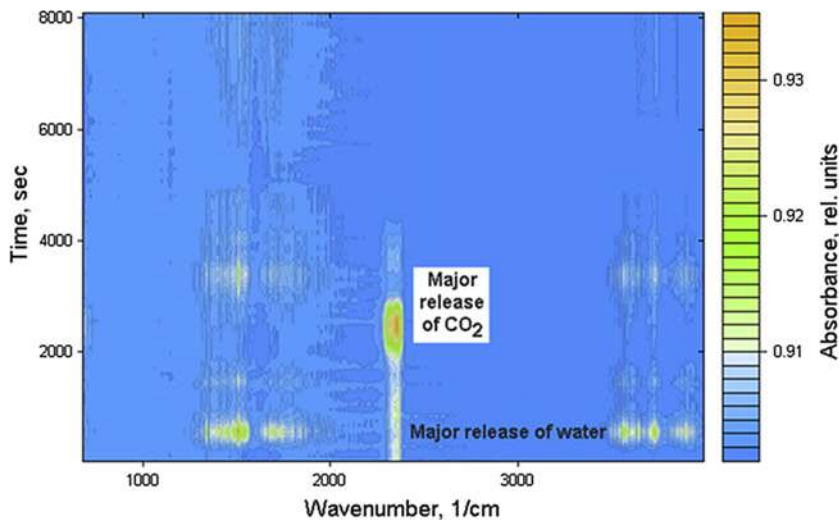


FIGURE 3.19 Projection of the process shown in Figure 3.18 indicating areas of major water and CO_2 release from laterite ore sample.

of thermal analysis, it might be possible to compare different specimens and to understand the processes behind the reduction of metal oxides and the production of ferroalloys.

3.1.5 Basics of Heat Transfer in Ferroalloys Processing

Heat and mass transfers are of extreme importance in all industrial processes, including ferroalloys smelting. Heat transfer includes the transportation of energy driven by temperature difference, and it might be realized by one of the following mechanisms (see Table 3.3): conduction, convection, and radiation. The first and third mechanisms do not involve mass transfer.

3.1.5.1 Heat Transfer via Conduction

Heat conduction in solids usually takes place via lattice vibrations (phonons) and electrons (especially in metals and semiconductors). Typical for heat conduction, the heat flux is proportional to the temperature gradient and material thermal conductivity (Fourier's law):

$$q \left[\text{W/m}^2 \right] = -\lambda \nabla T. \quad (26)$$

For many solid materials, thermal conductivity might be approximated by a linear function of temperature—for example, for magnesite (MgO) brick in air, $\lambda = 6.16 - 0.00267 \cdot (T - 273)$ in $\text{W}/(\text{m}\cdot\text{K})$. Let's suppose a smelting furnace has a cylindrical, multilayer wall (e.g., furnace steel shell, refractory lining, frozen charge or slag). In the stationary case (steady heat flux) across the wall, expanding equation (26), the resulting heat flow (in W/m^2) might be calculated as

$$q_{wall} = \frac{T_{in} - T_{out}}{\frac{1}{\alpha_{in}d_1} + \sum_{i=1}^{n-1} \frac{1}{2\lambda_i} \ln \frac{d_{i+1}}{d_i} + \frac{1}{\alpha_{out}d_n}}, \quad (27)$$

where d_i refers to the diameters of respective layers i , λ_i is the thermal conductivity of the i layer, and α_i is the convection coefficient inside and outside of the wall of the furnace. Convection coefficients are temperature dependent; for example, for a metallic shell or brick wall contacting with ambient air (20°C), $\alpha_{out} \sim 7.7743 + 0.0661 \cdot (T - 273)$, $\text{W}/(\text{m}^2\text{K})$, and this approximation already accounts for radiative losses as well. In high-temperature heat transfers, the inner convection coefficient is normally very high for turbulent flow and thus the term $1/\alpha_{in}$ might often be neglected.

3.1.5.2 Heat Transfer by Radiation

Heat transfer by radiation takes place through the transport of photons (electromagnetic radiation), which solid surfaces can absorb or reflect. Any body with a temperature above absolute zero emits thermal radiation. Surface-to-surface radiation may be hindered by shadowing and diffuse reflections between radiating surfaces. This is the only heat transfer mechanism able to operate in a vacuum and it requires only that photon flux reaches the surface. The radiative heat flux is proportional to material emissivity (degree of “gray”) and the difference of absolute temperatures of emitter T_1 and receiver T_2 in fourth power (Stefan-Boltzmann law; $T_1 > T_2$):

$$q[W/m^2] = C_F \sigma \varepsilon_s (T_1^4 - T_2^4), \quad (28)$$

where $\sigma = 5.67 \cdot 10^{-8} \text{ W}/(\text{m}^2\text{K}^4)$ is the Stefan-Boltzmann constant, C_F is the viewing (shading) coefficient (depending on a mutual arrangement of radiating and receiving surfaces), and ε_s is the total emissivity (unitless, 0–1). When the emissivity is unity, the heat flux emitted corresponds to the black body radiation. If radiative surfaces are somewhat obstructed or shadowed from the view of each other, the coefficient C_F is introduced, which accounts for this result so the effective heat flux is decreased. Some typical emissivities for different materials used in ferroalloys smelting are shown in Table 3.7.

3.1.5.3 Heat Transfer by Convection

Heat transfer via convection is now described for two scenarios. In the first, the fluid in motion carries away into some thermal energy, proportional to the net displacement of a fluid resulting from the fluid’s own velocity (see Table 3.2):

$$q[W/m^2] = \int_{T_2}^{T_1} \mathbf{u} \cdot \rho \cdot C_P dT \approx \mathbf{u} \cdot \rho \cdot (C_P(T_1) T_1 - C_P(T_2) T_2), \quad (29)$$

TABLE 3.7 Typical Gray Body Emissivities for Some Materials

Material	Gray Emissivity	Temperature Range, °C
Aluminum, oxidized	0.11–0.19	200–600
Aluminum oxide (corundum)	0.23–0.4	1200–1700
Calcium oxide	0.27	800–1300
Carbon	0.79–0.81	100–650
Chromium oxide	0.73–0.97	800–1300
Copper, oxidized	0.57–0.87	200–600
Molybdenum	0.096–0.292	700–2600
Steel, polished	0.55–0.61	900–1100
Steel, oxidized	0.8	200–600
Tungsten	0.053–0.307	300–2200
Water	0.95–0.963	0–100

where fluid local velocity vector is \mathbf{u} , fluid density ρ , and specific heat C_P , with temperatures at outlet and inlet, respectively, being given (density and velocity might be assumed constant if they do not significantly vary with temperature).

Another form of convective heat transfer occurs for heat dissipation from a solid surface to a fluid, where the heat transfer coefficient and the temperature difference across a hypothetical film describe the flux:

$$q \left[\text{W/m}^2 \right] = \alpha_{conv} \cdot (T_{surf} - T_{fluid}), \quad (30)$$

where α_{conv} is the effective convection coefficient, and $\text{W}/(\text{m}^2\text{K})$ is defined in the same way as in (27).

3.1.5.4 Generalized Heat Transfer Equation

For a fluid, the resulting combined heat equation becomes

$$\rho C_P \left(\frac{\partial T}{\partial t} + (\mathbf{u} \cdot \nabla) T \right) = -(\nabla \cdot \mathbf{q}) + \sum_i \sum_j \tau_{ij} \mathbf{S}_{ij} - \frac{T \partial \rho}{\rho \partial T} \Big|_p \left(\frac{\partial p}{\partial t} + (\mathbf{u} \cdot \nabla) p \right) + Q_s, \quad (31)$$

where ρ is the density (kg/m^3), C_P is the specific heat at constant pressure ($\text{J}/(\text{kg} \cdot \text{K})$), \mathbf{u} is the velocity vector (m/s), \mathbf{q} is the conductive heat flux vector (W/m^2), p is pressure (Pa), τ is the viscous stress tensor (Pa), \mathbf{S} is the strain rate tensor ($1/\text{s}$) equal to $\frac{1}{2}(\nabla \mathbf{u} + \nabla \mathbf{u}^T)$, and Q_s represents other heat sources, such as electromagnetic or joule heating (W/m^3). The other sources might also include terms such as those that have arisen from species diffusion (as the sum of partial

molar enthalpies by respective molar flux of the species), but these play a role only when there are species fluxes with substantially different enthalpies.

The generalized equation assumes that the mass of the fluid is conserved. The left part of the equation describes the rate of change of the stored heat (energy) in the material in time plus the contribution arising from convective heat inflow. The right part summarizes the contribution of conduction, radiation, viscous heating effects, and adiabatic heating from pressure work and other sources. In metallurgical practice, viscous heating and adiabatic heating are in most cases negligible and could be omitted.

For convection transfer between solid (walls) and fluid media, four cases might be outlined. They are combinations of either natural (no external forces besides gravity) or forced (blowing, mixing, etc.) convective fluid motion along an external (open) wall (surface) or an internal wall (tubes, pipes, closed reactors). Fluid flow in all these cases might be either laminar or turbulent. These conditions specify the dependence of the convection coefficient α_{conv} , for which no general expression could be made (Themelis, 1995). The determination of convective parameters is sometimes very complex, and the traditional engineering method relies on the use of different nondimensional groups (similarity numbers) (Table 3.8).

For natural convection arising within the closed volumes (between walls of different temperatures), a heat flux equation for thermal conductivity might be used, if thermal conductivity is corrected by the Rayleigh factor $q_c \approx \lambda \frac{T_1 - T_2}{S} \cdot 0.18(Ra)^{0.25}$. For forced convection, functional dependencies

TABLE 3.8 Some Important Nondimensional Numbers

Number	Formula	Use
Nusselt	$Nu = \frac{\alpha L}{\lambda} = f(Gr, Re, Pr)$	Calculation of α from Nu value at given dimension L (pipe diameter, wall length, etc.) and fluid conductivity λ ; gives the ratio of total heat transfer to conductive heat transfer
Grashof	$Gr = \frac{\beta L^3 g \rho \Delta T}{\mu}$	Fluid volume thermal expansion coefficient β , density ρ , dynamic viscosity μ at given gravity g and temperature difference \rightarrow ratio of buoyancy to viscous forces
Reynolds	$Re = \frac{u L \rho}{\mu}$	Fluid flow with velocity $u \rightarrow$ ratio of inertia to viscous forces; laminar flow usually if $Re < 2300$, turbulent for $Re > 5000$; not used for natural convection
Rayleigh	$Ra = Pr \cdot Gr$	Ratio of natural bulk heat transport to convective heat transport (near walls of characteristic length L)
Prandtl	$Pr = \frac{\mu C_p}{\lambda}$	Ratio of momentum diffusivity to thermal diffusivity; for diatomic gases $Pr = 0.72$, for triatomic gases it is 0.8

of Nu are more complex. For example, a gas flowing around a flat plate at laminar conditions ($Re < 2300$ in pipes) has Nusselt number $Nu = 0.67 Re^{0.5} Pr^{0.333}$ and the same for liquid metal under turbulent conditions ($Re > 5000$ in pipes) $Nu = 0.59 Re^{0.61}$. More details about the nondimensional numbers and their application for heat and mass transfer coefficients normally relevant to metallurgical furnaces can be found in many handbooks (Bird et al., 2005; Incropera and De Witt, 1996; McCabe and Smith, 1976; Themelis, 1995; VDI, 1993).

3.1.5.5 Heat Generation

The last term in equation (31) is important for setting up the amount of heat (heat flow or power) generation in the metallurgical reactor (furnace), which is required to initiate, support, and fulfill the specific reduction reactions and to melt the charge and reaction products. This is connected with the power supply to a specific furnace and determines the size of the plant and the conditions for electrical transformers. In a set of six furnaces of 63 MVA-rated power, each easily may consume half of the power generated by a nuclear reactor station. Therefore, it is important to understand the principles of energy conversion into heat inside the furnace.

The properties of materials (charge components, metal, and slag) are usually temperature dependent, so equations like (31) become nonlinear. The electric current density vector in the furnace is expressed with the Maxwell-Ampere law:

$$\mathbf{J} = \nabla \times \mathbf{H} = \sigma (\mathbf{E} + \mathbf{u} \times \mathbf{B}) + i \omega \mathbf{D} + \mathbf{J}_{ext} \quad (32)$$

where σ is the electrical conductivity, \mathbf{H} is the magnetic field strength, \mathbf{E} is the electric field strength (the gradient of electrical potential $\nabla \varphi$), \mathbf{u} is the velocity vector of the media (defining magneto-hydrodynamic flow), \mathbf{B} is the magnetic induction, \mathbf{J}_{ext} is the external current density (if present), $\omega = 2\pi f$ is the frequency of electrical field (Hz), and \mathbf{D} is the electric displacement ($\mathbf{D} = \epsilon \cdot \epsilon_0 \cdot \mathbf{E} + \mathbf{P}$). Here ϵ is a real part of dielectric permittivity, ϵ_0 is the dielectric constant of the vacuum, and \mathbf{P} is the polarization vector (which might be neglected for conducting materials). If the medium (slag, metal, charge) is not moving ($\mathbf{u} = 0$) and the voltage applied is DC only ($f = 0$), equation (32) transforms into Ohm's law (Gasik et al., 2010). The general Maxwell equations with use of (32) will take the following form:

$$\begin{aligned} -\nabla \cdot ((i \omega \sigma - \omega^2 \epsilon \epsilon_0) \mathbf{A} - \sigma \mathbf{u} \times (\nabla \times \mathbf{A}) + (\sigma + i \omega \epsilon \epsilon_0) \nabla \varphi \\ - (\mathbf{J}_{ext} + i \omega \mathbf{P})) = 0 \\ (i \omega \sigma - \omega^2 \epsilon \epsilon_0) \mathbf{A} + \nabla \times ((\mu \mu_0)^{-1} \nabla \times \mathbf{A} - \mathbf{M}) - \sigma \mathbf{u} \times (\nabla \times \mathbf{A}) \\ + (\sigma + i \omega \epsilon \epsilon_0) \nabla \varphi = \mathbf{J}_{ext} + i \omega \mathbf{P} \end{aligned} \quad (33)$$

where \mathbf{A} is the vector magnetic potential, \mathbf{M} is the vector of the material's magnetic saturation, μ is the relative magnetic permittivity, and μ_0 is the

magnetic permittivity of the vacuum. These equations describe the complete electromagnetic behavior of current, potential, and magnetic parameters in any materials or media. When an electromagnetic field is interacting with a material, the power dissipated in that material has active (ohmic) and reactive (inductance, capacitance) parts. In metallurgical practice, only ohmic (joule) losses lead to material heating, unless high-frequency (RF or microwave fields) are used. The total power dissipation in the material in the domain Ω is defined by partial derivatives of electric and magnetic energies:

$$-\int_{\Omega} \left(\mathbf{E} \cdot \frac{\partial \mathbf{D}}{\partial t} + \mathbf{H} \cdot \frac{\partial \mathbf{B}}{\partial t} \right) d\Omega = \int_{\Omega} \mathbf{J} \cdot \mathbf{E} \, d\Omega + \oint_S (\mathbf{E} \times \mathbf{H}) \cdot \mathbf{n} \, dS, \quad (34)$$

with \mathbf{n} being the normal vector to the bounding surface S . The first part of the right-hand side is cycle-time-averaged joule heating (ohmic losses), and the second is reactive power (especially inductive losses). This joule heating is the major source of the heat in the ferroalloys' smelting furnace, and it gives the major positive contribution to the source term Q_s in equation (31). Other heat sources and sinks are mostly heat from reactions (oxidation of carbon, enthalpy of reduction reactions, melting, and solidification), balanced by heat losses through the walls, roof, exhaust gases, and tapped materials.

3.1.6 Basics of Mass and Momentum Transfer in Ferroalloys Processing

Mass transfer is a critical aspect of ferroalloys processing, as it controls the conversion of raw substances into other final products. In ferroalloys processing, mass transfer occurs mostly through chemical reactions (which cause significant concentration gradients, acting as driving forces), via phase separation and transformation. Most ferroalloys processes require external heat, which in turn affects both the reactions themselves and other physical processes connected with the system. Furthermore, most furnace operations require an optimized and steady production of product. This means that most mass balance applications require coupling to momentum and energy balances.

3.1.6.1 Diffusive Mass Transfer

The simple mass balance equation for any species might be written for a change of the species concentration c_i (mol/m^3) in time:

$$\frac{\partial c_i}{\partial t} = \nabla \cdot (D_i \nabla c_i) - \mathbf{u} \cdot \nabla c_i + R_i, \quad (35)$$

where D_i is the species diffusion coefficient, \mathbf{u} is the fluid velocity, and R_i is the respective reaction rate, which produces these species (as shown in the previous section for kinetics of the processes). The left-hand side and the first term on the right-hand side of equation (35) constitute Fick's law of diffusion. The

diffusion coefficients D (describing pure Fick's diffusion) are independent of concentration. However, in concentrated solutions or melts, where relative concentrations are of the same order of magnitude, all species interact with each other and themselves (Wesselingh and Krishna, 2000). Their diffusion coefficients are therefore species and concentration dependent, and they can also depend on temperature and pressure. In this case for n -component system, the complete diffusion process is described by the Maxwell-Stefan equation, expressing concentrations in terms of weight fractions (w_j) and molar fractions x_j (Bird et al., 2005; Wesselingh and Krishna, 2000):

$$\frac{\partial}{\partial t} (\rho w_i) + \nabla \cdot \left(\rho w_i \left(\mathbf{u} - \sum_{j=1}^n \tilde{D}_{ij} \left(\nabla x_j + (x_j - w_j) \frac{\nabla p}{p} \right) \right) - D_i^T \frac{\nabla T}{T} \right) = R_i,$$

$$x_j = \frac{w_j}{M_j} M_\Sigma, \quad \sum_{j=1}^n w_j = 1. \quad (36)$$

This equation includes also possible effects of pressure and temperature gradients, which might be significant in different parts of the furnace (e.g., near electrode working tips). The difficulty in direct use of this equation is application of the Maxwell-Stefan cross-diffusion coefficients, which are related to the Fick cross-diffusion coefficients D_{ij} in a complex way, requiring numerical calculations. For example, for a three-component system

$$\tilde{D}_{ij} = \frac{\frac{w_1(w_2 + w_3)}{x_1 D_{13}} + \frac{w_2(w_1 + w_3)}{x_2 D_{23}} - \frac{(w_3)^2}{x_3 D_{12}}}{\frac{x_1}{D_{12} D_{13}} + \frac{x_2}{D_{12} D_{23}} + \frac{x_3}{D_{13} D_{23}}}. \quad (37)$$

Another contribution to the species diffusion in ferroalloys processing might be important, especially in the case of DC furnaces or other situations where there are strong electric fields acting on fluids with charged species (metal and slag melts). This is the Nernst-Planck contribution of electromigration of charged species under the gradient of electric field ∇V , changing diffusion equation (35) to

$$\frac{\partial c_i}{\partial t} = \nabla \cdot (D_i \nabla c_i) - \mathbf{u} \cdot \nabla c_i + Z_i v_i F c_i \nabla V + R_i. \quad (38)$$

Here the additional term includes species charge Z , species ionic mobility v ($\text{s} \cdot \text{mol/kg}$), and $F = 96480 \text{ C/mol}$, the Faraday number. This equation is complemented by the electroneutrality condition and the conservation of electric current: $\sum_j Z_j c_j = 0$; $\nabla \cdot \mathbf{i} = F \sum_j Z_j R_j$.

3.1.6.2 Convective Mass and Momentum Transfer

The generalized Navier-Stokes formation for fluid flow (in the absence of chemical reactions or phase changes) combines conservation of mass

$$\frac{\partial \rho}{\partial t} + \nabla \cdot (\rho \cdot \mathbf{u}) = 0, \quad (39)$$

conservation of momentum

$$\rho \left(\frac{\partial \mathbf{u}}{\partial t} + (\mathbf{u} \cdot \nabla) \mathbf{u} \right) = \nabla \cdot [-p \mathbf{I} + \tau] + \mathbf{F}, \quad (40)$$

and conservation of energy (equation (31)). Here, \mathbf{I} is the unity tensor and \mathbf{F} is an external body force (e.g., gravity) acting on that fluid (Hauke and Hughes, 1994). When the fluid might be considered incompressible (constant density during the flow), the incompressible Navier-Stokes formulation will take the following form:

$$\rho \left(\frac{\partial \mathbf{u}}{\partial t} + (\mathbf{u} \cdot \nabla) \mathbf{u} \right) = \nabla \cdot [-p \mathbf{I} + \eta (\nabla \mathbf{u} + (\nabla \mathbf{u})^T)] + \mathbf{F}. \quad (41)$$

These Navier-Stokes equations (40, 41) describe the basic phenomena of mass and momentum transport. This is the practical case for all fluids under normal conditions and also for gases at low velocities, unless pressure is getting too high. Because fluids in ferroalloys processing (slags, metals) pass through zones with large temperature gradients, this causes significant convection forces because of buoyancy. Physically, fluids density changes with temperature and it formally contradicts with incompressible assumption. To provide a solution, the Boussinesq approximation was developed to treat such cases of buoyant flows without having to use a compressible formulation of the Navier-Stokes equations (Hauke and Hughes, 1994). It assumes that variations in density have no effect on the flow field except that they give rise to buoyant forces. The density in equation (41) is taken to be a reference value (ρ_0), except in the body force term, which is set to $\mathbf{F} = \mathbf{g}(\rho_0 + \Delta\rho(T))$. The extra density changing term here is the density difference due to its volumetric thermal expansion. This allows solution of differential equation (41) and determination of fluid velocities. The same formulation can be used for turbulent flow simulations, although in that case it requires the use of the averaged equations, resulting in a hierarchy of equations and statistical unknowns. To solve these equations for turbulent flow (high Reynolds number values), different models have been developed, such as the $k-\epsilon$ turbulence model (Hauke and Hughes, 1994). Solutions that involve Reynolds-averaged equations require dedicated computational fluid dynamics (CFD) algorithms.

3.2 FERROALLOYS COMPONENTS AND THEIR PROPERTIES

3.2.1 Metallic Melts

Metallic melts form in every ferroalloy process and they are the main product with targeted composition upon solidification. The structure of the metallic melt is a subject of intensive studies. According to common knowledge, the

structure of liquid metals and alloys consists of a short-range ordered packing of atoms, which is close to the same coordination structure as the same alloy in the solid nearly its melting temperature. This is usually analyzed by measuring the radial distribution function with various diffraction methods.

As many ferroalloy systems have several metallic elements in the solution, there is no simple or straightforward model that allows description of the atoms' location and their interaction with temperature and composition. A comprehensive review of the thermodynamic, quasi-chemical, and statistical models of metal melts is given, for instance, by Lupis (1983), Hillert (1998), Kubaschewski and Alcock (1979), and other publications. Experimental data clearly show that liquid alloys do have complex structures, which change with temperature and composition (Seetharaman and Sichen, 1994). This is reflected in the variation of all properties (viscosity, surface tension, electric conductivity, density, etc.). For example, the data for the liquid Fe-Si alloys show that for Fe-25% at. Si, the primary solid phase is α' -Fe₃Si but the liquid phase has a "mixture" of subsystems based on Fe and FeSi associates (Zubov and Gasik, 2002). For the melt of ϵ -FeSi phase, the liquid has ~90% of ϵ -FeSi associates and ~10% of chaotic (Fe,Si) liquid, whereas FeSi_{2.3} phase has, in the liquid state, chaotic (disordered) liquid (Fe,Si), quasi-eutectic FeSi-Si, and "extra" silicon atoms. Knowledge of the liquid melts' structure and composition is very important for selecting the proper ferroalloy composition, not only from the view of processing (lower metal activity) but in terms of the stability of the alloy as well (it should not disintegrate or undergo oxidation after tapping and storage).

In some cases, minor impurities are also important to control from the point of view of safety of ferroalloys handling. One of the well-known cases is phosphorus and arsenic impurities in high-silicon FeSi, forming phosphides and arsenides, which react with moisture releasing highly toxic PH₃ and AsH₃. Therefore, special norms were elaborated regulating marine transportation of FeSi alloys in closed compartments (Zubov and Gasik, 2002) to avoid personnel poisoning.

Thus, the role of metal solutions formation during ferroalloys smelting is essential and might be summarized as follows:

- When the metal is dissolved into another melt (its activity decreases), the Gibbs energy change of the reduction and dissolution reaction is more favorable for recovery of the metal from its oxide. The maximal benefit is achieved when the melt composition approaches the similar one as for the most stable compound in the system.
- The total free energy decrease leads to lowering of the reduction temperature, which requires less energy input.
- Decrease of metal activity means its lower partial pressure, which decreases metal loss with gas phase and vapors.
- Melt with lower activity does not react with CO gas to the same extent as pure metal, which in many cases might lead to undesired secondary carbides formation (e.g., 2Al + CO → Al₂OC or 7Cr + 6CO → Cr₇C₃ + 3CO₂).

- Introduction of dissolving metals allows formation of a ferroalloy of correct composition and properties, ensuring an optimal smelting process.
- Formation of the complex melt allows co-reduction of several elements and makes it possible to receive ferroalloys with several elements (FeSiCr, FeS-iMn, FeSiAl, etc.), which are otherwise difficult or not economic to produce separately (for example, there has been a proposal to receive pure manganese and silicon separately and then mix them together to alloy or deoxidize steel).

3.2.2 Oxide Melts (Slags and Fluxes)

Ferroalloy slags usually contain SiO_2 , ferroalloy metal oxides (MeO_x —process dependent, i.e., Mn, Cr, etc.), basic oxides (CaO , MgO , FeO , alkalis), and additional compounds (Al_2O_3 , P_2O_5 , S). Silica in slag melts is presented in tetrahedral units based on the $[\text{SiO}_4]^{4-}$ anion. There are five possible forms of silica tetrahedrons, the base tetrahedron $[\text{SiO}_4]^{4-}$ and four other types $[\text{SiO}_4]_n^{m-}$, where the number of joint apexes $n = 1 \dots 4$ and charges $m = 4-n$ (Gasik et al., 2009). The molar ratio of SiO_2 to the sum of metal oxides indicates the degree of polymerization (oligomerization, or short chain formation). It might be expressed by the reaction $n\text{SiO}_4^{4-} \rightarrow \text{Si}_n\text{O}_{3n+1-c}^{2(n+1-c)} + (n-1+c)\text{O}^{2-}$, taking into account the isomerization of silicate structures and formation of the complex tetrahedron networks.

Each metal oxide is considered to break a bond of the network of tetrahedral units by supplying an additional oxygen and charge, compensating the electron at the broken bond with the cation (Sridhar, 2002). When the ratio is equal to two, each tetrahedral unit has one unshared corner, leading to the network structure resembling an endless sheet. When the ratio decreases toward unity, the structure turns into endless chains (Sridhar, 2002). At lower ratios, the network breaks down further to form rings and ring groups and finally discrete units of silica compounds (Gasik et al., 2009), as shown in Table 3.9.

In complex silicates, alumina as amphoteric oxide accommodates itself in the silica network in silica-rich melts as AlO_4^{5-} , but it changes its role as network breaker in low-silica melts. Phosphorus oxide substitutes alkalis and integrates in the silica network as PO_4^{4-} (Sridhar, 2002). Besides the ratio of silica to metal oxides, metal cation charge and size also play a role: smaller size (Fe^{2+} , Mg^{2+}) and higher charge (Fe^{3+} , Al^{3+}) promote formation of (di)orthosilicates.

During ferroalloy smelting, the charge heats up and minerals start to react with each other. The lowest melting temperature compounds that are present or form in the charge establish the liquid phase, whereas other charge components remain solid. If the composition has many low-melting temperature phases (e.g., manganese ferroalloys with MnO-SiO_2 system), the first liquid slag phase forms in the top part of the charge in the furnace (for high carbon ferromanganese about 150 to 250 mm below the charge level). There, carbon starts to reduce oxides from the liquid slag. When the charge consists of components with high melting temperatures (in production of FeSi , SiCa , FeSiAl , or high

TABLE 3.9 Types of Silicate Network Structures Formed in the Slags (see Gasik et al., 2009)

Silicate	Example	Tetrahedron Type
Ortho	Olivine $(\text{Fe}, \text{Mg})_2[\text{SiO}_4]$	Isolated
Di-ortho	Aksinite $\text{Ca}_2(\text{Mg}, \text{Fe})\text{Al}_2[\text{Si}_2\text{O}_6]_2\text{BO}_3$	Twinned
Ring	$[\text{Si}_3\text{O}_9]^{6-}$, $[\text{Si}_4\text{O}_{12}]^{8-}$, $[\text{Si}_6\text{O}_{18}]^{12-}$, $[\text{Si}_{12}\text{O}_{20}]^{12-}$	Ring groups of 3, 4, 6, and 12 (6 + 6)
Chain	Wollastonite CaSiO_3 , rhodonite MnSiO_3	Finite single-phase 1D chains
Ribbon I	Tremolite $\text{Ca}_2\text{Mg}_5[\text{Si}_4\text{O}_{11}]_3(\text{OH})_2$	Ribbon formed by 1D chains
Ribbon II	Talc $\text{Mg}_3[\text{Si}_4\text{O}_{10}](\text{OH})_2$	Ribbons formed by 1D layers
Skeleton	Nepheline $\text{KNa}_3\text{Al}_4\text{Si}_4\text{O}_{16}$	Bonds formed by oxygen atoms

carbon FeCr), the liquid slag phase forms well below the charge level. There, substantial gas cavities form under electrodes where electric arcs are operating. In some cases (smelting of high carbon FeMn and FeSiMn), the furnace operates in the arc-less mode when electrodes are immersed in the slag and the heating proceeds in the resistance mode (joule heating), although some micro-arcs appear there locally because of variations in temperature (Gasik et al., 2009). Among the set of properties of ferroalloy slags, two parameters are the most critical for the smelting process: slag viscosity and electric conductivity.

3.2.2.2 Viscous Properties of Slags

The flow behavior of slags is an important factor in many metallurgical systems, influencing the efficiency of separation of slag from metal and matte phases, the extent of slag foaming, and the kinetics of metal smelting and refining reactions (Kondratiev et al., 2002). Viscosity (η , Pa·s) is a measure of the ability of a fluid to sustain shear stresses, and in most cases viscosities are independent of the shear rate (Newtonian fluids, described by the incompressible Navier-Stokes equation (38)). The viscosity links the shear stress and the fluid velocity gradient normal to the shear stress vector (Shridhar, 2002). Shearing of layers of a fluid involves bonds breaking, and thus viscosity is a thermally activated process, often expressed as an Arrhenius-type relationship characterized by a preexponential factor A and an activation energy E :

$$\ln \eta = \ln A + \frac{E}{RT} \quad (42)$$

The ranges of viscosities that are typically encountered in metallurgical systems include 10^{-3} – 10^{-2} Pa·s for liquid metals and 10^{-2} to 10^{10} Pa·s for slags. If the slag needs to be tapped from the furnace, its viscosity should be lower than 15 to 25 Pa·s for the free flow. Experimental methods of viscosity and other determinations of the thermophysical properties of slags have been reviewed by Aune et al. (2002) and for metallic melts by Seetharaman and Sichen (1994). A summary covering most of the published viscosity models suitable for use in metallurgical applications is given by Kondratiev et al. (2002) and Sridhar (2002).

Many models have been developed for predicting viscosity from chemical compositions and temperature; however, the performance of the various models varies depending on the range of viscosity covered. The current understanding of the structure of slags is insufficient to construct a reliable model, one capable of encompassing a wider range in viscosity (Sridhar, 2002). For engineering purposes, a correlation was suggested by Gasik and Gasik (2010)—first for electrical conductivity and later also for viscosity; it was recognized that the preexponential factor A in Arrhenius equation (39) is not constant but that it follows the Meyer-Neldel rule (Meyer and Neldel, 1937). This rule posits a linear dependence of the logarithm of A versus activation energy, so equation (42) might be rewritten as

$$\ln \eta = a_0 - \frac{E}{RT_0} + \frac{E}{RT}, \quad (43)$$

where a_0 is the true constant and T_0 is the characteristic Meyer-Neldel temperature (isokinetic temperature), when the parameter (viscosity in this case) is not dependent on the activation energy. The physics behind this rule is not clear, although different explanations have been suggested (Dyre, 1986). This dependence is known to be very fundamental and has been observed in different materials and conditions, including the diffusion process (Swalin, 1956). Gasik and Gasik (2010) analyzed data for different slags (Fig. 3.20) and found that almost all ferroalloy slag viscosities might be approximated using the equation

$$\eta = 0.1771 \exp\left(\frac{E}{R} \left(\frac{1}{T} - \frac{1}{2008}\right)\right), \quad (44)$$

where activation energy is composition-dependent. It was thought that this behavior might be due to formation of the silicate networks in slags, but it also holds in fluxes, which have no silica.

Using advanced statistical methods, it is possible to arrive at a prediction of the activation energy versus slag composition (Fig. 3.21), although more experimental data are needed to improve the reliability of this analysis (Gasik and Gasik, 2010).

3.2.2.3 Electrical Conductivity of Slags

Electrical conductivity of molten slags is critical for the correct selection of ferroalloys for the operation of furnaces. There are different theoretical models of

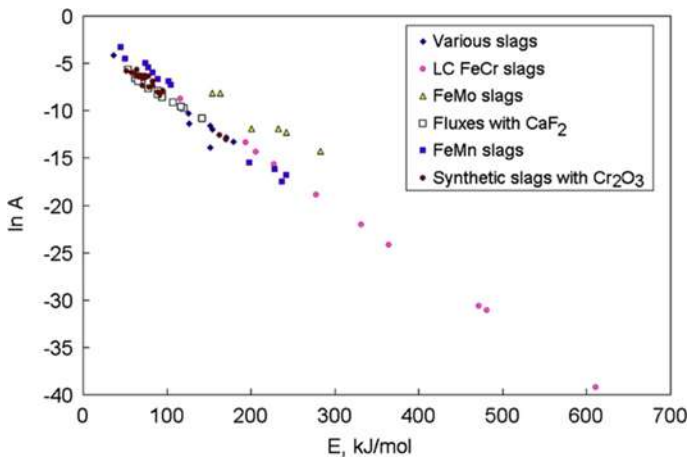


FIGURE 3.20 Dependence of the preexponential factor ($\ln A$) on activation energy E for the viscous flow of different ferroalloy slags. (Data collected by M. Gasik.)

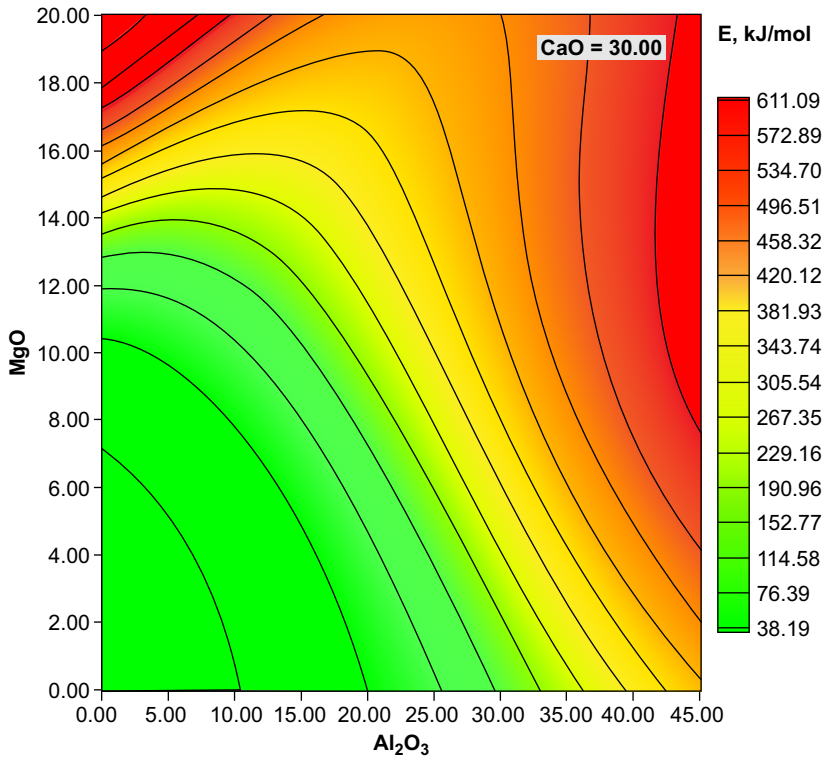


FIGURE 3.21 Predicted activation energy for the viscous flow of the $\text{MgO}-\text{Al}_2\text{O}_3-30\%\text{CaO}$ slags. Note this is just an illustrative example and should not be used in calculations. (Data provided by M. Gasik.)

the electrical conductivity of slags, based either on their treatments as ionic liquids (electrolytes) or on more simplified phenomenological correlations such as approximation using Stokes-Einstein-Nernst equations. However, in complex ionic melts it is difficult to assign specific values to parameters such as “particle radius” or “number of particles per unit volume with specific charge.” Many silicate slags exhibit complicated oligomerization of silicate networks where the “particle” definition makes little sense. The concept of optical basicity was intensively applied earlier, but as stated, it is not scientifically justified for slags with transition metals, which are essentially the basis of ferroalloys production.

For example, Segers et al. (1978) have experimentally measured electrical conductivities of the liquid slags in the CaO-MnO-SiO₂ system and represented specific electrical conductivity χ recalculated into equivalent conductivity Λ :

$$\Lambda = \frac{\chi V_m}{2(1 - N_{SiO_2})}, \ln \chi = \ln \Lambda + \frac{E}{RT}, \quad (45)$$

where V_m is the liquid slag molar volume, m³/mol, and N_{SiO_2} is the molar fraction of SiO₂. Equation (45) assumes that the electrical conductivity of slags using this system is ruled mostly by Ca²⁺ and Mn²⁺ (hence, in equation (45) the divider is 2 because of valence number 2+). Silica was assumed to exist in more complex tetrahedron forms like SiO₄⁴⁻ or Si₂O₇⁶⁻, and its effect on electrical transport was neglected. The data obtained by Segers et al. (1978) exhibited significant nonlinearity versus SiO₂ concentration or versus the “manganese module” $t = N_{MnO}/(N_{MnO} + N_{CaO}) = N_{MnO}/(1 - N_{SiO_2})$. Later analysis of these data (Gasik and Gavrilov, 2001) did not reveal such correlations of these plots with thermodynamic properties of these slags; neither did it show a clear dependence of the composition. Also questioned was the extent to which the assumption of basic +2 charge carriers is valid only within the whole composition range and the temperatures studied. The charge transfer in electrolytes must obey electroneutrality, even if partial charge transfer numbers might be different for different cations and anions.

By using an approach similar to the treatment of viscosity described earlier, Gasik and Gasik (2010) have shown that the electric conductivity of liquid slags also follows the Meyer-Neldel rule (Dyre, 1986; Meyer and Neldel, 1937). Figure 3.22 shows the dependence of the preexponential factor on the activation energy of electrical conductivity.

For the system CaO-MnO-SiO₂, electrical conductivity (Sm/cm) might be expressed as

$$\chi \approx 23.6 \exp\left(-\frac{E}{R} \left(\frac{1}{T} - \frac{1}{3550}\right)\right), \quad (46)$$

where activation energy depends on slag composition and might be predicted using advanced statistical analysis, for which rather good correlations have been obtained (Gasik and Gasik, 2010).

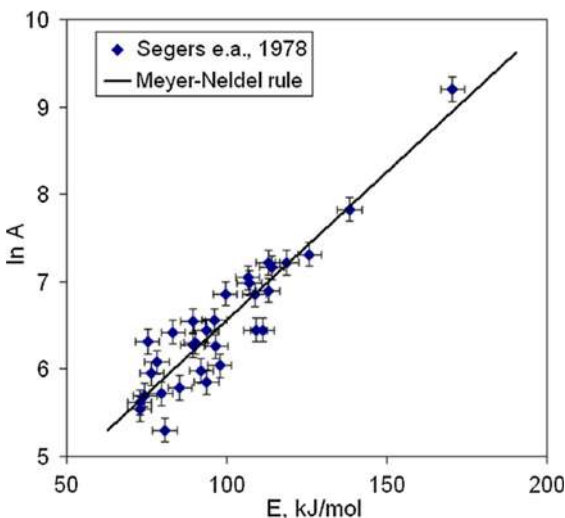


FIGURE 3.22 Dependence of the preexponential factor ($\ln A$) on activation energy E for the electric conductivity of slags of form $\text{CaO}-\text{MnO}-\text{SiO}_2$. (Based on the work of Gasik and Gasik, 2010.)

3.2.3 Carbon Reductants for Ferroalloys Processing

Carbon reductants play a critical role in ferroalloys processing. The basic requirements for the quality of carbon reductants are different for various ferroalloy groups and include the following indicators: (1) composition (solid [nonvolatile] carbon, volatile matter, moisture, and sulfur), (2) the amount and chemical composition of the ash (nonreducible oxides), (3) electrical resistance, (4) porosity, (5) physical and mechanical properties (size distribution, strength characteristics), and (6) reduction ability in respect to the oxides of the element in question.

According to the modern classification of raw carbons, there are several phases, which have different microstructure, properties, and possibly different geneses. Table 3.10 presents one of the known classifications based on different carbon mineral constituents, which are commonly found in coals (Zubov et al., 2001). Vitrinite components are usually the most important for determining the quality of produced metallurgical coke.

In Table 3.11 are listed some commonly used carbon reductant properties. However, these properties might vary for different producers depending on the carbon source, so this table gives a rather general idea about the differences in the reductant properties.

The reducing ability of carbon reductant is one of the most critical parameters, in addition to its electric resistance. The feasibility of a particular reducing agent to produce a specific type of ferroalloy is determined during industrial tests. Carbon reductant should have less potential for graphitization, because it causes a decrease in the reactivity of carbon, electrical resistance, and surface area, all of which affect the ability of the carbonaceous material to recover metals from oxides.

TABLE 3.10 Classification of Different Coal Components

Group	Characteristics
Vitrinite (V), semi-vitrinite (SV)	Glossy, colloidal structure; glassy fracture surface
Fusain or fusinite (F)	Tissue-like fiber and sooty structures
Liptinite (L)	Matt structures where soluble components were eluted
Alginite (ALG)	Products from organic-walled marine microfossils
Mineral impurities	Clay minerals, iron sulfides, carbonates, and the like

TABLE 3.11 Comparison of Properties of Different Carbon Reductants

Parameter	Coke	Nut-Coke	Half-Coke	Petrocoke	Charcoal
Ash A ^d (% wt.)	8–11	8–11	22–27	<1	<2
Volatiles VOC (% wt.)	<2	<1.5	4–6	7–9	10–15
Moisture W ^b (% wt.)	<0.5	<1.5	<2	<1	1.5–2.5
Total sulfur S, (% wt.)	<1	<1.5	<1	1–5	<0.05
Solid carbon C _t	>85	>85	>70	>85	>80
Reactivity at 1323 K, ml/(g·s)	>0.5	>0.9	>8	>0.3	>10
Resistivity, Ohm·m, for 3–6 mm	1–2	1–2	7500	3·10 ⁶	2·10 ⁶
Structural strength, %	>80	>85	>62	>62	>35
Density, g/cm ³ , real/apparent	1.82/0.91	1.95/0.93	1.58/0.93	1.41/1.12	1.4/0.40
Porosity, %/cm ³ /g	53.1/0.49	49.7/0.51	55.0/0.67	20.1/0.18	63.8/1.1
Ash composition, % wt.:					
SiO ₂	33–37	35–37	75–78	45–48	<2
Al ₂ O ₃	20–25	21–23	10–12	23–26	<4
CaO + MgO	3–5	3–5	3–5	9–11	40–45
Fe ₂ O ₃	30–35	30–35	7–9	13–15	<1
P ₂ O ₅	0.1–0.3	0.1–0.3	<0.05	0.5–1.0	5–6
K ₂ O + Na ₂ O	2–2.5	2–2.5	1–2	0.1–0.2	<0.5

Electrical resistivity of a reductant also impacts the resistivity of the whole charge in the furnace. It depends on the number and size distribution of cokes (or other reductants), ores, concentrates, fluxes, additives, and other components of the charge. Reducing the size of pieces of coke and ore components

increases the resistivity. Excessive shrinkage reduces the permeability of the pieces of the charge, resulting in a drop in performance and the economic indicators of the ferroalloy smelting. In practice, optimal particle size distribution of the charge is determined as a result of testing in batch furnaces at different particle distributions. Technologically, the electrical resistance of the charge has to be kept high enough to reduce the amount of electric current passing through the charge in favor of the current passing through the electric arcs, as they are the main heat source in the furnace.

Contrary to requirements for low electrical conductivity of carbon materials as reductants, for manufacturing carbon-based electrodes (self-baked, graphitized, composite), specific electric resistance must be as low as possible (Brandtzæg, 1985). This is usually achieved by performing calcination (high-temperature treatment over 2000°C) of carbon raw materials such as anthracite. The transformation of amorphous structures of anthracite into crystalline (graphite-like) material at high temperatures reduces the electric resistance, density, specific heat, degree of graphitization (crystal size), ash, and the contents of volatile organic compounds (VOC) (Celzard et al., 2000).

REFERENCES

- Aune, R.E., Hayashi, M., Nakajima, K., Seetharaman, S., 2002. Thermophysical properties of silicate slags. *Journal of Metals (JOM)* 11, 62–69.
- Bird, R.B., Stewart, W.E., Lightfoot, E.N., 2005. *Transport Phenomena*, second edition. John Wiley & Sons, 898 pp.
- Brandtzæg, S.R., 1985. Structural changes during calcinations of coke and anthracite. Doctoral Thesis. University of Trondheim, Norway, No. 45, 200 pp.
- Brown, M.E., Dollimore, D., Galway, A.K., 1980. Reactions in solid state. In: Bamford, C.H., Tipper, C.F. (Editors), *Comprehensive Chemical Kinetics*, volume 22. Amsterdam, pp. 340.
- Brown, M.E., 1989. *Introduction to Thermal Analysis. Techniques and Applications*. Chapman & Hall, London, 266 pp.
- Celzard, A., Mareche, J.F., Payot, F., Begin, D., Furdin, G., 2000. Electrical conductivity of anthracites as a function of heat treatment temperature. *Carbon* 38, 1207–1215.
- Dinsdale, A., 1991. SGTE data for pure elements. *CALPHAD* 15, 317–425.
- Dyre, J.C., 1986. A phenomenological model for the Meyer-Neldel rule. *Journal of Physics C: Solid State Physics* 19, 5655–5664.
- Flammersheim, H.J., Opfermann, J., 1999. Formal kinetic evaluation of reactions with partial diffusion control. *Thermochemical Acta* 337, 141–148.
- Gasik, M.I., Gavrilov, V.A., 2001. Silicothermy of manganese. *System Technologies*, Dniproprosvk, 512 pp.
- Gasik, M.I., Lyakishev, N.P., Gasik, M.M., 2009. Physical chemistry and technology of ferroalloys [in Ukrainian]. *Sistemnye Tehnologii*, Dnipropetrovsk, 494 pp.
- Gasik, M.M., 2001. Reduction processes kinetics and experimental methods. In: *Proceedings Seminaron Solid State Red-ox Reactions*. POHTO, Finland, Oulu, 40 pp.
- Gasik, M.M., Gasik, M.I., 2010. Multi-variation analysis and optimisation of electrical conductivity of MnO-CaO-SiO₂ slags. *Proceedings of the 12th International Ferroalloys Congress*. Editor: A. Vartiainen. Helsinki, Finland, 537–545.

- Gasik, M.M., Gasik, M.I., Urazlina Yu, O., Kutuzov, S.V., 2010. Modelling and optimisation of anthracite treatment in an electrocalcinator. Proceedings of the 12th International Ferroalloys Congress., Editor: A. Vartiainen. Helsinki, Finland, 339–347.
- Hauke, G., Hughes, T.J.R., 1994. A unified approach to compressible and incompressible flows. Computer Methods in Applied Mechanics and Engineering 113, 389–395.
- Hillert, M., 1998. Phase Equilibria, Phase Diagrams and Phase Transformations: Their Thermo-dynamic Basis. Cambridge University Press, Cambridge, UK, 540 pp.
- Incropera, F., DeWitt, D.P., 1996. Fundamentals of Heat and Mass Transfer, fourth edition. John Wiley & Sons, NY, 834 pp.
- Kondratiev, A., Jak, E., Hayes, P.C., 2002. Predicting slag viscosities in metallurgical systems. Journal of Metals (JOM) 11, 41–45.
- Kubaschewski, O., Alcock, C.B., 1979. Metallurgical Thermochemistry, fifth edition. Pergamon Press, Oxford, UK, 462 pp.
- Lupis, C.H.P., 1983. Chemical Thermodynamics of Materials. North-Holland, New York, 602 pp.
- McCabe, W.L., Smith, J.C., 1976. Unit Operations of Chemical Engineering, third edition. McGraw-Hill, NY, 1028 pp.
- Meyer, W., Neldel, H., 1937. Über die Beziehungen zwischen der Energiekonstanten ϵ und der Mengenkonstanten α in der Leitwerts-Temperaturformel bei oxydischen Halbleitern. [Upon dependence of the energy constant or quantity constant in temperature-dependent conductivity of oxide semiconductors] Zeitschrift für Technische Physik [J Techn. Physics] 18, 588–593.
- Ostrik, P.N., Gasik, M.M., 1993. Hydrogen reduction of $\text{MoO}_3\text{-Fe}$ mixes studied by stepwise differential isothermal analysis. Journal of Thermal Analysis 40, 313–319.
- Pelton, A.D., 2001. Thermodynamics and phase diagrams of materials. In: Kostorz (Ed.), Phase Transformations in Metals. G. Wiley-VCH, Weinheim, 724 pp.
- Pelton, A.D., 1988. A database and sublattice model for molten salt solutions. CALPHAD 12, 127–142.
- Saunders, N., Miodownik, A.P., 1998. CALPHAD, Calculation of Phase Diagrams, A Comprehensive Guide. Pergamon Materials Series, Oxford, 465 pp.
- Seetharaman, S., Sichen, D., 1994. Estimation of the viscosities of binary metallic melts using Gibbs energies of mixing. Metallurgical and Materials Transactions 25B, 589–595.
- Segers, L., Fontana, A., Winand, R., 1978. Conductivités électriques de mélanges de silicates fondus du système $\text{CaO-SiO}_2\text{-MnO}$. Electrochimica Acta 23, 1281–1286.
- Sridhar, S., 2002. Estimation models for molten slag and alloy viscosities. Journal of Metals 11, 46–50.
- Swalin, R.A., 1956. Correlation between frequency factor and activation energy for solute diffusion. Journal of Applied Physics 27, 554–555.
- Themelis, N.J., 1995. Transport and Chemical Rate Phenomena. Gordon & Breach Publishers, Basel, 370 pp.
- VDI - Verein Deutscher Ingenieure, 1993. Heat Atlas. VDI-Verlag GmbH, Düsseldorf.
- Wesselingh, J.A., Krishna, R., 2000. Mass Transfer in Multicomponent Mixtures. Delft University Press, Delft, 332 pp.
- Zubov, V.L., Gasik, M.I., 2002. Electrometallurgy of ferrosilicon. System Technologies, Dnipropteroovsk, 704 pp.
- Zubov, V.L., Ovcharuk, A.N., Gasik, M.I., 2001. Physico-chemical properties, structural characteristics of carbon reductants and their use in smelting ferrosilicon. System Technologies, Dnipropetrovsk, 144 pp.

Ferroalloys Processing Equipment

Isobel Mc Dougall

Tenova Pyromet, a Division of Tenova Minerals (Proprietary) Ltd. Johannesburg, South Africa

Chapter Outline

4.1 Introduction to Ferroalloys Processing Technology	83	4.1.9 Furnace Control	121
4.1.1 Ferroalloys Basic Furnace Design and Operation	85	4.1.10 Processing Hazards and Risk Management	122
4.1.2 Ferrochrome, Ferrosilicon, Ferromanganese, and Silicomanganese Furnaces	92	4.2 Equipment for Furnace Feed Processing	127
4.2.1 Agglomeration		4.2.2 Sintering of Manganese Ore	129
4.2.3 Preheating		4.2.4 Prereduction	131
4.1.3 Silicon Metal Furnaces	98	4.3 Downstream Processing	133
4.1.4 Ferronickel Furnaces	101	4.3.1 Refining	133
4.1.5 DC Furnaces	104	4.3.2 Casting	133
4.1.6 Electrical Supply and Operation	107	4.4 Other Furnaces for Ferroalloys Processing	136
4.1.7 Furnace Linings	119	Acknowledgments	138
4.1.8 Furnace Principal Operating Stages	120	References	138

4.1 INTRODUCTION TO FERROALLOYS PROCESSING TECHNOLOGY

The process by which ore is converted to a ferroalloy contains a number of steps. These include mining the ore, preparing the ore by processes such as crushing, screening, washing, grinding, or milling, and sometimes applying



FIGURE 4.1 General view of a ferroalloys smelter. (By permission of Tenova Pyromet, a division of Tenova Minerals [Pty] Ltd.)

beneficiation processes such as flotation, followed by smelting and refining. A general view of a ferroalloys smelter is shown in Figure 4.1.

Raw material is delivered to the smelter from the mine in bulk by rail, road, or sea. The raw materials required for ferroalloy smelting include the ore, reductants, and fluxing materials. These materials are delivered to a raw materials storage facility. Granular materials may be stored in an open stockpile or a bunker, from where they are retrieved and transferred by means of belt conveyors. Fine powdered materials are conveyed in pneumatic conveying systems. In a plant with multiple furnaces, there is generally a common bulk storage facility, with an arrangement of incline conveyors, shuttle conveyors, transfer conveyors, or skip hoists and intermediate bins to deliver material to the furnaces in the correct proportions at appropriate times. Feed bins containing the correct feed recipe are situated above the furnace roof. Where charging cars are used, the bins may be further from the furnace.

The smelting process may include preheating, prereduction, sintering, and pelletizing of the material prior to its introduction into the furnace. These processes receive feed material from the raw material handling facility and deliver processed material into the furnace. In larger furnaces, the raw material is fed into the furnace through feed chutes set into the roof, which facilitate the delivery of the material to a specific region of the furnace. In smaller furnaces, charging cars are often used for this purpose.

Irrespective of whether the furnace is circular or rectangular, AC or DC, the furnace shell is composed of a steel structure consisting of a base, sidewall, and roof. The base and shell are lined with refractory material to form a crucible, whereas the roof may be constructed of refractory material or may be of water-cooled steel or copper construction. The hearth is commonly cooled by forcing air across it by means of a dedicated fan. The sidewalls may rely on natural convection for cooling, or they may be cooled by forced air convection or by one of several different water-cooling methods, depending on the required intensity of heat removal. The simplest of these is film cooling, where a water

film runs down the outside of the steel shell. Spray cooling systems provide additional cooling by spraying jets of water onto the shell. Copper cooling elements with integral water passages provide the greatest intensity of water cooling. The copper cooling elements are set into the refractory lining. In these closed water circulation systems, the returning hot water is cooled in an indirect heat exchanger to avoid contamination of the cooling water. The cooling water system has its own pumps and ancillary equipment, and it may be fitted with an emergency water supply system, as a loss of cooling water to a furnace has potentially catastrophic consequences.

Electric current is introduced into the furnace by means of carbon electrodes, which receive power at relatively low voltage and high current from a voltage step-down arrangement connected to a high voltage (HV) supply. The electrodes are individually supported on a clamping mechanism, which allows the electrodes to be lowered into the furnace and additional sections added as they are consumed by the process. The contact shoes and bus bars through which current is supplied to the electrodes may be water cooled and may be connected to the same cooling water system as the furnace sidewalls.

Exhaust gas leaves the furnace through a duct, where it is cooled and the particulate matter removed prior to flaring to atmosphere. Waste heat boilers and other energy recovery systems placed downstream of the furnace are becoming increasingly common components of smelting plants.

Metal and slag may be tapped from a single tap hole, or there may be dedicated slag and metal tap holes opposite each other in the furnace, the slag tap holes usually being at a higher elevation than the metal tap holes. After metal is tapped from the furnace, it may be granulated, cast, or further refined. Slag from ferroalloy processes may be further processed to extract entrained metallic particles prior to being discarded. Some slags are suitable for use as aggregates for concrete.

In the following sections of this chapter, the equipment used for the smelting of ferroalloys will be described. [Section 4.1](#) describes furnace technology and operations, whereas [Section 4.2](#) discusses the more important processing steps, which may be applied to the raw materials at the smelter prior to their smelting in the furnace. Hydrometallurgical processes such as the concentrating of nickel ores are not included. [Section 4.3](#) describes the treatment of the product and slag after it leaves the furnace, and [Section 4.4](#) deals with other furnaces for ferroalloys production.

4.1.1 Ferroalloys Basic Furnace Design and Operation

The smelting of ferroalloys is commonly performed in electric arc furnaces. Although ferromanganese can be produced in a blast furnace in a manner similar to iron, the reduction of chromium and silicon from their oxides requires higher process temperatures and lower oxygen potentials than can be achieved in a blast furnace. To create the required high temperature and low oxygen environment, carbon electrodes are inserted into a mixture of ore, flux, and carbon

reductant in an electric arc furnace. The low-voltage, high-current arcs at the electrode tips create a zone of high temperature and low oxygen potential. No oxygen is blown into the furnace for the purpose of raising the temperature. Radiation from the arc zone impinges directly on the feed material, allowing the efficient transfer of energy from the arc to the feed material. As the arc is considerably shorter than that of an open-arc furnace, the bulk of the energy is transferred to the feed material by resistance (Joule) heating due to the flow of electric current through the furnace contents. Oxygen from the metal oxide combines with the carbon in the feed material to form carbon monoxide, liquid metal, and slag. An electric furnace operating in this manner is called a submerged arc furnace. A photograph of a furnace in operation showing the electrodes passing into the furnace charge is shown in [Figure 4.2](#).

In submerged arc processes, there is no visible arc. The electrode is immersed in the solid raw material with its tip immersed in the slag. The coke in the feed mix passes down into the slag, where reduction of oxides occurs as the molten slag mixes with the coke. Heating is predominantly due to the resistance of the slag, although some arcing may occur between the electrodes and the coke bed. In processes where a slag is not formed, such as ferrosilicon smelting, a short visible arc may exist. In a slag resistance furnace, the tip of the electrode protrudes into the slag, there is no arc, and the heat transfer is by joule heating. Raw material melts as heat is transferred from the slag with which it is in contact.

Submerged arc furnaces, although they all operate on the same general principles and use similar equipment, differ in the details of their construction and operation. The possible variations in a number of the important furnace parameters are summarized in [Table 4.1](#). However, the geometrical, electrical, and other parameters for a furnace for a particular application are dictated by the requirements of the process. Consequently, the variation in design between individual ferrochrome furnaces, for example, is relatively small, but silicon metal furnaces, for example, may differ substantially from ferrochrome furnaces in the details of their construction and operation. This also holds for small furnaces usually operating in resistance heating mode (arc-less) and used for refining operations.



FIGURE 4.2 The furnace in operation showing the electrodes passing into the furnace charge.
(By permission of Tenova Pyromet, a division of Tenova Minerals [Pty] Ltd.)

TABLE 4.1 Furnace Parameters

Parameter	Options
Overall shape	Circular or rectangular
Power supply	AC or DC
Arc type	Open, submerged, shielded, brush, resistance (no arc)
Number of electrodes (AC furnaces)	Single phase: 2 Three phase: 3, 6 (three pairs), 6 (2 × 3)
Number of cathodes (in DC furnaces)	1, 2
Roof	Gas-tight (hermetic), semiclosed, open
Sidewall cooling	Natural convection, forced air convection, water film cooling, water spray cooling, water-cooled copper elements

The design of an AC submerged arc furnace is based on the electrical power required to produce the required tonnage of ferroalloy. The required tonnage of alloy per year is decided based on the available ore and other economic factors. The specific energy requirement (SER) of the process (in kWh/ton) is determined by the process and the ore characteristics and is usually obtained by calculating a mass and energy balance. Representative figures for various processes are provided in **Table 4.3** (presented later). When the SER is known, and the required annual alloy production is known, the power (MW) rating of the furnace is determined by multiplying the kWh per ton by the number of tons per hour. Once the power (MW) rating of the furnace is known, the other parameters may be determined. Important considerations in the sizing of the furnace are the required electrode resistance and current. A number of empirical methods have been developed to describe the relationship between the various parameters such as electrode diameter and furnace resistance.

4.1.1.1 Kelly's Method

The relationship between the electrode diameter and the furnace resistance is characterized by empirical formulas ([Andreae, 1935](#) and [1950](#)) and refined by [Kelly \(1958\)](#). These researchers found that the furnace resistance is inversely proportional to the electrode diameter:

$$k = \frac{E\pi D}{I} \quad (1)$$

where k = electrode periphery resistance, E = electrode-to-ground voltage, I = current per electrode, and D = electrode diameter in inches.

TABLE 4.2 Typical “*k*” Factors for Submerged Arc Operations (Kelly, 1958)

Product	Typical <i>k</i> Factor
Phosphorus	0.75–1.0
HC FeCr (Low Si)	0.35–0.65
HC FeCr (High Si)	0.2–0.3
50% FeSi	0.24–0.34
CaC ₂	0.19–0.22
75% FeSi	0.16–0.2
FeCrSi	0.12–0.17
SiMn	0.1–0.15
FeMn	0.08–0.13

The proportionality constant *k* became known as the Kelly factor (Kelly, 1958). This factor is dependent on the process and the size of the furnace. Kelly factors have been published for a variety of furnace configurations. The values published by Kelly are included in Table 4.2. Due to the many economic changes that have taken place since the publication of Kelly’s paper, the actual values of the Kelly factor have been adjusted somewhat from those originally calculated in order to match the performance of much larger furnaces and new feedstocks (Barker, 2011). The Kelly factor is most often used when scaling up or down from a known operation.

Using equation (1), an initial estimate is made of the electrode diameter, electrode current and electrode voltage. The electrode size is also dependent on the anticipated current density that can be carried by the electrode. This is determined by experience based on the electrode type and the process. The choice of an appropriate value of the electrode-to-ground voltage is informed by the performance curve of the transformer.

The expected power factor $\cos(\phi)$ of the furnace is estimated, based on operating knowledge of other furnaces for this process. The power factor is largely determined by the process and the details of the placement of the major current-carrying components such as the electrodes and bus bar bundles. The furnace MVA rating may then be determined.

4.1.1.2 Westly’s Method

Westly (1974) developed a different approach to sizing furnaces and determining favorable electrical operating conditions. This method finds greatest

acceptance in slagless (flux-less) processes such as silicon metal and FeSi production. Based on the performance of operating furnaces, he showed that

$$I_{el} = C_3 P^{2/3} \quad (2)$$

where I_{el} is the electrode current in kA, C_3 is the factor appropriate to the particular smelting process, and P is the total power (VA) rating of the three-phase furnace in MVA. For example, for a ferroalloy process with 75% Si, a typical value of C_3 is approximately 10.5. The optimum electrode current for a 30 MVA furnace producing a 75% Si product would be thus $I_{el} = 10.5 \cdot 30^{2/3} = 101.4$ kA. From equation (2), the electrode-to-bath (phase) voltage in kV can be derived as

$$V_{ph} = \frac{\sqrt[3]{P}}{3 C_3} \quad (3)$$

Thus, for the same case phase voltage would be $V_{ph} = 30^{1/3}/(3 \cdot 10.5) = 0.0986$ kV = 98.6V. Westly's method has similarities to the method described in detail next.

4.1.1.3 Method by Gladkikh et al.

An example of parameters used for selection at some European (Russia, Ukraine) and Asian (Kazakhstan, China) ferroalloys plants is shown in Table 4.3 (Gladkikh et al., 2007). Note that other values might be reported (for example, specific energy demand might be lower if charge preheating or prerduction is used), but the procedure of furnace system design remains similar.

First, the required transformer power (in kVA) is calculated:

$$P = \frac{G \cdot A}{24 \cdot K \cdot \cos(\varphi)} \quad (4)$$

where G is the desired furnace productivity for the alloy, t/day, A is the specific energy demand (SER), kWh/t alloy (Table 4.3), and K is the repair time correction factor, accounting for plant availability (usually adopted as $\sim 0.94 \pm 0.01$, meaning $\sim 6\%$ of the year time is allowed for furnace repair and maintenance). The power factor $\cos(\varphi)$ is first adopted as 0.84 ± 0.02 . Then the product $\cos(\varphi) \cdot \eta_{el}$ is selected from the table, taking into account that higher transformer power usually leads to lower $\cos(\varphi) \cdot \eta_{el}$ product values. The electrical efficiency η_{el} is normally in the range 0.84 to 0.90 (again, higher efficiency is selected for lower power systems).

The active furnace power (kW) is then estimated:

$$P_{act} = P \cdot \cos(\varphi) \cdot \eta_{el} \quad (5)$$

and the nominal phase voltage (V) is determined per one electrode:

$$V_{ph} = C \cdot (P_{act}/k_{el})^n, \quad (6)$$

where C is the coefficient in Table 4.3, which depends on the material, process type, and electrical regime of the smelting, and k_{el} is the number of the

TABLE 4.3 Parameters for Ferroalloys Furnace Design*

Ferroalloy Type	Product $\cos(\phi) \cdot \eta_{el}$	SER, A, kWh/t alloy	Process Parameter C			Nominal Current Density j , A/cm ²
			Flux	Flux-less	Electrode Factor EP	
18% Si	0.70–0.68	2000–2200	—	3.0–3.1	1.42–1.99	7.0
25% Si	0.71–0.69	2700–2800	—	3.05–3.15	1.43–1.99	7.0
45% Si	0.72–0.70	4700–4900	—	3.2–3.3	1.50–2.00	7.0
65% Si	0.73–0.71	7400–7700	—	3.35–3.40	1.57–2.02	7.0
75% Si	0.74–0.72	8800–9200	—	3.4–3.5	1.60–2.03	7.0
90% Si	0.76–0.74	12 500–13 500	—	3.5–3.7	1.65–2.04	8.4
CaC ₂	0.72–0.70	2500–3000	—	3.0–3.5	1.44–1.50	6.8
FeSiCa	0.68–0.66	12 000–13 000	6.7–7.7	—	1.34–1.41	12.0
HC FeMn	0.68–0.65	3800–4100	7.3–8.3	—	1.54–1.49	7.6
HC FeCr	0.75–0.73	3450–3600	8.0–8.6	—	1.44–1.50	7.6
FeSiMn	0.69–0.67	4100–4700	5.7–6.7	—	1.34–1.41	7.6
FeSiCr	0.72–0.70	6200–6500	7.2–7.4	—	1.53–1.72	7.6

*When a range is shown, the lower limit is for lower power and the higher limit is for high power furnaces.

electrodes in the furnace (3 or 6). The n value is 0.25 for flux processes (high amount of slag—volumetric power distribution) and 0.33 for flux-less processes (low or no slag—surface power distribution).

Once a calculation like the preceding one has been performed or an appropriate Kelly's factor has been chosen, an initial estimate can be made of the electrode current and consequently the electrode diameter. The relationship between electrode diameter and electrode current is based on the properties of the carbon electrodes to be used. The current in the electrode (kA) is determined as follows:

$$I = \frac{P_{act}}{3 \cdot V_{ph} k_{el}} \quad (7)$$

and the calculated electrode diameter (mm) is determined as follows:

$$d_{calc} = \frac{EP \cdot I}{V_{ph}} \quad (8)$$

where the EP factor is selected from Table 4.3. The calculated diameter is usually rounded up to the nearest number as multiples of 50. The check of the calculation's consistency is made by evaluating the product $\cos(\varphi) \cdot \eta_{el}$ with the formula:

$$\cos(\varphi) \cdot \eta_{el} = \frac{1}{\sqrt{R^2 + X^2}} \cdot \frac{R^2}{R + r} \quad (9)$$

where R (ohm) is the active resistance of the furnace hearth, r (ohm) is the active resistance of the short circuit impedance of the supply network ("short net"), and X (ohm) is the total reactive resistance of the furnace circuit. Values of r commonly vary from 0.2 mOhm for low power transformers (<17 MVA) to 0.14 for higher power (33 to 63 MVA). Values of X , respectively, vary from 1 to 0.8 mOhm (depending on the transformer and the network short circuit fault rating characteristics). The product calculated by equation (8) should not deviate more than $\pm 5\%$ from the value adopted at the beginning of calculations; otherwise the calculation should be iterated once more.

The furnace diameter is determined by the required hearth power density, which is calculated by dividing the MW rating of the furnace by the surface area of the hearth. An appropriate value of this variable for a particular furnace is selected based on experience in other furnaces for this process and the desired sidewall cooling method. The pitch circle diameter of the electrodes and the electrode-to-wall distance are two other important furnace dimensions, the selection of appropriate values for which is based largely on experience of similar furnaces. For example, the distance between the lining and electrode is close to the electrode diameter value, but it can be $\pm 20\%$ more or less depending whether the process is flux or flux-less, whether the furnace is rotated, and so on. The diameter of the hearth similarly is close to the pitch diameter plus three times electrode diameter, again also higher or lower by $\pm 30\%$ versus process type and furnace design.

In the case of DC furnaces, the Kelly factor plays no part because electrode resistance is determined almost entirely by the length of the open arc and is process independent. The DC electrode current circuit has no inductive reactance and the furnace power factor is a function only of the rectifier design and operating point. The values of parameters such as the hearth power density and the electrode current density also differ significantly from those used for AC furnaces (Barker, 2011).

4.1.2 Ferrochrome, Ferrosilicon, Ferromanganese, and Silicomanganese Furnaces

Traditionally, smelting furnaces have been three-phase AC furnaces, although DC furnaces are increasing in popularity. The most common furnace type for ferrochrome (FeCr), ferrosilicon (FeSi), ferromanganese (FeMn), and silicomanganese (FeSiMn or SiMn) is a circular AC furnace with three electrodes arranged in a triangular configuration. Electric current is introduced into the furnace by three electrodes. The electrodes receive power from a single three-phase transformer or three single-phase transformers. Figure 4.3 shows a photograph of the inside of a ferrochrome furnace shell taken during construction. The lining and the electrodes are visible.

The base of the shell is usually flat and may be welded or bolted to the cylindrical section. The shell holds the refractory lining together and provides a certain degree of resistance to thermal expansion of the crucible.

These ferrochrome, ferromanganese, ferrosilicon, and silicomanganese furnaces employ a carbon lining in contact with the molten metal on the hearth and sidewalls, with various grades of aluminosilicate bricks used to form an insulating lining between the carbon and the shell. In the slag zone, the lining



FIGURE 4.3 Circular AC ferrochrome furnace showing the lining and electrodes. (By permission of Tenova Pyromet, a division of Tenova Minerals [Pty] Ltd.)

may include graphite tiles bonded to the shell to provide a thermally conductive layer between the bricks and the shell, with carbon bricks and aluminosilicate bricks on the hot face. The carbon lining may be made of large carbon blocks, which are machined to fit together. A thick layer of carbon ramming material may be used instead, as the cost is lower, but carbon ramming is generally less resistant to wear. The freeboard region above the slag is usually made of less expensive aluminosilicate bricks, as the conditions are generally less severe. The furnace lining shown in Figure 4.4 is a typical ferroalloy furnace refractory lining.

The furnace crucible is designed to maintain a balance between retaining sufficient heat to maintain the desired temperatures in the crucible, limit the heat losses from the furnace, and maintain a safe refractory and shell temperature. To achieve this balance, the shell may be cooled. Water and air are the most common cooling media, although oil may also be used. The use of oil carries a fire risk, however. The shell floor plates are supported on a set of steel rail sections or I-beams resting on the foundation, which consists of reinforced concrete plinths spaced at intervals to allow forced air cooling of the floor plates. Water is not used to cool the hearth because of the explosion risk associated with contact between water and liquid metal or slag. The simplest application of cooling water on the sidewall of the furnace is in the form of a water film on the outside surface of the shell. Water is poured or sprayed onto the shell near the top of the wall and runs down the shell into a channel welded to the lower shell. Channel cooling, in which water is pumped through channels welded to the shell, provides an enhanced capacity for heat removal. The cooling water circuit is a closed system containing treated water. Water is cooled in a heat exchanger or cooling tower. There is often an emergency

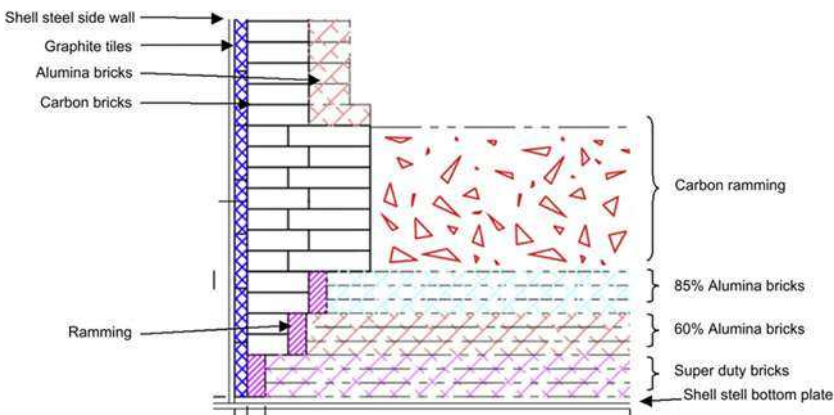


FIGURE 4.4 Section through the lining of a typical ferroalloy furnace. (By permission of Tenova Pyromet, a division of Tenova Minerals [Pty] Ltd.)

cooling water system, which is activated in the event of failure of the pumps or other components of the cooling system, in order to prevent excessive temperatures on the furnace.

The furnace roof is exposed to high temperatures and heat loads. The roof is built of water-cooled steel sections, where the cooling water pipes or passages form part of the structure. As ferroalloy smelting processes produce carbon monoxide and other noxious gases as by-products of the reduction process, the furnace roof may be made as gas tight as possible to contain this noxious gas. The furnace is operated under a small negative pressure to prevent leakage of gas. These closed roofs are common in ferrochrome furnaces, where the closed design reduces the hexavalent chrome (Cr^{6+}) content of the dust emissions in addition to preventing the release of carbon monoxide. A seal, typically made of sand, is fitted between the top of the shell and the furnace roof to provide a gas-tight seal. A closed roof for a ferrochrome furnace is shown in [Figure 4.5](#). In this design, the cooling water pipes contribute to the structural strength of the roof.

A semiclosed roof on a FeCr furnace is shown in [Figure 4.6](#). The roof panels are of water-cooled steel. The openings in the roof provide access for manual charging of raw material into the furnace. A small negative pressure is maintained in the exhaust gas system attached to the roof structure to assist with removal of gases and fumes, preventing leakage of these fumes into the building.

The feed system delivers raw materials and reductants to the furnace in the correct proportions. These systems may vary in complexity from simple manual systems in which batches of material are measured manually and delivered to a bin, from where the mix is fed into the furnace using wheelbarrows or a small front end loader, to fully automated systems of bins with



FIGURE 4.5 Closed roof on a FeCr furnace. (By permission of Tenova Pyromet, a division of Tenova Minerals [Pty] Ltd.)



FIGURE 4.6 Semiclosed roof on a FeCr furnace. (By permission of Tenova Pyromet, a division of Tenova Minerals [Pty] Ltd.)

weighing systems and automatic feeders. Most modern furnaces employ some level of automation in their raw material handling and batching processes.

Ore and reductants are delivered to a raw materials storage facility. Granular materials may be stored in an open stockpile or a bunker, from where they are retrieved and transferred by means of belt conveyors. In a plant with multiple furnaces, there is generally a common bulk storage facility, with an arrangement of incline conveyors, shuttle conveyors, transfer conveyors, or skip hoists, and intermediate bins to deliver material to the furnaces in the correct proportions at appropriate times. Screens may be fitted to the bins to prevent ingress of oversized particles or excessive fine particles.

Raw materials are conveyed from the storage area to day bins above the furnace. Electromagnets may be installed above the conveyors to remove tramp iron. A sampling system may remove samples of feed material for analysis. Each day bin is dedicated to a specific raw material. The material is drawn from the day bins by means of vibrating feeders, which discharge into weigh hoppers to facilitate the preparation of the required blend of material. Conveyors transfer blended material to the feed bins above each furnace.

Where furnace feed material is preheated, it passes from the day bins into the preheaters, which replace the feed bins. The preheaters are thermally insulated. Two types of preheating systems are in use. In the single rotary preheater, the feed material is fed into segments of the preheater in sequence. The outlet of each segment is connected to the feed chutes of a sector of the furnace. In a multiple preheater arrangement, each preheater forms an individual furnace feed bin, feeding a particular sector of the furnace. Feed material for ferrochrome is often preheated, although manganese ores are generally unsuitable for preheating.

Feed chutes connect the bottom of the feed bins to the furnace. The lower sections of the feed chutes, where they protrude below the furnace roof, may be

water cooled or thermally insulated. They are usually fitted with wear liners to accommodate the abrasive feed material. Hydraulic chute gates are installed in the feed chutes, providing the ability to shut off the feed system to the furnace. Furnaces of this type are choke fed. This means that, under normal operating conditions, the feed chute is always open to the furnace and there is a pile of feed on top of the slag. As this material is consumed, it is replaced by material from the feed bin without the need for any control interventions. The feed piles surround the electrodes and generally extend almost to the furnace roof. The greater proportion of the feed material is fed into the center of the furnace between the electrodes.

During the furnace operation, gas and fumes at a high temperature are generated in the furnace freeboard. Gas leaves the furnace through exhaust gas ports in the furnace roof. In closed (hermetic or gas-tight) furnaces the CO gas is not combusted prior to leaving the furnace. After quenching and scrubbing, the furnace off-gas may be combusted in the preheater, where the heat is used to preheat the feed material. Carbon monoxide (CO) gas, which is a product of the reduction process, is explosive in air at concentrations between 12% and 75%. Hydrogen gas may be formed if there is high moisture content in the feed or if there are water leaks. It is explosive in air at concentrations between 4% and 75%.

Furnace pressure is usually controlled to slightly below atmospheric pressure by means of a damper in the exhaust gas ducting to ensure that exhaust gas does not escape from the furnace through any apertures. The gas ducting is optimized to prevent the settling of dust in the duct. Inspection hatches are provided where possible to allow for inspection and cleaning of the inside of the ducting. However, these are only accessible when the furnace is off due to the dangers inherent in the CO gas.

The ducting close to the furnace, where the gas is hottest, may be water cooled or it may be refractory lined to protect the structure from the hot gas. The exhaust gas ducting is usually provided with expansion joints to accommodate thermal expansion. From the furnace, the gas is ducted to a gas cleaning plant, where it is cooled and particulate material is removed. In addition to dust, volatile tars released by the reductants must be removed by the gas cleaning system. In furnaces with closed roofs, wet scrubbing systems are usually used.

In a wet scrubbing system, the gas is quenched to saturation temperature and particles are removed as the gas is mixed with water. A wet venturi scrubber usually has two venturi sections. In the first venturi section, the gas is quenched and coarse particles are removed. Approximately 80% of the dust particles are removed from the furnace off-gas in the first gas cleaning stage. In the second, high-energy venturi, fine particles are removed. Entrained water droplets are separated from the gas by means of a cyclone situated after the second stage venturi. Clean water is used for gas cleaning. The dust-laden water leaving the scrubber flows to a collector sump from where the slurry is pumped to a slurry water treatment plant.

The furnace exhaust gas is drawn from the furnace and through the gas cleaning system by an induced draft fan train. A motorized damper upstream of the gas cleaning plant controls the furnace pressure. The pressure in the exhaust gas system is controlled by means of the damper and a variable speed drive on the fan to maintain both the required furnace pressure and the required pressure drop across the gas cleaning system. A recirculation line from the outlet of the scrubber may be included in the upstream ducting to control the gas temperature and flow rate to ensure safe and optimal operation of the scrubber. Gas leaving the scrubber is sufficiently clean to meet stringent environmental emissions requirements. From the scrubber, gas is returned to the preheater if one is employed, or it enters the stack, where it is flared. If an energy recovery system such as a waste heat boiler is employed in the downstream process, the gas is sufficiently clean at this point to enter the system. Upstream from the gas cleaning plant a bypass line leads to an emergency stack where the raw gas may be flared when the gas cleaning plant is not operational.

In open and semiclosed furnaces, dilution air is drawn into the furnace roof to facilitate combustion of the CO gas and the reduction of the exhaust gas temperature. After this combusted gas leaves the furnace, it is cooled in a radiant heat cooler (also known as a trombone, serpentine or hairpin cooler), prior to entering a bag filter plant where the dust is removed.

A trombone cooler consists of a series of vertical pipes and bends creating a radiant heat transfer area through which the gas temperature can be reduced to a level below that required for auto ignition (630°C for CO) and suitable for safe operation of the bag filter plant. There is usually a bypass duct across the cooler, fitted with a normally closed damper, which may be used to isolate the cooler for maintenance.

The operation of a ferroalloy furnace may be considered semicontinuous. The furnace is choke fed with raw feed material, and operates at an essentially constant power. Tapping of metal and slag is performed periodically.

Metal and slag are usually tapped from a single tap hole. Tap hole blocks are manufactured from carbon and graphite and extend from the hot face of the lining through the shell. The sidewall lining is thickened locally around the tap hole block. The furnace tap hole may be drilled open, with the final breakthrough accomplished using an oxygen lance. The drill is mounted on a pivot pedestal adjacent to the furnace. The tap hole is closed by means of a clay gun mounted on the same pedestal. There may be a fume extraction system located above the tap hole to capture some of the fumes released during the tapping process. The extraction system is connected to a dedicated gas cleaning plant to clean the fumes prior to exhausting into the atmosphere. A ferrochrome furnace and its tapping bay are shown in [Figure 4.7](#). The tap hole is in the center of the photograph, with the clay gun and drilling machine visible on the left. The fume extraction hood is mounted above the tap hole.

During tapping, slag and metal may be separated by means of a skimmer. Metal leaving the furnace travels along a launder section where the metal



FIGURE 4.7 A ferrochrome furnace viewed from the tapping bay. (By permission of Tenova Pyromet, a division of Tenova Minerals [Pty] Ltd.)

passes below the skimmer block and into a ladle from where it is removed to a casting bay. In the casting bay, metal may be cast into iron molds or it may cascade into casting beds made of river sand, fine feed material, or slag. The metal solidifies to form ingots, which are removed by means of an overhead crane once they have cooled sufficiently. Ferrochrome and ferrosilicon may be granulated in water as an alternative to casting.

Slag is diverted from the skimmer block via a side launder. The slag may be collected into a ladle or it may flow along a slag launder to a slag pit, where it is water cooled. The cooled slag is removed from the slag pit to the metal recovery plant or the slag dump by heavy vehicles. Molten slag can be transported to the slag dump in ladles on custom-made slag pot carriers.

4.1.3 Silicon Metal Furnaces

Silicon metal is usually smelted in circular AC furnaces, with typical capacities of 25 MVA and diameters of 10 m. Although they are generally similar to ferrosilicon furnaces, they embody some unique design features to accommodate the requirements of the process.

The furnace shell is a reinforced steel structure with the base and sidewalls welded together. The base of the shell is usually dished to follow the curve of the refractory lining of the hearth. This configuration provides a constant hearth thickness resulting in a uniform hearth temperature and even heat transfer from the hearth. The shell is mounted on a rotating table, allowing the entire crucible to rotate through 360 degrees, at a speed of between 1 to 8 degrees per hour. The table is mounted on a set of wheels, and is driven by a geared motor assembly. The rotating shell permits access for the rabbling cars to the entire circumference of the shell over a period of some days. Stoking or rabbling is

performed periodically in order to break the crust and to agitate the raw material to promote even processing of feed and gas formation. As the electrodes are fixed to the building structure and do not rotate with the shell, the rotation of the shell allows the electrodes to evenly burn away silicon carbide formed in the reduction process in the colder regions further from the reaction zone which has accumulated on the sidewalls, thus maintaining a consistent crucible size and shape. The shell, rotating mechanism, and tap hole fume extraction ducting of a silicon metal furnace are shown in Figure 4.8.

The sidewalls of silicon metal furnaces are usually uncooled, with heat transfer occurring purely by natural convection. The reinforcing ribs and stiffeners act as cooling fins, thus assisting in the cooling of the shell. Forced air-cooling may be applied to the base, although this is not as common as in other ferroalloy furnaces.

The furnace lining is based on an inner crucible made of high quality carbon material, in a similar manner to ferrosilicon and other ferroalloy furnaces. High-quality alumina bricks are used between the crucible and the shell and in the freeboard region. As these furnaces have no forced cooling on the shell, the lining design is optimized to remove the required heat from the crucible while maintaining a safe shell temperature. The shell usually has an angled top section, which facilitates the flow of air across the shell and into the furnace roof (smoke hood).

Multiple tap holes are set into the sidewall at regular intervals. Tap holes are usually made of carbon blocks protruding through the shell. Silicon metal tapping may be a continuous operation or a batch operation with tapping taking place approximately every 2 hours. Silicon metal is tapped into refractory lined ladles, which are preheated by means of gas burners. Ladles are mounted on ladle carriages, which are transported to the casting bays by small tractors.

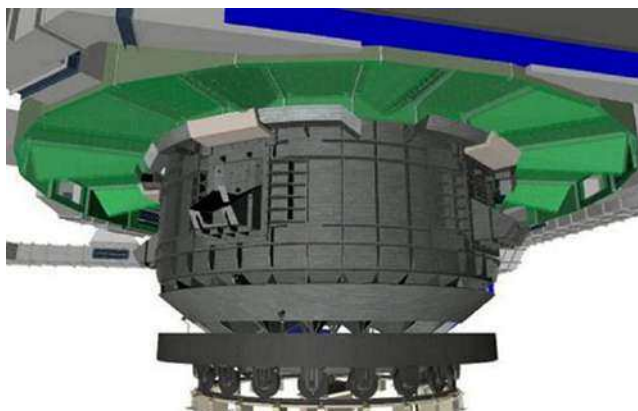


FIGURE 4.8 Shell, rotating mechanism, and tap hole fume extraction ducting of a silicon metal furnace. (By permission of Tenova Pyromet, a division of Tenova Minerals [Pty] Ltd.)

The furnace tap hole may be opened using a stinger, which is connected to a bus bar system from the furnace transformers, or by means of a hydraulic drill. Many producers favor the drill, as it creates a more accurate and consistent hole, whereas the stinger tends to create a large hole after repeated operations. The equipment is suspended from an overhead rail, where the floor is required to provide 270-degree access around the furnace for the tapping operator. An alternative to the permanent floor is the use of a mobile platform, which can be moved 360 degrees around the furnace to provide tapping access to the tap hole in use. This platform moves on a set of rails adjacent to the ladle car rails. The tap hole is closed by means of a clay gun.

A tapping fume extraction hood may be installed on the underside of the operating floor around the full circumference of the furnace, to be able to extract fumes from any position where the tap-holes may be located. A removable plate with a castable refractory may be provided above the tap hole to deflect the flames, hot gas, and fumes generated during tapping into the tapping fume extraction hood. The hood is divided into compartments. During the tapping process, only the compartment above the working tap hole is opened. This ensures that the fumes generated during the tapping process are effectively extracted to the furnace bag filter plant or into a separate dedicated bag filter plant. The fume extraction duct includes a hood, which extracts fumes from the ladle refining station.

Silicon metal furnaces are generally of a semiclosed construction. The furnace roof and smoke hood do not rotate with the furnace shell but are fixed to the building. The annular gap between the top of the furnace shell and the smoke hood allows for ingress of dilution air. As this air mixes with the CO, SiO₂ and SiO produced by the smelting process, the gas is oxidized and leaves the furnace as CO₂. The furnace off-gas contains SiO₂ (silica) dust, also known as condensed silica fume, which is a saleable byproduct of the process.

The furnace roof generally consists of horizontal water-cooled steel panels suspended from the building structure and vertical smoke hood doors and panels. These form a structure which makes allowance for ports through which the electrodes pass, one or more off-gas ports, and multiple feed ports through which the feed chutes protrude into the furnace. Panels in the central area between the electrodes are manufactured from a nonmagnetic stainless steel to avoid electromagnetic heating, and are insulated from each other to prevent stray currents circulating in the roof. Roof and side skirt panels may employ a plate and baffle construction, or they may be fabricated entirely from thick walled steel pipes. The inside of the smoke hood and roof, including the side skirts and lifting doors, is lined with a high temperature refractory castable to protect the steel from the high temperatures generated by the combustion of the CO gas. The smoke hood is fitted with water-cooled doors, which may be raised and lowered hydraulically to provide access for the stoking car and for maintenance. The furnace roof and smoke hood of a silicon metal furnace is shown in [Figure 4.9](#). This design has two exhaust gas ducts.

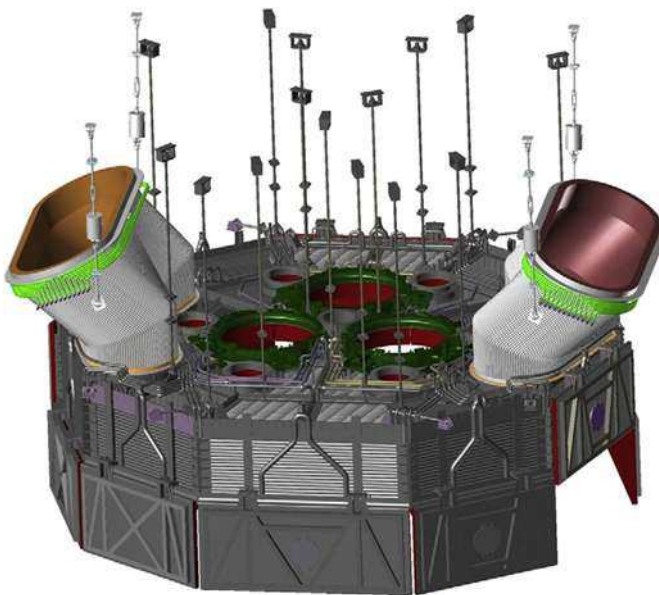


FIGURE 4.9 Smoke hood of a silicon metal furnace. (By permission of Tenova Pyromet, a division of Tenova Minerals [Pty] Ltd.)

On leaving the furnace, the gas is cooled in a radiant heat cooler prior to entering a bag filter plant where the dust is removed from the gas. In the bag filter plant, the dust-laden air passes through a number of filter bags in which dust particles are captured. The solid particulate matter remains on the filter cloth while cleaned air is passed into the connecting ductwork to the main induced draft (ID) fan which discharges into the clean gas stack. The filter bags are cleaned regularly. The dust dislodged from the filter bags is collected in the bag filter hoppers and removed to a storage silo. The temperature of the gas entering the bag filter plant is controlled by allowing some recirculation of colder downstream gas. Provision is made for bypassing the bag filter plant by sending gas to the emergency stack. The hot gas may be used in a waste heat boiler or other energy recovery system in preference to the radiant heat cooler.

4.1.4 Ferronickel Furnaces

Ferronickel is smelted from calcined nickel oxide in circular or rectangular AC furnaces. Furnaces are typically large, with power ratings of up to 120 MVA (75 MW). Rectangular furnace configurations are generally used for the larger furnaces. Ferronickel furnaces may be operated in a shielded-arc mode or as slag resistance furnaces. The typical hearth power densities of the order of 200 kW/m^2 combined with the degree of superheat of the slag normally necessitate the use of cooling elements made of copper on the sidewalls.

In a rectangular or six-in-line furnace, six electrodes are arranged in a line along the center of the furnace. The electrodes are connected in pairs, two adjacent electrodes being fed from the positive and negative connection of the same phase. The metal tap holes are located on one end wall, at a lower elevation to the slag tap holes, which are located at the opposite end of the furnace. In a rectangular furnace, the shell does not provide the same structural support to the lining as in a circular furnace. Rectangular furnaces are therefore held together by a system of steel tension rods and springs. A schematic view of a section through a six-in-line furnace is shown in Figure 4.10, and a cross-section of the smelting plant is shown in Figure 4.11.

The base plate of a ferronickel furnace is usually flat, with a dished hearth. In a circular furnace the dished hearth is saucer-shaped, whereas in a rectangular furnace the hearth is dished only across the short axis of the furnace. The slag produced by the process is chemically aggressive to refractory lining materials, necessitating particular attention being paid to the choice of lining materials and generally resulting in shorter lining life than in other ferroalloy smelting processes. Carbon linings are not used. The brick in contact with metal and slag is usually a low porosity magnesia chrome refractory brick.

The base plate is cooled by forced air ventilation, whereas the sidewalls are fitted with copper cooling elements with integral water passages, which are set into the refractory lining. These provide the capacity to remove heat fluxes $>200 \text{ kW/m}^2$ through the sidewalls and are a feature of linings employing a “freeze lining” (autogenous lining) design, where a layer of frozen slag protects the sidewall refractory from attack by the molten slag. The sidewall at the interface between the metal and slag is particularly vulnerable to damage as it is alternately exposed to metal and slag. Erosion or corrosion of the lining is limited by cooling the refractory sufficiently that a stable layer of frozen slag forms on the hot face of the cooler. The slag is

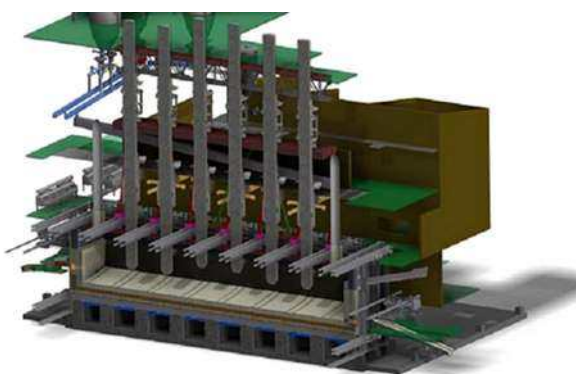


FIGURE 4.10 Schematic view of a six-in-line furnace crucible. (By permission of Tenova Pyromet, a division of Tenova Minerals [Pty] Ltd.)

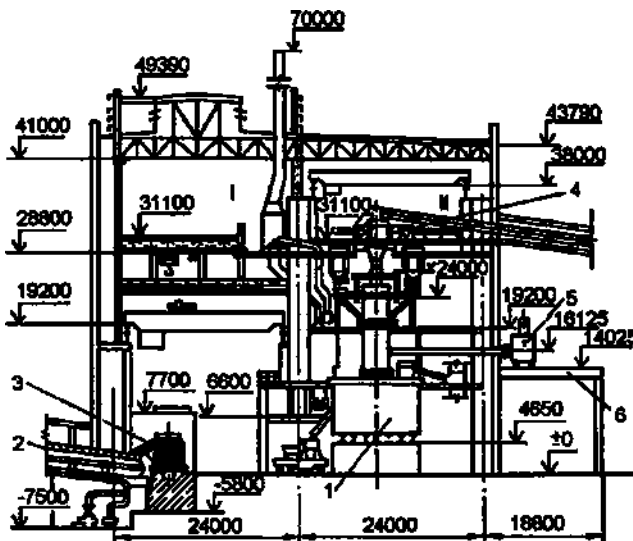


FIGURE 4.11 Schematic of a typical smelting plant with high-power rectangular furnaces of 63 MVA. I, tapping yard; II, furnace section; 1, furnace; 2, casting machine; 3, ladle; 4, conveyer charge feeder; 5, electric transformer; 6, power section support. Dimensions in mm. (By permission of Gladkikh *et al.*, 2007.)

chemically inert when frozen, and therefore acts as a refractory barrier between the furnace contents and the lining.

Copper coolers have been produced in a variety of geometric configurations. They may be broadly classified into two types: shallow cooled, where the copper element is inside the furnace but the water passages are located on the outside of the furnace, and deep cooled, where both the copper element and the water passages are inside the furnace. The cooling water circuit is a closed system containing treated water. Water is cooled in a heat exchanger or cooling tower. There is often an emergency cooling water system, which is activated in the event of failure of the pumps or other components of the cooling system in order to prevent excessive temperatures on the furnace.

The furnace roof is constructed of brick or refractory castable or a combination of brick and castable. Rectangular furnaces may be fitted with arched roofs, where the arch terminates in a skewback mounted on the top of the sidewall. The arch is compressed using an arrangement of buckstays and springs. Circular furnaces may be fitted with domed roofs, but these are generally only suitable for small furnaces. Suspended bricks are common, where each brick is suspended from a hanger attached to a steel roof structure. Apertures for the electrodes, feed ports, sounding ports, and exhaust gas ducts are provided in the roof refractory. The furnace roof may be made gas tight if the process produces a significant amount of CO, although this is not always necessary.

Metal is tapped periodically from the metal tap holes into a refractory lined launder, which discharges into a ladle. The tap hole blocks are water-cooled copper elements into which the refractory of the tapping channel is set. This configuration extends the campaign life of the tapping channel. The metal tap holes are opened and closed by means of a tap hole drill and clay gun, mounted on rails above the tap holes.

Slag tap holes are 700 to 1000 mm above the metal tap holes, and they are situated across the furnace from the metal tap holes. The slag tap holes are opened and closed by means of a tap hole drill and clay gun, mounted on rails above the tap holes. Slag is tapped periodically into launders, from where it may be transferred into ladles, dumped into slag pits, or granulated using a high volume of pressurized water. The slag launders may be refractory lined, or they may be water cooled.

Raw material in the form of hot calcine is received from the rotary kilns in calcine containers mounted on transfer cars, which run on rails between the kilns and the furnace. The containers are lined with thermally insulating castable to retain the temperature of the calcine and to protect the steel structure of the containers. The calcine bins are lifted using an overhead crane and discharged into feed bins, which are similarly lined with thermal insulation. The system is provided with multiple containers, cars, and cranes so that any feed bin may be filled at any time.

Multiple feed bins are arranged around the furnace to provide optimal positioning of the feed chutes. Feed material discharges into the furnace in batches through the feed chutes via gas-tight valves. The batching method may range from completely manual to fully automatic. The height of the feed piles in the furnace is monitored and used to control the batching process.

In open furnaces, dilution air is introduced into the freeboard of the furnace crucible to combust the CO gas generated by the reduction process and to reduce the gas temperature. Exhaust gas leaves the furnace in a water-cooled steel duct. Further downstream, where the gas is cooler, a refractory lined duct may be used. In a similar manner to other ferroalloy smelting processes, exhaust gas passes through a radiant heat cooler prior to entering the bag filter plant. An induced draft fan draws exhaust gas through the ducting. After the bag filter plant, the system vents to a stack. An emergency stack is provided through which gas may be vented into the atmosphere should the gas cleaning plant not be available. Ferronickel furnaces may also be hermetic, where the gas leaving the furnace is cooled in a wet scrubber prior to flaring in the exhaust stack.

Tapping fume from the slag and metal tap holes is extracted from above the tap holes and launders and introduced into the exhaust gas duct, where it cools the gas and provides additional dilution air.

4.1.5 DC Furnaces

The use of DC arc furnaces for the smelting of ferrochrome has increased. Whilst the operating temperatures are the same for AC and DC furnaces,

the raw material feed requirements differ. AC furnaces are choke fed and require lumpy feed material in order to provide a sufficiently porous bed to facilitate the upward percolation of the generated gas through the feed material. Too great a proportion of fine material in an AC furnace will reduce the porosity of the bed and result in pressure excursions and unstable operation. DC furnaces operate with an open slag bath and can therefore accommodate fine feed material which falls directly into the slag bath. A further consequence of the open bath operation is that lower grade, and consequently cheaper, reductants may be used. DC furnaces can operate at higher power densities than AC furnaces. A DC furnace is therefore usually smaller than the corresponding AC furnace of the same power rating. DC furnaces provide capital cost savings compared to AC furnaces where there is a large proportion of fine feed material, as these materials may be fed directly into the furnace, thus obviating the need for briquetting or other agglomerating equipment. This cost saving is offset against the higher cost of a transformer rectifier over an AC transformer and the more expensive graphite electrode technology, which is usually used.

The DC furnace operates with an open arc, which may be 700 mm long, unlike the submerged arc found in an AC furnace. Fine feed material is fed around the circumference of the electrode. A certain proportion may be fed through the center of the electrode. The feed material is deposited on top of the molten slag, but there may not always be sufficient to cover the slag bath. Conditions on the surface of the slag are generally quite turbulent, with slag splashes forming accretions on the roof and upper sidewalls. The roof and upper sidewalls may be exposed to direct radiation from the arc and the surface of the slag bath, representing a substantial heat load on these components. The sidewalls are cooled using serpentine cooling channels welded to the outside of the shell. This cooling may be supplemented by copper plate coolers (embedded into the refractory lining) to ensure that a layer of frozen slag is maintained on the sidewalls. The base of the furnace is cooled by forced air convection. The shell of a DC arc furnace is shown in [Figure 4.12](#). The cooling water channels on the sidewall are visible. The rectangular holes in the upper shell allow the copper coolers to pass through the shell.



FIGURE 4.12 The shell of a DC furnace. (By permission of Tenova Pyromet, a division of Tenova Minerals [Pty] Ltd.)

A DC furnace requires at least two electrical connections: a cathode and an anode. The conventional current (electron flux) passes from the cathode to the anode. Most of the actual current is carried by electrons moving from the graphite electrode tip (cathode) to the slag bath (anode) under the influence of the electric field between the electrode tip and the slag bath. The result is that in a DC furnace, an electrode operated as a cathode shows much less wear than an electrode operated as an anode.

A single prebaked graphite electrode similar to those used in AC furnaces forms the cathode. The anode is embedded into the lining of the hearth, which usually has a concave dished shape. The two most common anode configurations are a conductive hearth and a pin anode. A conductive hearth is formed by using carbon or carbon-coated bricks and enhancing the electrical conductivity of the hearth bricks by the inclusion of thin steel plates between bricks. The anode pin configuration utilizes four copper anodes protruding some distance into the hearth. The anodes are connected by means of a copper plate near the base of the hearth.

The DC furnace generally has a gas-tight roof in the same way as the AC furnace, and the raw material handling, off-gas handling, and tapping equipment is the same for both furnace types. A DC furnace is shown in Figure 4.13. The single graphite electrode with its clamping mechanism and the gas-tight, water-cooled roof are visible in the center of the picture.



FIGURE 4.13 General view of a DC furnace. (By permission of Tenova Pyromet, a division of Tenova Minerals [Pty] Ltd.)

DC furnaces are not used for the smelting of ferromanganese and silico-manganese because the high vapor pressure of manganese results in unacceptable metal losses in the gas phase.

4.1.6 Electrical Supply and Operation

Furnaces receive power from the electrical substation by means of a high voltage supply, in the kilovolt range appropriate to the furnace MVA rating. The voltage is reduced to that required by the AC furnace by means of a single, three-phase, step-down transformer or three single-phase, step-down transformers. Power from the substation is supplied to a DC furnace by means of a transformer-rectifier.

The low tension current is carried from the transformers to the electrodes by air-cooled bus bars or water-cooled copper bus tubes. Flexible conductors are fitted between the ends of the bus bars and the transformer flag connections to avoid placing mechanical loading on the transformer connection flags. Cooling water is piped to the bus tube ends by nonconductive flexible piping in order to insulate the piping system from the bus tubes. The bus bars terminate at fixed positions around each electrode. Flexible water-cooled copper conductors are used to carry both current and cooling water from these terminations to the terminals for the contact shoe riser tubes on the electrodes. These flexible conductors are shown in Figure 4.14.

The electrical insulation of conductors from each other and the furnace structure, as well as the insulation of the furnace from the building structure, is an important detail of furnace design. The large magnetic fields generated by



FIGURE 4.14 Flexible water-cooled copper conductors at the electrodes. (By permission of Tenova Pyromet, a division of Tenova Minerals [Pty] Ltd.)

the electrode current give rise to induced currents in magnetic materials in their close proximity. It is good practice to use nonmagnetic materials, such as stainless steels, for the furnace steelwork close to the electrodes.

4.1.6.1 AC Furnaces

The incoming voltage is reduced to that required by the AC furnace by means of a single three-phase, step-down transformer or three single-phase, step-down transformers. Voltage changes on the secondary side of the transformers are made using on-load tap changers.

The supply to the primary side of the transformers may allow star/delta switching to increase the secondary voltage range, thereby increasing the flexibility of the transformer. The star configuration is used when low electrode currents are used—for example, during startup or electrode baking schedules. The star/delta switching equipment is located in the furnace building for convenient access. Switching between star and delta is performed at the star/delta switch location, and it is never done remotely from the control room. The transformer secondary windings are connected to the three furnace electrodes in the delta configuration with the delta closed at the contact shoes on the electrodes.

AC furnaces may be circular or rectangular. Most AC furnaces are powered from a three-phase electrical supply. The most common furnace type for ferrochrome, ferromanganese, ferrosilicon, and silicon metal is a circular AC furnace with three electrodes arranged in a triangular configuration.

Rectangular or six-in-line furnaces are used in the smelting of ferronickel, high-carbon ferromanganese, and silicomanganese. In these furnaces, the electrodes are arranged in a line along the center of the furnace. The electrodes are connected in pairs, two adjacent electrodes being fed from the positive and negative connection of the same phase. Although three-electrode circular furnaces and six-in-line rectangular furnaces are the most common, a number of variations of these furnace configurations have been built. These include three-in-line rectangular furnaces, which are electrically identical to the circular three-phase furnace, and single-phase furnaces with two electrodes or one electrode and a bottom connection.

The current in an AC furnace passes through an electrode, through the arc, and into the conductive material in the bath, predominantly the molten metal, from where it passes into the other electrodes to close the circuit. Different arc configurations and operating modes are possible, based on the electrical properties of the feed material and slag.

The uncorrected power factor $\cos(\varphi)$ of most submerged arc ferroalloy furnaces lies in the range of 0.75 to 0.85, which is fairly low. For economic reasons, the power factor can be improved to approximately 0.95 by the installation of power factor correction capacitors.

With their short arcs and resistance heating component, submerged arc furnaces cause much less flicker and harmonic distortion than the much more common scrap melting furnaces in the steel industry. Due to the conductivity of

steel, scrap-melting furnaces are forced to generate their heat almost entirely from long arc operation, which necessitates extensive measures to reduce flicker and harmonic distortion on the electrical supply system.

4.1.6.2 DC Furnaces

DC furnaces are increasing in popularity for some processes. A single carbon electrode similar to those used in AC furnaces forms the cathode. Due to the high current density, the cathode is usually a prebaked graphite electrode. Söderberg (self-baked) electrodes are not used. The anode is embedded into the lining of the hearth. A DC furnace usually has a relatively long open arc, operating in a similar manner to a steelmaking electrical arc furnace.

A DC arc furnace is powered by a single transformer connected to the utility which powers the 33 MV bus, in turn transferring power to the furnace power supply and auxiliary loads. A vacuum circuit breaker is used to feed power to two rectifiers through a furnace transformer. The rectifiers produce the resulting DC voltage. Reactors ensure low ripple content in the DC current, providing arc stability and reducing harmonic levels.

The negative DC voltage output from the rectifiers is transferred to the electrode column by means of water-cooled copper bus tubes and flexibles. The copper flexibles are connected to copper contact shoes, which transfer the DC voltage to the graphite electrode. Contact between the copper contact shoes and the graphite electrode is maintained by means of a pressure clamping system. The positive DC voltage output is transferred to the copper anode dish by means of water-cooled copper flexibles.

Due to the positioning of the single power supply and asymmetrical bus tubes, high asymmetric magnetic fields are present inside the DC furnace, particularly in the arc zone. This causes skewing of the electrical arc, resulting in uneven refractory wear. This may result in premature failure of the furnace refractory lining. For this reason, magnetic compensation is provided to correct the arc skewing.

4.1.6.3 Electrodes

The electrode column provides the path through which electrical power is transferred from the switchgear to the material in the furnace. Current passes into the furnace from the transformers through bus bars or water-cooled bus tubes into a number of copper contact shoes placed around the circumference of the electrode. The contact shoes are clamped onto the electrode by means of a pressure ring designed to force the contact shoes against the electrode in order to provide good electrical contact for the transfer of current. The electrodes extend through the roof of the furnace and are submerged in the raw material inside the furnace (Fig. 4.15).

The electrode column includes a supporting structure for the electrode and a clamping mechanism. The clamping mechanism may be hydraulically or pneumatically powered or it may be connected to a winch. During operation,

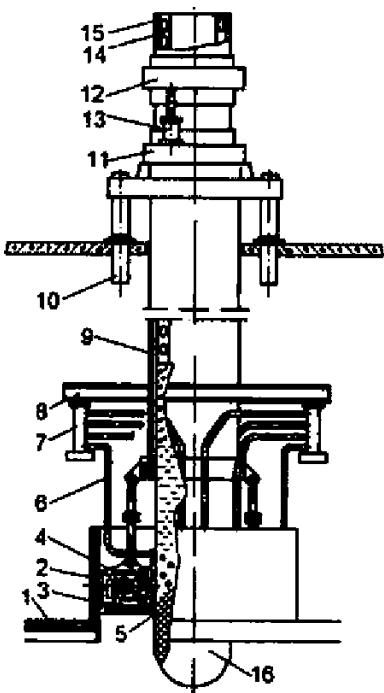


FIGURE 4.15 Schematic of the electrode (self-baked or Söderberg type) and its support.
 1, furnace roof; 2, water-cooled electrode seal; 3, thermal seal; 4, pressing mechanism; 5, copper contact shoes; 6, current flexible connectors (“short net”); 7, movable shoe; 8, traverse; 9, shield; 10, hydraulic lift; 11, fixed ring of the slipping mechanism; 12, movable ring of the slipping mechanism; 13, hydraulic cylinder; 14, steel shell fins; 15, steel shell; 16, electrode.
 (By permission of Gladkikh et al., 2007.)

electrodes may periodically be moved up or down by a few centimeters during operation to assist in the control of the furnace by increasing or decreasing the bath resistance, an activity termed *regulating*. This is achieved by raising or lowering the clamp assembly.

As the electrode is carbonaceous, it is consumed in the furnace. To compensate for this erosion of the electrode, it is fed into the furnace by a process called *slipping*. During this routine activity, one electrode clamp is released and the electrode, fully gripped by the other clamp, and is moved up or down by a precise amount, slipping it through the open clamp. Slipping is performed at regular intervals. The operating resistance of the furnace is determined by the furnace contents as well as the height of the electrode tip in the furnace. In a submerged arc furnace, the reaction zone tends to form near the electrode tip. With a short electrode, the reaction zone will be higher in the furnace than when the electrode is long. Likewise, moving the electrode up or down will cause short-term variations in conductivity, but these conductivity variations tend to disappear as the reaction zone reestablishes itself around the new electrode tip position. Electrode seals are provided where the electrodes enter the furnace roof. They may be active, using a compressed air powered bellows arrangement, or passive, fitted with a fiber rope seal. It is good practice to provide a heat shield around the electrodes above the furnace roof. This heat shield protects the steel building structure from radiant heat emitted by the

electrode. Dust shields may be fitted over the contact shoes to prevent the accidental ingress of feed material and dust.

Three types of electrodes are used (Gasik, 1984). The optimal electrode type for any application is determined by requirements such as the required current density, the electrode diameter, and capital and maintenance costs. The electrical conductivity and diameter of an electrode determine its current carrying capacity. Electrodes used in DC furnaces can carry more current than the same electrodes used in AC furnaces, as AC current tends to concentrate on the surface of the electrode, the so-called skin effect. In AC furnaces, smaller-diameter electrodes can accommodate a higher current density than can larger-diameter electrodes. The skin effect becomes pronounced at electrode diameters greater than 1000 mm.

Søderberg (Self-Baked) Electrodes

Søderberg electrodes were invented in 1919 to overcome the size limitations of prebaked electrodes. This self-baking electrode consists of two parts, namely a steel casing and the carbon core. The casing is a relatively thin steel tube, fitted with a number of fins, which protrude part of the way into the core. The purpose of the casing is to contain the paste before it is baked and to provide a path for the flow of current into the paste. In addition, the casing has sufficient mechanical strength to withstand the force of the clamping device and the pressure ring. Once the carbon has baked, the casing is no longer required. As the temperature of the electrode increases, the casing oxidizes and all of the current is conducted through the carbon.

The core material is typically calcined (thermally treated) anthracite (~60%) or coal and coke (<40%) in a pitch or tar binder (up to 25% over carbon materials). This unbaked or green paste is fed into the electrode from the top in an unbaked form, either as briquettes of 0.5 to 1.5 kg each (Gasik, 1984) or in larger cone-shaped cylinders (up to 1 ton each). As the electrical current passes from the contact shoes into the casing and fins and paste, the resistive heating component causes the paste to soften and then bake. The green paste has a very low electrical conductivity and thermal conductivity. Green paste softens at a temperature of 50° to 80°C and spreads to fill the casing. During baking, at a temperature of 350° to 500°C, the paste undergoes a change of state accompanied by a loss of volatiles and a change of state of the pitch binder. This results in an increase in both the electrical and thermal conductivities of the material. The paste changes from electrically nonconductive to conductive as it bakes and acquires sufficient mechanical strength to support itself and to withstand the forces applied by asymmetric feed piles in the furnace and other factors. The schematic of the electrode zone structure is shown in Figure 4.16 (Gladikh et al., 2007).

The first zone (<70°C) has electrode paste being heated and sintered. In the second zone (70° to 350°C) the binder (pitch) becomes liquid; it then starts coking in the third zone (350° to 550°C). The last zone consists of baked

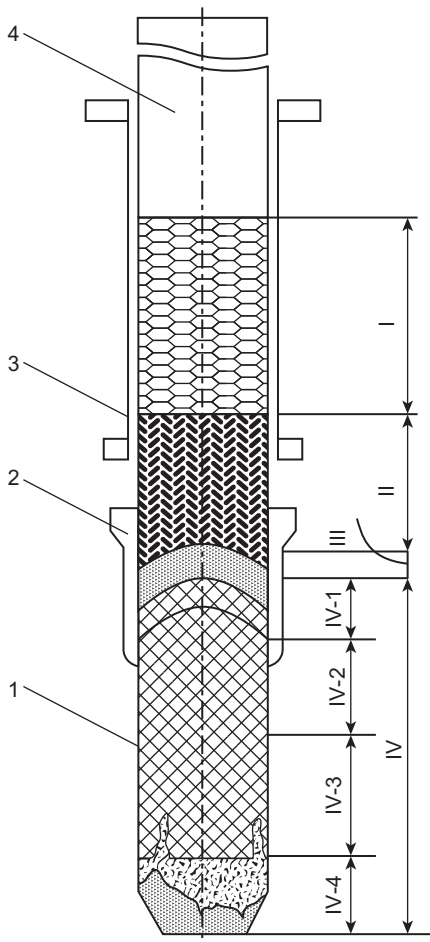


FIGURE 4.16 Zonal structure of the Söderberg electrode. I, solid paste; II, “liquid” paste; III, coking zone; IV, backed electrode (with four subzones); 1, electrode; 2, contact shoe; 3, shield; 4, electrode shell. (By permission of Gladkikh *et al.*, 2007.)

electrode, and in this region four subzones have been experimentally identified (Gasik, 1984), which are not based on the paste state but rather on the electrode material structural changes: the peak of the volatiles’ removal at 550° to 900°C (zone IV-1), the relative stability zone at 850° to 1450°C (IV-2), the zone of carbon graphitization and ash minerals reduction at 1450° to 2500°C (IV-3), and the working tip at 2500° to 2700°C (IV-4).

The resulting baked paste forms a solid carbon electrode through which the current passes into the furnace. Typical properties of Söderberg electrode paste are listed in Table 4.4.

The carbon electrode is able to carry a high current and to withstand the high temperature generated inside the furnace. In processes such as ferro-chrome and ferromanganese smelting, the electrodes carry a high current, electrode consumption is high, and baking occurs within the annulus enclosed

TABLE 4.4 Typical Properties of Søderberg Electrode Paste

Property	Value
Unbaked Paste	
Density	1600 kg/m ³
Volatile content	12–16%
Softening point	50–80°C
Melting point	100°C
Ash	<8.5%
Thermal conductivity	2.5 W/mK
Baked Paste (baked at 1000°C)	
Density	>1350 kg/m ³
Electrical resistivity (room temperature)	70 μΩm
Electrical resistivity (1000°C)	40 μΩm
Thermal conductivity	8 W/mK
Crushing strength	20 MPa
Bending strength	3–5 MPa
Maximum current density	7 A/cm ²

by the contact shoes. In ferronickel smelting, the electrodes carry a relatively low current, and the ambient temperature below the furnace roof assists baking.

As the tip of the electrode is consumed by the process, the length of the electrode is maintained by “slipping” the electrode a short distance. It is good operating practice to perform short slips, typically of the order of 20 mm, every hour, rather than performing one longer slip per shift. Long slips may be performed if required to correct a short electrode or to recover from an electrode break. These require the electrode to run under reduced current for a period of time until the paste is adequately baked. Slipping is performed by closing the fixed clamp on the electrode column and releasing the moving clamp. The moving clamp is moved upward by the required distance, and is closed against the casing. The fixed clamp is then released and the electrode is allowed to move down by the required distance. Casing segments are generally approximately 1.5 m long. As the casing moves down in to the furnace, additional segments are welded into place at the top of the electrode column. This activity is performed while the furnace is under load. Insulated barriers protect the welder from accidental contact with other electrodes or

the building structure. Additional paste is loaded from above using an overhead crane.

The baking process is directly affected by the operating conditions within the furnace. As these conditions are not always the same and may not always be optimal for electrode baking, poor quality electrodes may result, which may give rise to electrode breaks. Electrode breaks are classified into two main categories, namely hard breaks, which occur in the baked electrode, and soft or green breaks, which occur where the paste is unbaked. Hard breaks may range in severity from minor, for example where a relatively short section of the tip breaks off, to major, where the whole electrode tip section, a metre or more in length, breaks off. Hard electrode breaks may be caused by a number of factors:

1. Thermal stresses or thermal shock, where the surface of the electrode is exposed to a sudden change of temperature, which creates a severe temperature gradient through the thickness of the electrode. This may lead to cracking and spalling of the electrode.
2. Underbaking, where the paste is inadequately baked and the electrical current carrying capacity of the electrode as well as its mechanical strength is inadequate.
3. Overbaking, where the paste dries out too much during baking, leading to a brittle electrode
4. Unbalanced lateral mechanical forces on the electrode due to asymmetric feed piles
5. Paste segregation, where the anthracite particles and the binder separate before baking. This leads to a mechanically weak and brittle electrode, as there is nothing holding the anthracite particles together.

Green breaks are almost always major events, as significant quantities of electrode paste are dumped into the furnace, where they may ignite and cause damage to the furnace. Green breaks are usually caused by damage to the casing.

Special operating procedures are adopted to enable recovery from all but the most minor of hard breaks. These usually involve operating the furnace at reduced load for a period while performing “long” slips, which may be up to 1000 mm, on the affected electrode in order to expedite the lengthening of the electrode. Particular care must be taken to ensure that the resulting electrode is adequately baked before full current is restored.

Søderberg electrodes may be manufactured in a wide range of diameters. As they are made of relatively simple fabricated steel members, they are not restricted to standard sizes. In addition, they are not subject to the size limitations imposed by the prebaking process, and have been manufactured in diameters up to 2000 mm or rectangular (oval) to 3000×750 mm. They are less expensive than graphite electrodes, as their materials of construction are not as expensive. As the electrode paste is less conductive than graphite, the current density which can be sustained by a Søderberg electrode is lower than that of a graphite electrode.

A typical electrode column for a Søderberg electrode used in a ferroalloy furnace is shown in Figure 4.17. The upper electrode column houses the clamping, slipping, and regulating arrangements, whereas the lower electrode column contains the electrical contact shoes and ancillary equipment. The electrode passes through the center of the electrode column.

The electrode column is supported on the support frame, which is attached to the furnace building structure. The hydraulic cylinders used for regulating and slipping are fixed to the support frame. There are two electrode clamps. The

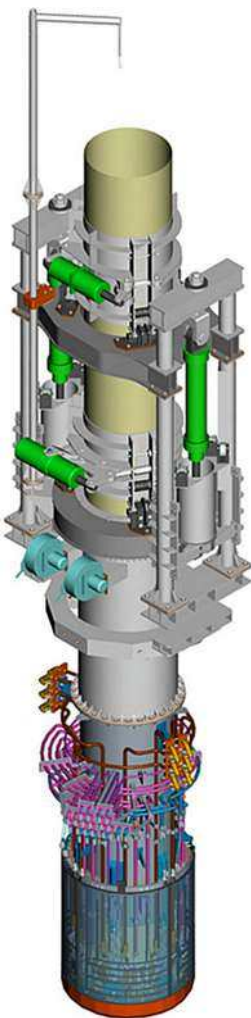


FIGURE 4.17 A Søderberg electrode column. (By permission of Tenova Pyromet, a division of Tenova Minerals [Pty] Ltd.)

upper clamp, which is normally open, is attached to the building structure. The lower clamp is normally closed and is attached to the hydraulic cylinders, allowing it to move up and down as required. The mantle is a shroud around the electrode through which warm air is forced by the mantle air fans. This air assists in heating the electrode paste. The contact shoe assembly is suspended from the mantle assembly.

The lower electrode column comprises the contact shoes, pressure ring, copper skirts, heat shields; and electrode seal. The heat shields and electrode seal are not shown in [Figure 4.17](#).

The contact shoes are water-cooled copper segments, which transfer the electric current through the bus tubes and flexibles to the electrode. They are forced against the electrode casing by a pressure ring, a segmented arrangement of hydraulically operated bellows. The copper skirts fully enclose and protect the lower part of the contact shoes from the furnace environment. The heat shields are situated around the outside of the contact shoes and bus tubes, and protect the contact shoes, bus tube risers, and pressure ring from radiant heat from the inside of the furnace as well as protecting the live electrical components from ingress of foreign objects and dust. When the electrode is in its normal operating position, the lower part of the lower electrode column protrudes through the roof into the furnace. The electrode seal forms a gas-tight seal where the heat shields pass through the furnace roof. The entire electrode column is isolated from the furnace building structure by multiple layers of electrical insulation material.

Söderberg electrodes are more common than prebaked electrodes in ferroalloy smelters and are used in high-carbon ferrochrome, ferromanganese, silicomanganese, ferrosilicon, and ferronickel production. They are generally not used in DC furnaces, as they are unable to sustain sufficiently high current densities.

Prebaked (Graphitized) Electrodes

Prebaked electrodes are manufactured in a range of diameters, lengths, and grades. The electrodes are manufactured by pressing the green mixture of anthracite or needle coke and a binder into a mold, after which they are fired and subsequently graphitized in a furnace in a neutral or reducing atmosphere. The maximum diameter of a prebaked electrode is limited by the ability to successfully graphitize the green electrode. The controlled conditions under which they are baked result in homogeneous quality, reducing the likelihood of breaks during operation due to poor electrode baking.

Prebaked electrodes are produced in a variety of grades. Although all are made of carbon particles in a tar pitch binder, the grade of carbon used affects the final degree of graphitization of the electrode and hence its thermal and electrical conductivity, but also its cost. The thermal and electrical conductivities and diameter determine the maximum current density that the electrode can carry. Anthracite and semigraphite carbon electrodes are available in

diameters from 700 mm to 1400 mm. Graphite has a considerably higher electrical conductivity, facilitating the use of a high current density in the electrode. Graphite electrodes are available in various grades and in diameters from 150 to 800 mm. Typical properties of various grades of prebaked electrodes are listed in **Table 4.5**.

Prebaked electrodes are supplied in sections. These sections are joined together by means of a threaded connection piece called a nipple on the end of each section. When the top of the electrode reaches a predetermined height, new sections are screwed onto the top of the electrode.

In earlier designs, graphite electrodes were supported by a hydraulically operated column and a cantilevered conductive arm. DC arc furnaces were subject to approximately 30 minutes downtime daily, as it was necessary to switch the furnace out for the purpose of joining a new section of electrode onto the existing column. Technological advances have resulted in the use of an automated electrode joinder for handling and joining the graphite electrode sections in conjunction with a central hydraulically operated electrode column for application with a DC smelting furnace, thus eliminating the furnace downtime normally associated with electrode joining. A schematic layout of such an electrode column is shown in **Figure 4.18**. The electrode column is supported and regulated by hydraulic cylinders. The slipping device uses springs to apply the clamping pressure and hydraulic cylinders to release the pressure to allow for slipping or back slipping. A suitable overhead traveling crane is required for lifting graphite electrode sections from ground level to the electrode floor, where jointing takes place.

TABLE 4.5 Typical Properties of Prebaked Electrodes

Grade	Diameter (mm)	Electrical Resistivity ($\mu\Omega\text{m}$)	Current Carrying Capacity (kA)	Maximum Current Density (A/cm^2)
Anthracite	700	37	30–36	9
	1005		46–52	6.6
Semigraphite	700	29	36–40	11
	1005		55–62	7.5
Graphite—high power	350	6.5	16–24	24
Graphite—ultra high power (UHP)	550	5	48–70	28
	700		80–100	25
Graphite—UHP for DC furnaces	550	5	65–78	32
	800		122–146	28

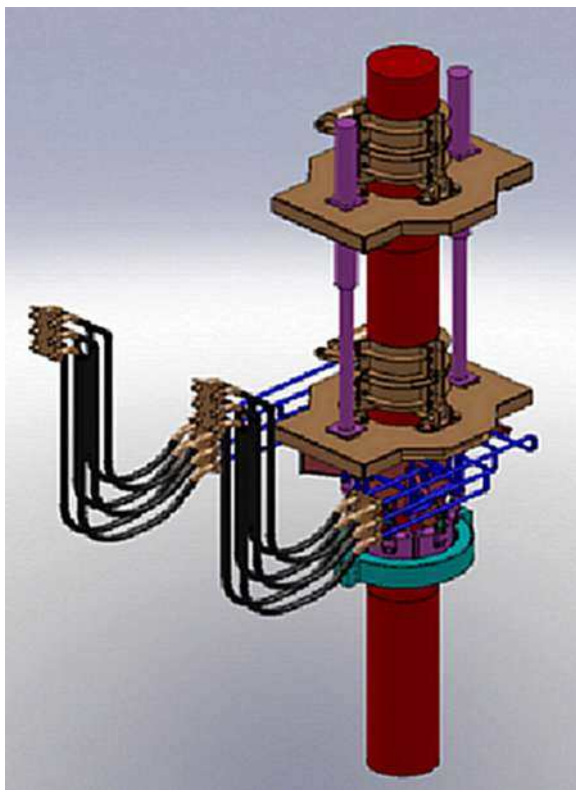


FIGURE 4.18 Electrode support column for a graphite electrode in a DC furnace. (By permission of Tenova Pyromet, a division of Tenova Minerals [Pty] Ltd.)

The high electrical conductivity of graphite electrodes renders them suitable for use in DC furnaces, and the absence of any metallic components in contact with the furnace renders all grades of prebaked electrodes suitable for use in silicon metal furnaces, although their relatively high cost is a disadvantage.

Composite Electrodes

The composite electrode was invented to fulfill a need for an iron-free self-baking electrode. These electrodes are used in low iron ferrosilicon and in silicon metal production, where the additional iron introduced by a Søderberg electrode casing is a contaminant in the product and reduces the grade of the metal.

The composite electrode has a central prebaked graphite core surrounded by a steel casing, the annulus between them being filled with Søderberg paste. The casing does not have fins. The graphite core is supported in a clamping assembly and is replenished using standard electrode sections with threaded nipples, as with conventional graphite electrodes. Current is introduced into the

electrode by means of contact shoes, which are forced against the casing, as in a Søderberg electrode. The electrode paste, which fills the space between the casing and core, bakes in the contact shoe region as a result of the resistive heating in the casing and paste due to the current. The baked Søderberg paste bonds well to the graphite, but not to the steel casing. The casing is supported by an independent clamping arrangement. Slipping is performed on the graphite clamping assembly rather than the casing assembly. Both the graphite core and the baked Søderberg electrode move downward during slipping, extruding the electrode through the casing, as the casing remains at its original height. The electrode below the furnace roof therefore consists only of baked carbon. The casing clamping device provides the capacity to slip the casing with the carbon electrode should this be necessary for recovery from electrode breaks or other upset operating conditions.

The composite electrode is able to carry a higher current density than can a corresponding Søderberg electrode due to its graphite core, but is free from the maximum size limitations of the graphite electrode. The support structure and control equipment is more complex than for either a prebaked or a Søderberg electrode, however.

4.1.7 Furnace Linings

The material of construction of the lining varies from process to process and is determined by considerations such as the operating temperature of the process and the chemistry of the contents of the furnace. Refractories are sophisticated technical ceramics that are tailored to suit the demands of high temperatures, thermal cycling, mechanical stresses, and chemical attack imposed by smelting processes. Although linings are, to a certain extent, consumable items with a finite life, the choice of an appropriate lining and careful attention to installation details is an important aspect of furnace construction due to the cost of the refractory material combined with the cost of the plant downtime required to reline a furnace and the potentially catastrophic nature of a lining failure. The most common constituents of refractory bricks and monolithics are magnesia (periclase), alumina (corundum), silica and chromite, in some cases in combination (e.g., chromia-magnesia bricks). Silicon carbide and carbon are also used. The materials used in various parts of the lining are chosen for their thermal properties as well as their resistance to thermal shock, resistance to wear, their mechanical strength, or their resistance to chemical attack by the processing. Lining wear is one of the major causes of furnace failure.

Refractories, like most other engineering materials, expand on heating and contract on cooling. This effect is more pronounced in the hotter regions of the furnace, and in particular in the hearth bricks. Differential expansion between the upper and lower surfaces of the hearth may cause the bricks to bow upward, to the extent that the denser molten metal may displace them. If the furnace lining is free to expand, gaps will form between individual bricks on cooling,

providing a path for metal or slag to run out of the furnace. If the lining is restrained against any movement, the force exerted on the shell by the refractory may be sufficient to damage the shell. This problem is usually overcome by accommodating a percentage of the expansion by a compressible material between the lining and the shell, usually carbon expansion paste or compressible refractory board, and by the use of expansion papers, which are inserted between bricks. As the lining is heated for the first time, the paper burns away and the bricks move into the gaps left by the paper. The balance of the expansion is constrained by the shell, which prevents the formation of gaps between bricks on cooling. A similar principle is employed in rectangular furnaces, except that the restraining force is applied to the lining by means of tension members such as tie rods and springs. A vertical force may be applied in a similar manner to reduce the formation of gaps between courses of bricks. This vertical force applied by springs has been applied to both rectangular and circular furnaces. The tensioning springs on a circular furnace are shown in Figure 4.19. The restraining force is sufficient to prevent the formation of gaps between bricks, but does not attempt to prevent thermal expansion of the lining.

4.1.8 Furnace Principal Operating Stages

The steps in the production of ferroalloys include preparation of the feed material, charging the furnace with feed, heating the feed material, reducing oxides to metal in the furnace, tapping metal, and tapping slag. This may be followed by further treatment of the metal and slag outside the furnace as well as cleaning of the exhaust gas.

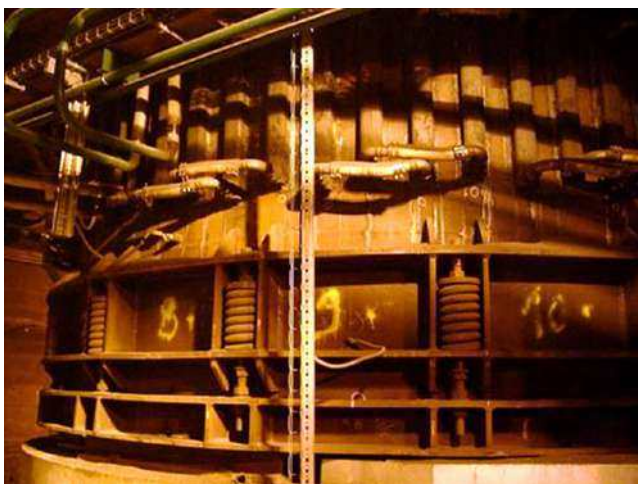


FIGURE 4.19 Tensioning springs on a furnace. (By permission of Tenova Pyromet, a division of Tenova Minerals [Pty] Ltd.)

The two extremes of furnace operation are batch mode and continuous operation. Few modern ferroalloy smelting furnaces operate in a pure batch mode where a batch of material is fed and processed, and all the metal and slag is tapped out of the furnace before more material is fed into the furnace. However, many posttapping processes, which take place in ladles or ladle furnaces, are true batch processes. In these processes, material is tapped from the furnace into the ladle furnace where it is kept warm by three electrodes whilst the conditioning process takes place. This may include blowing of oxygen and the introduction of minor alloying elements. Ladle furnaces are tapped by lifting the electrodes and tilting the entire furnace crucible once the metal conditioning phase is complete.

Most submerged arc furnaces operate in a semicontinuous mode. This is possible due to sophisticated furnace automation. The automated feed system delivers the chosen mix of feed materials into the furnace in batches based on the mass of each component at a suitable rate for the process and power setting of the furnace. In most furnaces, this means that there is a thick layer of solid feed material on top of the slag. This ensures that there is always sufficient material to efficiently absorb the heat generated by the electrodes as well as serving to protect the furnace roof and freeboard from radiation from the slag and electrodes.

The reduction process during which the raw material is converted into product and slag takes place while the furnace temperature is within a suitable range and while there is material to process. As the raw material is processed, the metal and slag levels rise. Metal and slag are tapped from the furnace at regular intervals, usually based on the number of kilowatt-hours absorbed supported by chemical analysis where relevant. The metal and slag levels inside the furnace cannot be measured directly. The amount tapped and the duration of the tapping cycle depends on the size of the furnace and the ladles. The height of the electrodes is regulated to accommodate the rising and falling slag level.

4.1.9 Furnace Control

The quality of the product and the life of the furnace crucible are enhanced when stable conditions are maintained within the furnace. A furnace operating in a stable manner exhibits very small variations in metal and slag temperature, electrode current, electrode resistance, and electrode immersion. In addition, the electrode currents and voltages are balanced. This leads to a more consistent quality of the product, consistent electrode quality, and a reduction in the number of electrode breaks (Braun et al., 1998).

Industrial process control systems are installed to automate the operation of the furnace and ancillary equipment. The plant is fitted with appropriate instrumentation to monitor and control the equipment. This instrumentation includes flow meters, thermocouples, level sensors, pressure sensors, limit switches, and comprehensive instrumentation of the electrical operating

parameters of the furnace and its auxiliaries. The output from these sensors is captured by a supervisory control and data acquisition (SCADA) system, which displays the state of each system on a computer screen in the control room and stores the data on a historian system, from where trends may be extracted. A programmable logic controller (PLC) is used to automate routine functions, such as feeding batches of raw materials, starting pumps, and shutting down systems. The PLC is also programmed to raise alarms when conditions exceed predetermined limits and to automatically initiate corrective actions such as shutting down a pump if the bearing temperature is too high or tripping the furnace electrical supply if the emergency stop button is pressed.

Many furnaces are equipped with an intelligent furnace control system in addition to the PLC. These systems contribute an additional degree of sophistication to the furnace automation, allowing automatic control of the furnace to a power (MW or MVA), current, or resistance set point as well as automating the slipping of electrodes. This is achieved by controlling the voltage on the electrodes and the resistance of the furnace circuit. The benefits of automatic furnace control include more stable furnace operation and enhanced electrode management, resulting in fewer electrode breakages and temperature fluctuations in the furnace. An example of a SCADA display summarizing furnace electrical parameters for a PLC-based furnace control module is shown in [Figure 4.20](#).

4.1.10 Processing Hazards and Risk Management

Smelting plants, and furnaces in particular, are fraught with potential safety hazards. The presence of bulk material handling equipment, high-voltage electrical systems, extremely high temperatures, and molten metals, as well as noxious and explosive gases, exacerbates the usual risks encountered in an industrial plant. Many of the hazards can, to a greater or lesser extent, be reduced by careful furnace design. Other hazards are managed by restricting access to certain areas; the application of electrical or mechanical interlocks, alarms, and emergency stop buttons; or the use of suitable personal protective equipment.

The active management of the risks associated with smelter operation—in order to provide a plant in which the safety of employees is maximized and damage to the environment is minimized—is an important responsibility of smelter management. To this end, the production of and strict adherence to safe operating procedures, the vigilant monitoring of process parameters and equipment condition, and regular furnace maintenance are of paramount importance.

4.1.10.1 Hazardous Gases

Carbon monoxide (CO) is produced during the reduction of metal oxides. It is toxic, and inhalation of the gas can cause death. For this reason, many furnaces are gas tight and are operated below atmospheric pressure to prevent leakage of



FIGURE 4.20 Typical screen for a PLC-based furnace control module. (By permission of Tenova Pyromet, a division of Tenova Minerals [Pty] Ltd.)

carbon monoxide. Access to the furnace is usually restricted while furnaces are in operation and CO monitors are often installed above the furnace roof. When it is necessary to enter an area where CO gas is likely to be present, a suitable CO monitor should be worn and accepted safety procedures for work of this nature should be followed.

In addition to its toxicity, CO gas is explosive at concentrations between 12% and 75% in air. It is flammable, with an auto-ignition temperature of 630°C. The gas-handling system is usually designed to prevent sparks, which could ignite the gas. The gas-handling system is also usually provided with rupture discs or other devices for preventing damage to the system in the event of an explosion or pressure surge.

Sulfur dioxide (SO₂) may also be produced if there is sulfur in the ore or if it is a product of the oxidation of sulfurous compounds, for example where sulfur is removed with gases in high-silicon alloys smelting via silicon sulfides. It is poisonous, but is not flammable. A respirator with suitable cartridges should be worn if this gas is present.

The volatiles contained in the pitch used as binders in Søderberg electrode paste are generally carcinogenic. Paste briquettes and cylinders should be

stored in well-ventilated spaces, and excessive exposure to these fumes should be avoided.

Additionally some other compounds might present safety and health hazard in some cases. The examples of this might be chromium (VI), nickel, manganese compounds, and nonmetallic impurities (As, F, Se, etc.) when particular ores are being treated. The fugitive emissions control of the smelting furnaces is continuously being improved (Gunnewiek et al., 2010).

4.1.10.2 Molten Metal and Slag

The temperature of the molten metal and slag contained in the furnace is in the range of 1200°C to 1800°C. Consequently, any activity involving handling of slag or metal is hazardous. It is usual to prevent access to areas near, below, or above the tap holes, launders, and ladles while tapping is in progress (Els et al., 2010). Operators performing lancing and tap hole plugging operations must wear suitable personal protective equipment, and respective safe working procedures should be enforced. Figure 4.21 shows an operator performing a manual tapping operation.

Access should also be restricted in areas where ladles containing metal or slag are transported or where the hot metal or slag is being cooled. Water used for quenching of ingots may boil and produce steam.

Both metal and slag can burn through the furnace, resulting in damage to equipment. Fires may start if flammable materials are in contact with molten slag or metal. Access to the base of the furnace is usually restricted, and measures should be in place to contain any spillages in order to prevent damage to personnel or equipment. Emergency procedures, including evacuation



FIGURE 4.21 Manual tapping operation. (By permission of Tenova Pyromet, a division of Tenova Minerals [Pty] Ltd.)

procedures, provision of escape routes and the provision of firefighting equipment, should be implemented.

4.1.10.3 Water

The presence of water near the furnace presents its own potential hazards. Water leaking into the furnace from the cooling system may rapidly turn to steam on contact with molten slag or metal, resulting in an explosion. Steam explosions inside furnaces can cause significant damage to the furnace roof, electrode column, and building. Similarly, explosions may occur if slag or metal splashes into water puddles near the launders or ladles or if there are leaks in water-cooled launder sections.

Slag and metal granulation systems are particularly vulnerable to explosions caused by changes in the ratio of metal or slag to water. Design features such as emergency water systems are implemented, as well as safety interlocks, which prevent the use of the granulation system in the event of a shortage of water.

4.1.10.4 High Voltage and High Current

It is usual to restrict access to the transformers and electrical switchgear while they are energized. When it is necessary to perform maintenance of high voltage (HV) or medium voltage (MV) equipment, elaborate safety interlock systems prevent accidental contact with live electrical parts.

The electrode columns carry large electrical currents during operation. Although they are electrically insulated from the building and furnace structure, which is not at the same electrical potential, the full length of the electrode is not usually insulated. It is usual to prohibit access to the furnace roof near the electrodes while the furnace is in operation by barricading the area. Bus bars and bus tubes are usually wrapped in insulating material in areas where accidental contact is possible. Caution should always be exercised when working near a furnace, as the furnace crucible may not be earthed, and the furnace may not be at the same potential as the building. Dust, feed material spillages, or other foreign objects may cause unintended current paths or accidental earthing of live parts.

4.1.10.5 Repairs and Maintenance

As a result of the restricted access to many parts of the furnace during operation, and the potential hazards, routine furnace maintenance presents a more complex problem than on many industrial plants. Thoughtful furnace design such as the provision of redundant equipment such as a duty and a standby pump and the provision of access points for lifting gear can improve the ease of maintenance of the facility to some extent. In spite of the challenges faced by maintenance personnel, routine inspection, preventive maintenance, and the timely repair of equipment will contribute significantly to the safe and

efficient operation of the furnace as well as the attainment of its desired availability.

Regular visual inspections of the plant by operating staff in the course of their normal duties are an important mechanism for maintaining a healthy furnace. In particular, the identification, investigation, and repair of faulty instrumentation will enhance the ability of the automated control systems to control the furnace in a stable manner and may be critical to the safety of personnel in the event of an emergency situation such as a furnace runout. In particular, all alarms registered by the control system should be investigated. The number of alarm signals generated by the control system should be optimized in order to alert control room staff to important issues without inundating them with nuisance warnings. In a similar manner, water leaks and other minor equipment malfunctions should be reported in a timely manner and their severity assessed to determine the optimal scheduling for maintenance activities.

Many furnaces are powered down for short periods on a regular schedule to provide opportunities for routine maintenance tasks, which cannot be performed while the furnace is live. When electrical power to the furnace is switched off, the furnace begins to cool slowly. As the furnace cools, the refractory lining cools and the electrodes cool from the outside inward. This cooling causes thermal stress in these brittle materials and causing gaps to open between individual bricks as they shrink. The duration of a furnace shutdown is therefore limited to the shortest time in which the required work may be done. A shutdown of up to 4 hours usually has no effect on the lining or electrodes, whereas longer shutdowns require more careful management. Cold shutdowns, where the furnace is drained and allowed to cool, are required if major repairs are to be performed. The furnace must be heated slowly until it reaches its operating temperature after such a shutdown.

Very little routine maintenance is required on the furnace crucible itself. Routine tapping channel replacement, particularly on metal tap holes, is performed regularly. In some furnaces, the outer tapping blocks are replaced on a weekly basis. The procedure becomes more complex when the repair goes deeper into the furnace. Replacement of the entire tapping channel usually requires a cold shutdown, which may extend to several days.

Repairs to electrode or transformer equipment require a complete shutdown and extensive electrical isolation of components. It is not necessary for the furnace to be cold, as these parts are all situated outside the furnace. However, if there is the danger of CO gas above the furnace roof, appropriate precautions must be taken to ensure that the environment is safe before maintenance staff can access the furnace roof.

Routine relining of refractory lined launders may be performed between tapping and does not necessitate powering down the furnace. Other routine maintenance tasks, such as cleaning filters and servicing pumps, can be performed while the furnace is in use.

4.2 EQUIPMENT FOR FURNACE FEED PROCESSING

The efficiency of some processes can be significantly enhanced by proper partial processing of the feed material before it enters the furnace. This may be accomplished by three broad categories of activity, namely agglomeration of fines, prereduction of ore, and preheating of raw material. One or more of these techniques may be applied to the same stream of feed material. Various techniques exist for agglomerating fine material into pellets, which are more easily processed in the furnace. A number of prereduction processes have been developed in which the reduction of the ore begins in the solid-state reaction prior to the material entering the furnace. Preheating often utilizes the calorific value of the CO in the off-gas stream to improve the energy efficiency of the furnace.

Ferromanganese and silicomanganese raw material may successfully be pretreated by sintering the ores into a sinter cake. Ferrochrome ore fines may be briquetted in a cold process, or pelletized. The feed may successfully be pre-reduced and fed into the furnace while it is hot. In addition, the feed, either lumpy or briquetted, may be preheated without a prereduction step. Quartzite, the raw material for silicon metal production, is unsuitable for agglomeration and preheating. However, as the silicon metal smelting process in the furnace is not as easily disrupted by fine feed material as other processes, fine material may be fed directly into the furnace.

Whether or not a particular pretreatment process will be effective in a particular context is heavily dependent on the mineralogy of the ore. It is usual to conduct extensive laboratory tests on a particular ore to determine whether it can successfully be agglomerated or whether it can effectively be prereduced.

4.2.1 Agglomeration

The raw material for the smelting of ferrochrome, ferromanganese, silicomanganese, and other ferroalloys in submerged arc furnaces is preferably lumpy (i.e., the particle size of the feed is 25 to 150 mm). In these processes, a small amount of fine material (particle size less than 6 mm) may be introduced into the furnace. However, if too much fine material is introduced, it reduces the permeability of the charge, which prevents the release of CO gas and may cause pressure excursions inside the furnace. A certain amount of fine material is generated by attrition of the lumps of ore in the raw material handling system. This excess fine material, which contains valuable minerals, cannot be processed directly and is wasted unless it can be agglomerated.

Ferrochrome fines may be agglomerated by means of a briquetting process or by the making of sintered pellets. The resulting briquettes or pellets are required to exhibit a high cold strength, so that they do not crumble during handling and do not disintegrate when dropped into an arc furnace, as well as a high hot strength, so that they do not crumble prematurely on heating. The briquetting or sintering process is not accompanied by prereduction of the ore.

Ferromanganese and silicomanganese ore fines may be agglomerated as sintered pellets in a similar manner to ferrochrome. However, it is more usual to pass the material through a sintering machine and produce a sinter cake.

4.2.1.1 *Briquetting*

In the briquetting plant, chromite ore fines are dried in a rotary dryer and stored in a silo. The dry ore is discharged into a mixer, where it is mixed with suitable binders. Each component enters the mixer from a bin fitted with weighing equipment in order to achieve the correct proportions in the mix. From the mixer, the material is fed into a double roll briquetting press where it is pressed into small pillow-shaped molds. Briquettes have typical dimensions of the order of 50 mm. The green briquettes are released from the molds and conveyed to a curing shed, where they are allowed to cure for a period of time, typically 24 to 48 hours. The cured briquettes are fed into the prereduction kiln, preheater, or furnace in the same way as the lumpy ore.

Various organic and inorganic binders may be employed. The most common binding material is a mixture of lime and molasses. However, various cements and resins, fuel oil, molasses, starch, dextrin, hydrated lime, bentonite, and sodium silicate have been used. The purpose of the binder is to glue the fine ore particles together in order to obtain the desired cold and hot strength. The cold strength of a briquette is a measure of its ability to resist crumbling during handling before it has cured, whereas the hot strength is a measure of the resistance to crumbling, chipping, or fracture in the raw material handling system of the furnace and, in particular, in the feed chutes and as the material drops into the furnace. As binders are consumed in the process and therefore do not add value directly to the final product, they must also be relatively inexpensive and easy to obtain. In addition, they must not introduce any undesirable trace elements into the furnace. The success of the briquetting process depends on the identification of a binder which provides optimal properties for a particular ore. Wear of the briquetting molds as a result of the abrasive nature of the ore can be a significant cost to the briquetting operation.

4.2.1.2 *Production of Sintered Pellets*

Chromite ore with a small amount of coke is ground wet in a ball mill, after which the resulting slurry is de-watered. It is mixed with a binder before being fed into a rotating drum or disc pelletizer, where it forms balls. Pelletizing occurs due to the rolling motion of the pelletizer without the application of pressure. The fines adhere to each other because of the moisture. The green pellets are screened to select the required size. Undersized particles are returned to the inlet of the pelletizer.

Green pellets are charged into a sintering furnace, which may be a vertical shaft furnace, although horizontal traveling grate sintering furnaces where the pellets are conveyed on a perforated steel belt are more common. After the raw

pellets enter the furnace, they are heated gradually to between 300°C and 350°C, which removes the water from the pellets and allows the binding material to form chemical bonds. The heat required for this operation is obtained from hot air, which is drawn through the grate past the pellets. As the pellets progress into the furnace, the temperature is increased to the sintering temperature of 1250°C to 1350°C where the metallic ores are fused together. Heat for this stage of the process is supplied by gas burners and the coke. Waste CO gas from the submerged arc furnace or natural gas or liquefied petroleum gas may be used. As the pellets move through the downstream section of the furnace they are cooled. The sintering furnace operates as a counterflow heat exchanger. Cold air enters the sintering furnace in the cooling section, where it is drawn through the grate and past the pellets, thereby cooling them. After cooling the pellets, the gas flows into the heating section where heat is transferred to the pellets. The sinter furnace operates at a negative pressure, with airflow driven by induced draft fans. The exhaust gas is cleaned in a venturi scrubber, cyclone, or bag filter plant after leaving the furnace. Dust is returned to the sinter plant feed system. Pellets are discharged onto a conveyor that takes the sintered pellets past a series of screens to the storage bins. Undersized pellets are returned to the sinter plant feed system. Sintered pellets may be used as feed for kiln prerduction, fed into a preheater, or fed directly into the furnace.

4.2.2 Sintering of Manganese Ore

The sintering process employed for manganese ore and the siliceous ores used to produce silicomanganese results in partial reduction of MnO₂, Mn₂O₃, and Mn₃O₄ in the ore to MnO by reaction with carbon in addition to agglomerating the fine ore and coke. New technology also utilizes addition of fluxes, such as magnesia-rich components, to improve mineral composition of the sinter and increase manganese reduction efficiency (Kutsyn et al., 2012). The energy released by this exothermic reaction is utilized to drive the sintering process. The use of sinter cake as a portion of the furnace feed leads to improved furnace performance, as the bed is more stable and less prone to eruptions. Additional benefits include reduced power consumption and improved manganese recovery as well as the ability to utilize fine material, which would otherwise have gone to waste.

In the sinter plant, raw material such as ore fines, coke or coal, dust from the furnace off-gas system, and binding material are discharged from feed bins in the correct proportions through weigh feeders and conveyed to a blending system. The raw materials are blended in a rotating mixing drum. Undersized material from the sinter process is added to the mixing drum. Moisture is added by means of fine sprays to promote agglomeration of the materials. This process is known as nodulizing.

The sinter strand is an endless chain of unlinked pallet cars, which are made of a wear-resistant material. The base of a pallet is slotted to allow air to

pass through the sinter bed. Sidewall plates prevent material from falling off the sides. The pallet cars are pushed along the frame of the sinter machine on wheels, driven by a series of drive sprockets mounted on the sides of the machine, which engage on the wheels of the cars. The drive mechanism is usually located at the cold end of the sinter machine. When the pallet cars reach the end of the sinter machine, they are driven around the discharge section by a second set of drive sprockets and return on the underside of the machine. A tensioning mechanism is provided to compensate for thermal expansion.

Two streams of material are fed onto the sinter strand, a hearth layer (made of sinter returns sized between 6 and 15 mm) and the sinter mix, which is placed on top of the hearth layer by a roll feeder with a leveling plough. The sinter strand passes below an ignition arch where the carbon in the mix is ignited by means of fuel oil, gas, or furnace off-gas. The exothermic reaction by which the higher manganese oxides are reduced to MnO in the presence of carbon and air provides further energy to drive the sintering of the feed. The sinter burns through vertically while the bed moves horizontally toward the discharge end. Air or a mixture of hot CO-laden furnace off-gas and dilution air is drawn through the pallets by induced draft fans. The sinter cake attains a temperature of about 850°C after sintering.

After the sintering process is complete, the sinter cake is cooled. Cooling may occur on the sinter strand, or the material may be discharged off the sinter strand onto a crash deck and into a spiked roll crusher, which reduces the lumps of sinter cake to a size smaller than 150 mm, prior to discharging the lumps onto a dedicated cooling strand. In both cases, cooling is performed by forcing ambient air through the material from below. The cooling area is supplied with its own fans and wind boxes. The sinter cake cools to a temperature of less than 100°C at the end of the strand.

After on-strand cooling, when the material reaches the end of the sinter strand, the material is discharged off the pallet cars onto a crash deck, which guides the sintered material into the spiked roll crusher. As the crash-deck is subject to severe impact and abrasion, it is lined with wear-resistant material. The finger crusher reduces the lumps of sinter cake to a size smaller than 150 mm. From the spiked roll (finger) crusher the sinter cake passes over a 75-mm screen, the oversized material being crushed in a roll crusher to less than 75 mm. The material then passes on to a further screening system, where the product is separated into return fines, the hearth layer, and the sinter product. The return fines are conveyed back to the sinter feed mixing drum, while the sinter product is conveyed to the day bins for the furnace.

Dust in the waste gas from sintering is removed using an electrostatic precipitator, whereas dust from the on-strand cooling is removed in cyclones. Dust from the raw material handling system is removed in a bag filter. This dust is returned to the sinter feed mixing drum for recycling.

4.2.3 Preheating

In ferrochrome smelting in closed furnaces, the feed material may be preheated before it enters the furnace. Lumpy ore, briquettes, sintered pellets, and pre-reduced pellets may all be preheated successfully. The energy used to preheat the feed material comes from the combustible CO contained in the furnace exhaust gas.

A number of different preheating technologies exist, although all operate on the same principle. Rotary kilns have been used for preheating ore and pellets. However, the availability of the rotary kiln is generally lower than that of the furnace. Preheating is therefore more generally performed in a shaft kiln situated above the furnace. A single shaft kiln may be employed, or multiple shaft kiln preheaters may be used, each processing a portion of the feed material. The shaft kiln has an integral surge bin, thereby providing a buffer between raw material feed and smelting. The preheater discharges into the feed chutes and thence directly into the furnace.

A three-dimensional view of a preheating system employing three preheater shaft kilns is shown in [Figure 4.22](#). Each kiln receives raw material feed from a feed bin, which is fitted with level indicators to continuously monitor the level of the feed material in the bin, and a position switch to stop the rotary conveyor at the specific bin when loading the feed material into the bin.

Quenched and scrubbed furnace exhaust gas passes through a booster fan (which provides the required volume flow and pressure) to the preheater



FIGURE 4.22 Ferrochrome preheating system located above the furnace. (By permission of Tenova Pyromet, a division of Tenova Minerals [Pty] Ltd.)

combustion chamber, where it is mixed with additional fresh air, supplying oxygen required to burn the gas. The CO gas is burned, after which it passes through the feed mix to heat the feed. Some of the exhaust gas from the preheater vessels is recirculated and mixed with the hot gas as it passes over the feed mix. The amount of furnace exhaust gas, fresh air, and recirculated gas is controlled in order to obtain the required temperature of the feed material. The exhaust gas from the preheater is cleaned in a venturi scrubber before being recirculated back to the combustion chamber or exhausted to the atmosphere. The temperature of the feed discharge from the preheater may be between 500°C and 700°C, although it is usually controlled in a much smaller range. The preheated raw materials are choke-fed into the furnace through a number of feed chutes. Each feed chute is fitted with a hydraulically operated rod gate, which is used to ensure that the feed chute remains full of material at all times to maintain the gas seal on the furnace.

The preheating of the furnace feed material reduces the power required for smelting inside the furnace, substantially reducing the specific power consumption of the process. In addition, any moisture contained in the feed material is removed prior to the material entering the furnace. This further reduces the specific power consumption and results in more stable furnace operation. The utilization of the calorific value contained within the CO gas further improves the overall energy balance of the process. The burning of the CO gas to heat the incoming material represents an efficient way of utilizing this energy whilst safely disposing of the noxious CO gas.

4.2.4 Prereduction

Prereduction refers to any partial reduction of the ore that is performed as a processing step prior to the feed mix entering the furnace. The sintering of manganese and silicomanganese ores is, to some extent, a prereduction process, as MnO₂ is reduced to MnO. In ferrochrome smelting, chromite ores may successfully be prereduced using a number of similar technologies, employing either a rotary kiln or a rotary hearth furnace. Up to 30% of the chromium and 90% of the iron may be reduced in this manner.

The prereduction processes used in the processing of ferrochrome start with the production of pellets. In the rotary kiln technology, sintered pellets containing ore, reductants, and fluxes enter the kiln where they are heated to 1450°C, at which temperature some of the chromite and much of the iron is reduced. Hot prereduced pellets are discharged into the furnace.

In the rotary hearth furnace prereduction technology, ore, reductants, and fluxes are milled to less than 100 µm before being blended, mixed, and fed into a pelletizing plant. The green pellets are dried using exhaust gas from the rotary hearth furnace. The pellets are sintered, reduced, and cooled in controlled zones with a maximum zone temperature of 1450°C in the rotary hearth furnace. The reduction occurs in stages in the different zones. Additional hot air is

introduced into the rotary hearth furnace to control the temperature and the composition of the atmosphere in order to provide conditions conducive to the optimal reduction of chromium and iron oxides and minimization of reoxidation of the metals. Once the material has passed through the rotary hearth furnace, it is discharged onto a steel belt cooler. The cooler operates under a nitrogen-rich atmosphere, which prevents the pellets from reoxidizing and cools the pellets to approximately 600°C before they are discharged onto a second steel belt cooler, which further cools the pellets to between 100° to 150°C. The finished product is conveyed and stored in an enclosed section of the furnace raw material bunkers. These pellets may be preheated or they may be fed cold into the submerged arc furnace. Energy for the sintering and pre-reduction process is provided by the oxidation of the CO in the exhaust gas of the submerged arc furnace.

4.3 DOWNSTREAM PROCESSING

After the hot metal is tapped from the furnace into a ladle, it may be refined therein, after which it is cast and sized before being dispatched to the customer.

4.3.1 Refining

Ladle refining of ferroalloys is performed by injecting gas into the ladle to adjust the chemical composition of the product. This may be done from above using a lance, or it may be done from below through a porous refractory plug situated at the base of the ladle. The gas may be air or oxygen or a combination of the two gases. In silicon metal production, this process reduces the calcium and aluminum contents.

4.3.2 Casting

The traditional method of solidifying the metal is to cast it into molds where it is allowed to cool slowly. The molds may simply be a casting bed of metal fines shaped to form molds. Alternatively, cast iron molds may be used. The casting bed is arranged on an incline so that metal from the ladle passes down a runner from where it cascades into the molds. Once cast into the molds, the metal is allowed to cool. It may be allowed to cool naturally, or it may be sprayed with water to cool it more rapidly. [Figure 4.23](#) shows the tapping of alloy into a series of molds.

A more sophisticated casting system employs cast iron molds arranged in a casting line, which moves past the ladle placed in a tilting station. The iron molds may be lined with a layer of metal fines to protect them from thermal shock induced by the rapid contact with molten metal. The layer of fines should be sufficiently thick to prevent contamination of the product by the mold and to allow easy removal of the solidified ingot. Once cast into the



FIGURE 4.23 Tapping of FeCr into molds directly from the tap hole. (By permission of Tenova Pyromet, a division of Tenova Minerals [Pty] Ltd.)

molds, the metal is sprayed with water to cool it more rapidly as it travels on an incline. When each mold reaches the top of the incline, the solid ingot or pig falls into a bin, breaking up as it does so. In some applications, the metal is kept in the iron mold only for the time needed for the surface to solidify sufficiently for it to hold its shape, after which it is de-molded and spray cooled. The residence time of the metal in the mold is typically 30 minutes. This practice reduces wear on the iron molds. Once the metal is sufficiently cold, it is crushed. The first stage of crushing often involves breaking the ingots into smaller sizes using a jackhammer, after which the pieces are sent to a crusher, usually a jaw crusher followed by a roll crusher. The crushed material is classified into the required sizes prior to dispatch. The crushing process is both capital and labor intensive and does not add much value. In addition, it produces fines, which have a lower market value than the larger pieces. The fines may be recycled into the furnace, used as molds, or stockpiled.

Some metals, such as silicon, ferrosilicon, ferrochrome, and ferronickel, may be granulated in water in preference to casting and crushing. During the granulation process, the hot metal is poured into a large amount of cold water, which breaks it up into droplets, which rapidly solidify. This may be achieved by pouring the metal into a jet of water at high pressure or by pouring the metal onto a water-cooled disc or a refractory brick, from where the resulting droplets fall into a tank of cold water. Control of the water to metal ratio is critical for the safe operation of the equipment and can typically be in the region of 20:1 or more. The essence of the granulation process is the rapid removal of heat from the molten metal. Loss of granulation water or any

accumulation of hot metal can result in steam explosions, which may cause damage to equipment and danger to personnel. The granulation process releases steam and might also release hydrogen gas. The metal granules are dewatered and dried, after which they are classified and dispatched to the customer. They do not require further crushing. The particle size produced by granulation may be varied by adjusting the operating parameters of the granulation system, but it is also dependent on the composition of the metal and the trace elements present in the metal being granulated. Ferrosilicon and ferrochrome may produce granules in the 20- 30-mm range, whereas silicon metal can be produced in granules up to 20 mm. Atomizing is also used to produce ferrosilicon powder. Ferromanganese and silicomanganese are generally unsuitable for granulation.

Thin layer casting of silicon metal and ferrosilicon is a different approach in which the molten metal is cast by pouring a thin layer up to 100 mm thick onto a water-cooled copper plate, where it begins to solidify rapidly. One of the available technologies uses a cooled vibrating copper table for the first stage of cooling, from where the material is discharged onto two vibrating iron tables placed in series, where it begins to break up as it cools. The competing technology utilizes a cooled copper plate in the form of a rotating carousel. The material is solid within 60 seconds of casting. Once the material leaves the casting table or carousel, it is cold enough to pass to the sizing equipment. No crushing is required as it breaks up during the cooling process.

The microstructure of a metal is affected by the rate at which it is cooled. In general, the faster it is cooled, the smaller the grain size, and the more homogeneous the metal, as impurities do not have time to congregate in the areas which solidify last. A further consequence of the rapid cooling and small grain sizes is that the material particles are less brittle, with a resulting reduction in the percentage of fines produced and improved resistance to disintegration during handling in downstream processes. In addition, there are economic benefits to the elimination of the crushing operation.

Slag is tapped from the furnace in quantities equal to or greater than the metal produced and therefore presents a material-handling problem of a similar nature and size to that of the metal. The simplest method of slag disposal is to empty the ladle into a slag pit, where the slag is allowed to cool naturally. Once it is solid, it is removed by means of a crane or front-end loader and taken to a crushing plant. Slag is often processed in a metal recovery plant, where entrained metal particles are removed by jiggling, after which it may be dumped on a stockpile or it may be used in refractory bricks or as an aggregate in concrete or as filling material for road construction or similar applications. Granulation of slag is a viable alternative to casting and crushing. It solidifies and breaks up the material in one step, reducing handling. Slag processed in this manner is in a suitable form for the recovery of entrapped metal.

4.4 OTHER FURNACES FOR FERROALLOYS PROCESSING

A special class of furnaces is used for production of ferroalloys using reduction by silicon. Such ferroalloys (refined ferrochrome, low-carbon ferromanganese, manganese metal, etc.) have limiting carbon (and sometimes iron) content, which restricts the use of self-baked electrodes. An example of such a furnace for smelting of metallic manganese is shown in Figure 4.24 (Gasik et al., 2009).

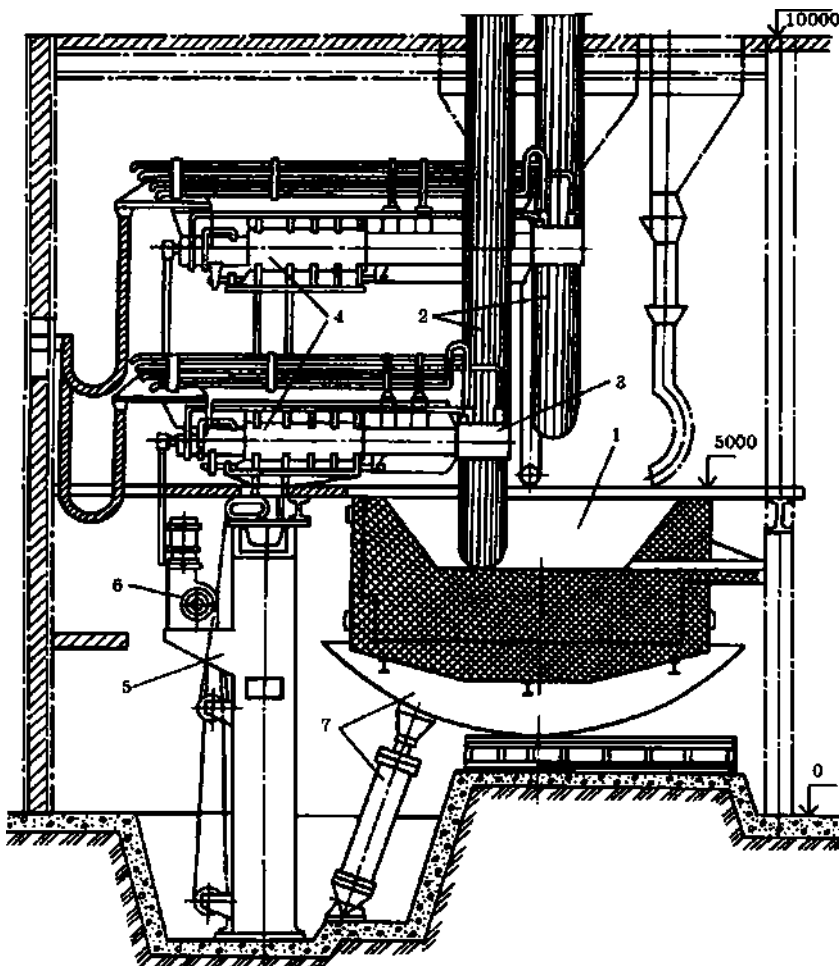


FIGURE 4.24 General view of the refining furnace for smelting of metal manganese (>95% Mn). 1, hearth; 2, graphitized electrodes; 3, contact device; 4, electrode holder shoulder; 5, telescopic support; 6, lifting mechanism; 7, tilting mechanism. Height marks are in mm. (By permission of Gasik et al., 2009.)

Known as *refining furnaces*, these furnaces usually operate at low power, typically less than 10MVA, and without an arc, in the resistance mode. Magnesia lining is the common feature, and the process is usually periodic. A similar type of furnace is employed for aluminum reduction processes (chromium metal, low-carbon FeCr, FeTi, FeNb, etc.), where the exothermic release of the heat of reaction of metal oxides with aluminum is not sufficient to melt the charge and the alloy, and some external heat supply is required.

Where the exothermic release of heat is sufficient, for example, in processing of ferromolybdenum by reduction with aluminum and silicon, the process might be carried without furnace. In this case the reactor is of a refractory-lined shaft type, which works periodically and is opened or disassembled after each heat (Gasik et al., 2009). The charge is loaded into the shaft (Fig. 4.25), located at the top of a sand bed with a space left (the receiver) for liquid metal.

There are also different types of hearth, such as tilting or water-cooled ones, for smelting of special ferroalloys and master alloys. The benefits of their use are simplicity and the possibility of processing melts with low impurities levels. However, the application of such off-furnace technologies is naturally limited to mixtures which can be exothermally reduced with a sufficient amount of heat being released. Sometimes they are combined with external heating or ignition by the top two or three electrodes.

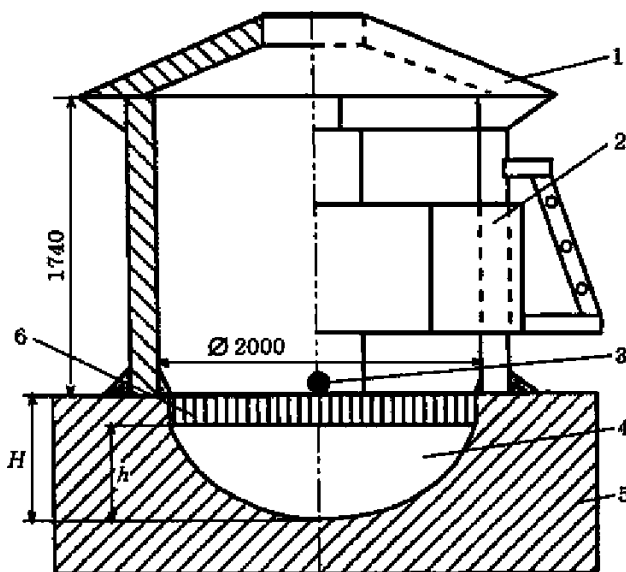


FIGURE 4.25 Smelting shaft for ferromolybdenum production. 1, shaft cover; 2, charge; 3, tapping hole; 4, metal ingot; 5, sand bed; 6, over-ingot slag; H, the height of the metal receiver; h, the height of the metal ingot. Dimensions are in mm. (By permission of Gasik et al., 2009.)

ACKNOWLEDGMENTS

The author wishes to acknowledge the assistance received from Mr. R. Bruce Nourse, Mr. Alec Jamieson, and other colleagues at Tenova Pyromet.

REFERENCES

- Andreae, F.V., 1935. The reactance of large rectangular three-phase electric furnaces. *Journal of the Electrochemical Society* 67 (1), 151–168.
- Andreae, F.V., 1950. Design and control of ferroalloy furnaces. *Transactions of the American Institute of Electrical Engineers* 69, 557–562.
- Barker, I.J., 2011. Some considerations on future developments in ferro-alloy furnaces. *Journal of the South African Institute of Mining and Metallurgy* 111 (10), 691–696.
- Braun, W., Nettleton, T., Jamieson, A., 1998. Advanced Furnace Control. In: Proceedings of Congress INFACON 8. China, Beijing, pp. 332–336.
- Els, L., Coetzee, C., Vorster, O., 2010. Design of Tapping Fume Extraction Systems for Ferroalloy Furnaces. In: Proceedings of Congress INFACON-XII. Helsinki, Finland, pp. 131–141.
- Gasik, M.I., 1984. Electrodes for ore-reduction furnaces, second edition. Metallurgia, Moscow, 248 pp.
- Gasik, M.I., Lyakishev, N.P., Gasik, M.M., 2009. Physical Chemistry and Technology of Ferroalloys [in Ukrainian]. Dnipropetrovsk: Sistemnye Tehnologii, 494 pp.
- Gladkih, V.A., Gasik, M.I., Ovcharuk, A.N., Proidak, Yu.S., 2007. Electric Furnaces for Ferroalloys [in Russian]. Dnipropetrovsk: Sistemnye Tekhnologii, 295 pp.
- Gunnewiek, L., Ravary, B., Cowx, P., Woloshyn, J., 2010. Continuous Improvement for Fugitive Emissions Control. In: Proceedings of Congress INFACON-XII. Helsinki, Finland, pp. 121–129.
- Kelly, W.M., 1958. Design and construction of the submerged arc furnace. *Carbon and Graphite News*, Union Carbide, 5, No. 1.
- Kutsyn, V.S., Gasik, M.M., Gasik, M.I., 2012. Thermodynamic computer modeling of phase transformations in complex oxide systems, equivalent to manganese agglomerates made by existing and developed technologies. *Metallurgical and Mining Industry* 4 (3), 16–24.
- Westly, J., 1974. Resistance and Heat Distribution in a Submerged-arc Furnace. In: Proceedings of the First International Ferroalloys Congress (INFACON), South African Institute of Mining and Metallurgy. Johannesburg, South Africa, pp. 121–127.

Electric and Thermal Operations of Furnaces for Ferroalloys Production

Gudrun Saevarsdottir

Reykjavik University, Reykjavik, Iceland

Chapter Outline

5.1 Introduction to Furnace Operations for Ferroalloys Processing	139	5.4.2 Electric Arc Models	156
		5.4.3 Resistive Heating	160
		5.4.4 Current Paths and Distribution of Heat Dissipation	162
5.2 Basics of Electric Circuit Theory	140	5.5 Electric Operations and Control of the Furnace	165
5.2.1 Direct and Alternating Current and Voltage	140	5.5.1 Power Control	166
5.2.2 Resistive Circuits	143	5.5.2 Electrode Control	166
5.2.3 Reactance Circuits	143	5.6 Environmental Issues of Ferroalloys Furnace Operations	170
5.2.4 Impedance and Power in AC Circuits	145	5.6.1 Particulates Emissions	170
5.3 Ferroalloy Smelting Furnaces as Electrical Circuits	147	5.6.2 Gaseous Emissions	173
5.3.1 DC Furnaces	147	5.6.3 Heat Emissions and Losses	174
5.3.2 AC Furnaces	148	References	174
5.4 Modes of Heat Dissipation in Furnaces	153		
5.4.1 Electric Arc	153		

5.1 INTRODUCTION TO FURNACE OPERATIONS FOR FERROALLOYS PROCESSING

Ferroalloys are produced in several types of furnaces, depending on the chemistry as well as the thermal and electrical parameters of the specific process. The

most used are submerged arc furnaces (SAFs) and resistance-heating furnaces (RHF), where heating of the charge, slag, and alloy proceeds by the application of electric current. In these electric furnaces, the tips of electrodes protrude into the furnace hearth and become hidden by a burden (charge) of raw materials, which have been fed into the furnace from the top. The burden typically is partially transformed by chemical reactions appropriate for the respective reaction zones in the furnace at the local temperature and pressure. The main difference between SAFs and RHF is whether or not an electric arc is present at the tip or along the side of the electrode. For example, in silicon and ferrosilicon production, the temperature required for the process to run with an acceptable silicon yield is above 1900°C. This requires an intense heat source and therefore dictates the formation of an electric arc, rather than heating by ohmic resistance (joule heating). The latter proceeds when electric current is conducted through the charge or slag surrounding the electrodes. Several ferroalloys smelting processes do not require an arc in order to reach the necessary thermodynamic conditions, but in many cases there are strong indications that an arc may nevertheless be present, such as in ferrochromium or ferromanganese production.

As the sole purpose of the electric current passing through the SAF is to release heat to fuel the chemical processes in the furnace, the current can be either AC or DC. The most common configuration for an industrial scale furnace is three-phase AC, where three electrodes are embedded into the furnace raw material charge. Three AC-current phases separated by a phase shift of 120° pass through the respective electrodes and cancel out at a star point located in the center of the furnace. One phase AC is used mostly in smaller laboratory or pilot scale furnaces, and it requires a top and a bottom electrode. DC furnaces also require a bottom electrode in addition to the consumable electrode from the top. Both small scale and large industrial scale DC furnaces are in operation around the world.

An extensive description of the design of SAFs and RHF, along with the associated subprocesses, is presented in Chapter 4. This chapter describes in more detail the electrical operation of the furnace with the goal of creating the optimal thermal conditions, and it provides a complementary analysis of the environmental effects.

Before addressing the electric particularities for different furnace designs, a brief introduction to electric circuit theory as relevant to understand the furnace circuit is given. Even though electric arcs will distort the sinusoidal current and voltage waveforms, for practical purposes of furnace circuit analysis this will be minimal and the treatment described here can be considered generic and applicable to all submerged arc furnaces.

5.2 BASICS OF ELECTRIC CIRCUIT THEORY

5.2.1 Direct and Alternating Current and Voltage

Any electric network consists of electrical elements such as voltage and current sources, resistors, inductors, capacitors, transmission lines, switches,

transformers, and other electrical equipment. An electric circuit is an electric network where all components are connected into a closed system so that the current will have a return path (Schultz, 2006). Real electrical systems show complicated responses to different types of current and voltage input because of the formation of electric and magnetic fields. The properties of electric systems that can be attributed to these physical phenomena are called reactance. In the analysis of real circuits, a simplifying assumption is made by assuming that these properties are lumped into simple electrical elements such as inductors and capacitors.

Electric current is the flow of electric charge through a conductive medium and has the units of charge pr. time unit. The SI unit for electric current is ampere (A), which is equivalent to 1 coulomb of charge passing per one second. Time invariant current is called direct current (DC). A common convention for DC current, which is applied here, is to denote the current by I . A periodic, time-dependent current, where the flow of moving charges is periodically reversed, is termed alternating current (AC). The most commonly applied AC form is using a periodic sinusoidal form. Other AC current waveforms occur in special applications, but a sinusoidal AC waveform is the form in which electric power is produced and delivered to homes and businesses, and this type of current is considered further in this chapter (Schultz, 2006). Deviations are due to nonlinear components such as the electric arcs found in submerged arc furnaces.

Sinusoidal AC and voltage can be written as

$$i(t) = I_0 \sin(\omega t + \phi_i), \quad u(t) = U_0 \sin(\omega t + \phi_u), \quad (1)$$

where t is time, I_0 and U_0 are the maximum values (amplitude) of current and voltage, ω is the angular frequency derived from the frequency f of the AC ($\omega = 2\pi \cdot f$), and ϕ_i and ϕ_u are the phase angles for the current and voltage, respectively, and describe current and voltage values at zero time (Fig. 5.1). The period of AC repetition is $\tau = 1/f$ (e.g., for 50 Hz frequency of standard electricity supply, the period of one oscillation will be 20 ms). In resistive circuits that have no reactance, the phase angles are identical for current and voltage. In the presence of unbalanced reactance, they are not, as the voltage is phase-shifted with respect to the current.

The $i(t)$ and $u(t)$ are the real current and voltage values as a function of time. In the analysis of electrical circuits, it is convenient for mathematical purposes to use complex notation to describe the cyclic circulation of i and u . As harmonic functions are often represented in circular form, a vector corresponding to an instant value of either current or voltage might be written using Euler's formula:

$$i(t) = I_0(\cos(\omega t + \phi_i) + j\sin(\omega t + \phi_i)) = I_0 e^{j(\omega t + \phi_i)}, \quad (2a)$$

$$u(t) = U_0(\cos(\omega t + \phi_u) + j\sin(\omega t + \phi_u)) = U_0 e^{j(\omega t + \phi_u)}, \quad (2b)$$

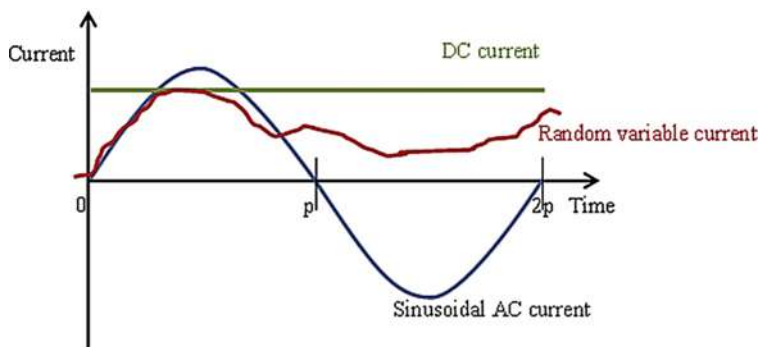


FIGURE 5.1 Examples of DC, sinusoidal AC (with a period of $2p$), and random current plots.

where $j^2 = -1$ is the imaginary unit. The imaginary parts of the current and voltage do not have a physical manifestation, but they are defined to simplify the mathematical analysis of the system (Schultz, 2006). They allow current and voltage to be displayed in a form of so-called phasors, as illustrated in Figure 5.2. When phase shifts of current and voltage are different, current and voltage vectors are rotating with a constant angle difference between them (Fig. 5.3).

The acting value of current and voltage, also known as the root mean square (RMS) value, is defined as an integral of half-period divided by the half-period

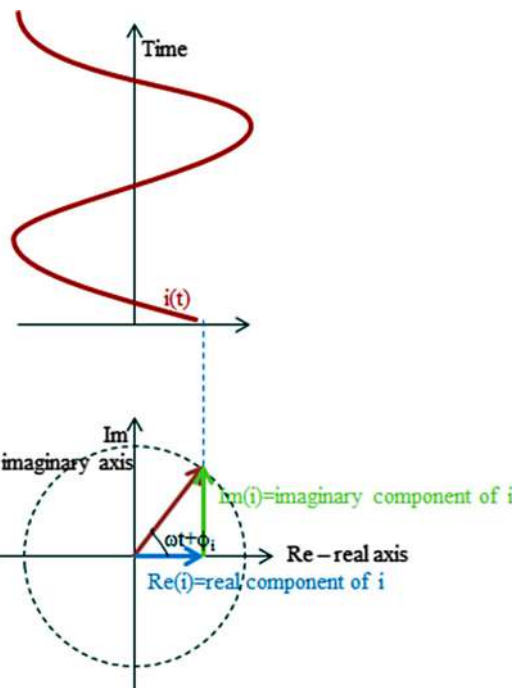


FIGURE 5.2 Illustration of a phasor representation of AC with a sinusoidal waveform.

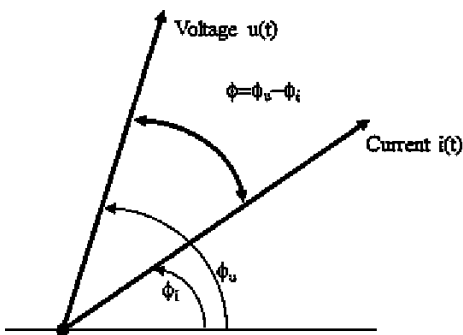


FIGURE 5.3 Illustration of the phase angle difference between AC and voltage.

time (p ; see Fig. 5.1), which for a sinusoidal waveform is $U_{RMS} = U_0/\sqrt{2}$, $I_{RMS} = I_0/\sqrt{2}$. Using this RMS value it is possible to denote the relation between alternative current, voltage, and power in a way that is analogous to the DC representation. Another more compact shorthand notation of the Euler representation of the current and voltage is $i(t) = I_{RMS} \angle \phi_i$, $u(t) = U_{RMS} \angle \phi_u$.

5.2.2 Resistive Circuits

The simplest form of an electric circuit is the resistive circuit, which contains a power source and a resistance R but no reactance. The SI unit for a resistance is Ohm (Ω). The voltage drop over the resistance is simply $U_{RMS} = I_{RMS} \cdot R$, and the power dissipated to heat in the resistance is $P = U_{RMS} \cdot I_{RMS} = R \cdot (I_{RMS})^2$. A purely resistive circuit will in the AC case not affect the phases of the current and voltage ϕ_i and ϕ_u , so the current and voltage over a pure resistance will be in phase with one another $u(t) = i(t) \cdot R$.

5.2.3 Reactance Circuits

Inductive reactance appears as a result of the energy stored in a magnetic field and released from this field, caused by current flowing through the circuit. Inductance is denoted by L and the SI unit is henry (H). The voltage over the self-inductance in a circuit is proportional to the rate of change in the current or more specifically the derivative of the current with proportionality constant L :

$$u(t) = L \frac{di(t)}{dt}. \quad (3)$$

In the case of DC, which is time invariant, no voltage is associated with inductance, as the DC time derivative is zero by definition. For AC, however, the complex representation will give the following form:

$$u(t) = L \frac{di(t)}{dt} = jL\omega \cdot i(t). \quad (4)$$

Comparing this equation with the one presented earlier for pure resistance, it might be assumed that the combination of parameters L , frequency ω and imaginary unit j , linking voltage and current has the same meaning of resistance as for R . However, in this case it is frequency-dependent inductive resistance $X_L = \omega L$. The RMS voltage over an inductance is therefore written as $U_{RMS,L} = jX_L \cdot I_{RMS}$

As follows from the representation of phasors (see Figs 5.2 and 5.3), the multiplier j means that the voltage vector would be ahead of the current vector by 90° ($+\pi/2$). The same might be also seen as delayed current: when voltage over inductance changes, the current is delayed by 90° because of the inevitable creation of a magnetic field in inductance, which stores energy. This energy is purged back to the circuit in the next half-period (Schultz, 2006).

Electric capacitance is the ability of a system to store electric charge. In the case of a parallel plate capacitor, the capacitance is proportional to the area of the plates and inversely proportional to the distance between them. If the charges on the plates are $+Q$ and $-Q$ and U is the voltage between the plates, the capacitance C is given by $C = Q/U$. The capacitance has the SI unit farad (F). Capacitative reactance appears because of the energy stored in the electric field formed by the charges collected on the capacitor plates (for inductance it was a magnetic field). The stored charge is proportional to the integral of the current applied to it over the half-period time (charging), so the relation between current and voltage over a capacitor with capacitance C becomes

$$u(t) = \frac{1}{C} \int_0^P i(t) dt. \quad (5)$$

In reality, an accumulated electric charge does not pass through a capacitor (Schultz, 2006). For AC current, the charges will just oscillate between the parallel plates of the capacitor, but a DC current will not pass through it. Therefore, a capacitance functions as a circuit breaker unit for DC. For AC however, the complex representation of the integral will give the following form of the equation:

$$u(t) = \frac{1}{C} \int i(t) dt = -\frac{j}{\omega C} i(t). \quad (6)$$

Similar to the resistance and inductance, here the capacitative reactance may be defined as

$$X_C = -\frac{1}{\omega C} = -\frac{1}{2\pi f C}. \quad (7)$$

Respectively, the RMS voltage over a capacitor is $U_{RMS,C} = jX_C \cdot I_{RMS}$, but X_C has negative sign as opposed to X_L . So for the inductance, the voltage over a capacitance is phase-shifted by $+90^\circ$ from the current, but in the case of the

capacitance, the voltage lags -90° ($-\pi/2$) behind the current. This might be seen as the delayed voltage rise over a capacitor, because at some applied current some time is needed for charges to accumulate and the capacitor to be charged, and this electric energy storage delays rising of the voltage.

The total reactance in a circuit is a combination of the inductive (X_L) and capacitative (X_C) reactances:

$$X = X_L + X_C = \omega L - \frac{1}{\omega C}. \quad (8)$$

Note that the capacitative reactance is subtracted from the inductive reactance. This is a very important feature, which is systematically utilized in the design of electric power systems, as a method to compensate for inductive reactance and minimize the reactance of the system (Schultz, 2006).

5.2.4 Impedance and Power in AC Circuits

The total impedance, denoted by Z , describes the opposition from a circuit to the passage of current given an applied voltage, which as follows from Ohm's law is $Z = U_{RMS}/I_{RMS}$. The impedance is a combination of the reactance and the resistance in a circuit: $Z = R + jX$. Thus, impedance is a complex parameter and the two components, resistance (active) and reactance (reactive), are orthogonal in the complex plane. As any complex variable, it can also be characterized by its length $|Z|$ and the angle ϕ :

$$Z = R + jX = |Z|e^{j\phi}, \quad |Z| = \sqrt{R^2 + X^2}, \quad \phi = \arctan(X/R). \quad (9)$$

From this definition it follows:

$$U = (R + jX) \cdot I = (R + j\omega L - j\frac{1}{\omega C}) \cdot I = |Z|Ie^{j\phi} \quad (10)$$

or for current and voltage in the complex formulation:

$$U_0 e^{j(\omega t + \phi_u)} = |Z|e^{j\phi} \cdot I_0 e^{j(\omega t + \phi_i)} = |Z|I_0 e^{j(\omega t + \phi_i + \phi)}, \quad \phi = \phi_u - \phi_i \quad (11)$$

The angle shift ϕ determined by the ratio of R and X is the phase angle between current and voltage in the circuit (see Fig. 5.3), leading up to the important concept of the power factor. The relation between total impedance Z , resistance R , and reactance X is shown schematically in Figure 5.4 together with corresponding voltage drops (Hochrainer, 1970).

As Figure 5.4 shows, voltage drop over capacitance is subtracted from the voltage drop over inductance, and their difference is the reactance voltage, which does not contribute to active heating. The power dissipated as heat in a circuit is the product of the current through a resistance I_{RMS} and the voltage over the resistance $U_{RMS} = I_{RMS} \cdot R$. The voltage over the whole circuit also includes the voltage over the reactance, so instead of the real power, the product of the instant, time-dependent voltage and current gives the apparent power

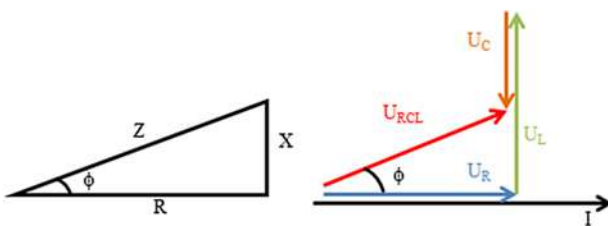


FIGURE 5.4 Phasor representation showing the impedance in a circuit and corresponding voltages over the different component types.

$s(t) = u(t) \cdot i(t)$. Expanding the harmonic functions of voltage and current and rearranging the real terms allows writing the expression for $s(t)$ as

$$\begin{aligned} s(t) &= u(t) \cdot i(t) = \frac{U_0 I_0}{2} (\cos(\phi) \cdot (1 - \cos(2\omega t)) + \sin(\phi) \cdot \sin(2\omega t)) \\ &= p(t) + q(t). \end{aligned} \quad (12)$$

The first term $p(t)$ of the expression is always positive and is called real (or active) power; the second term has a time-averaged value zero and is termed reactive power $q(t)$. The reactive power represents energy, which is stored in electric and magnetic fields and swings back and forth in the system at every period without doing any useful work. The mean value of the real power term can be expressed as

$$P = \frac{U_0 I_0}{2} \cos(\phi) = U_{RMS} \cdot I_{RMS} \cdot \cos(\phi) \quad (13)$$

Therefore, this equation has the same form as for the power in a DC circuit apart from the additional power factor $\cos(\phi)$, which is a very important parameter for all AC electric power systems. Figure 5.5 shows the current and voltage and the apparent power $s(t)$ in two cases: with no reactance and no phase shift between current and voltage, and with some phase shift (Hochrainer, 1970).

In the first case ($\phi = 0$), the apparent power always has a positive value. When phase shift is nonzero, the apparent power will take negative values during those time intervals where current and voltage have different signs. This means that at negative apparent power, the reactance in the circuit is returning the reactive power previously stored as energy in electric or magnetic fields.

Similar to real power, the acting value of the reactive power could be written as $Q = U_{RCL,RMS} \cdot I_{RMS} \cdot \sin(\phi)$. Apparent, real, and reactive power functions may also be represented in a complex plane as a vector diagram, in the same way as for current and voltage. The average (acting) apparent power is $\bar{S} = \bar{U}_{RCL,RMS} \cdot \bar{I}_{RMS}^* = P + jQ = S \angle \phi$. The apparent power is expressed in volt-amperes (VA) and the reactive power in volt-ampere reactive (VAr), to differentiate it from real power, which is always expressed in watts (W). In submerged arc furnace design, the electric equipment for the furnace must be designed with a capacity for both the reactive power and the real power.

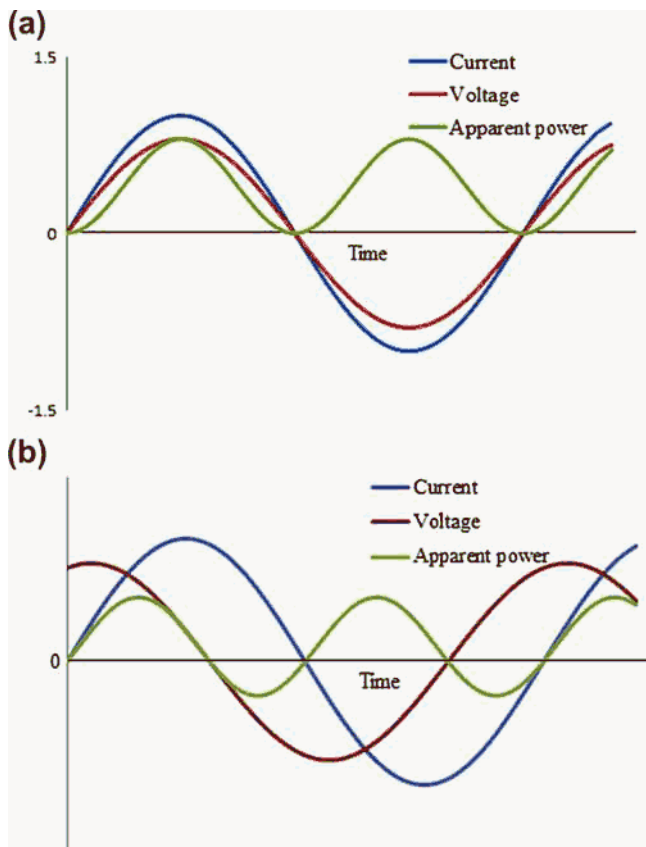


FIGURE 5.5 Apparent power for a real circuit where there is no phase shift between current and voltage (a) and with a phase shift of ϕ between current and voltage (b).

5.3 FERROALLOY SMELTING FURNACES AS ELECTRICAL CIRCUITS

5.3.1 DC Furnaces

The electric circuit and an associated load curve for DC furnaces allow for the simplest description of circuit and characteristics on the secondary side (“short net”; see Chapter 4), after the power rectifying equipment. A simplified schematic of the electric circuit for a DC furnace is shown in Figure 5.6.

The current in the circuit is $I = U_0/(R_{int} + R_{load})$, where R_{int} is internal resistance of the circuit itself, R_{load} is the load (useful) resistance, and U_0 the voltage delivered by the rectifying equipment on the secondary side. Respectively, the power over the load-bearing resistance is

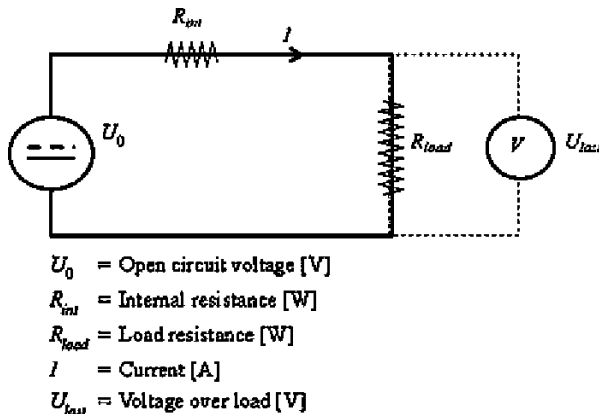


FIGURE 5.6 Schematic illustration of a DC furnace circuit.

$$P = R_{load} \cdot I^2 = \frac{R_{load} \cdot U_0^2}{(R_{int} + R_{load})^2}. \quad (14)$$

Maximum power is theoretically obtained when $R_{load} = R_{int}$, with values for voltage and current as $U_{load} = U_0/2$, $I_m = U_0/(2R_{int})$ and $P_m = U_0^2/(4R_{int})$. An attractive feature of DC furnaces is that inductance, which leads to a lowering of the power factor in large AC furnaces, does not have a similar effect in DC. Therefore, large furnaces supporting high currents can be designed without concern for low power factor and phases interaction, complicating the electrode control operations. Also, the absence of a skin effect and proximity effect enables a more efficient utilization of the whole electrode cross-sectional area for current conduction. There are furnace producers that have designed industrial DC furnaces where the location and movement of the electric arc is controlled by external magnetic fields. The main disadvantage of the DC furnace, apart from expensive rectifying equipment for converting low-voltage AC to DC, is the necessity of the bottom anode. The bottom anode is a critical and sensitive part of the DC furnace design.

5.3.2 AC Furnaces

Most industrial AC furnaces are of the three-phase type, with three or six consumable electrodes penetrating the furnace charge from above, each carrying separate phases that are phase displaced by 120° from one another. For six-electrode furnaces; the phases are directed to every pair of the electrodes (Valderhaug, 1992). Also, smaller one-phase AC furnaces exist on laboratory or pilot scales (e.g., Larsen, 1996).

The currents from the three phases cancel out at a star point within the furnace, and no bottom electrode is required. When discussing the electrical characteristics of AC furnaces, it is useful to make a simplifying analogy with

a one-phase circuit, which is justified for a symmetric configuration. For a one-phase AC furnace following analyses I and U , always refer to RMS values (i.e., $I = I_{RMS}$ and $U = U_{RMS}$).

5.3.2.1 One-Phase AC Circuit

Figure 5.7 is a schematic of a one-phase AC furnace circuit. The resistances in the system are divided into two resistances based on their usefulness. The load resistance R_p in this case is the lumped resistance in the charge and eventual electric arc. The heat dissipated by the current running through the load resistance represents the useful power, which supplies heat needed for the chemical reactions in the furnace.

Resistance in the outer circuit serving the furnace as well as the resistance in the upper part of the electrode are not in use for the process and therefore termed as a loss resistance r . The real power in the furnace is $P = I^2(R_r + r)$.

A typical SAF has relatively low voltage and high currents, and therefore a considerable magnetic field is generated around the electrodes, conductors, and other equipment. A significant amount of energy is stored in this magnetic field and is pumped in and out of the circuit as the current alternates. This reactive power Q_L causes a phase shift between the current and voltage in the system. The associated lumped reactance $X_L = \omega L$ is a characteristic of the furnace and is distributed all through the furnace and current carrying equipment rather than concentrated in a coil. In the simplified schematic of the circuit it is, however, substituted by a representative coil with an inductance L . There is very little capacitance on the secondary side of the furnace, and eventual capacitive reactance is usually neglected and the total reactance is $X = X_L$. The current in the circuit is calculated from the voltage delivered to the circuit:

$$I = \frac{U_2}{Z} = \frac{U_2}{\sqrt{X^2 + R^2}}. \quad (15)$$

The voltage share caused by the reactance is proportional to the derivative of the current and is therefore for a sinusoidal current source phase-shifted by $+90^\circ$ from the voltage over the resistance that is in phase with the current. The overall voltage is a combination of the real voltage and the reactive voltage and is therefore phase-shifted by an angle ϕ with regard to the current. This phase shift increases with increased reactance in the furnace circuit (see Fig. 5.5).

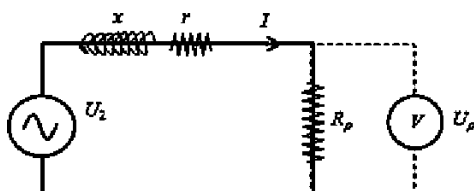


FIGURE 5.7 Schematic of a one phase AC circuit as discussed in this section.

Total active power P [kW], reactive power Q_L [kVAr], and apparent power S [kVA] depend on the resistance R as follows:

$$P = RI^2 = \frac{RU_2^2}{X^2 + R^2}, \quad Q_L = XI^2 = \frac{XU_2^2}{X^2 + R^2}, \quad S = \sqrt{P^2 + Q_L^2}. \quad (16)$$

The real furnace power P can be also expressed in terms of the power factor $\cos(\phi)$ as $P = S \cdot \cos(\phi)$, or in terms of current as $P = \sqrt{S^2 - Q_L^2} = \sqrt{U_2^2 I^2 - X^2 I^4}$. The useful power P_ρ , which is explicitly developed in R_ρ and released as heat in the charge and the arc, is

$$P_\rho = R_\rho I^2 = \frac{R_\rho U_2^2}{X^2 + (R_\rho + r)^2}. \quad (17)$$

The maximum total active power in the furnace is obtained for $R = R_\rho + r = X$ and it is equal to

$$P_m = \frac{U_2^2}{2X} \quad (18)$$

with the current at this full load point,

$$I_m = \frac{U_2}{\sqrt{2X}}, \quad (19)$$

and the charge voltage $U_\rho = R_\rho I$. The circuit loss resistance r might be measured with the electrode lowered in the furnace so that it reaches direct contact with the bottom electrode and the charge is short circuited ($R_\rho = 0 \rightarrow R = r$). The associated short circuit current is

$$I_s = \frac{U_2}{\sqrt{X^2 + r^2}} = \sqrt{\frac{2X^2}{X^2 + r^2}} I_m \quad (20)$$

and impedance is $Z_k = \sqrt{X^2 + r^2}$. It is easily shown that the maximum useful charge power is achieved when $R_{pm} = Z_k$ leading to the maximum charge power and the current:

$$P_{pm} = \frac{Z_k U_2^2}{X^2 + (Z_k + r)^2}, \quad I_m = \frac{U_2}{\sqrt{X^2 + (Z_k + r)^2}}. \quad (21)$$

For very low loss resistance ($r \ll X$), $Z_k \approx X$ and, respectively,

$$I_{sc} = \frac{U_2}{X} = \sqrt{2} I_m, \quad P_{pm} = P_m = \frac{U_2^2}{2x}, \quad I_{pm} = I_m = \frac{U_2}{\sqrt{2X}}. \quad (22)$$

With these, the most important parameters of a one-phase AC furnace, it is possible now to address the three-phase AC furnace.

5.3.2.2 Three-Phase AC Furnace

The standard Knapsack connection for a three-phase furnace is shown in Figure 5.8. One three-phase transformer or three single-phase transformers are coupled in a delta connection and are attached to the furnace electrodes at the same point where each pair of transformers is connected to one another.

The electrodes form a star circuit with a floating neutral point (zero point) where the sum of the instantaneous currents is zero: $i_1 + i_2 + i_3 = 0$. The complete three-phase circuit is shown in Figure 5.9. As the figure shows, the reactance in the furnace is distributed into inductances in the respective phases and also in the triangular delta connection.

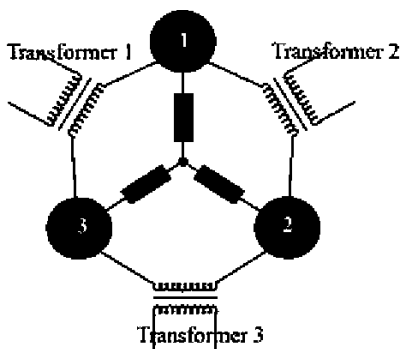


FIGURE 5.8 Three symmetrically configured one-phase transformers in a Knapsack connection with the three electrodes connected at a floating star point.

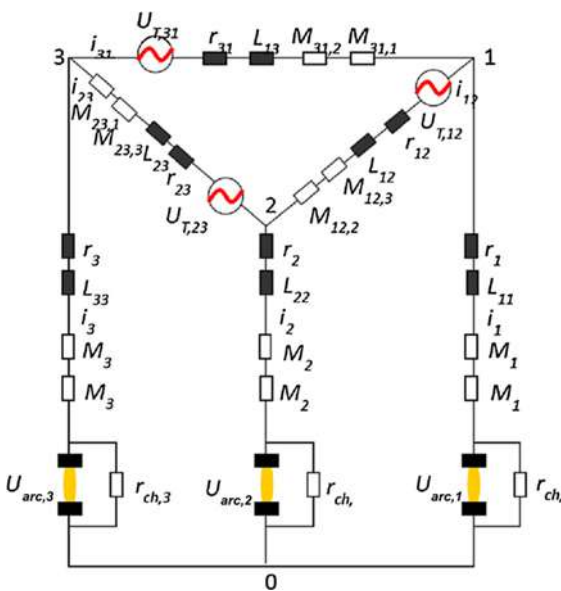


FIGURE 5.9 A schematic of a complete three-phase AC-furnace circuit with resistances, reactances, and mutual reactances shown as lumped circuit elements.

On the secondary side of the transformer windings there is no capacitance, so there reactance is only due to inductances L_{12} , L_{23} , and L_{13} , hence there $X = X_L$. Also, the presence of mutual inductances ($M_{ij,k}$) should be noted—they represent the induced voltage in a phase, due to the magnetic field generated by the current passing through the other two phases. This property of the three-phase circuit turns out to be quite important in the furnace operation, as it represents an interaction between the phase currents, which complicates the electric control of the furnace. A change in the current passing through one phase affects the current passing through the other two (Valderhaug, 1992). This phenomenon is further discussed when the electric operation of the furnace is addressed.

In the case of a symmetric furnace operation, the three-phase furnace circuit can be simplified into three one-phase equivalent circuits, where the currents are decoupled from one another and resistance and reactance have been merged into their lumped counterparts (see Fig. 5.7). The mutual inductances $M_{ij,k}$ are lumped into the phase inductance L_k , which can be justified when all conditions are symmetric. The delta-connected secondary voltage here is replaced by line voltages $u_{Tij} = U_2/\sqrt{3}$. Thus, the open-circuit voltages of the transformer secondaries have equal RMS values and a 120° phase delay between them. In this context, R is then termed *phase resistance* and X the *phase reactance*, both usually written in units of $\text{m}\Omega$. For these conditions, the phase current is

$$I = \frac{1}{\sqrt{3}} \frac{U_2}{\sqrt{X^2 + R^2}}, \quad (23)$$

the furnace real power is

$$P = 3 \cdot RI^2 = \frac{R \cdot U_2^2}{X^2 + R^2}, \quad (24)$$

and the reactive power is

$$Q_L = 3 \cdot XI^2 = \frac{X \cdot U_2^2}{X^2 + R^2}. \quad (25)$$

As for one-phase AC furnaces, the active power in the furnace can be written in terms of the transformer secondary voltages and phase current: $P = \sqrt{3U_2^2I^2 - 9X^2I^4}$. The useful power dissipation in the furnace charge is

$$P_\rho = 3 \cdot R_\rho I^2 = \frac{R_\rho U_2^2}{X^2 + R^2} \quad (26)$$

with the apparent power $S = \sqrt{3} U_2 \cdot I$, $S = P/\cos(\phi)$. The reactance X in an SAF increases with increasing furnace size and phase current. Large industrial furnaces of 40 to 50 MVA may have a reactance that substantially surpasses the resistance, leading to a relatively low power factor of less than 0.6.

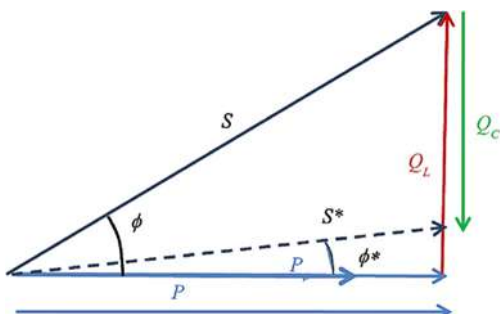


FIGURE 5.10 A vector diagram illustrating how capacitative compensation on the primary side of the transformer windings is used to swallow the reactive power and elevate the power factor. This is done at SAF facilities to meet the requirements of the power distribution utility.

Even though the power factor cannot be compensated on the secondary side, it must be on the primary side. As most of the reactance is inductive, it can be compensated by arrangements of capacitor batteries, which deliver their reactive power on the low-current primary side of the delta connection. This is necessary to protect the transport grid from the power factor and satisfy predetermined criteria from the power distributor (Schultz, 2006). Properly designed capacitor compensation can increase the power factor toward unity as seen from the grid. This is illustrated in a vector diagram in Figure 5.10.

It is not practical to compensate with capacitance on the high current secondary side of the transformers, and therefore the whole furnace circuit must be designed with extra capacity to accommodate for an apparent power S , which greatly exceeds the active power P . Also the induced fields in the furnace complicate the electrode operation associated with the electric control, as will be discussed in Section 5.5.

5.4 MODES OF HEAT DISSIPATION IN FURNACES

There are two main modes of heat dissipation in ferroalloys smelting furnaces. All furnaces have a part of the electrode current passing through the charge burden, molten slag, and metal. This will involve resistance heat dissipation, also called joule heating. In some processes, an electric arc will also be present, with a significant part of the heat dissipation. This is required for some types of the processes depending on the need for a high-temperature heat source for the chemical reactions, although arcing might be also found in other cases where it is not specifically required.

5.4.1 Electric Arc

An electric arc is formed when high electric field strength (voltage gradient) over normally nonconductive material, such as a gas, causes an electric breakdown of the material, which increases the conductivity in the medium. In the case of arc discharge for a gas, the ionization of the gas molecules introduces positively charged ions and electrons that enable electric current to pass through

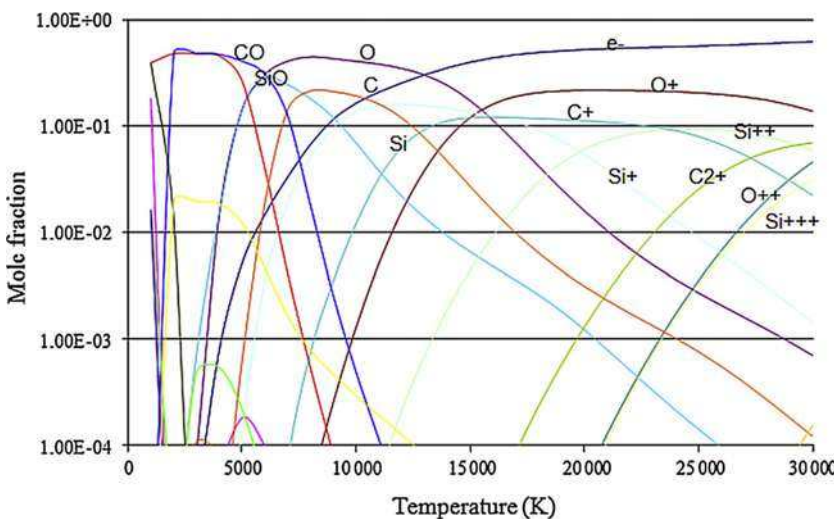


FIGURE 5.11 Density of different species present in a gas composed of Si-O-C plasma of 1:2:1 composition, as can be found in the crater of a Si-producing electric arc. In this gas mixture, some Al and Ca contaminant (not shown here) are present (Saevarsdottir et al., 2001b)

the medium. The ionized gas (plasma) is generally defined as a special state of matter in addition to solid, liquid, and gaseous states. Electric arcs in SAFs are formed at atmospheric pressure, which requires the formation of thermal plasma, which means that ions and electrons have the same kinetic energy (Chen, 1990). In less dense plasmas, electrons may be at a higher temperature than the heavy particles. For air and most other gases, the temperatures required for sufficient ionization for thermal plasma formation are above 8000 K.

As an example, Figure 5.11 shows the density of species as a function of temperature in a Si-O-C plasma (molar ratio Si:O:C = 1:2:1), which is the approximately expected gas composition in the crater of a silicon smelting furnace). A commonly faced arc temperature in an SAF is above 20 000 K, which means that heat released in the arc can support reactions requiring extremely high temperatures to run.

An industrial arc with a voltage of 100 V would typically not be much longer than 10 cm, and there may be more than one arc burning in parallel from the same electrode (Reynolds, 2011). Figure 5.12 shows a photograph of a 5-cm-long low current DC arc (2000 A) with a normal polarity where the top electrode is cathode (a) and a photograph of three arcs burning in parallel (b). (Courtesy of R. Jones and Q. Reynolds, Mintek, South Africa.)

The electromagnetic forces in the arc acting on the plasma are the strong drivers for fluid flow, so velocity of the plasma from the cathode toward the anode in the arc is high and pressure at the anode end is significant. Velocities can approach sonic speed, even though the sound velocity is much higher for

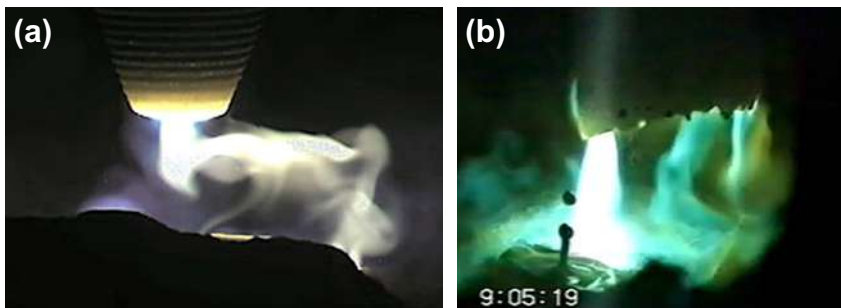


FIGURE 5.12 Photographs of (a) a 5-cm-long low-current (2000A) DC arc with a normal polarity where the top electrode is cathode and (b) three arcs burning in parallel. (*Courtesy of Q.G. Reynolds and R. Jones, Mintek, South Africa.*)

thermal plasma than for air at standard conditions. The heat released in the arc due to resistive dissipation, $P_a = R_a \cdot I^2$, is transported from the arc to its environment mainly through convection and radiation approximately equally distributed (Saevarsdottir et al., 2001a). However, a significant fraction of the heat is also delivered to the anode with particles impacting its surface (Palsson et al., 2007) as well as through proximity radiation, so the anode will receive a significantly more substantial heat load as compared to the cathode.

Although the electric arc serves as a resistive heat dissipater in the furnace, it has some characteristics that separate it from normal resistors. Primarily its resistance is nonlinear, as it depends on the current that passes through it. Therefore, the arc resistance varies over the 20 ms AC period (at 50 Hz frequency), being highest when the current passes through zero and lowest when the current passes through the sinusoidal maximum. As the temperature required for full ionization in the plasma is very high, the level of cooling and the temperature of the surrounding environment will affect the characteristics of the arc. When the current passes through zero, the heat dissipation by the current passing through the arc will not be sufficient to balance the heat loss by radiation and convection. Colder environments will lead to a higher variation in the arc resistance within the arc period, increasing the nonlinear properties of the electric arc. Figure 5.13 shows how the arc voltage dynamics will qualitatively change over a half period depending on the temperature of the surroundings, assuming that the current is imposed with a sinusoidal waveform.

In the case of large submerged arc furnaces, a high inductance will ensure a sinusoidal current waveform and nonlinearity will be reflected in the voltage waveform. Figure 5.14 shows the dynamic current-voltage characteristics for this same case (the so-called Lissajous curve).

This nonlinearity gives rise to harmonics in the voltage and current waveforms of the SAF, which can be utilized to deduce the level of arcing in the furnace. An example for a silicon smelting furnace is shown in Figure 5.15 during a period of charge smelting.

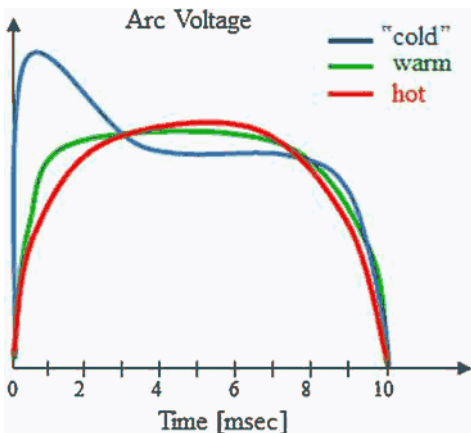


FIGURE 5.13 Qualitative illustration of arc voltage dynamics over a half-period (10 ms) depending on the temperature of the surroundings.

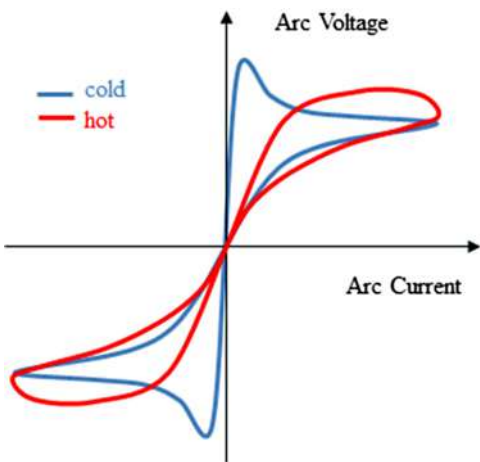


FIGURE 5.14 Qualitative illustration of the dynamic current–voltage characteristics for the case in Figure 5.13 (Lissajous curve).

5.4.2 Electric Arc Models

To understand and predict both the heat transfer from and the electrical characteristics of electric arcs, significant effort has been put into the modeling of electric arcs (Saevarsdottir et al., 2001b). The nature and the level of detail depend mostly on the purpose and application of the modeling. Arc models can be roughly divided into four categories:

1. Momentum source models, where the arc is represented by a momentum source and a heat source included in fluid dynamic reactor models.
2. Black-Box arc models, where attempts are made to simulate the current–voltage dynamics of the arc by fitting parameters on a linear model to

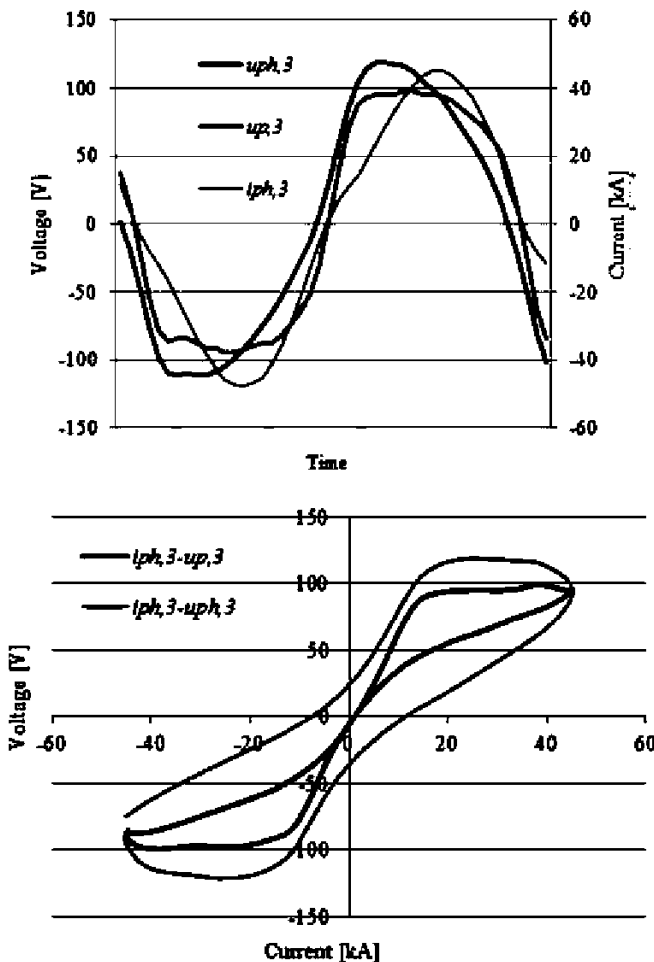


FIGURE 5.15 Current and voltage waveforms for an industrial electric arc in a Si-metal furnace during a period of melting down the charge. A Lissajous curve showing the current voltage relation for an electric arc.

empirical data. No physical justification is required in this category of models. Examples of this type are the Cassie (1939) or Kema arc models.

3. Semophysical models, where there is a simplified physical view of the arc, based on physical data for plasma properties and the underlying physical phenomena, such as the velocities and radiation.
4. Magneto-hydrodynamic (MHD) models, where the Navier-Stokes equations for energy and impulse balance in the system are coupled with source terms obtained from the Maxwell equations for the electromagnetic fields.

A short description of these respective categories follows. For the purposes of the electric operation of the furnace at the engineering level, the simple black-box approach is probably sufficient, as it does not postulate any specific plasma physics parameters be adopted.

5.4.2.1 Momentum Source Models

In the modeling of arc-heated thermochemical reactors where temperature and flow fields are desired but other arc characteristics are less important, it may be sufficient to replace the arc in the computational domains by a momentum source in the momentum equation and a heat source in the energy equations, which reasonably represents the heat dissipation in the electric arc. An example of this methodology is given by [Ravary et al. \(2003\)](#).

5.4.2.2 Black-Box Models

The so-called phenomenological models were the first type of AC arc models to be established. The purpose of such models is mainly to describe the arc as a nonlinear circuit element when calculating current voltage characteristics. These models are based on very rough assumptions of the physics, and parameters are adjusted empirically. Pioneers in this field were [Cassie \(1939\)](#) and [Mayr \(1943\)](#), but their models were established for circuit breakers. The derivation of the model is based on a rough energy balance, a derivation that results in the following differential equation:

$$R \frac{d}{dt} \left(\frac{1}{R} \right) = \frac{1}{\tau} \left(\frac{u_{arc} i}{P_{arc}} - 1 \right) \quad (27)$$

Here the arc resistance R is related to the time constant τ for the arc (which can be derived from the assumed internal energy for the arc), P_{arc} is the power dissipated in the arc, u_{arc} is arc voltage, and i is arc current.

5.4.2.3 Channel Arc Models

A channel arc model (CAM) is a simplified physical model, based on the assumptions that the arc column might be approximated as a conducting cylinder and with a prescribed radial temperature distribution. The cylinder is supposed to have a constant radius R_a apart from a small region at the cathode surface where the arc expands from a cathode spot with a smaller radius R_c ([Fig. 5.16](#)). The CAM for AC is based on a DC arc model taken for the condition that at each instant of time the arc strives toward the equilibrium state of the DC arc with the same current. The power dissipated in the arc due to resistive heating in the steady case is equal to the power lost through convection and radiation.

Temperature-dependent physical properties of the arc gas are used to calculate the resistance and other necessary parameters. Convection in the arc is induced by the fluid flow, and the average velocity field for a predetermined

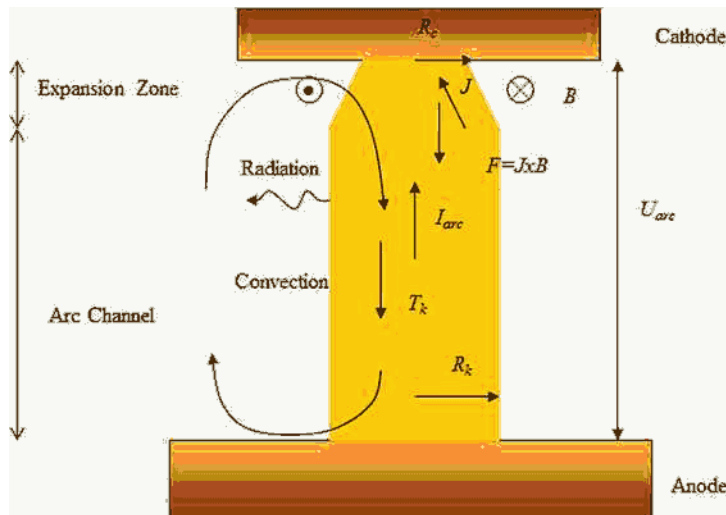


FIGURE 5.16 A schematic illustration of a CAM. (Based on Saevarsdottir et al., 1999.)

velocity profile is calculated from the Lorenz force on the current as it expands from the cathode spot into the electric arc channel. The arc temperature and radius have to be chosen such that the energy conservation is satisfied, but there are many values for temperature and radius that would satisfy this requirement. Thus, an additional constraint is imposed, which is that the power dissipation is minimized. This requirement is called Steenbeck's minimum criterion (Steenbeck, 1932). The CAM targets to obtain reasonable arc dynamics using physical principles from a relatively simple model with a small computational time (Larsen, 1996; Saevarsdottir, 2002; Saevarsdottir et al., 1999).

5.4.2.4 MHD Models

This model relies on a magneto-hydrodynamic (MHD) description of the arc behavior. This requires a coupled numerical solution of the Navier-Stokes equation for the conservation of mass, energy, and momentum, with a force term derived from the interaction of the arc current with the magnetic field in the momentum equation, and a heat source term obtained from ohmic dissipation caused by the electric current flowing through the arc. For these source terms, the Maxwell equations must be solved for the magnetic field and current distribution in the arc. The numerical solution procedure requires substantial computational power. In some geometries, the real three-dimensional system might be simplified to two-dimensional-axial symmetry and the problem solved in two dimensions, but important dynamics and instabilities are lost. Reliable time- and pressure-dependent physical data for the operating gas and its composition are required to obtain useful results. For example, a noble gas

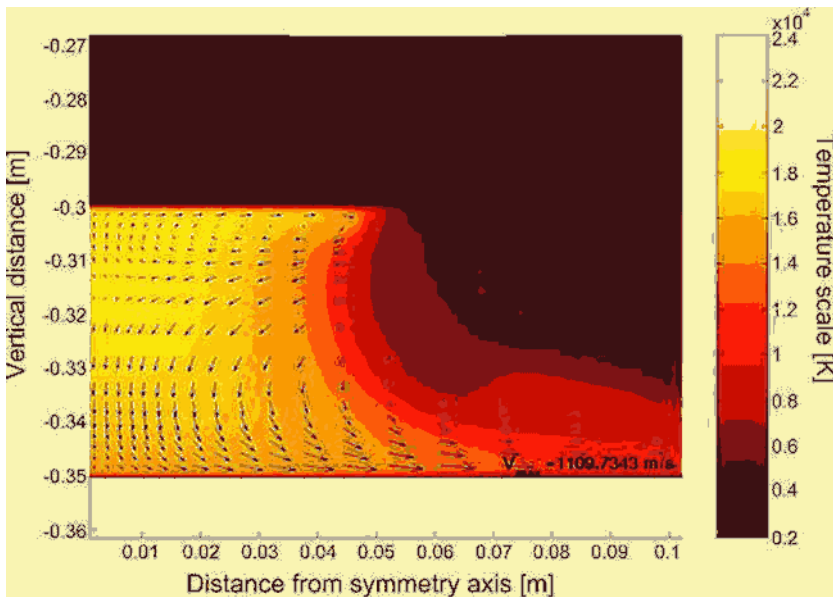


FIGURE 5.17 Temperature and velocity fields from MHD 2D-axisymmetric model for a 5-cm-long arc in SiO:CO 1:1 atmosphere at 100 kA.

like argon (which requires no extra energy for molecular dissociation) will really facilitate arc formation and reduce the nonlinearity of the arc characteristics as compared to air or other di-atomic gases. Thus, the heat required for ionization of argon is much smaller than for molecular gases, and less heat is lost from the arc through convection. Considerable work has been done on MHD modeling of electric arcs, and this clearly gives the most accurate description of the heat transfer and current voltage dynamics for the arc if the model is based on accurate assumptions and physical data. Figure 5.17 shows calculated temperature and velocity fields from an MHD model for a 5-cm-long arc with 100 kA current in a 50% SiO-50% CO atmosphere.

5.4.3 Resistive Heating

As the term *submerged arc furnace* indicates, the top electrodes are submerged in the furnace burden. The burden is composed of a charge of partially reacted and chemically processed raw materials. The initially electrically insulating raw materials in the charge become electrical due to their transformation and melting (Valderhaug, 1992). Electric current passes from the electrodes through the charge to the other electrodes in the furnace in addition to passing through a slag or a coke bed if present in the furnace. Heat is released according to $P_\rho = R_\rho \cdot I^2$. The charge resistivity is different for different

ferroalloy processes and even for the same process it will depend on the charge composition and materials selection (carbon reductant, grain sizes, bulk density, etc.). Direct measurement of the resistivity is also complicated by the variability of the properties depending on the reaction zones within the furnace. Different estimates on the average charge resistivity ρ (in $\Omega \cdot \text{m}$) for different processes have been obtained (Downing and Durban, 1966) (Table 5.1). The tabulated resistivity is calculated based on the simplified geometry from Morkramer (1961), so it should be interpreted comparatively rather than exactly.

It is assumed that all conduction happens from the tip of the electrode, which is formed as a half-sphere of diameter d . This is rationalized by a lower conductivity for a less mature charge in the upper zones of the furnace (Morkramer, 1961). The current is assumed to distribute with equal current density in all directions from the half sphere. With a simplifying assumption that the resistivity ρ is uniform in the charge and that the current spreads evenly in the half-sphere to a radius $r >> d$, the phase voltage (the voltage drop from the tip of the electrode to the furnace bottom) would be

$$U_\rho = \frac{\rho \cdot I}{\pi \cdot d} \quad (28)$$

By measuring the phase voltage and current, the bulk resistivity of the charge may thus be calculated for given electrode diameters.

TABLE 5.1 Estimated Resistivity for Operating Furnace Charge for a Range of Processes

Product	Charge Resistivity ρ [$\Omega \cdot \text{m}$]
FeMn standard	0.0020–0.0032
FeSi 75	0.0040–0.0050
FeSi 50	0.0060–0.0085
CaC ₂	0.0048–0.0056
Fe	0.0030–0.0060
FeCr with 4–6% C and 2% Si	0.0087–0.0162
FeCr with 4–6% C and 6% Si	0.0050–0.0075
FeCrSi	0.0030–0.0053
SiMn	0.0025–0.0037
P	0.0190–0.0250

5.4.4 Current Paths and Distribution of Heat Dissipation

The main goal of furnace operation is to get good stable operating conditions with a high yield of the produced metal, as well as low energy consumption and as few emissions as possible of dust, harmful gases, and substances. There are many different aspects to furnace operation. Of paramount importance are the selection and feeding of raw materials. The furnace charge must be properly distributed and mixed, through external stoking for an open or semiclosed furnace or by some automatic mechanism of moving the charge in the case of a closed furnace. This will prevent or remedy the eventual segregation of raw materials in the charge, close undesirable vent channels through the charge, and thereby enhance the contact of the process gases with the half-processed raw materials, condensing some gases and enabling reactions with others. Regular and successful tapping of the produced metal from the furnace is also of great importance as metal accumulated in the furnace may reoxidize back to slag under certain conditions.

5.4.4.1 Current Paths in the Furnace

The furnace resistance in an SAF or RHF is controlled by shifting the electrode up and down (Valderhaug, 1992). Lowering the electrode tip further down into the furnace will shorten the current path and improve the electrode contact with hotter and more conducting zones within the furnace, thereby decreasing the phase resistance but avoiding direct submersion into molten metal, as this will lead to a shortcut and electrical breakage. Eventual arcs will also be shorter with lower resistance, which leads to the same result. Raising the electrode has the opposite effect: the current path gets longer, the current will be more evenly distributed through less conductive charge, and there will be less arcing. Therefore, a high electrode holder position will cause higher phase resistance P_p , more diffuse and distributed heat dissipation in the furnace, and lower maximum temperatures. For ferroalloy processes where an electric arc is necessary, this may cause an insufficient heat release in the arc itself and therefore an inactive hot zone of the furnace. The consequences are slower reaction rates in the hotter metal-producing regions of the furnace and unfeasible thermodynamic equilibrium conditions leading to loss in metal recovery in the process.

In real furnaces, current distribution paths are, of course, much more complex than assumed in the simplified charge resistance (see Table 5.1). An example of the resistance heating operation mode (an RHF) current distribution is shown in Figure 5.18 for a three-phase AC furnace with a 13-m-wide hearth, 1100-mm self-baking electrodes, and 12 MVA nominal power. This model case includes molten metal, slag, and a coke-rich top layer.

As the model shows, the highest current density is indeed observed around the electrode tip, between the electrodes, and within the molten metal (up to 10^6 A/m^2), whereas close to furnace walls it drops as low as 0.003 A/m^2 . One,

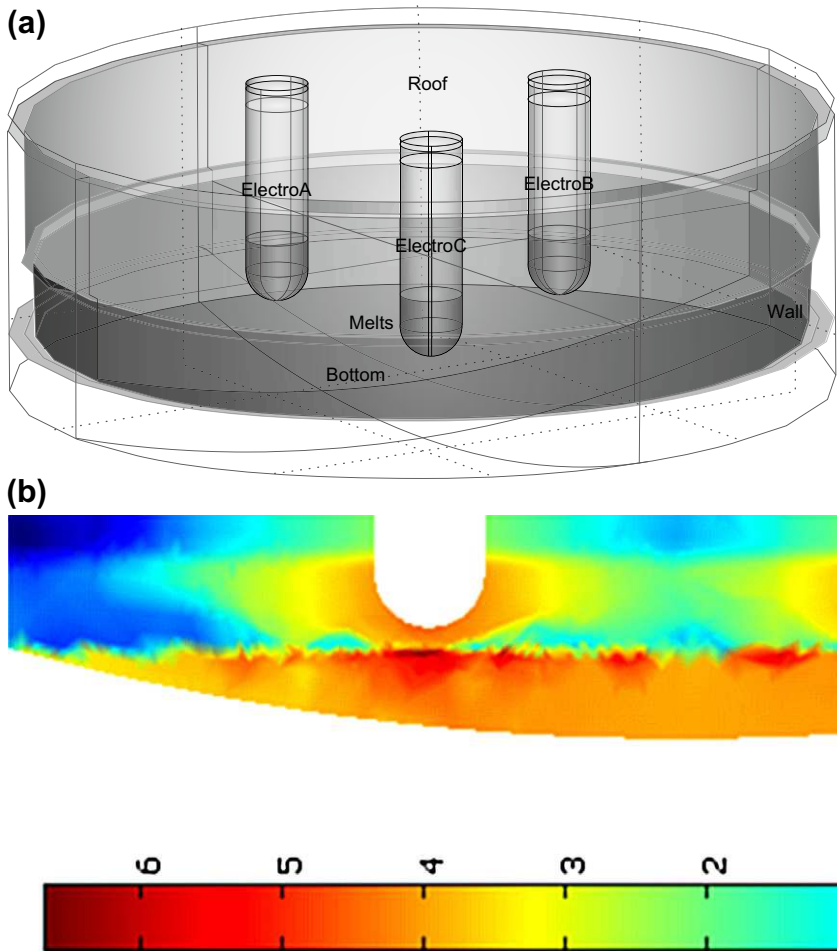


FIGURE 5.18 An example of RHF model geometry (a) and calculated current density distribution (for a cross-section) in logarithmic scale (b), calculated by M. Gasik. Numbers in the color scale are logarithms of the current density in A/m^2 .

however, should not make a false conclusion about the heat dissipation in the hearth, as, for example, very high current densities in metal do not necessarily result in excessive heat dissipation because the specific resistance of metal is much lower than that of slag or charge, so active power release there is also low.

5.4.4.2 Heat Distribution in the Presence of an Arc

If the process involves arcing, it can be assumed that the phase current splits up between the charge and the arc. This can be modeled by representing the charge

and arc by their respective resistances connected in parallel with each other and in series to a series resistance as illustrated in Figure 5.19 (Saevarsdottr and Bakken, 2010).

For this phase, the load-bearing operating resistance will then be given by equation

$$R = r + \frac{R_a \cdot R_{ch}}{R_a + R_{ch}}, \quad (29)$$

and the heat dissipation for each location will be in accordance with the magnitude of the resistance. The total active power P for the phase will be the sum of the power released in the arc P_a , in the charge P_{ch} (altogether constituting the useful active power P_p in the furnace), and power released in the series short circuit (e.g., electrode) resistance P_s : $P = P_s + P_a + P_{ch}$.

The power released in the charge P_{ch} heats up and melts the charge material and drives endothermic reactions in the upper regions in the furnace. Other heat sources in the area include possible exothermic reactions between process gas and raw materials, oxidation of carbon reductants, condensation of gases, and transfer of thermal energy from the reaction gases passing through.

The arc power P_a is released at $T \sim 20000$ K and enables endothermic chemical reactions that require high temperatures to be thermodynamically feasible. It is important to have sufficient temperatures in the high-temperature regions of the furnace to drive the metal generating reactions at a rate that is in balance with other reactions in the furnace that are supported by the charge current heat dissipation and other heat sources.

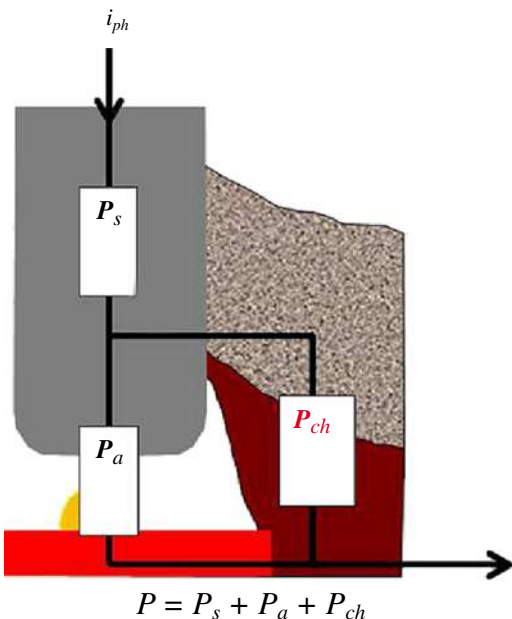


FIGURE 5.19 Equivalent circuit versus crater configuration in the presence of an arc.

The load resistance R_ρ is written as $R_\rho = R_a \cdot R_{ch} / (R_a + R_{ch})$, so P_ρ may be written in terms of R_ρ and the load voltage U_ρ as $P_\rho = U_\rho^2 / R_\rho$. The charge power P_{ch} and arc power P_a can be found in the same way: $P_{ch} = U_\rho^2 / R_{ch}$, $P_a = U_\rho^2 / R_a$. The ratio between the power released in the charge and the total effective power is

$$C = \frac{P_{ch}}{P} = \frac{U_\rho^2 / R_{ch}}{U_\rho^2 / R} = \frac{R}{R_{ch}}, \quad (30)$$

which is sometimes called Westly's heat distribution coefficient (Schei et al., 1998). A number of methods have been used in an attempt to evaluate current distribution between arc and charge in furnaces. For example, one method is based on the assumption that the percentage of harmonics in the phase voltage signal was inversely proportional to C . This method applied to a silicon furnace indicates that arc current in a Si furnace is passing by 80% to 90% through the arc. Direct measurements on pilot furnaces and industrial furnaces producing silicon indicate arc current fractions ranging from 30% to 35% up to 50% to 60% (Saevarsdottr and Bakken, 2010; Saevarsdottr et al., 2007).

The heat distribution coefficient C tells the fraction of the electric power dissipated in the charge (Schei et al., 1998), and as discussed previously this fraction should not exceed the maximum for a given process. This enables a balanced furnace operation where the reactions in the different zones run at coordinated rates, so for a particular charge composition with certain conductivity, there is an optimal phase resistance that represents the optimal C value (C_{opt}). If the raw materials in the furnace are changed (and thus electrical resistivity is changed), the overall phase resistance must be adjusted to maintain C_{opt} value. When $C >> C_{opt}$, there is a risk that there will be too little arc current and too much heat dissipation in the charge. That will lead to excessive slag generation in the furnace and reduced metal production. The slag generation will result in bad tapping and reduced sensitivity of the phase resistance to electrode movements as well as excessive consumption of the electrodes along the sides rather than at the tip of the electrodes.

If the operating resistance is lower than the optimal value ($C < C_{opt}$), the furnace must be run at a higher current to maintain the power load and production rate. This may push electrodes, transformers, bus bars, and other electric equipment beyond the current limits they were designed for, increasing wear and need for extra maintenance. Also, electrode failure risk increases if the phase current exceeds a sensible range.

5.5 ELECTRIC OPERATIONS AND CONTROL OF THE FURNACE

To maintain well-balanced furnace operation and at the same time the optimal and efficient production rate, and high yield for a given furnace design, electric operation is of uttermost importance (Valderhaug, 1992). The power delivered

to the furnace can be controlled by changing the transformer tap positions and by adjusting the electrode holder positions (HPs). Thus, the distribution of power dissipation in the furnace is influenced as discussed previously. Changing the raw materials selectively for electrical purposes can also be seen as electric control, but this is sometimes done in the case of abnormal furnace operation or when the electrode holder position is already too low or high without the target phase current being reached. Another feature that eventually influences the electric operation is the electrode slip control, but over time the slip rate should mainly compensate the electrode consumption.

5.5.1 Power Control

The electric power is fed to the furnace through transformers that normally are connected in the standard Knapsack configuration (see Fig. 5.8). Under special conditions—for example, at startup—the transformers can be connected in a star connection, but under normal operation the Knapsack delta prevails. The transformers convert the high voltage and low current on the primary side to a level fit for the furnace, and the transformer outlet settings determine the voltage level delivered in the delta connection. As the transformer outlet tap positions are adjusted, the power delivered to the furnace changes accordingly as resistance in the furnace is not influenced by this, and current will change with the voltage. Under normal operation, all three transformers have the same settings, providing the furnace with symmetric conditions. Biased settings might occur, but this is not recommended, as it will inevitably lead to circulating unbalanced currents in the delta connections that will not be detected with standard measurements and can lead to equipment failure.

An example of industrial furnace electrical operations is shown in Figure 5.20, which represents a sunflower plot of about 4000 data logs over a month (data analyzed by M. Gasik).

The data shown in Figure 5.20 pertain to the furnace with the geometry and current density distribution shown in Figure 5.18. The furnace is operated for a slag treatment process and the furnace load is targeted for the desirable process temperature range and is therefore operated at a much lower load than its design capacity. As shown, the furnace's active power is proportional to the supplied current that is typical for furnaces operating in resistance mode. The dashed-line ellipse outlines the furnace operational window, but there are also outlying points owing to various causes (shortcuts, charge hanging, improper electrode movement or breakage, external reasons such as maintenance, etc.).

5.5.2 Electrode Control

Assuming that a given voltage is delivered to the delta from the transformers, currents in the furnace are managed by changing phase resistance, which is achieved by controlling the electrode tip position in the furnace. This is done

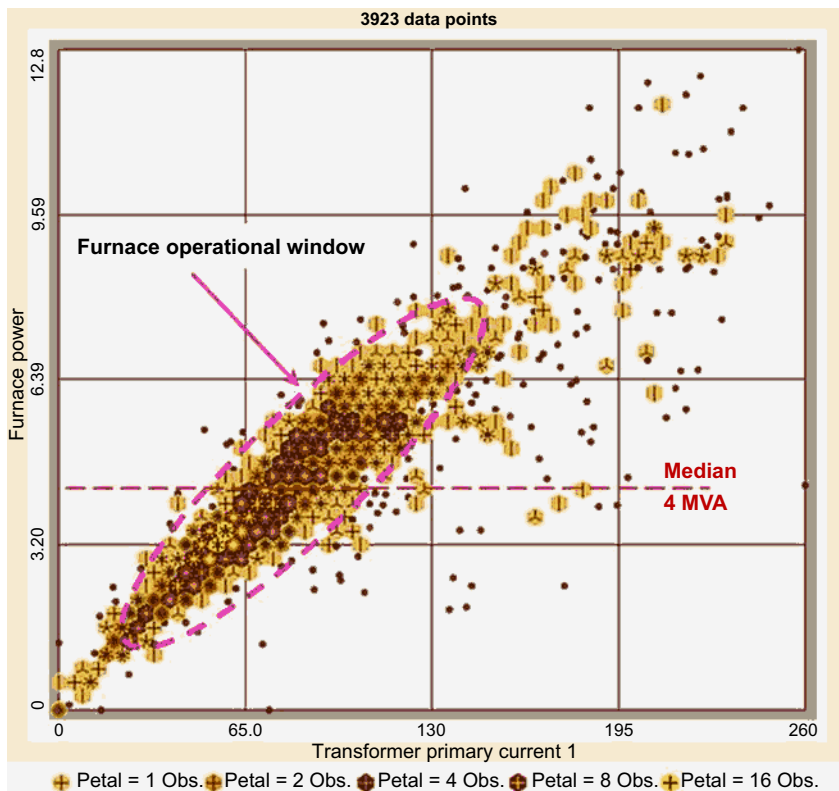


FIGURE 5.20 Data logs of the RHF furnace: power (MVA) versus transformer primary current (A). Each “flower” is a collection of measurements, grouped by number of appearances in this category. The color of the flower and number of petals (*lower legend*) represent how many observations were made at a given set of conditions.

by manipulating the electrode holder positions (HPs) up and down, raising and lowering the phase resistance accordingly. As the phase voltage is more or less determined by the transformer settings, phase current and resistance are interlinked by Ohm’s law. There are two strategies for regulating the furnace: resistance regulation and current regulation. Both are based on traditional dead-band regulation. There is a target value for the parameter, a so-called set point, but it is allowed to vary within a predetermined range called a dead band. If the parameter moves out of the dead band range and remains out of limits over a predetermined waiting time, the action of moving the electrode up or down is initiated as illustrated in [Figure 5.21](#). This movement will continue for a certain running time, which is equivalent to a certain displacement of the electrode tip.

In the case of current regulation, there is a target set point for the phase currents, and the dead-band regulation is designed to keep all phase currents

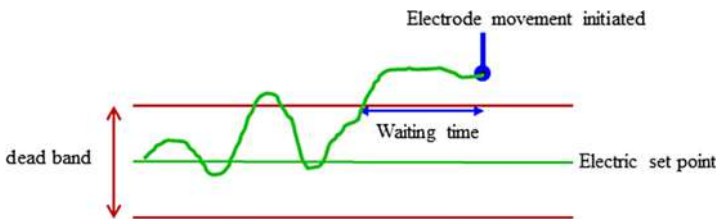


FIGURE 5.21 The concept of dead band regulation, showing the set point, dead band, and waiting time.

within limits. If the current rises above the limit, the electrode is raised to increase the phase resistance and decrease the current. The obstacle is that the change in current in this one phase will influence the currents in the other two phases, through both the floating star point in the furnace and the inductive coupling of the phases. As a consequence, a change in holder position in one phase will be transported to the other phases leading to disturbance in furnace operation, which in the worst case would lead to continuous movement of electrodes, if it is being controlled by automatics. This can be compensated for by using a larger dead band or a decoupling algorithm, but this represents a drawback in this approach to furnace regulation. The level of interaction between the phases depends on the furnace power factor $\cos(\phi)$ —the smaller the power factor, the stronger the phase interactions. As the power factor tends to decrease with increasing size of the furnace, this interaction will be more pronounced for large furnaces with a high power load.

The main advantage for the current regulation approach is that the phase current measurement is robust and reliable and done on the primary side of the transformers. Another benefit is that when current is the control parameter, there is less risk for the current to exceed the design limits for the electrode or other equipment. This can be an issue in particular for furnaces that are run at a load exceeding their initial design target value.

The issue of phase coupling can be overcome by regulating directly for the phase resistance rather than the phase current. The resistance is a physical parameter in the furnace, which is not directly influenced by the inductance in the furnace. The complication here is that to determine the phase resistance for the furnace, both the phase current and the phase voltage need to be known. A reliable measurement of the phase current is available, but measuring the phase voltage from the contact clamps to the bottom of the furnace is more complicated. One approach to do this is by using the Böckmann compensation (Schei et al., 1998), where the voltage drop from the contact clamps to the furnace bottom is measured, and induced currents are compensated for by loop connections (Fig. 5.22).

The weakness of the Böckmann compensation is that it may not be sufficiently robust for it to be reliable as a control parameter. Some resistance

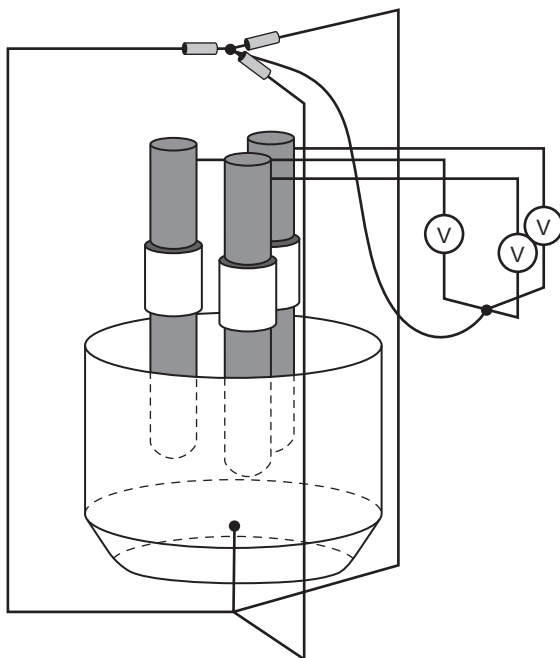


FIGURE 5.22 An illustration of the setup for Böckmann compensation. (*Modified from Schei et al., 1998.*)

control systems suffice by measuring the contact clamp voltage and use assumptions to deduce a phase voltage. This approach is more robust, but it may be inaccurate in cases when the assumptions are not valid. However, stable operation without the complicating phase interactions has been obtained at a number of smelters that have operated their furnaces with resistance control using this deductive method for evaluating the phase voltage.

An example for the furnace shown in Figure 5.18 and its active power distribution (see Fig. 5.20) can be found in Figure 5.23, which shows the dependence of the phase voltage on the phase current for one electrode (data analyzed by M. Gasik). This sunflower plot represents the same data logs as for active power (see Fig. 5.20) and for the same charge and process type illustrates that when an electrode goes down, resistance drops, and voltage decreases with increasing phase current (solid arrow). The group of the most observations indicates the operational window of this furnace as 65 to 90 V and 20 to 30 kA phase current. When the electrode goes up, resistance increases and so voltage drops, leading to lower current (dashed arrow).

A too-low electrode position (closer to molten metal surface) leads to much higher currents and it indicates to the operator that it might be wise to consider raising the electrode to avoid overheating and possible undesirable short circuits.

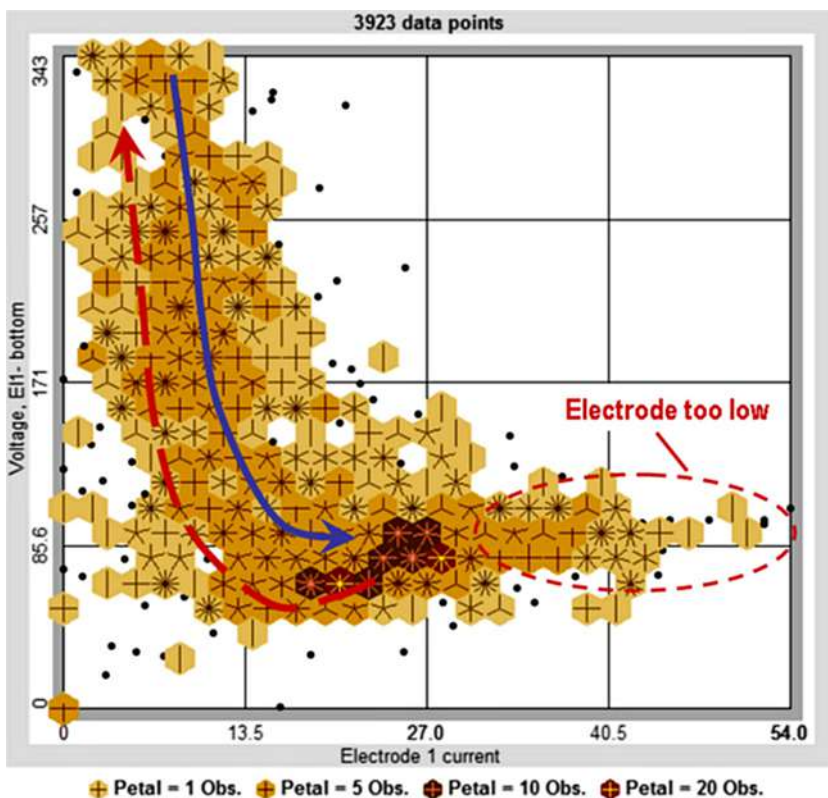


FIGURE 5.23 Data logs of the RHF furnace as one electrode phase voltage (V) versus phase current (kA) for the furnace data shown in Figures 5.18 and 5.20. The blue and red arrows show the lowering and elevation of the electrodes, respectively.

5.6 ENVIRONMENTAL ISSUES OF FERROALLOYS FURNACE OPERATIONS

A number of emissions are associated with ferroalloys production in electric furnaces. The use of modern smokehoods and vents associated with fume treatment makes it possible to substantially reduce most of the harmful emissions and thus the environmental impact of the production facilities, improving the working environment. In this section, various major emissions sources are listed and means of their mitigation discussed.

5.6.1 Particulates Emissions

Particulates are generated by the smelting process in the furnace, tapping, metal refining, and casting. Some dust is also generated during raw material and smelting products storage and handling, preprocessing, crushing, and blending.

The most significant contribution to the production of particulates is the smelting process in the furnace. For example, in silicon and ferrosilicon production, SiO gas from the process burns in oxygen as it mixes with air at the top of the furnace burden, forming amorphous microsilica particles. The microsilica particles are collected in the baghouse filters and are a valuable side product from the process (see Chapter 6 for more details). Also, fine dust in the raw materials is entailed in the gas flow through the charge and carried to the surface. The flue gas from the furnace is drawn through the smoke hood to a duct where the gas must be cooled down before it enters the baghouse filters. The temperature and composition of the gas depends on the extent of enclosure of the furnace. In an open furnace, the gas will be very greatly diluted with air, and therefore a high volumetric flow rate at a moderate temperature will not have a very high dew point due to the dilution. Semiclosed or closed furnaces, on the other hand, will have less dilution, a lower volumetric flow rate in the duct, and higher temperatures. In this case it is more critical to keep the temperature above the acid dew point: due to the presence of SO₂ in the flue, gas acid droplets will form, causing severe corrosion on heat exchange surfaces and damage to the baghouse filter system. An example of sulfuric acid formation conditions is shown in Figure 5.24, versus SO₂ content and gas temperature. It shows that high sulfuric oxide concentrations lead to an increase of sulfuric acid pressure and thus higher dew points.

The heat must be removed from the exhaust gas before it enters the filters, cooling it down to a maximum of ~175°C. Figure 5.25 shows the principle

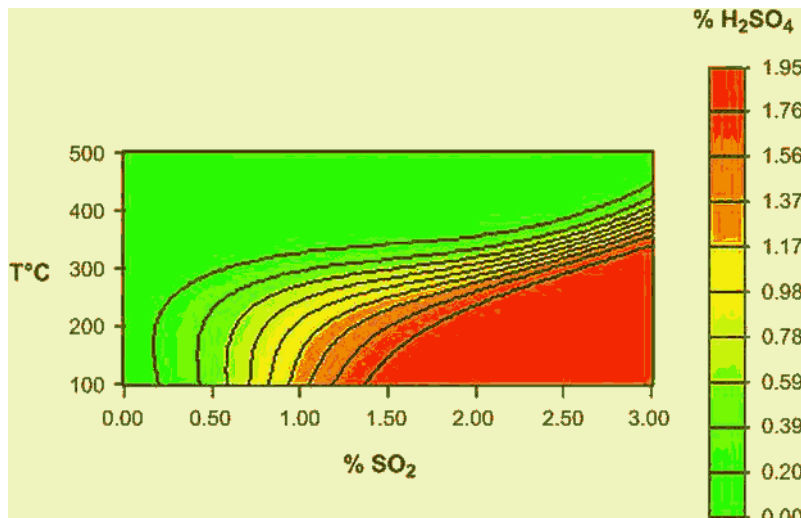


FIGURE 5.24 Approximated sulfuric acid content (vol. %) in a dust-free flue gas (85% CO₂, 4% H₂O, 4% O₂, 0.5% CO, balance N₂) versus SO₂ concentration and gas temperature at cooling. Higher values indicate a more favorable acid mist formation. (Data provided by M. Gasik.)

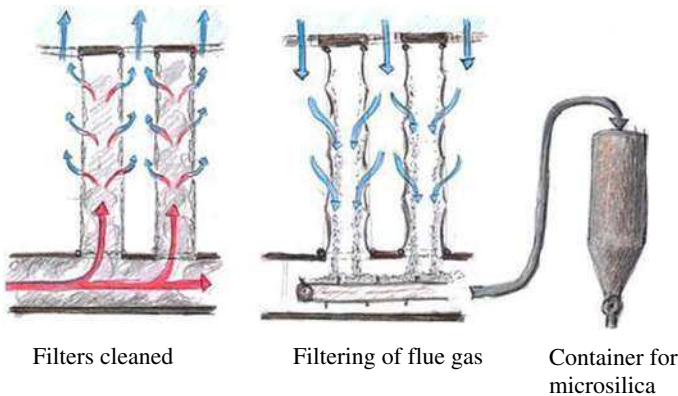


FIGURE 5.25 A schematic drawing of the baghouse filter operation for the removal of microsilica particles from the flue gas from silicon alloy processes. (*Courtesy of Dr. Þorsteinn Hannesson, Elkem Iceland.*)

behind the operation of a baghouse filter system as used in ferroalloy production plants.

During tapping, fumes from the furnace will escape through the tapping hole, burn in the oxygen, and form dust. Ideally, exhaust systems should be installed at the sites where all of these activities take place, removing the dust from the working environment. **Figure 5.26** shows the design and operation of a “dog house” smoke vent system located in the tapping area at an Elkem facility.

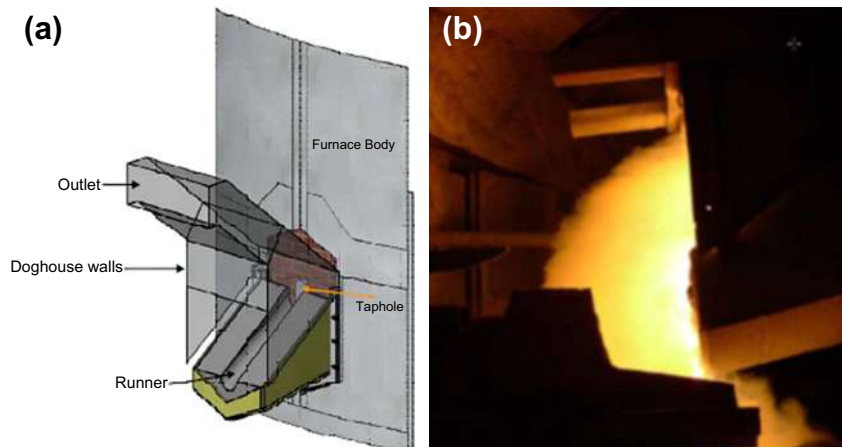


FIGURE 5.26 A schematic (a) and operation (b) of a smoke hood and vent system designed for the tapping area (“dog house”) hood installed at an Elkem factory. (*Reproduced with permission from Tveit et al., 2008.*)

TABLE 5.2 Example of Dust Chemical Composition (wt. %) from Some Ferroalloys Smelting Processes

Component	FeSi75...90	Si	FeSiCr	HC FeCr
Fe ₂ O ₃	<0.2	<4	<5	<15
Cr ₂ O ₃	—	—	<1	<5
Al ₂ O ₃	<0.5	<3	<6	5–10
SiO ₂	>96	80–96	75–95	15–35
SiC	<1	<4	—	—
CaO	<0.4	<4	<5	<5
MgO	<1	<3	<20	15–25
Carbon	<1.5	<6	<5	3–15
SO ₂ + P ₂ O ₅	<0.5	<1.5	—	—

In some processes, slags generated in ferroalloy production have high usable metal content and they are recycled so that specific dust collection and handling is not needed. In some other processes where slags are formed with a too-high content of minerals with a high volumetric phase transformation mismatch (e.g., calcium orthosilicate), a self-disintegrating slag is produced, which will cause dust generation as it breaks down. Mitigating means are needed to deal with this issue (Verein Deutscher Ingenieure, 2010). Similar measures should be taken if the metal product is crushed and screened. This will cause the generation of fine dust, which is difficult to collect and recycle. Metallic dust can be highly flammable and should be treated accordingly. Also, an air extraction system should be fitted and ducted to a dust collection device. Table 5.2 summarizes the chemical composition of particulate emissions from a number of ferroalloys smelting processes.

5.6.2 Gaseous Emissions

Ferroalloys production also generates gaseous and vaporous emissions. Most of the emissions originate in the furnace itself. Due to the high process temperatures, various metals may be present in the flue gas, if they have entered the process via raw materials or other sources. The most significant gaseous emission from these processes is sulfur dioxide originating from the carbon raw materials in the process. The concentration in the flue gas depends on the sulfur content in the carbon materials, as well as the level of dilution of the flue gas entering the process. For silicon and FeSi smelting, the common levels of SO₂

in off-gases are below 50 to 60 mg/m³. Carbon monoxide in the process gases will burn in the presence of air and form carbon dioxide. Also, hydrocarbons from the raw materials will burn to form water and carbon dioxide. Thus, residual CO levels are normally below 30 to 85 mg/m³.

Due to the high temperatures in the furnace, nitrogen oxides (NOx) are formed both in the furnace and at the tap hole during tapping. Their content might be up to 80 to 120 mg/m³. There are minor quantities of unburned organic pollutants (Verein Deutscher Ingenieure, 2010) such as benzene, 1,3-butadiene, and PAH, as well as traces of PCB and PCDD/F, which mainly originate from raw carbonaceous materials, carbon-contained charge briquettes, and electrode paste components. Their concentrations in treated waste gas are normally very low, 0.01 to 0.07 mg/m³. Other pollutants such as nonferrous metals typically are well below 0.001 to 0.010 mg/m³, as they are normally well captured and recycled.

5.6.3 Heat Emissions and Losses

In ferroalloys production processes, heat is lost in a number of ways. It is removed from the furnace structure, smoke hood, and electrode equipment using cooling water as well as through radiation and convection from the steel lining of the furnace. However, the most significant heat loss stream is the flue gas from the process. For example, in silicon and FeSi production, the energy carried by the flue gas from the furnace is more than the electric energy delivered to the furnace (see Chapter 6), and the temperature in the flue gas, 400° to 700°C, represents a high heat recovery potential (Hjartarson et al., 2010; Schei et al., 1998).

Heat recovery systems for electric power production have been successfully implemented at a number of facilities. The investment and operation is costly and complicated by the amount of dust in the flue gas, which causes severe fouling on heat exchange surfaces, which in turn creates additional maintenance costs. Heat in cooling water from smoke hood and electrode equipment as well as casting equipment can be used as a heat source in applications where low-grade direct heating is desirable, such as in greenhouse cultivation, aquaculture, or district heating with the aid of heat pumps.

REFERENCES

- Cassie, A.M., 1939. Theorie nouvelle des arcs de rupture et de la rigitité des circuits. [New theory of breaking arcs and stability of circuits] Proceedings Session on Large Electric Systems, CIGRE Rep. 102, 14 pp.
- Chen, F.F., 1990. Introduction to Plasma Physics and Controlled Fusion, Vol. 1: Plasma Physics, second edition. Plenum Press, NY, 421 pp.
- Downing, J.H., Durban, L., 1966. Electrical conduction in submerged arc furnaces. Journal of Metals 3, 337–344.

- Hjartarson, H., Palsson, H., Saevarsottir, G., 2010. Waste heat utilization from a submerged arc furnace producing ferrosilicon. Proceedings of Conference INFACON-XII, Helsinki, Finland. 739–748.
- Hochrainer, A., 1970. Einige Bemerkungen zum Stromnulldurchgang in Wechselstromschaltern. [Some noticeable loading calculations for the zero crossing in AC switches] Elektrotechnik und Maschinenbau 87, 15–19.
- Larsen, H.L., 1996. AC electric arc models for a laboratory setup and a silicon metal furnace. Doctoral Thesis 55. NTNU, Trondheim, 244 pp.
- Mayr, O., 1943. Beiträge zur Theorie des statischen und des dynamischen Lichtbogens. [Contributions to the theory of static and dynamic arc] Archives für Elektrotechnik 37, 588–608.
- Morkramer, K.L., 1961. Dimensionierungsgrundlagen von Elektro-Reduktionsöfen. [Dimensioning principles of electrical reduction furnace] Elektrowärme 19, 110–116.
- Palsson, H., Saevarsottir, G.A., Jonsson, M.T., Bakken, J.A., 2007. Thermal effects on carbon based electrodes close to a high current electric arc. Proceedings of Conference INFACON-XI, New Dehli, India. 695–702.
- Ravary, B., Bakken, J.A., Gonzales-Aguilar, J., Fulcheri, L., 2003. CFD Modeling of a plasma reactor for the production of nano-sized carbon materials. Journal of High-Temperature Material Processes 7, 139–144.
- Reynolds, Q.G., 2011. The Dual-electrode DC Arc Furnace – Modeling Insights. Proceedings of the Conference of Southern African Pyrometallurgy 2011, 33–46.
- Saevarsottir, G., 2002. High-current AC arcs in silicon and ferrosilicon furnaces. Doctoral Thesis 56. NTNU, Trondheim, 248 pp.
- Saevarsottir, G., Bakken, J.A., 2010. Current distribution in submerged arc furnaces for silicon metal. Proceedings of the Conference INFACON-XII, Helsinki, Finland. 717–728.
- Saevarsottir, G.A., Bakken, J.A., Sevastyanenco, V.G., Gu, L.P., 2001a. High-power AC arcs in metallurgical furnaces. Journal of High Temperature Material Processes 5, 21–44.
- Saevarsottir, G.A., Bakken, J.A., Sevastyanenco, V.G., Gu, L.P., 2001b. Arc Simulation Model for Three-phase Electrometallurgical Furnaces. Proceedings of the Conference INFACON-9, Quebec, Canada. 253–262.
- Saevarsottir, G., Larsen, H.L., Bakken, J.A., 1999. Modeling of industrial AC arcs. Journal of High- Temperature Material Processes 3, 1–15.
- Saevarsottir, G., Magnusson, T., Bakken, J.A., 2007. Electric arc on a coke bed in a submerged arc furnace. Proceedings of the Conference INFACON-XI, New Delhi, India. 572–582.
- Schei, A., Tuset, J.K., Tveit, H., 1998. Production of High-silicon Alloys. Tapir forlag, Trondheim, 63 pp.
- Schultz, M.E., 2006. Grob's Basic Electronics, tenth edition. NY: McGraw-Hill, 1286 pp.
- Steenbeck, M., 1932. Energetik der Gasentladungen. [Energetics of gas discharges] Physikalische Zeitschrift, 809–815. XXXIII.
- Tveit, H., Berget, K.H., Førde Møll, M., 2008. The Silicon Process – The Need for a Major Upgrade of the Internal Environment and Fugitive Emissions. Proceedings of the Conference on Silicon for the Chemical and Solar Industry X, Oslo, Norway. 25–34.
- Valderhaug, Aa. M., 1992. Modelling and control of submerged-arc ferrosilicon furnaces. Dr. Ing. Thesis 83. NTNU, Trondheim, 348 pp.
- Verein Deutscher Ingenieure, 2010. Emission Control, Carbothermic and Metallothermic Production of Ferroalloys and Silicon Metal. VDI e.V., Dusseldorf, 72 pp.

Ferrosilicon and Silicon Technology

Merete Tangstad

Norwegian University of Science and Technology, Trondheim, Norway

Chapter Outline

6.1 Introduction to Silicon and Its Ferroalloys	179	6.3.1 Basic Principles of Operation	198
6.1.1 Properties of Silicon	180	6.3.2 Smelting Process	201
6.1.2 Silicon Interaction with Other Elements	181	6.4 Casting and Refining Operations	211
6.2 Raw Materials, Silicon, and Ferrosilicon Compositions	186	6.4.1 Casting	211
6.2.1 Sources of Silica	186	6.4.2 Refining of Silicon and Ferrosilicon	212
6.2.2 Carbon Reductants	191	6.5 Energy Savings and Environmental Issues in Silicon and Ferrosilicon Production	215
6.2.3 Compositions of Silicon and Ferrosilicon	195	6.5.1 Energy Recovery	215
6.3 Silicon and Ferrosilicon Smelting Technology	198	6.5.2 Emissions Control	217
		References	219

6.1 INTRODUCTION TO SILICON AND ITS FERROALLOYS

In the liquid state, silicon has metallic properties regarding thermal and electrical conductivity, but in the solid state, it is a semiconductor and is called a metalloid. Due to its visual similarities in color and reflectance, it is often, misleadingly, referred to as a metal. Also when it comes to the production process, silicon may be produced in equipment used for metals production, such as manganese alloys and chromium alloys, and thus it is grouped with these alloys.

Before the 19th century, all elements discovered were produced by reduction with either hydrogen or carbon, but the later discovery of electrolysis has

allowed the extraction of potassium, sodium, calcium, barium, strontium, cadmium, and aluminum. In 1824, silicon was produced by the Swedish chemist Jöns Jacob Berzelius, and he named the new material “silicium.” As this material was closer in properties to boron and carbon than materials like magnesium and calcium, the Scottish chemist Thomas Thomson renamed it “silicon” some years later. In the literature, both names are still in common use in some countries.

The development of the industrial process of silicon production took almost a century (Schei et al., 1998; Vishu et al., 2005). With the development of the electric arc furnace by Paul Héroult, the first commercial plant was started in the United States in 1907, where high silicon ferrosilicon and silicon could be produced industrially. Frank Tone of Carborundum Co. was the first to commercialize the production of silicon. In the 1920s, silicon use in aluminum alloying increased steadily. In the 1930s, silicon application in chemicals and silicones increased, and the next boost for silicon came after the 1950s for photovoltaic applications, followed by the modern-day silicon demand in electronics. To be used as a semiconductor, silicon needs to be pure, and hence the metallurgical grade Si (MG-Si) must be further refined to fulfill requirements. Whereas MG-Si usually has 98.5% to 99.5% Si, the impurity content in photovoltaic devices, such as solar cells, must be in the ppm level and in electronic devices the impurity content must be in the ppb level. The most used refining method for both products is the Siemens process, where the Si is transformed to silicon–chlorine gases, which are distilled and then reduced to silicon.

The development of ferrosilicon technology corresponded with progress in the steel industry. In the 19th century, low silicon ferroalloys (~20% Si), known as silvery pig iron, were produced in blast furnaces, but since the 1920s all production has been moved to submerged arc electric furnaces, as they alone offer the only possibility of high silicon ferroalloys smelting.

6.1.1 Properties of Silicon

Silicon is the second, after oxygen, most abundant element in Earth’s lithosphere, occurring naturally in the form of silica (silicon oxide) and silicates and constituting over 25% of the crust. Silicon belongs to group IV of the periodic table with an atomic weight of 28.08 and an external electron shell configuration of $3s^23p^2$. As an analog of carbon, silicon might have oxidation states between 1 and 4, the latter being the most stable. Silicon lattice has a cubic, face-centered (FCC), diamond-type structure with lattice period 0.54307 nm at ambient conditions, giving silicon a density of 2.33 g/cm³. The melting point of silicon is 1414°C, and the boiling point is 3250°C. The density of liquid silicon is temperature dependent (Schei et al., 1998): $\rho_{liq} = 2553 - 0.45(T - T_m)$ in kg/m³, with T_m being the melting temperature. Liquid silicon solubilizes most elements to a low degree, and hence the density will not greatly depend on dissolved elements. However, if

iron is present, it will dramatically affect the density. At 1450°C the density of the Fe-Si alloys might be given as $\rho(\text{FeSi})_{\text{liq}} = 7106 \cdot \exp(-0.0107 \cdot \% \text{ Si})$ in kg/m³, where silicon content is expressed in wt. %.

6.1.2 Silicon Interaction with Other Elements

The interaction of silicon with oxygen and their compounds (silicon oxides) forms the basis not only for most metallurgical processes, but also for almost all known Earth minerals based on silicates. Silicon forms two oxides: silica (SiO_2) and silicon monoxide (SiO). Silica may exist in several phase modifications (quartz, cristobalite, tridymite, etc.), the transformations for which are shown in Section 6.2.1. At ambient conditions, β -quartz modification is the most stable. Silicon monoxide is metastable in its condensed state and easily decomposes to silicon and SiO_2 , but it is stable in a gas phase at higher temperatures. A detailed analysis of the phase equilibria and thermodynamics relating to the Si-O system was made by Schnurre et al. (2004). They considered the stable condensed phases in this system at normal pressure as quartz, cristobalite, and liquid, besides solid and liquid silicon. The Si-O phase diagram and the enlarged silicon-rich region are shown in Figure 6.1.

The solubility of oxygen in solid and liquid silicon has been studied extensively as it is important for high-quality silicon production. Data analyzed (Schnurre et al., 2004; Tang et al., 2010) show that the three-phase equilibrium $L = (\text{Si}) + \text{cristobalite}$ is a eutectic reaction, where the eutectic composition was calculated as 47.3 ppm O (at.) in solid solution and 54.2 ppm O (at.) in the liquid phase, but the eutectic temperature is only 0.003 K below the melting point of silicon. As Schnurre et al. (2004) pointed out, this extremely small melting point depression is certainly beyond any experimental determination and a direct consequence of the variation of assessed oxygen solubility in solid and liquid silicon (Tang et al., 2010). Thus, in many published phase diagrams, liquidus and solidus lines are practically indistinguishable near the pure silicon composition.

With carbon silicon forms one stable silicon carbide molecule (SiC). The phase equilibrium diagram Si-C is shown in Figure 6.2.

Silicon carbide does not melt but decomposes peritectically at ~2545°C. Gas phase over SiC has a complex composition, which depends on temperature (at 2000 K gas phase contains % (vol): 86.5 Si, 6.1 SiC_2 , and 7.4 SiC). The density of silicon carbide is 3.22 g/cm³ and besides two phase modifications α - SiC (hexagonal, $a = 0.3078 \text{ nm}$, $c = 0.2518 \text{ nm}$) and β - SiC (cubic, $a = 0.43596 \text{ nm}$), the α - SiC might exist in different polytypes (Fig. 6.3). The number of known polytypes is about 240, and they are formed by different arrangements and stacking of the layers into a single structure.

The most typical categories are 6H, 15R, and 4P (the digit tells the number of stacked layers, and the letter identifies the type of stack, hexagonal [H] or rhombohedral [R]), although some other forms also have practical value—for

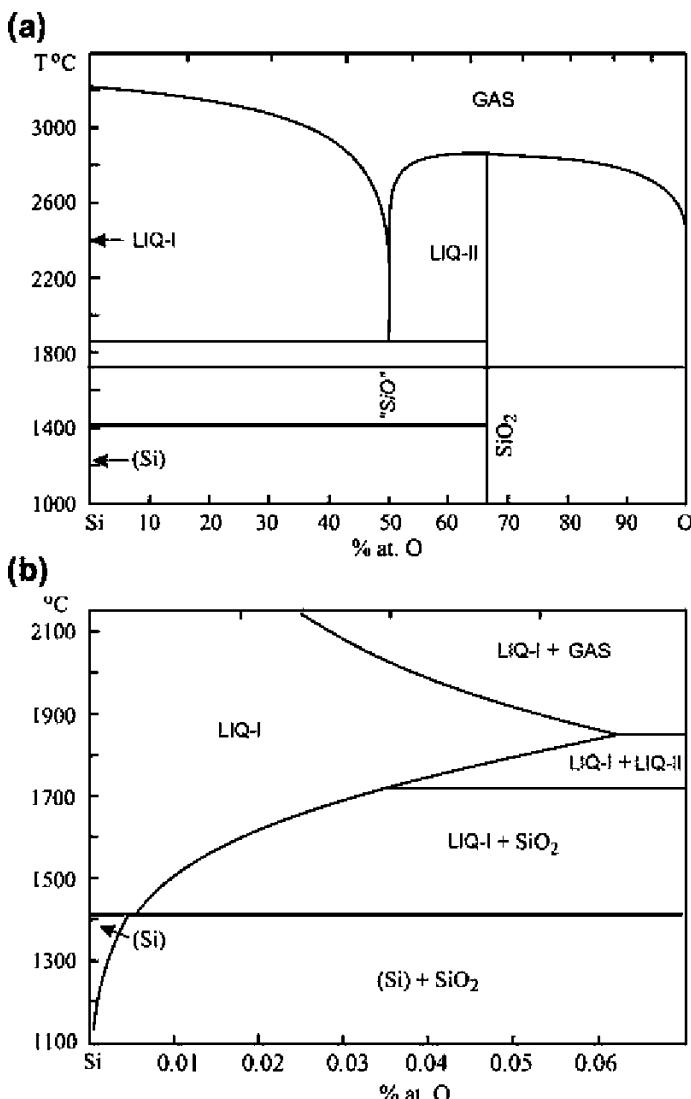


FIGURE 6.1 The equilibrium Si-O phase diagram (a) and its enlargement for the Si-rich domain (b).

example, polytype 9T crystallizes from very pure silicon melts (Inoue et al., 1971). In the SiC lattice, every carbon atom is placed into the tetrahedron of four Si atoms, and every Si atom, respectively, into C-tetrahedron. Tetrahedra [SiC₄] and [CSi₄] might be stacked in parallel or antiparallel, forming similarly oriented 2-4 hyperlayers (Gasik and Gasik, 2011). The β -phase transforms into α -SiC at temperatures over 2100°C. The density of α -SiC is temperature

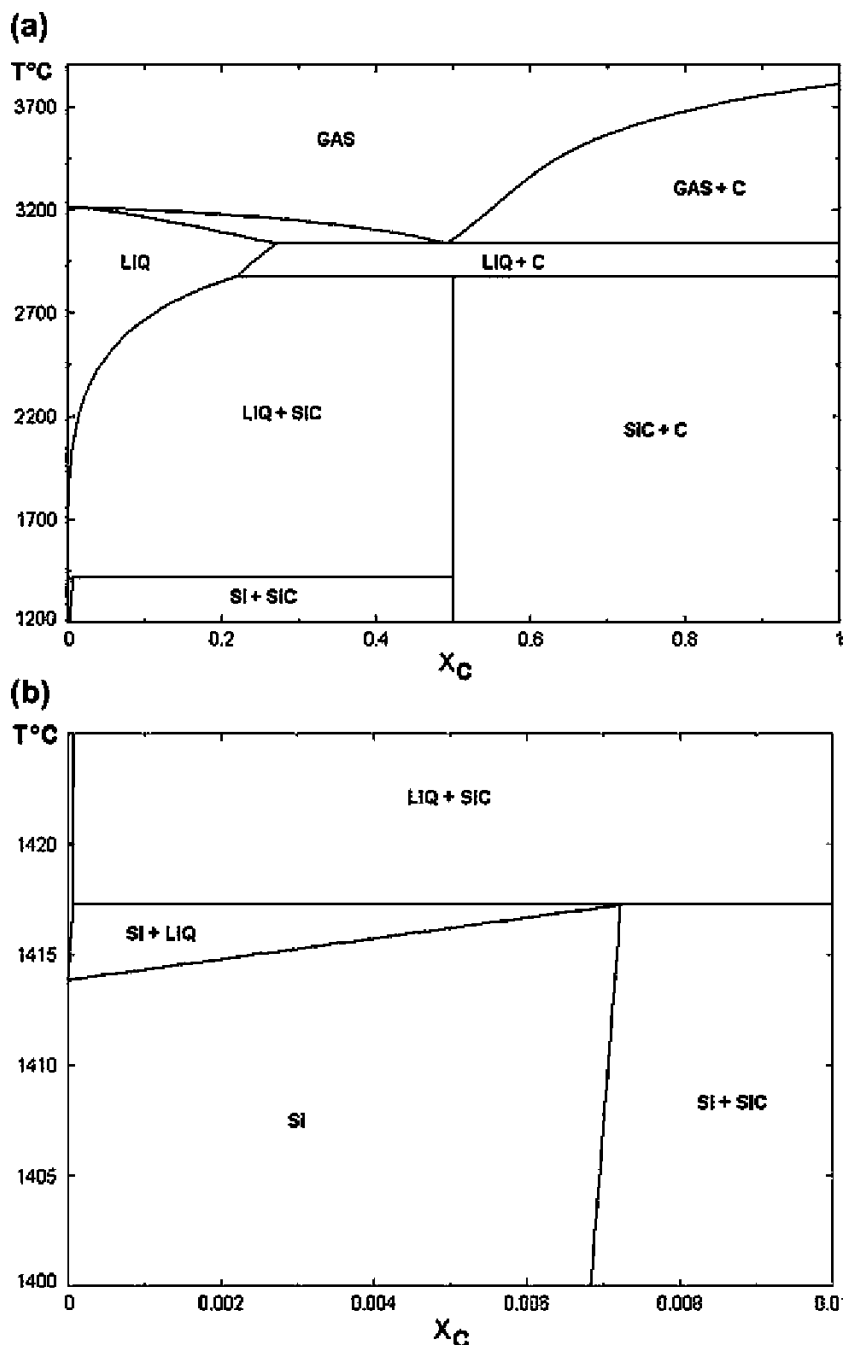


FIGURE 6.2 The equilibrium Si-C phase diagram (a) and its enlarged part in the Si-rich domain (b).

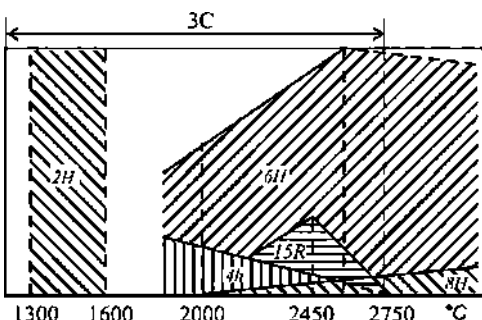


FIGURE 6.3 Approximate share of coexisting SiC polytypes. (From Gasik and Gasik, 2011.)

dependent and could be given for α -SiC as $\rho_{\alpha\text{-SiC}} = 3211 - 0.056 \cdot T(\text{°C})$, in kg/m^3 . Pure silicon carbide is colorless, but the presence of impurities gives green or gray color tints. In the furnace, produced silicon will be saturated with carbon and oxygen, as both SiC and SiO_2 are present in much excess in the high temperature zone. As the melt temperature is decreased during tapping and solidification, the solubility will decrease so SiO_2 and SiC precipitate. The solubility of oxygen is higher in the presence of iron (in ferrosilicon), but the solubility of carbon is lower compared to that for pure silicon.

Like oxygen and carbon, sulfur has very low solubility in silicon ($< \sim 10^{-8}\%$), but it forms volatile sulfides SiS and SiS_2 . Sulfur also reacts with SiC over 900°C with the formation of SiS_2 and CS_2 . These interactions are important for understanding the behavior of sulfur in the furnace, as sulfur is brought into the process with coke and other charge materials.

There are also a number of other impurity elements that will follow with the raw materials into the furnace and dissolve in silicon. The solubility is especially important when it comes to the solidification process, either during casting or in the refining step. The solubility of some elements is shown in Figure 6.4, which shows that among others, B, As, and P have relatively high solubility and their concentration will hence not be reduced dramatically during a directional solidification step. Tang et al. (2010) did an assessment of solubility, the activity coefficient, and the diffusivity of various elements in silicon.

The equilibria in the Si-O-C system are the most critical for understanding the development of the silicon oxide reduction process in the smelting of silicon and ferrosilicon. In this system, equilibrium solid phases are SiO_2 (solid or liquid), Si (solid or liquid), SiC (solid), carbon, and the gas phase (CO, CO_2 , SiO, SiO_2 , O₂, SiC, SiC_2 , Si_2 , Si_3 , C₂, C₃, Si_2C , Si_2C_2 , Si_3C , etc.). As the industrial furnace is highly reducing, the main gas species will be CO and SiO. The main reactions in the Si-O-C system might be presented as equilibrium SiO pressure versus temperature (Fig. 6.5). Note that this figure does not show the true predominance phase diagram, but an expression of different equilibrium reactions, which defines zones of eventual coexistence of different phases.

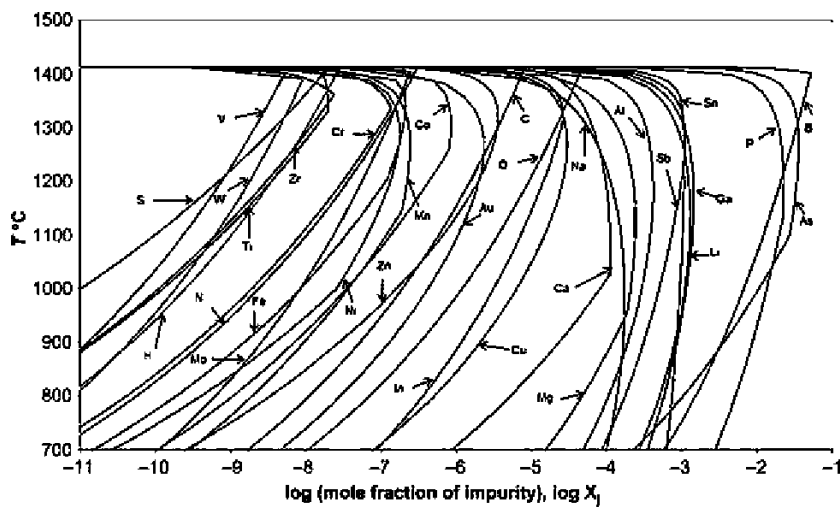


FIGURE 6.4 Solubility of different impurities in silicon. (From Tang *et al.*, 2010.)

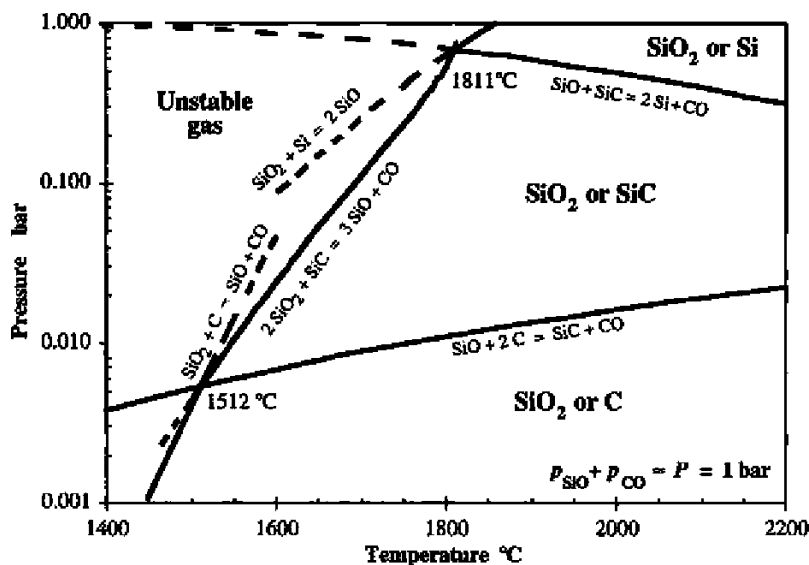


FIGURE 6.5 Partial SiO pressure versus temperature for equilibrium with different condensed phases at a total gas pressure of 1 atm. (From Schei *et al.*, 1998.)

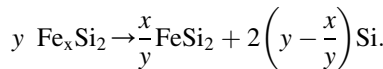
With this diagram, the conditions for silicon reduction might be understood at reasonably high temperatures ($>1800^\circ\text{C}$) and high SiO partial pressures. A higher SiO pressure and a higher temperature will increase the driving force to produce silicon. Carbon is only present at low temperatures and low SiO

pressures—when SiO pressure increases, carbon will react to form SiC . Hence, in a furnace where temperatures are well above 1000°C , SiC will be the stable carbon-containing phase in the system.

With Gibbs energy minimization, the phase predominance diagrams have been constructed for this system at prescribed temperature and total pressure (Gasik and Gasik, 2010). All solid phases were taken as pure substances, but gas was considered as real, not ideal. An additional feature is computing on the isobar of $P = 1$ bar, which is shown in Figure 6.6 as a line of plus signs (+++).

The interaction of silicon with iron is the basis for the formation of FeSi alloys in a wide range of compositions. Silicon is a ferrite-stabilizing element and narrows the γ -Fe stability area (Fig. 6.7).

The maximum solubility of silicon in γ -Fe is 1.63% wt. Si. The two-phase region ($\alpha + \gamma$) extends to 1.94% Si. A number of silicides are formed in the Fe-Si system: Fe_3Si , Fe_2Si , Fe_5Si_3 , FeSi , and FeSi_2 . The latter exists in two modifications: high-temperature FeSi_2 (HT) at 937° to 1220°C and low-temperature FeSi_2 (LT), which is below 937°C . The high-temperature phase is a nonstoichiometric compound, which exists in a certain range of concentrations of silicon, usually described as $\text{FeSi}_{2.3}$. However, it has been shown that the correct structural formula of this silicide is Fe_xSi_2 , which transforms to an LT-phase below 937°C according to the reaction (Zubov and Gasik, 2002):



Silicide Fe_3Si has a wide composition range, two modifications, and an ordering-disordering transformation (Fig. 6.8). A strong interaction between iron and silicon in the solid state is reflected also in the liquid. At 1600°C , the thermodynamic stability of clusters (associates) in the Fe-Si melt was determined to correspond to the following ratios: $[\text{FeSi}]:[\text{Fe}_3\text{Si}]:[\text{FeSi}_2]:[\text{Fe}_5\text{Si}_3] = 17.2:6.6:1.9:1$, respectively, indicating that equimolar concentration FeSi is the most favorable.

6.2 RAW MATERIALS, SILICON, AND FERROSILICON COMPOSITIONS

6.2.1 Sources of Silica

Silicon and its ferroalloys are produced by reducing silica-rich raw materials (quartzite or quartz) with carbon. Relatively pure silica (SiO_2), more frequently known as the mineral quartz, is usually found in pegmatite or hydrothermal bodies. The ore body containing the mineral quartz and smaller amounts of gangue is currently referred to as quartzite. Quartzite is typically formed metamorphic to quartz-rich sandstone. Hence, the terms *quartz* and *quartzite* are both used to describe the raw material for silicon production. From the

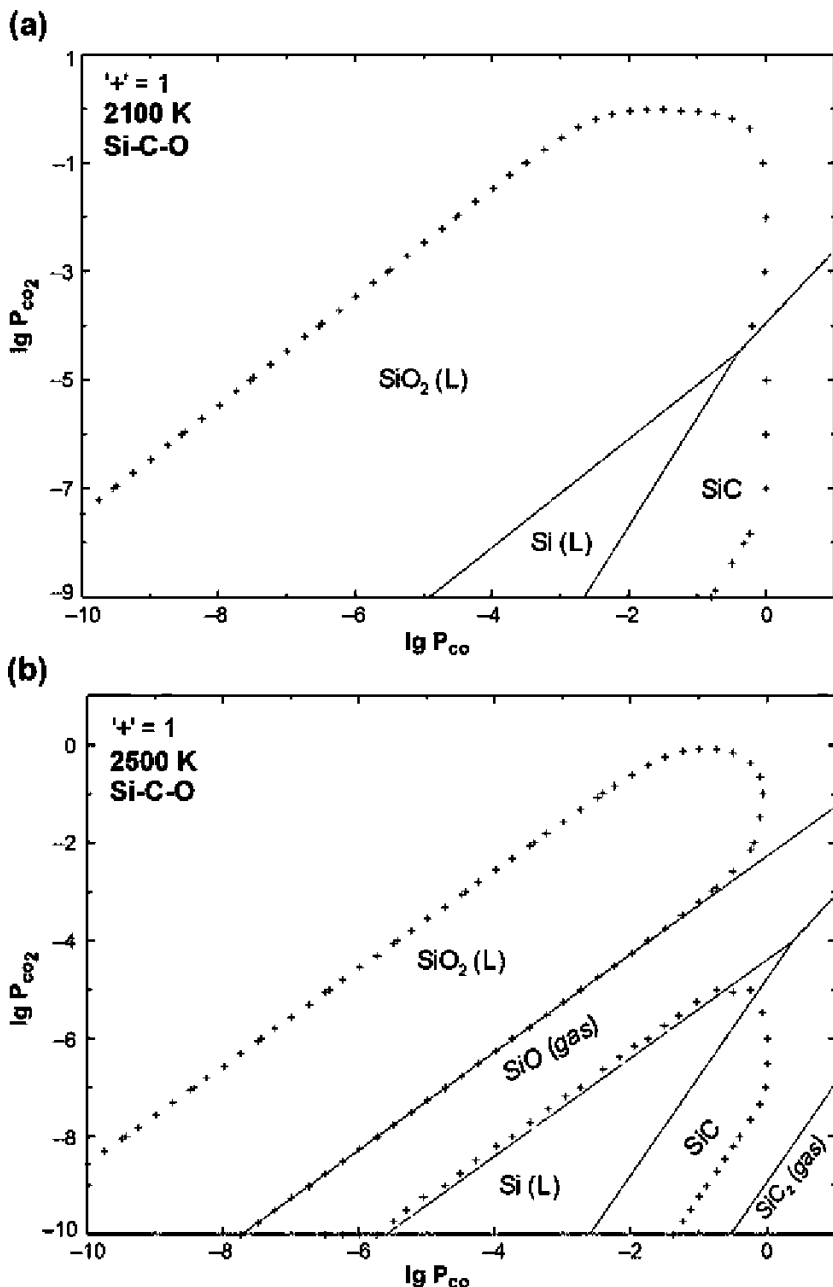


FIGURE 6.6 The phase predominance diagrams in the Si-O-C system for 2100 K (a) and 2500 K (b).

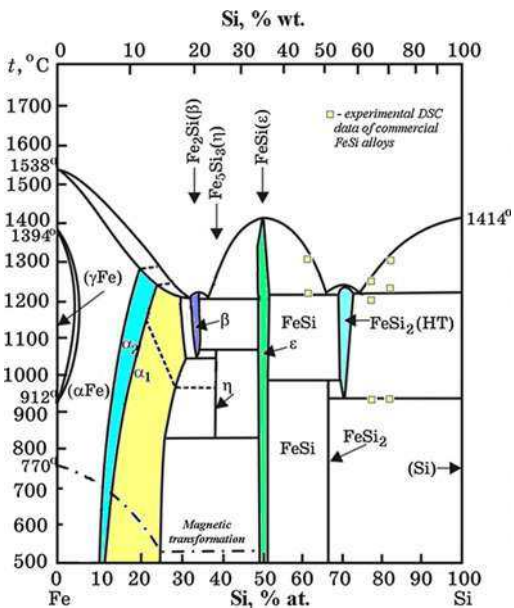


FIGURE 6.7 Equilibrium Fe-Si diagram. Experimental data (by M. M. Gasik) are shown for commercial FeSi alloys with 45%, 65%, and 70% Si.



FIGURE 6.8 Example of thermal expansion of quartz specimen during heating between 1750° and 1800°C.

metallurgical considerations, quartzite is used for more impure materials, whereas quartz is used for the purer ore bodies.

The most stable phase of silicon oxides is quartz (SiO_2), having a melting point of 1726°C and a boiling point of 2275°C. Silicon oxide SiO_2 also has several modifications that are more stable in a certain temperature range (Zubov and Gasik, 2002). The sequence of the quartz transformations might be presented as in Table 6.1. Transformations of quartz on heating and cooling are accompanied by a change in volume that sometimes leads to a premature cracking of quartz grains (quartzite) at the top of the furnace.

TABLE 6.1 Schematic of Basic Quartz Phase Transformations

α -quartz	α -tridymite	α -cristobalite	
(870°C) →	(1470°C) →	(1720°C) →	Melt
↓ 574°C	↓ 163°C	↓ 180–275°C	↑
β -quartz	β -tridymite	β -cristobalite	Glass (quenched)
	↓ 117°C		
	γ -tridymite		

It is worth noting that silica phases might have other structural forms but they have less metallurgical relevance. Transformations shown in Table 6.1 by vertical arrows are usually fast and the volume changes during these transformations are normally <1%. Transformations shown by horizontal arrows are slow and the change of volume between different phases is significant (e.g., α -quartz → α -tridymite adds 14% to 15% to the volume). Asaly (2006) found that after 10 minutes at 1550°C different quartz types would have between 0% and 10% of cristobalite. After 5 h holding at this temperature, the difference between various quartz types was gone, and they all had about 80% of cristobalite fraction.

As β forms of silica normally have higher stability, most quartz minerals appear in β form, vein quartz, quartz sand, sandstone, quartzite, flint, and so on. The basic structural unit of the crystal quartz is a silicon–oxygen tetrahedron $[\text{SiO}_4]^{4-}$. The distance Si–O is equal to 0.162 nm, and the nearest oxygen atoms are separated by 0.264 nm, resulting in an angle O-Si-O of 109.028°. Tetrahedrons can form a variety of more complex structural configurations, as described in Chapter 3 in more detail.

Many silica-contained minerals might be used for silicon-rich ferroalloys production. However, for ferrosilicon, quartzite is the most common and, for silicon smelting, quartz is the only feasible option, taking into account properties, availability, and purity. For the product and process requirements, the following properties are considered most important (Schei et al., 1998): chemistry (e.g., Al, Ti, P, Fe, and Ca content), lump size (10 to 150 mm preferable), mechanical and thermal strength (sometimes considered in combination), and softening behavior. Some elements from quartz will end up in the silicon metal, and thus the chemical composition of the oxide is perhaps one of the most important characteristics. These elements are typically more noble than Si, and among them the presence of iron, titanium, and boron is not desirable in silicon. Iron, of course, is not the concern in FeSi alloys. The quartzes used for silicon production typically contain more than 99% SiO_2 , with major impurities being Al (<0.5), Fe (<0.3), alkali (<0.25), and Ti (<0.02) species.

The lump size distribution is the most important parameter affecting the operation of the furnace. The mechanical strength of quartz is important during

transportation and handling, as well as the thermal strength during heating inside the furnace. [Aasly \(2006\)](#) reported that the fines generation and the strength of the material are dependent on the following major causes: type of quartz, mining procedures, and handling operations during transportation. It was found that even when the drilling and blasting conditions were similar during quartz mining, the resulting quartz product might give different levels of mechanical strength and stability.

Various mechanical loads are applied to quartz during transportation, and the most damaging one is the mechanical stress during drops (total drop height sometimes is ~70 m from the vessel to the furnace). The friability index is used to measure of the mechanical strength of the unheated quartz and is meant to assess how much of the quartz is disintegrating during transport ([Aasly, 2006](#)). A Hannover drum is used for tumbling the samples for given time and rate. After tumbling, the material is sieved, and a quantitative measure is found—for example, the percentage that still has the size of the original material and the dust (fines) formation as ~2 mm fraction.

The strength of the quartz raw material on heating is linked with the raw quartz properties: with a high content of microcracks from mining and transport, such quartz might disintegrate more easily during heating. The material will more or less disintegrate at elevated temperatures for different reasons ([Aasly, 2006](#)). Below the α - to β -quartz transformation (573°C), a decrepitation will occur due to fluid inclusions and the opening of microcracks. At temperatures 900° to 1000°C, decrepitating occurs again due to mica inclusions in the quartz, and over 1300°C all quartz types fracture. The formation of fines was found to increase with the cristobalite formation in quartz.

Although the chemical composition, size distribution, and the mechanical strength are the most used characterization methods for quartz feasibility for smelting in the furnace, other parameters may also be important, such as softening and melting temperature and the volume expansion of quartz.

The softening and melting of various quartz samples may affect the furnace operation. If the quartz used is melting too high in the furnace (i.e., its melting temperature is too low), it will form a sticky mass with the rest of the charge materials. This will prevent gas flow through the charge and hence gas channels will form, leading to a high SiO percentage loss and low Si output. Formation of the liquid slag phase up in the furnace might redirect some electric current paths, taking power off the arc and disturbing arc formation and overall thermal balance of the furnace. Of different investigated industrial quartz samples, heated in CO and nitrogen gas, none of them showed softening tendencies before 1800°C. However, some of them showed high volume expansion, which is believed to correlate to the transformation from quartz to cristobalite as shown in [Figure 6.8](#). It can also be noted that the volume expansion in some of the material is much higher than the

before-mentioned 15% increase, which thus might also be due to other causes.

Quartzites are a group of minerals that consists of quartz and other silica-rich minerals (opal, chalcedon, quartz) accompanied by different clay materials. Quartzites also have 4% to 9% of bounded water. Clays are usually particles $<10\text{ }\mu\text{m}$, composed of silica (30% to 70%), alumina (10% to 40%), and water with impurities of Fe_2O_3 , TiO_2 , CaO , MgO , K_2O , and Na_2O . Clays are the major source of alumina in quartzites, so they cannot be used directly in silicon and high-Si ferrosilicon smelting. The most typical clay minerals are kaolinite $\text{Al}_2\text{O}_3 \cdot 2\text{SiO}_2 \cdot 2\text{H}_2\text{O}$, dickite $\text{Al}_4[(\text{OH})_8\text{Si}_4\text{O}_{10}]$, nacrite $\text{Al}_4[(\text{OH})_8\text{Si}_4\text{O}_{10}]$, hydromuscovite $\text{K}_x(\text{H}_2\text{O})_x[\text{Al}_2(\text{AlSi}_3\text{O}_{10})_x(\text{OH})_{2-x} \cdot (\text{H}_2\text{O})_x]$, and illite $(\text{MgFe})_2(\text{Si},\text{Al}_4)\text{O}_{10} \cdot [(\text{OH})_2 \cdot \text{H}_2\text{O}]$. The last two are major sources of alkalis in ferrosilicon production. Some typical compositions of quartzites reported from Commonwealth of Independent States (CIS) countries are summarized in Table 6.2 (Gasik and Gasik, 2011).

6.2.2 Carbon Reductants

The choice of carbon reduction material is based on the following three main factors: process, product, and environmental considerations. The material must have the properties needed to achieve a high Si yield in the furnace and it must meet the product specifications. This means that the conditions for impurity elements in the raw materials (as, e.g., phosphorus) must be met. The reduction material will naturally cause the emissions of CO_2 . This is inevitable with today's technology. Some elements in the reduction materials will be reduced or evaporated in the process and follow the off-gases. Mercury is one element that will end up in the off-gases and should be avoided in the raw materials.

Besides general requirements for carbon reductants for ferroalloys (Chapter 3), in silicon and ferrosilicon smelting the additional most important requirements are size and SiO reactivity. The size of the particles will affect the permeability of the charge burden as well as the SiO reactivity. If the carbon particles are too fine, a high SiO reactivity will be obtained, but at the same time the gas permeability will decrease. Also smaller particles ($<1.5\text{ mm}$) may be taken by the gas flow, thus decreasing the process availability of the carbon added. The size of the carbon material is typically between 1 to 30 mm, according to Schei et al. (1998).

Myrvågnes (2008) investigated SiO reactivity, and the following summary is based on his work. His review showed that there are a number of recipes for carbon mixes that are used worldwide in Si smelting furnaces (Fig. 6.9). Based on a costs and availability, the reduction material can be based on fuels like coal or charcoal. Some producers also use petroleum coke. Metallurgical coke is not much used, as it gives lower SiO reactivity.

All producers use woodchips to increase the permeability of the burden. As shown later, the large number of condensates in the silicon furnace may easily

TABLE 6.2 Some Typical Compositions of Quartzite Minerals

Origin	Composition, % wt.						
	SiO ₂	Fe ₂ O ₃	Al ₂ O ₃	CaO	MgO	TiO ₂	P ₂ O ₅
Russia/Ural-1	98–99	0.3–0.4	0.25–0.45	—	—	—	—
Russia/Ural-2	98–98.5	0.41	0.24	0.7	—	0.14	—
Russia/Ural-3	97–98	0.2–0.4	0.9–1.3	0.2–0.4	0.1–0.3	—	—
Russia/Center	96–98	0.7–0.9	0.8–1.2	0.3–0.6	0.04–0.2	0.07	—
Russia/South	96–98	0.4–0.9	0.2–1	0.3–0.7	0.1–0.3	—	—
Russia/Siberia	98.4	0.4	0.5	0.52	0.35	—	—
Georgia	96–96.5	1–2.6	0.2–0.5	0.7	0.2–0.5	—	—
Ukraine/East	97.5–98.5	<2	<1.7	0.8	—	—	—
Ukraine/Center	97–98	0.5–1	0.4–1.2	0.2–1.	0.2–0.4	—	—
Ukraine/West	98–98.6	0.1–0.2	0.4–0.7	—	—	—	—
Kazakhstan/East	95–99	0.2–2.8	0.4–1.9	0.1–0.2	0.03–0.2	0.02–0.06	0.01–0.02
Uzbekistan	95–96.5	0.2–1.4	0.8–1	0.2–1.3	<0.15	—	—

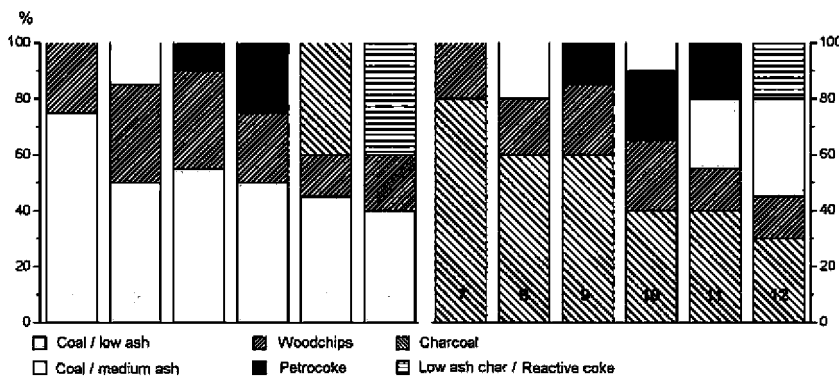


FIGURE 6.9 Comparison of various recipes of carbon reductants for silicon production by different sources. (From Myrvågnes, 2008.)

clog the voids in the burden. Hence, compared to other metallurgical furnaces, extreme measures, like using woodchips, must be taken to ensure good permeability. The typical raw materials used in silicon production are thus coal, charcoal, petroleum coke, and char for reduction purposes and woodchips for permeability (Myrvågnes, 2008).

Coal is a fossil carbonaceous material that is fairly commonly used as a reductant in the silicon process. Properties of coal are determined by organic materials from which it is the solid product, conditions at the time of deposition, and parameters that influence the maturity (see Chapter 3). The main properties of coal affecting both the process and the purity of the produced metal are rank, maceral composition, and amount and origin of mineral inclusions in the coal.

Metallurgical coke is the solid residue after a controlled carbonization of bituminous coal. As most of the metallurgical coke is used in the blast furnace production of pig iron, the main requirements are high strength and low reactivity toward CO₂. As properties of metallurgical coke do not correlate well with the requirements for reduction materials in the silicon process, char and reactive coke are used more commonly than metallurgical coke.

Char constitutes carbonization products from wood, activated carbons, or coal that do not pass through a plastic stage during pyrolysis and carbonization. Chars can be differentiated from metallurgical cokes by the level of anisotropy, with the former being isotropic and the latter characterized by a high degree of anisotropy.

Charcoal is a reduction material of biological origin and has been produced for centuries if not millennia. Charcoal for the silicon smelting process is produced by pyrolysis and carbonization of wood at moderate heating rates. The process can be divided into the following main stages: heating and drying (<110°C), wood endothermic (110° to 270°C) and exothermic (270° to 400°C)

decomposition, charcoal formation with some residual tar ($\sim 400^\circ\text{C}$), completion of carbonization ($\sim 500^\circ\text{C}$), and finally gasification and the degradation of charcoal (500° to 1000°C).

Petroleum coke (petrocoke) is a by-product of the oil refining process, generated in delayed coking. The heavy fractions from crude oil distillation are heated to $\sim 500^\circ\text{C}$ with partial cracking, generating lighter hydrocarbons and a solid residue, which is petroleum coke. The petroleum coke is usually divided into sponge-, shot- and needle-like coke.

Including woodchips in the raw materials recipe results in a higher permeability in the furnace, thus contributing to a better distribution of the gas flow through the burden and minimizing the effects of blowing.

In the silicon smelting process, one important property of the reduction material is its ability to react with SiO gas to increase the silicon yield in the furnace: $2\text{C} + \text{SiO(g)} = \text{SiC} + \text{CO(g)}$. Several models of mechanism of this reaction have been investigated, and it was found that the rate-determining step would be a mixture of gas diffusion in and out to the reaction zone and the chemical reaction itself. [Myrhaug \(2003\)](#) compared different theoretical models and found that some particles like charcoal could be described by the shrinking core model, whereas metallurgical coke did not follow the same typical topochemical model. When describing a packed bed, the shrinking core model gave the best result.

In addition to the single particle reactivity, tests of industrial materials usually show more correct results as several particles can be investigated simultaneously. One method commonly used to test for industrial carbon materials used in the silicon industry is the SINTEF reactivity test. In this test, the off-gas composition is measured and correlated with materials reactivity. The reactor contains three distinct parts: first a SiO generator, then a reaction chamber, and, on top, a condensing chamber. These reactors are placed in a vacuum graphite tube resistance furnace. In the SiO generator, the pellets made of fine ground α -quartz (SiO_2) and SiC powder are loaded and heated in Ar gas to a fixed temperature where they produce gas with 4.5% CO and 13.5% SiO according to the reaction $2\text{SiO}_2 + \text{SiC} = 3\text{SiO(g)} + \text{CO(g)}$. This gas enters the reaction chamber where the tested reduction material is placed in a bed. The SiO in the gas will react with carbon material to produce more CO: $\text{SiO(g)} + \text{C} = \text{SiC} + \text{CO(g)}$, and the SiO concentration in the reacted gas phase should decrease.

If a highly reactive material is used and all SiO gas is consumed, the off-gas from the carbon bed will contain very low amounts of SiO gas. When all tested carbon material is consumed and transformed into SiC, the off-gas will again contain 13.5% SiO, as SiO has no reaction anymore with SiC. The transition period from low SiO content to high SiO content in the off-gas is thus fast for high reactivity materials. If a low reactive carbon material is used, the transition from low SiO content to high SiO content is slower. Hence, a measure of reactivity might be the amount of unreduced SiO gas present

until the CO content reaches 10%. After the gas leaves the reaction chamber, it cools in the condensation chamber where the SiO decomposes into SiO₂ and Si in alumina tubes. The reactivity of different carbon reductants measured by this method could be roughly ranked as “charcoal > coals > cokes,” although various groups of raw materials have similarly closer reactivities. Myrvågnes (2008) determined that the most important parameters affecting the SiO reactivity were the rank of the coal, the ratio of fusible macerals versus infusible macerals, the density, and the amount and composition of mineral matter (ash).

6.2.3 Compositions of Silicon and Ferrosilicon

Silicon and ferrosilicon can be used in a number of applications and can be divided into four main product groups.

First, in steelmaking, silicon application has many features. As an alloying element, it provides solid solution strengthening in HLSA and some other steels, improves high-temperature oxidation resistance (Cr-Mo-V and stainless steels with 1% to 2% Si), and ensures lower electric losses in electric steels (e.g., “soft magnetic” steels in transformers, electric motors, and generators). Deoxidation and alloying of steel and cast iron is the largest application of ferrosilicon. Ferrosilicon reduces the oxidation of valuable elements like Cr in stainless steel production. It is also used as an alloying element to increase the elasticity, tensile yield, and annealing resistance in steels. In cast iron it is used, together with other elements, as an inoculant to induce graphite nucleation. Although the main type of silicon addition in steelmaking is in the form of ferrosilicon (FeSi) and ferrosilicon–manganese (FeSiMn), some other silicon ferroalloys are also frequently used (Vishu et al., 2005; Young, 2001).

Second, a large part of the produced silicon is used as an alloying element in aluminum to enhance the mechanical properties of cast and wrought aluminum alloys. As iron is a detrimental element in aluminum, the iron content of the silicon for these purposes must be controlled.

The third important area is the utilization of silicon in the chemical industry to produce silicones and similar derivatives. Silicones can be liquid oil, grease, rubber, and solid resin and are chemically inert, water repellent, and stable up to 400°C. They are used for medical applications, electric insulators, protective coatings, hydraulic fluids, and lubricants. The most important property of the silicon to this group of customers is the content of impurity elements, but the structure and grain/lump size of silicon are also important. Besides pure silicon, some high silicon ferrosilicon may be used.

Finally, as a semiconductor, silicon is widely used as a raw material in the electronics industry. For these applications, purity and dopants control are critical factors, and hence the metallurgical grade Si (MG-Si) must be further refined to fulfill its requirements. Although MG-Si usually has silicon content

from 98.5% to 99.5% Si, the impurity content in, for example, solar photovoltaic devices must be in the ppm level and for electronic devices it must be in the ppb level. The most used refining method for both products is the Siemens process where the raw material silicon is transformed to silicon–chlorine gases, which are distilled and then reduced back to pure silicon.

Since the beginning of the 21st century, the production of silicon has increased gradually from 1.1 million to almost 1.8 million tons, as shown in Table 6.3. The major producing country is China, which accounted for almost 50% in 2010. Other major producers are Brazil, Norway, the United States, and France. These five countries account for more than 80% of the world's silicon production. The remaining 20% is covered by countries that have a minor production, such as Australia, Canada, Germany, Russia, South Africa, and Spain. Roskill (2011) reported that the four companies producing the most silicon were Ferroatlantica, Dow Corning, Elkem Bluestar, and Globe Specialty Metals.

TABLE 6.3 The World Production of Silicon, Thousand Tons (based on data obtained by Roskill, 2011)

	2001	2002	2003	2004	2005	2006	2007	2008	2009	2010
Australia	32	32	32	32	32	32	32	32	32	32
Bosnia-Herz.	—	—	2	3	8	16	13	13	11	16
Brazil	112	133	181	220	229	226	225	220	154	240
Canada	30	35	40	40	40	40	40	40	24	47
China	400	500	600	660	650	730	820	820	780	820
France	90	85	85	85	85	100	120	118	90	125
Germany	28	25	28	29	29	30	29	29	28	30
Laos	—	—	—	—	—	—	1	3	7	10
Norway	135	153	207	193	179	150	145	160	110	160
Russia	70	70	65	65	58	60	55	61	18	46
South Africa	39	43	49	51	54	50	50	49	51	50
Spain	30	27	28	25	35	32	32	33	15	30
Ukraine	5	5	8	8	8	8	5	5	5	5
United States	131	108	134	144	143	148	150	150	130	150
Total	1102	1216	1459	1555	1550	1622	1717	1733	1455	1761

TABLE 6.4 Composition of Metallurgical Silicon

Grade	wt. %, max (except for silicon)				
	Si	Fe	Al	Ca	Fe+Al+Ca
Si99	99	0.4	0.4	0.4	1
Si98	98	0.7	0.7	0.6	2
Si97	97	1	1.2	0.8	3
Si96	96	1.5	1.5	1.5	4

Some typical compositions of metallurgical silicon are shown in Table 6.4, and typical compositions of ferrosilicon are shown in Table 6.5. Note that practical compositions of commercial alloys, especially for minor impurities, may vary depending on the types and purity of the raw materials used. Some producers might require higher standards if the raw materials and processes allow so.

TABLE 6.5 Composition of Ferrosilicon (maximal content for all elements except Si and Al), balance—iron

FeSi Type	wt. %							
	Si	Al	P	S	C	Mn	Cr	Ti
FeSi10	8–13	<0.2	0.15	0.06	2	3	0.8	0.3
FeSi15	14–20	<1			1.5	1.5		
FeSi25	20–30	<1.5			1	1		
FeSi45	41–47	<2	0.05	0.05	0.2	1	0.5	0.3
FeSi50	47–51	<1.5		0.05		0.8	0.5	
FeSi65	63–68	<2		0.04		0.4	0.4	
FeSi75Al1	72–80	<1	0.05	0.04	0.15	0.5	0.3	0.2
FeSi75Al1.5		1–1.5					0.3	
FeSi75Al2		1–2			0.2		0.3	0.3
FeSi75Al3		2–3					0.5	
FeSi90Al1	87–95	<1.5	0.04	0.04	0.15	0.5	0.2	0.3
FeSi90Al2		1.5–3					0.2	

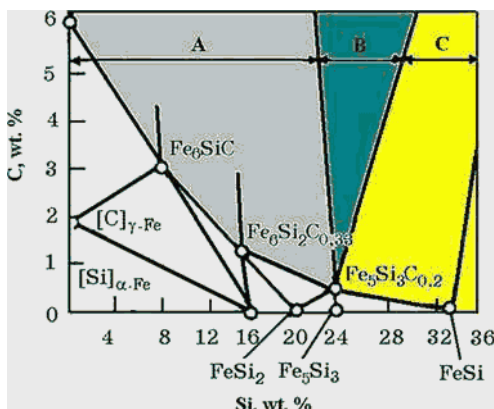


FIGURE 6.10 Influence of silicon concentration on carbon solubility in Fe-Si-C alloys at 1760°C. Excess solid phases in equilibrium with the melt are graphite (zone A), SiC (zone C), or both (zone B).

In the Fe-Si-C system, the solubility of carbon depends on temperature and silicon content, decreasing with higher silicon concentrations. Until ~24% wt. Si carbon solubility in melts decreases almost linearly. Iron, silicon, and carbon are able to form complex silicocarbides (Nowotny's phases) $\text{Fe}_x\text{Si}_y\text{C}_z$, where composition depends on the ferrosilicon grade. When carbon solubility is exceeded, the melt will be in equilibrium with graphite (zone A), graphite and SiC (zone B), or SiC (zone C) (Fig. 6.10). Thus, higher FeSi grades have much less carbon than low Si grades.

At high temperatures, both carbon and silicon dissolve well in iron, but on cooling excess phase (C or SiC) precipitates from the melt. To avoid fine graphite (<22% Si) or SiC (>24% Si) inclusions inside the ferrosilicon, the alloy is held in the ladle before casting.

Ferrosilicon (especially with lower Si content) may be granulated by pouring a controlled molten stream of alloy into a tank of water. The resulting granule size ranges from 0.2 to 2 mm. Low Si grades (<20% to 25% Si) are magnetic, which is an advantage in handling. These are used primarily as furnace blocks and are added in the form of controlled-weight piglets for initial deoxidization (Vishu et al., 2005). This type is also furnished in powder form for ore beneficiation (flotation in heavy suspensions). High aluminum ferrosilicon is used for the production of spheroidal gray iron to control and minimize the formation of carbides and decrease section sensitivity by refining graphite size and distribution. In ductile iron it is also known to be effective in minimizing carbide formation while increasing nodule count (Vishu et al., 2005).

6.3 SILICON AND FERROSILICON SMELTING TECHNOLOGY

6.3.1 Basic Principles of Operation

Silicon and ferrosilicon are produced carbothermally in electric arc furnaces. The major difference between silicon production and ferrosilicon production is,

of course, the presence or absence of iron in the system. Iron lowers the activity of silicon in the metal; hence, the major difference will be that ferrosilicon can be produced at a lower temperature, the Si yield will be higher, and the power consumption per ton of metal will be lower. However, the chemical reactions and the zones in the furnace are believed to be similar in the two processes, although for low Si ferrosilicon there will, of course, be additional differences.

Although the production is relatively simple in principle, the industrial process, which needs to be safe, environmentally sound, and effective, is much more complicated. As a high temperature is needed for production, silicon is produced in electric melting furnaces. This is the heart of the smelting plant. As shown in [Figure 6.11](#), the plant consists of the following production units in addition to the furnace:

1. The mix unit where the raw materials are weighed and mixed before they enter the raw material silos.
2. The electrical system giving energy to the furnace
3. The off-gas units that cool down and remove the off-gas from the furnace
4. The processing units where produced liquid silicon is refined cast and crushed. These parts of the plant are often referred to as the downstream units or post tap hole units, as they come after the furnace—that is after the tap hole—in the value chain.

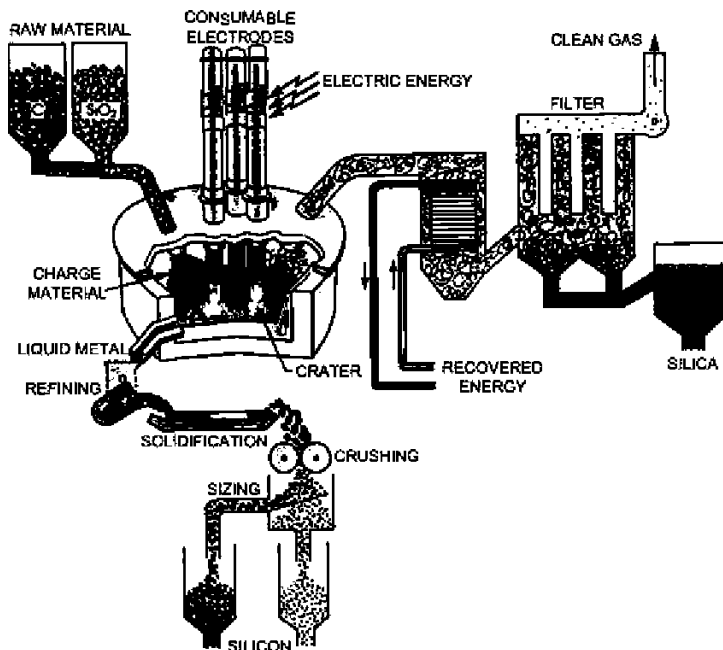


FIGURE 6.11 The schematic of the silicon smelting plant process. (*From Schei et al., 1998.*)

The electric energy is fed into the furnace through three electrodes, which are slowly consumed during production. In ferrosilicon smelting, electrodes are usually of the self-baked, Söderberg type, which are continuously replaced. Chapter 4 provides more details about self-baked electrodes technology. As they contain a steel shell that dissolves in metal, self-backed electrodes cannot be used in pure silicon production and prebaked electrodes are applied. For large-scale silicon furnaces, a composite electrode has been developed. These electrodes are made with a graphite core to secure the strength of the electrode. On the outer part, the less expensive carbon paste is used. The electrode is “extruded” through a steel casing to avoid adding iron to the silicon.

The off-gas plants consist of a cooler and a dust filter. Some plants also include an energy recovery unit. As energy is one of the main resources defining the profitability and sustainability of a process, energy recovery is expected to be a vital part of all plants in the future. From the furnace the gas species are mainly CO and SiO gas, and when these gases meet the air above the charge, they will exothermically oxidize to CO₂ gas and solid SiO₂. These reactions heat the fresh raw materials, keeping the temperature on top of the furnace between 700° and 1300°C. A higher temperature of the off-gas provides better energy recovery efficiency.

When the SiO-rich gas is oxidized, it forms “silica fume” or microsilica, consisting of solid, almost spherical SiO₂ particles, with an average size of only ~0.15 µm. In addition to the silicon, microsilica is an important by-product, which is used in the cement industry. The microsilica increases the strength and lifetime of the concrete. As an example, to strengthen the concrete in one of the highest buildings in the world, the Petronas Twin Towers in Kuala Lumpur, Malaysia, the Norwegian ferrosilicon company Finnfjord delivered about 4800 ton of microsilica.

Silicon is produced at temperatures above 1800°C in the furnace, so it stays in liquid form. The molten silicon is tapped into ladles. While the silicon is still liquid, the impurities less noble than silicon (Al, Ca, etc.) can be removed in an oxygen refining process to the form of oxides (slag). This is done by bubbling oxygen or air through the molten silicon. Silicon may also be oxidized, and the extent of the silicon oxidation is controlled by the rate of oxygen addition. However, if very small amounts of CaO and Al₂O₃ are present, the oxides will form inclusions (particles) in the molten silicon and do not actively move to form a separate slag phase. To prevent this, a flux CaO-SiO₂ is added to absorb the oxides. The oxide layer, whose density depends on the slag composition, will form on either the top or the bottom of the liquid silicon.

After the refining process, the liquid silicon is cooled and solidified. One typical method is to cast the silicon in big beds lined with solid silicon fines. This will prevent the silicon from being contaminated by other lining materials. When the silicon has solidified, it is crushed to a more convenient size. Some plants also granulate parts of the production by very gently pouring the liquid

silicon into a water pool. The product is thereby transformed into granules of a more homogeneous size. Liquid silicon in water has the potential to create violent explosions; hence, the granulation plant is situated in bunkers, which restrict the formation and possible direction of the explosion gases.

One of the important parameters controlled and adjusted by the furnace personnel is the submersion depth of electrodes. It depends also on the voltage switch and changes in the composition of the charge feed. Excess carbon reductant in the charge reduces the electrical resistance, so the depth of immersion of the electrodes in the charge decreases. A lack of reductant leads to an increase of electrical resistance and moves the electrode down (i.e., to deeper submersion). Significant deviations in the depth of immersion of the electrodes are a clear evidence of abnormal furnace operation, requiring changes in voltage steps or in the charge composition (Zubov and Gasik, 2002).

Typical symptoms of insufficient reductant in the charge are electrical current oscillations, unstable position of the electrodes in the charge, gas emission concentrated near the electrodes, increase of the charge sintering and number of gas fistulas, tapping of viscous slag, and partial furnace gases escape through the tapping hole. These lead to the thinning of the diameter and length of the working tip of the electrodes and an increase in the top charge temperature from 500°–600° to 1000°–1200°C with an increase in silicon losses due to SiO and dust. Delayed actions would cause a suspension of slag tapping and difficulties in closing the tap hole. The process might be restored by adding a “light” charge portion (with excess carbon reductant) under electrodes and by adjusting the operating voltage step.

Typical symptoms of reductant excess in the charge are rising of electrodes, narrowing of the crucibles (craters), avalanches of charge around the electrodes, sounds of electric arcs, difficulties in slag, and alloy tapping due to high SiC content. These symptoms might be caused by violations on short electrodes. Another cause is operation on electrodes that are too short (Shkirkontov, 2009a and 2009b).

Signs of good silicon/ferrosilicon furnace operation progress are (1) uniformly charge flow in all areas, without zones of over-sintered charge; (2) a deep position of electrodes; (3) positive gas pressure; (4) optimal temperature on the charge top (for ferrosilicon this could be below 500° to 600°C); (5) hydrogen content of the off-gas <5%, oxygen <1%; and (6) a constant off-gas flow rate. Too-high gas pressure is often due to a lack of reducing agent and the formation of large quantities of SiO (Gasik et al., 2011).

6.3.2 Smelting Process

6.3.2.1 Reactions in the Furnace

The core of the production process is the melting furnace. The furnace in general consists of a steel casing, lined on the inside with a material that can withstand high temperatures, mechanical stress when raw materials move

continuously through the furnace, and chemical wear when molten oxides/metals flow through it (Chapter 4 provides more details of furnace design, and Chapter 5 explores their electrical operation principles).

Electrical energy is fed into the process through electrodes. In AC furnaces for silicon and ferrosilicon smelting, the electric current flows from one electrode, through a gas cavity, down into the liquid bath, and up the next electrode. The gas cavity is formed around the electrodes' tip, and there an electric arc is ignited. The arc itself is a high-temperature plasma, up to 20 000 K, and is the source of heating in the arc furnace, increasing the temperature of the charge materials to 1800° to 2000°C. The DC closed furnace technology for smelting silicon has also been demonstrated, and significant effort has been put into its development (Vishu et al., 2005).

Most furnaces are semiclosed, which means the furnace has a partly open hood above the furnace chamber. The advantage of such a furnace is that one has access to the materials in the furnace through big hatches. An important part of the furnace operation is shifting the material to the high-temperature areas in the furnace, called stoking. In the silicon furnace, the production of condensates in the upper part of the burden is important to obtain a high silicon yield. However, the same condensate glues the charge and prevents a natural descent in the furnace. The stoking of the charge is thus an important part of the furnace's operation. Some industrial furnaces are also divided horizontally in the middle where one part rotates. This also contributes to a better raw material descent in the furnace.

The formal brutto-reaction of silicon reduction from silica is $\text{SiO}_2 + 2\text{C} = \text{Si} + 2\text{CO}$, but as shown previously, formation of SiO gas and solid SiC has a large influence on the whole process. In the furnace, raw materials are added from the top at ambient temperature and are quickly heated to 700° to 1300°C by the rising hot gas that burns at the top of the furnace. The raw charge materials are mainly SiO_2 and carbon. According to the equilibrium, SiO_2 will start to react with C to form SiC above 1500°C. Two solid particles of silica and carbon share only a small contact surface, and they will react with each other very slowly unless they were preliminarily mixed and supplied as briquettes or pellets.

From the high temperature area of the furnace, SiO gas rises to the cooler top area, where it reacts with carbon $\text{SiO(g)} + 2\text{C} = \text{SiC} + \text{CO(g)}$. This reaction is very important, because otherwise SiO gas will leave the furnace through the exhaust system and will oxidize to silica fume. The formation of SiO needs substantial energy, and if a lot of SiO gas leaves the furnace, the silicon yield is low and the power consumption becomes very high. If the residence time of SiO gas is long enough, even in the areas without carbon it will be disproportionate to silica and silicon ("condensates"): $2\text{SiO(g)} = \text{Si} + \text{SiO}_2$.

The materials that now sink down through the furnace into the high temperature area will consist of SiO_2 , C, SiC, and some Si. Pure silica melts at 1723°C forming a viscous liquid. In the high temperature area (~2000°C), the

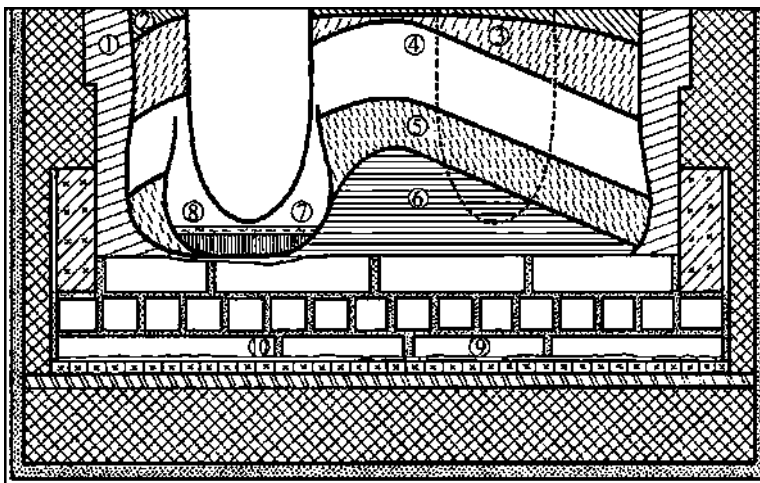


FIGURE 6.12 Cross section of the excavated open arc furnace after smelting silicon: 1, frozen lining; 2, sintered charge; 3, partially molten charge; 4, partially metallic charge; 5, molten and metallized charge; 6, SiC-rich crust; 7, silicon melt; 8, slag; 9, glassy phase; 10, slag penetrated under carbon bricks lining.

total process (unbalanced) may be described as $\text{SiO}_2 + \text{SiC} + \text{C} \rightarrow \text{Si} + \text{SiO(g)} + \text{CO(g)}$. It is important not to add too much carbon into the process zone as extra SiC will be formed and it may accumulate in the furnace (“freezing”). Figure 6.12 illustrates the results of the excavation of the industrial 16.5 MVA, silicon smelting furnace (Gasik and Gasik, 2011), indicating the main observed zones.

The mixture of SiO_2 , SiC , and condensate behave as a bridge, stopping the further descent of raw materials. Below this region it will therefore develop a void around the electrode. In the bottom of this void, there will be a liquid silicon pool containing SiC particles. From the bridge of liquid SiO_2 , drops of SiO_2 will fall down in the pool and react with SiC to form liquid Si and SiO gas. Heat is generated from electric current forming an arc between the electrode and the liquid silicon pool. In the cavity, a slight overpressure of 1 to 1.04 atm is measured (Kadkhodabeigi et al., 2011). When there is overpressure, internal avalanches and gas channels may be formed, leading to high off-gas temperatures and high SiO content. The temperature of the top of the charge could be as high as 1300°C , but it is very dependent on how much SiO will be condensed to Si and SiO_2 (Ringdalen and Tangstad, 2012).

Laboratory experiments have found that the rate of SiO formation from SiO_2 and SiC is more than two to three times faster than the $\text{Si} + \text{SiO}_2 \rightarrow 2\text{SiO(g)}$ reaction. If the contact area between the reactants changes dramatically, this may, of course, change the SiO production rates in the industrial furnaces. At lower furnace levels, SiO will mostly condense to a brown condensate (SiO_2 and Si) (Fig. 6.13).

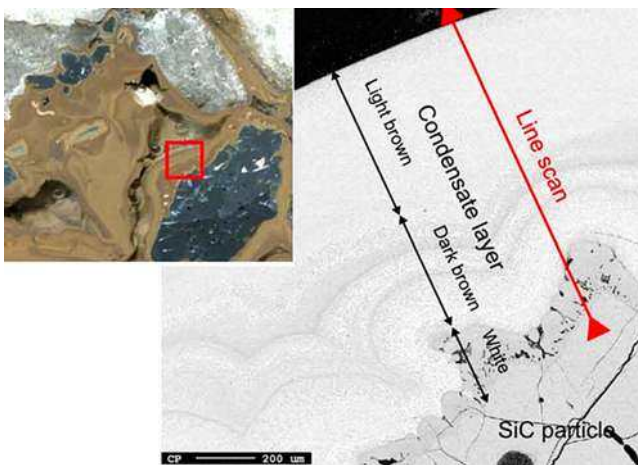


FIGURE 6.13 Macroscopic and microscopic views of condensate produced in a 50-kVA induction furnace.

This brown condensate may have various colors based on the size of the spherical silicon particles, and larger Si spheres give a darker color. A thin white condensate layer might be observed covering these particles (see Fig. 6.13), and its composition is $\text{SiC} + \text{SiO}_2$ coming from the reaction of SiO and CO in the gas phase. White condensate is believed to form when the temperature and SiO pressure are lower than they are for the formation of brown condensate. As the brown condensate is heated, silicon particles will coalescence into larger drops and leave the condensate area when the temperature exceeds the melting temperature of quartz.

Laboratory experiments show that condensate from SiO gas will create a layer that can hold the weight of the charge located above, and thus create a cavity. So the formation of the cavity due to SiO condensation is important in addition to the crater formed around the electric arc (Myrhaug, 2003).

The previous excavation of an industrial ferrosilicon furnace showed only one large crater around each electrode (Schei et al., 1998). However, in the more recent industrial excavation (Ringdalen and Tangstad, 2012) the layers of condensate outside the SiC crater wall were also found in addition to a condensate layer between the charge mixture and the crater. These layers could have been formed by SiO gas from the crater, which flowed from the bottom and outside the crater walls. They contribute to building up the crater and may also be of importance for the rate of the reactions that take place. The SiO condensation can take place close to the crater walls where the estimated temperature is 2000°C . Of note, two cavities, one for the arc crater and one built up by condensate, can be found in even larger furnaces or furnaces with other temperature distributions.

In small furnace experiments, the condensate cavity was found to grow downward from the position of the condensation temperature. This contradicts that described in earlier studies (Schei et al., 1998), where the cavity was believed to grow outward from the consumption of materials around the electrode tip. After the stoking process, where the materials are mechanically pushed into the cavity, both mechanisms may contribute to the cavity formation; a new charge roof will form due to condensate formation, and the materials below this condensate roof will be consumed by the arc from the electrode tip.

6.3.2.2 Peculiarities of Ferrosilicon Smelting

Ferrosilicon is usually smelted in closed submerged arc furnaces with power of 22 to 93 MVA (Fig. 6.14); example parameters are shown in Table 6.6 (Gasik and Gasik, 2011).

The silica source for producing ferrosilicon is usually quartzites of lump size 20 to 80 mm, subjected to prewashing, crushing, and grading if needed. Quartzites suitable for smelting of ferrosilicon must contain not less than 97% SiO₂ and not more than 1.5% Al₂O₃. The carbon reductant is usually nut-coke of 5 to 20 mm in size, but as mentioned previously, different producers may have their own local reductant recipes. The reductant should possess high electrical resistance and high reactivity in relation to SiO₂ and SiO reduction, and constant moisture content (Batra, 2003). Approximate charge composition, energy demand, and silicon yield for ferrosilicon smelting in closed furnaces are shown in Table 6.7 (Gasik et al., 2011).

The presence of iron during the carbothermic reduction of quartzite lowers the partial pressure of SiO required for reduction to silicon and reduces its activity due to the formation of Fe-Si solutions. Thus, the losses of SiO from the furnace top decrease as the iron content of ferrosilicon increases, so it is typical to have silicon recovery of greater than 90% to 95% for <50% Si grades of ferrosilicon (Vishu et al., 2005).

Ferrosilicon production is a nearly slag-free process (the silicate-based slag amount does not exceed 3% to 5% of the alloy mass). However, the tapping of ferrosilicon and slag through one tap hole might be complicated by changes in the slag composition. The slag is heterogeneous, consisting of silicate-based melts (48% to 50% SiO₂, 20% to 25% Al₂O₃, 15% to 18% CaO), suspension of silicon carbide (10% to 15%), and the metallic inclusions of ferrosilicon alloy. Silicate component is formed from silica and impurity oxides (Al₂O₃, CaO, MgO) contained in quartzite and coke ash. Silicon carbide forms as an intermediate product of silica reduction by carbon, as shown earlier. Depending on the silicate melt chemical composition, the slag can be solidified in different concentration fields of anorthite (CaO·Al₂O₃·2SiO₂, melting point 1553°C) and gehlenite (2CaO·Al₂O₃·SiO₂, melting point 1545°C) of the CaO-Al₂O₃-SiO₂ system (Fig. 6.15).

Anorthite-area compositions, including the presence of SiC particles, have higher viscosity and a lower ability to separate from metal. Therefore, lime is

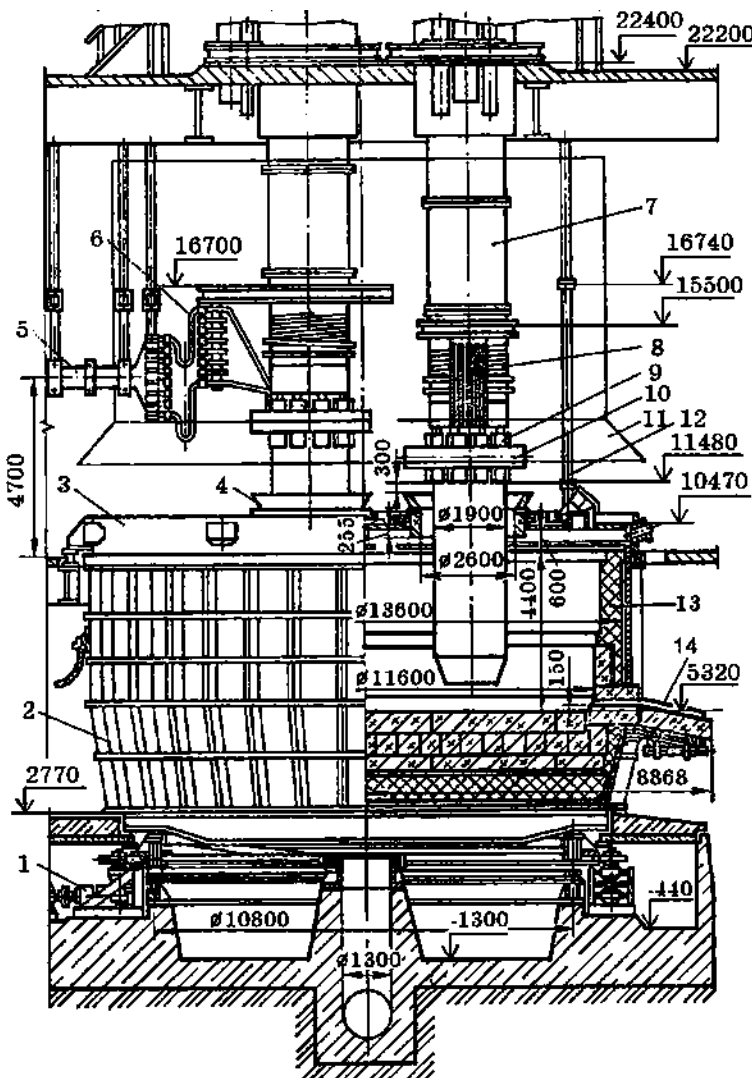


FIGURE 6.14 Round hearth 63 MVA power furnace: 1, mechanism of furnace rotation; 2, furnace shell; 3, arc furnace; 4, feeding funnel; 5, short net; 6, short net flexible bus bars; 7, electrode holders; 8, secondary current leads; 9, electrode contacts; 10, pressure ring; 11, furnace hood; 12, suspension; 13, refractory lining; 14, tap hole.

periodically added to increase basicity and to move slag composition into the gehlenite area.

Ringdalén and Tangstad (2012) reported the results of the excavation of an industrial ferrosilicon furnace (Fig. 6.16). They confirmed the existence of one large cavity around each electrode with walls made up of SiC and small

TABLE 6.6 Examples of the Furnace Parameters for Smelting Ferrosilicon

Parameters	Furnace A	Furnace B	Furnace C
Furnace power, MVA	27	40	80
Hearth depth, mm	2900	3500	5000
Hearth diameter, mm	6800	8700	11 600
Electrodes diameter, mm	1400	1500	1900
Electrodes current, kA	85	103	172
Power factor $\cos(\phi)$ (with compensation)	0.93–0.94	0.91–0.92	0.89–0.90
Electrical efficiency	0.91	0.915	0.89

TABLE 6.7 Typical Materials and Energy Demand for Smelting of Ferrosilicon in Closed Furnaces (per one basis ton of alloy)

FeSi Alloy	FeSi20	FeSi25	FeSi45	FeSi65	FeSi75Al1
Quartzite, kg	370	552	931	1568	1930
Iron chips, kg	810	780	658	343	250
Coke, kg	200	280	438	720	845
Electrode paste, kg	10	8	16	43.3	54
Electric energy, MWh/t	2.1	2.7	4.8	7.4	8.8
Silicon yield, %	94–95	97–98.5	98–99	92–94	91–93

amounts of quartz. Several gas channels existed within the walls, creating a layered structure. The channels started at the bottom of the crater, where they were widest. The gas flow appeared to move from the bottom of the crater, through the channels, up to the charge material.

Condensate occurred both in vertical layers outside the crater walls and in a horizontal layer high up through the furnace. Lumpy silica was found only in the upper 20 cm of the charge mixture and below this, the silica component was generally disintegrated. Most of the silica phase was transformed from quartz to cristobalite (Ringdalen and Tangstad, 2012).

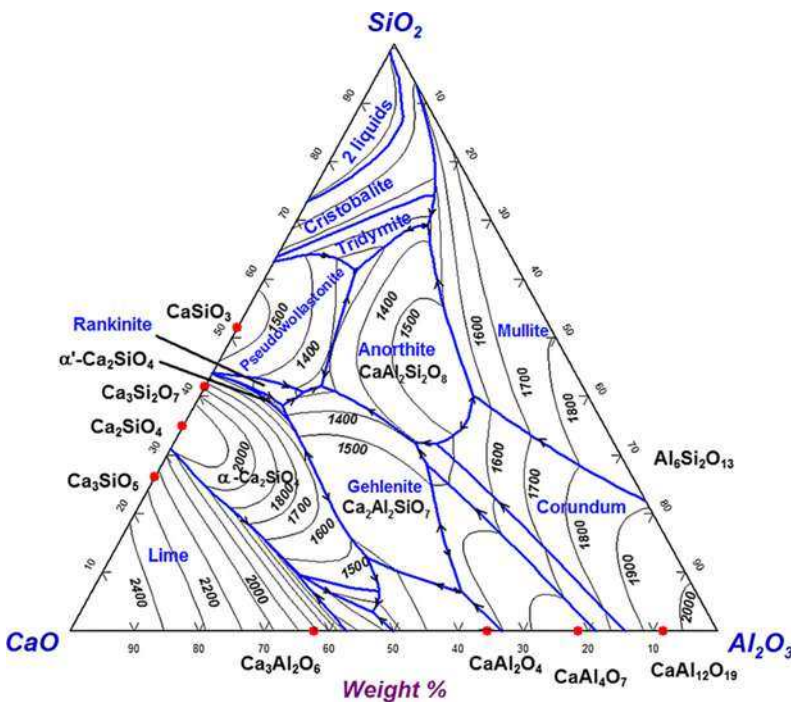


FIGURE 6.15 Diagram of phase equilibria (liquidus projection) in the system $\text{CaO}-\text{Al}_2\text{O}_3-\text{SiO}_2$. Solid lines, boundaries of coexisting mineral phases; thin lines, isotherms (calculated with FactSAGE 6.2).

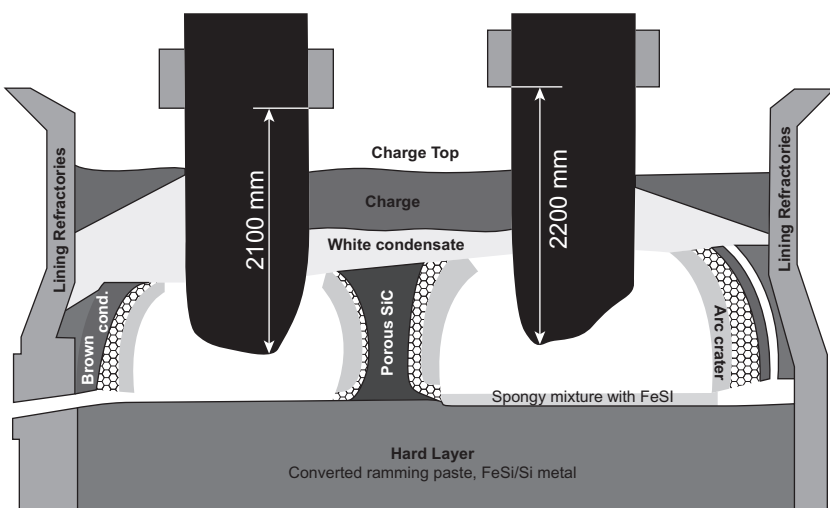


FIGURE 6.16 The distribution of material during the excavation of an industrial FeSi furnace of 7 m diameter. (*Ringdalen and Tangstad, 2012*).

6.3.2.3 Silicon Yield, Energy Demand, and Costs

The silicon yield (i.e., the ratio of silicon tapped from the furnace to the silicon added into the furnace) can be described as follows:

$$\text{Si yield} = \frac{\text{Mass Si tapped}}{\text{Mass Si tapped} + \text{Mass Si in SiO leaving the furnace} + \text{Mass of Si in accumulated SiC}}$$

In balanced operated silicon smelting, the accumulation of SiC in the furnace will be close to zero and it is a valid assumption for some time. Hence, the Si yield will first of all depend on how much silicon is produced (reduced) in the high temperature zone, and second, will depend on how much of the SiO gas can be captured in the low temperature part of the furnace.

In an ideal case with 100% Si yield, no SiO gas leaves the furnace and no SiC is accumulated. The theoretical enthalpy change to heat up silica and carbon from ambient temperature to produce silicon melt at 1800°C and CO gas at 1000°C would be 9.854 MWh/t Si. If the silicon yield is zero, which means all silicon is lost as SiO gas at 1000°C, this value would be 9.01 to 9.02 MWh/t Si. Thus, energy required for the process is inversely proportional to the Si yield (Fig. 6.17).

The Si yield has a significant effect on both the used electric energy costs as well as the fixed costs. With a lower energy consumption per ton of silicon produced, the tonnage will increase with a given furnace capacity in MVA.

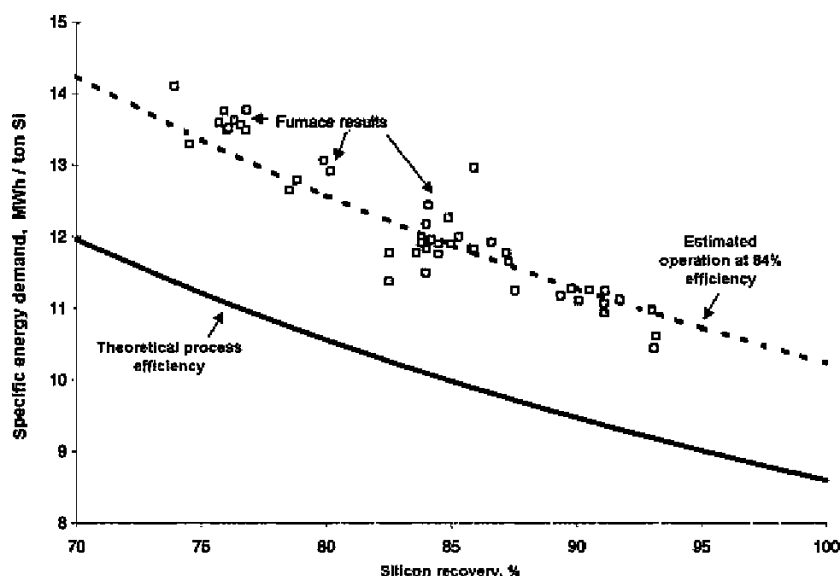


FIGURE 6.17 Measured and calculated energy demand for silicon production. Dashed line was fit with an assumption of energy efficiency of 84%. (Data from Schei et al., 1998.)

These numbers are, of course, very dependent on the individual raw material prices in each of the countries where the silicon is produced. However, changes in Si yield will affect the cost almost linearly in any case.

The most important factors affecting the Si-yield in the furnace were identified by Schei et al. (1998) as temperature in the cavity, SiO reactivity of the carbon reductant materials, and temperature in the low temperature zone. If the high temperature zone is “cold” (~1800°C), the SiO partial pressure is high and the silicon yield will be low (33%), as most of it will be recirculated in the furnace reducing from SiO to SiC and back. If the high temperature zone is “hot” (1950° to 2000°C), the partial pressure of SiO is closer to CO, which fits better the stoichiometry of the process, leading to nearly theoretical 100% silicon yield. This shows that it is important to obtain a high temperature in the high temperature zone, to therefore obtain a low SiO pressure to produce the same amount of silicon.

In the preceding example, it was assumed that all C in the low temperature zone was reacted to SiC. However, this reaction extent is determined in the furnace by kinetics. The rate is determined first by the distribution of the SiO gas in the burden (i.e., the permeability of the burden), second by the size of the carbon materials, and last by the reactivity of the carbon materials.

High carbon reactivity toward SiO gas is vital to obtain a high Si yield of the process. When this is high, the SiO gas is captured by the carbon in the upper regions of the furnace and will react according to the reaction: $\text{SiO(g)} + 2\text{C} = \text{SiC} + \text{CO(g)}$. At these conditions very little SiO gas will escape from the furnace at equilibrium (<1% as shown by Fig. 6.5). However, the practical limitations of the reaction due to kinetics dictate these losses typically at about 10% to 20%.

The reaction $2\text{SiO(g)} = \text{Si} + \text{SiO}_2$ also catches a lot of SiO gas produced in the high-temperature zone, and this reaction is directly affected by the temperature and condensation area. To obtain a high rate of the condensation reaction, the gas has to be evenly distributed in a charge with as low a temperature as possible.

The bigger the void around the electrode, the smaller the distance between the void and the top of the charge. A small zone for the preliminary reactions leads to less reaction of SiO gas with the carbon materials. This is due to a high temperature on the surface and because of a low number of carbon particles for the gas to react with. At regular intervals, the furnace is therefore stoked (i.e., a new, cold charge is mechanically forced into the void to collapse it). This treatment of the oven is necessary to reduce the SiO loss.

An increase in the carbon content of the charge will capture more silicon, but at the same time generate more accumulated SiC in the bottom and edges of the furnace. This will eventually lead to SiC buildup in the furnace. The electric energy is then developing heat higher up in the furnace, which is a problem, as shown earlier for abnormal ferrosilicon operations. In the worst case, the furnace has to be stopped in order to remove the SiC-buildup. The optimum

carbon addition will give the highest Si-yield and hence the lowest energy consumption.

6.4 CASTING AND REFINING OPERATIONS

6.4.1 Casting

Unlike the methods used for iron and steel castings, similar procedures for silicon and ferrosilicon require much more care and development. Besides ferrosilicon, which is usually used almost exclusively for steelmaking, silicon has a wider range of applications (aluminum alloys, chemical industry, electronics, etc.), which dictates different quality requirements in chemical composition (impurities—trace elements) and grain size (especially fines).

Silicon going to the chemical industry ends up in a bed requiring a sizing between 100 and 200 μm where the silicon reacts with chemical agents. This is a surface reaction and hence elements catalyzing/retarding this reaction are of importance. The quality of the silicon will also affect the reaction rate. Some phases do not react, and hence the selectivity of the material also varies. In particular, phases containing Fe, Al, and Ca give a low selectivity and are thus not desired. Besides total content of trace elements, their distribution on grain boundaries versus solution in the Si crystals is important.

The total number of fines, as this particularly affects the total oxygen content in the metal, is the next critical issue. The number of fines formed depends on the strength of silicon, which again is dependent on phases in the metal and their grain size. For conventional diffusion-driven solidification, the grain size is proportional to the inverse cubic power of time, as shown by Schei et al. (1998).

Homogeneity of the metal regarding both element distribution and phase distribution is critical. Although the liquid Si/FeSi has a homogeneous distribution of trace elements, they will segregate during solidification due to their partition ratios (segregation coefficients) between solid and liquid phases. The solubility of the elements is in most cases lower in the solid phase than in the liquid phase. When the first part of the melt starts to solidify, the initial trace element content will be very low in the solid phase; hence, its content in the liquid phase will increase. As more of the slab is solidified, the content in the liquid phase gradually increases. The recently solidified part will be in equilibrium with this high content liquid, so the content in the solid phase will increase as the solidification proceeds. Within this formalism, the trace element content in the solid (C_s) will depend on the fraction already solidified (f_s), the specific segregation coefficient k_o , and the initial trace element content (C_0) according to the Gulliver-Scheills equation:

$$C_s = k_o C_0 (1 - f_s)^{(k_o - 1)}$$

TABLE 6.8 The Segregation Coefficient k_o of Some Elements in Silicon

Al	$2 \cdot 10^{-3}$ – $2.8 \cdot 10^{-3}$	Cu	$4 \cdot 10^{-4}$ – $8 \cdot 10^{-4}$	P	0.35
B	0.8	Fe	$6.4 \cdot 10^{-6}$ – $6 \cdot 10^{-5}$	Sn	0.016
C	0.05–0.07	N	$7 \cdot 10^{-4}$	Ti	$2 \cdot 10^{-6}$ – $3.6 \cdot 10^{-4}$
Ca	$8 \cdot 10^{-3}$	Ni	$8 \cdot 10^{-6}$ – $3 \cdot 10^{-5}$	Zn	$1 \cdot 10^{-5}$
Cr	$1.1 \cdot 10^{-5}$	O	0.25–1.4		

The segregation coefficients for metals are usually very low as shown in Table 6.8, whereas for elements like C, O, B, and P they are in the order of unity. This means the same content of these trace elements will be in the solid and in the liquid phase, so the content should be similar throughout the cast product.

However, the solidification direction during casting of metallurgical grade Si and FeSi is usually not fixed, so the distribution of trace elements might not be according to the ideal state of Gulliver-Schell's equation. The practice shows that the distribution of trace elements may vary with a factor of 5 through the silicon ingot, and the slower the solidification, the larger the variation in trace element content. Among the casting and atomizing methods investigated for silicon solidification, many options have been developed and tested (Table 6.9).

Processes for casting ferrosilicon are quite similar to those used for silicon. During solidification of the standard grade of 75% ferrosilicon, silicon crystallizes initially, followed by solidification of the ϵ -phase. The transformation of the ϵ -phase to stable FeSi_2 is accompanied by an increase in volume, which can lead to disintegration of the alloy in the range of 45% to 65% Si alloy (Vishu et al., 2005). The microstructure of $\text{FeSi}45$ alloy has FeSi phase, non-stoichiometric Fe_xSi_2 , and that of $\text{FeSi}65$ extends to Fe_xSi_2 phase and pure silicon. Trace elements may form excess phases, which have a complex chemical composition. They are usually crystallized at the grain boundaries of iron silicides (Zubov and Gasik, 2002).

Substandard ferrosilicon fractions can be converted into commercial products by recycling them with the original charge in FeSi smelting furnaces, by briquetting, pelletizing, or remelting in induction furnaces. Some technologies have been developed and implemented for briquetting ferrosilicon fines.

6.4.2 Refining of Silicon and Ferrosilicon

6.4.2.1 Trace Elements Distribution

The feed materials going into a furnace are carbon materials and quartz, both containing trace elements. These elements will be present in one of the three flows passing out of the furnace: metal, silica in the off-gas, and gas.

TABLE 6.9 Reported Methods of Silicon Casting and Atomizing
(from Nygaard, 2006)

Method and Developer	Features
Atomizing in inert gas (Elkem Meraker); 800 t were produced in the pilot plant	Very high cooling rate and small particles that in principle can be used directly in the chemical industry. High productivity, but feasible product yield was not high; increased costs.
Air granulation (Fesil), forming ~1 mm bullet particles	The layer of oxidized silicon on each particle was high to develop further production.
Water granulation (Elkem, Fesil, Silicon Smelters, Becancour Silicon)	A number of crucial requirements that must be met to prevent explosions, but they cannot be avoided, so many producers have now stopped this method due to the instability of the process.
Cooling down in water sloping channel (Mintek); forming large lumps (4–8 × 20–50 mm diameter)	The sloping channel is filled with about 10 mm of water, allowing poured liquid metal to slide along the bottom and to form lumps. No full-scale process was reportedly built in a silicon plant.
“Cast to shape” in copper molds (Elkem trial).	The molds were rod-shaped, allowing rods to fall out and break up into pieces ~10 × 10 mm. This process was never introduced into production, and costs were too high.
Casting on flat copper plates (Becancour Canada, Ferroatlantica)	Rotating copper plates or flat copper plate in the bottom of a vibrating feeder. Oxygen content is believed to be very low; fines fraction is three times lower versus cast and crushed material.
Casting in cast iron molds	Silicon dissolves iron; volume expansion may create cracks in the molds, silicon fines must be used to protect the molds. However, it introduces a high amount of oxygen.
Multiple layer casting (first layer cast onto the bed of fines, subsequent one on top of the previous layer)	Probably the cheapest solidification method. Each layer is typically 5–15 cm. The effect of fines and oxygen is reduced versus the first layer. Not very rapid cooling as with other methods, but low cost.

Sometimes also smaller quantities of slag may be tapped together with the metal. Most of the impurities introduced into the furnace via the raw materials and any other sources are transferred to the product. Myrhaug (2003) has shown an example of the distribution of trace elements in silicon smelting (Fig. 6.18). Such partition figures, however, vary from furnace to furnace, but they reveal the major trends in elements distribution.

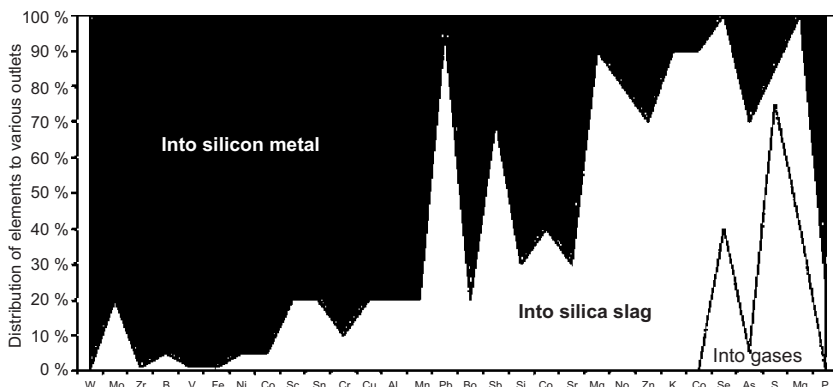


FIGURE 6.18 Example of a trace element partition between different products of silicon smelting. (From Myrhaug, 2003.)

Most trace elements follow the boiling-point model, which states that the elements with the lowest boiling temperature will go to the gas phase, the elements with a slightly higher boiling temperature will condense on the microsilica or stay in the slag, and the ones with the highest boiling points will mostly go into the metal. Some elements deviate from the boiling point model and vary significantly between measuring campaigns. As the trace element content is close to the analytical limits, it is believed that the deviation is mostly due to analytical inaccuracy at these low levels. To produce high purity grades of silicon and ferrosilicon, the tapped alloy is refined by different methods.

6.4.2.2 Refining Processes

Typical elements that must be controlled in silicon are Fe, Ca, and Al. As Ca and Al are less noble than Si (have higher oxygen affinity), they can be removed by oxidation. Iron, however, can only be controlled by limiting the Fe content in the raw material as in the quartz and the carbon reductant ash. For some grades, the content of oxygen and carbon can also be of importance. Ferrosilicon, titanium, and chromium might be also limited if their content in raw materials is initially high.

Oxygen for refining might be introduced as gas or air (blown from a lance or via a plug in the ladle) or as oxides (e.g., Fe_2O_3 in the case of ferrosilicon refining). In either case, thermodynamics is based on the reaction of dissolved Al and Ca with oxygen species, giving alumina or CaO , which is absorbed by the special slag phase. Due to the low content of impurities in the metal phase, slag composition and temperature are essential to provide the thermodynamic driving force for the reactions.

The equilibrium between the melt and slag is achieved when a certain amount of aluminum in the alloy is reached and alumina content in the slag $\text{CaO}\text{-}\text{Al}_2\text{O}_3\text{-}\text{SiO}_2$ (and its viscosity) is increased. Common slag compositions are based in the triangle $\text{SiO}_2\text{-}\text{CaSiO}_3\text{-}\text{CaO}\cdot\text{Al}_2\text{O}_3\cdot\text{SiO}_2$ (anorthite) (see

Fig. 6.15). Thus, to reach lower aluminium content, slag treatment might be repeated two or three times, but this leads to higher silicon losses and increased electrical energy consumption. To improve the refining procedure, slag may additionally have some CaO and CaF₂ as flux to reduce its viscosity, while blowing oxygen-containing gas into the melt. Although aluminum in this case is removed more efficiently, more silicon is also oxidized. There were also methods of refining ferrosilicon that involved applying mixtures of siderite (FeCO₃) with fluorspar. Siderite decomposes on heating to FeO (oxidizes aluminum) and CO₂ (provides gas for efficient mixing), whereas fluorspar decreases viscosity. As the final level of refining is dictated by the product specification, the result does not depend on the method used. However, the heat balance and the cost may, of course, be affected by the method preferred.

Oxygen and carbon are present in the metal only as ppm quantities, hence in the solidified product most of the carbon and oxygen are present as oxides and carbides (Tang et al., 2010). However, the total oxygen and carbon content is also higher than the liquid solubility given by the phase diagram, and hence it shows that, already at liquid state, the melt contains some oxides and carbides. Reported oxygen contents are between 0.04% and 0.70% (Schei et al., 1998). Oxygen is a specific concern for silicon used in the chemical industry. During refining, the use of viscous crusty oxide films (adding CaO or CaO with silicates) to activate the bottom slag should be avoided throughout the process, to avert “over-oxidation” and to add an inert gas that will keep gas bubbles from collapsing before reaching the slag layer. Operating at a high degree of turbulence and adding fluorspar at the end of the blow will help to keep the oxygen content low.

Contrary to silicon production, the oxygen solubility increases and the carbon solubility decreases when the iron content in FeSi is increased. When the metal is tapped from the furnace, the carbon content is assumed to be close to the solubility limit at these temperatures. As the temperature decreases during pouring, stirring, and casting, SiC (or graphite for alloys with <22% Si) will be precipitated. The resulting carbides end up in the lining and in the slag phase. As Al₂O₃-CaO-SiO₂ slags wet SiC well, slag additions are efficient to remove formed SiC particles from the metal.

The contamination of chemical-grade silicon with small amounts of the oxide slag was found to be detrimental to the silicon performance. Therefore, oxide slag must be removed from molten silicon by phase separation during casting. This can be improved by controlling the process to generate an oxide slag with suitable viscosity, density, and melting point (Vishu et al., 2005).

6.5 ENERGY SAVINGS AND ENVIRONMENTAL ISSUES IN SILICON AND FERROSILICON PRODUCTION

6.5.1 Energy Recovery

In energy balance calculations, the reference state is usually taken for the highest oxidation step of each element at 25°C. The energy flow going into the

furnace can be divided into several streams, namely electric energy and the latent energy contained in the charge materials. The electrical efficiency of the furnace versus the incoming energy on the transformer primary circuit is estimated as 85% to 90% depending on the furnace power and design. About one fourth of the electrical power loss is in the leads (bus bars) and transformers, and about half of the loss is in the electrodes. Solid carbon reductant brings into the process about 9 MWh/ton and coke volatiles bring in about 13.8 MWh/ton of CH₄, assuming volatiles are converted into methane.

The outgoing energy flow is divided into the following streams: energy in the off-gas, in the products like slag and metal; chemical energy plus latent heat at 1600°C; and energy removed with cooling water.

An example of the energy balance for a 10-MW furnace is shown in Table 6.10. The chemical energy flow is of the same order as the electrical energy input to the furnace, and about 85% of it is converted into the chemical energy of the products. As the temperature in the off-gas in a silicon furnace is high, half of the energy is in the off-gas as thermal energy. The gas on the top of the furnace contains CO₂, N₂, and unreacted O₂, in addition to the minor species like NO_x, SO₂, and so on.

The temperature in the off-gas is dependent on how much of the CO and SiO gas is oxidized and how much surplus air is in the off-gas. Usually all CO and SiO is oxidized to CO₂ and SiO₂(s). The temperature of the off-gas is calculated based on 1400°C for the gas coming from the charge and 80% Si recovery. If the air inlet is limited, the temperature can reach more than 2500°C. However, this is seldom the case and the temperature is usually much lower due to excess air that cools the off-gas. This is also important due to the temperature limitations in the filter bags.

There has been continuous development in the silicon industry to reduce energy consumption, especially by increasing the Si yield, and increase energy recovery by utilizing the energy in the hot water and making extra electricity

TABLE 6.10 Example of a 10-MW Silicon Smelting Furnace Energy Flow Balance (from Kamfjord, 2012)

Incoming Streams	MW	Outgoing streams	MW
Electricity	10	Smelting products	7.33
Solid carbon	8.41	Off-gas energy	11.14
Coke volatiles	3.28	Cooling water	2.87
		Other losses	0.34
Total in:	21.68	Total out:	21.68

from the high temperature off-gas flow. Hot water utilization depends on the country's conditions. For example, in Norway it is used to grow flowers, to produce fish, and to keep public areas free from snow.

Also, some plants recover the energy in the off-gas by producing electrical energy. From the off-gas share of 11.14 MW shown in [Table 6.10](#), directed into the boiler, about 75% (8.35 MW) might be recovered as steam. When this steam is used to run a turbine and generator of total 25% efficiency, about 2 MW of electricity can be produced, which is 20% of the electric power consumed by the furnace originally. For hot water, about 90% of the electrical energy can be recovered.

The energy streams are dependent on the raw materials used and the operation of the furnace, so they naturally vary over time. For example, within 48 h of furnace operation, energy flow in the products and off-gas varies by about $\pm 15\%$ of the furnace effect. These variations have to be taken into account when designing energy recovery units.

6.5.2 Emissions Control

The emissions from a plant can be divided in two groups: controlled emissions and diffuse emissions. Controlled emissions of energy and materials are those going through the stack and other off-gas handling systems. Diffuse emissions of energy and materials are those that are not captured by the off-gas systems and hence are distributed randomly ("diffused") through the plant.

Controlled solid emissions from ferrosilicon production are mainly fines containing the off-gases. The precipitator's dust from dry gas cleaning has usually 80% to 95% SiO_2 , 1.5% to 9% Al_2O_3 , 0.4% to 2.7% CaO , 1% to 5% MgO , <0.5% Fe_2O_3 , and <2% others. This dust, with an average particle size of 5 μm , has a very high specific area ($\sim 2000 \text{ m}^2/\text{g}$) and low bulk density (180 to 230 kg/m^3). It has been estimated that 10% to 15% of all silicon losses during the smelting of FeSi75 contains in these fines ([Zubov and Gasik, 2002](#)).

Determining the rational use of silica dust captured during gas cleaning is one of the urgent tasks in ferrosilicon production to save material resources and to improve the efficiency of environmental objectives. The principal health hazard is caused by the crystalline form of silica (quartz) used as a raw material, as it is the chief cause of disabling pulmonary fibrosis, such as silicosis ([Vishu et al., 2005](#)). Different methods of dust utilization are being studied, like the application in the cement for constructions and the preparation of "liquid glass" (sodium silicates) by an aqueous caustic treatment. This includes ceramics production, sorbents, manufacturing of silicon tetrachloride, abrasive SiC and Si_3N_4 , and so on.

Diffuse or fugitive emissions occur wherever materials are exposed to handling. They may be solid materials, like raw materials and produced metal, or liquid metal. In the solid state, the fume will come from the abrasion of the



FIGURE 6.19 Examples of fugitive emissions from ladle before casting (*left*) and during tapping (*right*) (Kamfjord, 2012).

solid material, whereas in the liquid state, evaporation will be the main source. Splashing may also contribute but is believed to be of minor significance.

The three main drivers for reducing diffuse emissions are to increase the health of the workers at the plant, to reduce the cost of production, and to reduce the environmental footprints of producing silicon and silicon alloys. Compared to the workers at FeMn and FeCr plants, the workers at Si/FeSi plants have reduced respiratory capacity with a factor of 2, and this is correlated to the work operations and earlier exposure. This was recognized a long time ago (Swensson et al., 1971) and many measures are being taken to quantify and to reduce the diffuse emissions. Typical examples of fugitive emissions are presented in Figure 6.19, which shows smoke from a ladle used during transport and tapping (Kamfjord, 2012). At every step—from raw materials handling to smelting and reduction, casting, and crushing—fume, dust, and energy are released to the surroundings.

In Table 6.11 these emissions have been quantified (Kamfjord, 2012). The two major pollution time periods are during casting and during tapping, but the leaks from the furnace process and the crushing, screening, and packing processes are also quite high.

During environmental monitoring campaigns in tapping and casting areas, the average dust load in the air was 6 to 12 mg/Nm³; however, when the dust content was measured only in areas where it had been observed, the numbers were 23 to 45 mg/Nm³ and 223 mg/Nm³ outside of the tapping area and above the casting area, respectively. Therefore, it has been concluded that fugitive emissions occur mostly when ladles are transported in the plant after tapping

TABLE 6.11 Major Emissions in the Silicon Smelting Plant

Process Stage	Share of Diffusive Emissions, %	Share in Internal Pollution, %	Emission Type
Materials handling to storage	0–5	0	Fume—transportation, conveyers, etc.
Materials transport to furnace	0–5	5–10	Fume—mixing, transportation
Furnace processes	10–20	5–20	Smoke and fume—escaping from furnace gas system
Tapping	20–40	30–50	Smoke and fume—tapping
Casting	20–40	15–25	Smoke and fume—liquid metal handling
Crushing, screening, packing	5–15	5–15	Metallic fume
Off-gas systems	5–10	0–5	Fume and smoke escaping gas systems
Off-gas collected products packing	0–5	5–10	Fume—passage into work environment

and during the casting process, probably due to the purge gas stirring and refining operations. Intensive gas collection in suction hoods is therefore required over the ladles and in similar locations (Kamfjord, 2012).

REFERENCES

- Aasly, K., 2006. Properties and behaviour of quartz for the silicon process. Ph.D. Thesis 236. NTNU, Trondheim, Norway, 187 pp.
- Batra, N.K., 2003. Modelling of ferrosilicon smelting in submerged arc furnaces. Ironmaking & Steelmaking 30 (5), 399–404.
- Gasik, M.I., Gasik, M.M., 2011. Electrothermal silicon technology. Dnipropetrovsk: National Metallurgical Academy of Ukraine, 487 pp.
- Gasik, M.M., Gasik, M.I., 2010. Thermodynamic analysis of the dominant phase equilibria in M(Si, Cr, Al)-O-C systems. Russian Metallurgy (Metally) 6, 548–556.
- Inoue, Z., Ueno, S., Tagai, T., Inomata, Y., 1971. A new polytype of silicon carbide 9T. Journal of Crystal Growth 8 (2), 179–183.
- Kadkhodabeigi, M., Tveit, H., Johansen, S.T., 2011. Modeling the tapping process in submerged arc furnaces used in high silicon alloys production. ISIJ International 51 (2), 193–202.
- Kamfjord, N.E., 2012. Mass and energy balances of the silicon process – Improved emission standards. Ph.D. Thesis 162. NTNU, Trondheim, Norway, 139 pp.

- Myrhaug, E.H., 2003. Ph.D. Thesis 67. Non-fossil reduction materials in the silicon process – properties and behaviour. NTNU, Trondheim, Norway, 226 pp.
- Myrvågnes, V., 2008. Analyses and characterization of fossil carbonaceous materials for silicon production. Ph.D. Thesis 30. NTNU, Trondheim, Norway, 232 pp.
- Nygaard, L., 2006. Silicon solidification techniques for the chemical industry. Proceedings of the Conference on Silicon for the Chemical Industry, NTNU, Trondheim. 12–15 June 2006, 71–78.
- Ringdalén, E., Tangstad, M., 2012. Reaction mechanisms in carbothermic production of silicon, study of selected reactions. Proceedings of the International Smelting Technology Symposium, Hoboken, NJ: John Wiley & Sons, 195–204.
- Roskill International, 2011. Silicon and Ferrosilicon: Global Industry Markets and Outlook, thirteenth edition. 268 pp.
- Schei, A., Tuset, J.K., Tveit, H., 1998. Production of High Silicon Alloys. Trondheim: Tapir Forlag, 363 pp.
- Schnurre, S.M., Gröbner, J., Schmid-Fetzer, R., 2004. Thermodynamics and phase stability in the Si–O system. Journal of Non-Crystalline Solids 336, 1–25.
- Shkirmontov, A.P., 2009a. Theoretical principles and energy parameters in ferrosilicon production with an increase in the electrode spacing and the distance from the electrodes to the bath. Metallurgist 53 (5–6), 373–379.
- Shkirmontov, A.P., 2009b. Energy parameters of ferrosilicon production with larger-than-normal values for the electrode gap and electrode spacing under factory conditions. Metallurgist 53 (9–10), 642–647.
- Swensson, A., Kvarnström, K., Bruce, T., Edling, N.P.G., Glömme, J., 1971. Pneumoconiosis in ferrosilicon workers – a follow-up study. Journal of Occupational Medicine 13 (9), 427–432.
- Tang, K., Øvreliid, E.J., Tranell, G., Tangstad, M., 2010. Thermochemical and kinetic databases for the solar cell silicon materials. Proceedings of the Congress Infacon-XII, Helsinki, Finland. 2, 619–629.
- Vishu, D., Kroupa, M., Bittar, R., 2005. Silicon and silicon alloys, chemical and metallurgical. In: Kirk-Othmer Encyclopedia of Chemical Technology, volume 21. John Wiley, NY, pp. 1104–1122.
- Young, L.E., 2001. Ferroalloys: production and use in steelmaking. In: Encyclopedia of Materials: Science and Technology. Elsevier, pp. 3039–3044.
- Zubov, V.L., Gasik, M.I., 2002. Electrometallurgy of Ferrosilicon. Dnepropetrovsk: System Technologies Publ., 704 pp.

Manganese Ferroalloys Technology

Merete Tangstad

Norwegian University of Science and Technology, Trondheim, Norway

Chapter Outline

7.1 Introduction to Manganese Ferroalloys	222	7.5 Smelting Technologies for Manganese Alloys	240
7.1.1 History and Background of Manganese	222	7.5.1 Basics of Reduction Processes	240
7.2 Properties of Manganese and Its Compounds	222	7.5.2 Outline of Industrial Practice	242
7.2.1 Properties of Manganese	222	7.6 Technology of Ferromanganese	247
7.2.2 Interaction of Manganese with Oxygen and Carbon	223	7.6.1 High-Carbon Ferromanganese Production	247
7.2.3 Interaction of Manganese with Other Elements	225	7.6.2 Production of Commercial Silicomanganese (FeSiMn)	250
7.2.4 Manganese in Oxide Systems and Slags	229	7.6.3 Post-Tap Hole Processing for FeMn and SiMn	252
7.3 Manganese Ores Processing and Reduction	231	7.6.4 Production of Manganese Metal	253
7.3.1 Manganese Ores	231	7.7 Refining Operations for Low-Carbon Manganese Ferroalloys	256
7.3.2 Agglomeration Processes	234	7.7.1 Production of Low-Carbon Ferromanganese	256
7.4 Manganese Ferroalloys	238		
7.4.1 Manganese Alloy Specifications	238		
7.4.2 Impurities in Manganese Alloys	240		

7.7.2 Production of Low-Carbon Silicomanganese	258	7.10 Energy Use in Manganese Ferroalloys Processing	262
7.8 Manganese Ferroalloys		7.11 Potential Hazards of Operations	263
Postprocessing	259	Acknowledgments	265
7.8.1 Casting	259	References	265
7.8.2 Crushing and Sieving	260		
7.9 Nitrided Manganese Ferroalloys	261		

7.1 INTRODUCTION TO MANGANESE FERROALLOYS

7.1.1 History and Background of Manganese

Manganese is a relatively common element in the earth's crust. The average concentration reaches nearly 0.1%, and it is the twelfth most abundant element and fourth most abundant of the metals in commercial use. Manganese occurs in nature mainly in the form of oxide, carbonate, and silicate minerals. Paintings pigmented with manganese oxide can be traced back 17 000 years. Later, in ancient Greece, the presence of manganese in steel gave the Spartans superior steel weapons. In 1774, Swedish chemist Carl Wilhelm Scheele was the first to recognize that manganese is a separate chemical element, and in the same year his colleague Johan Gottlieb Gahn isolated an impure sample of the element by reduction of MnO₂ (pyrolusite) with charcoal. In 1816, it was found that adding manganese to iron made it harder, without making it more brittle. At the beginning of the 19th century, scientists began to explore the use of manganese in steelmaking, with patents being granted for its use.

Because about 90% of all manganese produced is consumed in the steel industry, the world demand for manganese depends directly on the needs of the steel industry, which is typical for most ferroalloys. There are numerous grades of steel, and each grade requires a different amount of manganese. The average unit consumption of manganese per ton of steel is currently about 10 kg. There is some direct consumption of manganese ores and sinter in the blast furnaces where pig iron is produced, but manganese is mainly consumed in the form of ferromanganese, silicomanganese, and manganese metal. Only about 5% of the manganese used in steel production is introduced into the blast furnace.

7.2 PROPERTIES OF MANGANESE AND ITS COMPOUNDS

7.2.1 Properties of Manganese

There are four modifications of manganese known at ambient pressure: complex cubic structure α -Mn ($a = 0.89124$ nm, 58 atoms in the basic lattice,

density 7.44 g/cm^3) below 727°C ; complex cubic β -Mn in the range 727° to 1090°C ($a = 0.6289 \text{ nm}$, 20 atoms in the basic lattice, density 7.29 g/cm^3); FCC γ -Mn at 1090° to 1138°C ($a = 0.3855 \text{ nm}$ at 1100°C , density 6.37 g/cm^3); and those above 1138°C —BCC δ -Mn ($a = 0.3075 \text{ nm}$ at 1143°C , density 6.28 g/cm^3). The melting point of manganese is 1244°C and the boiling point is 2150°C . It can have valences from $1+$ to $7+$, of which $2+$ and $4+$ are the most common. The pure metal is grayish white, resembling iron, but it is harder and very brittle. Manganese (Mn) and iron (Fe) are close neighbors in the periodic system, with element numbers 25 and 26 and atomic weights of 55 and 56, respectively.

Manganese is added to steel for the following reasons: it is used as an alloying element to improve strength, toughness, and hardness; it is used for sulfur control whereby it combines with sulfur and controls the morphology of sulfides; and, lastly, it is used for oxygen removal. Manganese stabilizes the austenite in steel, although it is less potent than nickel. It lowers the temperature of austenite transformation into ferrite and improves the response of steel to quenching. The effect of manganese in forming austenite is improved by combining it with nitrogen, which is also an austenite-forming element (Matricardi and Downing, 1995).

Manganese plays a key role in steels because of its ability to combine with sulfur: manganese sulfide avoids the hot shortness of the steel and prevents the interstitial liquid formation of iron sulfide.

Manganese is a milder deoxidizer than silicon and aluminum but enhances their effectiveness due to the formation of stable manganese silicates and aluminates. Silicomanganese (SiMn) is a more effective deoxidizer than is the case with individual additions of ferrosilicon and ferromanganese. Deoxidation with silicomanganese results in cleaner steel as the liquid manganese silicate formed coalesces and thus separates more easily from the melt, compared to solid SiO_2 formed during ferrosilicon deoxidation. This feature also reduces the problems with nozzle clogging during casting.

7.2.2 Interaction of Manganese with Oxygen and Carbon

Manganese forms several oxides, of which only monoxide (MnO) is stable at high temperatures. The unstable higher oxides MnO_2 , Mn_2O_3 , and Mn_3O_4 predominate in manganese ores. Higher manganese oxides such as Mn_2O_7 are very unstable and easily decompose even at room temperatures. MnO_2 and Mn_2O_3 dissociate in solid state to lower oxides when heated. Figure 7.1 shows areas corresponding to oxides and metal stability at different oxygen potentials versus temperature, and Figure 7.2 presents the phase equilibria diagram at 1 atm air (0.21 atm oxygen partial pressure).

Reduction of MnO to liquid metallic manganese is far more difficult than reduction of FeO to iron; and reduction of MnO to form solid manganese, analogous to the sponge iron formation in the Fe-O system, is not practically possible.

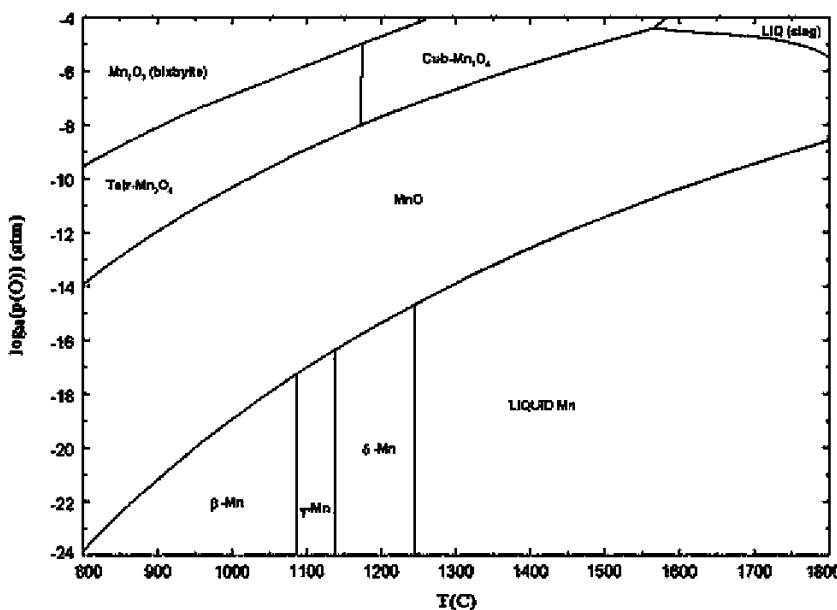


FIGURE 7.1 The stability phase diagram of the Mn-O system.

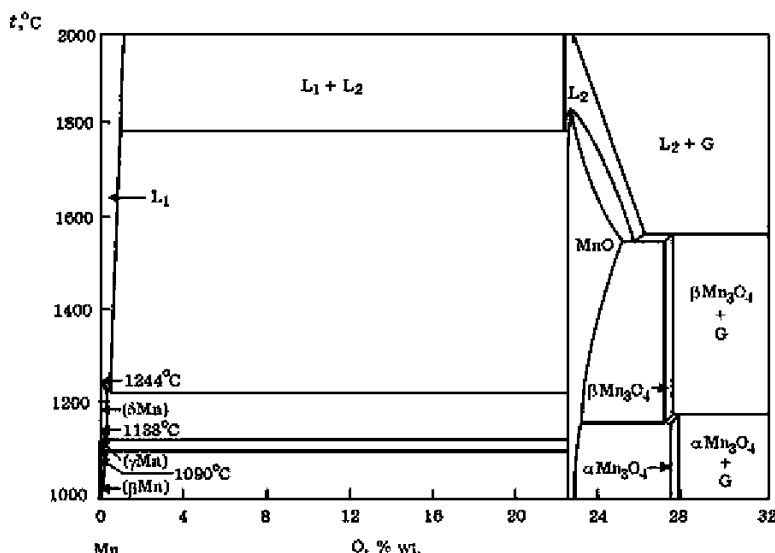


FIGURE 7.2 The phase equilibria in the Mn-O system at 1 atm air conditions.

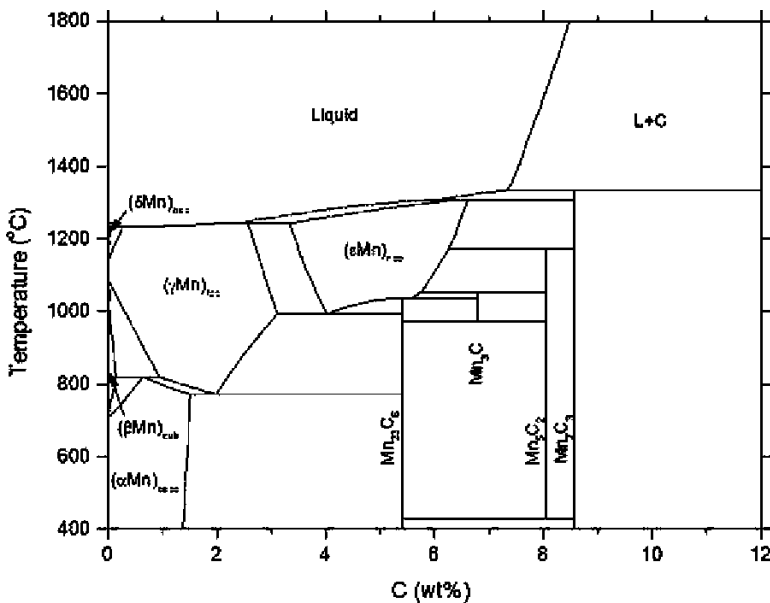


FIGURE 7.3 Calculated Mn-C phase diagram using the SINTEF ferroalloy database (Olsen et al., 2007).

The Mn-C equilibrium phase diagram is shown in Figure 7.3. Manganese and carbon are completely miscible in liquid state, but, as opposed to the Fe-C system, the liquidus temperature increases with increasing carbon content from 1237°C up to 1297°C at 7.34% C. This composition corresponds to alloy in equilibrium with graphite and the carbide Mn₇C₃. Stable carbides are formed during solidification—for example, Mn₂₃C₆, Mn₃C, and Mn₇C₃. Most manganese carbides (particularly Mn₅C₂) are unstable in reaction with moisture, but it is found that 5% Fe is sufficient to stabilize the alloy in wet air and 10% Fe is sufficient to avoid reaction with water. Among manganese carbides, Mn₃C is the most stable in respect to environmental conditions.

7.2.3 Interaction of Manganese with Other Elements

In the Mn-Fe system, manganese stabilizes austenitic structure forming a large area of FCC γ -(Fe, Mn) (Fig. 7.4). Both manganese-rich and iron-rich solid solutions have a wide range of homogeneity. There is complete miscibility in the liquid state, and the system shows very small deviation from ideal behavior. Manganese and iron are not found to form any stable intermetallic compounds.

Manganese and silicon are completely miscible in the liquid state. The minimum eutectic temperature at the Mn-rich side is 1038°C at $X_{Si} = 0.175$ (11.2 wt% Si). Several silicides are formed during solidification (Fig. 7.5). Manganese silicide compositions (Gasik et al., 2009) have been updated—for

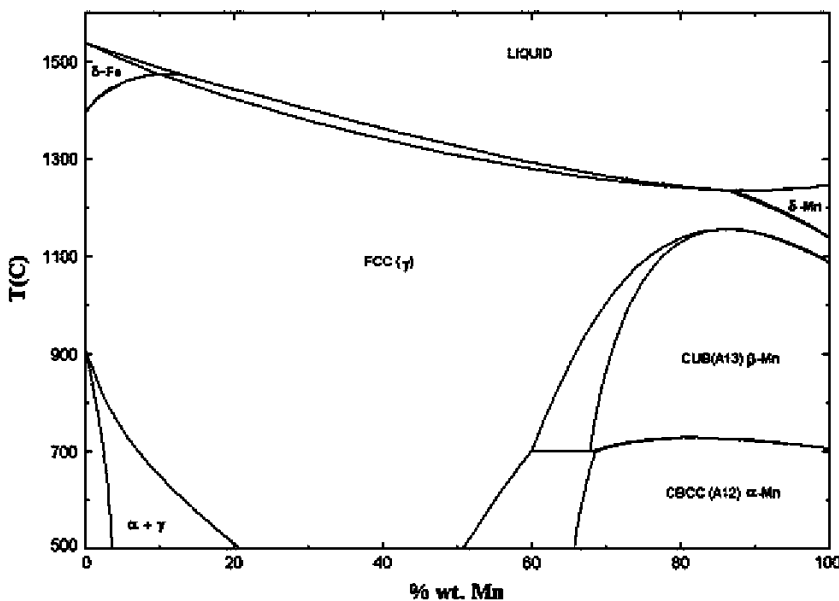


FIGURE 7.4 The phase equilibrium diagram of the Fe-Mn system.

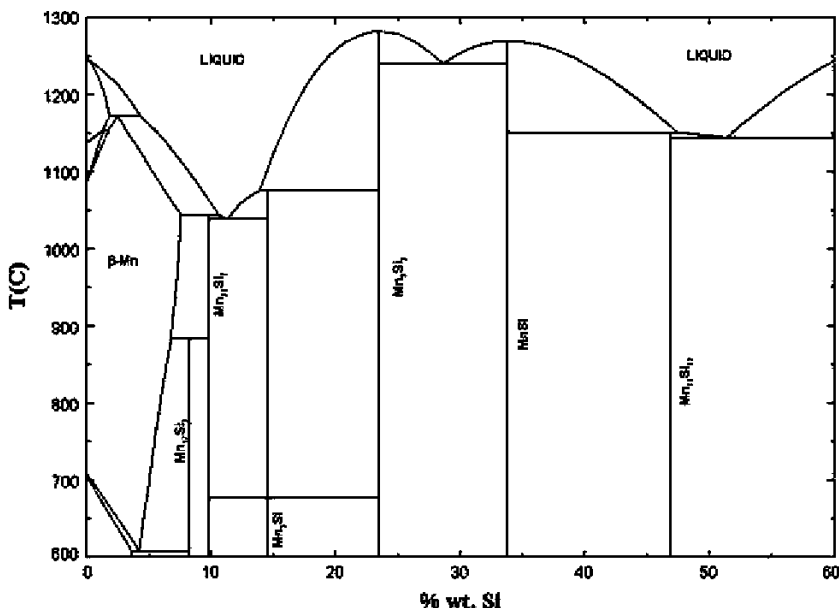


FIGURE 7.5 The phase equilibria in the Mn-Si system (up to 60% wt. Si).

instance, the MnSi_2 formula is being expressed now more correctly as $\text{Mn}_{11}\text{Si}_{19}$, Mn_6Si as $\text{Mn}_{17}\text{Si}_3$ (R-phase), and Mn_9Si_2 as $\text{Mn}_{33}\text{Si}_7$ (ω -phase). Some of these silicides have a certain homogeneity range, particularly at high temperatures (not shown in Fig. 7.5).

With phosphorus, manganese forms several stable phosphides such as Mn_3P , Mn_2P , Mn_3P_2 , and MnP , but no solid solutions (Fig. 7.6). In the liquid state there is a strong interaction between Mn and P atoms.

With sulfur, manganese forms two stable sulfides, MnS and MnS_2 . Sulfide MnS has a high melting temperature of 1610°C , and this is one of the reasons why manganese addition is effective for reducing the harmful effect of sulfur in steels. As with phosphorus, sulfur is practically insoluble in solid manganese.

Nitrogen and manganese form rather complex equilibria (Fig. 7.7). Besides nitrides Mn_4N , Mn_5N_2 , Mn_3N_2 (also expressed as Mn_6N_4), and Mn_6N_5 , there are wide homogeneity ranges in austenitic γ -Mn and ξ - Mn_5N_2 phases. These equilibria are important for processing nitrided manganese ferroalloys.

From the point of view of manganese ferroalloys processing, one of the most important systems is Mn-Fe-Si-C, as it eventually forms the basis of all manganese alloys. These alloys are high-, medium-, and low-carbon ferromanganese, often abbreviated to HC-, MC-, and LC-FeMn, as well as silico-manganese (SiMn) and to some extent metallic manganese (>96% Mn). Pure manganese has a high vapor pressure in its liquid state (above 1246°C), although the boiling point is 2060°C , so the addition of iron, silicon, and carbon has an appreciable effect on decreasing Mn vaporization at temperatures used for production and refining processes.

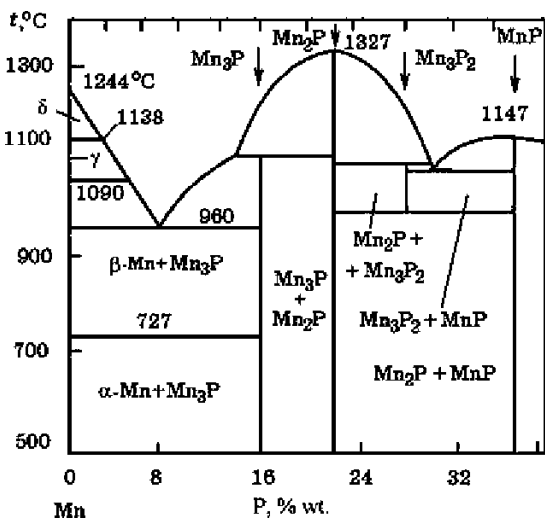


FIGURE 7.6 The phase equilibria diagram Mn-P.

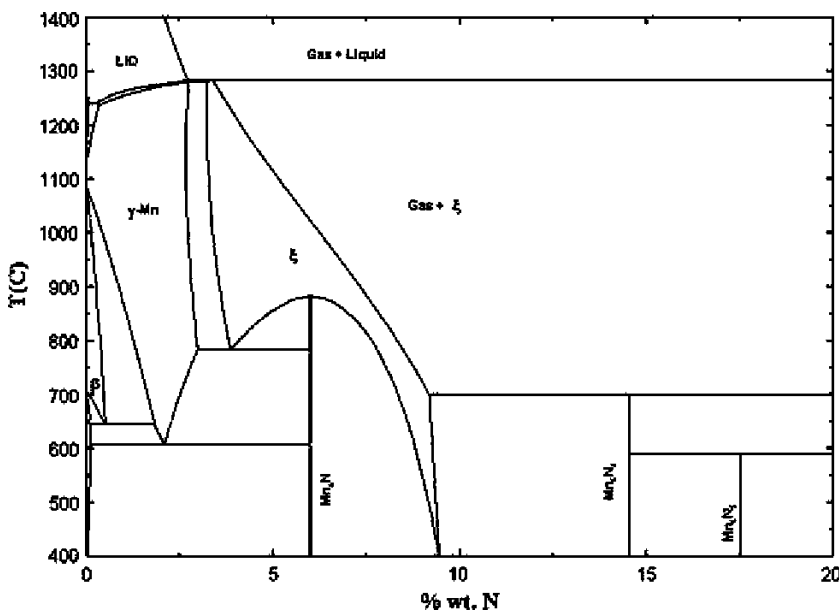


FIGURE 7.7 The phase equilibria diagram Mn-N at 1 atm pressure.

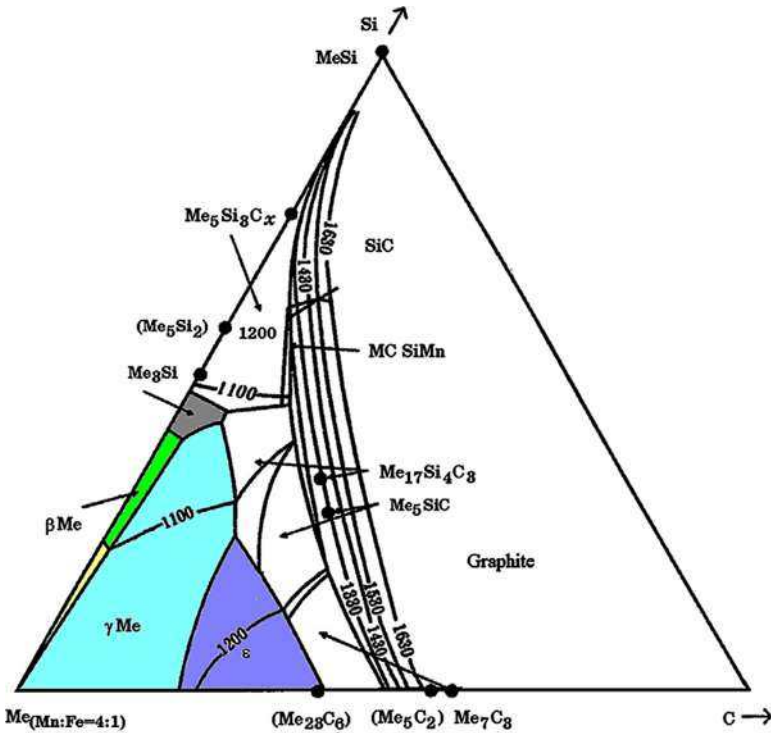


FIGURE 7.8 The liquidus projection in the Mn-Fe-Si-C system (weight ratio Mn/Fe = 4).

Tang and Olsen (2002) analyzed phase equilibria and reactions in the Mn-Si-C system. Contrary to the Fe-Si-C system, in the Mn-Si-C system carbon solubility is higher, but it also decreases with an increase of silicon content. As for iron, for liquid Mn-Si-C alloys with low silicon content (<16% to 23% Si wt., depending on temperature), the equilibrium solid phase is carbon (graphite), whereas at higher concentrations it is silicon carbide. Graphite and SiC might coincide in equilibrium where the Nowotny phase $Mn_5Si_3C_x$ may appear (Olsen et al., 2007). Figure 7.8 represents the liquidus projection of the Mn-Fe-Si-C system in the metal-rich corner for the ratio Mn/Fe = 4. Complex silicocarbides $[Mn, Fe]_{17}Si_4C_3$, $[Mn, Fe]_3SiC$ might appear in equilibrium with graphite.

7.2.4 Manganese in Oxide Systems and Slags

Manganese monoxide forms two compounds with silica: rhodonite $MnSiO_3$ and tephroite Mn_2SiO_4 (Fig. 7.9). They have rather low melting temperatures and this is one of the reasons why manganese-silicate charge components usually melt first before reducing to metal.

The main slag elements when producing FeMn and SiMn alloys are Mn-, Si-, Ca-, Mg-, and Al- oxides. Calculated liquidus projection relations for the ternary MnO - SiO_2 - CaO system are shown in Figure 7.10. Many commercial ores will, after agglomeration and prerduction, also fall into the system MnO - SiO_2 - Al_2O_3 . Calculated phase and liquidus relations for the MnO - SiO_2 - Al_2O_3 system are shown in Figure 7.11.

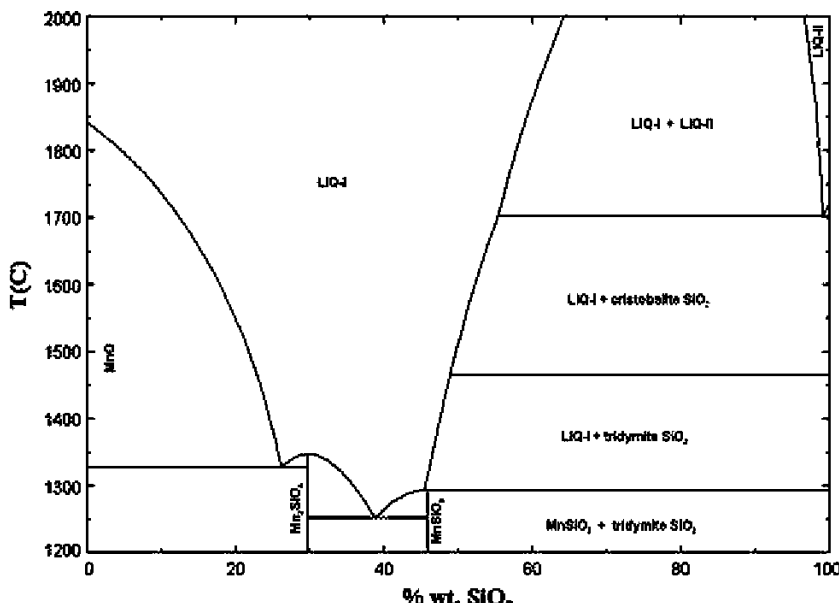


FIGURE 7.9 The phase equilibria diagram in the MnO - SiO_2 system.

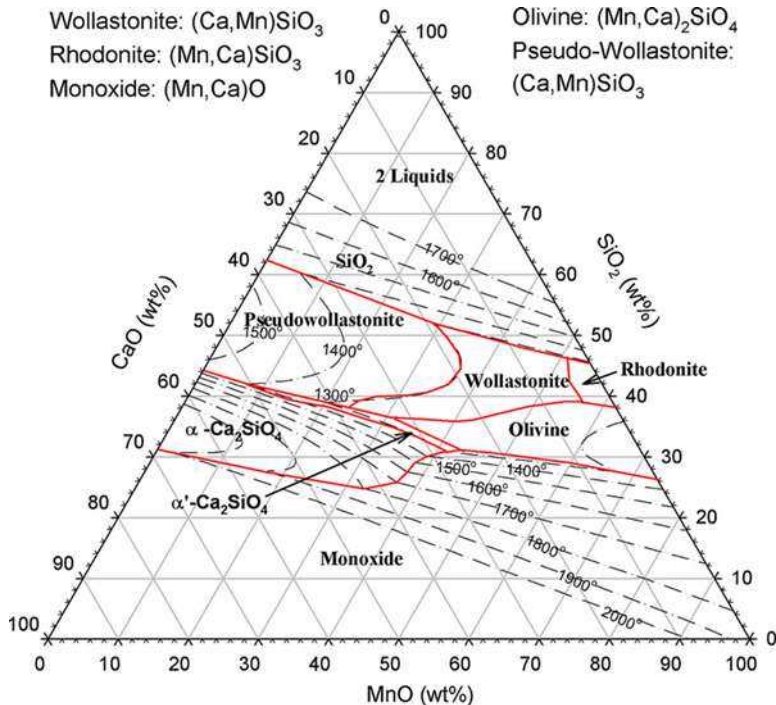


FIGURE 7.10 Calculated phase and liquidus relations for the MnO-SiO₂-CaO system using the FACT oxide database.

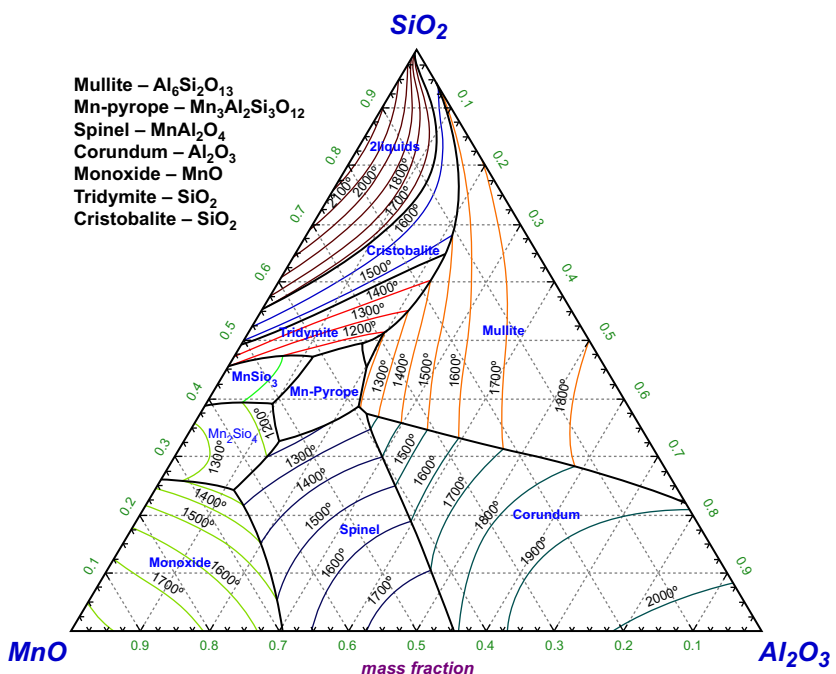


FIGURE 7.11 Calculated phase and liquidus relations for the MnO-SiO₂-Al₂O₃ system using the FACT oxide database.

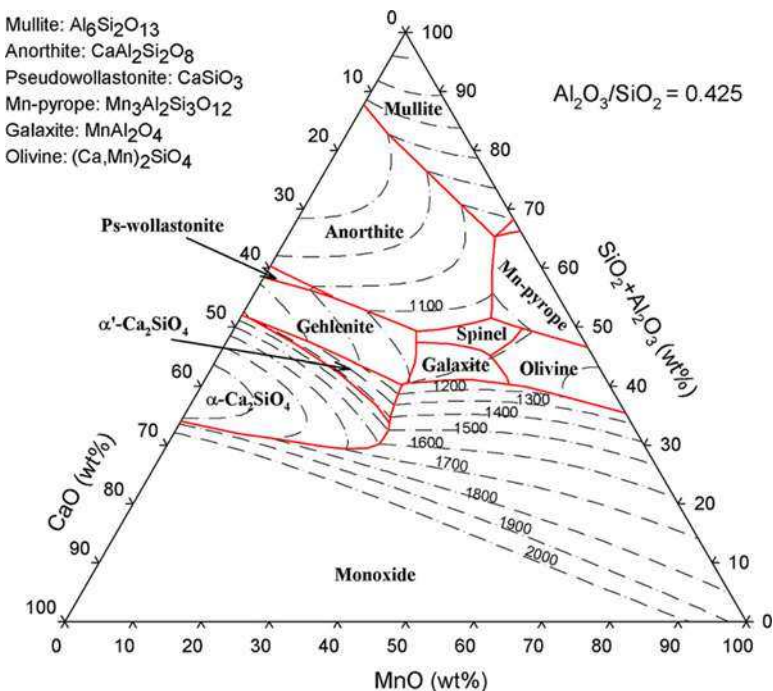


FIGURE 7.12 Calculated phase and liquidus relations for the $\text{MnO}-\text{SiO}_2-\text{CaO}-\text{Al}_2\text{O}_3$ (weight ratio $\text{Al}_2\text{O}_3/\text{SiO}_2 = 0.425$) system using the FACT oxide database.

In many manganese ferroalloys smelting and agglomeration processes, basic fluxes like lime or dolomite are often added. This shifts phase equilibria and leads to new, important phase fields. Examples of calculated phase and liquidus relations for the $\text{MnO}-\text{SiO}_2-\text{CaO}-\text{Al}_2\text{O}_3$ (weight ratio $\text{Al}_2\text{O}_3/\text{SiO}_2 = 0.425$) system are shown in Figure 7.12.

7.3 MANGANESE ORES PROCESSING AND REDUCTION

7.3.1 Manganese Ores

Manganese occurs in nature in the form of minerals. More than 300 minerals are said to contain some manganese, but only a small number have high manganese content. The manganese mineralogy is complex because manganese occurs in divalent, trivalent, and tetravalent states. The most common manganese minerals are oxides, carbonates, and, appearing less frequently, silicates and sulfides (Matricardi and Downing, 1995). Manganese minerals of significant abundance and economic importance are listed in Table 7.1.

TABLE 7.1 Most Known Manganese Minerals

Mineral	Chemical Formula	Mn Content
Oxide Types		
Pyrolusite	MnO ₂	63.2
Vernadite	MnO ₂ ·H ₂ O	44–52
Braunite	3(Mn,Fe) ₂ O ₃ ·MnSiO ₃	48.9–56.1
Braunite II	7(Mn,Fe) ₂ O ₃ ·CaSiO ₃	52.6
Manganite	γ-MnOOH	62.5
Psilomelane	(K,Ba)(Mn ²⁺ Mn ⁴⁺) ₈ O ₁₆ (OH) ₄	48.6–49.6
Cryptomelane	(K,Ba)Mn ₈ O ₁₆ ·xH ₂ O	55.8–56.8
Hollandite	(Ba,K)Mn ₈ O ₁₆ ·xH ₂ O	42.5
Todorokite	(Ca,Na,K) (Mn ²⁺ Mn ⁴⁺) ₆ O ₁₂ ·xH ₂ O	49.4–52.2
Hausmannite	(Mn,Fe) ₃ O ₄	64.8
Jacobsite	Fe ₂ MnO ₄	23.8
Bixbyite	(Mn,Fe) ₂ O ₃	55.6
Carbonate Types		
Manganocalcite	(Mn,Ca)CO ₃	<20–25
Oligonite	(Fe,Mn)CO ₃	23–32
Rhodochrosite	MnCO ₃	47.6
Silicate Types		
Rhodonite	MnSiO ₃	42
Tephroite	Mn ₂ SiO ₄	54.4
Sulfide Types		
Alabandine	MnS	63.2
Gauerite	MnS ₂	46.2

Braunite and braunite II are common complex silicate minerals usually occurring in association with bixbyite, hausmannite, and pyrolusite in deposits such as the Postmasburg and Kalahari manganese deposits of South Africa where braunite is the principal manganese mineral. Rhodochrosite is a common carbonate mineral in various ores.

There are only a limited number of workable deposits of manganese ores. The most important land-based manganese ore deposits are located in the Republic of South Africa, Australia, Gabon, Brazil, China, India, and in the Commonwealth Independent State (CIS) countries of Ukraine, Kazakhstan, and Georgia. The manganese ores are characterized by their content of manganese, iron, and various impurities. The main types of ores are metallurgical ($>35\%$ Mn; high-grade ores with a manganese content above 48% are within this category), ferruginous (15% to 35% Mn; high levels of iron), and mangano-ferrous ores (in fact, iron ores with 5% to 10% Mn). The metallurgical ores are mainly used for direct production of high carbon ferromanganese and silicomanganese alloys, whereas the last two categories are used especially in blast furnaces for adjusting the manganese content of produced pig iron. There might be a substantial variation of ore composition even within the common deposit. For example, Georgian Tchiatura-oxide type ores have 15% to 43% Mn, 13% to 58% SiO_2 , 2% to 4.5% Fe_2O_3 , and 0.7% to 5.5% Al_2O_3 with the average manganese content ~27% (Gasik et al., 2009; Matricardi and Downing, 1995).

Metallurgical grade ores are produced from open pit and underground operations by conventional mining techniques. Ores are crushed and screened, and washed if necessary. Heavy media separation can be used for ores with a high content of silica and alumina gangue. The average manganese recovery in this operation is usually between 60% and 75%.

Metallurgical grade manganese ores contain typically 40% to 50% manganese. Another important parameter is the manganese-to-iron ratio (Mn/Fe), which is required to be >7.5 by weight for the production of standard ferromanganese alloy with 78% Mn. Extra iron might always be introduced as steel chips and recycled scrap. There are also limitations on alumina and silica contents, as excessive slag formation in the furnace increases the electric energy consumption. Ores and concentrates with more than 10% SiO_2 are suitable for use in SiMn production. In some deposits, high phosphorus content is also a concern, and it must be removed before smelting because most of the phosphorus remains in the finished product. South African manganese ores are characterized by low phosphorus content, but, for example, Nikopol ore deposits (Ukraine) have 0.15% to 0.30% P in oxide-type ores and up to 0.6% P in carbonate-type ores (Gasik, 1992). Other physical and chemical properties are also important, such as the level of volatiles and the excess oxygen content. Sulfur is not a problem, neither for metallurgical nor for environmental reasons, as sulfur forms manganese sulfide, which is dissolved and usually removed with the slag.

Most of the mines have sinter plants, where fines are agglomerated. Sintered material is well suited for use in ferromanganese furnaces because it is mechanically strong and thermally stable, allowing the gas to disperse evenly throughout the preheating and prerduction zone. The sintering also results in saving energy if the ore is of the carbonate type. If, on the other hand, oxide-type ores are sintered, most of the beneficial heat from the exothermic

prereduction that usually takes place inside the furnace is lost and the energy consumption will increase. However, the use of fluxed sinter, by the addition of dolomite or MgO-contained materials, has been introduced and shown to improve both sinter plant and smelting operations (Kutsyn et al., 2012).

A blend of manganese ores is, in most cases, used when manganese ferroalloys are produced either in electric submerged arc furnaces or in blast furnaces. The choice of ores depends on chemical and physical properties as well as on economic factors. Table 7.2 shows the average analyses of some important metallurgical ores (Gasik, 1992; Gavrilov and Gasik, 2001; Matriardi and Downing, 1995; Olsen et al., 2007; Samuratov et al., 2010; Tangstad et al., 2004). It is evident that there are important differences in the chemical composition of the various ores. For example, some ores have an unfavorable Mn/Fe ratio but rather low phosphorus content, so a proper ore dressing process must be applied on a case-by-case basis.

After mining, ore is crushed and screened into various particle size fractions ranging from fines (<6 mm) to lump ore (<75 mm). The proportion of fines is often as high as 30% to 70% of the total. Screened ores are upgraded by various methods to produce concentrates. The most common physical separation methods are washing, high-intensity magnetic separation, separation by gravity concentration, and separation by flotation, which makes use of the different surface properties of the minerals. An example for particle size distribution for Nikopol ore concentrates is shown in Table 7.3 (Gasik, 1992).

7.3.2 Agglomeration Processes

Experience has shown that smooth and efficient operation of manganese ferroalloys smelting furnaces is achieved when close sizing control is practiced on the raw materials. The raw materials must secure good permeability for the gas to be distributed through the burden. Fines in the raw materials are particularly detrimental, causing poor charge porosity, which will result in high power consumption per ton of alloy, excessive fume and dust losses, and low productivity. Alloy producers prefer lump and agglomerated ores. High-quality fines are often agglomerated, normally by the use of a sintering process either at the mine or at the customer's plant.

Sintering, pelletizing, and briquetting are three principal technologies used for the agglomeration of ores and concentrates.

Pelletizing is a more difficult process for manganese ores than for most iron ores. It requires higher temperatures ($>1150^\circ$ to 1250°C) to produce strong enough manganese ore pellets, which makes it a more expensive process. On heating of green pellets, manganese dioxide (MnO_2) and manganic oxide (Mn_2O_3) dissociate in endothermic reactions that impose additional fuel consumption. Fine grinding of the material would also be necessary for pelletizing. Consequently, pelletizing appears to be a rather expensive solution for manganese ore, particularly compared with iron ore, although there are

TABLE 7.2 Typical Compositions of Some Manganese Ores (major components)

Deposit	Type	Mn	SiO ₂	Fe _{tot}	MgO	Al ₂ O ₃	CaO	H ₂ O	P
Nikopol (Ukraine)	Oxide	29–43	11–24	1–3	0.8–2	1.4–3.3	4–10	0.5–2.5	0.15–0.3
	Pyrolusite	47.5	8.6	0.65	0.6	1.6	2	<1	0.2
	Carbonate	22–28	13–16	1.5–3	1.5–2.2	1.7–2.3	7–13	0.5–1.5	0.3–0.6
Tchiatura (Georgia)	Oxide	30–44	6–17	0.7–4	1–2.5	1.3–2.6	3.8–5.5	n.r.	0.1–0.4
	Pyrolusite	28	17.6	1.3	1.5	2.9	8.2	n.r.	0.20
	Carbonate	23–25	16–17	1.3	2.5	2	10	n.r.	0.15
Comilog (Gabon)	Pyrolusite	46–51	4–8	3–4.7	<0.3	5.5–7.5	<0.2	<9	<0.1
Groote Eylandt (Australia)	Pyrolusite	48.8	7	4.2	0.1	4.2	0.1	2.7	0.1
Gloria (South Africa)	Carbonate	39.1	5.7	5	3.8	0.3	12.7	0.4	0.02
Mamatwan (South Africa)	Carbonate	37.8	4	4.6	3.5	0.5	14.7	1	0.02
Zapadny Kamys (Kazakhstan)	Fe-Mn type	17–19	40–42	5–6	1–1.5	5–6.5	1.2–1.7	n.r.	0.035

n.r., not reported.

TABLE 7.3 Typical Particle Size Distribution, % wt., of Beneficiated Nikopol Manganese Ores

Size Class, mm	Gravitational Oxide Concentrates	Oxide-Carbonate Concentrate
+25	2.5–10.5	—
25–8	10–33	—
8–5	15–36	—
5–3	5–20	63–68
3–0.5	14–42	17–20
0.5–0.2	5–14	—
–0.2	<3.5	13–16

known attempts to pelletize fine manganese ores (flotation enriched) into 12 to 15 mm size pellets using low-temperature drying.

Briquetting is of less importance for conventional concentrates but is of some interest for agglomeration of manganese-bearing wastes and undersized ore and carbon materials at the production plant. The sintering and pelletizing processes are associated with high capital investment and the high cost of grinding and burning. Briquetting is, in contrast, a cold bonding process and consequently less capital intensive than pelletizing, and it does not need extra milling of materials. Bitumen, cement, molasses, and lime, alone or in combination, have been tested as binders for making briquettes. Reasonable results have been reported for briquetting of concentrates with 3% to 6% humidity (using 7% to 10% lignosulfate as a binder) when pressing at 9 to 10 MPa and drying at 130° to 140°C (Gasik, 1992). The presence of carbon reductant raises the briquette softening temperature up to 1250° to 1400°C.

Agglomeration by sintering has become the leading technology for processing manganese ore. Phase transformations in manganese sinter are not as well known as respective ones in iron ore sintering, which are hindered by a lack of reliable information of the equilibria in complex oxide systems. For instance, in the CaO-MnO-MgO system the solid phase is only of the monoxide type (MeO), but in the presence of MnO there is a miscibility gap leading to separation of CaO-rich and MgO-rich solutions (Woermann and Muan, 1970). It might be caused by manganese oxidation, as in this system oxygen potential should be below 10^{-9} atm to ensure the stability of Mn^{2+} . This system, with addition of silica, is even less studied, especially in the solid-state regions relevant for sinter production. Mechanisms of low-temperature transformations

at 600° to 1200°C as well as the exact mineral structure of some forming phases (donpeacorite, kanoite, substituted pyroxene, and clinopyroxene) are still a subject of discussion (Bohlen et al., 1980; Kutsyn et al., 2012; Petersen et al., 1984; Phase equilibria diagrams, 2001).

The traveling grate technology is the traditional way to produce manganese sinter, such as at the TEMCO ferroalloy smelter plant (Australia), Samancore Manganese Mamatwan mine (South Africa), COMILOG manganese mines (Gabon), and Vale mines (Brazil). This equipment is most suitable for larger capacities. Alternatives are the new steel belt sintering technology developed for smaller capacities (Outokumpu Corp., Finland) or stationary pan sintering (Vale in Mo i Rana, Norway and previously also by Eramet Sauda, Norway). The down-draught sintering in stationary pans is an old established practice capable of producing good-quality sinter for smaller tonnages.

Sintering and pelletizing upgrades the manganese content of the ore through the loss of oxygen from manganese oxides and other volatile species as bound water and carbonates. An example of nonfluxed and fluxed compositions of agglomerates is shown in Table 7.4 (Gasik, 1992; Kutsyn et al., 2011).

Agglomerate compositions similar to those shown in Table 7.4 usually result from the mixture of proper ores and concentrates, depending on the raw materials parameters and requirements for final basicity, stability, and composition. As an average, about 1 to 1.3 t of sinter is processed per 1 m² of the sinter machine in 1 hour. One ton of ready sinter usually requires 1.2 t of manganese concentrate, 120 kg of coke, 5.6 Nm³ of natural gas, and 85 to 95 kWh of electric energy (Gasik et al., 2009). A burden less oxidized, but with better physical characteristics and favorable mineral composition, may result in improved furnace operation compared with an oxidized burden of poor physical quality. When manganese ferroalloys are manufactured on a scale that does not allow the use of large sinter plants at the metal producer's plant as in iron making, the sintering of fines is often carried out at the mine. Sintering at the metallurgical plant makes it possible to use fine ores that are otherwise unusable, as well as fines produced by rescreening classified ores, bag-house dust, sludge from gas cleaning plants, and fines from screening of carbon materials. Coke fines are used as the main energy source in the sintering process. If the smelting furnace is covered and equipped with CO gas collection, the CO gas

TABLE 7.4 Example of Composition of Nonfluxed (AMN) and Fluxed (AMO) Manganese Sinters from Nikopol Ores, % wt.

Type	Mn	SiO ₂	Fe ₂ O ₃	Al ₂ O ₃	CaO	MgO	P	S	K ₂ O+Na ₂ O
AMN	43–50	19–28	2–4	2–3	2–4	1–2	0.12–0.2	0.1–0.2	1–2.5
AMO	36–40	16–25	3–6	2–3	3–8	6–10	0.15–0.2	0.1	1–2.5

can also be used as energy in the sintering plant and for preheating the smelter feed. Sinter is extensively degraded during handling and transportation and should therefore be produced near the utilization point. Addition of proper fluxes (higher MgO contents) was shown to improve mechanical properties of fluxed sinter and resist its degradation in storage (aging due to calcium orthosilicates) by creation of a larger fraction of monoxide phase (Kutsyn et al., 2012).

7.4 MANGANESE FERROALLOYS

7.4.1 Manganese Alloy Specifications

The primary use of manganese is in the steel industry where manganese is added mainly in the form of ferroalloys. Several different types of manganese alloys have been developed and are being marketed (Maticardi and Downing, 1995). These alloys may be divided into the following major categories:

- Ferromanganese FeMn, high- (HC), medium- (MC), and low-carbon (LC)
- Silicomanganese SiMn (or ferrosilicomanganese FeSiMn)
- Metallic manganese Mn
- Nitrided manganese alloys (nitrided manganese MnN and silicomanganese SiMnN)

The number of alloy specifications is large. Some suppliers list more than 20 different products. The alloys vary in manganese, carbon, silicon, phosphorus, and nitrogen content. Because of the scarcity of low phosphorus manganese ores, many users, especially alloy steel manufacturers, will pay a premium for low phosphorus alloys. Typical examples of alloy specifications for most commercially used manganese ferroalloys are shown in Table 7.5 (Gasik, 1992; Gasik et al., 2009; Olsen et al., 2007).

High-carbon FeMn is the traditional form of manganese added to steels, but its application is mostly limited to unalloyed and low-alloyed carbon steels. Medium and low carbon ferromanganese are used where the carbon content must be controlled and cannot be reduced after the addition of the ferroalloy. These grades are mainly produced by oxygen refining of high carbon ferromanganese and by a silicothermic process involving the reaction between silicon in crude SiMn alloy and manganese ore. The consumption of refined alloys with reduced carbon content is increasing due to increasing production of low carbon steels. In 2010, the worldwide production of refined ferromanganese (< 2% C) was 1.5 Mt. The use of silicomanganese is expected to advance at a faster rate than high carbon ferromanganese consumption. Silicomanganese adds less phosphorus, carbon, aluminum, and nitrogen to the steel compared to a mixture of standard high carbon ferromanganese (HC FeMn) and ferrosilicon with 75% Si (FeSi75). Standard quality silicomanganese (SiMn) is used in most silicon and manganese-containing steels where the combination of carbon,

TABLE 7.5 Typical Composition of Major Commercial Manganese Alloys
(maximum content, wt. % unless shown otherwise)

Alloy	Grade	Mn	C	Si	P	S	N
HC-FeMn	78	78–82	7.5	1	0.05*; <0.2–0.35	0.03	
	75	>75	<6–7	<4–6	0.05*; 0.45	0.03	
	70	>70	7	6	0.06	0.03	
MC-FeMn	88	85–95	2	3	0.4	0.03	
	85C1	85	1–1.5	1	<0.1–0.3	0.03	
	75C2	75	1.5–2	2–2.5	<0.2–0.35	0.03	
LC-FeMn	90	95	0.2	1	0.07	0.05	
	85C0.5	85	0.5	2	<0.2–0.3	0.03	
FeSiMn (commercial)	Si25	>60	0.5	25–35	0.05	0.01	
	Si22	>65	1	20–25	0.1	0.02	
	Si17	>65	2.5	15–20	0.1	0.02	
	Si12	>65	3.5	10–15	0.2	0.03	
FeSiMn	Crude [†]	Bal.	<0.05–0.15	>27	<0.05–0.07	0.02	
Metal Mn	998 [‡]	99.8	0.04	—	0.003	0.003	
	997 [‡]	99.7	0.06	—	0.05	0.10	
	965	96.5	0.10	0.8	0.05	0.05	
	95	95	0.20	1.8	0.07	0.05	
MnN	92N6 [‡]	92	0.1	—	0.005	0.1	>6
	87N6	87	0.2	1.8	0.07	0.05	>6
	89N4	89	0.2	1.8	0.07	0.05	>4
	91N2	91	0.2	1.8	0.07	0.05	>2
SiMnN	7N	>60	3.5	9–17	0.1	0.02	>7
	5N	>60	3.5	9–17	0.1	0.02	4–7

^{*}For premium grades only.[†]As reductant for smelting Mn, max. 2.3% to 2.8% Fe.[‡]Only for Mn made by electrolysis.

manganese, silicon, and trace elements fits the final steel analysis in an economical way. The use of low carbon silicomanganese in stainless steels and alloy steels provides a more economical production route, where a combination of manganese and silicon is required in a low carbon steel product.

Metallic manganese is produced by two methods: electrolytic and electro-thermal. Electrolytic manganese is the purest form of manganese and has a minimum content of 99.8% Mn. This hydrometallurgical method is not considered here. Electrothermal manganese is produced by the reduction of dephosphorized manganese slag melt with silicon from crude SiMn in the presence of flux (lime). For this purpose, SiMn has a limited amount of iron (Gasik, 1992). It is used in the production of aluminum and copper alloys, for special grades of stainless steel and other special steels, and for electronic applications. Aluminum alloys constitute the largest nonferrous metallurgical use of manganese. Manganese improves the corrosion resistance of aluminum. Aluminum alloys with a Mn content of 1% or more are widely used in beverage cans and in food-handling equipment. Manganese bronzes are copper-based alloys, strengthened by small additions of manganese (up to 4.5%). These alloys are used for marine propellers and fittings as well as gears and bearings.

7.4.2 Impurities in Manganese Alloys

The trend toward the production of higher-quality steels with fewer impurities increases the pressure on producers of manganese alloys to improve the quality of their products by tighter specifications on harmful elements—particularly carbon, sulfur, and phosphorus (see Table 7.5). Commercial production of manganese alloys from ordinary raw materials inevitably introduces many impurities in the final metal, although in smaller amounts. Typical concentrations of a number of these constituents are given in Table 7.6.

7.5 SMELTING TECHNOLOGIES FOR MANGANESE ALLOYS

7.5.1 Basics of Reduction Processes

Manganese ores will always contain some iron oxides. Reduction of the iron oxides in the ore is probably almost complete when the temperature reaches 1200°C. The product will be a carbon-saturated iron alloy with an increasing content of manganese at increasing reductions in temperature. The last reduction step, $\text{MnO} \rightarrow \text{Mn}$ metal, will take place in the liquid state with MnO being dissolved in the oxide melt and the produced manganese metal continuously dissolved in the liquid carbon-saturated Mn-Fe-C metal. Both MnO and SiO₂ are partially reduced from the slag to form the metal phase.

Besides manganese oxides and silica, the manganese ores normally also contain Al₂O₃, CaO, and MgO. Coke ash also contains SiO₂, Al₂O₃, and smaller amounts of CaO and MgO. In addition, CaO- and MgO-containing

TABLE 7.6 Typical Concentration of Other Impurity Elements in Manganese Ferroalloy (Olsen et al., 2007)

Alloy	wt. %		ppm												
	O	N	Al	Ca	Mg	Ti	Cr	Co	V	Ni	Cu	Zn	S	B	H
HC FeMn	0.2	0.03	50	100	300	80	200	220	400	220	130	80	20	< 5	20
MC FeMn	0.4	0.12	50	100	3000	40	350	270	400	280	150	10	40	< 5	15
LC FeMn	0.4	0.12	50	100	2000	50	750	290	450	280	170	10	30	< 5	15
MC SiMn	0.15	0.005	150	200	350	2000	320	110	250	300	75	15	90	220	15
LC SiMn	0.15	0.005	150	100	200	2500	300	70	250	300	75	15	30	220	15

fluxes are usually added to the raw material mixture. These oxides will end up in the slag phase. They are considered to be irreducible, and they maintain their mutual ratio in the slag during the reduction process, this being of great importance for the thermodynamic and physical properties of the slag phase.

As follows from the Fe-Mn-Si-C system equilibria (e.g., see Fig. 7.8), graphite remains the stable phase coexisting with carbon-saturated alloy melts until the Si-content reaches a certain value (approximately 18% for Mn-Si melt; this depends on temperature). Then silicon carbide replaces graphite as the stable carbon-containing phase.

The important factors that control the degree of manganese reduction are the slag basicity, which in practice is expressed as $(\text{CaO} + \text{MgO}) / (\text{Al}_2\text{O}_3 + \text{SiO}_2)$, and CO partial pressure. An increase of basicity and a decrease of CO pressure will reduce the MnO content of the slag considerably (Olsen et al., 2007). Even though experimental results may provide a basic image of the equilibrium compositions of metal and slag for a given system, it will still be difficult to determine the exact quantities and compositions of the reaction products. The reason is that the final state of a given system is dependent not only on chemical equilibrium but also on stoichiometric restrictions (i.e., the materials balance).

Carbonates present in the charge or added as flux decompose between 300° to 900°C. The higher manganese oxides that predominate in manganese ores (MnO_2 , Mn_2O_3 , and Mn_3O_4) are relatively unstable and easily reduced in solid state. These are exothermic reactions producing a considerable amount of heat and thereby preheating the charge materials in the furnace. Iron is always present in manganese ores, and the reduction of iron oxides runs parallel to the reduction of higher manganese oxides. At temperatures above 1150°C, reduced iron forms a liquid alloy, dissolving carbon and assisting in the reduction of manganese due to lower Mn activity in the metal phase. Considerable smelting of the remaining oxide mixture starts at ~1250°C, and the final reduction of MnO to manganese metal will take place with solid carbon in the coke bed. This is also the case for the reduction of silica to silicon metal. Some carbon will dissolve in the metal up to carbon saturation.

The manganese reduction reaction is highly endothermic and will consume approximately two thirds of the supplied electric energy for HC FeMn production and one third for SiMn production. The CO gas will heat the descending raw materials in the furnace. Because a reduction of the higher manganese oxides with CO gas is exothermic, these reactions will contribute to the temperature increase in the prereduction zone.

7.5.2 Outline of Industrial Practice

Manganese ferroalloys are commercially produced by the carbothermic reduction of manganese oxide ores in submerged arc furnaces (SAFs). The blast furnace process is still marginally used for high carbon FeMn production, where the coke serves as a reducing agent as well as an energy source. Blast

furnace smelting has serious disadvantages, such as high coke consumption (~1500 to 2000 kg/t of alloy, which is five to six times higher than in electric furnaces) and high losses of manganese in slag and off-gases. The electric furnace practice offers several advantages, such as a higher overall yield of Mn from the ores, less carbon consumption, lower-quality reducing agents, and greater flexibility in its ability to produce different grades of alloys. In addition, basically the same furnace might be switched to a flexible production of either HC FeMn or SiMn on demand.

All manganese ferroalloys are processed, in principle, by either the discard slag method (sometimes called the flux process) or the duplex (also known as the flux-less) method. These two methods are not, however, directly dependent on the number of added fluxes but rather on the final basicity of the slag. Both can be realized with or without fluxes, depending on the raw materials. The first method is quite similar to the blast furnace practice and it aims to reduce manganese into the alloy in one stage, usually with assistance of basic fluxes (CaO, MgO) or using a basic ore decreasing silica activity in the slag and increasing the activity of MnO. For high-carbon ferromanganese discard slag practice (flux), manganese recovery is ~80%, and about 15% to 20% MnO remains in the slag, which is dumped, as it is not economical to recover more manganese at such concentrations.

The second method, the duplex process, is more common. There is normally a blend of several ores to achieve a required composition of produced metal and slag. The tapped slag will contain as much as 30% to 50% MnO. The MnO-rich slag is reprocessed for the production of silicomanganese or metal manganese in the second stage (Fig. 7.13). In this way, the MnO content of the discarded slag can be reduced to ~5% MnO, and an overall manganese recovery is increased to 85% to 90% with less coke required.

The interior of a furnace producing high carbon ferromanganese consists of two main zones: the top prerection zone (low temperature) and the lower coke bed zone (high temperature). In the prerection zone, raw materials are heated through heat exchange with ascending hot gases, and solid-state reduction of higher manganese oxides to MnO by CO gas takes place. Due to the exothermic nature of these reactions, temperature increases lead to melting of the partially reduced manganese ore (Tangstad et al., 2010). In the coke bed zone, prereduced and molten ores and fluxes fuse together to form an oxide melt (slag). This zone has a bed of solid coke, liquid slag, and liquid metal. These phases may be present in various configurations depending on the history of the operation. The coke bed starts approximately at the tip of the submerged electrodes. The relative amount of coke in the charge mix determines whether the coke bed increases, decreases, or is stable in size. In addition to being the chemical reduction agent coke also acts as the heating element of the process where the electric current runs and joule energy is produced, determining temperature distribution. The production rate, product quality, and stability of the furnace operation are mainly determined by parameters in the coke bed.

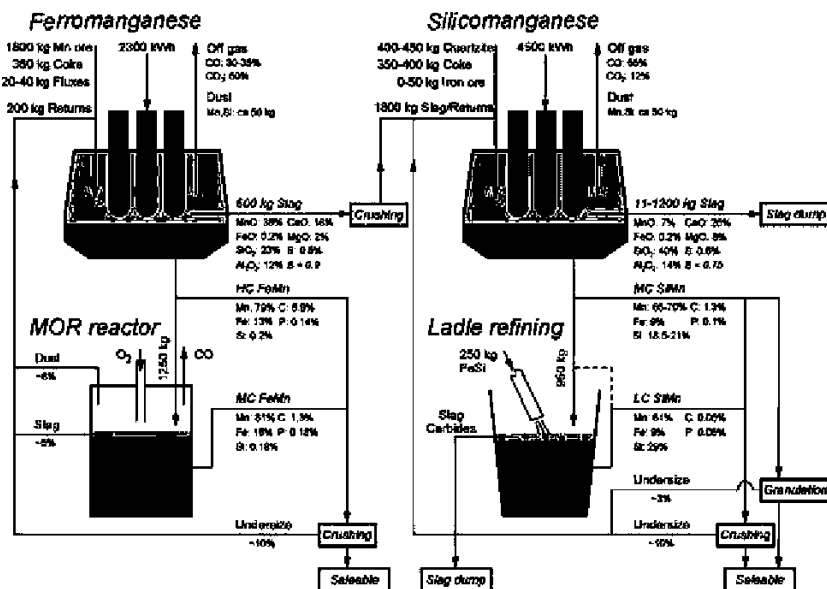


FIGURE 7.13 Duplex (double stage) production of HC FeMn and SiMn, with refining processes (Olsen et al., 2007).

Due to the different densities of coke, slag, and metal, the various layers are often described in the literature as consisting of separate layers. However, from excavations of single-phase pilot-scale furnaces and industrial furnaces, it has been proven that coke is present all the way down to the metal layer, due to the weight of the above located charge materials. The slag-to-coke ratio in the coke bed increases with decreasing distance to the metal layer. Also, vertical columns of almost pure slag have been found in the center of the coke bed. The structure of this zone may vary from “dry coke” (with no slag) to coke lumps more or less evenly dispersed in the slag, which hence have no mutual contact. The shape and size of the coke bed may also vary from horizontal layers to bell-shaped and conical shapes depending on raw materials, slag chemistry, and most of all on the preceding furnace operation (i.e., whether the coke volume in the furnace is increasing, decreasing, or is in a stable state). The electrode tips are normally located around the upper level of the coke bed, and the current distribution is mainly determined by conditions in this zone. If raw materials are changed in type, the existing ore inside the furnace will be replaced much faster than the existing coke. Depending on the coke bed volume, a complete change to new coke in the furnace may take several weeks.

The generation and transfer of heat in the furnace determine the performance. Electric energy must be converted into heat in those regions where the thermal energy is mainly consumed. Enough energy should be supplied

to the lower regions to give sufficient conditions of slag and metal for easy tapping. The main factors that affect the energy distribution and consequently the process temperature are a naturally electric energy supply, a balance of enthalpy of chemical reactions, and internal heat exchange and transfer of heat by circulating substances, such as Mn(g), K(g), and CO-rich gases.

For normal furnace operation, the electrodes are submerged relatively deep in the furnace, and due to the large difference in electric resistivity, most of the current will run through the coke bed. The main part of the electric energy is dissipated in the coke bed area close to the electrodes. This means that the rate of raw material flow and metal production is at its maximum close to the electrodes, where also the gas flow rate will be high. Despite the turbulence and high temperature gradients in the reaction zone, it has been found during the excavation of furnaces that the slag composition changes gradually throughout the coke bed; hence, it is believed that the horizontal movement of coke, slag, and gas is very small.

Commonly, bulk manganese alloys are produced in three-phase submerged arc furnaces, which have a three-electrode (Søderberg type, or self-baking) circular or a six-electrode rectangular geometry. Most of the modern production of manganese alloys takes place in covered furnaces rated from 20 to 90 MVA power capacity ([Table 7.7](#)).

Examples of the construction of the last two furnaces described in [Table 7.7](#) ([Gasik et al., 2009](#)) are shown in [Figure 7.14](#) (rectangular type) and [Figure 7.15](#) (circular type).

TABLE 7.7 Parameters of Some Industrial Furnaces for Smelting of HC FeMn from Plants in Norway and Ukraine ([Gasik, et al., 2009; Olsen et al., 2007](#))*

Furnace Type	Circular	Circular	Rectangular	Circular
Rated power, MVA	45	45	63	75
Electrodes	3	3	6	3
Electrode section, mm	Ø 1700	Ø 1900	3000 x 750	Ø 2000
Electrode current, kA	120	133	112	160
Electrode pitch, mm	4000		3300	4300
Hearth depth, mm		8800	3190	7300
Hearth size, mm	Ø 12000	Ø 15000	20340 x 6000	Ø 15000
Power factor			0.91	0.92

*Empty cells mean no data have been provided.

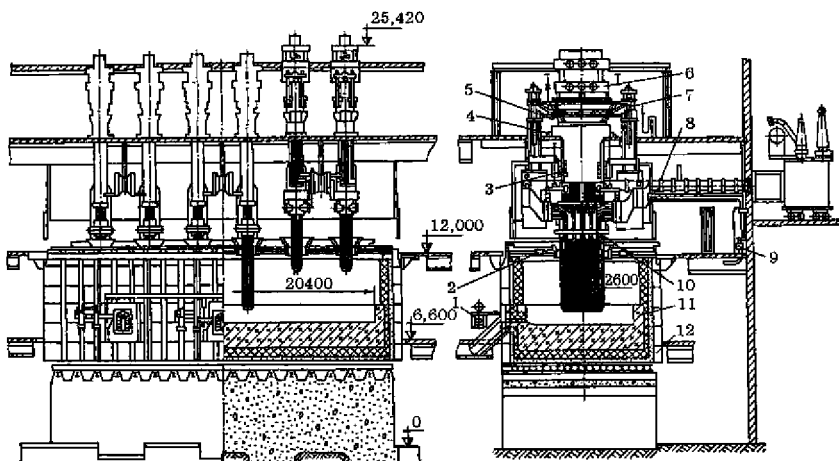


FIGURE 7.14 Rectangular 63 MVA furnace for manganese ferroalloys (dimensions in mm): 1, tap hole device; 2, furnace cover; 3, electrode holder support; 4, gaskets; 5, hydraulic shift system; 6, electrode shift mechanism; 7, hydraulic lift; 8, “short net” (secondary circuit); 9, water cooling system; 10, electrode holder; 11, lining; 12, furnace shell.

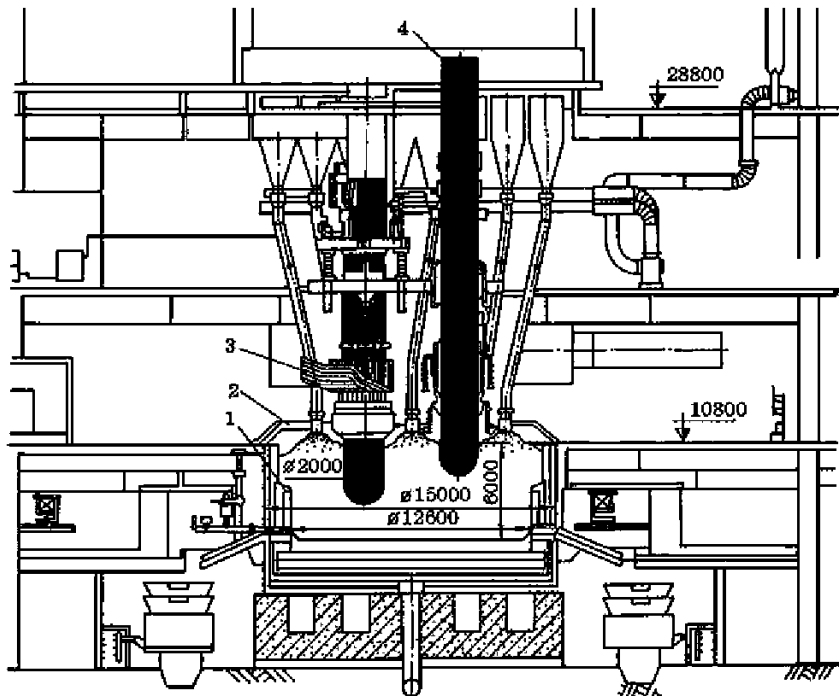


FIGURE 7.15 Circular furnace (75 MVA) for manganese ferroalloys (dimensions in mm): 1, carbon blocks lining; 2, furnace cover; 3, short net; 4, electrode.

The raw material mix is transported to hoppers above the furnace from where it is fed by gravity through chutes passing through the furnace cover. Produced slag and metal may be tapped simultaneously from the same tap hole, or separately in different slag and metal tap holes arranged at a vertical distance of 0.5 to 1 m.

When high-phosphorus ($>0.2\%$ P) manganese ores are utilized, it is not usually feasible to remove phosphorus at the stage of ore-dressing or agglomeration. In this case, the electrometallurgical method is sometimes used first to reduce phosphorus and iron from the oxide melt with a minor amount of coke into a by-product metal, leaving most of the manganese in the refined slag, which then will be used for further processing into FeMn, SiMn, or metal manganese. The process is carried out in circular closed furnaces (Fig. 7.16) continuously, with periodic tapping of slag (38% to 42% Mn, 0.010% to 0.017% P) and metal (50% to 55% Mn, 1% to 3% Si, balance Fe, C, and P). There, ~90% of the total amount of phosphorus and iron present is reduced into the metal.

7.6 TECHNOLOGY OF FERROMANGANESE

7.6.1 High-Carbon Ferromanganese Production

High carbon ferromanganese is commercially produced by the carbothermic reduction of manganese ores, primarily in electric submerged arc furnaces. The produced metal typically contains around 72% to 82% Mn and 7% C (see Table 7.5), and the slag contains around 40% MnO (duplex process). An increasing part of the metal is refined to medium or low carbon ferromanganese after smelting. Different raw material components are weighed out based on chemical analyses of ores, fluxes (dolomite, limestone), and carbonaceous agents (coke), and on the desired composition of alloy and slag. These basic fluxes are added to give the slag suitable chemical properties, smelting temperature, and viscosity in order to secure good furnace operation and a high manganese yield. Blending ores from different sources is a common practice—for instance, to obtain a specific Mn to Fe ratio in the metal (e.g., 7:1 for high carbon ferromanganese with 78% Mn). Independent producers in ore-importing countries have considerable flexibility in the blending of ores to produce a given product at the lowest production cost. For instance, the Fe and P content of the metal is determined and controlled by the composition of the ore mix, as iron oxides and undesired oxides of phosphorus are easily reduced. Also, the slag basicity is important because it controls smelting properties and the content of unreduced MnO in the slag.

Examples of HC FeMn smelting by flux and flux-less processes are shown in Table 7.8 (Gasik, 1992). Note that the parameters of these processes greatly depend on the ores used, furnace type, slag basicity, and furnace operation methodology.

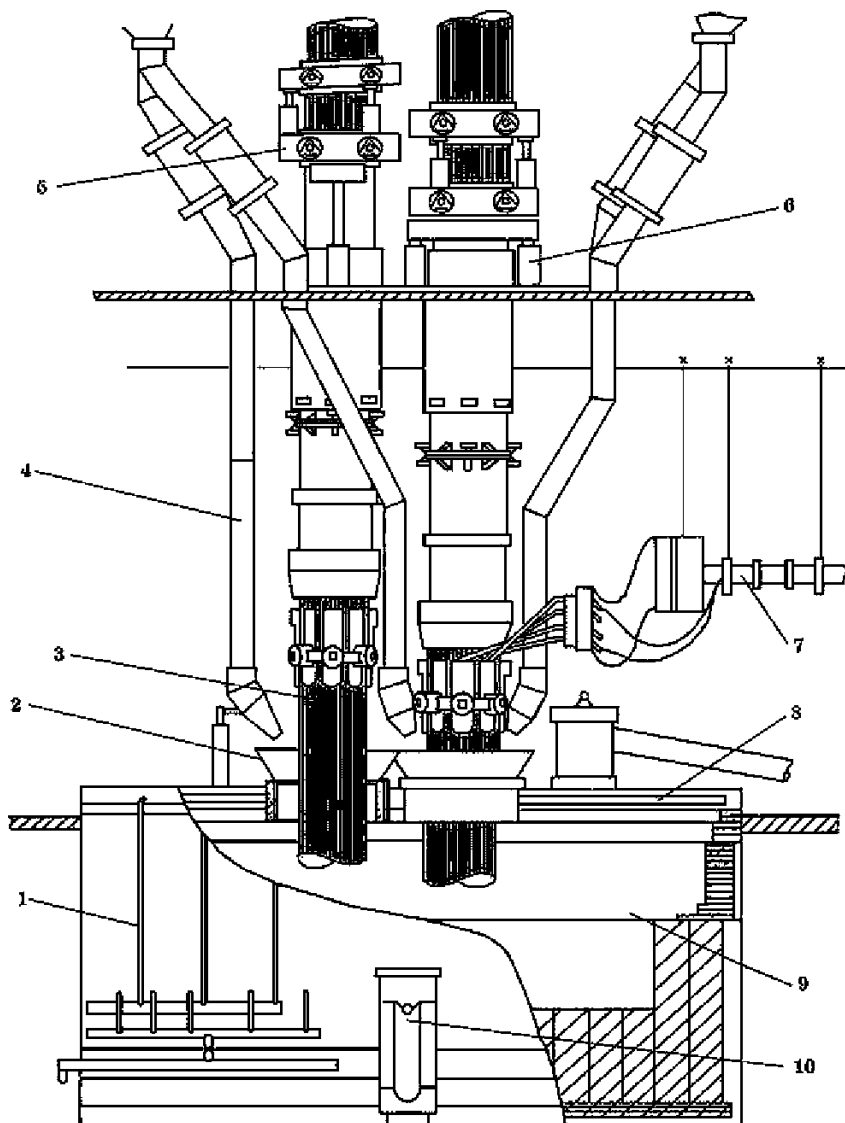


FIGURE 7.16 General view of the 22.5 MVA furnace for phosphorus removal from the manganese slag: 1, furnace shell; 2, charge feeding funnel; 3, self-baking electrodes; 4, charge feeding ducts; 5, electrode holding and shifting mechanisms; 6, hydraulic shifting cylinders; 7, short net; 8, furnace cover; 9, hearth; 10, tap hole and guide.

Optimized ferromanganese furnace operation assumes a necessary high load, a minimum of coke and energy consumption, stable and expected metal and slag composition with a high yield of manganese and minimized greenhouse gases, and noxious compounds emissions. Whereas the power consumption is

TABLE 7.8 Comparison of Basic Parameters of Smelting of HC FeMn by Different Process Types (per 1 ton of alloy with 78% Mn; n.r. = not reported)

Parameters	Discard method		Duplex method	
	Plant A	Plant B	Plant C	Plant D
Specific consumption, kg/ton				
Concentrate or agglomerate (48% Mn)	1950–2060	2750–2970	n.r.	n.r.
Coke	550–580	350–420	360	306
Iron ore pellets	110	85	—	—
Limestone	700	—	—	—
Electrode paste	10–21	12–22	12	6.6
Electric energy, kWh/ton	3300–3900	2200–3500	2400	2150
High-MnO slag (48% Mn basis), kg/ton	—	900–1300	n.r.	n.r.
% Mn in slag	12–15	35–38	31.2	33.1
Slag/metal ratio	1.2–1.3	0.8–0.9	0.64	n.r.
Manganese yield, %	76–82	97–99	76.7	81.5

determined mainly by reactions in the prereduction zone, the stability of the operation is determined by the coke bed size and the reactions taking place in the coke bed zone. A biased carbon balance (coke loads that are too high or too low) will result in erroneous electrode positions and an upset of the heat distribution between the charge zone and the reaction zone. This will most often lead to operational problems with less metal yield and a lower load, and thus reduced tonnage. These factors are important for the economy of the process.

If the correct mixture of ores and fluxes fails to be added, this will be easily detected by the slag and metal analyses and may be corrected relatively quickly. However, if the added quantity of carbon is incorrect, this may not be readily noticed. Even with good chemical analyses and weights of raw materials, there can easily be 1% to 2% inaccuracy in the carbon quantity added. In a 40 MW FeMn furnace producing 400 tons of HC FeMn per day with a coke consumption of 330 kg coke per ton of alloy, a total of 132 tons of coke will be added every day. With an inaccuracy rate of 2%, the furnace may be “undercooked” or “overcooked” by ± 2.6 tons/day. After 2 weeks of “overcoking” there will be a buffer of more than 35 tons of coke in the furnace. Hence, even if a good mass balance is calculated, this is only one of several necessary means to secure the right quantity of raw materials.

7.6.2 Production of Commercial Silicomanganese (FeSiMn)

Silicomanganese (SiMn) is also produced by the carbothermic reduction of raw materials in electric submerged arc furnaces of the same type as used for the production of HC FeMn. The size of the SiMn furnaces is usually in the range 15 to 63 MVA (actual power 13 to 57 MW), giving 80 to 340 tons of alloy per day. Operation of the SiMn process differs from the FeMn process, as higher process temperatures are needed to attain the wanted silicon specification content in the metal (see [Table 7.5](#)). Basically there are no differences between commercial and crude SiMn production except the charge composition and process temperature. The SiMn production is often integrated with the manufacture of HC FeMn so that the high-MnO slag from the HC FeMn production (or from the phosphorus removal smelting) is reprocessed in the production of SiMn. In this way a high total yield of manganese is achieved (see [Fig. 7.13](#)).

In addition to manganese slag, Mn ore (agglomerate), and coke, other components of the charge are quartzite, FeSi or Si-melts, or off-grade qualities. The ratio of raw ore to Mn slag varies from plant to plant, depending on the ore quality and availability (for high-grade ores with low phosphorus production, the use of MnO-rich slag might not be required). The major flux used is dolomite or dolomite-limestone.

During smelting, iron and manganese oxides are reduced first, as in the HC FeMn process, but the reduction of silicon requires higher temperatures (1600° to 1650°C). Carbon-saturated alloys are in equilibrium with either graphite (<20% to 23% Si) or SiC (at higher silicon concentrations), whereas a major amount of carbon is combined into Nowotny's phase $(\text{Mn},\text{Fe})_5\text{Si}_3\text{C}_x$ ([Gasik et al., 2009](#)). The higher the silicon content, the lower the carbon level would be, similar to the Fe-Si-C and Cr-Si-C systems. As high silicon content in the alloy requires more energy, for SiMn alloys >30% Si addition of silicon wastes from the ferrosilicon industry is being practiced ([Olsen et al., 2007](#)). These wastes are relatively cheap sources of silicon, so this practice can even be favorable for the production of standard SiMn because it greatly reduces the specific energy consumption and consequently increases the production capacity of the furnace. The example of the SiMn smelting parameters is shown for 33 to 63 MVA furnaces in [Table 7.9](#) ([Gasik, 1992](#); [Gasik et al., 2009](#); [Olsen et al., 2007](#)). The specific power consumption for the production of standard SiMn from a mixture of Mn-ore, HC FeMn, slag, and Si-rich metallic remelts is typically 3500 to 4500 kWh/ton of metal, depending primarily on how much of the metallic part of the charge is added to the feed. The power consumption will increase with the Si-content of the metal produced and also with the produced amount of slag per ton of metal.

Although the use of high-MnO slag with low phosphorus might ensure lower phosphorus content in SiMn, an excess supply of the slag is not feasible as it has a relatively low melting temperature compared with Mn-ores. Therefore, a too-

TABLE 7.9 Example of SiMn Smelting Parameters (basis 17% Si in the alloy)*

Parameters	Phosphorus Content in SiMn, %			
	<0.20	0.25–0.35	0.40–0.55	>0.60
Specific Consumption, kg/ton				
Manganese ore (48% Mn basis)	900–1200	1250–1400	1350–1400	1650–1670
Manganese slag (48% Mn basis)	650–850	300–360	150–180	—
Coke	310–415	320–425	320–410	320–395
Quartzite	250–285	260–330	260–305	260–300
Flux (dolomite, limestone)	100	<50	—	—
Recycled materials and Mn slags	160–200	200–235	190–250	150–220
Electrode paste	27–30	24–26	24–26	23–25
Electric energy, kWh/ton	3900–4300	3800–4100	3800–4000	3600–3900
Maximal Mn content in slag, %	10–12	11–12	11–13	12–13
Slag/metal ratio	1.6	1.5	1.4	1.3
Manganese yield, %	75–77	79–81	80–82	82–85

*Phosphorus content roughly indicates the share of low-P, high-MnO slag used in the charge, which affects other parameters.

high share of MnO slag will tend to give lower process temperatures, which will limit the practically achievable Si-level (usually <20% Si).

The economy of silicomanganese smelting is enhanced by minimizing the Mn loss as metal inclusions and MnO dissolved in the slag. The discarded slag from the SiMn process normally contains 5% to 10% MnO for the best practice (Olsen et al., 2007), although in some plants low-grade raw materials do not allow this level to decrease below 11% to 14% MnO (Gasik, 1992). To reduce the overall losses of the processes, any amount of metal fines and remelts from the production process are usually recycled back to the furnace. Industrial experiments have demonstrated that a reasonable increase of MgO in the slag would improve manganese recovery significantly. For example, Kutsyn et al. (2012) have shown that the addition of waste slag from ferronickel smelting in an SiMn flux-less process increased MgO in the slag up to 10% to 12% and allowed a decrease of MnO in tapped slag from 30–35% to 15–20% with optimal coke additions. It is expected that MgO additions shift slag mineral equilibrium composition toward the primary monoxide phase (MeO) instead of olivine or rhodonite (MeSiO_3), thus enhancing the activity of MnO for reduction.

7.6.3 Post-Tap Hole Processing for FeMn and SiMn

Both ferromanganese and silicomanganese furnaces are tapped every 2 to 3 hours. Even for duplex practice, there is a substantial amount of slag (Tables 7.8 and 7.9), so especially in the case of larger furnaces there are often separate tap holes for slag and metal. In the case of tapping through the same tap hole, slag and metal have to be separated outside the furnace, either by a skimmer in the runner or by cascade tapping. Both methods utilize the difference in density of slag and metal.

By the use of a skimmer, the flow from the furnace is blocked in such a manner that slag and metal are forced in different directions. In cascade tapping, a ladle for metal and one or more slag pots are placed in series, so that the flow from the furnace cascades from one container to the next. Separation occurs as the metal stays in the ladle, whereas the slag passes on to the pots. At the end of the tap, some slag remains in the ladle. The remaining slag has to be removed (e.g., by tilting the ladle and dragging off the slag with a manual or mechanical rake).

The typical temperature of the slag when it leaves the furnace is 1400° to 1500°C for HC FeMn and 1550° to 1650°C for SiMn (~19% Si). The metal temperature is ~50°C lower in both cases. The liquidus temperature at which the metal starts to solidify is for all alloys in the range of 1200° to 1300°C. For HC FeMn, the temperature interval between tapping and solidification is limited to ~100°C, which is enough to avoid extensive buildups (“sculling”) on the ladle walls. However, for SiMn this value might exceed more than 300°C, which causes additional challenges. Casting at such high temperatures leads to slow solidification and creates more carbides precipitates. The solubility of carbon strongly depends on the temperature, and during cooling and solidification a considerable

number of carbides will precipitate and float toward the top of the melt. In this case, the final metal will be strongly segregated with carbide-forming elements. This phenomenon is the most troublesome at high silicon contents (>20%), because below this limit carbides will not form at these conditions.

7.6.4 Production of Manganese Metal

For manganese metal (see Table 7.5), carbon and iron contents are limited, so contrary to HC FeMn and SiMn production, carbon cannot be used here as a reductant. Manganese metal is thus produced by silicon reduction of high-MnO slag from which phosphorus has been removed. The silicon source is usually crude silicomanganese alloy, which differs from commercial SiMn mainly by limited iron content. The liquid Si-rich metal is mixed with liquid MnO slag with the addition of flux (CaO). The three-stage technology of metal manganese production is shown in Figure 7.17 (Gasik, 1992).

The first stage is very similar to the smelting of HC FeMn in large furnaces by a process like the one described above, and it includes production of HC FeMn (<0.70% P) and high-MnO slag (36% to 38% Mn, 20% SiO₂ and <0.012% P). The slag is tapped and split into two streams: one (liquid slag) is transferred and poured into a neighboring furnace for Mn production, and the second is solidified and then used for the smelting of crude SiMn alloy.

This solid slag is mixed with quartzite, coke, and dolomite flux to produce SiMn. Again, the chemistry of the process is similar to that used for the production of commercial SiMn, but here the attention is paid to iron, carbon, and phosphorus control. Due to this limitation, self-baking electrodes cannot be used and are substituted by graphitized electrodes; also, furnace lining is made of magnesite instead of carbon blocks (Gasik et al., 2009) (Fig. 7.18).

The charge for SiMn smelting consists of 800 kg of slag, 270 to 290 kg quartzite, and 340 to 360 kg of coke. During smelting, the yield is about 60% for Si and 83% to 85% for Mn. Target silicon content in the alloy is >25% Si, normally 27% to 29% Si. Slag formed in this stage has up to 10% to 11% MnO and is partially recycled in commercial SiMn and FeMn smelting.

The last stage includes mixing of liquid MnO slag, crude SiMn, and flux (CaO). Here, manganese oxide is reduced by silicon: MnO + Si + CaO → 2Mn + CaO·SiO₂ (formed SiO₂ is bound in the slag by lime to decrease its activity and to assist the reduction process). Lime addition also improves the thermal effect of manganese reduction.

The process is carried out in a tilting furnace (see Fig. 7.18), the same as used for SiMn smelting (5 to 7 MVA capacity). It includes the following steps: preparatory stage, loading of ~one third of the total SiMn amount on the bottom, pouring of liquid MnO slag, loading of lime, melting, loading of the remaining ~two thirds of SiMn, complete melting (and reaching the required temperature), and blowing of the melt by oxygen to remove extra

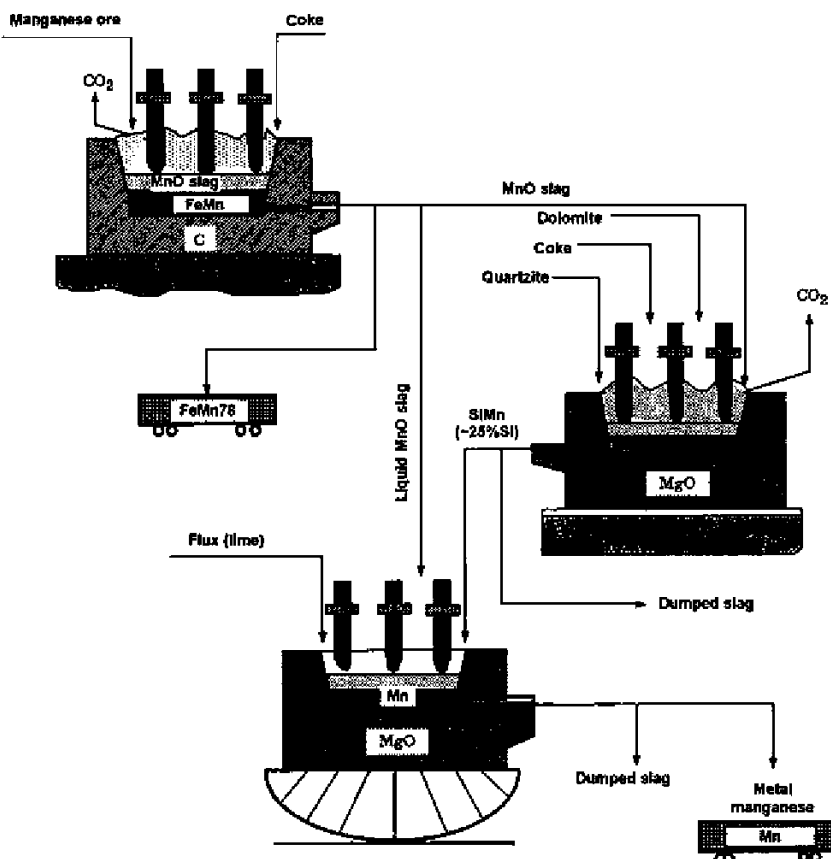


FIGURE 7.17 Three-stage technology of metal manganese: (1) production of dephosphorized MnO slag and HC FeMn, (2) smelting of crude SiMn, and (3) smelting of metal manganese from liquid slag and SiMn (*From Gasik, 1992.*)

silicon from the metal melt. The process time is about 3 to 3.5 h and it requires 2040 to 2090 kg of MnO slag, 640 to 660 kg of crude SiMn, 1600 to 1650 kg of lime, and 2550 to 2600 kWh of electricity per 1 ton of manganese (Gasik, 1992). These values indicate that the slag-to-metal ratio in this stage is high, 3.6 to 4 depending on the required Mn grade and the quality of the charge materials.

The resulting metal manganese has 96% to 97% Mn, <0.15% C, <1.2% to 1.4% Si, <2% Fe, <0.02% S, and <0.05% P. The slag from this stage has a rather high manganese content (11% to 14% MnO) and high basicity, which leads to excessive slag dusting upon cooling. This is due to phase transformation $\beta\text{-}2\text{Ca}\cdot\text{SiO}_2 \rightarrow \gamma\text{-}2\text{CaO}\cdot\text{SiO}_2$, giving +12% volume change. Different additions for slag stabilization have been suggested (Gasik et al., 2009).

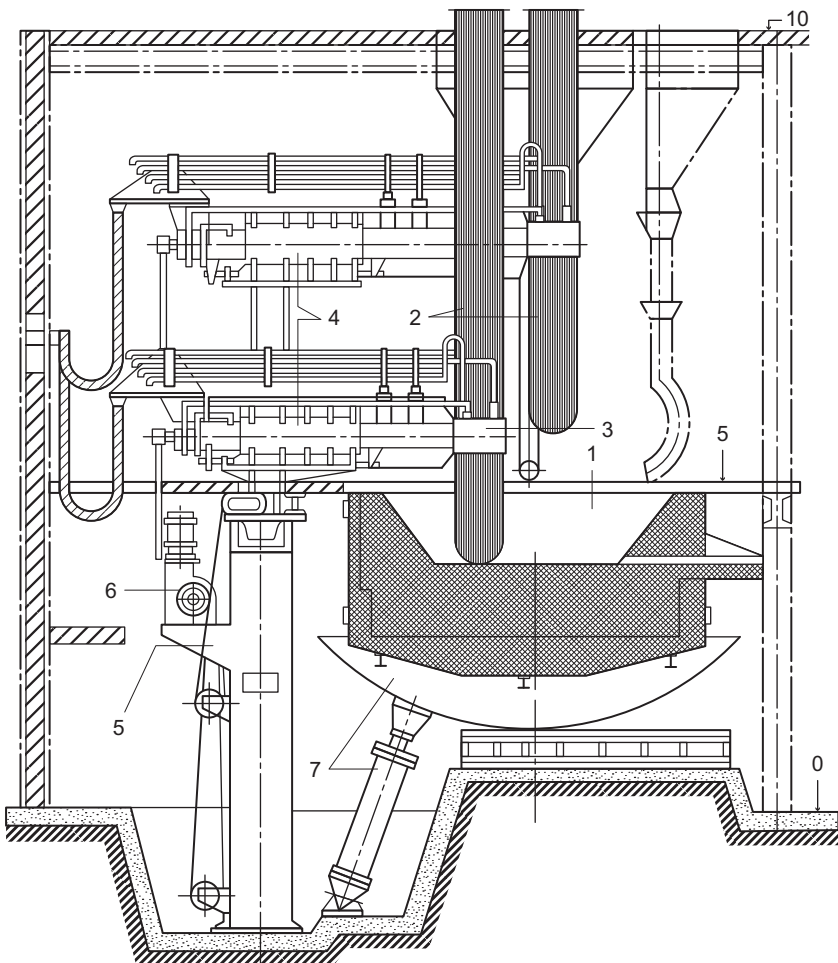


FIGURE 7.18 Furnace of 5 MVA capacity for the smelting of crude SiMn and metal manganese:
1, hearth; 2, electrodes; 3, short net contacts; 4, electrode holder sleeve; 5, telescopic stand;
6, lifting mechanism; 7, tilting mechanism.

In some cases, the desulfurization of metal manganese is being carried out. The usual sulfur content in manganese is only 0.01% to 0.02%, but for several applications this is too high. For example, the processing of iron-free vibration-damping alloy Mn-Cu-Ni (75% Mn) or magnetic shape memory (MSM) alloy Ni-Mn-Ga requires less than 0.001% to 0.005% S in manganese. For sulfur removal, molten manganese is treated by using a synthetic slag (40% CaO, 20% Al₂O₃, 28% CaF₂, and 12% Na₃AlF₆), which has a high potential for sulfur removal (Gasik, 1992).

7.7 REFINING OPERATIONS FOR LOW-CARBON MANGANESE FERROALLOYS

7.7.1 Production of Low-Carbon Ferromanganese

Low-carbon ferromanganese (LC FeMn) alloys are preferred, for example, for the production of low-carbon and other special grades of steel where close control of carbon is essential. Two principal methods of producing LC FeMn are in commercial operation. The first method includes the silicochemical reduction of manganese ore and MnO-rich slag, and its chemistry is very similar to that in the processing of metal manganese described previously. The second method involves blowing of the high carbon FeMn alloy with oxygen. This manganese oxygen refining process (MOR) has been in use in Norway and the United States since 1976. This process is in principle similar to the oxygen steelmaking processes.

7.7.1.1 Silicochemical Reduction

The first method utilizes SiMn as a reductant, and its composition determines the final carbon concentration in the alloy. It appears that SiMn with more than 22% Si at 1500°C is required to produce LC FeMn with a maximum of 0.8% C. Lime flux is added to increase basicity ($\text{CaO}/\text{SiO}_2 = 1.1$ to 1.3) and to decrease SiO_2 activity in the slag. The process might be realized in two versions. In the first version, the high-MnO slag with low phosphorus content is produced as for flux-less HC FeMn and metal manganese processes. Then slag (and possibly an manganese ores mixture) is reduced by a mixture of commercial and crude SiMn, for which usually some crashed SiMn undersieves are additionally used to decrease costs (Gasik, 1992). As the allowable iron content in LC FeMn is higher than in metallic manganese, this allows use of lower-grade SiMn and the manganese yield is normally higher than in the metal manganese three-stage process (see Fig. 7.17).

In the second version of the process, the SiMn is reduced outside of the furnace, in the ladles (Fig. 7.19), and two ladles with a counterflow of slag and SiMn are used to enhance the process. Two separate furnaces are used, one slag smelting furnace for preparing the oxide melt containing 55% MnO, and the other a conventional submerged arc furnace for producing the silicomanganese alloy.

Because the silicochemical reduction of slag is exothermic, the heat of the reaction is normally sufficient to cover the heat losses in the process. Any iron oxides in the manganese ore/sludge will also be reduced, consuming silicon. An iron-free slag with a high content of MnO will give the highest content of Mn in the final alloy. As Figure 7.19 shows, some ferrosilicon is added to the metal to raise the Si content to 30%. This high Si metal meets in ladle I slag from ladle II with 30% MnO. Equilibrium is established to give a waste slag with 5% MnO and a metal with 20% Si. The partly reacted SiMn alloy, now with 20% Si, is mixed in ladle II with the MnO-rich slag mixture received from the slag-

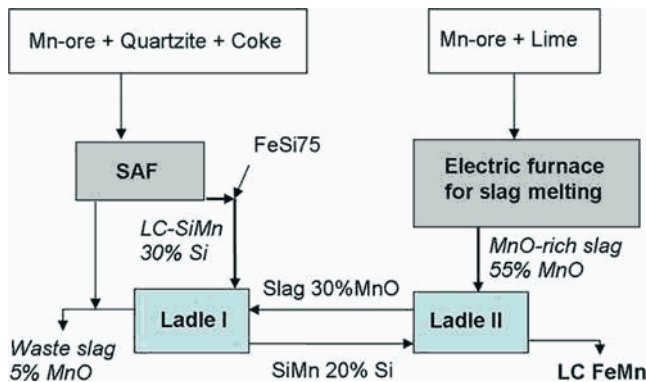


FIGURE 7.19 Flow sheet diagram for the silicothermic production of LC FeMn.

melting furnace. Assuming that the slag/metal equilibrium is established, resulting in the 30% MnO slag and the final alloy product, LC FeMn, with 1% Si and less than 0.5% C, will be obtained (Olsen et al., 2007).

Due to thermodynamic conditions, 25% to 30% MnO in the final slag is necessary to obtain a final metal with 0.5% C and less than 1% Si, which might be the upper limit according to alloy specifications (Olsen et al., 2007). Fluxing of the slag with MgO and Al₂O₃ was found to lower the residual MnO concentration of the slag provided that equilibrium was established. A moderate addition of MgO has a favorable effect on the silicon–manganese distribution, indicating that the presence of MgO increases the activity coefficient of MnO and decreases the activity coefficient of SiO₂. To increase the rate and yield of the silicothermic process, ladles with a stirring capability such as a shaking ladle can be used in an effort to improve the efficiency of the process.

7.7.1.2 Decarburization of High Carbon Ferromanganese

In this process, HC FeMn alloy (~7% C, <1% Si) is decarburized by blowing the metal in its liquid state with oxygen gas or with oxygen-argon mixtures. This manganese oxygen refining (MOR) process is in many ways similar to the basic oxygen steel process (BOF) where liquid cast iron is decarburized by blowing with oxygen in a converter. One important difference is the process temperature: due to the high affinity of manganese for carbon and oxygen, the necessary temperature of the manganese refining process has to be >1750°C, which is 200° to 250°C higher than is needed for the steel process. The much higher temperature leads to several challenges, such as refractory attack, casting of superheated metal, and slag-metal separation. Another problem encountered is the high vapor pressure of manganese leading to excessive evaporation and oxidation by excess oxygen. Oxidized manganese is collected mainly as Mn₃O₄ in the gas cleaning system. The oxide dust can be agglomerated and recycled to the FeMn furnace for recovery of Mn. Some of the

TABLE 7.10 Mechanisms of HC FeMn Decarburization by Oxygen Blowing (MOR)

Stage	1	2	3
Temperature °C	1350 → 1550	1550 → 1650	~1650
Temperature increase rate	High	Average	Low
Oxygen reacts with	Mn > C	C > Mn	Mn > C
Mn loss rate	High	Low	High
Limiting mechanism	Oxygen transfer	Oxygen transfer	C transfer to gas/liquid interface

oxidized manganese may dissolve in a slag phase and thus fluxing agents can be added to adjust the properties of the slag. Additional silicon reduction of MnO (e.g., with FeSi75) will be necessary to recover Mn at the end of the process. MOR process slag often contains about 65% MnO, and it can also be recycled to the FeMn furnace together with other collected manganese values such as ladle sculls, splash, and spills. The economy of the MOR process is highly dependent on the recovery of manganese in the refined alloy. The total yield of manganese is typically about 92% (fume, 5%; slag, splash, and sculls, ~3%).

The MOR method allows practical achievement of ~0.5% to 1% C in the alloy if the temperature reaches 1800°C and CO pressure reaches 1 atm. Oxygen dilution with argon should be considered if further decarburization is desirable. The decarburization of ferromanganese takes place by three different mechanisms in sequence, summarized in Table 7.10 (Olsen et al., 2007).

It is believed that manganese is lost by evaporative mechanisms. The manganese vapor is oxidized to MnO mist by oxygen that was not consumed for CO formation. As the process continues, the manganese loss decreases gradually and reaches a minimum at the end of the first stage of decarburization. During the second stage, the rate of manganese loss increases slowly. Finally, after transition to the third period of decarburization, the loss of manganese again increases quickly with time (Olsen et al., 2007).

7.7.2 Production of Low-Carbon Silicomanganese

For required SiMn alloys with less carbon than usually obtained from the standard process, the effect of decreasing carbon solubility while increasing silicon content is utilized. Instead of separate smelting, LC SiMn is made by adding FeSi to standard SiMn in the ladle. As the silicon content in the melt increases, the equilibrium shifts toward the formation of silicon carbide (SiC).

Due to the lower density of the carbide compared to the metal, the precipitated particles will float to the top of the melt, where they can be captured by a slag layer, which subsequently is removed from the ladle.

Although it is possible to add FeSi or other silicon sources into the furnace, this might lead to unstable furnace operations. On the other hand, the ladle method increases the expenditure of FeSi due to losses of SiC to the slag. Thus, the plant optimum might be a combination of these two methods.

7.8 MANGANESE FERROALLOYS POSTPROCESSING

7.8.1 Casting

Manganese ferroalloys can be poured from the casting ladle either over the lip or through a bottom gate. Top pouring allows higher rates but has no good control on the captured unwanted inclusions of slag and carbides. Bottom tapping is the opposite: the flow rate is low and can, with the more sophisticated variants of gates, be throttled and stopped. Slag and carbides remain in the ladle, as they, due to lower density, tend to float in the opposite direction of the downward metal stream. The drawback is a somewhat higher cost of the equipment and occasional difficulties with opening the gate, but lip pouring is always a possible option.

High-carbon FeMn and SiMn alloys usually undergo layer casting, where the liquid metal is filled into a casting bay for a number of subsequent taps. Metal fines are used as the bed material, and new layers are cast on top of the preceding casts. With a bay area adjusted to the tap size and provided that this is fairly constant, it is possible to obtain a quite even thickness of the layers with the requested size in one direction. When full, the casting bay is emptied by a wheel loader and prepared for a new series. The method is suitable even for large tonnages. The metal may require some cooling before the bay can be emptied and reused.

Refined qualities are usually cast and stored separately according to the analysis for each tap, and for this purpose casting in sand molds is suitable. This is a series of interconnected forms prepared in, for example, olivine sand. The liquid metal is filled from one end; optionally a skimmer between the first two forms can prevent slag and carbides from contaminating the rest of the set. Compared to layer casting, the thickness of the metal tends to increase and become more difficult to adjust even with careful preparations, and the cooling time is longer as the sand is a good insulator. Special attention should be given to superheated metal (e.g., MOR-treated FeMn with temperatures exceeding 1750°C). Removal of the large amount of surplus heat puts extraordinary demands on the casting equipment, and manganese fuming is considerable from the large surface of the cast.

When sufficiently cooled the metal blocks are removed from the molds by crane equipment or a wheel loader with forks. Notably, the timing of this

operation is often crucial, as too-hot metal “bleeds” and too “cold” metal breaks into pieces. If the available time between taps is insufficient for the molds to be emptied and prepared, casting is alternated between two sets of molds. The method is less suitable for large tonnages as it is rather space consuming and labor intensive (Olsen et al., 2007).

Other methods used to some extent involve chill cast and mold conveyors (3 to 10 m/min moving speed). These options require more sophisticated equipment and thus involve higher investment and operating costs. They are also more vulnerable and more often likely to be out of operation. However, they offer rather fast cooling and an even thickness of the metal, and the cast can be made thinner. Special cast iron molds are usually used, and the efficiency of this method is strongly affected by the lifetime of the molds.

7.8.2 Crushing and Sieving

For meeting the customer’s demands in respect of the sizing of ferroalloy lumps, respective crushing and sieving procedures are utilized. Usually jaw and cone crushers in combination and roller crushers are used. The latter can be used for materials that already have the right size in one direction. Besides eliminating the secondary crusher, a notable feature of the roller crusher is that it generates fewer fines (Olsen et al., 2007).

Unavoidably, any crushing process gives a fraction of undersized material, which to a limited extent is sold, possibly at a discount. For manganese alloys the size limit of fines is usually set to 10 mm, although some customers accept fines as small as 4 mm at a full price. The remaining fines can be used as bed material or coolant additions in the ladle, or they can be recycled as feedstock on the furnace.

Table 7.11 gives typical size distribution of various crushed alloys, showing that 22% to 30% of the crushed metal must be recycled, one way or another. It should be noted that these numbers include bed materials, which, especially on HC FeMn and SiMn, might account for as much as 5%, thus reducing the actual generated fines figures accordingly.

An alternative “net shape casting” technique was developed to eliminate the need to subsequently crush the metal, similar to the process of granulation (water atomization) of ferrosilicon. The control of the flow rate of metal that enters water and a sufficient water amount to be present as coolant agent are critical parameters to monitor. For example, Elkem ASA developed a similar method for granulation of SiMn (“Mansil”). The granules produced are dense discs with a diameter up to 30 mm and thickness up to 10 mm. This was found to be close to the optimum size when considering the rate of dissolution of the alloy in liquid steel. The mechanical strength of these granules is high due to the rapid solidification, and the macro-segregation tends to be lower than with traditional casting methods. Finally, the fraction of undersized material (-3 mm) with this method can be as low as 3%.

TABLE 7.11 Examples of Size Distribution of Crushed Alloys (Including Bed Materials)*

Fraction, mm	Alloy, % in Size		Utilization				
	Fraction	FeMn	SiMn	Charge	Ladle	Bed Material	Sale
0–1	8.5–9.5	9.8	All				
1–4	3.5–5.7	9.4	Some	Some	Most		
4–10	7.3–11	10.3		Some	Most	Some	
10–25	18–21.3	17.2					All
25–50	30.1–33.4	29.4					All
50–80	23.5–27.1	24.1					All

*Equipment: jaw crusher and cone crusher.

7.9 NITRIDED MANGANESE FERROALLOYS

Nitrided manganese and silicomanganese (see Table 7.5) with 2% to 8% N are used for different steel grades, especially austenitic stainless grades (20Cr-10Mn-4Ni, 18Cr-12Mn-5Ni, etc.), which have 0.5% to 0.8% N and additionally may contain Nb and V, which improve steel properties at subzero temperatures. Manganese here is used, together with nitrogen, as an efficient nickel substitute (Gasik, 1992).

As nitrogen solubility in liquid manganese is much lower than in solid (particularly γ -Mn), the production method is based on the solid-state reaction of manganese with nitrogen. Crushed in a nitrogen atmosphere, manganese (< 2 mm) is first put into trays and evacuated at 200°C and <150 Pa. Hydrogen contained in manganese is released, which makes higher active surface areas of the powder beneficial for the next reaction with nitrogen. Then the temperature is raised to 800°C and pure nitrogen gas is entered into the furnace. The reaction of nitrogen with manganese is exothermic, and the temperature in the manganese layer increases to 900° to 950°C with partial sintering of the grains. The product is cooled down in a nitrogen atmosphere and the whole process time is about 70 h (Gasik et al., 2009). Manganese yield is 97% to 98% in this process. Metal manganese from silicon reduction and from electrolysis might be used, resulting in different purity grades and manganese content. For 1 ton of MnN, the requirements are 1030 kg of metal manganese, ~150 m³ nitrogen, and 1180 kWh electricity (depending on the vacuum furnace type and parameters).

Nitrided SiMn (14% to 25% Si) is used for similar purposes. Nitrogen here is usually present as complex nitride Mn_{2.05}Si_{2.35}N_{3.6} and carbon as carbide

$(\text{Mn}, \text{Fe})_{23}\text{C}_6$. As nitrogen is added, silicon and manganese contents in SiMnN decrease slightly (see Table 7.5). Solid-state nitriding is a very efficient method for obtaining complex ferroalloys with nitrogen, especially of the Fe-Mn-Cr-V-Nb-N system. Nitrogen content may be up to 10% wt., and these ferroalloys have been proven in steelmaking to be a universal source of nitrogen for stainless steels and alloys.

7.10 ENERGY USE IN MANGANESE FERROALLOYS PROCESSING

As in all electrothermal ferroalloys processing, the costs of manganese ferroalloys are directly correlated with the specific energy consumption (kWh/ton of alloy) due to a higher tonnage but, of course, also related to the cost of electrical energy.

From the point of the reduction process, the largest energy demand would be imposed when MnO is the only manganese oxide in the raw materials, as the reduction reaction is highly endothermic. On the other hand, reduction reactions of the higher manganese oxides (MnO_x , where $x > 1$) with CO gas are all exothermic. For instance, about 20% energy reduction for this process might be achieved if the Mn_3O_4 sinter is fully replaced by MnO_2 ore.

The addition of carbonate ores leads to higher energy consumption, as might be expected. Carbonates are normally present as the added fluxes (CaCO_3 and MgCO_3) and to a lesser extent as MnCO_3 in some manganese ores. Decomposition of the carbonates is endothermic: if 100 kg of CaCO_3 is added per ton of alloy produced in order to increase the total content of basic oxides, the energy consumption will increase by ~70 kWh. In practice, however, CO_2 produced from this reaction may react with carbon in coke according to the Boudouard reaction $\text{CO}_2(\text{g}) + \text{C} \rightarrow 2\text{CO}(\text{g})$, and hence increase the specific energy consumption even more. The same effect is created by moisture present in raw materials: 10% of water in the charge would require an additional ~150 kWh to evaporate. Theoretically, the difference between high rates of the prereduction reactions, defined as 100% prereduced ore, will decrease electricity demand by about 400 kWh per ton of alloy compared to a very low prereduction rate. However, industrial practice shows a reduction of ~160 kWh/ton when the prereduction degree of the ore is between 20% to 60% (Ishak and Tangstad, 2007).

From the point of view of heat transfer in the process, higher temperature of the materials leaving the furnace would naturally require higher specific energy consumption. A rough estimation might be made as +50 kWh for an additional 100°C of tapped slag and metal temperature and +70–80 kWh for additional 200°C in off-gas temperature.

In silicomanganese smelting, more energy is required to reduce silicon, and the higher the % Si in SiMn, the higher the specific energy demands. For example, energy cost to produce 18% of silicon in the metal is about the same as the cost to produce 100% Mn. Hence, the cost of producing SiMn with 18% Si from oxides is about twice the cost of producing FeMn. Adding metal (cheap

TABLE 7.12 Example of the Energy Balance (off-gas temperature is taken as 150°C)

Input	kWh/ton	Output	kWh/ton
Electric energy	1992	Gas (sensible heat)	42
Carbon reductant	2708	Gas (chemical enthalpy)	776
		Metal (chemical enthalpy)	2897
		Metal (sensible heat)	363
		Slag (sensible heat)	181
		Slag (chemical enthalpy)	317
		Carbonates decomposition	122

silicon sources, remelts, etc.) to boost production is very efficient for decreasing specific energy numbers.

Other energy flow sinks are usually heat losses from the equipment (~20% of total) and cannot be significantly exploited. However, it is possible for the plant to control material losses: a 5% loss of metal in the slag will increase the apparent energy consumption by 5%. **Table 7.12** shows an example of the process energy balance for FeMn smelting.

Besides the chemical enthalpy of the metal, the next major form of energy that can potentially be recovered is chemical potential in the gas, especially CO and hydrogen. In closed furnaces this value may be quite high, and many producers sell the gas directly as a by-product. The most challenging issues for recovering this energy are the dust in the gas and the relatively low and varying temperature in the off-gas. In **Table 7.12**, the off-gas is assumed to be at 150°C (equivalent to ~42 kWh/ton of alloy). If the off-gas temperature is increased to 600°C, its potential energy content will increase to 213 kWh.

The latent heat of slag and metal is usually lost to the surroundings as the metal and slag are cooled and solidified. However, some plants heat water with this energy, which is exploited in adjacent fish farming and the heating of houses, streets, and facilities around the plant.

7.11 POTENTIAL HAZARDS OF OPERATIONS

Some elements of risk are always attached to high temperature smelting and reduction processes. They could be of a general nature, such as accidents caused by metal and slag penetration through furnace and ladle linings, and danger of CO gas poisoning, CO gas explosions, and hot metal-water explosions. The production of HC FeMn in closed furnaces involves special hazards

due to occasional eruptions, blowouts, and explosions taking place inside the furnace. Blows or eruptions of minor strength may have no dramatic effect, but more violent eruptions (sudden ejection of solid, liquid, or gaseous products from the furnace interior), on the other hand, may have dramatic effects and cause great damage. A more violent and instantaneous ejection of material, accompanied by rapid gas expansion, is considered to be an explosion. Although the occurrence of such incidents is rare, they have caused extensive damage to equipment and severe injuries.

Virtually all reported serious eruptions have been traced to a set of conditions that resulted in a hangup or bridging of the charge materials so that their normal downward movement was interrupted or retarded. As electric energy continues to be supplied to the furnace with little or no movement of the charge due to the bridging, a cavity forms under and around the electrode, particularly after tapping of the furnace. When conditions change, allowing the bridge to collapse (usually during or shortly after a tapping), large quantities of unreacted mix may enter the superheated cavity. The effect of the sudden contact between relatively cold raw materials and the hot liquid slag is an instantaneous dissociation of oxides, carbonates, and moisture, followed by explosive reactions evolving oxygen, CO, and hydrogen. These reactions can be extremely violent, and as they normally take place rather deep in the furnace charge, large amounts of hot materials may be thrown out of the furnace by the gaseous reaction products.

Industrial experience has shown that such dangerous situations may arise when the furnace condition prevents an even distribution of the escaping gases in the charge and an even regular downward movement of the raw materials in the furnace. Excessive moisture in the charge materials, particularly if present with excessive fines, will tend to intensify the densification of the charge, promote mix segregation, and inhibit uniform downward movement of the charge. Any leakage of water into the furnace has the same effect, so moisture control is a vital item to monitor closely.

Bridge formation and blocked raw material movement may also be a result of excessive amounts of alkalis (Na, K) and zinc in the charge materials. ZnO is reduced in the furnace hot zone and gaseous Zn is formed. Zn vapor condenses in the colder part of the charge mix normally as ZnO. Banks and bridges are formed, and the flow of materials becomes nonuniform. Occasionally, the area under the bridge may be overheated and the bridge collapses, bringing some of the unreacted raw materials directly into the superheated zone. A similar circulation of alkalis (i.e., K₂O) may take place with the same result. The agglomeration effect of Zn- and K-vapor has also been investigated by [Sli-zovskiy \(2012\)](#).

To minimize the causes for densification and bridge formation (minimizing the effect of a bridge collapse if it occurs), the chemical composition of the raw materials is of major importance, especially the content of higher oxides and carbonates in the charge. The type of ore influences largely the amount of gas

produced in a possible blowout. A highly oxidized ore has traditionally been considered to be an advantage in ferromanganese smelting, as the net exothermic process through dissociation of oxygen and the subsequent reaction with carbon monoxide will result in reduced consumption of electrical energy. However, at the same time, the risk of explosions and eruptions connected with the use of highly oxidized ores has been recognized. Apparently, a certain threshold value exists for the content of high-oxidized ore in the burden, under which such ore can be used without any hazard.

The choice of reductants is clearly also of high importance for the prevention of explosions in furnaces. The number of fines in the reductants is probably of even higher importance than the content of ore fines for gas permeability and thereby for the general furnace condition and specifically for the bridging mechanism in the charge. Coke fines normally carry much more moisture than do ore fines, and coke dust itself represents an explosion hazard through the possibility of ignition.

When ferromanganese is produced in open furnaces, the operator can estimate the risks of eruptions by visual observation of the charge condition and mix-flow from the hoppers. Through easy access to the charge surface, the operator may be able to direct corrective intervention, such as the breaking of crusts and the distribution of charge on the furnace surface. With the introduction of closed furnaces, the operator's visual contact with the furnace top has been removed, taking with it the possibility of direct corrective intervention. Also, the furnace units have gradually grown in size, thereby dramatically increasing the severity of blows and eruptions when such events take place.

ACKNOWLEDGMENTS

Much of the material in this chapter is taken from the book *Production of Manganese Ferroalloys*, by Olsen, S., Tangstad, M., and Lindstad, T. (2007), Trondheim: Tapir Forlag. The author acknowledges Tapir and SINTEF for giving permission to use these materials.

REFERENCES

- Bohlen, S.R., Essene, E.J., Hoffman, K.S., 1980. Update on feldspar and oxide thermometry in the Adirondack Mountains, New York. Geological Society of America Bulletin 91 (2), 110–113.
- Gasik, M.I., 1992. Manganese. Metallurgya, Moscow, 608 pp.
- Gasik, M.I., Lyakishev, N.P., Gasik, M.M., 2009. Physical chemistry and technology of ferroalloys [in Ukrainian]. Sistemnye Technologii, Dnipropetrovsk, 494 pp.
- Gavrilov, V.A., Gasik, M.I., 2001. Silicothermy of Manganese. System Technologies, Dniprope-trovsk, 512 pp.
- Ishak, R., Tangstad, M., 2007. Degree of pre-reduction without coke consumption in industrial furnaces. Proceedings of the Conference INFACON XI, New Delhi, India. 268–280.
- Kutsyn, V.S., Gasik, M.M., Gasik, M.I., 2012. Thermodynamic computer modeling of phase transformations in complex oxide systems, equivalent to manganese agglomerates made by existing and developed technologies. Metallurgical and Mining Industry 4 (3), 16–24.

- Kutsyn, V.S., Polyakov, O.I., Gasik, M.I., 2011. Electric and technology regimes of large-scale manganese ferroalloys smelting in high-power furnaces. *Ekonomika, Dnipropetrovsk*, 316 pp.
- Matricardi, L.R., Downing, J., 1995. Manganese and manganese alloys. In: Kirk-Othmer Encyclopedia of Chemical Technology, 4th Edition, volume 15. John Wiley, 963–990.
- Olsen, S., Tangstad, M., Lindstad, T., 2007. Production of Manganese Ferroalloys. Tapir Forlag, Trondheim, 248 pp.
- Petersen, E.U., Anovitz, L.M., Essene, E.J., 1984. Donpeacorite $(\text{Mn},\text{Mg})\text{MgSi}_2\text{O}_6$ – a new orthopyroxene and its proposed phase relations in the system $\text{MnSiO}_3\text{-MgSiO}_3\text{-FeSiO}_3$. *American Mineralogist* 69 (5–6), 472–480.
- Phase Equilibria Diagrams, 2001. Oxides. In: Roth, R.S. (Ed.), American Ceramic Society, vol. XIII, 468 pp.
- Samuratov, Ye., Baisanov, A., Tolymbekov, M., 2010. Complex processing of iron-manganese ore of Central Kazakhstan. Proceedings of the Conference INFACON-XII, Helsinki, 517–520.
- Slizovskiy, D., 2012. Agglomeration in ferromanganese submerged arc furnaces with focus on K and Zn deposition. Ph.D. Thesis, NTNU, Trondheim, Norway, 216 pp.
- Tang, K., Olsen, S.E., 2002. Manganese and silicon activities in liquid carbon-saturated Mn–Si–C alloys. *Steel Research* 73 (3), 77–82.
- Tangstad, M., Calvert, P., Brun, H., Lindseth, A.G., 2004. Use of Comilog ore in ferromanganese production. Proceedings of the Conference INFACON-X, Cape Town, pp. 213–222.
- Tangstad, M., Leroy, D., Ringdalen, E., 2010. Behaviour of agglomerates in ferromanganese production. Proceedings of the Conference INFACON-XII, Helsinki, Finland, pp. 457–465.
- Woermann, E., Muan, A., 1970. Derivation of approximate activity-composition relations in $\text{MgO}\text{-MnO}$ solid solutions. *Materials Research Bulletin* 5 (10), 779–788.

Technology of Chromium and Its Ferroalloys

Mihail I. Gasik

National Metallurgical Academy of Ukraine, Dnipropetrovsk, Ukraine

Chapter Outline

8.1 Properties of Chromium	268	8.3.4 Technology of Ultra-Low-Carbon FeCr	303
8.1.1 Phase Equilibria with Major Chromium-Containing Systems	268	8.3.5 Technology of Nitrided Ferrochromium (FeCrN)	305
8.1.2 Phase Equilibria with Chromium Oxide	276	8.4 Production of Metallic Chromium and Its Alloys by Aluminum Reduction	307
8.2 Chromium Raw Materials and Their Processing	280	8.5 Environmental Issues of Chromium and Its Ferroalloys Processing	312
8.2.1 Chromium Minerals Overview	280	8.5.1 Human Health Hazards of Chromium and Its Compounds	312
8.2.2 Chromium Resources Overview	283	8.5.2 Dust and Wastewaters Treatment from Chromium Ferroalloys Processing	313
8.2.3 Chromium Ores and Chromites Processing	285	8.5.3 Fire and Explosion Hazards of Chromium Ferroalloys	314
8.3 Chromium Ferroalloys Technology	289	References	314
8.3.1 Technology of Low-Carbon Ferrochrome	289		
8.3.2 Technology of Medium-Carbon Ferrochrome	297		
8.3.3 Technology of Ferrosilicochrome (FeSiCr)	299		

8.1 PROPERTIES OF CHROMIUM

Chromium is element no. 24 of the IVb subgroup of the periodic table, along with its analogs molybdenum and tungsten. It has atomic mass 51.996 and an external electron configuration of $3d^54s^1$, leading to stable valences of +2, +3, and +6. Chromium's density is 7.19 g/cm³, its melting temperature is 1870°C, and its boiling point is about 2469°C. Chromium has BCC lattice, which is stable throughout the range of solid chromium stability (i.e., it does not have stable phase transformations in the solid state).

Chromium is one of the most versatile and widely used alloying elements in many steels and alloys. It imparts corrosion and oxidation resistance, is a mild hardenability agent, improves wear resistance, and promotes the retention of useful strength levels at elevated temperatures. Chromium is the basis of all stainless steels (about 70% of all chromium used in steelmaking belongs to stainless steels). It is also an important part of low-alloyed constructional alloy steels (1% to 3% Cr) and ball-bearing steels. Chromium is also used in various tool steels, superalloys, and other specialty metals. Besides chromium's ability to form protective oxide (Cr_2O_3), which is the main reason for its use in stainless steels, it forms hard carbides, which are employed in wear-resistance applications.

8.1.1 Phase Equilibria with Major Chromium-Containing Systems

Carbon and chromium form several carbides, which have been a subject of many investigations. The commonly observed carbides in the Cr-C system are $Cr_{23}C_6$ (5.68 wt. % C; sometimes also referred as Cr_4C), Cr_7C_3 (9% C), and Cr_3C_2 (13.3% C). The types of crystalline lattices and their parameters for chromium carbides have been determined as complex BCC for $Cr_{23}C_6$ ($a = 1.066$ nm), hexagonal for Cr_7C_3 ($a = 1.401$, $c = 0.425$ nm), and orthorhombic for Cr_3C_2 ($a = 1.147$, $b = 0.5545$, $c = 0.283$ nm) (Bolgar et al., 1973). Chromium carbides have more complex crystalline structures than the carbides of Ti, Zr, V, or Nb. Additionally, metastable chromium carbide has been identified to form in binary Cr-C alloys at rapid solidification or quenching (Inoue and Matsumoto, 1979). This Cr_3C carbide has a structure similar to that for metastable iron carbide (cementite Fe_3C) with lattice parameters $a = 0.458$ nm, $b = 0.512$ nm, and $c = 0.680$ nm. The Cr-C phase equilibria diagram is shown in Figure 8.1. The solubility of carbon in solid chromium is low (Lyakishev and Gasik, 1998; Zemskij and Fokin, 1967).

With oxygen, chromium forms a wide range of oxide phases with different molar ratios Me:O from 3:1 to 1:3, which is typical for its analogs (Mo and W). These oxides have different thermal stability. High-oxygen compounds (Me:O < 2:3, such as CrO_3 , Cr_8O_{21} , Cr_5O_{12} , and CrO_2) dissociate almost completely already at relatively low temperatures and thus are not relevant to

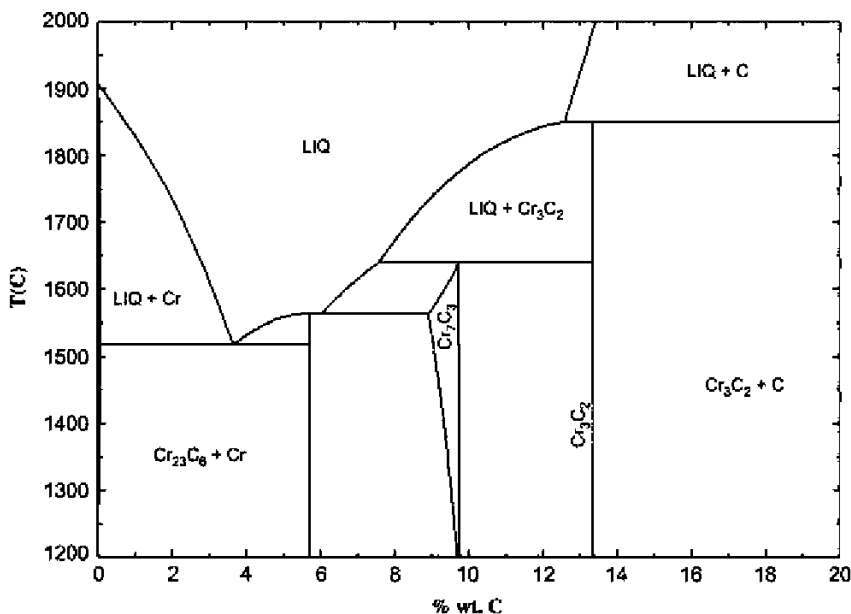


FIGURE 8.1 The carbon–chromium phase equilibria diagram.

ferrochromium processing, although they may form during cooling of Cr-containing gases and fumes or the oxidation of chromium-rich alloys. These intermediate oxides are sometimes considered to be chemical compounds of chromium chromate and polychromates. For example, Cr_5O_{12} might be presented as $\text{Cr}_2(\text{CrO}_4)_3$, $\text{Cr}_6(\text{Cr}_{10}\text{O}_{30})$, and $\text{Cr}_4(\text{Cr}_7\text{O}_{27})$ (Lyakishev and Gasik, 1998; Rode, 1962).

The stability of oxides increases with an increasing Me:O ratio with trivalent chromium oxide Cr_2O_3 being the most stable. Oxides Cr_3O_4 (tetragonal lattice of rutile-type with $a = 0.4421$ and $c = 0.2916$ nm) and CrO (cubic lattice with $a = 0.412$ nm) are stable at high temperatures only. Upon cooling they usually decompose to Cr and Cr_2O_3 . Oxide Cr_3O_4 might be also considered as a chromium chromite, CrCr_2O_4 or $\text{CrO} \cdot \text{Cr}_2\text{O}_3$. The practically relevant oxide Cr_2O_3 has the structure of corundum $\alpha\text{-Al}_2\text{O}_3$ type, but was also found to have a tetragonal lattice when it exists in the form of mineral eskolaite (Lyakishev and Gasik, 1998).

Oxygen solubility in solid chromium is low (~0.013 wt. % O at 1500°C), and oxygen lowers chromium's melting point. A version of the phase diagram of the Cr-O system is shown in Figure 8.2.

The oxide liquid phase may form over 1663°C in equilibrium with either chromium or chromium oxides. Over 1875°C two liquids (metal-rich and oxide-rich “ CrO ”) might co-exist in a wide range of oxygen compositions. Note that the explicit appearance of “ CrO ” at the phase diagram depends on

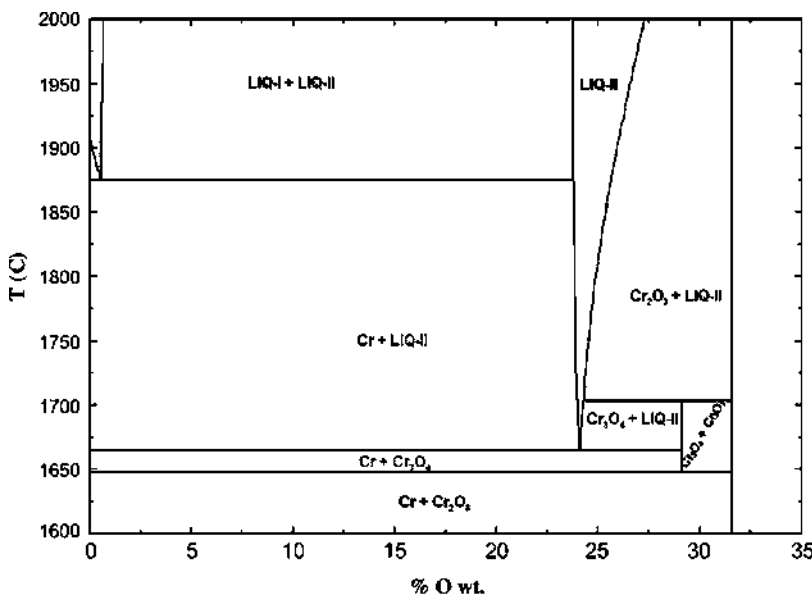


FIGURE 8.2 The phase diagram of the Cr-O system.

the selection of the gas phase, especially oxygen potential (Fig. 8.3). For theory as well as the practice of producing alloys of the Cr-Fe system (FeCr and chromium-rich steels), the thermodynamic properties of chromium monoxide (CrO) are also of interest. This oxide is usually stabilized in the presence of silica (acidic slags), where the ratio $\text{Cr}^{3+}/\text{Cr}^{2+}$ is decreasing (Gasik et al., 1970; Lyakishev and Gasik, 1998). This might be shown in the Cr-O phase dominance diagram as function of temperature for the Cr-O system (see Fig. 8.3). Here chromium oxides are supposed to be pure phases and the theoretical stability area of the CrO in this binary system appears to be in this case over 1710°C and in the limited range of equilibrium oxygen potentials.

For chromium reduction from oxides, thermodynamics of the Cr-O-C equilibria is of high importance. Let's consider the isothermal sections of this phase dominance diagram for different temperatures (Fig. 8.4). Here cross marks (+) indicate the isobar line—the total pressure in the system, which was fixed to be 1 atm. If these cross marks exist anywhere in the phase stability field, this means there is a thermodynamic possibility of obtaining this phase in the system.

Table 8.1 shows numerical data of these equilibria. Here the equilibrium type means only these phase areas, which are being crossed by the isobar line (Fig. 8.4 shows the coordinates of the crossing points as logarithms of partial pressures of CO and CO_2). The respective triple points (if they exist) are

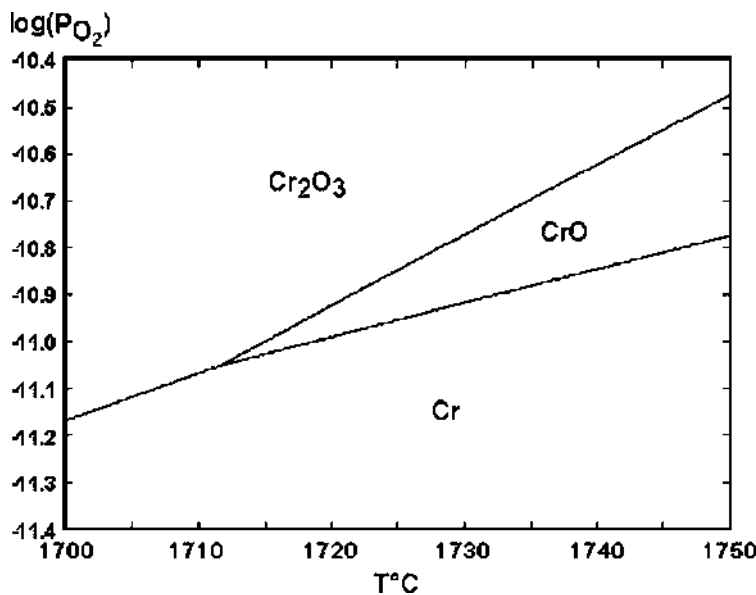


FIGURE 8.3 Triple point in the Cr-O system at high temperatures (calculated with HSC Chemistry ver. 7.1).

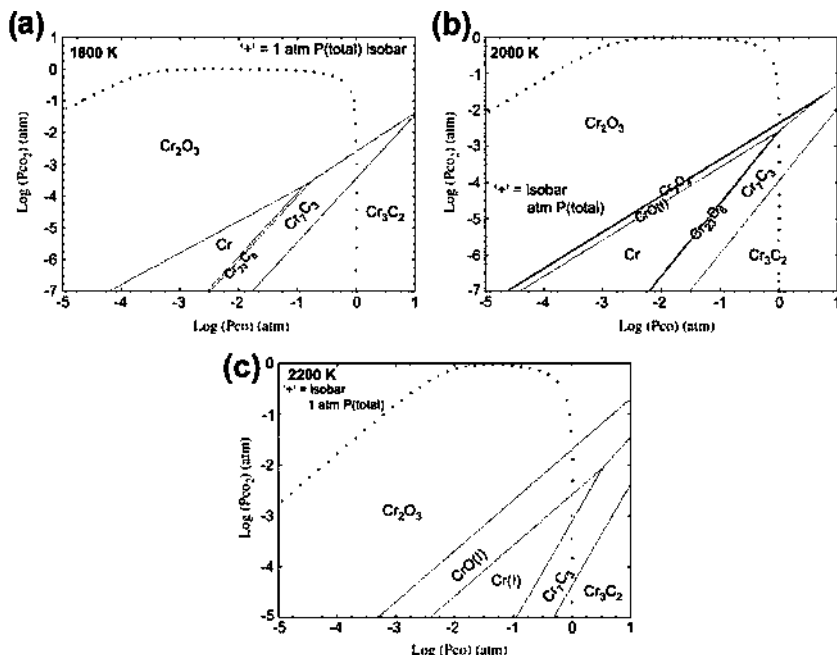


FIGURE 8.4 Phase stability diagram for the Cr-C-O system at 1800 (a), 2000 (b), and 2200 K (c).

TABLE 8.1 Types of Equilibria in the Cr-O-C Systems at Different Temperatures

T, K	Equilibrium Type	$\log P_{CO}$	$\log P_{CO_2}$	Invariant point	$\log P^*_{CO}$	$\log P^*_{CO_2}$
1800	$Cr_3C_2-Cr_7C_3$	-0.000926	-3.44615	$Cr-Cr_7C_3-Cr_2O_3$	-1.18413	-4.04745
	$Cr_7C_3-Cr_2O_3$	-0.000926	-2.59538			
2000	$Cr_3C_2-Cr_7C_3$	-0.000694	-3.95231	$Cr-Cr_7C_3-Cr_3O_4$	-0.11428	-2.68805
	$Cr_7C_3-Cr_3O_4$	-0.000694	-2.54154	$Cr_2O_3-Cr_7C_3-Cr_3O_4$	0.80694	-1.53731
	$Cr_3O_4-Cr_2O_3$	-0.000694	-2.34410			
2200	$Cr_3C_2-Cr_7C_3$	-0.031746	-4.37345	$Cr-Cr_7C_3-Cr_3O_4$	0.74921	-1.5993
	Cr_7C_3-Cr	-0.031746	-3.11248			
	Cr_3O_4-Cr	-0.031746	-2.35589			
	$Cr_3O_4-Cr_2O_3$	-0.031746	-1.75923			

summarized with their coordinates. Note that triple points might not be located at the isobar line, and this means they will not be accessible at these temperatures at ambient total pressure.

The conclusions one could make on the basis of these diagrams are as follows. First, at 1800 K it is not possible to get metallic chromium in the Cr-C-O system but only oxide Cr_2O_3 (at high CO_2 fractions) or carbides Cr_23C_6 and Cr_3C_2 (at high CO fractions) if the total system pressure of 1 bar (atm) is maintained. According to the data in Figure 8.3, an increase of temperature to 2000 K leads to the appearance and extension of the Cr_3O_4 and CrO areas. At the even high temperature of 2200 K, CrO seems to not be stable anymore, as metallic chromium is now possible (yet within a very limited range of pressure of CO_2). Therefore, even though chromium might be reduced by carbon at high temperatures and normal pressure, it is unlikely to be practically feasible for pure metal production due to difficulties in local control of the gas atmosphere. Furthermore, these diagrams do not explicitly show that in these conditions a significant part of the chromium compound is present in the gas phase. Thermodynamics of the Cr-C-O equilibria justifies that the most practical method of chromium reduction by carbon might be realized by decreasing chromium activity in the melt with the addition of iron or silicon.

The system Cr-Si has been studied for many years and several compounds have been reported: Cr_2Si , Cr_3Si_2 , $CrSi$, Cr_2Si_3 , $CrSi_2$, and Cr_2Si_7 . Later, not all of them were confirmed and reliable data exist for Cr_3Si , Cr_5Si_3 , $CrSi_2$, and to some extent $CrSi$. Depending on the thermodynamic data used, different versions of the Cr-Si phase diagram have been published. One of the versions as calculated by the authors is shown in Figure 8.5. The solubility of chromium in solid silicon is very low (possibly <0.06 ppm below 1300°C),

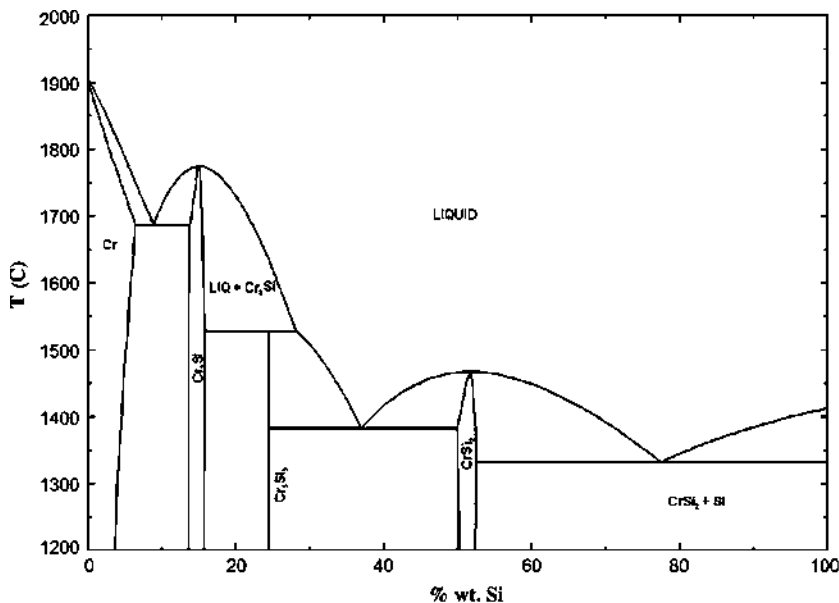


FIGURE 8.5 Phase diagram of the Cr-Si system.

but solubility of silicon in solid chromium is of an order of 1.36% wt. at 1650°C.

In the ternary system, Cr-Si-C besides carbides and silicides (including SiC), a ternary nonstoichiometric compound (known as the Nowotny phase), Cr₅Si₃C_x, is also formed. The crystalline lattice of the Cr₅Si₃C_x is more defective and includes fairly large voids. Saturation of Cr₅Si₃ with carbon results in the formation and stabilization of the hexagonal Cr_{5-x}Si_{3-y}C_{x+y}. Saturation of binary Cr-Si alloys with carbon gives not only Cr₅Si₃C_x but also carbides Cr₇C₃ and Cr₃C₂. Only the silicides CrSi and CrSi₂ do not change their structure after carburization. In carbon-saturated alloys at a constant temperature, the carbon solubility is a linear function of silicon content. The formation of SiC occurs when a melt is oversaturated with carbon on the liquidus surface. Having lower density, SiC is precipitated at cooling and segregates up to the surface of the melt.

In the presence of iron, these phases have been reported as (Cr, Fe)₁₄Si₄C₃ (15% to 18% wt. Fe) and (Cr, Fe)₅Si₃C₆ (23% to 30% wt. Fe) (Kosyrev and Olsen, 1995). These phases appear in equilibria in the carbon-saturated Cr-Fe-Si melts (Fig. 8.6) and play an important role in all chromium ferroalloys processing where reduction by carbon and silicon is involved.

In the chromium-nitrogen system, two stable nitrides are known: Cr₂N (β -phase, HCP lattice type with $a = 0.4582(\pm 3)$, $c = 0.4460(\pm 20)$ nm) and CrN (γ -phase, cubic structure with $a = 0.415$ nm) (Fig. 8.7). The nitride Cr₂N has

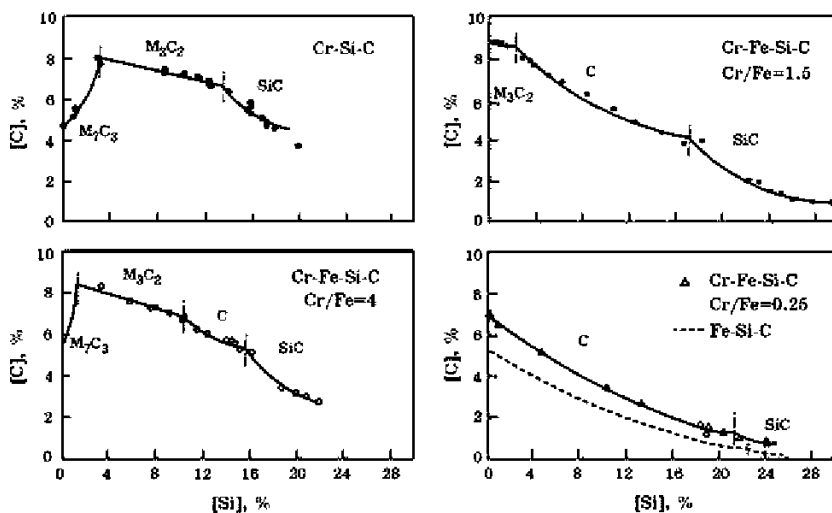


FIGURE 8.6 Phase equilibria and solubility of carbon and silicon at 1600°C in the Cr-Fe-Si-C system (Gasik et al., 2009).

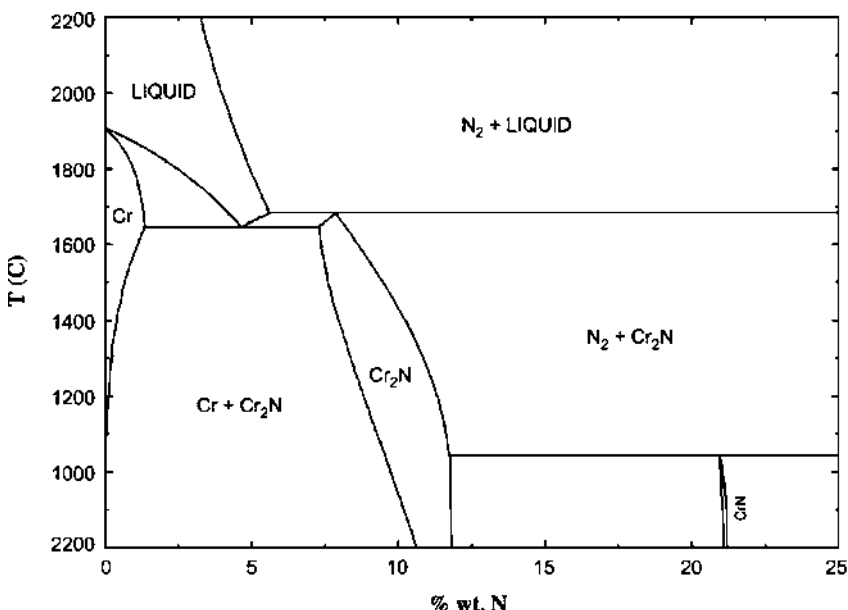


FIGURE 8.7 Phase diagram of the Cr-N system at 1 atm pressure of nitrogen.

a homogeneity region in the range 11.3 to 11.9 wt. % N. Nitride CrN is nearly stoichiometric with a high enthalpy of formation, which makes its thermal stability compatible with nitrides like TaN. Nitrogen dissolves in solid chromium in small amounts. The equilibrium nitrogen content in liquid chromium is higher than in solid chromium, but it decreases with temperature due to the exothermal nature of the reaction of interaction of molecular nitrogen with chromium melt. The dissolution of nitrogen in chromium significantly lowers its melting point (eutectics ~1650°C; see Fig. 8.7).

During the reaction of nitrogen with metallic chromium at 960° to 1200°C and $P_{N_2} = 1$ to 2 MPa, it is also possible to form a nonstoichiometric nitride Cr_2N_x ($x < 1$) (Lyakishev and Gasik, 1998). Such specimens with 8 to 11 wt. % N usually have a multiphase structure with a solid solution of nitrogen in Cr, Cr_2N , CrN, and Cr_2N_x . The latter phase does not form at nitrogen concentrations >11% wt. The Cr_2N_x phase is assumed to be the product of the disproportion of Cr_2N with the formation of a nitrogen-lean solid solution based on the Cr_2N lattice.

With phosphorus chromium forms several phosphides (Cr_3P , Cr_2P , CrP , CrP_2), which are stronger than similar phosphides of iron. The solubility of phosphorus in solid chromium is low, and phosphorus removal from the chromium-rich melts by oxidation is not efficient.

Sulfur forms stable chromium sulfides CrS , Cr_3S_4 , and Cr_2S_3 , as well as two metastable sulfides, Cr_7S_8 and Cr_3S_6 .

For the equilibrium of chromium with other metals, iron and aluminum are the most important cases. The Fe-Cr system is one of the basics for ferrochromium and chromium steel production, and it forms a basis for the whole study of chromium metallurgy (Lyakishev and Gasik, 1998; Mills and Grieveson, 1976; Witusevich et al., 1987). The Fe-Cr phase equilibrium diagram is shown in Figure 8.8.

The maximum solubility of chromium in the iron-rich γ -FCC phase is observed at ~980°C at 11.4 wt % Cr. When chromium exceeds ~13.5 wt. % Cr, only the α -BCC phase is stable (see Fig. 8.8). The positions of the phase boundaries are affected considerably by the impurities present, such as nitrogen and carbon.

The BCC solid solutions of the Fe-Cr system near equimolar composition tend to form the σ -phase. It exhibits a tetragonal crystalline lattice ($a = 0.8800$, $c = 0.4544$ nm) at a nominal content of 46.5 at. % Cr. This phase is usually considered to be undesirable in the Cr-rich steels and alloys as it causes excessive brittleness. The σ -phase exists in equilibrium with three types of BCC solutions: α -phase (ferrite) at apex, α' (iron-based ferrite), and α'' (chromium-based ferrite). They all have the same BCC structure but different composition and lattice parameters. The experimental validation of such transformations is always challenging, as it requires a long equilibration time—for example, equilibration times of even 11 years at 500°C have been reported (Zubkov et al., 1990).

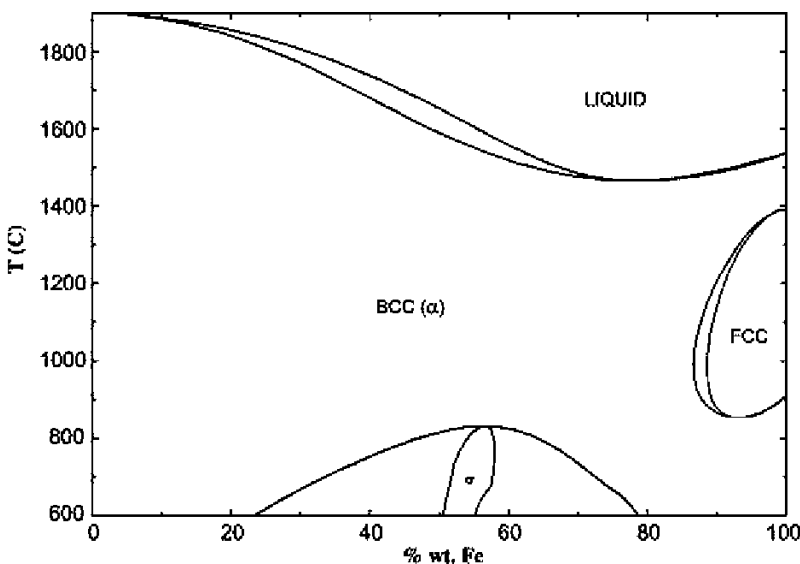


FIGURE 8.8 Phase diagram of the Cr-Fe system.

The chromium-aluminum equilibrium is important for processing metallic chromium by reduction of the oxide with aluminum. This system has several intermetallic compounds (Fig 8.9). Some of these phases described by exact stoichiometric ratios could be represented by other ratios of chromium and aluminum atoms. The solubility of Al in BCC chromium is rather broad, but solubility of chromium in FCC aluminum is limited to ~0.5 wt.% Cr at a peritectic equilibrium of 651°C.

8.1.2 Phase Equilibria with Chromium Oxide

In the $\text{Cr}_2\text{O}_3\text{-Al}_2\text{O}_3$ system, chromium oxide does not form intermediate phases with alumina, given that a region of continuous solid solutions exists below the solidus line, at least above 1500 K. At lower temperatures, the solid solution tends to decompose into two isomorphic chromia-rich and alumina-rich solutions. The region of coexistence of these two solutions is about from 15% to 25% to 50 to 70 mol. % Cr_2O_3 , but the exact phase boundary positions remain the subject of discussion.

Reliable data on the phase equilibria in the chromia-silica system and the presence of metallic chromium in contact with the silicate melts are important for optimizing the slag modes of reducing processes in the production of chromium ferroalloys. These data are of a great theoretical and practical interest for the production of chromium-containing steels and oxidative decarburization of high-carbon ferrochromium in converters. Under the

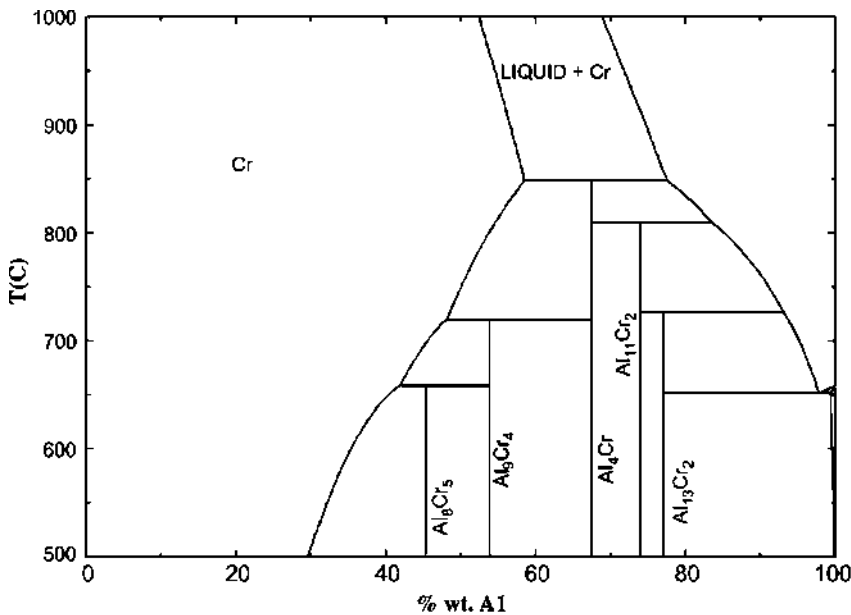


FIGURE 8.9 Phase diagram of the Cr-Al system.

conditions of a high oxidative potential of the gaseous phase and the absence of a metallic chromium-containing melt, silica does not react with Cr_2O_3 .

In reducing conditions (a low oxidative potential of the gaseous phase and the presence of metallic chromium), the interaction of silica with chromium oxide (Cr_2O_3) is accompanied by the reduction $\text{Cr}^{3+} \rightarrow \text{Cr}^{2+}$, followed by the formation of, a silicate melt “ CrO ”- SiO_2 . Here a hypothetical phase diagram (Fig. 8.10) shows where “ CrO ” oxide is used instead of Cr_2O_3 . As shown for the Cr-O system, in purely acidic (silica-rich) environments, the ratio $\text{Cr}^{3+}/\text{Cr}^{2+}$ is substantially decreased, leading the Cr^{2+} form to be in equilibrium with silica-rich melts. As CrO is not an independent stable phase at normal conditions, it is described by the $\text{Cr}_2\text{O}_3 + \text{Cr}$ composition in silica-lean areas. Figure 8.10 also shows the region of existence of chromium silicate Cr_2SiO_4 . Although approximate, it explains some of the technological methods employed in the production of chromium ferroalloys and steels.

The opposite of silica, calcia as a basic oxide shifts equilibria toward higher chromium valences in the presence of oxygen. CaO forms calcium chromite (CaCr_2O_4) with Cr_2O_3 at high temperatures in the chromium-rich area (Fig. 8.11). This chromite is not stable at lower temperatures and its composition also has been reported as $(\text{Ca}_2\text{Cr}_3)\text{Cr}_{10}\text{O}_{20}$ —that is, as mixed calcium-chromium chromite (Dechterov and Pelton, 1997). Upon the increase of CaO content, the ratio $\text{Cr}^{6+}/\text{Cr}^{3+}$ gets higher and calcium chromate CaCrO_4 is formed. Further, two more complex compounds (calcium chromite-chromates)

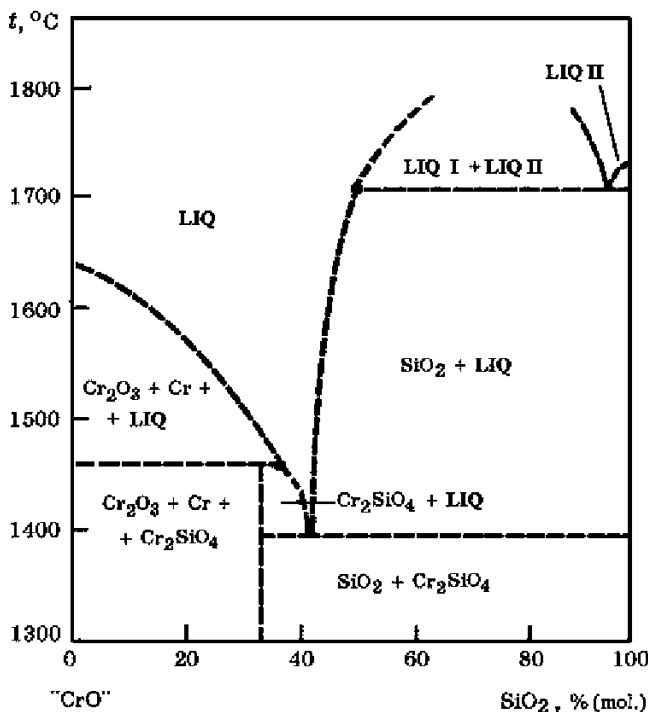


FIGURE 8.10 The “CrO”- SiO_2 phase diagram.

of composition $9\text{CaO} \cdot 4\text{CrO}_3 \cdot \text{Cr}_2\text{O}_3$ and $3\text{CaO} \cdot 2\text{CrO}_3 \cdot \text{Cr}_2\text{O}_3$ have been identified. It was also suggested that this diagram should be treated as a part of the ternary equilibrium $\text{CaO-Cr}_2\text{O}_3-\text{CrO}_3$ (Kaiser et al., 1992; Lyakishev and Gasik, 1998). For example, Kaiser et al., (1992) identified compositions $\text{Ca}_5(\text{CrO}_4)_3\text{O}$ to be stable in air between 776° and 959°C , $\text{Ca}_3(\text{CrO}_4)_2$ between 882° and 1253°C , and $\text{Ca}_5(\text{CrO}_4)_3$ between 1140°C and 1297°C , but unstable in reducing conditions.

The substantial decrease of the liquidus temperature ($<1775^\circ\text{C}$) in a range of compositions (30% to 60% Cr_2O_3) is utilized for calcia-chromia melts processing during low-carbon FeCr production by mixing FeSiCr and $\text{CaO-Cr}_2\text{O}_3$ melts.

Besides equilibria of chromia with CaO and SiO_2 , the system $\text{Cr}_2\text{O}_3-\text{MgO}$ is one of the most important systems in the production of ferroalloys and steels. In this system only one compound (magnesium spinel MgCr_2O_4) is formed, but MgO has a wide solubility range, decreasing with lower temperatures (Fig. 8.12). Magnesium chromite was also reported to have some homogeneity range.

The binary systems with Cr_2O_3 discussed previously do not explicitly appear as such in ferroalloys processes but they form a basis for ternary and

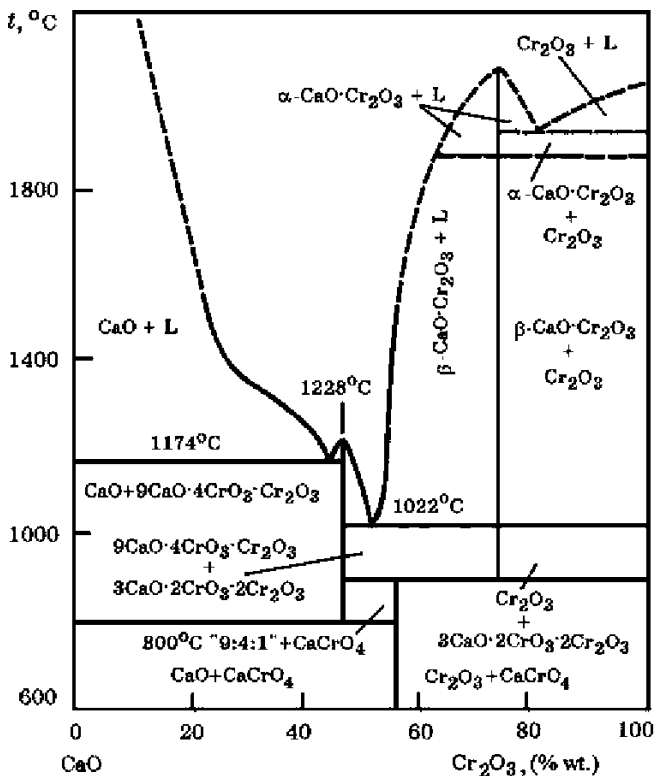


FIGURE 8.11 The CaO-Cr₂O₃ phase diagram.

more complex combinations. The most important ones are briefly presented in this chapter.

In the ternary system Cr₂O₃-Al₂O₃-SiO₂, a large region of corundum solid solutions and also a narrow long field of mullite (3Al₂O₃·2SiO₂) have been reported (Lyakishev and Gasik, 1998). The triple eutectic liquid composition has 6% wt. Al₂O₃ and 1% wt. Cr₂O₃. Eventually no ternary compounds appear in equilibrium here. Due to the mutual solubility of alumina and chromia (corundum phase), alumina possibly does not affect the Cr²⁺/Cr³⁺ ratio as much as silica does.

On the contrary, in the ternary system Cr₂O₃-CaO-SiO₂, there is a ternary compound 3CaO·Cr₂O₃·3SiO₂, which corresponds to the natural mineral uvarovite (Ca₃Cr₂Si₃O₁₂), which belongs to the garnet group. If chromium is present in the 3+ oxidized state (oxygen potential in the gas phase is sufficiently high), the liquid phase has a miscibility gap into two liquids: nearly pure silica and silica-rich melt with 27% wt. CaO and ~1% wt. Cr₂O₃.

However, as was noted for binary systems, the level of oxygen potential, the presence of metallic chromium, and slag basicity (CaO/SiO₂ ratio) have

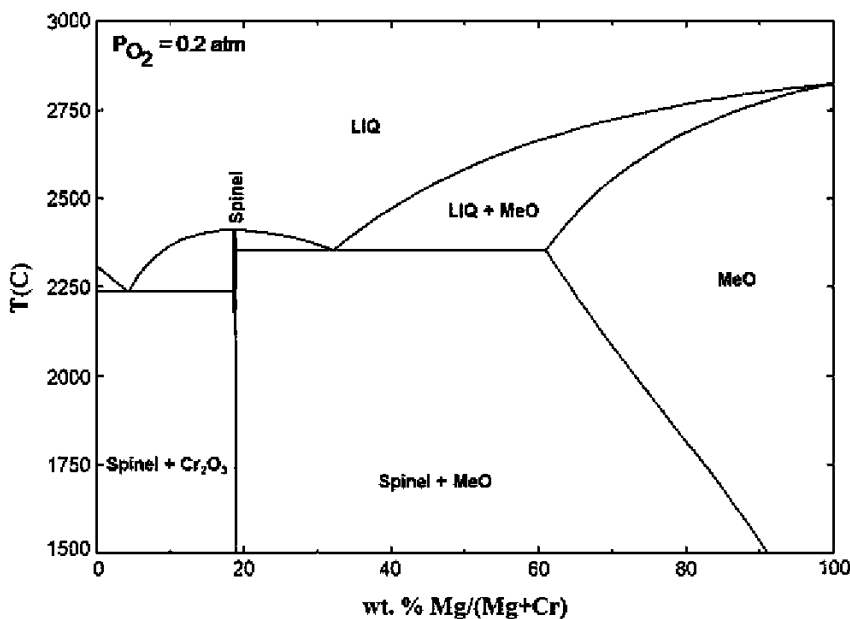


FIGURE 8.12 The $\text{MgO-Cr}_2\text{O}_3$ phase diagram at $P_{\text{O}_2} = 0.2 \text{ atm}$.

a strong effect on the chromium oxidation state, which might change from +2 (“ CrO ”) to +6 (CrO_3). Experimental studies (Villiers and Muan, 1992; Xiao and Holappa, 1993) have confirmed that for realistic conditions, more correct liquidus and solids equilibria could be achieved if this system is considered as a quaternary one: $\text{CaO-CrO-Cr}_2\text{O}_3-\text{SiO}_2$.

For the system $\text{Cr}_2\text{O}_3\text{-MgO-SiO}_2$, no ternary compounds have been reported, but a large miscibility gap was found. The major phases in this system are essentially chromia, MgO , and MgCr_2O_4 adjacent to the binary $\text{Cr}_2\text{O}_3\text{-SiO}_2$.

The substitution of different oxides has various effects on chromia activity (Xiao and Holappa, 1993). As might be expected, the substitution of CaO in slags by MgO lowers the activity of chromium oxides but does not significantly affect the $\text{Cr}^{2+}/\text{Cr}^{3+}$ ratio. Minor additions of alumina increase the activity of chromium oxides, whereas higher amounts do not produce such effect. This shows that slags of ferrochromium processing might have rather different behavior if their composition varies during the process.

8.2 CHROMIUM RAW MATERIALS AND THEIR PROCESSING

8.2.1 Chromium Minerals Overview

Knowledge of the chromium ore minerals proper and their associated rocks-forming minerals is needed to explore new chromite fields and to predict the

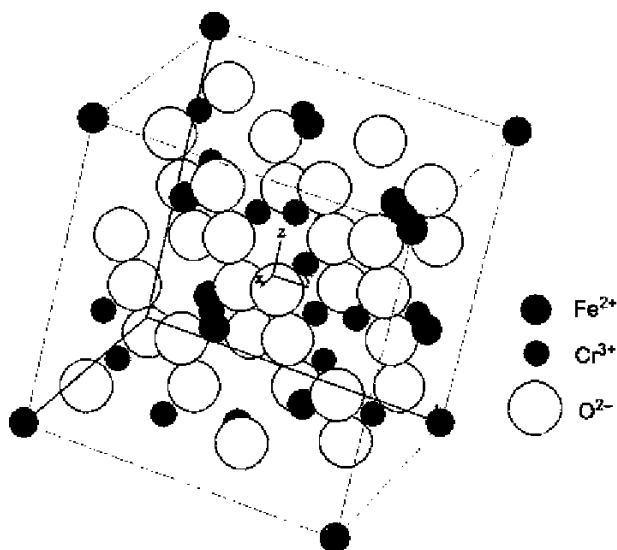


FIGURE 8.13 Crystal lattice of FeCr_2O_4 spinel structure (lattice parameter 0.88 nm).

efficiency of individual methods for the beneficiation of chromite ores. It is important also to know the physicochemical properties of individual mineral fractions of chromite ores and preparation of ore (or concentrates) for electric smelting, the fabrication of refractory materials, and the production of chemical compounds of chromium. The leading minerals of common chrome ores are chromium spinelides, which belong to the spinel group (natural spinel mineral MgAl_2O_4). All of these minerals crystallize in space group $Fd\bar{3}m$. The spinel group includes not only oxides, but also certain sulfides Cr_3S_4 , FeCr_2S_4 (daubreelite), and others. A unit cell of a spinel lattice contains 8 AB_2O_4 units (i.e., $\text{A}_8\text{B}_{16}\text{O}_{32}$). These 32 oxygen atoms constitute the closest cubic packing of 64 tetrahedral and 32 octahedral positions (Fig. 8.13). Out of 96 cation sites per unit cell, only 24 are included in this face-centered cubic cell.

A distinction is drawn between normal, inverse, and mixed structures of spinel. In a normal spinel, bivalent A^{2+} cations occupy tetrahedral sites and trivalent B^{3+} cations are located in octahedral sites. In inverse spinels, the octahedral A^{2+} cations occupy tetrahedral positions, and half of the B^{3+} cations (in the ideal case) are in octahedral sites. The normal and inverse arrangements of cations in natural spinels represent the ultimate limits of spinel structures when the spinel structural formula is presented in the form $(\text{B}_x\text{A}_{1-x})_{\text{tetr.}}(\text{A}_x\text{B}_{2-x})_{\text{oct}}\text{O}_4$. Normal spinel has $x = 0$ and inverse spinel has $x = 1$. Natural spinels are usually classified into four mineral species as series with Al^{3+} , Fe^{3+} , Cr^{3+} , and Ti^{4+} . All spinels with normal and inverse structures form solid solutions that are stable at certain temperatures and pressures (Lyakishev and Gasik, 1998).

TABLE 8.2 Approximate Composition of Chromium Spinelides from Different Countries*

Country	Content, wt. %				Ratios	
	Cr ₂ O ₃	Fe ₂ O ₃	MgO	Al ₂ O ₃	Cr/Fe	MgO/Al ₂ O ₃
Russia	30.54	27.38	24.16	17.92	1.12	1.35
Ukraine	37.15	19.16	18.06	20.78	1.94	0.87
Kazakhstan	60.765	1.845	15.695	8.32	32.93	1.89
Turkey	43.47	18.36	22.39	15.76	2.37	1.42
Greece	39.52	14.37	23.17	22.93	2.75	1.01
South Africa	46.63	11.97	22.75	18.63	3.90	1.22
India	55.2	16.7	14.1	14	3.31	1.01
Pakistan	49	14.37	22.29	14.33	3.41	1.56
Philippines	31.62	15.17	23.83	29.38	2.08	0.81
Canada	48.22	16.17	22.12	12.9	2.98	1.71
Cuba	28.46	13.57	24.29	33.68	2.1	0.72
Brazil	41.1	15.17	21.95	20.78	2.71	1.06

*There might be a large variation depending on the ore type (Karnouchov et al., 2001).

For example, chromites from certain ore deposits in Kazakhstan include chromium spinelides with a predominant content of $(\text{Mg}, \text{Fe})\text{Cr}_2\text{O}_4$, which contains some Al^{3+} in octahedral sites. The structural formula of chromium spinelides might be expressed as $(\text{Mg}_{5.44}\text{Fe}_{2.56})(\text{Cr}_{12.64}\text{Al}_{2.78}\text{Fe}_{0.58})\text{O}_{32}$. The composition ratios of chromium spinelides from different countries are shown in Table 8.2.

The following minerals might accompany chromium spinelides: chrome dioxide, chrome actinolite, chrome garnet (uvarovite $\text{Ca}_3\text{Cr}_2\text{Si}_3\text{O}_{12}$), kammererite $(\text{Mg}, \text{Fe}^{2+})_5\text{Al}(\text{Si}, \text{Al})_4\text{O}_{10}(\text{OH})_8$, clinochlore $(\text{Mg}, \text{Fe}^{2+})_5\text{Al}(\text{Si}, \text{Al})_4\text{O}_{10}(\text{OH})_8$, rhodochrome, serpentine (chrysotile $3\text{MgO}_2\text{SiO}_2 \cdot 2\text{H}_2\text{O}$), chrysotile asbestos, actinolite $\text{Ca}_2(\text{Mg}, \text{Fe}^{2+})_5\text{Si}_8\text{O}_{22}(\text{OH}, \text{F})_2$, magnetitecalcite $\text{MgCO}_3 \cdot \text{CaCO}_3$, antigorite $(\text{Mg}, \text{Fe})_3\text{Si}_2\text{O}_5(\text{OH})_4$ olivine $(\text{A}, \text{B})_2\text{SiO}_4$, magnetite Fe_3O_4 , quartz, opal, pyrite FeS_2 , chalcopyrite CuFeS_2 , goethite FeOOH , limonite $(\text{FeO}(\text{OH}) \cdot n\text{H}_2\text{O})$, and hydrous ferruginous aluminosilicates. Chromite ores of certain deposits contain minerals of the platinum group (Ir, Ru, Pt, Pd, and Rh), especially in South Africa and Zimbabwe, often found as inclusions in chromite silicate matrix.

TABLE 8.3 Classification of Chromite Ores

Category	Type	% Cr ₂ O ₃	% SiO ₂
Commercial	High	58–62 50–58	0.3–3 3–8
	Medium	38–50	8–15
	Low	25–38	15–24
Noncommercial	Low	<25	>25

The mineral and gangue components have different magnetic susceptibilities, which makes it possible to use various magnetic separation methods. Typical values of magnetic susceptibility of chromium spinelides in Kazakhstan deposits are 35 to 70. Gangue minerals might have much higher values (asbestos with fine magnetite inclusions has 2260) or much lower values (chlorides 10 to 11, magnesite 2.5, calcite 5).

Depending on the concentration of chromium spinelides and overall composition of chromium ore (i.e., the content of Cr₂O₃), the deposits are subdivided by way of convention into commercial and noncommercial types (Table 8.3). High grades might be essentially processed without or with a little dressing procedure; other types require proper dressing technologies.

Chromium ores are also subdivided according to their physical state (strong, friable, pulverized, and silicified) and the chromites' grain size (coarse 7 to 15 mm, medium 1 to 7, and fine < 1 mm). So-called strong ores occupy ~80% of all chromite ores, friable ores occupy ~10%, and pulverized and silicified ores occupy 5% each (Lyakishev and Gasik, 1998).

The ores of certain sites might be enriched with or depleted in Cr₂O₃, as well as complementary SiO₂, Al₂O₃, MgO, Fe₂O₃, and CaO, even though they retained their original textural and structural characteristics. That makes it difficult to carry out selective mining and beneficiation. Therefore, it is essential to carry out the classification of chromium ores from commercial deposits, so as to be able to choose the most effective methods and parameters for dressing processes, to utilize ores and concentrates for smelting specific types of chromium ferroalloys, and to obtain chromium compounds and refractory materials.

8.2.2 Chromium Resources Overview

Reliable data on the explored world reserves of chromite ores are virtually absent, because different reviews and forecasts give widely different estimates of the reserves and production scale of chromite ore (Zhuchkov et al., 2010).

In some cases, where data are published they are not very compatible. In general, the republic of South Africa currently holds more than 70% (reserves 11 748 Mt, average 37% Cr₂O₃) of the world's known deposits and it is believed to be one of the world's leading suppliers. Neighboring Zimbabwe is the next major source with 25% (reserves 986 Mt, average 43.2% Cr₂O₃) of the known reserves. Other important chromite and ferrochromium producers are Kazakhstan (reserves 1316 Mt, average 50.2% Cr₂O₃), Turkey, Finland, and Brazil (reserves 72 Mt, average 22.3% Cr₂O₃). Other countries possessing explored commercial chromium ore reserves are Albania, Australia, Greece, India, Cuba, the Philippines, the United States, and Russia. Some deposits are being exploited in Armenia and Azerbaijan. The short summary of these chromite ore deposits is given below.

The main chromite resources of South Africa are associated with the Bushveld complex and the Witwatersrand system. The Bushveld complex represents deposits of chromite ores and platinoids situated in the Transvaal province in the territory of Rustenberg, Potgietersrust, Waterberg, and Leydenberg districts. The chromite deposit in the Bushveld complex is estimated at 2 billion tons.

The bulk of explored chromite reserves and their mining in South Africa are concentrated in the Rustenberg and Leydenberg districts. In the Republic of South Africa, chromite ores contain less Cr₂O₃ and have a lower Cr:Fe ratio, making them suitable mainly for the direct smelting of ferrochrome with a lower chromium content, the so-called charge chrome.

Chromites in Zimbabwe are mined mainly near the town of Selukwe. These Great Dyke range rocks are rich in iron and manganese, and also contain chromium, nickel, and other valuable metals. The metallurgical value of the chromites from the Great Dyke deposit varies from 40% to 50% Cr₂O₃ depending on the location. The major difference between Zimbabwe chromites and those of South Africa is that Zimbabwe ores have a higher Cr₂O₃ content and ratio Cr:Fe > 3:2. This makes them directly suitable for the smelting of commercial ferrochrome.

Turkey is one of the few countries that began mining and exporting high-grade chromites in the 1860s. The Guleman deposit chromites were the best in the world in terms of quality (52% Cr₂O₃). A large chromite ore deposit is situated near Eskisehir.

Finland occupies first place in Europe in terms of its amount of chromite, vanadium, and cobalt reserves; second place in terms of its titanium and nickel reserves; and third place in terms of its copper and pyrite reserves. The commercially exploitable chromite ore deposits are estimated at 165 million tons, although new deposits in the Kemi region have been recently examined. The mean Cr₂O₃ content is 26% with ratio of Cr:Fe = 1.5. Most chromite is used for the ferrochrome smelting factory at Tornio (this technology is somewhat unique, as liquid ferrochrome is used directly in steelmaking). The Cr₂O₃ content in the ore sent for concentration is 24% to 25% (Cr:Fe = 1.6 to 1.7) in the concentrates, the contents are 42% to 48% Cr₂O₃ and 2% to 5% SiO₂.

The commercial chromite ore deposits in the United States (reserves ~338 Mt) are located in Montana, Oregon, Alaska, and California. These are mostly low-grade ores (10% to 18% Cr₂O₃) and require dressing. Some deposits in Montana have ~25% Cr₂O₃, 7% SiO₂, and a ratio of Cr:Fe = 1.3 to 2.8. This ore is enriched to the concentrate grade of 42% to 44% Cr₂O₃, 17% Al₂O₃, and 3% to 4% SiO₂.

The ores in Russia (estimated reserves 486 Mt) contain mainly two types of chromite: medium (35% to 39% Cr₂O₃) and low-grade chromites (25% to 35% Cr₂O₃). Some chromites might have a higher content of Al₂O₃ (<20%). In the northern Ural region, chromites are of a high-chromium alumochromate type (Mg,Fe)(Cr,Al)₂O₄ (60% Cr₂O₃, 8.4% Al₂O₃, 12.84% FeO, and 5.52% Fe₂O₃). Chromite-bearing beds have also been discovered in Siberia and the Far East.

In Albania, rich deposits of chromium ore (48% Cr₂O₃ and 9% SiO₂) were discovered in the early 1930s near Lake Ohrid, in the vicinity of the town of Pogradec.

Australia has a large number of chromite fields, but they are low-grade types and, in most cases, require concentration processing. From 1930 to 1945, Australia was one of the major suppliers of chromite ores, producing 150,000 to 300,000 tons annually. The explored reserves of chromite ore in Australia have been estimated at 0.5 million tons.

Greek main deposits of chromite ore in Thessaly and the Chalcidice Peninsula have 40% Cr₂O₃, 12% FeO, 22% Al₂O₃, 18% MgO, and 5% SiO₂. Greece has one of Europe's largest chromite deposits at Skaumtsa.

A large chromite deposit in India is situated in Mysore, where reserves have been estimated at 1.32 million tons.

In Armenia, ore deposits in Shordzha having 22% to 33% Cr₂O₃ with the ratio MgO:Al₂O₃ ~1.4 have been reported.

Deposits of chromites in Azerbaijan (Geidar, Zandara) are medium grade (43% to 52% Cr₂O₃, 12% to 17% FeO, 5–6% SiO₂). There are, however, differences in alumina content from 10% to 17% (at chromia levels of 50% to 58%) to 23% Al₂O₃ with lower levels of Cr₂O₃ (<40%).

The chromite ores in Ukraine have a mean content of 30% Cr₂O₃, although there is a variation between different fields: medium grade (40% Cr₂O₃), low-grade (<25% Cr₂O₃), and noncommercial disseminated ones (6% to 15% Cr₂O₃). These chrome-spinelides belong to low-iron (Cr₂O₃:FeO = 2.4), high-chromium, medium-alumina varieties.

Some reserves in Greenland have been reported of order of 169 Mt with an average 21% Cr₂O₃ (Zhuchkov et al., 2010), but no specific details were given.

8.2.3 Chromium Ores and Chromites Processing

Chromite ores, as might many others, be mined by open-pit and underground methods. The share of underground mining varies between countries and deposits. The extracted ore is subjected to crushing and sorting (normally rich

TABLE 8.4 Typical General requirements for Chromite Ores

Customer Industry	Grain size, mm	% Cr ₂ O ₃	Others
Smelting of high-carbon FeCr	10–100	>49	
Smelting of low-carbon FeCr	0–10	>50	
Refractories (Cr-Mg bricks, etc.)	0.5–3 <0.5 – less 10%		<8% SiO ₂ , for high grades <3%
Chemistry (Cr compounds)	<0.5	>49	

ore containing more than 45% Cr₂O₃ is supplied to the processing plant, whereas lower-grades are subjected to different dressing procedures).

The main consumers of chromite ore are the ferroalloy, refractory, and chemical industries, which have different demands for the ore and the concentrates, both in terms of the impurity ingredients and in grain-size composition (Table 8.4).

A typical technological process of chromite ores enrichment includes a series of operations (Lyakishev and Gasik, 1998): screening of the input ore, slurry rinsing-off, and heavy media separation. The slurries formed are subjected to wet screening, dehydration, filtration, and drying. The major parameter, changing in these phases, is the SiO₂ concentration gradually changing to <7, 5, 3, and 1%. Because these low-silica concentrates are represented by finer fractions, it is important to prepare the product in lumpy forms (pellets, briquettes). It has been recommended that fine concentrate should be granulated and roasted (~1800°C).

The most common method is gravity concentration (heavy-media separation, screw separators, and concentration tables). Aside from the gravity method (in various modifications), flotation methods are used (separately or in combination with gravity methods), as well as concentration in a strong magnetic field. Magnetic concentration in a weak field is also used to extract magnetite from chromium ore before flotation or to extract it from chromium concentrate after flotation (Kurochkin, 1988; Lyakishev and Gasik, 1998). Wet high-gradient magnetic separation is usually thought to be the most promising method for improved performance. Chromite ore can be separated in a high-strength field, despite the presence of iron impurities. The choice of method depends on several factors, primarily the type of the gangue.

In some cases, separation and dressing methods are optimized to take into account other useful elements, such as PGM (platinum group metals) in South Africa, where noble metals extraction (besides chromium) is of high importance. Along with gravity-flotation and magnetic methods, hydrochemical (hydrometallurgical) technologies are being developed.

Besides these ore dressing methods, combined techniques are also possible, especially when the chromite quality is low. In India, low Cr:Fe ratio chromites are briquetted with coke and selectively reduced at 1250°C. Treated briquettes are crushed, ground, and leached, leading to the higher Cr:Fe ratio concentrates with chromium extraction exceeding 95%.

The authors have estimated that more than 75% of chromite ores are represented by fine fractions and the remaining share is represented by lumpy ores. Electric furnaces consume approximately two thirds of all mined chromite ore, and there the optimum operating conditions are achieved with large sorted chromite ore. For metallurgical processing of high-chromium concentrates, usually present in the finest forms, they have to be agglomerated. Although some successful experiments were made for smelting of ferrochromium in various metallurgical furnaces using fines, this technology has not yet been implemented on an industrial scale. For chromites agglomeration, three main methods are being exploited: sintering, palletizing, and briquetting.

Sintering technology originates from the similar method used for iron ores agglomeration. Many combinations of ores, carbon fuels, moisture content, and binders (bentonite) have been studied. An example of different versions of sinter charges is shown in Table 8.5. The addition of iron ore depends on the required Cr:Fe ratio, fines fractions, and chromite quality.

The pelletization of chromite fines and concentrates is usually based on mixing chromites, binder (bentonite), recycled material, and possibly coke fines and roasting at sufficiently high temperatures (1200° to 1300°C). It is known that roasting in air results in better pellet quality due to the oxidation of iron (2+ to 3+) taking the octahedral sites in spinel structure. A minor share of coke fines in the pellets gives the possibility of raising the temperature and gets more uniform temperature distribution inside the pellet. However, a better resistance to impact and abrasion was achieved in pellets with no fuel additions. During roasting, sulfur is removed from the pellets by 70% to 80% (due to oxidation of sulfides like pyrite). The remaining sulfur is of the sulfate type

TABLE 8.5 Example of the Charge Components for Chromites Sintering by Different Sources

Components	Russia (Ural)	India	Russia
Iron ore			15%–25%
Moisture	7.2%	10%	Not specified
Recycled material	33%	40%	
Coal	5%		Not specified
Coke dust		18%–20%	

TABLE 8.6 Some Examples of Chromite Pelletizing Technologies

Technology	A	B	C	D
Ore grain size	+150...300 mesh	Not specified	"Large"	Not specified
Water, %	12–14	Not specified	9	Not specified
Binder, %	bentonite 0.5–2	Caustic magnesite	Bentonite, filter cake	Lime 2–3, bauxite ore tails 4–5
Drying	150°C	380–400°C		187°C at 1.3 MPa
Roasting	700°–1000°C	Alternatively, 1700°C	1300°C	None

(magnesium and calcium sulfates). Some examples of pelletization technology parameters by different sources are shown in Table 8.6.

Briquetting as a method for agglomeration of fine fractions is widely used in ferrous and nonferrous metallurgy. Unlike sintering or pelletization, it is possible to make briquettes of single component (monobriquettes). In many cases, briquetting was reported to be commercially competitive with sintering or pelletization—the latter is associated with high capital investment, high cost of the grinding and roasting, demand for low SiO₂ content because of possible sintering of pellets when they are roasted in rotary kilns, and so on. The clear environmental advantage of briquettes versus lumpy ore is in the reduction of dust emissions by 1.5 to 2.5 times.

In developing a technology for briquetting of chromite ore, it is important not only to study the mineralogical and grain-size characteristics but also to make a proper choice of the type and quantity of the binder and the conditions for pressure and heat treatment of raw briquettes (Sen et al., 2010). It should be noted that it is very difficult to make recommendations about briquette quality with a particular charge and processing parameters, as well as whether they would be suited for effective smelting of ferrochrome in a submerged arc electric furnace (Pavlov et al., 2010). For example, briquettes in the furnace bath are also a current conductor, so extra coke in briquettes may lead to their premature destruction in the case of high current density. On the other hand, briquettes produced by this method are a good regulator of electric resistance in the charge.

Different compositions have been suggested for briquetting chromites using coal, tar resin, sulfite solution (lye), lime, and so on. One of the recommended briquetting methods is as follows (although it should be remembered that no defined remedy recipe exists for briquetting all types of chromite ores). The ore

of the 6 to 10-mm fraction is dried and mixed with hydrated lime to which mixture molasses is added at 35° to 40°C. The formed briquettes are 2 to 5 inches long, 1 to 2 inches thick, and 1.5 to 2.5 inches wide, and they are stored in piles; their strength increases slowly with holding, reaching maximum values (8 to 25 MPa) after 10 to 12 h. The briquettes retain their strength values even in humid conditions (for shipping and handling, >8 MPa is considered a sufficient limit). The exact mechanism behind the process of strengthening is not known, but some have speculated that it is related to calcium hydroxide carbonization or molasses transformations.

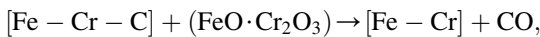
8.3 CHROMIUM FERROALLOYS TECHNOLOGY

The ISO 5448 standard has specified the composition ranges for both chromium and carbon. Ferrochromium is divided into three groups: high, medium, or low carbon. There are five major ranges of chromium content with averages of 50%, 60%, 70%, 80%, and 90% Cr with $\pm 5\%$ tolerances. The nominal composition of the high-carbon ferrochrome alloys is shown in Table 8.7. Typical high-carbon ferrochrome has 60% to 70% Cr, 6% to 8% C, and <5% Si (Chapter 9). Other commercial ferrochromium alloys are low-carbon (Table 8.8) and medium-carbon (Table 8.9) ferrochromium. Low-carbon grades of ferrochrome (<0.25% to 0.50% C) are mostly used to produce corrosion-resistant chromium-nickel and chromium (superferritic) steels. Explicit limitation of phosphorus content in low-carbon and medium-carbon FeCr is dictated by low phosphorus and sulfur demand in steels and difficulties of phosphorus removal from the steel melt bath after the addition of FeCr. All components of the charge are sources of phosphorus. Phosphorus of the charge materials is reduced also by chromium and practically completely transfers into ferrochrome.

Besides these bulk ferrochromium alloys (Daavittila et al., 2004), there are also specific grades of ferrosilicochrome (FeSiCr), ultra-low carbon FeCr, nitrided ferrochromium (FeCrN), and metallic chromium; their compositions and production technologies are described in other chapters.

8.3.1 Technology of Low-Carbon Ferrochrome

Low- and medium-carbon ferrochrome can be produced in several ways (Bobkova, 1991; Durrer and Volkert, 1972; Karnouhov et al., 2001; Lyakishev and Gasik, 1998). In some of them, the raw material is high-carbon ferrochromium, from which carbon has been removed via oxidation, either by chromite additions,



or by gaseous oxygen (converting),

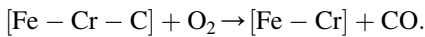


TABLE 8.7 Nominal Composition of High-Carbon FeCr Alloys*

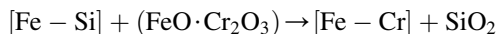
FeCr Grade	C, wt. %	Si, wt. %
FeCr...C50	4–6	<1.5
FeCr...C50LS		
FeCr...C50Si2		1.5–3
FeCr...C50Si2LS		
FeCr...C50Si4		3–5
FeCr...C50Si4LS		
FeCr...C50Si7		5–10
FeCr...C70	>6–8	<1.5
FeCr...C70LS		
FeCr...C70Si2		1.5–3
FeCr...C70Si2LS		
FeCr...C70Si4		3–5
FeCr...C70Si4LS		
FeCr...C70Si6		5–10
FeCr...C90	>8–10	<1.5
FeCr...C90LS		
FeCr...C90Si2		1.5–3
FeCr...C90Si2LS		
FeCr...C90Si4		3–5
FeCr...C90Si4LS		

*Note that “...” is replaced by the respective average chromium content. All grades have maximal sulfur content of 0.10% S except LS grade (“low sulfur”) for 0.05% S.

Low-carbon FeCr might be also produced by oxidation of FeSiCr melt with chromite:



as well as reduction of chromite with silicon (FeSi):



The latter method is similar to the previous process and historically it was developed first (Lyakishev and Gasik, 1998), but the chromium content therein

TABLE 8.8 Nominal Composition of Low-Carbon Ferrochromium Alloys*

Grade	C wt. %	Cr wt.%	P, wt. % max
FeCr...C01P	<0.015	45–75, 75–95 [†]	0.02, [†] 0.03
FeCr...C01			0.05
FeCr...C03P	0.015–0.03	45–75, 75–95 [†]	0.02, [†] 0.03
FeCr...C03			0.05
FeCr...C05P	0.03–0.05	45–75, 75–95 [†]	0.02, [†] 0.03
FeCr...C05			0.05
FeCr...C1P	0.05–0.1	45–75	0.03
FeCr...C1			0.05
FeCr...C2P	0.1–0.25	45–75	0.03
FeCr...C2			0.05

*All grades have <1.5% Si, <0.03% S, and <0.15% N.

[†]Maximal phosphorus content of 0.02% marked is for the highest chromium content (in the 75% to 95% Cr range).

TABLE 8.9 Nominal Composition of Medium-Carbon Ferrochromium Alloys*

Grade	C wt. %	Cr wt.%	P, wt. % max
FeCr...C10	0.5–1	45–75	0.05
FeCr...C10LP			0.03
FeCr...C20	1–2	45–95	0.05
FeCr...C20LP			0.03
FeCr...C40	2–4	45–95	0.05
FeCr...C40LP			0.03

*All grades have <1.5% Si and <0.03% S (except <0.05% S for non-LP grades).

is limited. It is also possible to combine several methods, such as reduction of quartz in the presence of high-carbon FeCr with production of FeSiCr, from which silicon is removed by adding chromite (the resulting slag has a high chromia content and is recycled back to the high-carbon FeCr smelting) (Karnouhov et al., 2001).

Low-carbon ferrochrome is also produced by aluminum reduction, which is discussed in Section 8.4 in more detail. However, in any of these methods, reduction products (either SiO_2 or Al_2O_3) dissolve in the slag, reducing the activity of chromium oxide and making further reduction more difficult. To compensate, increasing slag acidity lime must be added and thus both methods require a substantial amount of flux.

The aluminum reduction process might supply all the heat needed for the reactions exothermally and therefore might be carried out of the furnace, requiring no external heating. In practice, however, some heating is used to reduce the consumption of aluminum powder. Silicon reduction can be carried out exclusively in an electric furnace or by first smelting FeSiCr and mixing it with chromite melts in a ladle.

Reduction by silicon proceeds in the presence of lime (CaO), resulting in a decrease of silicon content in the metal melt (starting FeSiCr) and an increase of chromium in the metal and SiO_2 in the slag. As was mentioned in the description of the Cr_2O_3 -“ CrO ”- SiO_2 - CaO system, the ratio $\text{Cr}^{2+}/\text{Cr}^{3+}$ is very dependent on the slag basicity. Experimental data with different slag compositions (Durrer and Volkert, 1972; Lyakishev and Gasik, 1998) show that the Cr^{2+} fraction has a clear trend to drop at high basicity values (Fig. 8.14). Besides that, the distribution of Cr^{2+} in the volume of the slag is not uniform. In the surface layer of slag, the fraction of Cr^{2+} is below 20% to 25%, depending on the total chromium content in the slag, whereas close to the slag–metal interphase boundary it increases to 40% to 70%.

Therefore, during the process the ratio $\text{Cr}^{2+}/\text{Cr}^{3+}$, and activities of silica, MgO , and CaO in the chromite–lime slag change continuously, which is also

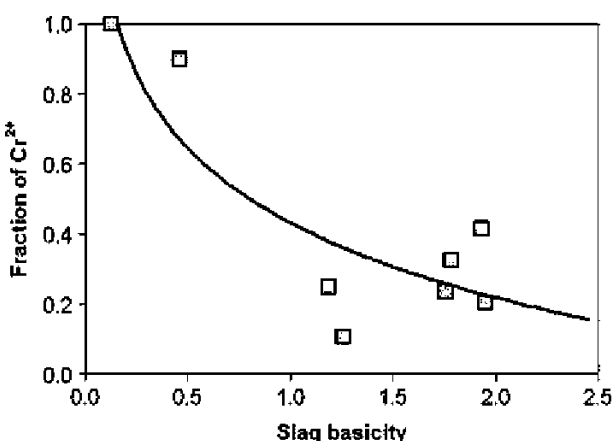


FIGURE 8.14 Molar fraction ratio $\text{CrO}/(\text{CrO} + 2\text{Cr}_2\text{O}_3)$ versus slag basicity expressed as $(\text{CaO} + \text{CrO} + \text{MgO} + \text{FeO})/(\text{SiO}_2 + \text{Al}_2\text{O}_3 + \text{Cr}_2\text{O}_3)$.

affected by oxygen from the furnace environment (the process is very sensitive to the oxidation-reduction potential of the gas phase). In the metal phase, activities of chromium, silicon, and iron also vary. This makes thermodynamic analysis of the reactions very challenging. Furthermore, the limiting silicon content (<1.5%) and the requirement of the highest possible chromium extraction set additional constraints in defining the optimal process conditions. As the reactions of Cr_2O_3 with dissolved silicon are exothermic, increasing process temperature leads to higher silicon content in the FeCr melt.

Process slags contain a substantial amount of MgO besides added lime. Excess lime dilutes slag, increases viscosity, and slows reaction kinetics in general. Excess MgO decreases possibilities for a silicon reaction with chromite, and therefore its content should be limited to 12% to 14% wt.

In practice, the conditions for producing low-carbon ferrochrome in electric arc furnaces are determined experimentally by varying the method of FeSiCr, chromite ore, and lime loading; charge composition; heating and electrical conditions; as well as the quality of refractories and electrodes. In the electric-furnace method of producing low-carbon ferrochrome by silicon reduction, there is a correlation between silicon content in the ferrochrome and Cr_2O_3 in the slag. In the conditions of industrial production of low-carbon ferrochrome, slags with lower basicity (<1.8), high-quality lime, and FeSiCr have provided the best results. Among these, the use of high-quality graphitized electrodes is an important factor (if the electrode quality is lacking, carbon particles might drop off into the slag melt). When the slag basicity is high, carbon may react with calcium and chromium oxides, forming their carbides, and these are a source of increased carbon in the ferrochrome. This sometimes justifies the production of ferrochrome with <0.03% C by mixing a slag melt with liquid or solid FeSiCr outside the electric arc furnace, despite the fact that it makes the processing organization more complex.

8.3.1.1 Furnace Method

The quality of the FeCr and the features of the whole process are very much determined by the method of loading the charge components into the furnace and the conditions used for the decision of the tapping moment. Different options have been utilized, such as: a) loading all components at once, b) loading all components except FeSiCr (for which the second part is added later), c) loading a small amount of FeSiCr to establish an electric load, and then adding other charge components and finally the rest of the FeSiCr. The following procedure has been considered the most appropriate (Table 8.10).

The processing of low-carbon FeCr is usually carried out in small furnaces (5 MVA) lined by magnesite (MgO) bricks. The furnace is loaded with the first part chromite ore, lime, and the first part of FeSiCr. After melting, the second part of FeSiCr, chromite ore, and lime is loaded, the melting is finished, and the metal and slag are tapped. The appropriateness of heat-tapping was earlier

TABLE 8.10 Comparison of Technological Operations of Smelting of Low-Carbon Ferrochrome

Ferrochrome Grade	FeCr...C2(P)	FeCr...C05(P)
Charge (1st/2nd period), kg		
Chromite ore	5200–5800/5200–5800	5600–5800/5600–5800
FeSiCr	1700–1900/1700–1900	2000–2400/1200–1400
Lime	4200–4700/4200–4700	3600–4000/3600–4400
First period:		
FeSiCr loading	700–1000 kg first	700 kg first, then 1300–1400 kg after ore–lime addition by 200–250 kg batches
Chromite ore–lime	With remaining FeSiCr	After first FeSiCr
Tapping	Slag only	None
Second period:		
FeSiCr loading	700–1000 kg first	400–500 kg first, then 800–900 kg after ore–lime addition
Chromite ore–lime	With remaining FeSiCr	With remaining FeSiCr
Tapping	Slag and metal	Slag (1 and 2 period) and metal
Additional operations	+25–50 kg FeSi at the end of each period	
Slag basicity	1.7–1.9	~1.7
% Cr ₂ O ₃	4–5	5–6
% CaO	48–51	45–46

judged according to the amount of electrical energy fed into the furnace, but more recently the direct measurement of silicon in the metal melt has been considered a more reliable control.

8.3.1.2 Off-Furnace Technology (Mixing Method)

For ferrochromium with the least carbon content, furnace graphitized electrodes have been identified as a major source of carbon, accounting for ~40% of

all carbon input. In this case, the chromite ore–lime melt is made in the furnace without reduction, and it is mixed with FeSiCr in a ladle, outside the furnace (the mixing method, also known as the Perrin process). During the melting of the chromite ore and lime mixture, the oxidation potential is high (no metal formed) and thus carbon content in the slag is low. During mixing, there are no graphitized electrodes and a large amount of heat is released due to exothermic reactions of chromium and iron oxides with silicon and of interaction of CaO with SiO₂. The heat release is high enough to allow the use of solid FeSiCr along with liquid FeSiCr.

The mixing process is highly turbulent, kinetically fast (at the beginning of the mixing stage), and efficient enough to remove silicon from the FeCr melt. The slag might be used in several ladles to enhance refining of the FeCr from silicon; however, the main objective of the mixing method is essentially low-carbon FeCr processing. The disadvantages of the mixing method are increased nitrogen content in FeCr and some more challenges to control chromium-rich emissions (dust, fumes, gases).

The charge materials used to produce low-carbon FeCr are chromite ore, lime, and FeSiCr. The starting charge materials have to be classified depending on phosphorus concentration, as phosphorus content affects the quality of ferrochrome. Besides these main charge materials, the returns from the gas cleaning units (cyclones) with 25% to 40% Cr₂O₃ are also used as charge components. FeSiCr is used in a liquid (melt) or solid (granules) form and its typical composition is 48% to 51% Si and 28% to 30% Cr, with the balance composed of Fe and impurities. The main requirement to FeSiCr is that phosphorus content should not exceed 0.02% wt.

Chromite ore and lime are fused in small electric furnaces (~5 MVA) lined with MgO bricks, and fed through graphitized electrodes. The ratio of chromite ore to lime is roughly 1:0.8, and the resulting melt has about 27% to 30% Cr₂O₃ and 40% to 45% CaO. To accelerate melt formation, a small fraction of FeSiCr is added to form silica for the purpose of reducing the liquidus temperature.

The chromite ore–lime melt is poured into a ladle (5 to 6 m³) with a magnesite lining. To decrease heat losses, the melt in the ladle is covered with slag from previous heats. The ladle with the melt is weighed and the amount of FeSiCr additions is calculated depending also on the content of Cr₂O₃ in the melt. The FeSiCr is poured into the ladle while it is on the scales. The pouring rate is adjusted to the rate of reduction processes in the ladle (~200 kg FeSiCr per minute). At the end of pouring, the contents of the reactor ladle are transferred to another ladle and then back to the first ladle. The number of pourings between ladles (up to six times) is determined by the rate of refining ferrochrome from silicon.

Another example of the smelting hardware in the Tchelyabinsk plant (Russia) includes a closed submerged arc furnace, 33 MVA (bath inner diameter 8.8 m, depth 3.5 m, electrodes 1500 mm) for smelting of FeSiCr and 16.5 MVA (bath inner diameter 4 m, depth 2.35 m, electrodes 500 mm) for

chromite ore–lime melt preparations. For the latter process, the chromite and limestone are preroasted in rotary kilns at 1100°C, and this hot charge is fed directly into the furnace. The chromite ore–lime melt is tapped at ~1900°C into a magnesite-lined ladle and is mixed with liquid FeSiCr in a 20 m³ ladle. The cross section of the chromite–lime melting and mixing plant is shown in Figure 8.15.

The specific consumption of raw charge materials for the production of 1 ton of low-carbon ferrochrome by mixing is 1750 kg of chromite ore (basis 50% Cr₂O₃), 570 kg of FeSiCr with 48% Si, 1370 kg lime, and 18 kg of electrodes. Electricity consumption varies, but the chromium extraction efficiency is ~80%.

The exothermal reactions of chromium reduction by silicon give about one fourth of total heat input in the balance, which is enough for raising the temperature of the process and melting the solid charge.

A version of the mixing process operation involves reaction in a converter with argon blowing (Lyakishev and Gasik, 1998). Here chromite–lime melt was poured into a converter, followed by the addition of FeSiCr and subsequent agitation by argon. To control melt temperature and to avoid overheating, a mixture of chromite and lime was added. The length of the converting cycle was from 10 to 30 minutes. The low-carbon FeCr obtained in this way had 0.02% C, 62.2% Cr, and 0.03% P with residual chromia content in the slag of 3% to 4%; however, the extraction of chromium was about 80% (i.e., not very different from the conventional mixing process without argon blowing).

Low-carbon ferrochrome is cast into iron molds into ingots with a thickness < 80 mm if no degassing is applied. Ferrochrome produced by mixing contains a substantial amount of dissolved gases (up to 30 cm³ per 100 g).

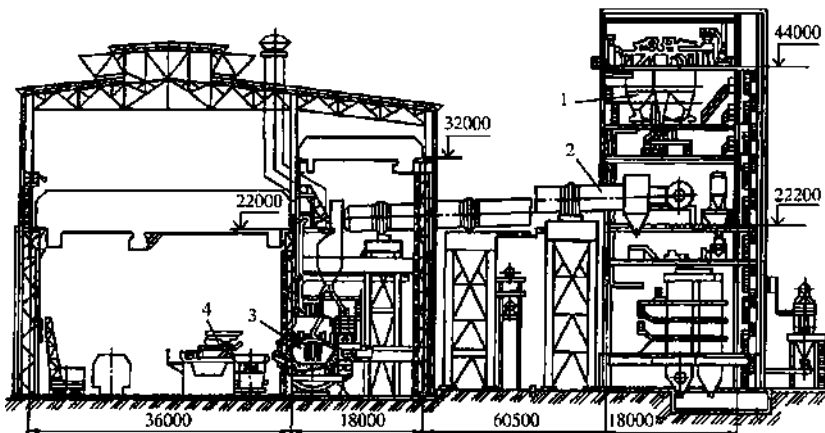


FIGURE 8.15 Cross section of the plant for melting of the chromite ore–lime melt and mixing process (dimensions in mm) using a preheated charge. 1, dosing equipment; 2, rotary kiln; 3, electric furnace; 4, ladles for mixing of ore–lime melt and FeSiCr.

Upon solidification, excess gases form cavities and small bubbles. This has a negative effect on ingots crushing (more fines and dust) as well as steelmaking (less dense FeCr lumps do not sink well enough in the steel bath, leading to excess chromium losses). Therefore, it is a common practice to carry out degassing of FeCr before its casting by subjecting the ladle to a vacuum treatment (<10 min). After that, the slag pots are filled first to 70% of their volume with liquid slag and the rest of the slag from the ladle is poured into separate slag ladles. After few minutes, when the slag lining has been formed, the FeCr melt is poured into ingots with a thickness of less than 150 mm.

The mixing method also allows production of master alloys that contain elements such as molybdenum, tungsten, and manganese, which are easier to reduce than chromium.

Similar to the furnace method, mixing might be carried out in different stages. For example, extra FeSiCr might be poured first into the oxide melt to get FeCr with a high silicon content. This melt is treated with extra oxide melt, reducing silicon content down to the required values but leaving slag with a high Cr₂O₃ content, which in turn is repeatedly treated with excess FeSiCr. Also, the mixing of different heats is being practiced.

Residual slag from low-carbon FeCr smelting has high basicity (CaO:SiO₂ > 1.6). This creates favorable conditions for the formation of calcium orthosilicate 2CaO·SiO₂ as the main mineral component of the slag. The polymorphic transformation of calcium orthosilicate upon cooling with more than 12% volume increase leads to slag self-crushing and excessive dusting (particle sizes <0.1 mm). To combat this problem, MgO and some other oxides (B₂O₃, BaO) are used to stabilize the mineral composition of the slag. Slags with basicity of 0.9 to 1.2 and 15% to 18% MgO have a stony structure, are characterized by high strength, and do not disintegrate with prolonged storage (Bobkova, 1991). However, separation of these slags from metal is more difficult and requires additional crushing and separation steps. Nonstabilized slags have sometimes been used as a calcium orthosilicate source (in molding sands binding, construction mixes, etc.). For example, there have been positive outcomes to the use of low-carbon FeCr dump slags in agriculture (fertilizing, increasing soil basicity), road construction (filling material), cement processing, and colored and special glass manufacturing, and as a pigment in paints (Karnouhov et al., 2001).

8.3.2 Technology of Medium-Carbon Ferrochrome

Medium-carbon ferrochrome is also a product of interest in the foundry industry and in steelmaking plants where refining capacity is limited but low silicon content is desired. Most of the medium-carbon FeCr is produced by the oxygen-converter method. It is based on carbon removal from liquid high-carbon ferrochrome (8% to 9% C, 0.3% to 0.5% Si, 0.04% P) with gaseous oxygen blowing (Karnouhov et al., 2001; Lyakishev and Gasik, 1998).

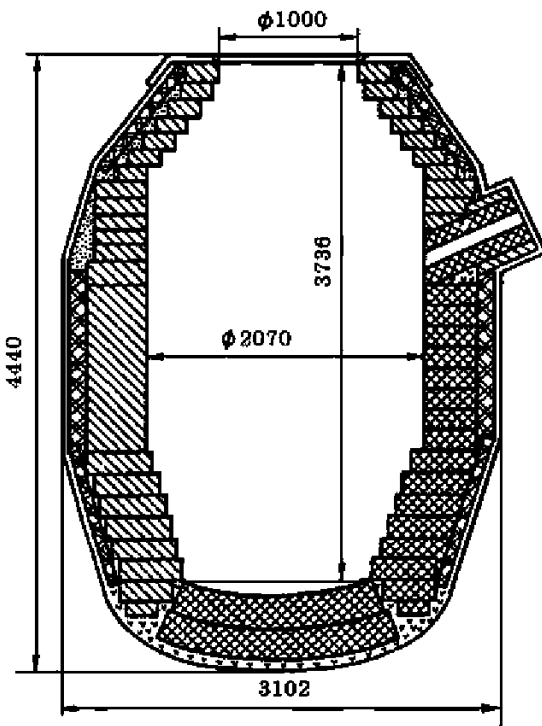


FIGURE 8.16 Dimensions (mm) of the top-blown converter for the production of medium-carbon ferrochrome.

A typical converter is the top-blown type and it has capacity of 15 tons of liquid FeCr (Fig. 8.16). The converter is lined with chromium–magnesite and periclase (MgO).

The idea of the carbon removal from the liquid FeCr is based on carbon oxidation during oxygen blowing. As FeCr has a limited amount of silicon, silicon oxidation cannot be used as a heat source (furthermore, the formation of silica would have negatively affected the lifetime and stability of the lining). The melt temperature at the beginning of the process is not sufficient for carbon oxidation, and it only starts to proceed together with chromium oxidation after some time. Carbon and chromium oxidize simultaneously, but at higher temperatures chromium oxide from the slag phase starts to react with carbon in the metal phase, releasing free chromium and CO (these reactions are endothermic and require higher temperatures). The ratio Cr:C in the melt during oxygen blowing is a function of melt temperature and might be approximated by $\log (\text{Cr/C}) = -10850/T + 7.12$ (Gasik et al., 2009; Lyakishev and Gasik, 1998). Increasing temperature by 200 K results in an equilibrium residual carbon decrease from 3.1% (1873 K) to 0.92% C at 2073 K. To reach high

temperatures, aluminum-rich scrap ~5 to 8 kg/ton is sometimes used (aluminum oxidation is highly exothermal).

The refining process is carried out by pouring 7 to 11 tons of liquid high-carbon FeCr into a converter (>60% Cr, <1% Si, <0.05% P— carbon content is not limited). For every ton of FeCr, 80 to 100 m³ oxygen is required. At the end of blowing, 600 to 800 kg of medium-carbon FeCr returns are added to cool down the melt; 15 to 20 kg of FeSiCr is also added to enhance slag reduction and decrease its viscosity. Tapping of metal and slag is carried into metal mold. For 1 ton of ready medium-carbon FeCr, about 1230 to 1260 kg of high-carbon FeCr is required at a chromium extraction efficiency of 80% to 82%.

8.3.3 Technology of Ferrosilicochrome (FeSiCr)

Ferrosilicochrome (FeSiCr) is an alloy of the multicomponent system Fe-Cr-Si with carbon, phosphorus, and sulfur as main impurities. The FeSiCr alloy is produced for two purposes: direct use in steelmaking (steel bath killing and alloying with chromium and silicon) and as a reductant in processing of low-carbon FeCr as described previously. The typical compositions of FeSiCr alloy are shown in **Table 8.11** (there are several national standards and plant norms for FeSiCr grades, especially when it is used in house for low-carbon FeCr production only).

The carbon content in FeSiCr for the production of medium-carbon ferrochrome is not regulated, as it is determined by the concentration of silicon in the alloy. Obtaining the alloy with the highest silicon content (>45%) and lowest carbon content (<0.05% C) is a challenging engineering operation. This alloy is intended for the production of low-carbon ferrochrome with <0.07% C (by the furnace method) and <0.03% C (by the mixing method with FeSiCr).

FeSiCr can be produced by a slag-less or slag (flux) process. In the first case, the reduction of silicon by carbon (coke) from quartzite charge proceeds in the presence of high-carbon FeCr (i.e., here chromium is not reduced, only silicon).

TABLE 8.11 Chemical Composition Requirements for Typical FeSiCr Alloy Grades

Grade	Si, wt.%	Cr, wt. % min	C, wt. %	P, wt. % max	S, wt. % max
FeCrSi13	10–16	55	6	0.04	0.03
FeCrSi20	16–23	48	4.5	0.04	0.02
FeCrSi26	23–30	45	3	0.03	0.02
FeCrSi33	30–37	40	0.9	0.03	0.02
FeCrSi40	37–45	35	0.2	0.03	0.02
FeCrSi48	>45	28	0.1	0.03	0.02

In the second method, chromite ore is added so both chromium and silicon are reduced simultaneously by carbon.

The slag-less process uses coke, quartzite, and high-carbon FeCr. Silicon is reduced by carbon from both coke and FeCr, and chemically the process is close to smelting of ferrosilicon with 45% to 65% Si. Silicon dissolves in the Fe-Cr-C melt and its activity is significantly lower than for FeSi alloy processing. As silicon reduction proceeds through several intermediate stages, gaseous SiO and solid SiC form. The concentration of SiO in the gas phase is high, 30 to 40 vol %, and might lead to losses of silicon and distortions of the closed arc furnace operations. The formation of very fine SiC particles is undesirable; therefore, the melt is soaked in a ladle for an hour to allow SiC to float to the top of the melt. Nevertheless, the quality of the FeSiCr alloy by this method is lower than it is with the flux process.

In the single stage slag (flux) method, chromite ore is charged instead of high-carbon FeCr. This leads to a complex mechanism of melt and slag formation. Their properties have an important role in the production of alloys with lower carbon content. The slag may have different silica content and various MgO:Al₂O₃ ratios, depending on the quality and composition of raw chromite ore. It has been recommended that the ratio MgO:Al₂O₃ should be raised if silica contents increase (~1 for 45%SiO₂ and ~1.2 for 50% SiO₂).

An example of the submerged arc furnace of 33 MVA is shown in Figure 8.17. This furnace has a water-cooled shell, a carbon bricks lining, and self-backed electrodes of 1500 mm diameter. An electric circuit includes a capacitor battery with 12 MVAR power per current phase.

It is necessary for every furnace to maintain a proper height of carbon lining. Specific recommendations depend on the type of ferroalloy being produced. If the height of carbon brick walls is too high, a slag–carbide “false bottom” buildup is formed due to the excess availability of carbon. In such cases, removal of additional upper carbon blocks allows FeSiCr production with improved indicators.

The slag-less process of FeSiCr smelting is performed in such furnaces using a charge of high-carbon FeCr, quartzite, and coke. Quartzite (20 to 80 mm) is required to ensure low water content and porosity, as well as high thermal and cracking resistance. Coke (5 to 25 mm) is supplied at some surplus (<5%). Table 8.12 lists the normalized charge materials expenditure (per 1 ton of FeSiCr) with different levels of silicon content for slag-less and slag processes.

The standard operating current of the furnace (see Fig. 8.17) is 90 to 100 kA and the power factor $\cos(\phi)=0.90$ to 0.95. With these conditions, the temperature of off-gases ranges from 550° to 750°C, which reflects normal furnace operation. In the case of deviations, gas temperature might rise to 1300°C, and this is an indicator of abnormal operation requiring operator intervention and parameters adjustment. The composition of gas emerging from the electrodes zone is 10% to 12% N₂, 5% to 7% H₂O, 4% to 5% CO₂, balance CO, and impurities. In abnormal cases where the temperature is very high, the

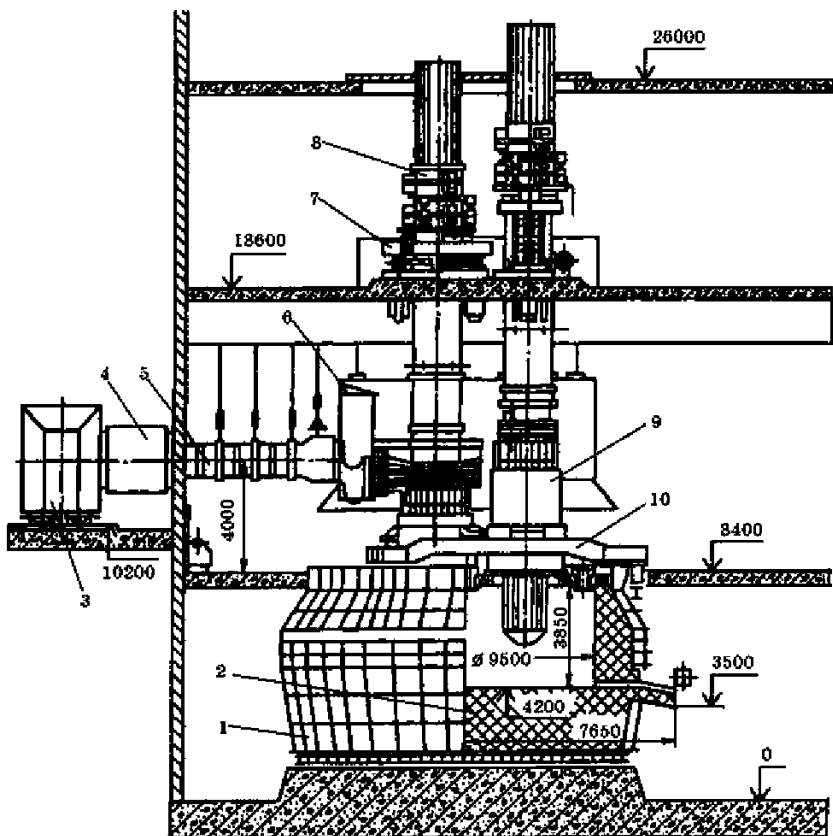


FIGURE 8.17 Submerged arc furnace of 33 MVA power for smelting ferrosilicochrome. 1, shell; 2, lining; 3, power transformer; 4, short net compensator; 5, short net; 6, screens; 7, hydraulic lift; 8, electrodes control and bypass mechanism; 9, electrodes holder; 10, furnace cover.

furnace operation is also disrupted by sublimes, forming alternating black/white layer deposits. Black layers are a combination of graphite (~16%), MgO (~40%), and SiO₂ (~40%); white layers are mixtures of oxides (~42% MgO, 23% SiO₂) and carbide (30% SiC). A high MgO content possibly originates from the oxidation of magnesium vapors given off from the reduction of magnesia. Sublimes have no MgO in the case of a slag-free process.

Slag-less FeSiCr smelting is a continuous process when the products are tapped every 1.5 to 2 h. The temperature of the liquid alloy at tapping is 1850° to 1950°C, dropping down to ~1600°C in the filled ladle. This temperature is much higher than that of the liquidus of the alloy (1320° to 1340°C) and such overheating is needed for soaking the alloy in the ladle for about an hour to allow formation, coagulation, and floating up of SiC inclusions (the carbon-saturated Fe-Si-Cr melt is in equilibrium only with silicon carbide). SiC inclusions have

TABLE 8.12 Charge Materials for Slag-Free (Top Rows) and Slag (Bottom Rows) Processes

Charge Materials, kg/t FeSiCr	Si, % wt.				
	13	23	33	43	50
Quartzite	298	520	742	965	1121
	634	881	1134	1323	1464
Chromite ore	not used				
	1908	1600	1420	1145	923
Coke	117	220	312	424	308
	543	575	625	678	712
High-carbon FeCr	1089	911	803	648	525
	not used				
Iron (steel) chips	8	41	62	93	115
	30	82	84	105	116

different origins, primarily as the result of SiO_2 reduction by carbon from the melt and secondarily as the result of the decreased solubility of carbon in liquid FeSiCr. There might also be external inclusions due to slag entrapping. Whereas these inclusions are the same for SiC compositions, the degree of their removal from the melt is different as they have a variety of particle sizes.

The duration of soaking in the ladle could be extended by preheating the ladle lining and by insulating the melt surface with a layer of high-basicity ferrochrome slag.

After the holding, FeSiCr alloy is cast into ingots or granulated by spraying the liquid alloy with a water jet. In the process granulating the alloy, the slag and SiC inclusions are washed off.

The slag amount in this process is 3% to 6% of the metal weight. The chemical composition of the slag varies significantly, due not only to furnace operation but also to chromite composition and the quality of other charge materials. Examples of FeSiCr process slag composition from three different plants are shown in Table 8.13. The “normal” slag composition is defined by SiC content that should not exceed 8% wt. The differences in the compositions shown are due to many factors. For example, some slags with a high content of BaO result from the use of quartzite in the Baikal deposit, which contains 0.2% to 1% BaSO_4 . Higher alumina (or a lower $\text{MgO}/\text{Al}_2\text{O}_3$ ratio) in the slag was achieved by adding bauxite or using chromite ore with $\text{MgO}/\text{Al}_2\text{O}_3 \sim 1$. Some

TABLE 8.13 Examples of Slag Compositions from FeSiCr Smelting*

Plant/Furnace	SiO ₂	Al ₂ O ₃	CaO	MgO	BaO	SiC	Cr ₂ O ₃
I	17–27	21–45	11–33	1.5–6.5	9–12	1–27	Not analyzed
II	36–51	14–28	2–18	2–8	—	7–70	0.5–6
III	26–32	17–25	12–20	1–2	12–20	8–11	2–6
IV	41–43	23–24	0.5–6	20–25	—	3–5	0.5–2

*Impurities not shown are mostly FeO (<4%).

furnaces operate with the addition of lumpy pegmatite rock (74% SiO₂, 13% Al₂O₃, 1.8% CaO, 10% (Na₂O + K₂O) and chromite ore with <20% MgO. The presence of alkalis decreases the viscosity of slags and improves the separation of metallic shots and SiC, leading to a higher alloy yield.

The mineral composition of the slags is governed by anorthite CaO·Al₂O₃·2SiO₂, gehlenite 2CaO·SiO₂·Al₂O₃, spinel MgAl₂O₄, and corundum Al₂O₃. Barium oxide (when present) tends to form celsiane BaO·Al₂O₃·SiO₂ and barium hexa-aluminate BaO·6Al₂O₃. Celsiane might also incorporate alkalis. The practical experience of ferroalloy plants indicates that FeSiCr slag containing inclusions of alloy and SiC should be utilized in the charge for producing high-carbon ferrochrome. The productivity of a 33 MVA furnace (see Fig. 8.17) with an operating active power of 28 to 30 MW is 120 to 130 ton FeSiCr per day.

8.3.4 Technology of Ultra-Low-Carbon FeCr

In some cases, the composition of standard low-carbon FeCr is not satisfactory for processing of special alloys and steels with an ultra-low carbon, hydrogen, and nitrogen content. Low-carbon FeCr with <0.03% C still has a too-high nitrogen content, significantly reducing the corrosion stability of Cr-Ni-Mo stainless steels, even when carbon in the steel does not exceed 0.015%.

A method has been developed to remove these impurities and oxide inclusions by subjecting solid FeCr lumps to a high-temperature treatment in a vacuum (Gasik and Polyakov, 1990; Lyakishev and Gasik, 1998). This method has been patented in many countries and has received widespread recognition, allowing production of FeCr with <0.015% C and <0.025% N. The principle of the method lies in solid-phase decarburization and the degassing of FeCr lumps with a starting carbon content of 0.10% to 0.15% in a vacuum (residual pressure 1.3 to 13 Pa) at 1350° to 1450°C in three-chambered resistance furnaces (Figs. 8.18 and 8.19). During the treatment carbon content drops from 0.10% to 0.02% C and nitrogen from 0.06% – 0.07% to <0.02% N. The ferrochrome

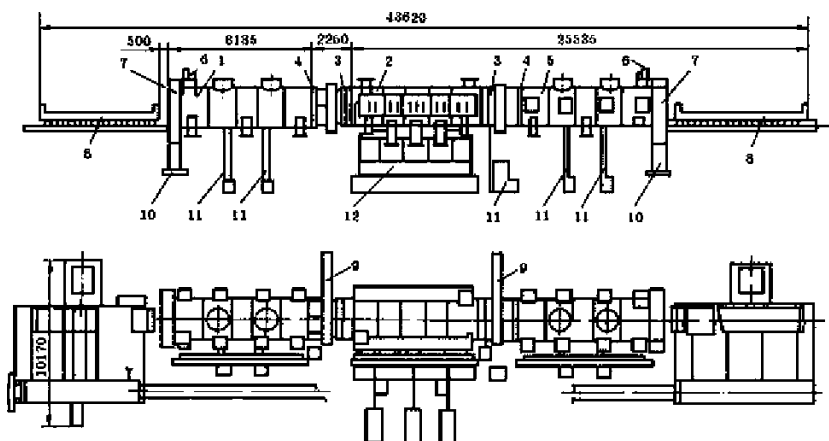


FIGURE 8.18 Vacuum furnace layout for processing ultra-low-carbon ferrochromium by the method designed at the Dnipropetrovsk Metallurgical Institute. 1, FeCr cooling chamber; 2, isothermal soaking chamber; 3, vacuum gates; 4, compensators; 5, preheating chamber; 6, cover lift; 7, cover; 8, carrier; 9, vacuum shields; 10, support; 11, low-vacuum pumps; 12, acceleration pumps.

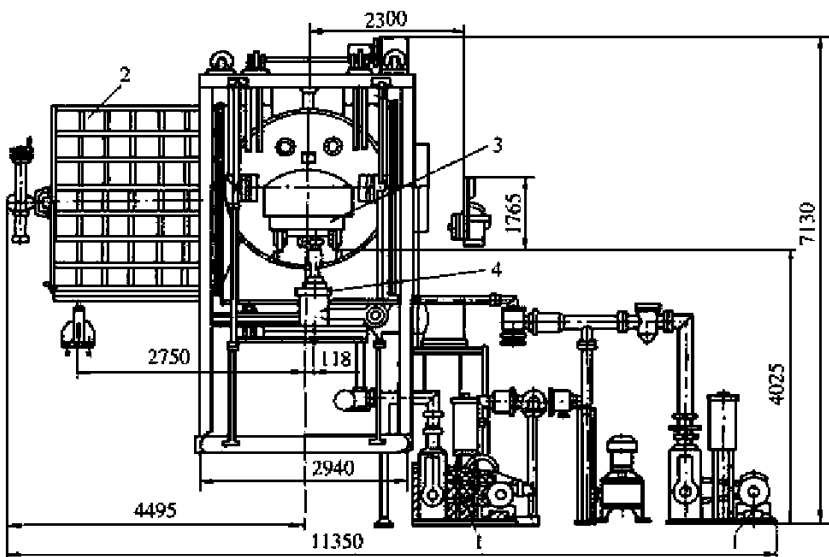


FIGURE 8.19 Cross section of the vacuum furnace for ultra-low-carbon FeCr processing (see Fig. 8.18). 1, pumps; 2, vacuum slag; 3, carrier; 4, carrier moving mechanism.

degassed by this process is also characterized by low concentrations of hydrogen ($\leq 7 \cdot 10^{-4}$ %), oxygen (≤ 0.04 %), and nonmetallic inclusions.

This furnace of 1.5 MW power operates at 1050°C in the first chamber and 1350° to 1450°C in the second chamber (the third chamber is used for cooling). The entire cycle time is 24 h. Carbon, nitrogen, hydrogen, and oxygen are removed by the diffusion mechanism. Oxide inclusions might be partially reduced in the vacuum. This method is only useful for solid-state FeCr refining, as liquid ferrochromium would have too many losses of chromium with vapors.

8.3.5 Technology of Nitrided Ferrochromium (FeCrN)

In the case of low-, medium-, or high-carbon ferrochromium, nitrogen content is usually limited (Tables 8.7 to 8.9). However, when making Cr-Ni-Mn and Cr-Mn stainless steels as well as some other special grades, part of the nickel is replaced by nitrogen, which stabilizes the austenite structure if properly dissolved in the FCC phase. It also improves some physical and mechanical properties of steels. The input of nitrogen into liquid steel from the gas phase is difficult and uneven, so the best way is to use nitrided ferroalloys (FeMn, FeCr, FeV), which might have up to about 10% wt. nitrogen. According to the method of nitrogen introduction in the ferroalloy, it might be classified as “molten” (nitriding proceeds in the liquid state) or “sintered” (nitriding proceeds in the solid state, e.g., by treatment of the alloy powder). The typical composition of these FeCrN alloys is shown in Table 8.14. On request, the alloy with a carbon content below 0.03% to 0.06% wt. C, phosphorus below 0.02%, silicon < 1%, and sulfur < 0.02% might be supplied.

The saturation of molten FeCr by nitrogen is performed while liquid low-carbon ferrochrome is soaked in a nitrogen atmosphere, traditionally in induction furnaces. Nitrogen dissolution in liquid FeCr is an exothermic process, and the solubility of nitrogen decreases with increasing temperature. Other elements also affect nitrogen solubility, such as the following:

1. Carbon decreases nitrogen solubility; in the Fe-70%Cr melt, solubility is described as $\log(\%) = 0.48 + 0.105(\%)$ at 1 atm and 1873 K.

TABLE 8.14 Nominal Composition of Nitrided FeCr, wt. %*

Grade	Cr	C	Si	P	N	S
Molten FeCr...CIN3	45–75	<0.10	<1.5	<0.03	2–4	<0.025
Sintered FeCr...CIN7					2–4	4–10

*Chromium content is chosen from 50%, 60%, or 70% Cr with $\pm 5\%$ tolerances (i.e., 45% to 75% wt. Cr).

2. Silicon decreases nitrogen solubility; in the Fe-70%Cr melt, the addition of 1.5% Si drops solubility by 0.2% to 0.25% N.
3. Titanium and vanadium increase nitrogen solubility limits but do not substantially affect the kinetics of the process.
4. Oxygen significantly affects nitrogen solubility; furthermore, it also decreases the solubility rate. Therefore, FeCr melt must be deoxidized before the nitriding procedure (also, nitrogen gas must be dry, with the least amount of water possible).

The melt composition also has an impact on nitrogen concentration. Figure 8.20 represents phase equilibria of nitrogen with the Fe-Cr system at 1600°C. As the figure shows, 2% to 4% wt. N fits solubility limits for alloys near the Fe-70%Cr compositions. For >80% Cr it is not possible to have a homogeneous liquid phase, as hexagonal packed (HCP) $(\text{Cr}, \text{Fe})_2\text{N}$ or BCC solid solution forms at this temperature. The liquidus–gas line defines practically achievable nitrogen concentrations.

Therefore, it is possible to reach higher nitrogen contents only in the solid state. However, despite a lower nitrogen content in the molten FeCrN, the resulting alloy has high uniformity of composition and high efficacy of nitrogen utilization when added into a steelmaking furnace or ladle.

“Sintered” FeCrN is produced from solid powder of either low- or high-carbon ferrochrome. In the latter case, high-carbon FeCr must be first

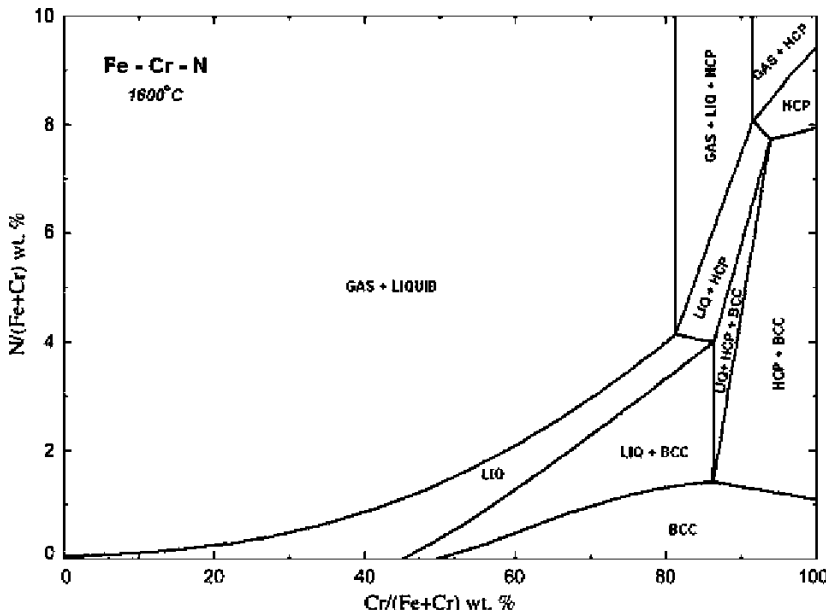


FIGURE 8.20 Phase equilibria in the Fe-Cr-N system at 1600°C.

decarburized in a vacuum to remove excess carbon. In this process as a rule, initial amounts of phosphorus and sulfur are retained in the alloy, so the quality of FeCrN by these impurities is determined by the quality of the initial ferrochromium. Although about 10% wt. N might be achieved in solid-state nitriding, the use of this alloy is not always reasonable due to increased nitrogen losses in steelmaking (particularly in a ladle) if the nitrogen content in the FeCrN is too high (lower efficacy).

Solid nitriding of high-carbon FeCr is carried out using lumpy FeCr briquettes at temperatures of 950° to 1050°C and 1 atm of nitrogen gas. This nitriding stage follows immediately after the vacuum treatment to remove carbon. Nitrided alloy cools down at low nitrogen pressure until 600° to 650°C; after that the cooling proceeds in air. Nitrogen in such FeCrN is present in the form of HCP $(\text{Cr}, \text{Fe})_2\text{N}$ and FCC $(\text{Cr}, \text{Fe})\text{N}$ phases.

Solid nitriding of low-carbon FeCr does not involve stages of decarburization, but the initial alloy has to be ground in smaller particles and then briquetted. This method is more economical as it does not require vacuum treatment and the homogeneity of FeCrN is higher than in the case of high-carbon FeCr. It is possible to use different starting alloys and obtain nitrided master alloys with Cr, Mn, and V.

Finally, it is also possible to get nitrided alloy simultaneously with smelting during reduction by aluminum in the presence of nitrogen, but this method usually does not allow more than 2% wt. N.

8.4 PRODUCTION OF METALLIC CHROMIUM AND ITS ALLOYS BY ALUMINUM REDUCTION

There are several methods of manufacturing pure chromium and its alloys by reduction of raw materials with aluminum. Practically, chromium chloride, iodide, and oxide might be used in alloys production. The main difference between chloride and iodide technology is that chlorides are being reduced (besides aluminum reduction; also use of sodium, magnesium, and zinc for chrome reduction has been developed), whereas iodides are thermally dissociated to pure chromium and iodine. The reduction of chromium oxide is commonly done using aluminum.

Metallic chromium is used to produce nickel- and cobalt-based superalloys and alloys with regulated low iron or without iron. There are also special chromium-rich alloys where iron content is limited. The properties of these alloys are very sensitive to impurities and therefore chromium, much like other pure components, has an extensive list of allowable limits (Table 8.15). This also puts additional demands on charge materials used for chromium processing (chrome oxide, aluminum powder, lime, etc.).

Basically all CrCl_3 reduction reactions are exothermic, so the process temperature rises by 200° to 250°C. This is beneficial, as the product mix is further subjected to vacuum distillation to remove resulting chlorides (AlCl_3 ,

TABLE 8.15 Nominal Composition of Metallic Chromium, wt. %*

Cr (min)	99A	99	98.5	98	97
Si	0.3		0.4	0.5	
Al	0.2	0.5		0.7	1.5
Fe	0.6			0.8	1.2
C	0.03			0.04	0.05
S	0.02			0.04	
P	0.02			0.03	
Cu	0.01		0.02	0.04	0.05
As	0.01				
Bi	0.0005				
Sb	0.008				
Zn	0.006		0.01		
Pb	0.0008		0.01		
Sn	0.004				
Co	0.005				
N	0.04	0.05			

*Empty cells means this impurity is not specifically controlled. Nitrogen content could be decreased to <0.015% wt. N on demand.

ZnCl_2 , MgCl_2 , or NaCl) over 950°C . Metallic chromium produced by this method normally has purity of 99.3% to 99.7% Cr.

The production of metallic chromium by the iodide method relies on a similar technique developed for pure titanium, hafnium, and other elements that form iodides capable of being properly refined and decomposed at heating. The interest in pure chromium made by this method is in low ductile-to-brittle transition temperature, which might reach $-50\ldots -65^\circ\text{C}$ for doped chromium or even -130°C if CrI_3 has been refined to achieve “extreme” purity of chromium, about 99.995% Cr. This method is rather expensive and is used only when special quality materials are demanded.

The most common metallurgical method is reduction of chromium oxide (98% to 99% Cr_2O_3) by other metals, especially aluminum. The classical method includes ignition or heating of the charge with chromium oxide, aluminum powder and sodium nitrate as an oxidizer. The mixture might be

composed as either exothermic (excess Al and NaNO₃) or endothermic (will require extra heating to keep the process). Use of nitrate, however, does not allow receiving chromium with less nitrogen. This might be improved by using magnesium as a reductant: heating up the mixture of magnesium and chromium oxide in an argon atmosphere leads to the evaporation of magnesium and the reduction of chromium powder with MgO as a side product. Another method is to replace sodium nitrate with calcium chromate CaCrO₄. The charge consisting of 37 kg of calcium chromate and 46 kg aluminum powder per 100 kg of chromium oxide was shown to achieve 0.03% to 0.05% N in the final ingot. This also could be carried out in an electric furnace, when at least part of the chromium oxide is melted first, forming slag with <50% CaO. Yet another method involves the reduction of chromium oxide with iron-less Cr-Si alloy, but the benefits of this method are questionable because iron-free chromium-silicon alloy requires a special preparation of its own. Thus, reduction of chromium oxide by aluminum is the most widespread process at the moment.

Theoretically, the reaction of chromium oxide with aluminum leads to the formation of metallic chromium and aluminum oxide. The latter starts to form solutions with the remaining chromium oxide, decreasing its activity and making further reduction more difficult. This is managed by adding flux (lime), which forms stable calcium aluminates and releases chromium oxide, improving reduction efficiency. Additionally, CaO decreases the liquidus temperature of the slag and (in oxidizing conditions) forms calcium chromite-chromate 9CaO4CrO₃Cr₂O₃, which is beneficial when making chromite-lime melts first. When the ratio CaO:Al₂O₃ = 0.5 to 1 in the ternary system CaO-Al₂O₃-Cr₂O₃, the saturation concentration of chromium oxide is normally below 8% wt., depending on temperature. Process slag additionally contains some MgO, SiO₂, and alkalis. The major factors affecting residual Cr₂O₃ content in the process slag are the ratio CaO:Al₂O₃ and the content of aluminum (its activity) in liquid chromium melt. For ~0.5% Al in the reduced chromium metal, the calculated equilibrium concentration of Cr₂O₃ in the slag varies from 0.001 to 0.5% wt.

Besides chromium oxide, formation of “CrO” should be taken into account, especially when the temperature is high and slag basicity is low. In this case, the calculated equilibrium concentration of “CrO” in the slag is about 1% to 2% wt. Experimental measurements, however, indicate that residual chromium content in slag is higher than expected by thermodynamic analysis, which might be limited for kinetic reasons. Some errors in residual chromium content in the slag might be due to the difficulty of metal droplets separation as slag is viscous and possibly heterogeneous (when Cr₂O₃ content is still high).

There are two technological methods of chromium oxide reduction by aluminum: off-furnace smelting and in an electric furnace. The principles of the processes are the same, but the charge composition and smelting procedures are different.

For the off-furnace method, about one tenth of the charge amount is loaded in a melting hearth and topped by the ignition mixture (magnesium and sodium nitrate). Upon ignition and formation of the melt, the rest of the charge is gradually loaded, trying to keep the charge melting rate in the range of 120 ± 10 kg/m²·min. For 1 t Cr, the materials consumption is 1650 kg of oxide, 630 kg of aluminum, and about 140 kg of sodium nitrate (lime content varies depending on the process). After the smelting has finished, the hearth is cooled down for about 10 h and the metal block is separated from the slag and crushed. Such chromium metal normally consists of 98% to 99.5% Cr, up to 1% Al, <0.3% Si, <0.6% Fe, <0.02% C, P, and S respectively, and <0.1% to 2% N. The extraction of chromium from oxide is about 90%.

In the case of special requirements for chromium purity, smelting and casting are carried out in under-pressure chambers (Fig. 8.21). There the charge consists of chromium oxide (>99% Cr₂O₃), aluminum powder, calcium chromate, and CrO₃ as an oxidizer (sodium nitrate is not used in this case). The charge is not loaded directly, but pelletized first at 400° to 500°C with the removal of water and possible carbon. The metal chromium that results from this method has 0.001% to 0.01% N, 0.001% to 0.01% C, <0.08% Fe, <0.03% Si and other nonferrous metals.

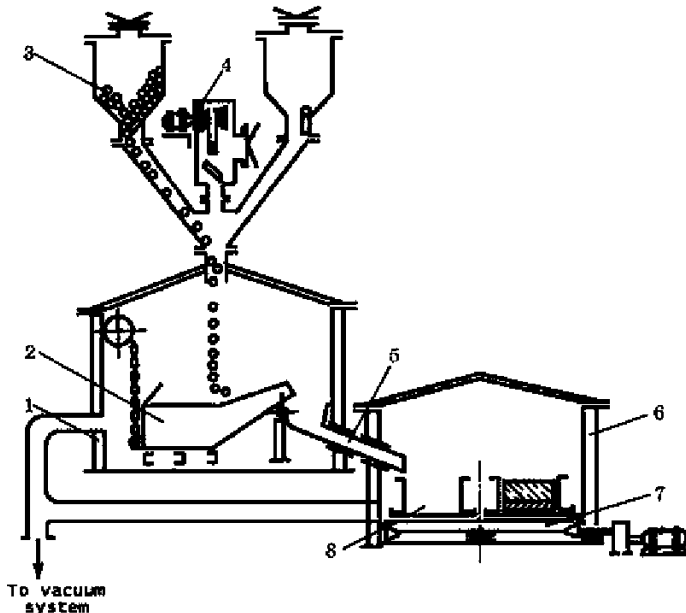


FIGURE 8.21 Two-chamber system for smelting pure chromium under a vacuum or inert atmosphere. 1, melting chamber; 2, tilting smelting ladle; 3, pellets storage; 4, ignition of the charge; 5, tapping channel; 6, casting chamber; 7, rotating table; 8, casting molds.

TABLE 8.16 Charge Composition for Low-Carbon FeCr Smelting Using Aluminum Reduction

Smelting Method	Off-Furnace	Furnace + Block	Furnace + Tapping of the Alloy
Charge materials, kg/t			
FeCr:			
Chromite	2215	1756	1640
Aluminum	710	466	445
Sodium nitrate	411	32	30
Lime		466	335

This technology for smelting of chromium has disadvantages such as low utilization of the smelter, high share of labor, and large consumption of refractories. Another version of this method is adapted to produce high-alumina slag in combined process. The smelting hearth (a tilting reactor) is lined by MgO bricks and has a seed of chromium metal up to 250 mm thick. The ignition proceeds in a method similar to the one described previously, but the melt is poured into an iron mold. Slag corresponding to approximate composition $\text{CaO} \cdot 6\text{Al}_2\text{O}_3$ forms an auto-crucible skull (“frozen lining”). The liquid slag is poured into an electric furnace, where lime and aluminum are added to ensure final chromium extraction.

The method could be also carried out essentially in an electric furnace, without the use of molds. As in the off-furnace method, one tenth of the charge is loaded into the furnace (without the ignition mixture) and the exothermic reactions are initiated by electric arc heating. Then about one fifth of the charge is added and the oxide–lime melt is formed in parallel with the reduction products (chromium melt). After formation of the melt, the rest of the charge is added. Upon completion, the cooling and separation of the chromium metal block is similar to that in the off-furnace process.

A tilting reactor is also used in the process of low-carbon (<0.04% C) ferrochromium (70% to 75% Cr) smelting using aluminum reduction. The main difference with the chromium smelting process described earlier is that chromite concentrate is used instead of pure chromium oxide (Table 8.16). Chromite concentrate for this process has 57% to 60% Cr_2O_3 , <2% SiO_2 , and about 10% Al_2O_3 and 14% MgO. The exothermic heat released during reaction is enough to reach melt temperatures above 2300°C. Chromium extraction using this process is about 90%. When lower-grade raw materials are used, it is still

TABLE 8.17 Typical Slag Compositions for Chromium Processing by Aluminum Reduction

Smelting Process	Cr (no lime added)	Cr (added lime)	Low-Carbon FeCr
Composition, wt. %	45% to 55% $\text{Na}_2\text{O} \cdot 11\text{Al}_2\text{O}_3$, 33% to 45% corundum ($\alpha\text{-Al}_2\text{O}_3$), <1% chromium spinel	75% to 80% Al_2O_3 , 6% to 12% CaO , 6% to 8% Cr_2O_3 <1.5 Na_2O	60% Al_2O_3 , 2% to 4% Cr_2O_3 , 10% to 13% CaO , 20% to 24% MgO , <1% FeO <1.5% SiO_2
Typical slag utilization routes	As raw material for making synthetic slag for ladle steel treatment		As raw material for production of high-alumina refractory cements (70% to 65% Al_2O_3 , 17% CaO)

possible to get standard low-carbon FeCr, but the utilization of chromium is also lower (70% to 80%) ([Eissa et al., 2010](#)).

The slag from aluminum reduction processes has different compositions, depending on the type of smelting method applied and the addition of lime ([Gasik et al., 2009](#)). These differences are summarized in Table 8.17.

8.5 ENVIRONMENTAL ISSUES OF CHROMIUM AND ITS FERROALLOYS PROCESSING

As for all ferroalloys manufacturing processes, ferrochrome and other chromium alloys production is accompanied by the formation of different emissions (dust, fumes, organic compounds, wastewaters). Technological, medical, and sanitation studies have been devoted to the study of the sources of gas and dust formation, the composition of dusts and their effect on the environment, and the health of personnel ([Lyakishev and Gasik, 1998](#); [Stockmann-Juvala et al., 2010](#)).

8.5.1 Human Health Hazards of Chromium and Its Compounds

As a trace element, chromium is necessary in physiological doses to regulate metabolic processes in the body, and a person's daily chromium requirement is 0.2 to 0.25 mg. However, when it enters the body in larger doses, chromium may have a toxic effect on the organism ([Lyakishev and Gasik, 1998](#)).

In a lump state, metallic chromium and all groups of FeCr and FeSiCr are nontoxic in the conditions of their transportation, storage, and use. Dust of metallic chromium and of all chromium ferroalloys might, however, be

hazardous with respect to its degree of action on the human body. Midander et al. (2010) have studied the surface composition of ferrochromium particles ($<63\text{ }\mu\text{m}$) and confirmed that the surface is composed mainly of chromium and iron oxides, but there is also some enrichment of silicon (a few percentages when the bulk content of silicon is 1 wt%). It was shown that FeCr alloys cannot be assessed on their biological response based on pure components data and specific studies are required. Very low amounts of chromium and iron ($<0.15\%$) were released from particles of FeCr and FeSiCr alloys in synthetic biological media of varying pH and composition, and this chromium was released as Cr^{3+} . Disruptions of the external respiratory function (bronchial permeability) as well as nose and skin irritation have been observed historically when workers have been occasionally exposed to high Cr-rich dust levels (Lyakishev and Gasik, 1998). It is unlikely that Cr^{6+} compounds would form in technological smelting processes, unless there is some malfunction or excess oxidation of chromium-rich dust in off-gas tracts and wastewaters.

Inhalation exposure limit values for chromium oxide Cr_2O_3 and metallic chromium were set in the human health hazard assessment of trivalent chromium compounds conducted by the World Health Organization (WHO) (Stockmann-Juvala et al., 2010). The conclusions were based on the repeated dose inhalation study. The limit value for workers has been set at 0.5 mg Cr/m^3 air. Based on the metal release and surface composition of ferrochromium, the same value was suggested as relevant for ferrochromium as well (Stockmann-Juvala et al., 2010).

8.5.2 Dust and Wastewaters Treatment from Chromium Ferroalloys Processing

Many data have been collected for dust emissions of ferroalloys plants (Kasimov et al., 1988). Dust composition varies significantly, not only by process type but also by the gas cleaning method (dry/wet) and the dust sampling position (after furnace, after bag filters, venturries, cyclones, electrostatic precipitators, etc.). In respect to Cr_2O_3 content, dust usually has the highest values when the alloy produced has maximum chromium content and a minimal amount of carbon and silicon. For example, bag filter dust was reported to have 23% to 37% Cr_2O_3 for low-carbon Fe-Cr, decreasing to 13% to 22% for high-carbon FeCr and further $<1\%$ for FeSiCr (Lyakishev and Gasik, 1998). Chromium normally is reported as Cr_2O_3 , although some part might be oxidized to a hexavalent state ($<1\%$ CrO_3). Similarly, silica content is the highest for silicon-rich alloys processes (for FeSiCr up to 85% to 90% SiO_2) and silicon-reduction methods. Other major dust compounds are usually CaO , MgO , Al_2O_3 , and FeO . Naturally when dust has high chromia content, recycling of the dust into the FeCr production (via pelletizing) improves chromium utilization. In this method the dust captured is added to chromite ore concentrate, coke fines, and binder. Pellets are fed into the preheated furnace, and this

might completely utilize chromium-containing dust (Lyakishev and Gasik, 1998).

Whereas dust from the furnaces off-gas forms in preferably reducing conditions, dust from the roasting of pellets or chromite-lime mixture forms in oxidizing conditions. This is the major source of Cr⁶⁺ compounds to be monitored. For instance, calcium chromite–chromate $9\text{CaO}\cdot 4\text{CrO}_3\cdot \text{Cr}_2\text{O}_3$ and calcium chromate CaCrO₄ were detected in the most finely dispersed fractions of the dust of chromite–lime roasting furnaces. Hexavalent chromium is known to be toxic and carcinogenic (lung tumors are typical), unlike trivalent chromium.

Typical wastewaters from the production of various chromium compounds and the treatment of chromite ores contain hexavalent chromium Cr⁶⁺. Existing water quality regulations have strict limits on the permissible contents of chromium of different valences. Different methods have been suggested for the removal of chromium from waters, such as treatment with formic acid (precipitation of insoluble chromium formiate), ferrous sulfate $\text{FeSO}_4\cdot 7\text{H}_2\text{O}$ (as the reducing agent for Cr⁶⁺), alkaline (NaOH) in the organic phase extraction (in the form of Na₂CrO₄), electro-coagulation, high-molecular ion exchange resin, activated carbon (absorption), bacterial method, and so on—even waste tin-plated metal cans (reduction of chromium followed by precipitation with limestone) (Lyakishev and Gasik, 1998).

8.5.3 Fire and Explosion Hazards of Chromium Ferroalloys

In a lump state, all chromium alloys are nonflammable and do not present fire or explosion hazards during their transportation, storage, and use. However, fine dust of the alloys may ignite depending on the degree of dispersion and the concentration of metallic particles. Experimentally it was established that for pure chromium dust aerosol, the flammability limit is 1000 mg/m³ air and ignition temperature 515°C and for FeSiCr (50%Si, 32%Cr) aerosols—1000 mg/m³ air and 625°C, respectively (Lyakishev and Gasik, 1998). On the contrary, no other ferrochrome alloy fines (<50 µm) explode or ignite in air <1000°C and <5000 mg/m³.

REFERENCES

- Bobkova, O.S., 1991. Reduction of metals by silicon. Metallurgia, Moscow, 173 pp.
- Bolgar, A.S., Turchanin, A.F., Fesenko, V.V., 1973. Thermodynamic Properties of Carbides. Kyiv: Naukova Dumka, 271 pp.
- Daavittila, J.M., Honkanen, M., Jokinen, P., 2004. The transformation of ferrochromium smelting technologies during the last decades. Journal of the South African Institute of Mining and Metallurgy, 541–549.
- Decterov, S., Pelton, A.D., 1997. Critical evaluation and optimization of the thermodynamic properties and phase diagrams of the CrO-Cr₂O₃-SiO₂-CaO system. Metallurgical and Materials Transactions 28B, 235–242.

- Durrer, R., Volkert, F., 1972. Metallurgie der Ferrolegierungen. Springer, Berlin, 506 pp.
- Eissa, M.M., El-Fawakhry, K.A., Mishreky, M.L., El-Faramawy, H.R., 2010. The aluminothermic production of extra low-carbon ferrochromium from low grade chromite ore. In: Proceedings of the Congress INFACON-XII. Helsinki, Finland, pp. 431–438.
- Gasik, M.I., Emlin, B.I., Khitrik, S.I., 1970. Thermodynamics of reduction of chromous oxide by silicon. Izv. VUZov SSSR, Chern. Metall. 3, 59–62.
- Gasik, M.I., Lyakishev, N.P., Gasik, M.M., 2009. Physical chemistry and technology of ferroalloys [in Ukrainian]. Dnipropetrovsk: Sistemnye Tehnologii, 494 pp.
- Gasik, M.I., Polyakov, O.I., 1990. Vacuum-thermal refining of ferrochrome. Problems of Special Electrometallurgy 4, 102–107.
- Inoue, A., Matsumoto, T., 1979. Formation of non-equilibrium Cr₃C carbide in Cr-C binary alloys quenched rapidly from the melt. Scripta Metallurgica and Materialia 13, 711–715.
- Kaiser, A., Sommer, B., Woermann, E., 1992. The system CaO–“CaCr₂O₄”–CaAl₂O₄ in air and under mildly reducing conditions. Journal of the American Ceramic Society 75, 1463–1471.
- Karnouchov, V.N., Voronov, Yu., I., Zaiko, V.P., Zhuchkov, V.I., 2001. Technology of low-carbon ferrochrome. Ekaterinburg: IMET UrO RAN, 482 pp.
- Kasimov, A.M., Rovenskii, A.I., Maksimov, B.N., 1988. Dust and gas emissions in production of main types of ferroalloys. Metallurgia, Moscow, 109 pp.
- Kosyrev, K.L., Olsen, S.E., 1995. Silicon and carbon in chromium alloys. In: Proceedings of the Congress INFACON-VII. Trondheim, Norway, pp. 329–338.
- Kurochkin, M.G., 1988. Processing of Chromite Ores. Novosibirsk, Nauka, 141 pp.
- Lyakishev, N.P., Gasik, M.I., 1998. Metallurgy of Chromium. Allerton Press, NY, 626 pp.
- Midander, K., de Frutos, A., Hedberg, Y., Darrie, G., Odnevall Wallinder, I., 2010. Bioaccessibility of ferro-chromium and ferrosilicon-chromium particles compared to pure metals and stainless steel – aspects of human exposure. In: Proceedings of the Congress INFACON-XII. Helsinki, Finland, pp. 43–51.
- Mills, K.C., Grievson, P., 1976. Activities of iron and chromium in liquid Fe-Cr alloys. The Journal of Chemical Thermodynamics 8, 545–550.
- Pavlov, A.V., Zavalishina, V.V., Grigoryan, V.A., Kosyrev, K.L., Chadaeva, O.V., 2010. Research of briquetting process of fine chromium ores. In: Proceedings of the Congress INFACON-XII. Helsinki, Finland, pp. 283–292.
- Rode, T.V., 1962. Oxygen compounds of chromium and chromium catalysts. AN USSR, Moscow, 279 pp.
- Sen, R., Mukherjee, D., Van Vuuren, J.J., DeVilliers, W., Banerjee, S., 2010. Research and development initiatives on the briquetting technology and its commercialization for Richards Bay plant. In: Proceedings of the Congress INFACON-XII. Helsinki, Finland, pp. 275–282.
- Stockmann-Juvala, H., Zitting, A., Odnevall Wallinder, I., Darrie, G., Santonen, T., 2010. Use of read-across in the health risk assessment of ferrochromium alloys under REACH. In: Proceedings of the Congress INFACON-XII. Helsinki, Finland, pp. 35–41.
- Villiers, P.R., Muan, A., 1992. Liquidus-solidus phase relations in the system CaO-CrO-Cr₂O₃-SiO₂. Journal of the American Ceramic Society 75, 1333–1341.
- Witusevich, V.T., Biletskij, A.K., Shumikin, V.S., 1987. Formation enthalpy of melts of the iron-chromium-carbon system. Zh. Fizicheskoi Khimii 61, 623–629.
- Xiao, Y., Holappa, L., 1993. Determination of activities in slags containing chromium oxides. ISIJ International 33, 66–74.
- Zemskij, S.V., Fokin, A.I., 1967. Study of solubility of carbon in solid chromium. Zh. Fizicheskoi Khimii 41, 93–97.

- Zubkov, A.A., Gomonov, P.A., Mogutnov, B.M., Shaposhnikov, N.G., 1990. Formation enthalpy of the sigma-phase in the iron-chromium system. *Zh. Fizicheskoi Khimii* 64, 534–536.
- Zhuchkov, V.I., Zayakin, O.V., Zhdanov, A.V., 2010. Utilization of substandard and off-grade raw materials for chromium and manganese ferroalloys production. In: Proceedings of the Congress INFACON-XII. Helsinki, Finland, pp. 311–315.

High Carbon Ferrochrome Technology

Johan Basson

Outotec South Africa, Centurion, South Africa

Jorma Daavittila

Outotec Finland, Espoo, Finland

Chapter Outline

9.1 Introduction	318	9.2.5 Open Arc DC Furnaces	344
9.1.1 High Carbon Ferrochrome and Its Production Base	318	9.2.6 Other Technology Routes	348
9.1.2 Uses and Applications of High Carbon Ferrochrome	326	9.3 Post Tap Hole Practices and Product Types	350
		9.3.1 Alloy and Slag Tapping	350
		9.3.2 Product Types	351
		9.3.3 Slag Handling and Utilization	353
9.2 Technology Routes for the Production of High Carbon Ferrochrome	328	9.4 Environmental Control and Occupational Health	354
9.2.1 Introduction	328	9.4.1 Environmental Impact of High Carbon Ferrochrome Production	354
9.2.2 Open/Semiclosed Submerged Arc AC Furnaces	331	9.4.2 Occupational Health Hazards	360
9.2.3 Closed Submerged Arc AC Furnaces	335	References	363
9.2.4 Prereduction and Submerged Arc AC Smelting	340		

9.1 INTRODUCTION

9.1.1 High Carbon Ferrochrome and Its Production Base

High carbon ferrochrome represents a group of alloys with a chromium content typically between 60% and 70% and a carbon content typically between 4% and 6%. To meet this specification the alloy requires a chromite ore with a high Cr/Fe ratio (>2). Since the commercialization of the argon oxygen decarburization (AOD) process, it also became possible to produce ferrochrome from lower-grade chromite ores, which are available in countries such as South Africa, India, and Finland. These ores typically have Cr/Fe ratios of 1.5 to 1.6 and result in ferrochrome with a chromium content of 50% to 55% (and recently even below 50%) and carbon content typically between 6% and 8%. Ferrochrome produced from these ores is generally referred to as *charge chrome* and is often included in the broad category of high carbon ferrochrome.

The silicon content in conventional high carbon ferrochrome is normally below 2%, whereas the thermodynamic equilibrium allows charge chrome larger flexibility in terms of silicon content, which can vary between 2% and 5%. The silicon content in the alloy is dependent on the chosen production technology route and the selected slag operating regime.

High carbon ferrochrome is an intermediate product and is used as a feed material in the production of value-added materials such as stainless steel. Typical product types for high carbon ferrochrome are crushed lumpy product with a silvery metallic appearance (Fig. 9.1) and irregular, flaky granulated product with a greenish appearance.

High carbon ferrochrome does not have a single specification, as the ores in different regions differ, which impacts on certain components in the alloy (e.g., Cr, Fe, and C). Furthermore, the smelting process (slag metallurgy or technology route) employed also impacts on particular components in the alloy (e.g., Si, S). Finally, the type of reductant used will also impact on particular components (e.g., P). Therefore, rather than a universal standard specification, producers generally have their own specifications, which depend on their particular process and set of raw materials. Minor elements in the alloy are not normally specified, but could attract premiums from particular specialty steel producers (e.g., Ti).

Nevertheless, there are two broad categories of specifications, which follow the classical distinction between high carbon ferrochrome and charge chrome. These illustrative specifications are shown in Table 9.1.

Sizing specifications are typically in accordance with the client's requirements, which, in some cases, depend on the transport and product-charging infrastructure at their facilities. A lumpy product would typically have a bottom size limit of 6 or 10 mm and top size limit of 50 mm or larger. Material below 6 or 10 mm is classified as fines and normally attracts a discount. Weight adjustments are made for moisture content.



FIGURE 9.1 Lumpy high carbon ferrochrome. (*Source: Outokumpu.*)

Granulated material follows the same size pattern, but the size distribution is not determined by the crushing and screening process but rather by the granulation process. Unlike the cast product, granulated material is porous and could entrap some moisture, which could be viewed as being a process risk for the client. Granulated material generally also has a lower bulk density.

High carbon ferrochrome is historically primarily produced in submerged arc AC furnaces, utilizing a number of process routes as shown in the next section. For obvious cost reasons these production facilities are primarily in countries with sufficient resources of chromite ore, but other factors, such as relatively cheap electricity, may also facilitate production in other countries.

TABLE 9.1 Typical High Carbon Ferrochrome Specifications

Alloy Type	Elements				
	Cr	Si	C	P	S
High Carbon Ferrochrome	60–70	<2	<8	<0.015	<0.02
		2–3	<6	<0.03	<0.04
				<0.05	<0.06
Charge Chrome	50–55	2–3	<8	<0.015	<0.02
		3–4		<0.03	<0.04
		4–5		<0.05	<0.06

The worldwide production of high carbon ferrochrome production is shown in the [Table 9.2](#).

The raw materials for high carbon ferrochrome comprise a combination of suitable chromite ores, reductants, and fluxes.

Chromite ores were described in Chapter 8, which shows the distribution of chromite ore reserves and resources to be heavily weighted toward South Africa, having more than 70% of measured reserves. For high carbon ferrochrome production, lumpy or agglomerated ores are generally suitable for larger or closed alternating current (AC) furnaces, whereas finer ore fractions can either be agglomerated or be used in smaller or open furnaces and also in direct current (DC) furnaces. The application of ores in different processes is described in the following sections. Ore composition has a direct impact on the resultant slag composition and volume, whereas the physical quality of the ore impacts on the metallurgical efficiency in the smelting furnace. The typical distribution of chromite ore production is shown in [Table 9.3](#).

Fluxes are generally required to modify the slag-forming components in the chromite ore into a slag with the appropriate compositional characteristics for the targeted process metallurgy, melting temperature, and suitable tapping properties. A wide range of fluxes is used and often depends on availability of fluxes in close proximity to the particular smelter. Common fluxes are quartzite, dolomite, and limestone.

Reducants are used to reduce the reducible components in the chromite ore to the metallic or carbide states, which form the alloy. A variety of reductants is used in the production of high carbon ferrochrome, and the selected reductants for a particular smelter would depend on the technology process applied, the availability of reductants, and the perceived cost-effectiveness of a particular reductant. Physically competent reductants, such as coke, are deemed to contribute to the formation of a coke bed in the furnace, which is particularly relevant to and beneficial for larger furnaces. Volatiles in reductants can result in tar deposition in off-gas cleaning plants of closed furnaces, which is detrimental to the operation of these plants. Reductants can be classified in terms of their reactivity for a particular process. This classification is often used to select appropriate reductants. The sizing of reductants is specified in accordance with a particular furnace, as it impacts directly on the operating resistivity of the furnace. As each furnace and process has an optimal operating resistivity, the reductant size specification is important. Reductants for high carbon ferrochrome production are normally selected from one or a combination of the following: coke, gas coke, char, coal, anthracite, and even charcoal or petroleum coke in some instances.

The metallurgical efficiency (expressed as % Cr recovery to the alloy) and electrical efficiency (expressed as specific electrical energy consumption) vary in accordance with a number of factors. The mineralogy of the particular

TABLE 9.2 High Carbon Ferrochrome Production 2001–2010 (gross weight—metric tons)

Country	S	2001	2002	2003	2004	2005	2006	2007	2008	2009	2010
Finland	p	236 710	248 180	250 490	264 492	234 881	243 350	241 760	233 550	123 310	238 195
Norway	p	82 600	61 100	—	—	—	—	—	—	—	—
Spain	p	—	—	—	—	—	—	—	—	—	—
Sweden	p	109 198	118 823	110 529	128 191	127 451	136 374	124 403	117 053	31 345	70 576
Turkey	p	41 480	—	24 603	24 956	15 500	55 900	58 846	66 492	36 263	50 878
Total W. Europe		469 988	428 103	385 622	417 639	377 832	435 624	425 009	417 095	190 918	359 649
Albania (e)	o	19 500	22 800	37 800	34 650	34 000	17 040	—	8 390	6 470	22 556
Croatia	p	—	—	—	—	—	—	—	—	—	—
Kazakhstan	p	526 985	629 907	755 146	819 511	907 670	928 177	1 070 000	955 202	938 675	1 073 237
Russia	p	38 099	26 393	76 230	147 164	295 000	304 312	345 092	261 808	135 770	241 080
Slovakia	p	5 371	4 869	1 901	1 712	867	19	—	—	—	—
Total E. Europe		589 955	683 969	871 077	1 003 037	1 237 537	1 249 548	1 415 092	1 225 400	1 080 915	1 336 873
S. Africa	p	1 939 584	2 288 652	2 721 630	2 960 258	2 505 611	2 818 400	3 535 871	3 238 985	2 316 754	3 663 275
Zimbabwe	p	276 963	289 998	261 095	218 065	257 271	213 512	200 833	151 729	73 600	156 118

(Continued)

TABLE 9.2 High Carbon Ferrochrome Production 2001–2010 (gross weight—metric tons)—cont'd

Country	S	2001	2002	2003	2004	2005	2006	2007	2008	2009	2010
Total Africa		2 216 547	2 578 650	2 982 725	3 178 323	2 762 882	3 031 912	3 736 704	3 390 714	2 390 354	3 819 393
Brazil	p	97 245	149 135	185 592	185 572	170 103	140 886	164 486	186 676	101 780	165 963
Total Americas		97 245	149 135	185 592	185 572	170 103	140 886	164 486	186 676	101 780	165 963
China	o	261 621	231 305	423 324	532 000	680 000	858 000	1 060 200	1 283 700	1 510 000	2 212 000
India	p	267 350	311 918	468 677	527 100	611 373	634 200	820 000	750 000	670 000	1 006 000
Iran (e)	o	8 430	15 000	17 000	17 000	17 000	17 000	17 000	10 000	9 000	3 389
Japan	o	104 300	87 700	6 600	5 700	1 900	3 500	300	—	—	—
Total Asia/M. East		641 701	645 923	915 601	1 081 800	1 310 273	1 512 700	1 897 500	2 043 700	2 189 000	3 221 389
Grand Total		4 015 436	4 485 780	5 340 617	5 866 371	5 858 627	6 370 670	7 638 791	7 263 585	5 952 967	8 903 267

S = sources; p = producers; o = industry organizations, others; — = no production; (e) = estimate.

Source: International Chromium Development Association (ICDA).

TABLE 9.3 Chromite Ore and Concentrate Production 2001–2010 (gross weight—metric tons)

Country	S	2001	2002	2003	2004	2005	2006	2007	2008	2009	2010
Finland	p	575 126	566 090	549 040	579 780	571 103	548 713	556 100	613 543	246 817	583 120
Turkey	o	368 012	313 637	229 294	506 421	858 729	1 059 901	1 678 932	1 885 712	1 770 029	2 206 533
Total W. Europe		943 138	879 727	778 334	1 086 201	1 429 832	1 608 614	2 235 032	2 499 255	2 016 846	2 789 653
Albania (e)	p	129 700	72 600	98 000	158 392	119 964	201 120	323 570	203 850	256 000	455 505
Kazakhstan	p	2 056 648	2 349 640	2 781 725	3 290 000	3 581 202	3 366 078	3 687 211	3 614 188	3 544 197	3 702 612
Kosova	p	—	—	—	—	—	—	—	—	2 000	9 500
Russia	p	69 926	74 300	116 455	320 200	772 000	966 095	1 007 181	913 050	416 036	457 124
Total E. Europe		2 256 274	2 496 540	2 996 180	3 768 592	4 473 166	4 533 293	5 017 962	4 731 088	4 218 233	4 624 741
Madagascar	p	51 900	11 000	45 040	77 386	140 847	132 335	122 260	117 115	113 569	115 275
South Africa	p	5 616 949	6 372 739	7 136 666	7 309 575	7 244 112	6 950 279	8 720 330	9 267 848	6 394 815	8 749 875
Sudan (e)	p	20 500	14 000	37 000	26 000	21 654	28 772	15 476	31 890	19 000	65 447
Zimbabwe	p	727 670	734 011	666 357	621 269	819 903	712 908	663 593	484 482	279 366	542 561
Total Africa		6 417 019	7 131 750	7 885 063	8 034 230	8 226 516	7 824 294	9 521 659	9 901 335	6 806 750	9 473 158
Brazil	p	418 423	279 684	510 640	622 755	616 534	604 145	625 627	753 326	725 681	762 000
Cuba	p	26 000	21 150	27 600	42 487	14 729	5 047	—	—	—	—

(Continued)

TABLE 9.3 Chromite Ore and Concentrate Production 2001–2010 (gross weight—metric tons)—cont'd

Country	S	2001	2002	2003	2004	2005	2006	2007	2008	2009	2010
Total Americas		444 423	300 834	538 240	665 242	631 263	609 192	625 627	753 326	725 681	762 000
Australia	p	11 800	132 665	138 826	265 987	241 865	260 112	253 400	224 809	131 941	186 917
China (e)	o	184 500	164 200	197 800	230 000	202 000	220 000	220 000	220 000	280 000	280 000
India	p	1 677 924	2 698 577	2 210 000	2 948 944	3 255 162	3 600 400	3 320 000	3 760 000	3 760 000	3 800 000
Pakistan	p	64 000	62 005	98 235	129 500	148 432	199 000	323 100	320 000	275 000	567 500
Philippines (e)	p	26 932	23 703	12 967	70 001	72 025	85 151	221 481	345 725	88 234	161 271
Vietnam (e)	o	105 026	113 957	143 518	194 909	78 915	73 037	103 828	55 885	37 105	58 675
Total Asia & Austral.		2 070 182	3 195 107	2 801 346	3 839 341	3 998 399	4 437 700	4 441 809	4 926 419	4 572 280	5 054 363
Iran (e)	o	104 905	80 000	120 000	183 171	223 623	244 603	185 758	188 032	255 129	350 537
Oman (e)	o	30 150	27 444	13 000	26 600	72 537	76 716	355 547	908 502	680 216	956 870
U.A.E. (e)	o	10 000	—	—	7 089	—	—	13 066	34 355	6 490	40 484

Total Mid. East	145 055	107 444	133 000	216 860	296 160	321 319	554 371	1 130 889	941 835	1 347 891
Grand Total	12 276 091	14 111 402	15 132 163	17 610 466	19 055 336	19 334 412	22 396 460	23 942 312	19 281 625	24 051 806
End Uses*	2001	2002	2003	2004	2005	2006	2007	2008	2009	2010
Metallurgical	10 768 124	12 688 135	13 825 672	16 261 958	17 833 420	18 324 097	21 476 787	22 565 916	18 307 558	22 837 358
Refractory	162 472	127 861	118 143	101 012	206 992	198 423	142 729	178 869	198 863	139 314
Chemical	1 000 390	863 645	768 027	752 735	510 788	454 856	327 642	530 960	323 397	463 179
Foundry Sands	345 105	431 761	420 321	494 761	504 136	357 036	449 302	666 567	451 807	611 955
TOTAL	12 276 091	14 111 402	15 132 163	17 610 466	19 055 336	19 334 412	22 396 460	23 942 312	19 281 625	24 051 806

S = sources; p = producers; o = industry organizations, others; — = no production; (e) = estimate; (r) = revised. Excludes production of concentrate derived from SA UG2.

*Production figures assumed 100% metallurgical when breakdown not available.

Source: International Chromium Development Association (ICDA).

chromite ore plays an important role, and the selected technology route is also a strong determinant. Furthermore, the selection of reductants and slag metallurgy will also impact on the process efficiencies. Illustratively the example of a mass and heat balance for high carbon ferrochrome (HCFeCr) production in a large closed furnace with preheated feed with typical process results is shown in [Table 9.4](#).

This mass and energy balance requires information on the ratios and analyses of feed materials, the furnace power input, the preheater outlet temperature, and the assumed silicon content in the alloy and calculates the distribution of elements to the slag and alloy phases, the electrical energy requirement, and the expected product masses (alloy, slag, and dust). Mass and heat balance models can be used to calculate the ratio of feed materials, the electrical heat requirements, and the efficiencies of a particular process, when actual results are used.

9.1.2 Uses and Applications of High Carbon Ferrochrome

Chromium is an essential alloying element for the production of all types of stainless steels and special alloy steels, on account of the special properties chromium imparts to these materials. The use of low carbon ferrochrome and ferrosilicochrome for chromium addition was common practice until the 1960s, the vacuum argon decarburization (VOD) process being commercialized in 1964 and the AOD process in 1968. In 1972, the Creusot-Loire Uddeholm (CLU) refining process was developed. These three processes, in particular the former two, introduced a revolution in the alloy steel production technologies. Quite a few other similar and modified processes have been developed subsequently.

With the advent of AOD and VOD technologies, the use of high carbon ferrochrome, for introducing chromium into steel with much improved process economics, was established. However, with the worldwide standardization of these technologies, not only the use of high carbon ferrochrome was established; it was also established that lower grades, with even less than 50% chromium content, can be efficiently used in the production of stainless steels and other special alloy steels. This resulted in the arrival of charge chrome as the most economical and established route of chromium addition to steels. Because the charge chrome production technology permits the use of lower-grade chromite ore, charge chrome was accepted as a suitable alloy for stainless steel production, in response to the depleting resources of high Cr /Fe ratio lumpy chromite ore.

High carbon ferrochrome is primarily used in the production of stainless steel. More than 90% of high carbon ferrochrome is used in the production of stainless steel ([International Chromium Development Association \[ICDA\], 2011](#)). The majority of the balance is used in the manufacturing of special steels (including high chromium steels).

TABLE 9.4 Typical Mass and Energy Balance for a HCFeCr Furnace

Mass and Energy Balance for Large Closed Furnace with Preheating										
Furnace power										56 MW
Preheated feed temperature										492°C
Cr	Fe	C	Si	SiO ₂	MgO	Al ₂ O ₃	CaO	Cr/Fe	T°C	Flow, t/h
Feed										
Pellets	30.43	19.13	0.00	3.97	10.60	13.03	0.47	1.59	492	26.86
Lump ore	24.41	13.73	0.77	11.17	16.10	11.60	1.20	1.78	492	15.11
Coke	0.65	87.30		6.27	0.10	3.07	0.33		492	8.64
Quartzite				95.33	0.37	0.83	0.33		492	5.54
Products										
Alloy	53.61	34.86	7.10	3.91				1.54	1580	18.40
Slag	8.81	3.83	0.72	31.33	23.66	24.92	1.58	2.30	1680	22.20
Dust	7.98	6.55	17.24	26.95	17.87	6.24	0.80	1.22	900	0.22
Gas phase			CO	CO ₂	H ₂	H ₂ O	N ₂	O ₂	T°C	Flow, Nm ³ /h
Furnace gas			84.82	6.01	5.96	0.40	2.81	0.00	900	12 654
Burner			83.45	5.91	5.87	2.00	2.77	0.00	45	3 215
Balance			83.45	5.91	5.87	2.00	2.77	0.00	45	9 646
Total furnace feed	469 700 tpa			Slag/alloy				1.21		
Total slag production	187 800 tpa			Total dust production				1 900 tpa		
Total alloy production	155 400 tpa			Paste consumption				1 173 tpa		
Cr recovery to alloy	84%			Specific energy consumption				3 070 kWh/t		

9.2 TECHNOLOGY ROUTES FOR THE PRODUCTION OF HIGH CARBON FERROCHROME

9.2.1 Introduction

When a particular technology route is selected, a number of considerations should be taken into account. However, previous practice or the known status quo in a particular organization often plays a determining role in the selection of a process route. The substantially different outcomes of different technology routes are therefore not always fully acknowledged in the decision-making process. The financial return on a particular capital investment primarily depends on the operating cost of the selected technology route and is normally less dependent on the initial capital investment cost.

Various technology routes are available for the production of high carbon ferrochrome. Some of these routes are established, whereas others are relatively recently commercialized. Intellectual property constraints and even patents make some of the technology options less accessible than others for outsiders. Although there are a large variety of technology routes, with a multitude of varying operating features, there are probably four groupings that cover almost all commercial processes for the production of high carbon ferrochrome. These groupings are as follows:

1. Open/semiclosed submerged arc AC furnaces
2. Closed submerged arc AC furnaces
3. Prereduction followed by closed submerged arc AC smelting
4. Open arc DC furnaces.

The considerations for technology selection are often determined by factors such as access to a particular technology, availability of raw materials, cost of electricity, and environmental and occupational health legislation. History has shown that companies most often continue with known, tested technology routes that fit into their existing portfolio. The industry seems to be risk averse and investments are seldom made in technologies that are perceived to be unproven. Few companies are prepared to assume the risk of investing in breakthrough technologies. Eventually most expansion decisions are strongly influenced by the cost of the investments, and not necessarily by the operating cost benefits associated with the selected technology.

A number of outcomes for a chosen technology route decision are hereafter briefly discussed to demonstrate what the expected results could be for different decisions. When efficiencies are quoted, typical results with South African chromite ores are used illustratively. Ores with different reducibility characteristics could result in different quantitative results. However, relative efficiencies remain valid.

9.2.1.1 Metallurgical Efficiency

On open furnaces with low-quality raw materials (e.g., unscreened lumpy ores), Cr recoveries to the alloy are generally below 80%. With screened lumpy ore,

together with briquetted fines, the chrome recovery should increase to about 80%. When lumpy and fine ore are replaced by pellets, the Cr recovery responds favorably and increases to about 85%. When the smelting process is preceded by prereduction, this efficiency parameter improves further to about 90%. A similar high level of Cr recovery is achieved when fine ore is smelted in the open bath of a DC arc furnace. Given the fact that the return on any investment is primarily determined by the operating cost, it is clear from these numbers how investment decisions could potentially benefit from higher-efficiency processes.

From the preceding discussion it becomes obvious that metallurgical efficiencies are directly related to the quality of the feed material directed to the furnace. In general, the better the physical strength of the ore are, the more favorable the furnace smelting conditions and resultant metallurgical efficiencies would be. Chromite ore is often friable and the mined product contains varying percentages of fine ore. To prevent the adverse effect of these fines in the furnace, the fine ore requires some form of agglomeration. The most common agglomeration processes are briquetting and pelletizing. Briquetting normally takes place at low temperatures and utilizes a binding agent such as lime and molasses, starch, or cement. Normally the binding process is not followed by a form of induration. The general shortcoming of using briquettes in a furnace is that the briquettes lose their strength at elevated temperatures, resulting in decrepitation and fines generation in the furnace. On the other hand, good-quality sintered pellets generally have good physical properties even at elevated temperatures and are internally porous, which results in metallurgical reduction performance even better than lumpy ore. Ores are sometimes classified in terms of a refractory index (RI), which indicates the ore's durability at the high temperatures in the reaction zone of the furnace, and therefore also its ability to take part in refining reactions within the molten slag bath.

The chosen slag metallurgy will also impact on the metallurgical efficiency. It is well documented that processes operating under highly basic slag conditions result in improved reduction of Cr_2O_3 , and therefore improved chromium recoveries. However, highly basic conditions reduce the electrical resistivity in the furnace burden, which may impact adversely on furnace operating conditions and power input. Highly basic conditions also favor desulfurization of the alloy and favor the production of a low Si alloy. On the other hand, processes operating under highly acidic slag conditions also result in improved reduction of Cr_2O_3 and therefore improved chromium recoveries. However, operating outcomes that are generally adversely affected by highly acidic conditions are slag/alloy separation, slag viscosity, and refractory lining wear. From these observations it is therefore clear that process metallurgy selection will also impact on equipment and process design.

9.2.1.2 Electrical Energy Efficiency

On smaller, open furnaces operating with unscreened raw materials, specific energy consumption is suboptimal for reasons explained later and could be as high as 4500 kWh/t. This number will improve substantially when screened

lumpy ore is used and when the furnace size is increased. When preheating is introduced to the pelletized feed to a large, closed submerged arc AC furnace, this efficiency will improve to about 3100 to 3200 kWh/t, depending on the level of preheating. When the smelting process is further preceded by prerection, the efficiency improves further to below 2500 kWh/t—which could be reduced further to below 2000 kWh/t when the level of prerection is maximized. It should be clear what the implications of these different levels of electrical energy efficiencies are in an environment of rapidly increasing energy costs.

It is therefore apparent that electrical energy efficiencies depend on a number of factors, of which the size of the furnace, the quality (including chemical composition) of the raw materials (especially the type of agglomeration), and the utilization of preheating or prerection are the most important. It must also be understood that the total energy requirement for the high carbon ferrochrome production process is driven by the process thermodynamics and remains fundamentally the same, regardless of the selected process route. What could change is the source of energy, which can either be electrical energy or some form of chemical energy (e.g., heat from the combustion of a type of fuel). This should be taken into account when prerection processes are considered.

9.2.1.3 Economy of Scale

If the large variation in furnace sizes (and capacities) from 5 to 135 MVA is taken into account, it will become clear that economy of scale benefits in terms of investment cost will apply, but normally the metallurgical and electrical efficiencies also improve as the furnace size increases. The general trend is still toward larger furnaces, and older, small furnaces are gradually being replaced with larger ones. A 135 MVA submerged arc AC furnace, such as the furnace commissioned by Outokumpu in Finland in 2012, can produce close to 250 000 tons of high carbon ferrochrome annually—more than the total plant output of many of the smaller plants. Larger furnaces require skilled operating personnel and strict raw material quality control compared to smaller furnaces. The choice therefore becomes a risk/return decision.

9.2.1.4 Capital Investment

There is a marked contrast in capital investment cost when the simple layout of a conventional open furnace is compared to a vertically integrated complex with facilities for ore preparation, induration, prerection, and smelting. Understandably, the contrast in investment cost has to be weighed against the benefits in operating efficiencies and economies of scale. In countries or areas where the chromite ore is predominantly fine, the ferrochrome producer has little choice but to consider technology routes that can

handle fine ore, such as DC arc smelting and routes based on ore agglomeration, or even prereduction. These technologies invariably require larger capital investment. However, as will be shown later, the appropriate parameter to consider is not the capital investment cost but the investment cost per ton of product.

9.2.1.5 Occupational Health

It is generally understood that open and semi-closed furnaces produce an order of magnitude more hexavalent chromium in the off-gas than closed furnaces due to the oxidizing conditions favoring hexavalent chromium generation. The occupational health effects of hexavalent chromium are described in more detail later. Regulatory constraints and occupational health risks could become a determining factor in terms of approval for new projects (as is the case in South Africa).

Summarized, some of the outcomes for the different process selections are shown in [Table 9.5](#). Note that numbers used in the table are based on the use of similar, comparable raw materials. The relative values are relevant, although the quantitative numbers may vary among countries and types of raw materials.

Furnace design principles and parameters apply to all ferroalloy furnaces, but the specific design parameters differ in accordance with the particular alloy. These parameters include dimensional and operating specifications such as the following:

1. Furnace diameter and height
2. Electrode spacing (pitch circle diameter [PCD])
3. Electrode diameter
4. Furnace operating power, resistivity, and electrode current.

In general, substantial benefits are to be gained when furnace size is increased to optimal. These benefits include economy of scale benefits, thermal and metallurgical efficiency benefits, and capital investment cost benefits. On the other hand, operating large furnaces requires increased levels of sophistication and quality control. Examples of these constraints are stringent raw material quality control and challenging electrode design and management. A typical schematic view of a submerged arc furnace is shown in [Figure 9.2](#).

The four representative groupings of technology routes are separately discussed in more detail in the following sections.

9.2.2 Open/Semiclosed Submerged Arc AC Furnaces

Open or semiclosed furnaces represent the most common, original type of submerged arc furnaces for the production of ferroalloys. These furnaces are generally smaller (typically <30 MVA) than closed furnaces. A large number of these furnaces have been in operation for a long time and originate from the early days of ferroalloy production. China and India are countries with

TABLE 9.5 Comparative Results for Different HCFeCr Process Routes

Type of Furnace	Metallurgical Efficiency (%Cr Recovery)	Specific Energy Consumption (kWh/t)	Economy of Scale (maximum size of single furnace/output from single furnace)	Occupational Health Indicator (indexed Cr ⁶⁺ generation)
Open AC furnace (without raw material screening)	70–75	4300	30 MVA/50 ktpa	10
Closed AC furnace (with pelletized feed and preheating)	83–88	3200	135 MVA/240 ktpa	1
Prereduction followed by closed AC furnace	88–92	2400*	66 MVA/160 ktpa	1
Closed DC arc furnace	88–92	4200	60 MW/110 ktpa	1

*Only electrical energy in the furnace; excludes fuel energy associated with prereduction kiln.

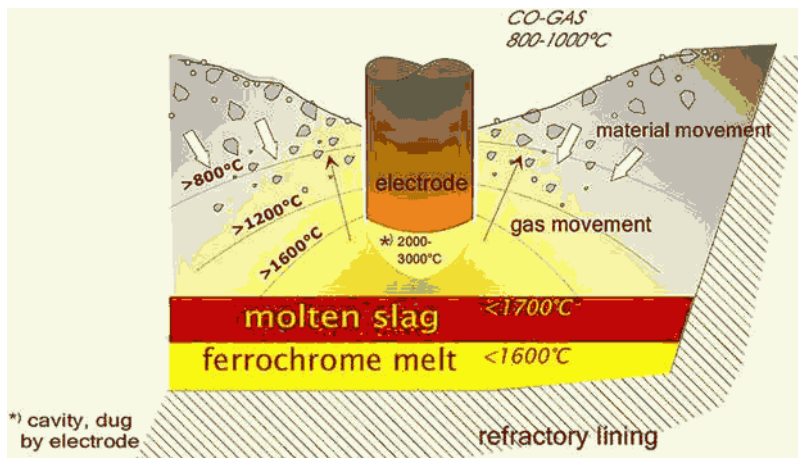


FIGURE 9.2 Schematic view of an AC submerged arc furnace. (Source: Outotec.)

a significant number of small, open furnaces. Other common characteristics of these furnaces are simple raw material feed systems, lack of gas cleaning equipment, and manual labor practices.

One of the most relevant characteristics of these furnaces is that they have less stringent requirements in terms of raw material quality and can successfully operate with high fines content in the feed materials. As a result of the lower-quality raw materials, open furnaces generally require frequent rabbling of the furnace bed to improve bed porosity and to break crust and bank formation. Eruptions due to the furnace bed condition are common on these furnaces. Rabbling of the furnace bed is done by means of a variety of methods, ranging from manual rabbling to mobile rabbling machines.

Generally, open furnaces have lower thermal and metallurgical efficiencies. Thermal inefficiencies result from suboptimal heat transfer in the furnace (due to erratic gas flow patterns) and higher heat losses through the furnace bed and sidewalls. Metallurgical inefficiencies also result from suboptimal gas flow and heat transfer in the furnace. Furthermore, a portion of the finer-sized raw materials (notably fine ore) is tapped with the slag, resulting in a substantial amount of unreduced material lost in the tapping process. This causes increased metallurgical chromium losses and could result in difficult tapping conditions.

Benefits of the operation of open furnaces are generally the simplicity of the operation (which could exclude screening of raw materials), easy access to the furnace bed and electrode equipment (which assists with maintenance), and visibility of the furnace bed (which provides a visual indication of the condition of the process). A further benefit is the low capital investment cost due to the simplicity of the layout and lack of sophisticated control systems. A typical flow diagram for this production process is shown in Figure 9.3.

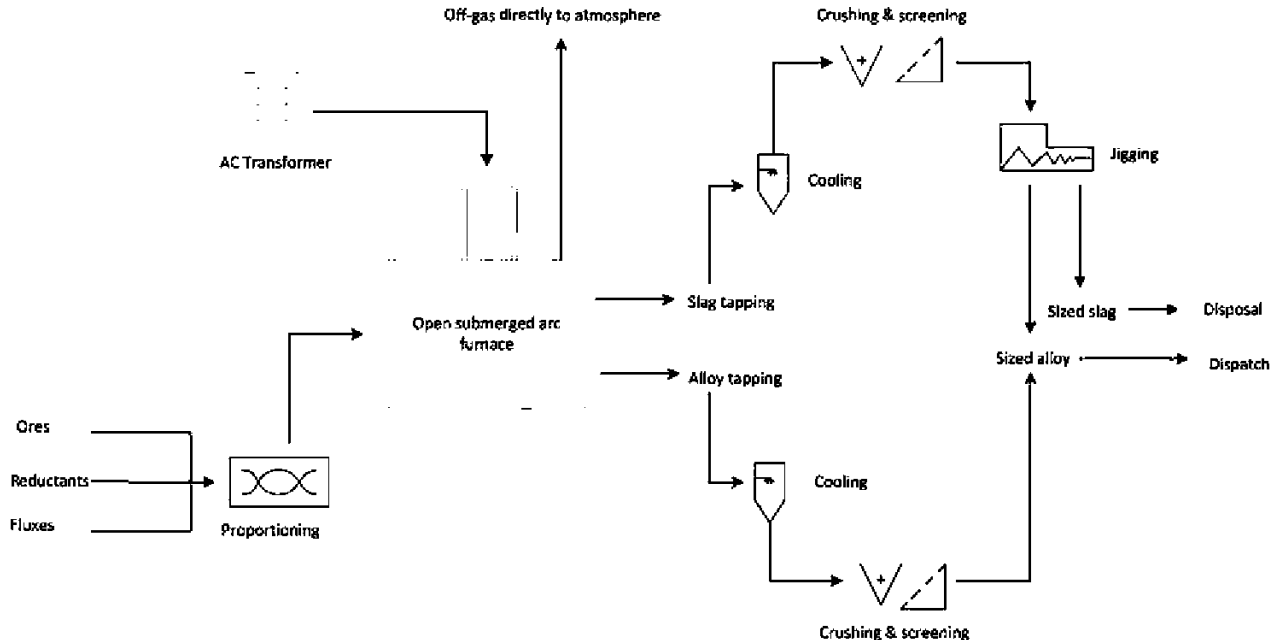


FIGURE 9.3 Typical flow diagram of an open furnace process route.

9.2.3 Closed Submerged Arc AC Furnaces

This technology route generally consists of submerged arc furnaces that are closed and generally larger (>30 MVA). A closed furnace has an airtight roof that prevents air ingress and combustion of the process gases. The gas scrubbing equipment is therefore sized for lower gas volumes than for open furnaces, and the process gas, consisting of primarily carbon monoxide (CO), can be utilized for its calorific value. Furnaces of up to 135 MVA are in operation, although few furnaces in operation presently actually exceed 78 MVA.

The size of these furnaces places constraints on the design and operating parameters. When Söderberg (self-baking) electrodes reach diameters approaching or exceeding 2000 mm, it becomes difficult to design operating conditions for effective baking of the electrodes. Also, due to the physical size of the furnace, it becomes critical to establish a porous furnace bed for effective process gas flow, which can only be achieved by stringent raw material quality requirements. Pelletized ore feed and coke form important success factors for large, closed furnace operation. The quality of the ore is essential for good process efficiencies and for the stable operation of the furnace. The raw material to the closed AC smelting furnace must therefore be in agglomerated or screened, lumpy form. The benefits of large, closed furnaces, when overcoming the mentioned obstacles, are economy of scale benefits (low unit capital investment cost) as well as improved metallurgical and electrical efficiencies.

An appropriate example of successful integrated large closed AC furnace operations can be found in the Outotec ferrochrome process (Fig. 9.4), as it covers all the principles for ore agglomeration, waste heat utilization, and maximization of furnace size. The most representative plant utilizing this technology is Outokumpu's ferrochrome plant in Tornio, Finland. The core of the following process description was provided by Outotec in November 2011.

Outotec's ferrochrome process consists of the smelting of high carbon ferrochrome in a closed and sealed submerged arc furnace, using mainly sintered pellets as raw material, preheating the furnace feed in a shaft kiln located above the furnace, cleaning the furnace gas in two venturi scrubbers and further in a CO filter (optional), and utilizing a portion of the produced CO gas for preheating and sintering of the pellets.

Raw materials to the smelter are chromite pellets and lumpy ore, coke as reductant, and quartzite for fluxing. Other fluxing agents may also be used depending on the ratio of slag forming components in the ore.

First, the pelletizing and sinter process for the chromite ore is briefly described (Fig. 9.5). Feed material is fed to the grinding mill to homogenize the raw material mixture. Coke is preferred as carbonaceous material, although char and gas coke are also successfully used as the main external energy source in the sintering process. Fine coke (<4 mm) is added to the ore concentrate before milling. In the milling circuit the concentrate mixture is wet milled in an

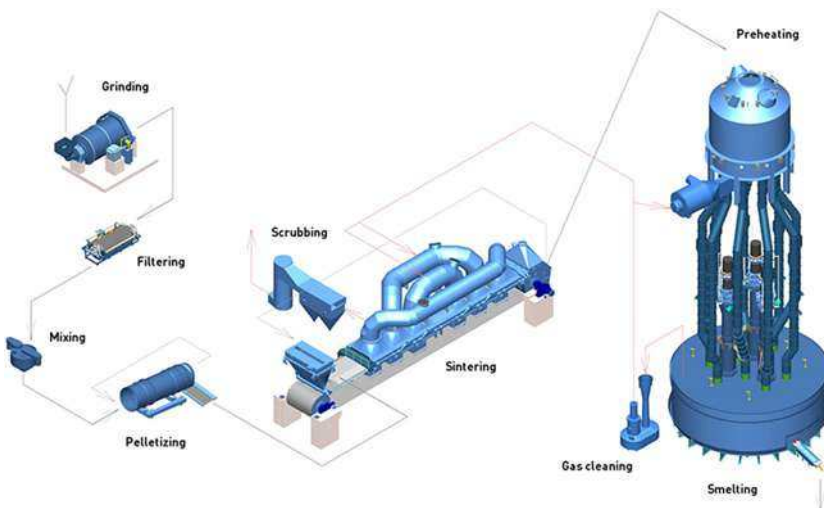


FIGURE 9.4 Flow diagram of the Outotec ferrochrome process. (Source: Outotec.)

open circuit ball mill (without recycling). The purpose of milling is to mill the mixture to a particular grain size distribution, which is suitable especially for pelletizing, but also for sintering. The grain size distribution required is >80% of the fraction less than 74 µm. Ceramic filters (i.e., capillary disc filters) are used to dewater the slurry from the mill into a filter cake. The moisture content of the filter cake is normally about 8.5% to 9%.

The filter cake is collected in a number of filter cake bins, which are equipped with disc feeders to measure and control the feed of material to the pelletizing circuit. Bentonite is used as a binding agent in the pelletizing process and is added in a very fine powder form to blend homogeneously with the filter cake. Dust from the pelletizing plant dust scrubber can be recycled and blended with the milled material. This dust is already in an oxidized form and its addition to the mill has an adverse effect on sintering. The total feed of already sintered recycling material must therefore be limited to a maximum range of 3% to 4% of the concentrate to ensure the production of good quality pellets. The proportioned materials are then well mixed in a mixer before pelletizing in a pelletizing drum, resulting in pellets with an average diameter of 12 mm.

The sintering furnace is a multicompartiment unit through which the green pellets are carried on a perforated steel conveyor belt. The counter-current flow of cooling gases carries waste heat from sintered pellets to those entering the front-end compartments. Sintered pellets are used as a bottom layer on the steel belt to protect it from excessive temperatures. The temperature of the bed is gradually increased to the sintering temperature, which, depending on the mineralogy of the ore, is about 1400° to 1500° C.

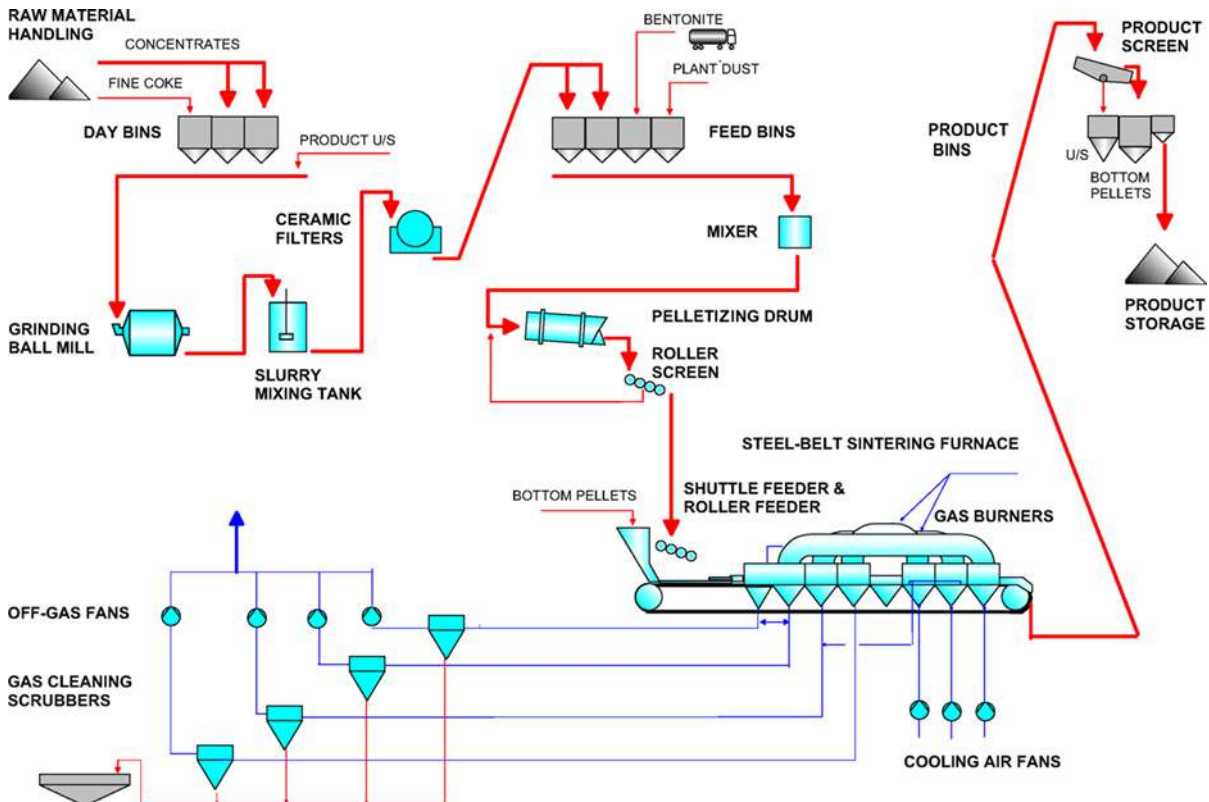


FIGURE 9.5 Flow diagram of the Outotec pelletizing and sinter process. (Source: Outotec.)

Sintered pellets are cooled in three cooling compartments by blowing air through the bed from below. Fresh sintered pellets are, together with bottom layer pellets, discharged onto a belt conveyor transporting them to pellet bins via a screening plant. During typical operation the produced pellets are screened at +6 mm and fed to fill the bottom layer feed bin at the front end of the sintering machine. The final product pellets are conveyed to the smelting furnaces.

Secondly, the ferrochrome smelting process is briefly described (Fig. 9.6). The ferrochrome smelting is based on using sintered chromite pellets as the main chromite source, blended with lumpy ore, although a 100% pellet feed can also be used. Pellets are typically produced from concentrate, which results in a high chromite content in raw material, lowering the slag-to-metal ratio. The chemistry of the chromite ore is also altered by preoxidation in the sintering process, which enhances the smelting step. The chromium recovery is improved and specific energy consumption lowered during the smelting of pellets compared to conventional smelting of lumpy or fine ores.

Good-quality metallurgical coke with a high fixed carbon is preferred, although char and gas coke are also successfully used in some operations. The use of coal and anthracite is not recommended because of the formation of tar in the preheating kiln and in the closed smelting furnace, which also adversely affects the furnace gas production and quality. The strength of the coke is

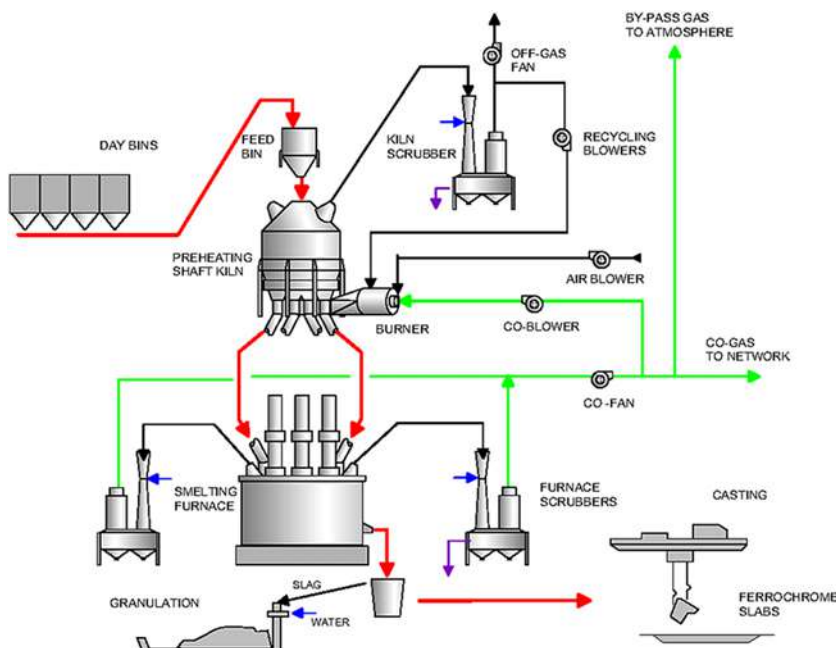


FIGURE 9.6 View of an HCFeCr furnace with a preheater. (Source: Outotec.)

important so that it can move through the preheating kiln and feeding systems without decrepitation. The silica content of the quartzite must preferably be high to minimize other slag-forming components. The physical quality must be such that it can be heated without decrepitation. The smelting process is based on an acidic slag composition. Some limestone or dolomite may have to be added for fine-tuning of the slag chemistry.

The batching system is critical for controlling the feed mixture to smelting; it has to be accurate and reliable. All raw material corrections for smelting are made in the batching station before preheating. The process after batching is a closed system.

The purpose of preheating is to eliminate the moisture from the feed charge mixture and to calcine and preheat it to as high a temperature as possible without igniting or oxidizing the coke. The Boudouard reaction ($C(s) + CO_2(g) \leftrightarrow 2CO(g)$), is the limiting factor. The preheating temperature in the shaft kiln is limited to 650° to 700°C depending on the reactivity of the coke, but the average temperature of the hot outlet material is typically about 450° to 550°C. The thermal power in preheating during normal operation is about 8 to 11 MW for a large furnace.

The Outotec preheating shaft kiln is a steel silo located above the smelting furnace (see Fig. 9.6). The material flows freely through the charging tubes to the smelting furnace. The material in the tubes and in the silo forms a gas seal between the gas spaces in the furnace and in the kiln. The charge material is preheated counter-currently by hot gas that is produced by combusting CO (carbon monoxide) gas in a separate combustion chamber. Preheating generally decreases the electrical energy consumption in the smelting furnace, but it also increases the CO content of the furnace gas and stabilizes the resistivity of the burden. Preheating improves the operation, production, and safety of the smelting process.

Smelting is carried out in a closed submerged arc furnace. The smelting furnace is closed with a flat roof. The furnace is sealed so that there is no combustion of gas and no gas leakage to the surroundings. The CO fan is used to control the pressure in the furnace under the roof to atmospheric level to avoid leakages. The electrode system comprises self-baking Söderberg electrodes, which are not moved extensively.

The specific energy consumption in the smelting furnace depends on the raw material quality. Good, sintered pellets represent high-quality feed that gives stabilized smelting conditions, high chromium recovery, and low specific energy consumption. The lumpy ore, which accompanies the pellets, must also be of high quality. With an increasing amount of fines and dust, the operation becomes unbalanced, which results in decreased power input and thus decreased production. High-quality pellets and lumpy ore allow high operational efficiency and facilitate the successful use of large furnaces.

The furnace is lined with highly heat conductive carbon-based freeze lining. The furnace shell is water-cooled and the furnace bottom is air-

cooled. The freeze lining forms a protective slag skull inside the surface of the lining. Because of skull, the life of the heat conductive linings is typically considerably higher than that of traditional linings. The thickness and profile of the furnace linings are monitored with a sophisticated lining monitoring system.

CO gas is formed in the furnace during reduction. The gas is extracted to two high-pressure venturi scrubbers. The CO gas is further cleaned with CO gas filters, and can then be widely used for heating purposes in the plant or be sent to a CO holding vessel. A CO holder in the network stabilizes the pressure in the line so that all the CO gas can be utilized effectively. The CO-rich off-gas can be used in electricity generation.

The produced ferrochrome and slag are tapped intermittently every 2 to 2½ hours into a ladle or double-ladle system. The alloy settles in the ladles while the slag overflowing the ladle flows via the slag launder to a water granulation installation. The granulated slag is then transported to a stockpile. The slag does not contain significant amounts of alloy or any harmful components. It is directly usable for secondary application purposes.

The alloy ladle is skimmed and the alloy is cast on an alloy fines bed. A fork truck lifts the solidified alloy as big ingots for cooling and for further sizing. The product is crushed in a jaw crusher to a sized product. The ladles are preheated with CO gas to minimize the scull formation.

The skimmed material, spillages, and sculls from the launders and ladles contain alloy. These are treated in a recovery plant, and the recovered alloy fines are returned to the cast beds.

The scrubber slurries contain some cyanides originating from the closed furnace reducing gas atmosphere. The overflow from the thickener is recycled to slag granulation for evaporation and decomposition of the cyanides. Virtually no hexavalent chromium is formed due to the reducing gas atmosphere in the furnace. Water from the granulation goes to settling ponds for recycling. Sand filters are used for cleaning of the recycled water.

9.2.4 Prereduction and Submerged Arc AC Smelting

The history of ferrochrome production includes a substantial number of initiatives to develop a successful prereduction process. These efforts range from laboratory scale testing to piloting and full-scale production. It is, however, accurate to state that most of these initiatives did not result in viable commercial processes. To develop a totally new process requires a strong commitment by an organization to fund the development work, as well as the patience for and financial commitment to the commercial optimization, which could take a long time—often more than a decade.

A number of development projects involved shaft furnaces. Professor Gasik (Sr.) performed extensive test work in Ukraine on blast furnaces in the 1970s, whereas Outokumpu performed selective iron reduction in shaft kilns as far

back as the 1960s. Other projects involved converters and fluidized bed reactors. Kawasaki performed prerduction of chromite ore successfully in a fluidized bed reactor, using methane and hot reaction gases. Outokumpu successfully demonstrated agglomeration and prerduction in a rotary kiln the 1970s.

In the 1980s, Krupp Industrietechnik performed successful prerduction of nonagglomerated chromite in a rotary kiln. This chrome direct reduction (CDR) process was subsequently commercialized by Middelburg Steel & Alloys in the late 1980s and this huge 120 000 tpa (throughput) plant was operated with mixed success during the 1990s. The cyclicity of the ferrochrome market and a lack of long-term commitment to resolve the remaining operational challenges resulted in this operation being discontinued.

The most successful chromite prerduction process proved to be the solid state reduction with carbon (SRC) process, developed by Showa Denko and successfully operated by their JV company with Nissin Steel, Shunan Denko, in Japan for a long period in the 1970s and 1980s. The technology was successfully replicated by CMI on its plant at Lydenburg, South Africa, in the mid-1970s. This plant is still operational under its present owner (Xstrata), albeit in a slightly modified fashion (referred to as the Premus process). Xstrata has subsequently built another plant (Lion Ferrochrome) in Steelpoort, South Africa, based on this technology, which has been in operation since 2007. A duplicate plant of Lion Ferrochrome was under construction in 2012. It should be mentioned that the original SRC plant in Japan operated at high levels of Cr metallization (approximately 70%), whereas the plants built in South Africa are operating at lower levels of Cr metallization (approximately 50%).

The Xstrata Premus process is used as the reference technology in this section. This technology is a slightly modified version of the SRC technology, originally owned and patented by Showa Denko. The core of the following process description was provided by Xstrata Alloys in November 2011.

The Xstrata plants at Lydenburg and Steelpoort (Lion) in South Africa are the only commercial, large-scale high carbon ferrochrome plants worldwide utilizing a prerduction step. Chromite ore concentrate, reductant (typically coke, but also char or anthracite), and binder (typically bentonite) are proportioned and dried prior to milling. The milling operation is closely monitored in order to ensure that the discharge is appropriately finely ground with a typical sizing of well over 90% less than the 74 µm required to achieve the requisite green pellet strength and subsequent sintering and prerduction performance.

Despite the relative differences in the work index of ore and reductant, the relatively large proportion of reductant added at lower density yields ultimately a similar size distribution of major constituents in the mill discharge, thus enabling sound pelletizing characteristics and appropriate prerduction kinetics.

Following dry milling, the fine milled material is moistened and pelletized on large diameter pan pelletizing units, yielding consistent, compact pellets

typically controlled between 12 and 18 mm in diameter. Close control of the pelletizing operation is important to ensure appropriate characteristics of both the moist green pellets together with their subsequent performance through the drying and preheating stages of the process, thus ensuring that the pellets entering the kiln have sound integrity and suffer minimal degradation during subsequent exposure to the high temperature prereduction environment of the kiln.

The prereduction process remains the core element of the Premus process. Conducted in 80 m long kilns, 5 m inside diameter, at temperatures exceeding 1300°C, the carbon-rich pellets progressively increase in temperature to a point where reduction of initially Fe species and subsequently Cr species can take place. The design of the kiln and integration of kiln and furnace units is such that operational conditions can be varied to optimally suit prevailing electricity availability and pricing conditions to ensure the maintenance of the most cost-effective operation possible. In this regard, kiln energy input is maintained at an optimally high level, with pellet ore and reductant proportion tailored to suit conditions of either higher degrees of metallization in the kiln, with corresponding minimum electrical energy requirement in the final smelting stage (a strategy suited to constrained supply of high-priced electrical energy), or more typically maximized kiln throughput at moderate levels of metallization to optimally complement the smelting capacity of the large 63 MVA downstream submerged arc furnaces, with corresponding high-alloy output rates.

At all times, the process is typically operated around a strategy that enables maximum energy input to the kilns to be maintained, with up- and downstream adjustments in operation to minimize overall alloy production costs.

Following prereduction, the hot prerduced pellets are discharged into refractory lined conveyor bins, where the residual components required for smelting (fluxes and carefully controlled carbon makeup requirements) are added and the hot charge is transferred into refractory lined furnace feed bins, located a relatively short distance above the furnace roof.

The hot charge containing prerduced pellets descends through refractory lined feed chutes into the closed furnace.

The raw material mixture makeup and hot transfer arrangement including furnace bins and transfer chutes are so arranged to ensure that the maximum practical retention of heat in the feed entering the furnace is achieved.

Although the furnace configuration is essentially that of a typical high-powered submerged arc smelter unit, specific allowance has been included in the design to cater to the different characteristics of a fully pelletized and prerduced charge under typical operating conditions, but with sufficient flexibility to accept cold charged prerduced pellets and even lump ore if required. The process is shown schematically in Figure 9.7.

Even though the Premus process capital cost is higher than the capital cost for a conventional process, it is claimed to have the lowest capital cost per

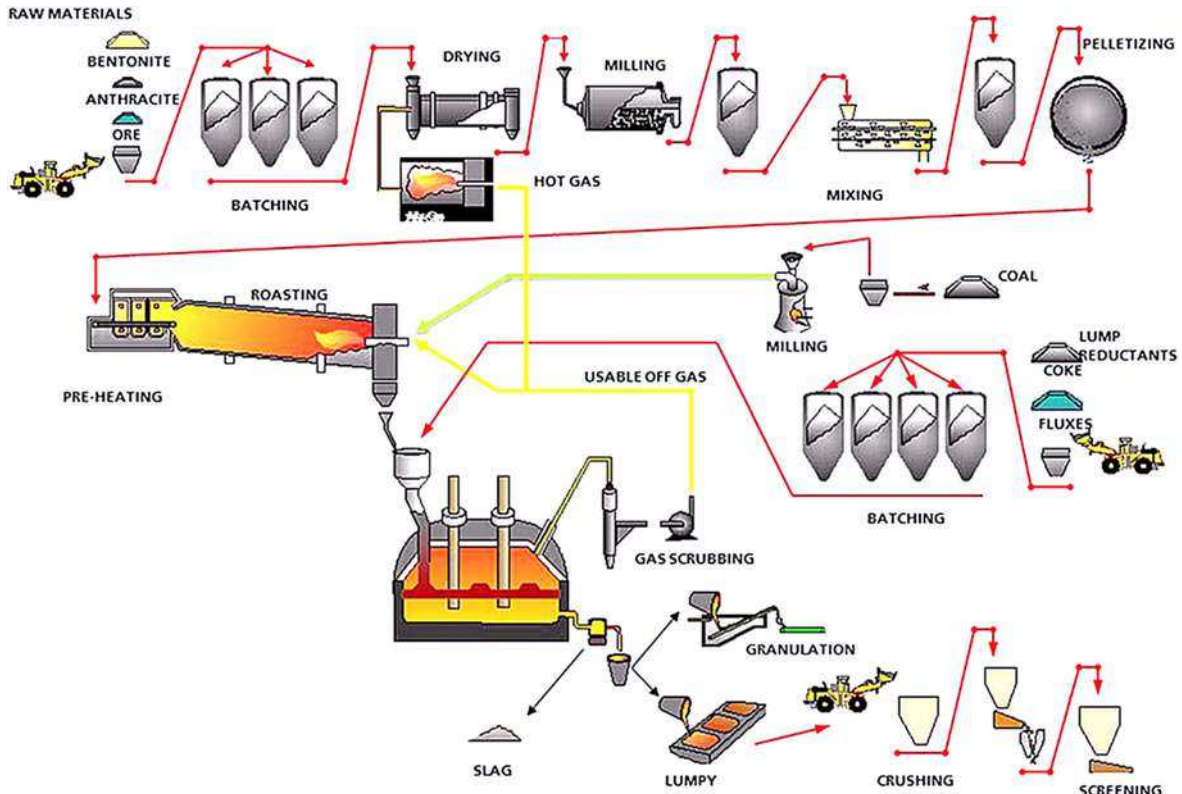


FIGURE 9.7 Flow diagram for the Premus ferrochrome process. (Source: Xstrata.)



FIGURE 9.8 View of the Premus plant. (Source: Xstrata.)

annualized ton of alloy compared to other alternative environmentally acceptable processes available. It is expected to also result in cost of production at the bottom of the cost curve for the foreseeable future. Not only does it result in superior efficiencies (typically 90% chromium recovery and 2.4 MWh/t specific electricity consumption in the smelting furnace), but it also provides important benefits such as low coke consumption and 100% chromite ore agglomeration, and it produces a low silicon product and good environmental results. A view of the Premus plant is shown in Figure 9.8.

9.2.5 Open Arc DC Furnaces

The history of commercial DC arc furnaces for high carbon ferrochrome production is strongly linked to the committed research program by the Council for Mineral Technology (MINTEK) in Randburg, South Africa, over a number of decades. Although numerous major organizations were involved in research work and even pilot scale testing, it was the MINTEK-based work that led to the commercialization of the technology. Selected facts from T. R. Curr's presentation have been used in the following two paragraphs (Curr, 2009).

MINTEK and Middelburg Steel & Alloys (now part of Samancor Chrome) conducted smelting trials on Tetronics's pilot transferred-arc plasma furnaces as far back as 1979–1980. Although these trials were metallurgically

successful, constraints with scale-up were experienced. At the time plasma torches could not be scaled up to larger than 5 MW due to excessive electrode wear.

In the 1970s, ASEA in Sweden developed high-power thyristor rectifiers and investigated the conversion of AC open arc furnaces to DC mode, principally for steelmaking. They identified a graphite cathode electrode arcing onto a slag/metal bath as the anode and devised an electrically conductive hearth and a hollow graphite electrode for finely sized iron ore smelting.

The process was metallurgically proven at Tetronics, and together with the scale-up potential of ASEA's DC arc furnace, it provided the synergies for a workable large-sized unit. This resulted in Middelburg Steel & Alloys converting an existing AC furnace at its Palmiet works (now Mogale Alloys) to a 12 MW DC arc furnace of ASEA design in 1984. It also resulted in MINTEK building a 1.2 MW pilot DC arc furnace in 1983, to support this development and extend it to other applications. The 12 MW furnace at Palmiet was upgraded to a 32 MW furnace in 1988. A 42 MW DC arc furnace (which was later upgraded to 60 MW) was built at Middelburg Ferrochrome in 1996 and was followed by another 60 MW DC arc furnace on the same site in 2009.

Swedechrome produced high carbon ferrochrome on a transferred plasma furnace with three 6-MW nontransferred torches between 1987 and 1990 in Malmö, Sweden (the Plasmachrome process). The operation only reached about 70% of design capacity and was shut down for economic reasons.

In 2012 a number of DC arc furnaces were in the planning and design phases in South Africa, awaiting electricity allocation from the capacity-constrained national electricity supplier, while at ENRC's Aktobe Ferrochrome Plant in Kazakhstan, four SMS Siemag designed 72-MW DC furnaces were commissioned during 2013. A substantial increase in new generation DC arc furnaces is expected to be commissioned in the second decade of the 21st century.

Due to the open bath nature of DC arc furnaces, the process operates on a thermal knife-edge and power/feed control is critical. When graphite electrode sections are joined off-line, the furnace availability is affected adversely. The high free board temperatures and direct contact of the molten materials with the refractory lining require special measures for the cooling of the roof and refractory lining. Copper cooling elements are typically installed in the bottom part of the lining and tap hole areas. Furnaces are operated with hollow electrode feed, side roof feed, or combinations thereof.

Fundamentally the benefits of DC arc furnaces (Fig. 9.9) for the production of high carbon ferrochrome are as follows:

1. Utilization of fine, nonagglomerated (lower-grade) ore
2. Utilization of fine, lower-value reductants (e.g., coal or anthracite)
3. High metallurgical efficiencies (chromium recovery)
4. Simplified furnace control (as it excludes burden characteristics).

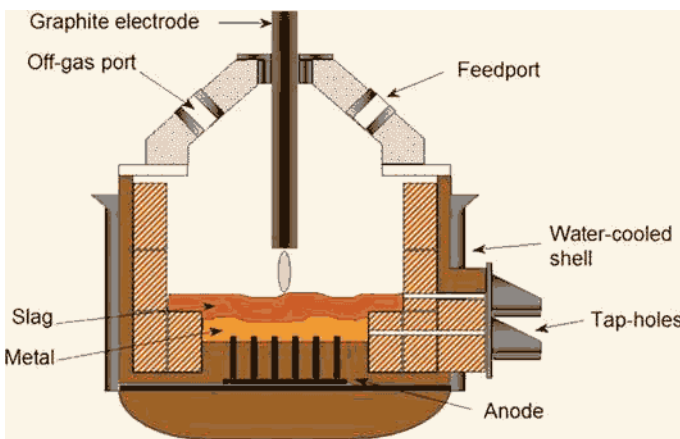


FIGURE 9.9 Schematic diagram of a DC smelting furnace. (Source: MINTEK.)

The DC arc technology route as practiced by Samancor Chrome is presented as the reference technology here. The specific process route selected is the application at the company's Middelburg Ferrochrome plant in Middelburg, Mpumalanga, South Africa, where two furnaces (both 60 MW) are in operation. Samancor Chrome provided the core of the following process description in November 2011.

At this plant the DC process is utilized for the efficient processing of chemically high-grade fine ores, as well as chemically low grade fine ores such as UG2 (Upper Grade 2) tailings from the platinum group metals (PGM) operations. In DC furnaces the input of power is not limited by the electrical conductivity of the materials being processed. This type of furnace can respond to process changes in a relatively short period. Very high temperatures can be attained; however, it should be pointed out that, at the same throughput and power flux, the thermal efficiency of the DC furnace is lower than that of the submerged arc furnace. Two factors are responsible for this effect: More energy is lost to the walls and roof of the furnace by radiation from the open arc and molten bath, and some vaporized material is lost to the off-gas stream from the arc-attachment zone.

The open bath system provides opportunities for excellent process and product control, as the use of an open bath permits greater control of the process metallurgy than in a choke-fed system.

In the case of Middelburg Ferrochrome, the DC furnace is fitted with a solid graphite electrode (contrasting with the hollow graphite electrode used by Mogale Alloys) supported by a hydraulically operated mechanical arm, which can be raised and lowered as and when required. These arms also serve as current conductors to the electrode.

The graphite electrode is centralized and an anode is embedded on a copper dish in the furnace hearth. The molten alloy in the furnace is in electrical contact with the anode. Energy is supplied to the furnace by means of an open plasma arc that impinges on the upper surface of the molten material. The arc is a sustained high velocity high temperature jet, driven by electromagnetic acceleration in the constricted region near the arc's root on the electrode surface. The arc is generated by interaction between the fluid flow, the thermal field, and the electromagnetic fields.

Important characteristics of a typical DC furnace power supply are (1) balanced three-phase load; (2) high-power utilization—constant power input into furnace; (3) ability to operate at reduced load; and (4) constant, stable arc.

Electrical operating parameters vary depending on the design capacity of the furnace. A typical DC power configuration consists of a medium voltage circuit breaker, rectifier transformer, DC isolator and earth switch, and DC reactor.

A transformer and rectifier supply a continuous direct current. The central graphite electrode forms the cathode and the hearth forms the anode. The anode and the metal bath are kept at earth potential, while the arc is struck between the cathode and the slag bath. Convection between the arc, a high-velocity jet of plasma (ionized gases and electrons) and the bath results in most of the energy transfer to the bath.

The balance of the energy transfer is achieved by resistive heating from the current flowing through the bath. The control of this open bath process is extremely critical, because of the ease with which unwanted reactions can become significant if a suitable temperature and feed distribution are not maintained.

The DC smelting process is an open-bath carbothermic reduction of metal oxides in the presence of slag. The following reaction sequence is observed. First, dissolution of metal oxides into the slag phase at the surfaces and within the bath, followed by the reaction of dissolved metal oxide with solid carbon at the slag interface. Formed metal droplets start to descend through the bulk slag phase to the bulk alloy phase, simultaneously reacting with the slag. Finally, the process approaches the equilibrium at the interface between the bulk slag and the alloy.

As the feed increases, the most probable rate-limiting step would be (1) dissolution of metal oxides in the slag or (2) reduction of the dissolved oxide by carbon, as both occur at the surface of the liquid slag bath.

It is a requirement with the DC arc furnace operation to balance the raw material feed rate with furnace power input. The feed into the furnace is therefore controlled from the raw material hoppers on a loss-of-weight basis, in order to continuously monitor and adjust the furnace feed rate to the required levels. The control system is such that the hoppers are never completely emptied, so that each feeder and partially filled hopper may serve as seal against the hot gases from the furnace. Typical feed characteristics are: the ore is fed dry at <1% moisture and

particle size –6 mm; limestone and quartzite are used for fluxing purposes. A mixture of lower-grade reductant blends of anthracite, coal, and char is used.

The high-temperature open bath operation enables separation of slag and metal, consistently giving a reasonably clean tapped alloy into the ingot molds. The furnace consists of two tap holes, positioned on opposite sides of the furnace. One tap hole is for alloy tapping, and the other is for slag tapping, with the slag tap hole at a higher level than the metal tap hole. Each tap hole is provided with an efficient tapping drill and clay gun combination, as the tap holes are normally closed against the flow.

Alloy is tapped at intervals equivalent to 70 to 90 t of alloy production. Alloy is tapped until the slag appears from the alloy tap hole. The furnace alloy level is managed by adhering to a regular tapping schedule (2 taps per shift) and the procedure of tapping alloy continues until the appearance of the slag. Visual monitoring of furnace levels and bath conditions is usually done on a daily basis through the inspection port situated on the furnace roof. This inspection is done during all electrode additions.

The tapped alloy is cast into ingots and the cooled ingots are transported to stockpiles by means of road tractors. The material is later crushed through a tertiary jaw crushing system. The fines generated though crushing are reused as molds for the ingot casting operation.

The resulting CO gas from the ferrochrome smelting process is collected though the off-gas duct. The furnace off-gas duct transfers the hot and dusty CO gas from the furnace off take (at approximately 1780°C) to an off-gas cleaning plant, where it is cooled, scrubbed, and washed to remove entrained dust.

Two options for cleaning of the off-gas are employed for the DC furnaces: a wet venturi scrubbing system and a disintegrator scrubber system. The cleaned gas is flared and the entrapped dust is settled in a clarifier; the resulting slurry is processed through a filter press. The solids are responsibly discarded and the clean water is pumped back to the plant water system. The process flow diagram for a DC high carbon ferrochrome smelting plant is shown in [Figure 9.10](#).

9.2.6 Other Technology Routes

In the early days of ferroalloy production, a number of other process routes were tested. These included various versions of shaft furnaces, rotary kilns, and converters. These process routes were typically part of an integrated stainless steel production line where “direct reduction” process routes were developed and where ferroalloys were not produced as intermediate products. In the late 1980s, an oxygen converter process was extensively studied and tested on a 30-tonnes-per-day scale by the Research Institute for New Smelting Technologies in Japan. Chromite ore fines were preheated in a rotary kiln and smelted in a top and bottom blown oxygen converter ([Izawa et al., 1992](#)). The Tecnored process was extensively researched and incorporated the production of cold bonded chromite and carbon pellets, which were indurated and prerduced in a shaft kiln by using gas from the

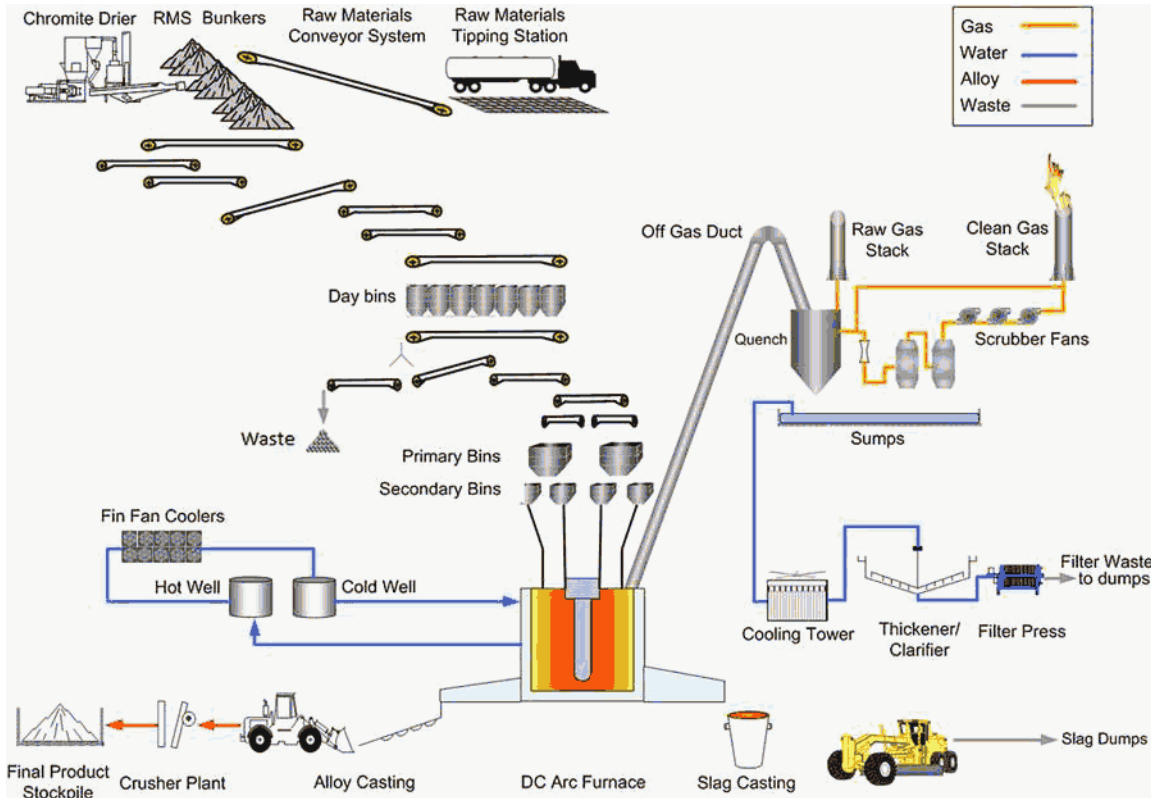


FIGURE 9.10 Process flow diagram for a DC smelting plant. (Source: Samancor Chrome.)

lower smelting zone, followed by the introduction of solid fuel and hot oxygen-enriched gas. The process was tested at pilot scale level and produced promising results (Contrucci et al., 1994). The SKF-developed Plasmachrome utilized nontransferred arc gas torches to supply superheated gas to a coke-filled shaft kiln, together with fine chromite and fluxes (Srinivasan et al., 1987). This process was commercialized and is briefly discussed in Section 9.2.5.

There are presently very few (if any) high carbon ferrochrome plants that do not utilize one of the four main technology routes described in the preceding sections or variations thereof.

9.3 POST TAP HOLE PRACTICES AND PRODUCT TYPES

9.3.1 Alloy and Slag Tapping

As limited superheating of either alloy or slag takes place inside a choke-fed submerged arc furnace, the selection of slag composition (and therefore liquidus temperature) is important for the slag to tap at a temperature that allows marginal superheating of the alloy. As mentioned earlier, the entrenchment of raw materials (especially fines) into the molten slag can also impact on the viscosity of the slag and the effective separation of molten alloy and slag in the furnace. This would impact on the tapping process.

The opening of the tap holes can take place manually, by using an oxygen lance, or mechanically, by using a tap hole drilling machine. The latter method contributes to the reduction of damage to the tap hole and surrounding refractories, whereas oxygen lancing can cause physical and oxidation damage. Tapping of a high carbon ferrochrome furnace takes place either through a single tap hole, where both alloy and slag are tapped simultaneously or via separate slag and alloy tap holes. In the case of tapping via separate tap holes, the furnace has to be sufficiently large to allow slag/metal separation to take place inside the furnace and to create a height differential for separate tapping. When separate tap holes are used, the alloy tap hole is normally closed when the first slag becomes visible. Under normal conditions the alloy level does not reach the height of the slag tap hole. Therefore, slag and alloy from this configuration are typically clean and minimal separation steps outside the furnace are required.

Tap holes are either closed manually, by ramming a clay or carbon-based plug into the tap hole, or mechanically, by using a mud gun to force a clay or carbon-based plug under high pressure into the tap hole. The process of mechanically opening and closing tap holes with high-quality tap hole material ensures that the tap hole is continuously refurbished and kept in good condition.

When a common tap hole is used for both slag and alloy tapping, a post-tap hole cleaning step is required to obtain slag-free alloy and also alloy-free slag. The most common practice is to tap into cascading ladles, which results in the alloy collecting in the first ladle and the slag overflowing into a slag ladle or into a slag pit. Alloy ladles are typically steel ladles with a refractory lining,



FIGURE 9.11 View of furnace tapping. (Source: Xstrata.)

whereas slag ladles are typically cast steel ladles without refractory linings. The layer of slag in the alloy ladle is separated from the alloy by a decanting and slag skimming operation. The alternative tapping arrangement is to tap the alloy directly into ingots or molds, in which case slag/metal separation can take place by utilizing a liquid skimming process situated between the tap hole and the molds, enabling the slag and alloy streams to be separated and handled separately. Slag and alloy can also be tapped directly into molds without skimming, but this technique results in slag-containing alloy ingots that have to be cleaned mechanically afterward. When alloy is tapped into ladles, this provides the opportunity for the alloy to be granulated (Fig. 9.11).

Where high carbon ferrochrome production facilities are adjacent to stainless steel plants, the option to transfer the alloy in liquid form to the end user is also available. The alloy is tapped in suitably designed ladles and, after taking measures to minimize heat loss from the ladles, the alloy is transported in liquid form to the stainless steel plant where it is fed directly into a converter, or other suitable vessel, and processing thereof commences immediately. Utilization of liquid high carbon ferrochrome provides substantial benefits in terms of energy savings, reduction of post-tap hole alloy losses, improved space utilization, and logistical simplification. Examples of liquid transfer being applied are at Outokumpu's Tornio works in Finland and between Samancor Chrome's Middelburg works and Columbus Stainless plant in South Africa.

9.3.2 Product Types

The most common product type for high carbon ferrochrome is a sized, lumpy product. This product type typically originates from the crushing and screening

of cast ingots into different size fractions. This product type can be offered to customers either in bags or in bulk.

An alternative product type is a granulated product. Granulation of high carbon ferrochrome generally takes place by pouring liquid high carbon ferrochrome into water. Solidification takes place immediately, and the resultant product comprises typically green-tinged, irregular particles. The benefits of this product route are the relatively low cost of granulation, reduced fines generation, and the speed of the operation. The relatively low popularity of this product type can be attributed to its lower bulk density, higher porosity, and the client's perception of the product being oxidized, based on the greenish surface color. The two most common granulation technologies used for high carbon ferrochrome granulation are Showa Denko (SDK) granulation and Granshot granulation.

The SDK technology was introduced by Showa Denko in Japan and comprises the controlled pouring of liquid high carbon ferrochrome into a strongly flowing stream of water. The energy of the water stream solidifies and breaks the high carbon ferrochrome into small particles, followed by further cooling and dewatering of the particles, resulting in granules. The size distribution of the particles can be controlled by regulating the casting rate, the water jet characteristics, and the profile of the pouring launder. CMI (now Xstrata) improved and modified this technology.



FIGURE 9.12 View of Granshot granulation process. (*Source: Uvån Hagfors Teknologi [UHT].*)

The Granshot granulation technology is owned by Uvån Hagfors Teknologi (UHT) (originally Uddeholm) and comprises the pouring of liquid high carbon ferrochrome through a nozzle in a tundish onto a refractory splash plate and the partly solidified droplets then drop into a cooling water tank (Fig. 9.12), from where they are pumped across a dewatering screen. Again, the size distribution of the particles depends on the size of the tundish hole and therefore the flow rate. Product from this process is generally more round and solid than product resulting from the SDK process.

9.3.3 Slag Handling and Utilization

The most common handling method for slag is to tap the slag directly into a slag pit filled with water. The slag solidifies, cools down, and is removed from the pit to a dump or stockpile area. Another method is to granulate the slag by allowing the slag to flow through a set of water jets. In the first method the slag solidifies in large lumps and requires crushing if further processing is required. In the second method the slag solidifies into small, stringy particles, which can readily be pumped and dewatered.

Depending on the slag and alloy properties, as well as the selected tapping configuration, the final slag still contains alloy particles entrapped in the slag. The alloy content in the slag is substantial and comprises typically 1% to 4% of the total alloy tapped. It is therefore normally viable to attempt recovery of this alloy from the slag. The most common recovery process is to crush the slag (in the case of the first slag-handling method) and recover the alloy particles in a wet jiggling process. In particular cases where the high carbon ferrochrome is sufficiently magnetic, magnetic separation techniques can also be applied. The quality of the product from the recovery process depends on the process settings, as a balance has to be found between alloy recovery and alloy product quality.

High carbon ferrochrome slag generally has favorable properties that could be utilized in various economically beneficial applications. It must, however, be emphasized that the permissibility of these applications may be differently regulated in different countries, which may impact on the permissibility of certain applications. In European conditions high carbon ferrochrome slag is certified to be chemically stable and compliant with regulations SFS 5904 and EN 13285. According to Outotec, successful applications for high carbon ferrochrome slag include the following:

1. Heat recovery
2. Road construction, both for the support layers (granulated slag) and the tarmac (crushed slag)
3. Refractory applications
4. Sandblasting
5. Mineral wool production.

9.4 ENVIRONMENTAL CONTROL AND OCCUPATIONAL HEALTH

9.4.1 Environmental Impact of High Carbon Ferrochrome Production

In terms of high carbon ferrochrome production, the main environmental focus is to reduce emissions of dust from stacks and tapping processes to prevent contamination of groundwater with hazardous components and to reduce/limit the release of carbon dioxide emissions to the atmosphere.

In terms of carbon dioxide emissions to the atmosphere, a number of sections in this chapter have shown that various technology-related options are available to reduce unit electrical energy consumption, and thereby unit carbon dioxide generation. This is commonly referred to as the carbon footprint of the operation. These options include the following:

1. Selection of more energy-efficient production routes (e.g., large, closed furnaces).
2. Utilization of CO process off-gas for preheating of the furnace feed, ore sintering (both of which improve the overall energy efficiency), and other heating applications, as well as electricity cogeneration. The latter particularly applies to countries where primary electricity is generated from fossil fuels.

In the following sections, various systems are described for the cleaning of furnace off-gas.

9.4.1.1 Gas Cleaning Systems

The gas cleaning systems may comprise different processes and methods depending on the specific plant requirements. The most common technologies utilized are venturi-type scrubbers, disintegrators, bag filters, and electrostatic precipitators.

Venturi-Type Scrubbers

A venturi scrubber is designed to effectively use the energy from the inlet gas stream to atomize the liquid being used to scrub the gas stream. This type of technology is a part of the group of air pollution controls collectively referred to as wet scrubbers. Venturi scrubbers are the most common gas cleaning systems on closed furnaces due to gas volumes being low in their noncombusted state. However, as emission requirements become more stringent, venturi scrubbers reach their efficiency limits and need to be improved technically to remain viable.

A venturi scrubber consists of three sections (Fig. 9.13): a converging section, a throat section, and a diverging section. The inlet gas stream enters the converging section and, as the area decreases, gas velocity increases in accordance with the Bernoulli equation. Water is introduced either at the throat or at the entrance to the converging section. The inlet gas, forced to move at

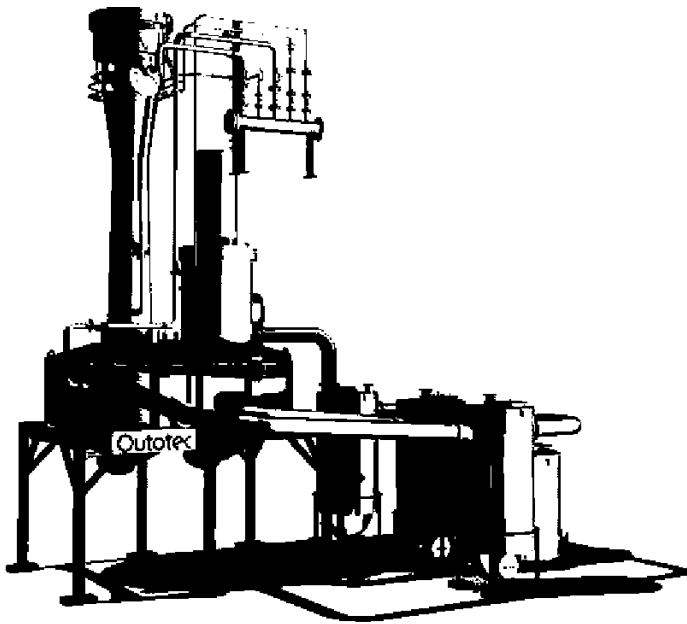


FIGURE 9.13 Schematic diagram of a venturi scrubber. (*Source: Outotec.*)

extremely high velocities in the small throat section, shears the liquid from its walls, producing a large number of very tiny droplets.

Particle and gas removal occur in the throat section as the inlet gas stream mixes with the fog of tiny liquid droplets. The inlet stream then exits through the diverging section, where it is forced to slow down. Venturis can be used to collect both particulate and gaseous pollutants, but they are more effective in removing particles.

Equipped with a water seal, the venturi scrubber is especially designed for handling explosive gases in the safest possible manner. This applies directly to closed submerged arc furnaces that produce CO gas. The efficient and secure operating principle is to both cool and clean the gas and to quench sparks from the furnace. The venturi scrubber is simple to operate, as it has no moving mechanical parts. Venturi-type scrubbers are primarily used on closed furnaces where the off-gas volume is low, which makes the venturi scrubber installation relatively small. The cleaning efficiency of venturi scrubbers typically complies with environmental requirements that stipulate that the outlet gas should contain less than 50 mg/Nm³ particulate content.

Disintegrators

As an alternative to venturi scrubbers, a disintegrator gas washing system (as patented and supplied by Theisen) has been installed on a number of ferroalloy

plants, including some high carbon ferrochrome furnaces. The Theisen disintegrator (Theisen, 2009) is a self-conductive wet separator with a particularly high efficiency separating rate, for solid particles and harmful gaseous pollutants. The volumetric performance ranges from $10 \text{ Nm}^3/\text{h}$ up to $150\,000 \text{ Nm}^3/\text{h}$, which is indicative of the flexibility of this high-performance wet separating machine.

The dirty furnace gas enters through two inlets, axially into the disintegrator housing, where a set of rotor and stators are arranged (Fig. 9.14). Spraying cylinders and the carrier disc are mounted on to the rotor shaft, which is supported by external bearings. Also attached to the carrier disc are the rotating impingement-bar cages. These incorporate the central stators, likewise fitted with impingement-bar cages that are rigidly bolted to the housing walls. The scrubbing fluid is conveyed through pipes to the spraying cylinder where it is atomized and then distributed over the entire rotor width. As a result of the centrifugal force of the rotor bars, the gas–fluid mixture is thrown against the stationary impingement bars of the stators, producing a fine scrubbing mist that covers all solids in the dust-laden gas. This process is repeated within each rotor and stator cage, thus achieving very high separating efficiency rates, even with the finest dust particles, by using a corresponding number of rotor and stator impingement-bar cages. Each Theisen disintegrator is always succeeded by a scrubbing fluid separator in which the scrubbing fluid droplets are separated from the cleaned gas.

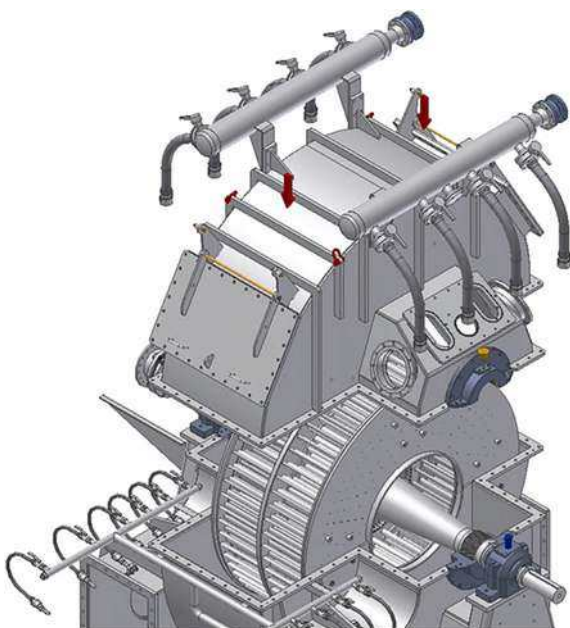


FIGURE 9.14 Schematic diagram of a disintegrator section. (Source: Theisen.)

Theisen scrubbers are generally more efficient in lowering the particulate content in furnace off-gas and levels of 10 to 20 mg/Nm³ are achieved. The installation is generally much larger than for an equivalent venturi system and therefore more expensive.

Bag Filter Plants

The use of bag filter plants is common for capturing the fume generated by open ferroalloy furnaces. Gas volumes are higher for these applications, as the CO gas is combusted on the furnace bed, resulting in increased volume. Whereas pressure-type bag filters have been the norm historically, the modern trend is toward suction-type bag filters (Actom, 2001).

Reverse air collectors are effective for various applications involving very fine dust and where low emissions are required. Bags are cleaned by reversing the airflow and blowing air back through the fabric. Of necessity the bag filter needs to be of multicompartiment design in order to isolate individual compartments for reverse air cleaning. The simple cleaning design involves few moving parts, resulting in low maintenance cost, low operating costs, and extended bag life.

Figure 9.15 illustrates a pressure type baghouse. The principle is the same as for a suction type, except that the fan is on the clean air side and the casing is of sealed construction, unlike pressure baghouses where the casing is typically an corrugated iron clad structure.

The generation and collection of dry dust from bag filter plants provides different challenges and opportunities than would be the case with slurry or sludge from wet venturi scrubbers. The dust contains hazardous components, such as hexavalent chromium, which causes occupational risk conditions when in contact with humans. Efficient collection, transport, and disposal processes have to be in place to prevent dust from disseminating into the atmosphere. In most countries with appropriate environmental pollution legislation, these handling and disposal processes have to be strictly controlled.

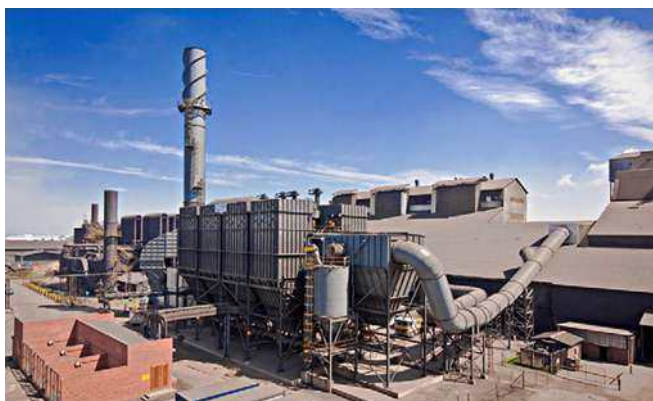


FIGURE 9.15 Bag filter plant. (*Source: Actom.*)

Bag filter dust has beneficial properties (including binder-enhancing characteristics) that allow the dust to be utilized in various industrial applications. Dust can be used as a cement extender in concrete applications and can also be included as a contributory binding agent in briquetting and pelletizing processes. Generally bag filters are more efficient than venturi scrubbers in terms of reduction of particulate content in the gas stream. Levels of < 20 mg/Nm³ are achievable.

Electrostatic Precipitators

Electrostatic precipitators function by electrostatically charging the dust particles in the gas stream. The charged particles are then attracted to and deposited on plates or other collection devices. When sufficient dust has accumulated, the collectors are shaken to dislodge the dust, causing it to fall with the force of gravity to hoppers below. The dust is then removed by a conveyor system for disposal or recycling. Depending on dust characteristics and the gas volume to be treated, there are many different sizes, types, and designs of electrostatic precipitators.

Electrostatic precipitation removes particles from the exhaust gas stream of a variety of industrial processes. Often the process involves combustion, but it can be any industrial process that would otherwise emit particles to the atmosphere. Six activity steps typically take place (Neundorfer, 2011):

1. Ionization: Charging of particles.
2. Migration: Transporting the charged particles to the collecting surfaces.
3. Collection: Precipitation of the charged particles onto the collecting surfaces.
4. Charge dissipation: Neutralizing the charged particles on the collecting surfaces.
5. Particle dislodging: Removing the particles from the collecting surface to the hopper.
6. Particle removal: Conveying the particles from the hopper to a disposal point.

For high carbon ferrochrome furnaces, electrostatic precipitators are not, however, commonly used, mainly for the following reasons: (1) fineness and high resistivity of the dust from an electric arc furnace can limit the dust removal efficiency, (2) risk of explosion because of high voltage sparking if there is CO in the gas during startup, and (3) relatively high investment cost because gas volume is small compared to typical electrostatic precipitator applications.

9.4.1.2 CO Gas Reticulation and Utilization

Closed furnaces invariably produce a noncombusted off-gas with high levels of CO content. This brings challenges in terms of safety and occupational health, but also opportunities in terms of potential utilization of the energy potential of the gas.

CO gas is potentially explosive when brought into contact with air and therefore requires a carefully designed and operated reticulation system. The

objective is to operate the closed furnace under slightly positive pressure to prevent ingress of air on the furnace roof and around the electrodes. Extreme care must also be taken during shutdown and startup processes on the furnace to prevent the development of explosive conditions. CO gas is furthermore extremely dangerous to inhale and has caused many deaths over the history of the industry. This risk is further exacerbated by the fact that CO gas is both invisible and odorless. Proactive measures must always be in place to prevent human exposure, such as the effective utilization of CO monitors in enclosed and high-risk areas.

CO gas has a high calorific value of approximately 3 kWh/Nm^3 and provides heat during combustion. This property makes CO gas amenable to applications such as ladle preheating, other gas burner applications, preheating of feed materials, sintering of chromite ore, and cogeneration of electricity.

Once upgraded and refined, CO gas can also be used in a number of applications such as the production of methanol, formic acid, dimethyl ether, synthetic natural gas (methane), and Fisher Tropsch wax. Of these options, the production of formic acid and Fisher Tropsch wax probably have the most potential for commercial viability, as indicated by Outotec in November 2011.

Electricity can be generated from furnace off-gas in internal combustion engines or steam turbines, both of which are well-proven, commercially viable processes. The particulate content in furnace off-gas from venturi scrubbers, and mostly from disintegrator plants as well, is not low enough to make the feed gas suitable for cogeneration engines. A further gas-cleaning step is therefore required. Although a number of potential technologies exist for this post-cleaning step, the most common filter process applied is the CO filter supplied and developed by Outotec (Fig. 9.16). The filtering element is a sintered HDPE

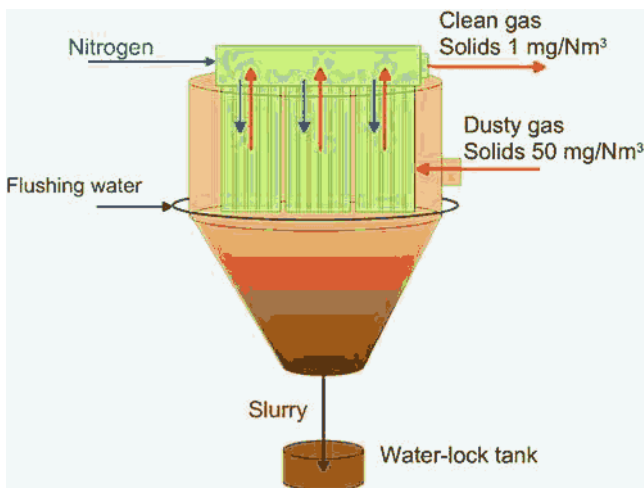


FIGURE 9.16 Schematic diagram of a CO filter. (Source: Outotec.)

material with minutely small pores. This filter reduces the particulate content in the gas to well below 5 mg/Nm³.

Electric power generation can take place via the illustrative configuration (provided by Outotec in November 2011) shown in Figure 9.17. Depending on the quality of the CO gas stream, additional electricity amounting to almost 20% of the combined furnace power can be generated.

Finally, sludge from wet scrubbing systems is normally pumped to water treatment, storage, and reticulation systems. The nature of the chemical treatment of the water is determined by the accumulation of hazardous or valuable components that collect in the furnace off-gas and are washed out by water in the scrubbing systems.

9.4.2 Occupational Health Hazards

9.4.2.1 Hexavalent Chromium

Chromium is encountered mainly in the following three oxidation states: metallic (Cr⁰), trivalent (Cr³⁺), and hexavalent (Cr⁶⁺). Hexavalent chromium, Cr⁶⁺, is formed in small quantities as a by-product during high carbon ferrochrome production. Certain Cr⁶⁺ species are regarded as carcinogenic, with specifically airborne exposure to these Cr⁶⁺ species being associated with cancer of the respiratory system (Beukes et al., 2012). Cr⁶⁺ formation in properly closed furnaces is very low, in some cases almost undetectable, whereas the prevalence is an order of magnitude higher in open, oxidizing furnaces.

As indicated by Beukes et al. (2012), Cr⁶⁺ can be generated during various ferrochrome production processes. With regard to Cr⁶⁺ content, fine particulate matter originating from the off-gas of high temperature processes can be regarded as the most significant Cr⁶⁺-containing waste material generated by the high carbon ferrochrome industry. Exposure to airborne Cr⁶⁺ by inhalation is also much more hazardous than other exposure routes, which further emphasizes the importance of these fine, potentially airborne materials. Studies have consistently shown that elevated chromium levels persist in the lungs for many years after the cessation of exposure. Cr⁶⁺ is able to penetrate the membrane of red blood cells, where it is reduced (Huvinen, 2002).

Measures to prevent or minimize the exposure of employees to risks associated with Cr⁶⁺ would therefore focus on design aspects to contain bag filter dust in closed collection and transport systems and to equip employees with appropriate protective equipment to prevent inhalation and exposure of the skin.

Ma and Garbers-Craig (2006) have reported on the formation, treatment, and stabilization of certain South African hexavalent chromium containing metallurgical wastes and pointed out that there are a number of different methods to deal with these wastes:

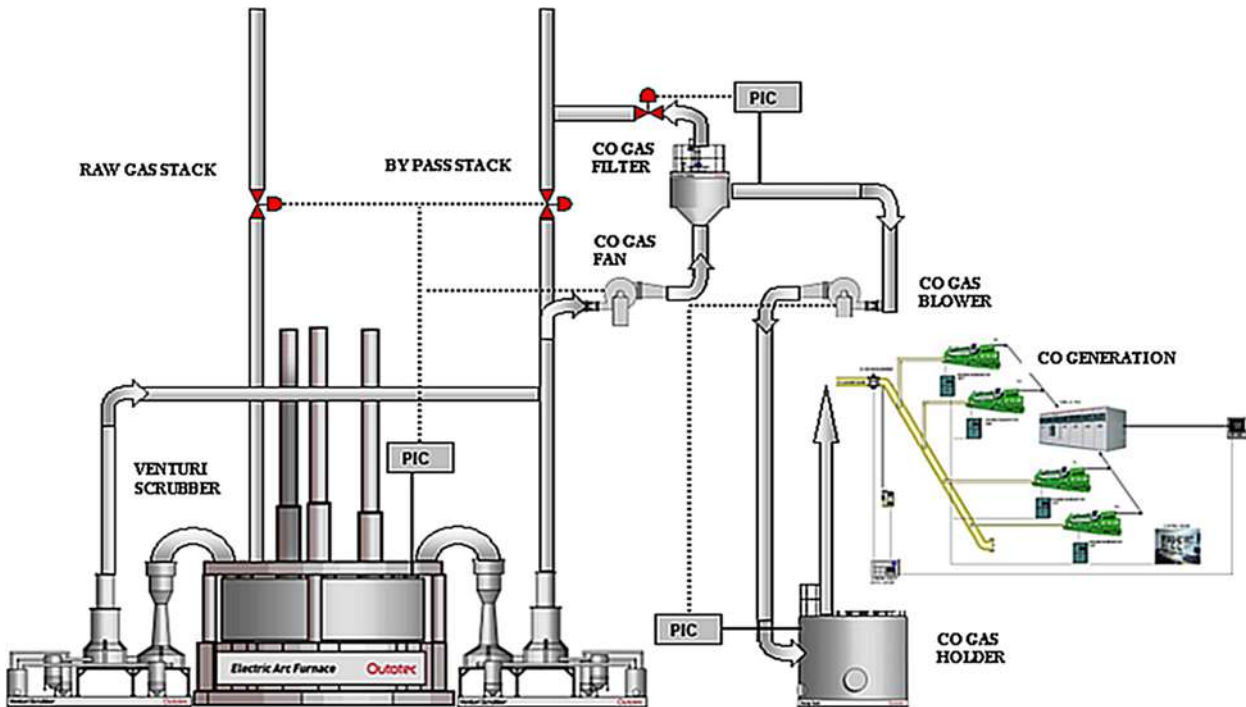


FIGURE 9.17 Schematic diagram of a cogeneration plant. (Source: Outotec.)

1. Minimization of the wastes at the source by optimizing the operational parameters
2. Direct recycling of certain materials to the furnace
3. Recovery processes, which include hydrometallurgical and pyrometallurgical methods
4. Solidification/stabilization methods—for instance, cementation and vitrification (formation of glassy state) processes
5. Use as a raw material in an appropriate product, such as fertilizer
6. Treatment and land filling.

Although these findings relate to South African plants, the trends are similar in all high carbon ferrochrome plants.

According to [Ma and Garbers-Craig \(2006\)](#), most of the above-mentioned treatment options are used at least to some degree within the South African high carbon ferrochrome industry on possible Cr⁶⁺ containing wastes. Minimization of the wastes at the source by optimized operational parameters is a prime objective of all SA high carbon ferrochrome producers, as minimized waste implies higher profitability. Direct recycling is also applied. However, direct recycling of furnace off-gas wastes (e.g., bag filter dust and scrubber sludge) to a high carbon ferrochrome smelting furnace could lead to the buildup of more volatile species, such as sodium and zinc, resulting in lower production capacity and even possibly the risk of explosions.

By far the most common process for dealing with possible Cr⁶⁺ containing waste in the SA high carbon ferrochrome industry is aqueous chemical Cr⁶⁺ reduction with suitable reducing agents (e.g., ferrous sulfate), with subsequent precipitation of the Cr³⁺ hydroxides and land filling in specially designed waste facilities.

In general, it can be stated that wet venturi scrubbers should be regarded as a better control mechanism for removing Cr⁶⁺-containing particulate matter from off-gas than bag filter systems ([Actom, 2011](#)). This belief stems from the fact that wet scrubbers immediately contact the particulate matter possibly containing Cr⁶⁺ with water during the capturing mechanism. This is in contrast to bag filter systems, which capture the particulates as dry matter. As mentioned previously, airborne Cr⁶⁺ is more hazardous than aqueous Cr⁶⁺.

9.4.2.2 Dust and Fumes

Besides the risk of Cr⁶⁺-containing dust explained previously, dust generation is a more general problem in high carbon ferrochrome production. Several processes contribute to dust generation, of which the following are the most prolific:

1. Raw material handling, including off-loading, crushing and screening, transportation, feeding to furnace bunkers
2. Leakages from furnace roof area, charging chutes

3. Furnace rabbling
4. Furnace tapping and casting
5. Final product (slag and alloy) removal
6. Wind-blown dust from stockpiles and roads.

Systems therefore have to be in place to limit dust generation (e.g., dust suppression systems) and to protect employees against dust exposure (e.g., dust masks, safety glasses). These measures are required to prevent unhealthy respiratory conditions and to improve working conditions for equipment and workers.

The most common processes producing hazardous fumes are paste loading and tapping. Both these processes have the potential to generate coal tar pitch volatiles (CTPVs), from the electrode paste and mud gun plugging mixture, respectively. Employees working in these areas should be equipped with appropriate protective masks to prevent inhalation of toxic fumes present in the CTPVs.

REFERENCES

- Actom Company, 2011 Website. www.actom.co.za.
- Beukes, J.P., Van Zyl, P.G., Ras, M., 2012. Treatment of Cr(VI)-containing wastes in the South African ferrochrome industry – a review of currently applied methods. The Journal of the South African Institute of Mining and Metallurgy, pp. 347–352.
- Contrucci, M. de A., Costa, P.H.C., Camargo, L.M.A., Marcheze, E.S., et al., 1994. The production of high-carbon ferrochromium by the TECNORED process. Proceedings XVth CMMI Congress, Johannesburg, pp. 217–220.
- Curr, T.R., 2009. The history of DC arc furnace process development. MINTEK.
- Huvinen, M., 2002. Exposure to chromium and its long-term health effects in stainless steel production. Kuopio University, Finland, pp 23–24.
- International Chromium Development Association (ICDA), 2011 website www.icdacr.com.
- Izawa, T., Katayama, H., Sano, N., 1992. Smelting reduction of chromite ore in an oxygen converter. INFACON 6 and the 1st International Chromium Steel and Alloys Congress, Cape Town. Vol. 2, South Africa, pp. 245–252.
- Ma, G., Garbers-Craig, A.M., 2006. A review on the characteristics, formation mechanisms and treatment processes of Cr(VI)-containing pyrometallurgical wastes. The Journal of the South African Institute of Mining and Metallurgy 106, pp. 753–763.
- Neundorfer, 2011. website www.neundorfer.com/knowledge_base/electrostatic_precipitators.
- Srinivasan, N.S., Santen, G.O., Staffansson, L.I., 1987. Plasmachrome process for ferrochrome production – thermochemical modelling and application to process data. Steel Research 58 (4), 151–156.
- Theisen Gas Cleaning Systems, South African Institute of Mining and Metallurgy seminar, University of Pretoria, 2009. Website www.theisen-muc.eu.

Technology of Ferronickel

Oleg Polyakov

National Metallurgical Academy of Ukraine, Dnipropetrovsk, Ukraine

Chapter Outline

10.1 Properties of Nickel and Its Compounds	367	10.3.1 Ferronickel and Its Smelting	371
10.2 Nickel Raw Materials	371	10.3.2 Refining and Casting of Ferronickel	373
10.3 Ferronickel Smelting and Refining	371	References	374

10.1 PROPERTIES OF NICKEL AND ITS COMPOUNDS

Nickel (atomic number, 28; atomic weight, 58.6934) belongs to group VIII of the periodic table and together with iron and cobalt is commonly referred to as the “iron triad.” Indeed properties of these three elements are rather close. The outer electron shell configuration of the nickel atom is $3d^84s^2$, so its common valence is +2, and less often +3. Nickel’s melting temperature is 1455°C, and its boiling temperature is ~2915°C. The density of nickel is 8.92 g/cm³ (i.e., slightly higher than that of iron).

Nickel is an important and widely used constituent of many alloy steels. It is a well-known solid solution strengthener and a promoter of high toughness, especially at low temperatures. Nickel has only one stable solid phase (FCC) in the whole practical temperature range, and its addition usually stabilizes the austenitic (FCC) structure in steels and alloys. This is an important application in stainless steelmaking (austenitic, martensitic, and duplex grade stainless steel compositions). Besides stainless, nickel is also widely used in low-alloys steels, and it is a major component of nonferrous, high-temperature-resistant superalloys and heat-, oxidation-, and corrosion-resistant materials.

With iron, nickel forms continuous solid solutions with austenitic (FCC) compositions (Fig. 10.1). In the liquid state, both elements have unlimited

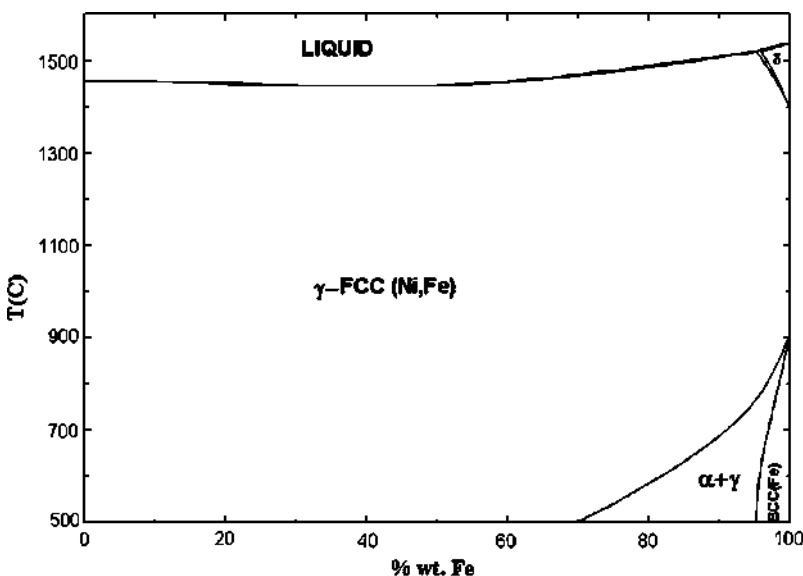


FIGURE 10.1 The equilibrium diagram of the Ni-Fe system. Magnetic transformations and possible intermetallics are now shown.

solubility. Earlier it was assumed that the Ni-Fe system's behavior is close to ideal solution, but then it was determined that the activity coefficient of nickel is lower than unity in alloys <40% Ni. There are also indications of the formation of an ordered FeNi_3 structure below 500°C, although this process seems to be kinetically limited and possibly of a metastable nature.

Like iron, nickel and carbon form carbide Ni_3C of a cementite type, but it is more metastable than Fe_3C and does not usually form easily. The stable phase diagram of the Ni-C system has a simple eutectic form with Ni-C eutectics at 1326°C (Fig. 10.2). Dashed lines in this diagram indicate approximate phase positions for metastable $\text{Ni-Ni}_3\text{C}$ equilibria.

With silicon, nickel forms several stable silicides, some of which have a noticeable homogeneity range (Fig. 10.3). Silicon also dissolves in considerable amounts of liquid and solid nickel (Sudavtseva and Zinevich, 2004).

A number of intermetallic compounds are formed between nickel and aluminum (Fig. 10.4). The solubility of aluminum in the solid nickel is much higher than nickel solubility in solid aluminum.

With sulfur, nickel forms four sulfides: Ni_3S_2 , NiS , Ni_3S_4 , and Ni_2S . The most stable nickel phosphides are Ni_5P_2 , NiP , NiP_2 , Ni_2P , and Ni_3P (Gasik et al., 2009). Phosphide Ni_3P is isomorphic to Fe_3P and Mn_3P .

Nickel dissolves a significant amount of oxygen (Fig. 10.5) and forms nickel oxides NiO and Ni_2O_3 . The latter completely decomposes to NiO above

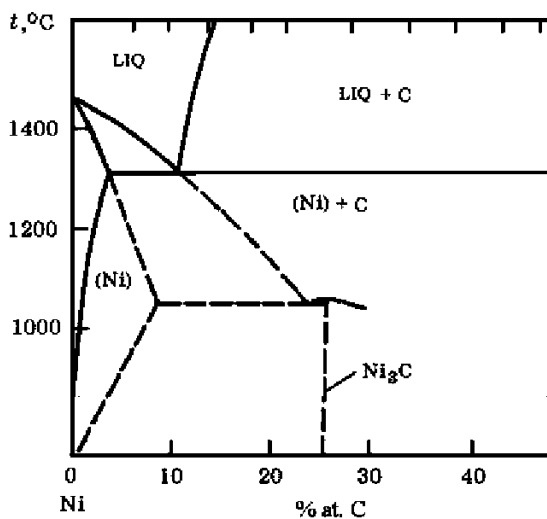


FIGURE 10.2 Stable and metastable equilibria in the Ni-C system.

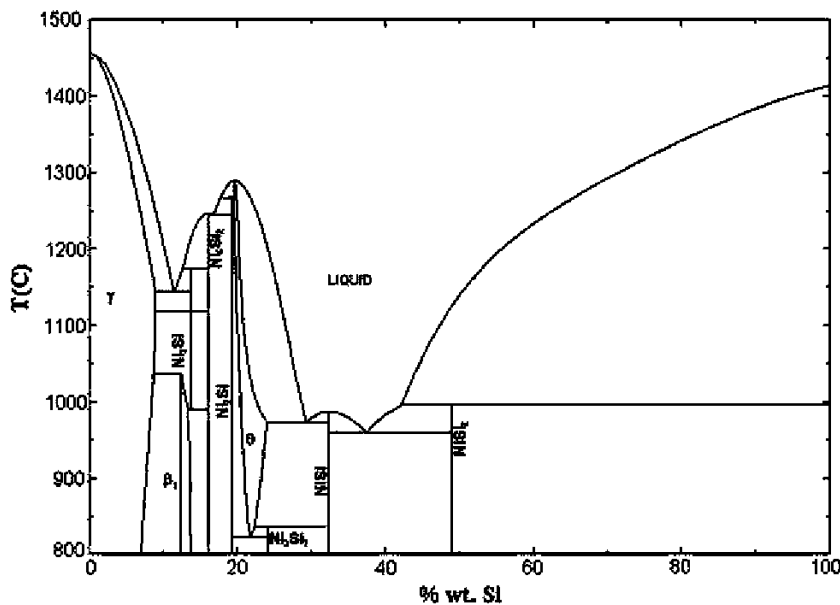


FIGURE 10.3 The equilibria in the Ni-Si system.

1100°C and thus is not normally observed in the materials present during the smelting of ferronickel. Nickel oxide also forms binary compounds with silica (Ni_2SiO_4) and ternary compounds with silica and calcia ($\text{CaNiSi}_2\text{O}_6$).

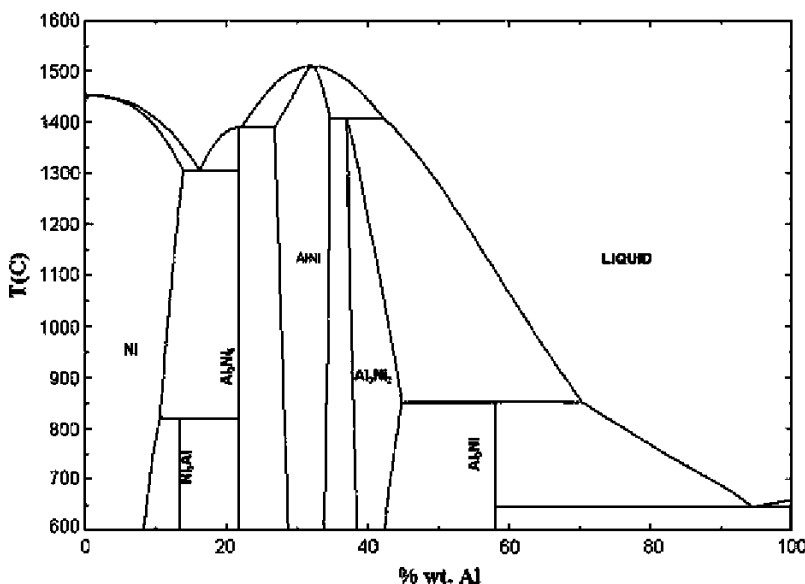


FIGURE 10.4 The equilibrium phase diagram of the Ni-Al system.

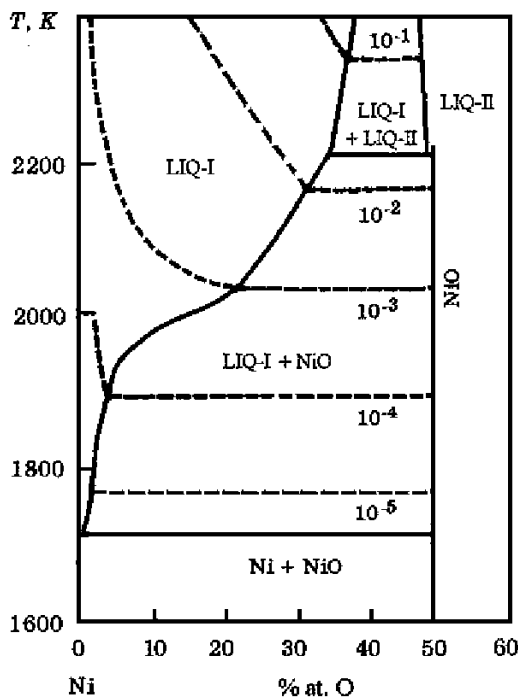


FIGURE 10.5 The equilibrium diagram of the Ni-O system. Dashed lines represent equilibrium oxygen pressure, atm.

10.2 NICKEL RAW MATERIALS

Nickel appears in two different mineral categories, namely the sulfide type and the laterite type (oxide–silicate). Among known sulfide minerals of commercial interest are violarite Ni_2FeS_4 , siegenite $(\text{Co},\text{Ni})_3\text{S}_4$, poldimitite Ni_3S_4 , fletchrite $\text{Cu}(\text{Ni},\text{Co})_2\text{S}_4$, and others. These ores might contain up to 4% Ni, but their availability is about 14% of the total known nickel reserves. Thus, recovery of nickel from laterite ores is getting more attention, as laterite might have up to 1% to 2% Ni. Depending on the composition of the gangue, laterite ores are classified into magnesia-, silicate-, and alumina-type varieties. There are also known reserves of iron ore (50% to 60% Fe and 1% to 1.5% Ni), which might be classified into limonite and saprolite ores. Limonite ore has 1.2% to 1.3% Ni, <0.1% Co, <0.1% MgO, and 45% to 50% Fe. Saprolite ores have 2% to 2.3% Ni, 0.01% to 0.05% Co, 15% to 20% MgO, and 15% to 20% Fe. In ferronickel production, both lean ores (<1% Ni) and relatively nickel-rich ores (2% to 3% Ni) might be used. The lean laterite ore (Ukraine) has (wt. %) 0.9 to 1 Ni, ~20 Fe, 0.05 to 0.10 Co, 32 to 44 SiO₂, 5 to 7 Al₂O₃, 4 to 6 MgO, <2 CaO, and 1 to 2 Cr₂O₃. The chemical composition of nickel ores varies widely from plant to plant—(% wt.): 1 to 3 Ni, 0.03 to 0.1 Co, 10 to 32 Fe, <28 MgO (Weisegar et al., 2005)—and thus different ores are blended.

Oxidized nickel ores are composed of many complex minerals, such as nontronite ($\text{Fe}[(\text{OH})_2\text{Al}_{0.33}\text{Si}_{3.67}\text{O}_{10}]\text{Na} \cdot (\text{H}_2\text{O})_4$), as a group of smectites. Their general formula might be represented as $\text{X}_{0.33}\text{Y}_2\text{Si}_4\text{O}_{10}(\text{OH})_2 \cdot 4\text{H}_2\text{O}$, where X is Ca or Na, Y is Fe³⁺, Al, Cr, Mg, Ni, Zn, Li. These mineral formations are usually composed of ~14% Al₂O₃, ~8% MgO, and small amounts of CaO, K₂O, and Na₂O, and in some cases also NiO and Cr₂O₃. Some of the clay-forming minerals are based on serpentine ($\text{Mg},\text{Fe},\text{Ni}_{8-x}\text{Al}_x\text{Si}_{4-y}\text{Al}_y\text{O}_{10}(\text{OH})_8$).

Potential future sources of nickel, cobalt, and manganese minerals are manganese nodules in the ocean. It is estimated that stocks of nodule in the Pacific Ocean have more than 10¹⁰ tons, containing up to 2.5% Ni, 0.1% to 2.6% Co, <1.9% Cu, and so on. However, all of these deposits are confined to the central regions of the deep ocean, so their exploration requires substantial investment and the development of new underwater mining technologies.

10.3 FERRONICKEL SMELTING AND REFINING

10.3.1 Ferronickel and Its Smelting

The standard ferronickel for steelmaking has a wide range of compositions, from 5% to 25% Ni, Table 10.1. Solar et al. (2008) noted two trends in nickel laterites processing, one favoring high-grade ferronickel (35% to 40% Ni) and the other favoring lower grades (20% to 25% Ni). Because the ores processed vary widely in terms of nickel content and other components, it is natural that both lower and higher reduction degrees are used. Low reductions imply higher

TABLE 10.1 Typical Composition of Ferronickel Alloys

Grade	Ni	Co	Si	C	Cr	S	P
FeNi10	5–15	0.3–0.6	<0.3	<0.1	<0.3	<0.08	<0.03
FeNi15	12–18	0.5–0.8	<0.4	1–2.5	<2	<0.1	<0.03
FeNi20	15–25	*	<0.4	1–2.5	<2	<0.4	<0.03

*Recommended value Ni/Co = 20–40.

slag losses and lower nickel recoveries but also lower power and reductant requirements, whereas higher reductions imply the reverse (Solar et al., 2008). In some cases, nickel scrap and remelts are added to low-grade FeNi to increase nickel content.

The technological scheme for ferronickel smelting in electric includes the following steps (Fig. 10.6): preparation and averaging of nickel ore; preparation, dispensing charge materials, and calcining the charge (ore, limestone, coal, and recirculated dust) in the rotating drum furnaces; FeNi smelting with a hot charge supply from rotary kilns, FeNi refining (sulfur removal) in the ladle, followed by purging with oxygen (first in a converter with an acid lining, then with the basic lining); and finally casting of refined ferronickel.

An example of the modern large-scale FeNi smelter was given by Rodd et al. (2010). The sources of sulfur in the charge are carbon reductant and heavy fuel oil (1.8% S) and phosphorus, mainly carbon reductant and nickel ore. The smelting of ferronickel using lean nickel ores usually starts with roasting (calcining) of the ore mixture with limestone (~one third of the ore), anthracite

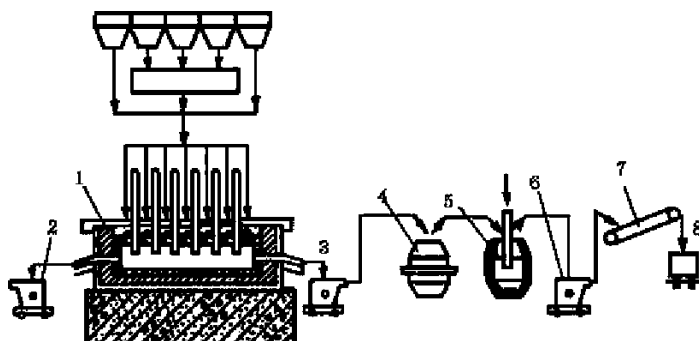


FIGURE 10.6 Flow sheet of ferronickel production: 1, submerged electric arc furnace; 2, slag ladle; 3, ladle for crude FeNi; 4, converter with acid lining (removal of excess Si and Cr); 5, converter with basic (MgO) lining for phosphorus removal; 6, ladle for refined ferronickel; 7, filling/casting machine; 8, storage.

(~1/10 of the ore amount), and recycled dust. Roasting is carried out in rotary kilns (~3 m in diameter, ~75 m in length, with a hot zone length of 9 to 12 m in the case of lean ore processing). The treatment temperature should not exceed 850°C to avoid stacking of the charge in the kiln. The hot roasted charge is fed into the submerged arc furnace of 50 MVA with six 1200 mm electrodes (Fig. 10.7) operating at a 30 to 40 kA current.

This furnace hearth has dimensions $\sim 25 \times 10 \times 5$ m, and it is lined with carbon blocks (see Fig. 10.7). The furnace has three tap holes for slag and three tap holes for FeNi. Other furnace types (e.g., the round type of 24 to 94 MVA) and novel developed DC furnaces (Jones et al., 1996) are also used for FeNi smelting (Walker et al., 2010). From 1 ton of roasted charge the yield of crude ferronickel is 120 to 140 kg and for slag it is 650 to 700 kg. The slag has <0.02% to 0.06% Ni, <0.02% Co and low basicity (50% to 52% SiO₂ versus 25% to 30% [CaO + MgO]), and its main utilization is as a construction material. Slag behavior and reactions during laterite smelting have been analyzed (e.g., by Utigard, 1994).

10.3.2 Refining and Casting of Ferronickel

Because crude ferronickel has a high sulfur content, it undergoes desulfurization in the ladle by sodium carbonate (soda): $[S]_{\text{FeNi}} + 2 \text{Na}_2\text{CO}_3 + [\text{C}] + [\text{Si}] = (\text{Na}_2\text{S}) + (\text{Na}_2\text{SiO}_3) + 3 \text{CO}$. The consumption of soda is ~4% to 5% by weight of FeNi metal, and a practically achievable degree of desulfurization is 50% to 60%.

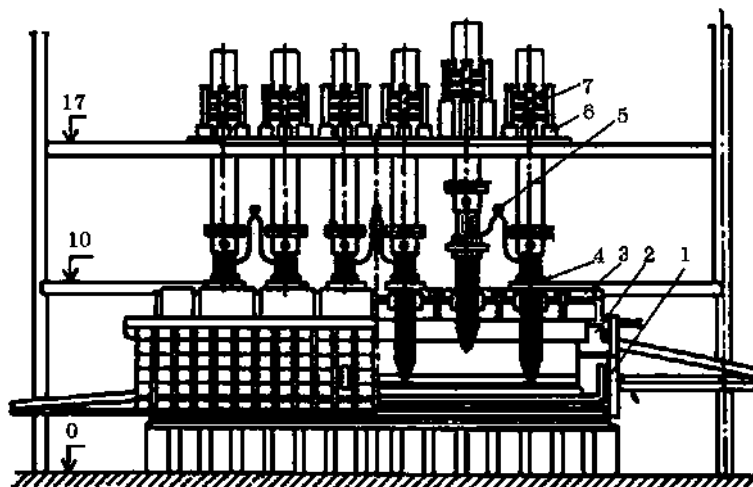


FIGURE 10.7 Ferronickel smelting furnace: 1, shell; 2, lining; 3, cover; 4, gaskets; 5, current bus bars; 6, electrode moving mechanism; 7, electrode shifting mechanism. Numbers indicate the height levels in meters.

Treated ferronickel is poured into the converter with acid lining and subjected to oxygen purge to remove excess chromium and silicon. An increase of silica in the slag facilitates the transition of chromium into the slag from ferronickel. This dump slag from refining ferronickel in an acid converter has the following composition (% wt.): 52 to 55 SiO₂, 15 to 25 Fe, ~1.7 CaO, 2 to 6 MgO, 1 to 8 Cr₂O₃, ~3 Al₂O₃, and <0.09 Ni. After this refining stage, ferronickel is poured into the next converter with a basic lining and subjected to conversion with oxygen purge to remove phosphorus. The oxidation of phosphorus in the main converter in the presence of highly basic slag is similar for phosphorus removal in conventional steelmaking. The converted basic slag has the following composition (%): 15 to 20 CaO, 5 to 10 SiO₂, 35 to 50 FeO, <0.05 Ni, <0.005 Co, and 1 to 10 Cr₂O₃. Acidic and basic slags are subjected to conversion of magnetic separation to remove trapped particles of ferronickel. Ferronickel is usually cast on conveyor machines in ingots of 25 to 35 kg weight. The specific energy consumption for processing 1 ton of dry lean nickel ore (1% Ni) is 810 kWh or 78 200 kWh per 1 ton of nickel. The use of richer ores (2.5% to 3.0% Ni) allows the decrease of specific energy consumption at least twofold (Novikov et al., 2005). The combined nickel yield into ferronickel is 88% to 93%.

Among alternative technologies of ferronickel smelting and refining, blowing molten iron and nickel ore mixture with reducing gas (Krasheninnikov and Leontiev, 2001) might be mentioned. The addition of 20% limestone allowed an increase of nickel content in the metal to 70%, in slag <0.1%, to achieve a nickel yield of 93%.

In the electric furnace development for ferronickel smelting, the trend is to go to higher-power furnaces (90 to 120 MVA), as the capital investment might decrease almost twice when compared to the cost of using low-power furnaces (Walker et al., 2010), but the operation of these furnaces also requires a proper turnover of materials and lower costs of electric energy.

REFERENCES

- Gasik, M.I., Lyakishev, N.P., Gasik, M.M., 2009. Physical chemistry and technology of ferroalloys [in Ukrainian]. Dnipropetrovsk: Sistemnye Tehnologii, 494 pp.
- Jones, R.T., Hayman, D.A., Denton, G.M., 1996. Recovery of cobalt, nickel and copper from slags, using DC-arc furnace technology. Proceedings of the International Symposium on Challenges of Process Intensification. 35th Annual Conference of Metallurgists, CIM, Montreal, Canada, 451–466.
- Krasheninnikov, M.V., Leontiev, L.I., 2001. Mathematical model of ferronickel processing by using gas blowing of oxide melt. Rasplavy (Melts) 2, 37–41.
- Novikov, N.V., Kapran, I.I., Sokolov, K.A., Ovcharuk, A.N., 2005. Material balance of ferronickel smelting using New Caledonian ore. Metallurgical and Mining Industry 3, 32–36.
- Rodd, L., Voermann, N., Stober, F., Wasmund, B., Lee, S.H., Lim, K.Y., Yoo, J.-H., Roh, S.-J., Park, J.-H., 2010. SNNC: a new ferronickel smelter in Korea. Proceedings of the Conference INFACON-XII. Helsinki, Finland, 697–708.

- Solar, M.Y., Candy, I., Wasmund, B., 2008. Selection of optimum ferronickel grade for smelting nickel laterites. CIM Bulletin 11, 1107.
- Sudavtseva, V.S., Zinevich, T.N., 2004. Thermodynamic properties of the Ni-Si melts. Izv. Ros. Acad. Nauk. Metally 3, 13–17.
- Utigard, T., 1994. An analysis of slag stratification in nickel laterite smelting furnaces due to composition and temperature gradients. Metallurgical and Materials Transactions 25B, 491–496.
- Walker, C., Koehler, T., Voermann, N., Wasmund, B., 2010. High power, shielded-arc FeNi furnace operation – challenges and solutions. Proceedings of the Conference INFACON-XII. Helsinki, Finland, 681–696.
- Weisegar, M.L., Onischin, B.P., Tsemehman, Sh, L., 2005. Pyrometallurgical treatment of oxide nickel ores. Electrometallurgy 2, 6–15.

Technology of Tungsten Ferroalloys

Michael Gasik

Aalto University Foundation, Espoo, Finland

Chapter Outline

11.1 Properties of Tungsten and Its Compounds	377	11.3.1 Reduction by Carbon and Silicon	382
11.2 Minerals, Ores, and Concentrates of Tungsten	380	11.3.2 Reduction by Aluminum	385
11.3 Technology for Producing Ferrotungsten	382	References	385

11.1 PROPERTIES OF TUNGSTEN AND ITS COMPOUNDS

Tungsten is one of the heaviest stable metals used commercially. It is located in the VIb subgroup of the periodic table, together with chromium and molybdenum. The atomic weight of tungsten is 183.85, and the external electronic configuration is $4f^{14}5d^46s^2$. Tungsten has one stable phase with a body-centered cubic (BCC) structure of $a = 0.3165$ nm and a density of 19.3 to 19.9 g/cm³. The melting point of tungsten is 3410°C and a boiling point is 5930°C, making it also one of the most refractory metals.

In metallurgy, tungsten is known for its tendency to form extremely hard and stable carbides, which is the reason for using tungsten as a component of high-speed and tool steels as well as many hard metal alloys (Durrer and Volkert, 1972). Tungsten finds a lot of applications as a pure metal and as a master alloy in special steels, superalloys, filaments, radiation shields, refractory applications, and so on. About half of the world's known tungsten reserves are estimated to be located in China, but important deposits also exist in Canada, the United States, South America (Bolivia, Peru), other parts of Asia

(Thailand, Myanmar, Kazakhstan, Uzbekistan, and Korea), and other places throughout the world (Australia, Russia).

The system W-Fe (Fig. 11.1) forms the basis of the industrial ferrotungsten alloy. Iron and tungsten react to form several intermetallic compounds, of which the most stable are the Laves phase (Fe_2W) and the μ -phase Fe_7W_6 . At the content of tungsten of >60% wt. in the industrial FeW alloy, the melting temperature exceeds 2200°C. Tungsten stabilizes the BCC lattice of iron, which might thus dissolve up to 30% to 34% wt. tungsten at subsolidus temperatures (see Fig. 11.1).

In the system W-C (Fig. 11.2), two stable carbides are known: W_2C (3.07% C, density 17.5 g/cm³) and WC (6.12% C, density 15.5 g/cm³). Both carbides have high melting temperatures and high hardness, which is exploited in tool steels and hard metals. Additionally in ternary Me-W-C systems, η -carbide ($\text{Me}_3\text{W}_3\text{C}$) might form in the case of deficit of carbon. This phase is usually brittle and has to be avoided in tools applications by correlating the ratios of carbon, tungsten, and other metals.

In the system W-Si, two stable silicides form (Fig. 11.3): W_3Si_2 (9.21% Si) and WSi (23.3% Si). Like similar molybdenum silicides, they have high melting temperatures. Mutual solubility of silicon and tungsten is low.

With oxygen, tungsten forms several oxides, of which the most stable are WO_2 (dark brown color), W_4O_{11} (dark blue color), and WO_3 (lemon yellow

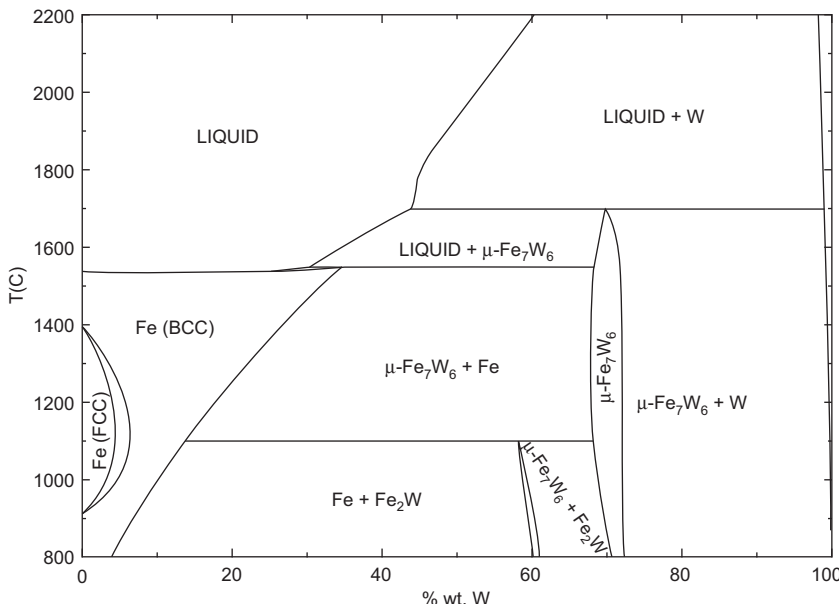


FIGURE 11.1 Phase diagram of the W-Fe system.

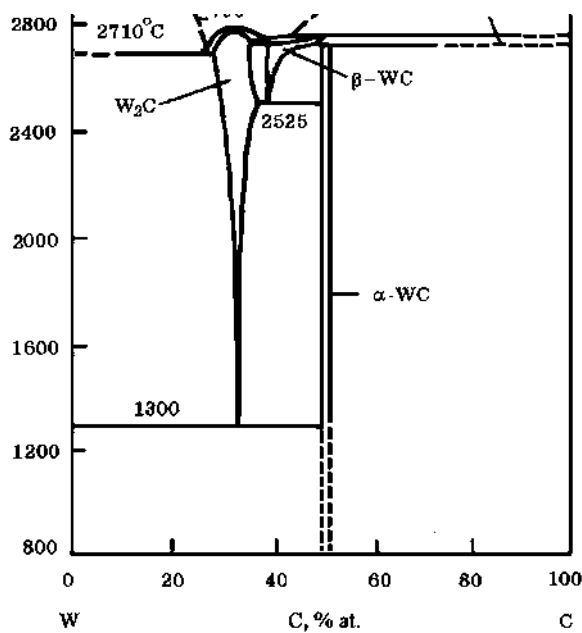


FIGURE 11.2 Phase diagram of the W-C system.

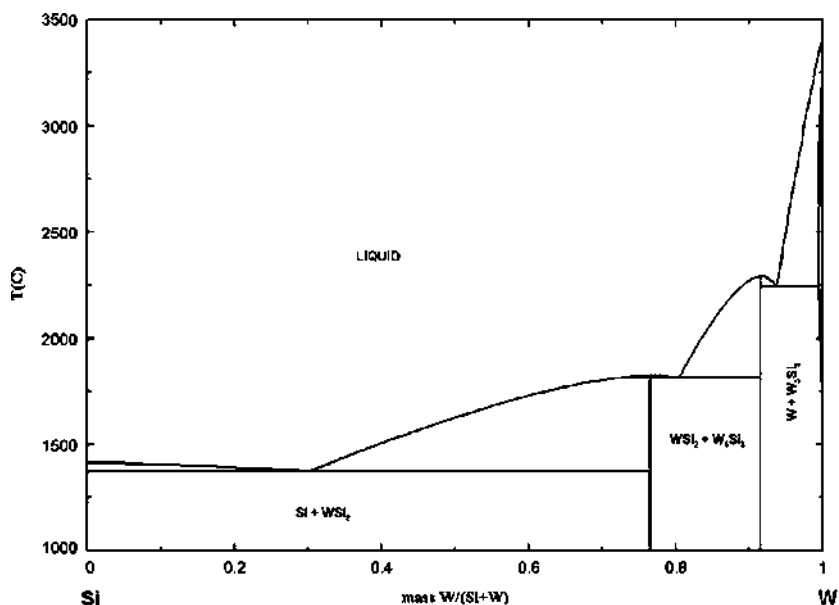


FIGURE 11.3 Equilibrium diagram of the W-Si system.

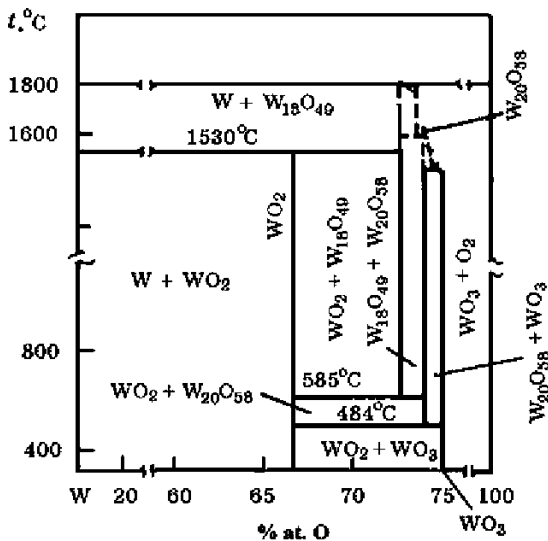


FIGURE 11.4 Equilibrium phase diagram of the W-O system.

color) (Fig. 11.4). Additionally, like molybdenum, it has a set of intermediate oxides like $\text{W}_{18}\text{O}_{49}$, $\text{W}_{20}\text{O}_{58}$, and so on, generally expressed by formula WO_{3-x} and sometime referred as “blue oxide,” which is an intermediate product of some hydrometallurgical and chemical processes of WO_3 extraction from ores and recycled materials.

Tungsten oxides can be reduced by hydrogen to tungsten metal or by carbon either to metal or to carbide phases. Figure 11.5 shows the example of the phase dominance diagram of the W-C-O system at 1500°C . The figure shows that it is thermodynamically possible to obtain metallic tungsten at this temperature using equilibrium with gas of 1% to 15% CO_2 . A higher CO_2 fraction moves equilibrium toward the oxide’s stability, whereas CO -rich gas will favor the formation of tungsten carbide.

11.2 MINERALS, ORES, AND CONCENTRATES OF TUNGSTEN

Several tungsten minerals have practical industrial importance, particularly ferberite FeWO_4 , hubnerite MnWO_4 , wolframite ($\text{Fe}, \text{Mn}\text{WO}_4$, and scheelite CaWO_4 . The first two have rare separate occurrences, as they usually form an isomorphic mixture—wolframite, in which manganese and iron can substitute for each other in the crystal lattice (Gasik et al., 2009). Wolframite has 76.5% WO_3 and has a density of 7.1 to 7.5 g/cm^3 . Scheelite has 80.6% WO_3 and has a density of 5.8 to 6.2 g/cm^3 .

Tungsten ores contain an average of 0.2% to 0.5% WO_3 , rarely exceeding 1% wt. Tungsten ores often include other minerals with molybdenum, tin,

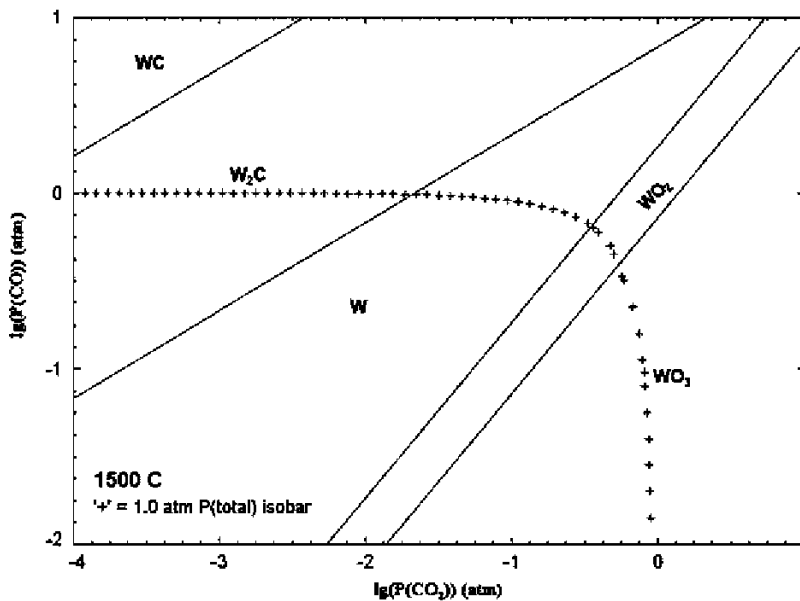


FIGURE 11.5 Phase dominance map of the W-C-O system at 1500°C. Cross marks indicate 1 bar total pressure isobar.

copper, arsenic, and so on. Dressed tungsten ores could be roughly divided into two classes depending on the leading mineral (either wolframite (hubnerite and ferberite) or scheelite type) (Table 11.1). Tungsten concentrates with high sulfur content (1% to 7%) are subjected to oxidizing roasting to decrease sulfur content below 0.1% to 0.5% S.

For processing of pure tungsten and its alloys, pure oxide WO_3 is extracted by a series of sophisticated chemical and hydrometallurgical operations on these concentrates. The side rocks here are represented by mostly quartz, calcite, and fluorite (Gasik et al., 2009).

TABLE 11.1 Typical Chemical Composition, % wt., of Tungsten Ore Concentrates

Ore Type	WO_3	MnO_2	SiO_2	P	S	As	Sn	Cu	Mo
Wolframite	60–65	15–18	<5	<0.05	<0.8	<0.05	<0.15	<0.1	<0.2
Scheelite	60–65	<1	<6	<0.03	<0.3	<0.02	<0.05	<0.1	<3

11.3 TECHNOLOGY FOR PRODUCING FERROTUNGSTEN

Standard ferrotungsten is available in several grades (Table 11.2). The major difference is defined by the alloy production method, which is reduction by either aluminum or carbon and silicon. This also determines the amount and distribution of impurities. The density of ferrotungsten is high (14 to 15.5 g/cm³), as is its melting temperature (~2700°C), so it dissolves in the steel-making furnace slowly and tends to sink at the bottom (Voronov et al., 2000).

The reduction of tungsten by carbon and silicon usually involves being preformed in small furnaces (3.5 to 5 MVA), and the liquid alloy is scooped out of the furnace with a specially designed spoon if the liquidus temperature is too high (this would prevent normal tapping, as the alloy would be solidified during this process). Higher-grade FeW alloy is usually made by aluminum reduction. Thermodynamically, tungsten has a low affinity for oxygen and from its oxides can be reduced with silicon, carbon, and aluminum.

11.3.1 Reduction by Carbon and Silicon

The smelting furnaces are lined with magnesite bricks, which are partially destroyed during the melting and replaced by ferrotungsten metal skull. The raw materials used in the process are tungsten concentrate (see Table 11.1), coke, granulated ferrosilicon (65% to 75% Si), steel chips, and recycled tungsten-containing slag. The composition of the charge is calculated taking into account that impurities would be transferred into the alloy in the following ratios, % wt.: Mo, 100; Cu, 100; As, 15; S, 15; and Sn, 30% of the amount in the smelting charge (Gasik et al., 2009).

By the nature of occurring physical and chemical processes, the smelting operations used are divided into three periods. After the third period, the bath in the furnace contains ferrotungsten melt (from the previous smelting) with 3%

TABLE 11.2 Typical Chemical Composition of Ferrotungsten Alloys, wt. %, Depending on the Production Method: A—Reduction by Aluminum, CS—Reduction by Carbon and Silicon

Method	W Content	Mo	Mn	Si	C	Al
A, high purity	85–90	<0.2	<0.1	<0.1	<0.05	<0.1
A, high grade	75–80	<0.4	<0.1	<0.5	<0.1	<3
A, low grade	70–75	<6–7	<0.3	<2	<0.7	<3–6
CS, high grade	70–75	<2	<0.3	<0.5	<0.3	<0.04
CS, low grade	65–70	<6	<0.6	<1	<0.6	<0.10

to 8% Si, 1.7% to 4.5% Mn, <2% C, and 50% to 55% W. At the beginning of the first period, this melt is refined from Si, Mn, and C by loading into the furnace tungsten concentrate, recycled tungsten slags, and dust (from the gas cleaning). Silicon, manganese, and carbon all reduce WO_3 to tungsten, which dissolves in the melt. Iron oxides reduce simultaneously. To reduce the viscosity of the melt, iron (steel) chips are proportionally added before filling the concentrate. The slag formed in the furnace at this stage has 16% to 23% WO_3 , 15% to 20% FeO, 28% to 32% SiO_2 , 10% to 15% MnO , 8% to 10% CaO , 1% to 3% MgO , and 2% to 4% Al_2O_3 . To improve the refining rate and increase metal temperature, the furnace is run on maximum power.

At the end of the first period, tungsten concentrate and coke are loaded with the purpose of obtaining the working slag with 10% to 12% WO_3 . Here reduction of wolframite and scheelite proceeds via carbon, but silicon and manganese remaining in the melt also take part in reduction reactions. By the end of the first period, the melt has a standard content of tungsten and impurities.

In the second period, which lasts 1 to 1.5 hours, the operating voltage is reduced in an attempt to preserve the heated metal and to keep it in a solid–liquid state. Also during the second period, the alloy is dredged using special machine constructions on site (see, for example, Fig. 11.6). The alloy from the furnace is taken with a spoon made of carbon steel, containing 50 kg of metal at each turn. The metal spoon is dipped into a water tank, cooled, and knocked to extract the ingot. To ensure even alloy pickup, the bath of the furnace is rotated.

The purpose of the third period is to reach the final reduction of WO_3 from the slag by silicon (ferrosilicon) to levels <0.25% WO_3 . The metal is enriched with silicon and manganese, reducing the tungsten concentration in the alloy from 65–75% to 52–55% W. When the tungsten oxide content in the slag reaches 0.25% (typically 0.05% to 0.15%), the furnace is held for 10 to 15 minutes; after that the slag is tapped. The final slag contains (by weight) 0.05% to 0.20% WO_3 , 0.3% to 2% FeO, 45% to 50% SiO_2 , 15% to 20% MnO , and 25% to 30% CaO . The metal left in the furnace after the third period and slag tapping typically has (by weight) 66% to 70% W, 5% to 7% Si, 0.7% to 2.5% Mn, 0.03% to 0.14% S, and 0.1% to 0.2% C. After the third period, the process is repeated.

If carbon, silicon, and manganese concentrations in the alloy are getting higher, the amount of the tungsten ore concentrate in the charge is increased. If WO_3 content in the slag is too high, more coke is added to increase metal and slag temperature—slag foams better; electrodes slip down; and the rate of C, Si, and Mn oxidation improves (Gasik et al., 2009).

To produce 1 ton of ferrotungsten by this method, ~1530 kg of tungsten concentrate (60% WO_3) is required. Additionally, ~108 kg of ferrosilicon (75% Si), 87 kg of coke, and 40 kg of electrode paste are consumed. The extraction degree of tungsten is high, typically >99%. The main cost share of the ferrotungsten process is the cost of the tungsten oxide concentrate (96% to 98% of

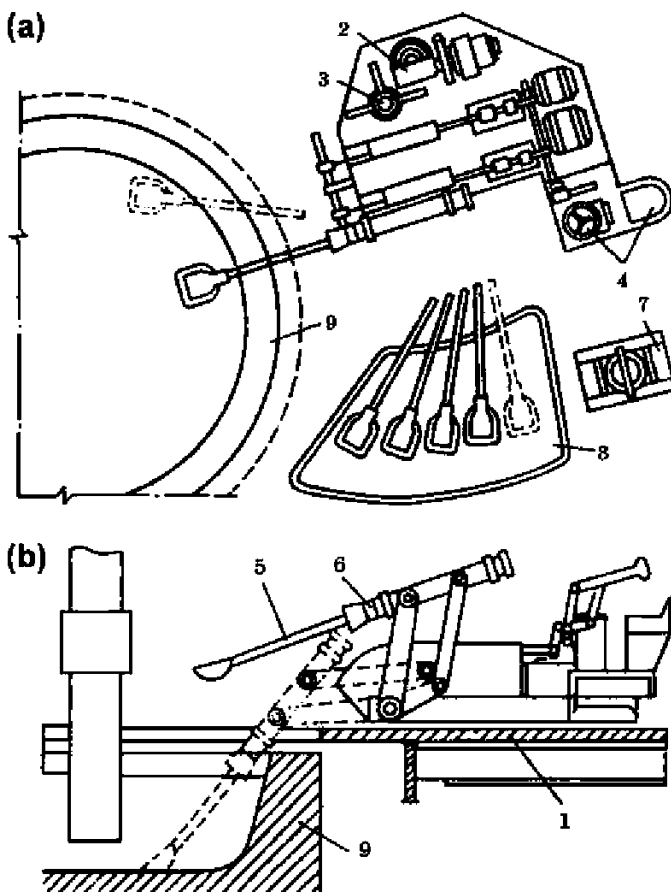


FIGURE 11.6 The machine for scooping of ferrotungsten (a, top view; b, side view): 1, working level; 2, turning mechanism; 3, axis of rotation; 4, remote control; 5, spoon; 6, holder; 7, device for ingot extraction; 8, stand; 9, electric furnace.

the total), so all possible measures are taken to reduce the loss of tungsten from the slag, waste gas, and dust. The vapors (mainly in the form of WO_3 and WO_2) are captured using a series of equipped cyclones and electrostatic precipitators. The collected dust is smelted separately, resulting in alloy (40% to 50% Pb, 45% to 50% Bi, and 5% to 8% Sn) and slag with 35% to 40% WO_3 . This recycled slag is fed into the FeW smelting furnace together with other furnace charges.

Some plants use a two-stage technology for FeW smelting. Here two furnaces are engaged: the first (1 to 3 MVA) melts tungsten and iron ore concentrates with carbon, leading to alloy with >80% W, 1.5% C, 1.5% Mn, 0.1% Si, and slag <0.15% WO_3 . The second furnace refines this alloy by

adding extra tungsten and iron ore concentrates, leading to the oxidation of carbon (decreases <0.4% C) and manganese (decreases <0.4% Mn) from the metal and to the formation of slag with 10% to 15% WO_3 , which is fed back into the first furnace. Tungsten losses with gas and dust in this process are about 3% to 4% (Gasik et al., 2009).

11.3.2 Reduction by Aluminum

Reduction by aluminum is used when the tungsten content in the alloy should be higher and other impurities (especially carbon) content should be lower. During reduction, oxides of tungsten, molybdenum, iron, and silicon are reduced into metal melt.

Despite the high exothermic effect of reduction reactions, the heat released is not enough to ensure formation of the metal melt and its separation from the slag because of the high melting point of ferrotungsten. Additional heat is provided from the furnace transformer of ~1 MVA power. The furnace lining is made of magnesite.

Scheelite concentrate (see Table 11.1) is the main component of the charge. On every 100 kg of scheelite charge, the following components are added: primary aluminum powder 23 kg, iron chips 3 kg, steel slag 4 to 5 kg, and lime 1 kg. Also to improve the recovery of tungsten, recycled scrap, slag residuals, and collected dust are added. Depending on the volume of the furnace, 2500 to 5000 kg of concentrate is smelted per one batch (Gasik et al., 2009).

For the aluminum reduction process, 1 ton of ferrotungsten requires ~1555 kg of scheelite concentrate, 345 kg of primary aluminum powder, 20 kg lime, and ~80 kg iron chips. The extraction of tungsten in this process is high (>99%).

Ferrotungsten mixed alloy (with increased molybdenum content) is also produced by remelting W and Mo metallic and oxide scrap with the addition of lime, iron chips, and FeSiAl as a reductant (Voronov et al., 2000). This mixed alloy (nonstandard) has ~20% to 25% Mo and 20% to 25% W, with <10% to 15% Si used for alloying high-speed steels where both tungsten and molybdenum are required. Similar technology is used for making Cr-30%W and Ni-30%W master alloys.

REFERENCES

- Durrer, R., Volkert, F., 1972. Metallurgie der Ferrolegerungen. (Metallurgy of Ferroalloys), Springer, Berlin, 506 pp.
- Gasik, M.I., Lyakishev, N.P., Gasik, M.M., 2009. Physical chemistry and technology of ferroalloys [in Ukrainian]. Dnipropetrovsk: Sistemnye Tehnologii, 494 pp.
- Voronov, Yu.I., Zaiko, V.P., Zhuchkov, V.I., 2000. Technology of ferroalloys with molybdenum. Ekaterinburg: IMET UrO RAS, 276 pp.

Technology of Molybdenum Ferroalloys

Michael Gasik

Aalto University Foundation, Espoo, Finland

Chapter Outline

12.1 Properties of Molybdenum and Its Compounds	387	12.3 Oxidative Roasting of Molybdenite Concentrates	392
12.2 Minerals, Ores, and Concentrates of Molybdenum	392	12.4 Technology for Producing Ferromolybdenum	393
		References	395

12.1 PROPERTIES OF MOLYBDENUM AND ITS COMPOUNDS

Molybdenum belongs to the subgroup VIb of the periodic table, and its atomic weight is 95.94 with an external electron shell configuration $4d^55s^1$. Its physical properties correspond well to its position between its analogs chromium and tungsten: a body-centered cubic (BCC) crystal lattice ($a = 0.314$ nm), a 2622°C melting point, a 4840°C boiling temperature, and a density of 10.23 g/cm^3 .

Molybdenum has many important uses in stainless steels, alloyed cast irons, and superalloys. It provides necessary hardenability in many heat-treatable alloys, such as pressure vessel steels. Together with tungsten, it is an important component of high-speed steels and other tool steels and hard metals. Molybdenum also improves the corrosion resistance of stainless steels and brittle fracture resistance for steels and cast irons (Voronov et al., 2000).

The Mo-Fe system equilibrium diagram is shown in Figure 12.1. Iron and molybdenum form several intermetallic compounds: FeMo (σ -phase), Fe_7Mo_6 , R-phase $\text{Fe}_{27}\text{Mo}_{26}$, and solid solutions. In the figure, the melting point of

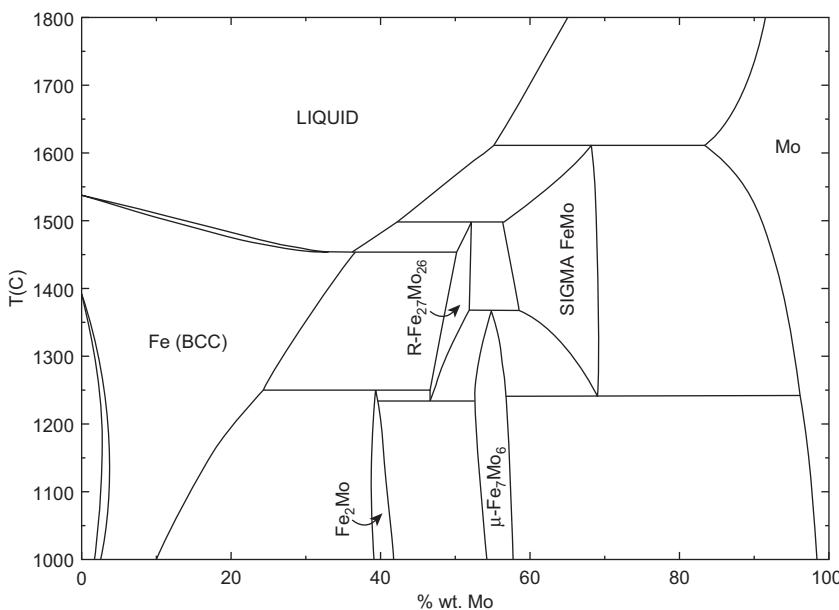


FIGURE 12.1 Equilibrium phase diagram of the system Mo-Fe.

iron-rich alloys is reduced up to ~37% wt. Mo, and after that it increases. The binary alloy with 55% to 58% wt. Mo melts at temperatures above 1650°C. The maximum solubility of iron in solid molybdenum is 15% Fe at 1610°C.

The equilibrium diagram of the Mo-C system is shown in Figure 12.2. Molybdenum with carbon forms two carbides, Mo_2C and MoC_{1-x} . These carbides have different phases, exhibiting coexistence at high temperatures. Small amounts of carbon are dissolved in the solid molybdenum with the formation of a solid solution. In the ternary system, the Mo-Fe-C formation of complex carbides $(\text{Fe},\text{Mo})_3\text{C}$, $(\text{Fe},\text{Mo})_{23}\text{C}_6$; η -phase $(\text{Fe},\text{Mo})_6\text{C}$; and $(\text{Mo},\text{Fe})_2\text{C}$ has been confirmed.

The diagram of the Mo-Si system includes several silicides (Fig. 12.3). Known silicides are Mo_3Si , Mo_5Si_3 , and MoSi_2 . MoSi_2 silicides exist in two modifications, and the temperature of the transformation $\alpha\text{-MoSi}_2 \leftrightarrow \beta\text{-MoSi}_2$ is ~1900°C. Molybdenum disilicide has an important application as a high-temperature heating element in different furnaces. The maximum solubility of silicon in Mo reaches 3.52% (at.) at 2053°C.

In the system Mo-Al, there are six known aluminides: MoAl_{12} , MoAl_6 , MoAl_5 , MoAl_4 , Mo_3Al_8 , and Mo_3Al (Fig. 12.4). Some of them might have composition homogeneity ranges.

With phosphorus and sulfur, molybdenum forms stable phosphides (Mo_3P , MoP_2) and sulfides (Mo_2S_3 , MoS_2 , and MoS_3). The first sulfide dissociates below 605°C, but MoS_2 is stable and forms mineral molybdenite, which is one

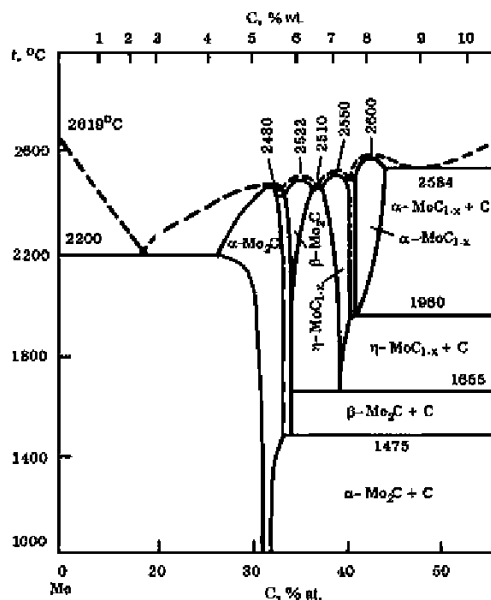


FIGURE 12.2 Equilibrium phase diagram of the system Mo-C.

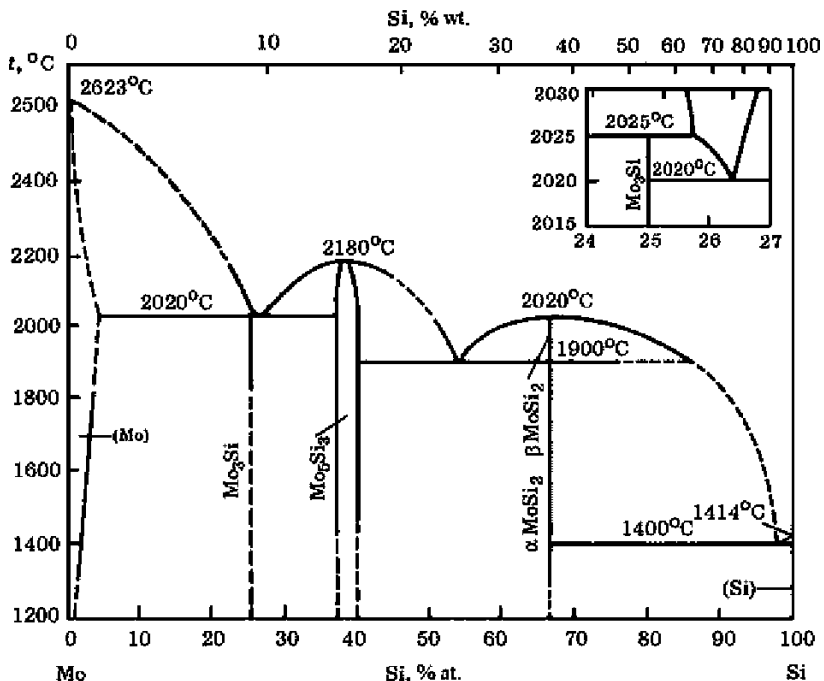


FIGURE 12.3 Equilibrium phase diagram of the system Mo-Si.

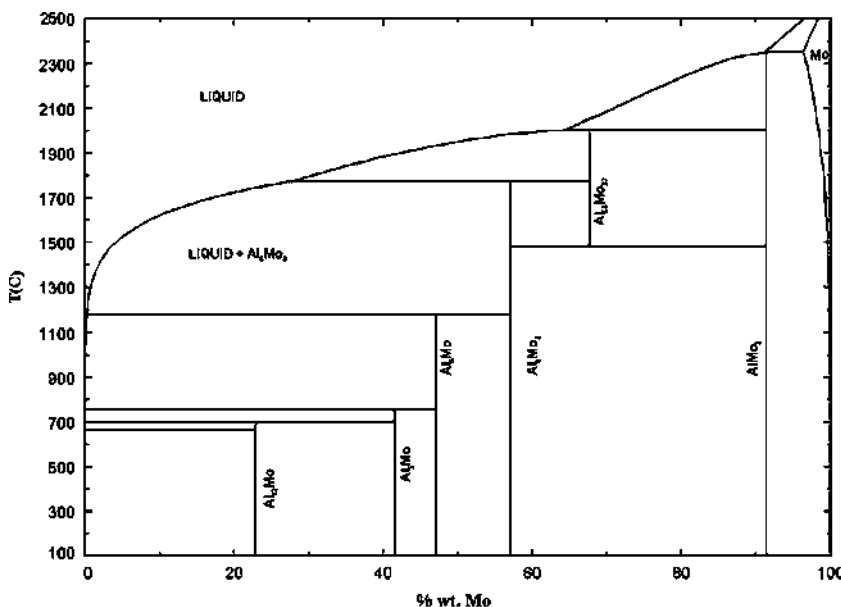


FIGURE 12.4 Equilibrium phase diagram of the Mo-Al system.

of the major molybdenum sources. Nitrogen does not dissolve in molybdenum in substantial amounts, so for nitriding it is possible for the ferroalloy used in powder form (Kirby and Fray, 1993).

Oxygen dissolves in solid molybdenum in small amounts, but like tungsten it forms many molybdenum oxides, of which the most known are yellowish white MoO_3 , brown MoO_2 , dark violet $\text{Mo}_{4}\text{O}_{11}$, black $\text{Mo}_{17}\text{O}_{47}$, violet $\text{MoO}_{2.8}$, dark blue Mo_8O_{23} , and Mo_9O_{26} (Fig. 12.5). When the O/Mo ratio increases, the melting temperature of the oxide drops and its vapor pressure increases; thus MoO_3 easily evaporates (sublimates) on heating before melting.

The evaporation of MoO_3 increases in the presence of water vapor; for example, at 690°C it is four times higher than in a dry atmosphere because of the formation of complex molecules $\text{MoO}_3 \cdot \text{H}_2\text{O}$. This has to be taken into account during the oxidative roasting of molybdenite MoS_2 concentrate. Oxide MoO_3 also tends to form trimer Mo_3O_9 , tetramer Mo_4O_{12} , and pentamer Mo_5O_{15} molecules in the gas phase near its melting point (Gasik et al., 2009).

Molybdenum has a relatively small affinity for oxygen and it can be reduced by carbon. However, the stability area of pure molybdenum is narrow, and thus molybdenum carbides also form during reduction (Fig. 12.6). As carbon content in ferromolybdenum is limited, the alloy should be produced by reduction with silicon or aluminum (Gasik et al., 2009).

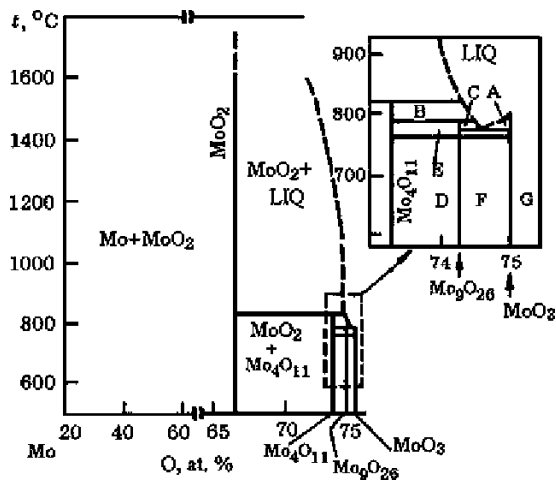


FIGURE 12.5 Equilibrium phase diagram of the system Mo-O. The insert shows details of phase areas: A = MoO₃ + L, B = Mo₄O₁₁ + L, C = L + Mo₉O₂₆; D = Mo₄O₁₁ + Mo₉O₂₃; E = Mo₄O₁₁ (β) + Mo₉O₂₆; F = Mo₉O₂₆ (γ) + MoO₃; G = Mo₉O₂₆ (β) + MoO₃.

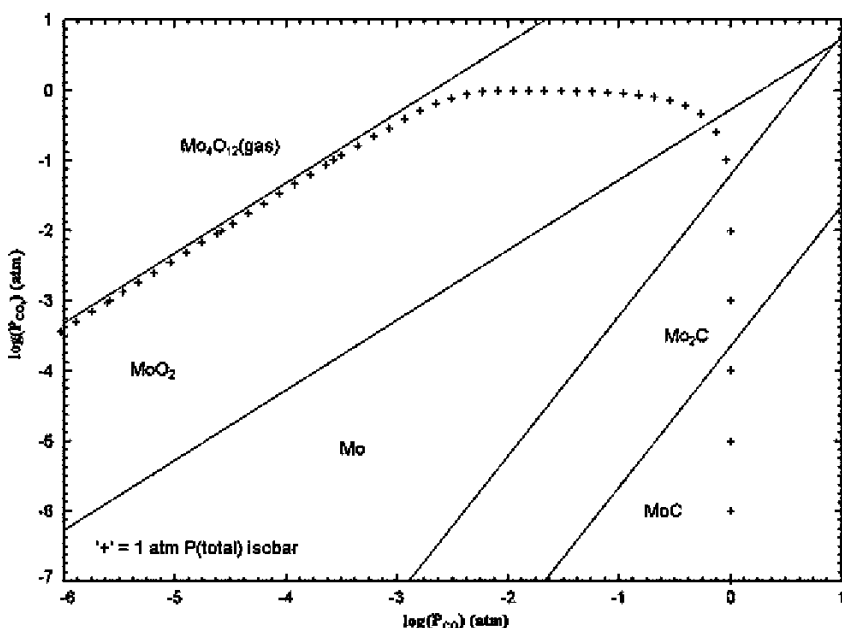


FIGURE 12.6 Phase dominance diagram in the Mo-O-C system at 1200°C.

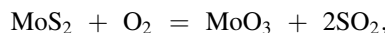
12.2 MINERALS, ORES, AND CONCENTRATES OF MOLYBDENUM

Known molybdenum minerals are molybdenite (MoS_2), povellite (CaMoO_4), wulfenite (PbMoO_4), molybdite (ferrimolybdite) ($\text{Fe}_2(\text{MoO}_4)_3 \cdot n\text{H}_2\text{O}$) ($n = 7-8$), and molybdenum scheelite ($\text{Ca}(\text{W},\text{Mo})\text{O}_4$). The most common mineral is MoS_2 , which is the main mineral of molybdenum in concentrates used to produce ferroalloys (Kummer, 1979). It is derived as primary ore (United States, Canada, China) or as a by-product of the extraction of other metals (copper) (United States, Chile, Mongolia). Various molybdenum ores are being recovered also in Russia, Kazakhstan, Uzbekistan, and the Caucasus region. Molybdenite (MoS_2) traditionally occurs in quartz veins, often in conjunction with scheelite (CaWO_4), wolframite ($(\text{Fe},\text{Mn})\text{WO}_4$), cassiterite (SnO_2), chalcopyrite (CuFeS_2), and other minerals such as those containing arsenic and bismuth. The ores are classified into simple (quartz-molybdenum), copper-molybdenum, and molybdenum-tungsten. Ordinary quartz-molybdenum ores contain about 0.1% to 1% Mo (Kummer, 1979; Gasik et al., 2009). The use of other minerals such as ferrimolybdite for direct smelting of ferromolybdenum from lean concentrates has been also reported by Pattnaik et al. (1981).

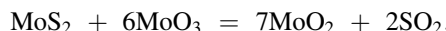
Polycrystalline (formed via substitution of other minerals) ores of molybdenum and tungsten contain molybdenite with scheelite (CaWO_4), pyrite (FeS_2), and chalcopyrite, although concentrations of the last two are usually minor (e.g., ores from Northern Caucasus). Molybdenite is normally removed first by flotation, but as scheelite (CaWO_4) and povellite (CaMoO_4) form an isomorphic mixture, molybdenum concentrates always have some tungsten. Depending on the grade, enriched concentrates have 45% to 60% wt. Mo, below 5% to 9% WO_3 , <0.03% to 0.07% As, <0.01% to 0.7% Sn, and <0.01% to 0.05% P. Major impurities, which vary significantly with ore-dressing degree, are silica (from <0.2% to 12%) and copper (from <0.01% to 2.5%). Because these concentrates have up to 35% sulfur, they have to be roasted to oxidize molybdenite (Voronov et al., 2000).

12.3 OXIDATIVE ROASTING OF MOLYBDENITE CONCENTRATES

During oxidative roasting of molybdenite concentrates, molybdenum sulfide transforms to MoO_2 and MoO_3 . The oxidation of the sulfur proceeds first with the formation of MoO_3 :



followed by the reaction of MoO_3 with molybdenum sulfide:



The oxidation of MoS_2 to MoO_3 is highly exothermic, so external heating is required only at the end of the firing process, when the amount of molybdenum sulfide is getting too low. Sulfides of other metals (FeS_2 , Cu_2S , ZnS , NiS , etc.) present as impurities in commercial molybdenum concentrates oxidize at the same time.

The roasting process is carried out in an oxidizing atmosphere in a vertical furnace with eight levels at a maximum temperature of 680° to 750°C to avoid evaporation losses of MoO_3 with gases. Despite the seeming simplicity of roasting of molybdenum concentrate, industrial realization of the process to get concentrate suitable for smelting of standard ferromolybdenum is a complex process. The quality and yield of the concentrate depend on many factors: mineralogy, particle size and composition of source concentrate, temperature distribution, oxidation potential of the gas phase, the duration of firing, and so on. The identification of a rational and optimal combination of factors is an important technological challenge. [Voronov et al. \(2000\)](#) describe this process in more detail.

Residual sulfur content in the concentrate should not exceed 0.05% to 0.15% S. This calcined (roasted) molybdenum concentrate should have at least 50% to 55% Mo, <0.03% to 0.05% P, <0.05% As, <0.6% to 1.5% Cu, 5% to 7% SiO_2 , <0.05% Sn, and <0.1% C ([Gasik et al., 2009](#)). Additionally, roasted concentrate contains 14% to 16% CaO , <3% FeO , <1.5% MgO , <0.7% Al_2O_3 , and 0.15% to 0.5% W. About one tenth of all molybdenum in this concentrate is present as MoO_2 , and the rest is present in the form of MoO_3 .

12.4 TECHNOLOGY FOR PRODUCING FERROMOLYBDENUM

Standard ferromolybdenum alloy has about 60% Mo, although grades with 50% to 58% Mo have been also produced on request. Also, ferromolybdenum with increased silicon content (<15% to 20% Si, >45% to 50% Mo) has been produced ([Voronov et al., 2000](#)). As the Mo-Fe phase diagram shows (see Fig. 12.1), such an alloy has a liquidus temperature of over 1800°C, but the first liquid phase forms around 1540°C (decomposition of FeMo sigma phase). A high melting temperature and high density of the alloys (9 to 9.3 g/cm³) represent a challenge of the addition of FeMo lumps into molten steel, although this challenge is less critical than it is for ferrotungsten. [Gourtsoyannis et al. \(1984\)](#) reported on the dissolution of molybdenum and ferromolybdenum in liquid steel. Pure Mo dissolves in stagnant steel baths at 1600°C at a rate of 0.4 mm/min, whereas the rate measured in an inductively stirred bath was 0.7 mm/min. By extrapolation it was calculated that ~1.2 min is needed for the dissolution of a 2" FeMo lump in a stirred steel bath at 1600°C.

Other impurities in ferromolybdenum are usually tungsten (0.3% to 0.8%), silicon (<0.5% for the highest grade and <3% for the lowest grade), copper (<0.5% and <2%, respectively), phosphorus (<0.05%), and sulfur (<0.15%).

Nonferrous metals accompanying molybdenum in minerals and concentrates (As, Sn, Sb, Pb, Zn, Bi) normally should not exceed 0.005% to 0.01% each (Gasik, et al., 2009; Voronov et al., 2000). Carbon content is limited to 0.05% for the highest grade and 0.5% for the lowest grade of the ferroalloy.

The smelting of FeMo is based on the reduction of molybdenum oxides with silicon and aluminum off-furnace, as the process is exothermic and the alloy ingot is solidified at the end of the smelting hearth. The following charge compositions have been employed commercially for FeMo processing (Table 12.1).

At the Chelyabinsk Electrometallurgy plant in Russia, the alloy is produced from the charge consisting of roasted molybdenum concentrate (50% to 55% Mo), granulated aluminum, iron ore and chips, and lime. The main reductant is FeSiAl alloy (60% to 65% Si and 10% to 12% Al), especially designed for this type of process to provide optimal heat release during reactions. The smelting hearth is charged and covered and the charge is ignited. This process of ferromolybdenum smelting consists of two periods: the first includes the reaction progress and gas and solid separation; the second consists of the separation of reaction products (metal and slag). The duration of the first period is regulated according to the specific heat release of the charge (kJ/kg of charge) based on industrial practice. It usually varies between 10 min (~2100°C) and 50 min

TABLE 12.1 Examples of Charge Compositions for FeMo Smelting (per 100 kg of MoO_3 in the Concentrate with 60% Mo)

Component	Al Reduction	SiCa Reduction	Al and Si Reduction	Si Reduction
Fe-75%Si	31.5	21–23		38
Granulated Al	9			5
FeSiCa		17–18		
Fe-45%Si-10%Al			65	
FeMo scrap				5.5
CaF_2			7	7.5
Lime				2.5
Iron (steel) chips	5–6	18		
Iron mill scale	29	16–18	35	51
MoO_3 captured dust				9.5

(~1760°C). Temperature of the melt in the first period determines the time of the second period (30 to 50 min) and the final result of melting. This time is needed to allow metal droplets to coagulate and to precipitate at the bottom of the hearth.

The liquid slag is tapped at the end of the process into the slag ladle via skimmer. Even though slag has a much lower density than ferromolybdenum alloy, metal droplets are not easily separated because of the high slag viscosity (Ivanov et al., 1984; Voronov et al., 2000) when slag has 60% to 70% SiO₂, 9% to 13% Al₂O₃, 7% to 11% FeO, and 6% to 9% CaO. The highest metal content in the slag is in the skimmer and stuck to the walls of the smelting hearth (slags with >0.3% Mo are recycled back to the process with ferromolybdenum scrap).

When processing low-grade concentrates (25% to 40% Mo), there is not enough exothermal heat to achieve reasonable amounts of reductant (Al and Si); in this case the process should be carried out in an electric furnace (Voronov et al., 2000). The charge is formed from low-grade concentrate, recycled slags, FeMo scrap, lime, and 65% Si ferrosilicon. Smelting in a 3.5 MVA furnace is carried out for 90 minutes (first period) with 30 minutes soaking for droplets removal. The best results were obtained with slags having CaO/SiO₂ = 0.85, giving <0.25% Mo in the slag and 50% to 51% Mo in the alloy. Although the molybdenum content is lower than in standard alloy, the process was reported to be efficient, as more expensive aluminum or FeSiAl alloy is not used.

All smelting processes release a substantial amount of fumes (~3% of used concentrate) containing MoO₃ and nonferrous metals; therefore, collected dust recycling is important. Typical dust composition as captured by electric filters has 10% to 15% Mo, <4% Bi, <10% Pb, <10% Zn, <0.5% Cu, 15% to 18% SiO₂, 10% to 12% FeO, <2% CaO, <5% MgO, and <7 Al₂O₃ as well as other impurities (As, Sn, Re, Cd, Se, Te, Ag, Au, etc.). Rhenium and noble metals have their special extracting technology. Collected dust was pelletized with coke, lime, and fluorspar and fed into a small furnace (0.5 MVA). The addition of lime combines molybdenum into CaMoO₄, decreasing losses with vapors and increasing the reduction temperature (so molybdenum retains in the slag phase). The slag contains 10% to 13% Mo, <2% Pb, <6% Zn, and <0.1% Bi. The by-product alloy has essentially bismuth (40% to 43% Bi) and lead (57% to 60% Pb) with little molybdenum (<0.01% Mo). In this way both slags and dust from the FeMo smelting are recycled.

REFERENCES

- Gasik, M.I., Lyakishev, N.P., Gasik, M.M., 2009. Physical chemistry and technology of ferroalloys [in Ukrainian]. Sistemnye Tehnologii, Dnipropetrovsk, 494 pp.
- Gourtsoyannis, L., Guthrie, R.I.L., Ratz, G.A., 1984. The dissolution of ferromolybdenum, feroniobium and rare earth (lanthanide) silicide in cast iron and steel melts. Proceedings of the 42nd Electric Furnace Conference, Toronto, Canada. 119–132.

- Ivanov, I., Donchev, I., Georgiev, A., 1984. Phase and structural studies of ferromolybdenum slags. Metalurgiya (Sofia) 39, 6–11.
- Kirby, A.W., Fray, D.J., 1993. Nitriding of ferromolybdenum powder. Journal of Materials Science Letters 12, 633–636.
- Kummer, J.T., 1979. Molybdenum. Bureau of Mines, Washington DC, 23 pp.
- Pattnaik, S.P., Mukherjee, T.K., Gupta, C.K., 1981. Ferromolybdenum from ferrimolybdate. Metallurgical and Materials Transactions B 12, 770–773.
- Voronov, Yu.I., Zaiko, V.P., Zhuchkov, V.I., 2000. Technology of molybdenum ferroalloys. IMET UrO RAS, Ekaterinburg, 267 pp.

Technology of Vanadium Ferroalloys

Michael Gasik

Aalto University Foundation, Espoo, Finland

Chapter Outline

13.1 Properties of Vanadium and Its Compounds	397	13.4 Technology of Ferrovanadium	405
13.2 Sources of Vanadium	401	13.4.1 Reduction by Silicon	405
13.3 Treatment of Vanadium Raw Materials	402	13.4.2 Technology of Ferrovanadium by Reduction by Aluminum	407
13.3.1 Chemical Treatment of Vanadium Raw Materials	404		
13.3.2 Metallurgical Processing of Vanadium Raw Materials	404	13.5 Technology of Other Ferrovanadium Alloys	407
13.3.3 Reduction of Vanadium from Oxides	405	13.6 The Technology of Nitrided Ferrovanadium	408
		References	409

13.1 PROPERTIES OF VANADIUM AND ITS COMPOUNDS

Vanadium is an element of the fifth group of the periodic table. Its serial number is 23, its atomic weight is 50.94, and its external electron configuration is $3d^34s^2$, which allows it to take valence states from +2 to +5. The melting temperature of pure vanadium is 1920°C, the boiling point is ~3400°C, and its density at 20°C is 6.11 g/cm³. Because of its high melting point, vanadium belongs to the refractory metals group (niobium, tantalum, chromium,

molybdenum, tungsten). Like most of the refractory elements, pure vanadium is ductile, but impurities usually make it brittle.

Vanadium is mainly used as an alloying addition to steel (already at 0.01% to 0.05% V), as it promotes the formation of finer grain size, increases hardenability, and improves wear resistance through the precipitation of its carbides and nitrides (vanadium is a strong carbide former, which causes carbide particles to form in the steel). These features are used in a large variety of steels (constructional grades, carburizing steels, rail steels, and especially in heat-resisting tool and die steels and special stainless steels). Vanadium is also an important beta-phase stabilizer for titanium alloys and other special alloys widely used in turbine motors, automobile parts, jet-aircraft engines, and so on, where high temperature creep resistance is a basic requirement (Baroch, 2005).

With iron, vanadium forms a continuous series of BCC (ferrite type) solid solutions with a minimum melting temperature (Fig. 13.1). Below 1250°C there is an area of σ -phase in a wide temperature range, which is similar to one forming in the Fe-Cr system.

In the system V-C (Fig. 13.2), there are three known vanadium carbides, of which V_2C and VC are rather refractory and have a substantial homogeneity range (somewhat similar to the W-C system).

With silicon, vanadium forms several silicides (Fig. 13.3), known as V_3Si , V_5Si_3 , V_6Si_5 , and VSi_2 , of which V_3Si has a noticeable homogeneity region around 21.4% to 25% (at.) Si.

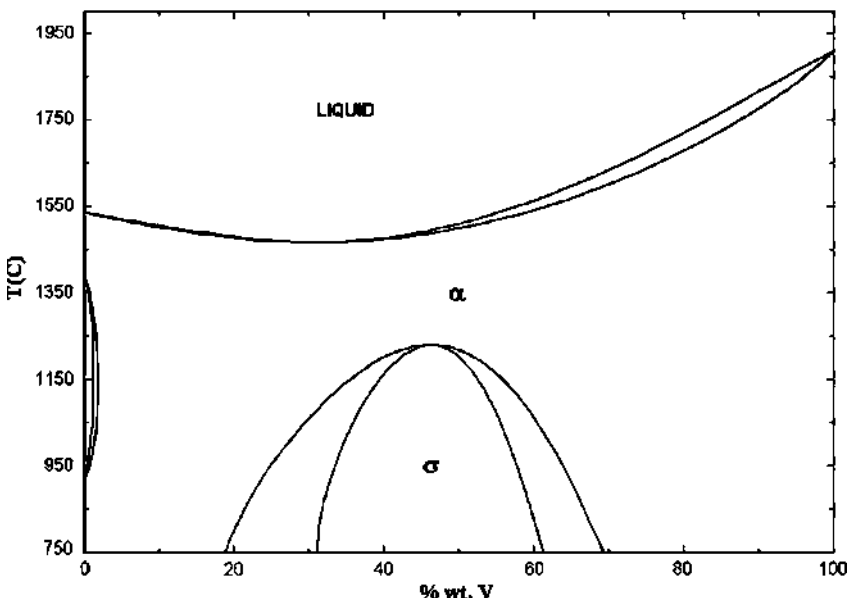


FIGURE 13.1 Equilibrium phase diagram of the Fe-V system.

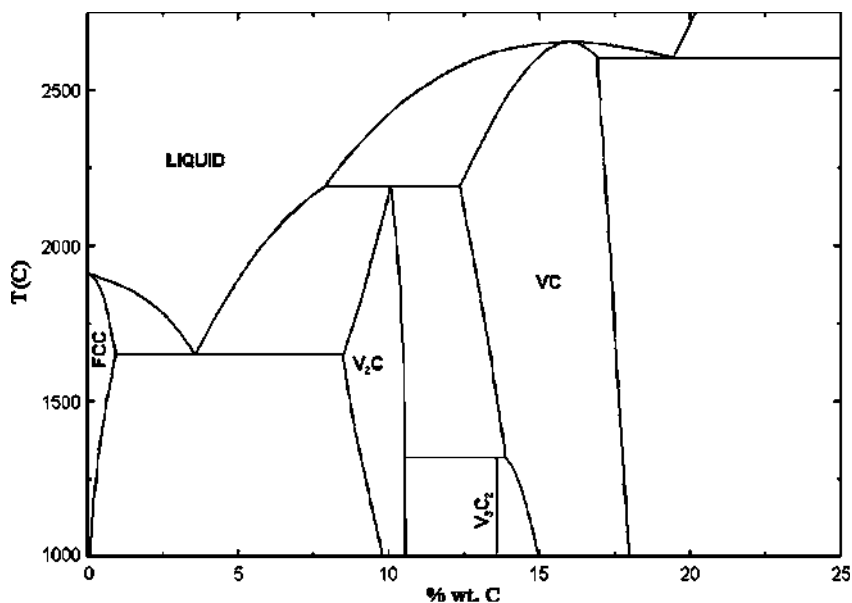


FIGURE 13.2 Diagram of the equilibria in the V-C system.

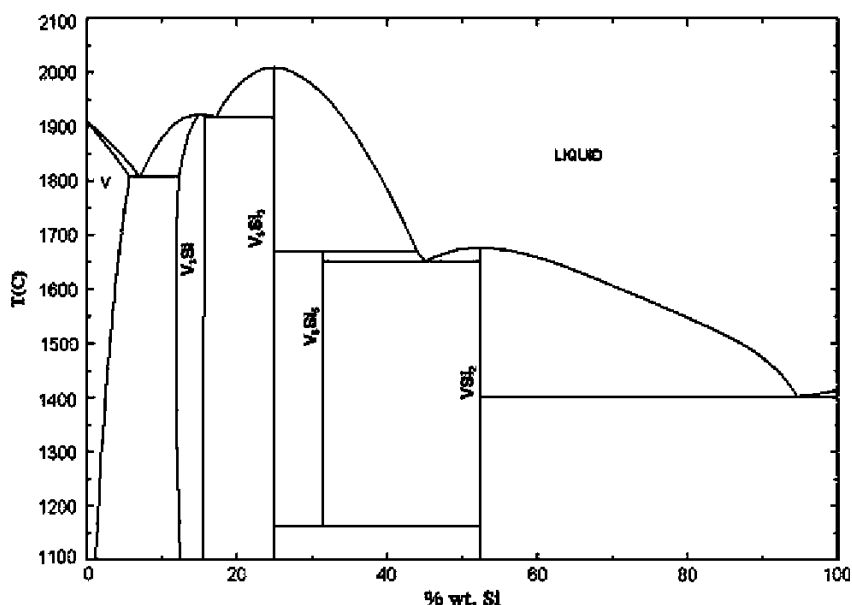


FIGURE 13.3 Diagram of the equilibria in the V-Si system.

Several intermetallics are known in the system V-Al (Fig. 13.4). Aluminide V_5Al_8 is the most refractory of those intermetallics.

The system V-O (Fig. 13.5) is rather complex, resembling similar equilibria in the Ti-O system. The most stable vanadium oxides are δ -VO, V_2O_3 and V_2O_5 . The density of oxide VO is 5.76 g/cm³, the density of V_2O_3 is 4.87 g/cm³, and the density of V_2O_5 is 3.36 g/cm³. With the increase in the oxidation state of vanadium, its oxides acquire more enhanced acidic properties and their overall chemical resistance increases. The higher vanadium oxides (Magnelli phases, as in the case of the Ti-O or Mo-O system) might be expressed by the common formulas V_nO_{2n-1} ($n = 3-6$) and V_nO_{2n+1} ($n = 3$ and 6). As Figure 13.5 shows, many vanadium oxides are characterized by rather wide homogeneity ranges.

Vanadium oxides form with iron oxide spinel FeV_2O_4 and $2FeO \cdot V_2O_3$ as well as a series of solid solutions with a wide range of homogeneities. With CaO, vanadium pentoxide has three known vanadates ($CaO \cdot V_2O_5$, $2CaO \cdot V_2O_5$, and $3CaO \cdot V_2O_5$) and at least five nonvariant equilibria and three eutectics, but this system has not yet been well studied throughout its concentration range. With alumina, V_2O_5 has one compound, $Al_2O_3 \cdot V_2O_5$ ($AlVO_4$), which melts incongruently at 695°C. Vanadium compounds are present in ores and slags in different forms, and it is customary to recalculate the amount of vanadium on the V_2O_5 basis.

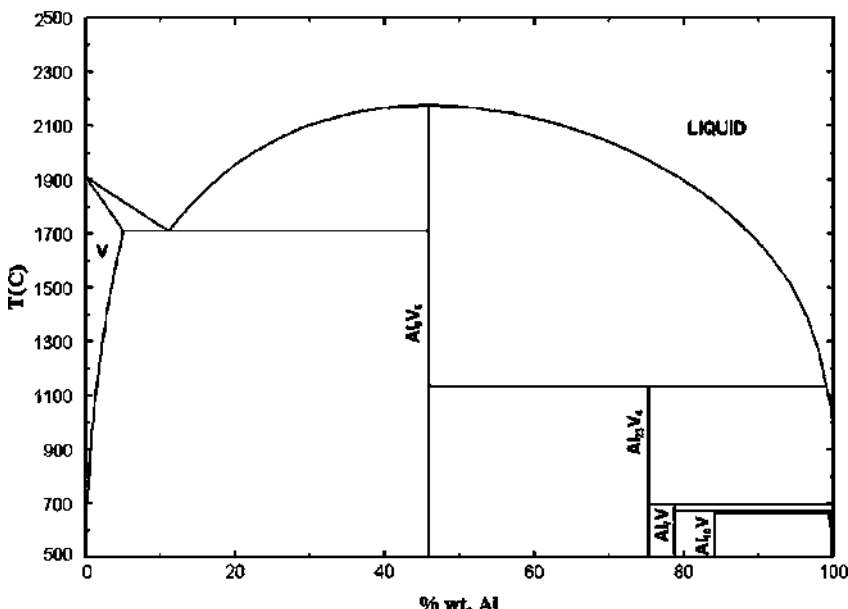


FIGURE 13.4 Equilibrium phase diagram in the V-Al system.

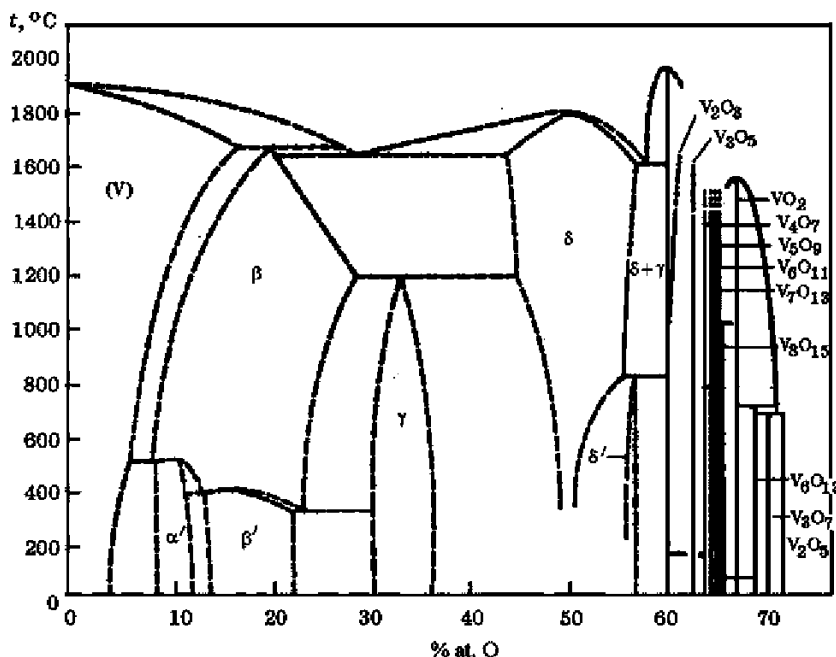


FIGURE 13.5 Combined diagram of the equilibria in the V-O system: α' - V_9O , β , β' - V_4O , γ - V_2O , and δ - VO .

13.2 SOURCES OF VANADIUM

Although it is abundant in Earth's crust and oil deposits, vanadium is, however, present in concentrations that make it too uneconomical to process it alone. Thus, most vanadium coming from primary sources is usually co-produced along with the recovery of other minerals or substances. Estimated world vanadium reserves are considered to be sufficient to meet vanadium demand into the 21st century based on the present demand. This does not account for the increased recovery of vanadium from fly ash, petroleum residues, slag, and spent catalysts (Baroch, 2005).

The most important minerals of vanadium are shown in Table 13.1. The vanadium minerals of industrial importance are mainly titanomagnetite, kulsonite, roscoelite, and carnotite. Industrial sources of vanadium are usually classified into the following groups and subgroups:

1. Vanadium ores, where vanadium might be considered to be the leading element ($>3\%$ V_2O_5), usually a subgroup of roscoelite
2. Complex vanadium ores of nonferrous and rare metals, 1% to 3% V_2O_5 (carnotite, vanadium bauxite)

TABLE 13.1 Some Important Minerals of Vanadium

Mineral/Group	Approximate Formula
Sulfides	
Patronite	V ₂ S
Bravoite	(Fe,Ni,V)S ₂
Sulvanite	3Cu ₂ S·V ₂ S ₆
Oxides	
Davidite	(Fe,Cr)(Ti,U,V,RE)O ₃
Roscoelite	K(V,Al,Mg) ₃ (AlSi ₃)O ₁₀ (OH) ₂
Kulsonite	(Fe,V) ₃ O ₄
Carnotite	K ₂ (UO ₂) ₂ (VO ₄)·3H ₂ O
Vanadinite	Pb ₅ (VO ₄) ₃ Cl
Descloizite	4(Cu,Pb,Zn)O·V ₂ O ₅ ·H ₂ O
Cuprodescloizite	5(Cu,Pb)O·(V,As) ₂ O ₅ ·2H ₂ O
Vanadiferous phosphate rock	Ca ₅ (PO ₄ ,VO ₄) ₃ (F,Cl,OH)
Titaniferous magnetite	(Fe,V,Ti) ₃ O ₄

3. Ferrous ores with <1% V₂O₅ (magnetite, titanomagnetite, oolitic limonite),
4. Other fossil fuels <1% V₂O₅ (mostly of petrochemical origin such as asphaltites, bitumen, shale oil, coal, some phosphates).

Most world vanadium ore deposits are located in South Africa, the United States, Russia, Australia, China, Mexico, and Venezuela, but vanadium can be recovered at any large-scale petrochemical industry (Xiao et al., 2010). A recently mapped Siberian deposit (in the Baikal-Amur region of Russia) was found to hold a substantial reserve of vanadium (more than 50 million tons), making this field somewhat unique in the world. This ore contains 25% to 35% Fe, 4% to 7% TiO₂, and 0.35% to 0.55% V₂O₅ (Gasik et al., 2009). Other potentially relevant impurities in this ore are copper (0.01% to 0.40%), cobalt, platinum, and palladium.

13.3 TREATMENT OF VANADIUM RAW MATERIALS

The main source of vanadium for metallurgy is titanomagnetite ores, which are dressed into enriched concentrates (see the example in Table 13.2) for

TABLE 13.2 Chemical Composition, %, Vanadium Ores and Concentrates

	Fe ₂ O ₃	V ₂ O ₅	TiO ₂	SiO ₂	Cr ₂ O ₃	Al ₂ O ₃	MnO	CaO	MgO	P	S
Ore (Russia)	32–38	0.1–0.7	4–14	4–16	<0.7	4–12	<0.3	2–7	4–8	0.01–0.02	0.01–0.06
Ore (Ukraine)	53–55	0.1–0.15	—	20	—	8	5	2	0.4	1	0.2
Concentrates	53–69	0.5–8	2–15	6–11	<0.1	2–7	<0.4	1–3	0.9–3	0.01–0.4	<0.04

metallurgical processing to produce V_2O_5 and ferrovanadium (Gasik et al., 2009) as well as vanadium-bearing slags (Lindvall et al., 2010).

The industrial technology of vanadium extraction from the titanomagnetite is based on multistep metallurgical and chemical repartitions obtaining commercial vanadium pentoxide (V_2O_5). In addition, vanadium is often recovered from uranium–vanadium ores and from ferrophosphorus as a by-product in the production of elemental phosphorus (Baroch, 2005), as well as from petroleum products (Xiao et al., 2010).

13.3.1 Chemical Treatment of Vanadium Raw Materials

Vanadium ores are usually crushed, ground, screened, mixed with NaCl or Na_2CO_3 (soda), and roasted at 850° to 1100°C for 2 to 3 hours. The purpose of roasting is to oxidize iron and vanadium components to the highest oxidation degree and to convert vanadium into the water-soluble form (NaVO_3). Sodium vanadate is readily soluble in water and in dilute acids and carbonates. Leaching of vanadium compounds from the calcined mixture is carried out in two stages with the precipitation of V_2O_5 . The first extract is treated with sulfuric acid to precipitate sodium hexavanadate ($\text{Na}_4\text{V}_6\text{O}_7$) at $\text{pH} = 2\text{--}3$, which together with other impurities forms a “red cake.” This product is converted to vanadium pentoxide of technical grade (87% to 90% V_2O_5 , 0.010% to 0.015% P, with the balance consisting mostly of Na_2O) by heating to 700° to 1000°C . To obtain higher purity, the second stage is used, whereby this red cake is treated with soda solution and purified from Fe, Al, Si, and other impurities first by pH adjustment. Finally, ammonium vanadate is precipitated and calcined to yield >99.5% V_2O_5 product (Baroch, 2005). In principle, a similar method is used for vanadium extraction from carnotite (together with uranium), but additionally there is usually a liquid–liquid extraction stage for vanadium and uranium separation.

13.3.2 Metallurgical Processing of Vanadium Raw Materials

Two main routes are used industrially for vanadium processing by metallurgical means: pig iron smelting in blast furnaces and pig iron smelting in submerged arc furnaces, followed by oxygen conversion into vanadium-rich slag. For the blast furnace technology (Gasik et al., 2009), there are some peculiarities compared to the conventional smelting of pig iron. For a more complete transition of vanadium in iron, the process is carried out at 1300° to 1350°C , and the basicity of slag is maintained at 0.8 to 0.9. The resulting cast iron contains ~0.45% V, 0.1% to 0.4% Si, and 0.2% to 0.3% Ti. About 80% to 85% of vanadium is reduced into the cast iron. This metal is blown by oxygen into converters producing slag with 12% to 24% V_2O_5 , 20% to 25% SiO_2 , and 30% to 45% FeO . The major form of vanadium in these slags is V^{3+} in vanadium spinels $(\text{Fe},\text{Mn},\text{Mg})\text{O} \cdot (\text{V},\text{Fe},\text{Al},\text{Cr})_2\text{O}_3$. The slag is used for vanadium

extraction by chemical methods (as described previously) or for smelting vanadium ferroalloys (Gasik et al., 2009).

The recovery of high vanadium slags from titanomagnetites is also realized by partially reducing vanadium ore with coal in large rotary kilns and then feeding this hot ore into a submerged arc electric smelting furnace. Here slag contains substantial amounts of titania, but the metal is similar to that obtained in blast furnaces. Conversion of the metal to vanadium-rich slag is the same with either the bottom or the top oxygen blowing method (Baroch, 2005).

13.3.3 Reduction of Vanadium from Oxides

Reduction of vanadium is in principle possible via carbon, silicon, and aluminum. Carbon reduction, however, ends up with the formation of high-carbon product due to the strong predilection of vanadium to form carbides (VC). Silicon and aluminum allow the formation of vanadium-rich metal. Aluminum reduction is very exothermic and requires some dummy load components to decrease specific heat generation during the process (Gasik et al., 2009).

13.4 TECHNOLOGY OF FERROVANADIUM

Depending on the content of impurities different ferrovanadium grades are produced (Table 13.3). As described previously, it is possible to obtain ferrovanadium by either silicon or aluminum reduction, and both processes are used commercially.

13.4.1 Reduction by Silicon

Ferrovanadium is produced by the reduction of V_2O_5 by silicon from ferrosilicon in the presence of lime in the electric arc furnace (3 MVA). The technology used for the smelting of ferrovanadium in the electric arc furnace utilizes three periods. The purpose of the first period is to restore vanadium from the current (return) fusion products of the third period of the previous heat. The charge, consisting of a recycled furnace slag, lime flux, ferrosilicon, aluminum, vanadium pentoxide, and iron chips, is loaded (Table 13.4). After the first period (80 to 100 min), V_2O_5 content in the slag is reduced to 0.25% to 0.35%, and the metal ends with 25% to 30% V, 20% to 24% Si, and 0.3% to 0.5% C. The slag with this low content of vanadium is tapped from the furnace.

In the second period, the basic operations are to restore additional V_2O_5 with silicon and aluminum to increase vanadium content in the metal >35% V and to decrease silicon content in the metal below 10% to 12% Si. Here the charge loaded in the second period is composed of vanadium pentoxide, lime, FeSi75, and aluminum (see Table 13.4). After melting, the mixture is stirred to accelerate the recovery of vanadium. At this time, the metal contains 6% to 8%

TABLE 13.3 The Composition of Ferrovanadium, % wt. max.*

Grade	V	Si	Al	C	S	P	As	Cu	Mn
FeV75C0.1	70–85	0.8	2	0.1	0.05	0.05	0.05	0.1	0.4
FeV75C0.15	70–85	1	2.5	0.15	0.1	0.1	0.05	0.1	0.6
FeV50C0.4	48–60	1.8	0.2	0.4	0.02	0.07	0.01	0.2	2.7
FeV50C0.5	48–60	2	0.3	0.5	0.02	0.07	0.01	0.2	4
FeV50C0.6	48–60	2	0.3	0.6	0.03	0.07	0.02	0.2	5
FeV50C0.3	>50	2	2.5	0.3	0.1	0.1	0.05	0.2	0.2
FeV50C0.75	>50	2	2.5	0.75	0.1	0.1	0.05	0.2	0.2
FeV40C0.5	35–48	2	0.5	0.5	0.05	0.08	0.03	0.4	2
FeV40C0.75	35–48	2	0.5	0.75	0.05	0.08	0.03	0.4	4
FeV40C1	35–48	2	0.5	1	0.05	0.1	0.03	0.4	6

*The two first grades (FeV75) are produced by aluminum reduction, others by silicon reduction.

Si and the slag contains 8% to 10% V₂O₅, and ferrosilicon and aluminum are loaded at this stage. When the metal composition reaches 35% to 40% V, 9% to 12% Si, and 0.4% to 0.6% C and the V₂O₅ content in the slag drops to <0.35% V₂O₅, the second period (~1 h) ends and the slag is tapped.

TABLE 13.4 Consumption of Charge Materials (kg) in the Smelting of Ferrovanadium

Materials	Smelting Period			Total
	1	2	3	
V ₂ O ₅ (technical grade 75%)	250	1000	900	2150
Lime	1100	2000	1000	4100
Steel chips	500	—	—	100
Recycled slag of the third period	1932	—	—	—
FeSi75	800	210	—	1010
Aluminum	50	55	—	105
Tapped metal from the previous period	—	1417	1866	—

In the third period (refining; 40 to 60 min) more lime and vanadium pentoxide are added (Table 13.4), and the purpose is to utilize reaming silicon in the metal to reduce more vanadium. The metal is tapped upon reaching <2% Si into a refractory-lined ladle. The slag from the third period (12% to 16% V₂O₅) is tapped into the skimmer and used in the first period of the next heat. Ferrovanadium is poured from the ladle into vertical cast-iron molds (Gasik et al., 2009).

13.4.2 Technology of Ferrovanadium by Reduction by Aluminum

The aluminothermic process for preparing a ferrovanadium alloy differs from silicon reduction processes in that the reaction is highly exothermic and it allows the production of ferrovanadium with low carbon content (0.02% to 0.06% C). The charge consists of vanadium pentoxide, aluminum powder, steel chips (iron scrap), and lime. The process might be improved with some additions of magnesia. Maximum metal output is achieved when lime content is about 30% to 40% by weight of the vanadium pentoxide amount. The metal contains 82% to 84% V, 1% to 2% Si, <0.05% P, 0.1% Ti, 1.5% Mn, and slag ends with <4.5% V₂O₅. Extraction of vanadium (yield) in the alloy is 90% to 96%.

The vanadium loss with the slag can be reduced by using additional heating at the end of the process. In this case the smelting starts in the furnace (350 kVA) with risen electrodes and proceeds normally without a power supply (Gasik et al., 2009). Upon finishing, the power is turned on and the slag and metal are heated and mixed to improve conditions for the recovery of vanadium and the deposition of metal drops. The dumped slag <1% V₂O₅ is tapped and the excess aluminum in the metal is reduced by the addition of a controlled amount of V₂O₅ and FeO. If the vanadium content in the slag remains high, it is recycled to the next heat.

Ferrovanadium can also be prepared by the thermite (exothermic) reaction, in which vanadium and iron oxides are co-reduced by aluminum granules in a magnesite-lined steel vessel or in a water-cooled copper crucible (Baroch, 2005). This method is also used to prepare vanadium master alloys.

13.5 TECHNOLOGY OF OTHER FERROVANADIUM ALLOYS

Ferrosilicovanadium (Table 13.5) is obtained directly from the converter slag in the electric furnace batch process by reducing vanadium with ferrosilicon with lime and fluorspar as fluxes. The process is carried out in a submerged-arc electric furnace with either silicon or carbon (for alloys with >2.5% C).

For alloying structural steels with vanadium and manganese, FeMnV alloys have been developed (Table 13.6). They are produced similarly to FeSiV, and their costs normalized to 1 kg of vanadium in them is 35% to 40% lower than for standard FeV alloys.

TABLE 13.5 Chemical Composition, % wt. of FeSiV Alloys

Grade	V	Si	Ti	Mn	Cr	C	P	S
			Max.					
FeVSi1	>10	14	3	10	2.5	1.5	0.1	0.03
FeVSi1A	>10	10–20	3	10	4	1.5	0.15	0.03
FeVSi2	>8	20	5	15	4	3	0.2	0.08

TABLE 13.6 Chemical Composition, % wt., of FeMnV Alloys

Grade	Mn	V	C	Si	P	S
			Max.			
FeMnV1	40–50	7–10	2.5	3	0.1	0.005
FeMnV2	45–55	4.5–6	2.5	3	0.1	0.005
FeMnV3	60–65	3–4.5	2.5	3	0.1	0.005
FeMnV4	45–55	4.5–6	6.5	5	0.1	0.005
FeMnV5	60–65	3–4.5	6.5	5	0.1	0.005
FeMnV6	75–78	1.5–2.5	7.5	5	0.1	0.005

13.6 THE TECHNOLOGY OF NITRIDED FERROVANADIUM

Vanadium actively reacts with molecular nitrogen (or other nitrogen-containing substances) above 700°C, forming nitride (VN). It is a refractory nitride (melting point ~2360°C) and an efficient hardener in steels when it forms in situ during thermal treatment (nitride (VN) or carbonitride (V[C,N])). Nitrided ferrovanadium can be obtained in different ways: (1) the solid phase method by saturation of the FeV alloy powder with nitrogen (6% to 8% N) at 900°C, (2) from the melt by blowing with nitrogen (3% to 4% N), and (3) by plasma nitriding (0.3% to 0.5% N). There are also methods of FeVN processing that utilize self-propagating high-temperature synthesis (SHS) on a small scale; nitriding can also be applied to FeSiV alloys.

The addition of nitrided FeV to the steel is accompanied by the dissolution of both vanadium and nitrogen, which recombines upon crystallization of steel ingots and during the subsequent heat treatment.

REFERENCES

- Baroch, E.F., 2005. Vanadium and vanadium alloys. In: Kirk-Othmer Encyclopedia of Chemical Technology, volume 24. John Wiley & Sons, New York, pp. 782–797.
- Gasik, M.I., Lyakishhev, N.P., Gasik, M.M., 2009. Physical Chemistry and Technology of Ferroalloys [in Ukrainian]. Dnipropetrovsk: Sistemnye Tehnologii, 494 pp.
- Lindvall, M., Rutqvist, S., Ye, G., 2010. Recovery of vanadium from V-bearing BOF-slag using an EAF. Proceedings of the Conference INFACON-XII. Helsinki, Finland, 189–195.
- Xiao, Y., Mambote, C.R., Jalkanen, H., Yang, Y., Boom, R., 2010. Vanadium recovery as FeV from petroleum fly ash. Proceedings of the Conference INFACON-XII. Helsinki, Finland, 179–88.

Technology of Niobium Ferroalloys

Mihail I. Gasik

National Metallurgical Academy of Ukraine, Dnipropetrovsk, Ukraine

Chapter Outline

14.1 Properties of Niobium	411	14.3 Technology of Niobium	
14.2 Sources of Niobium and Its		Ferroalloys	416
Reduction	415	References	419
14.2.1 Minerals of Niobium	415		
14.2.2 Reduction of			
Niobium	416		

14.1 PROPERTIES OF NIOBIUM

Niobium (an American term also referred to as columbium, Cb) belongs to the group V elements of the periodic table. It has number 41, an atomic weight of 92.9, a density of 8.57 g/cm³, and an atomic electron configuration of 4d⁴5s¹. The most stable compounds are formed with pentavalent niobium (+5), but there are also known compounds with oxidation states +4, +3, +2, and +1. The melting temperature of niobium is reported to be 2470°C, and the boiling point is 4927°C. The crystal lattice of niobium is body-centered cubic (BCC) with a = 0.3294 nm.

Niobium has become useful in steelmaking because of its ability to control carbides, nitrides, and material grain size, especially at elevated temperatures. Niobium in steels forms finely dispersed carbide NbC and nitride NbN. Niobium improves the resistance of stainless steels to intercrystallite corrosion, reaching its maximal value at mass ratios Nb/C > 10. Niobium alloyed (<1.5% Nb) chromium–molybdenum steels (2% to 13% Cr, <0.6% Mo) are often used in high-temperature applications such as for boilers. In low-alloyed steels, niobium is widely used as a microalloying element, which in combination with

controlled thermal-mechanical treatment is important for many varieties of high-strength, low-alloy (HSLA) steels. Minor niobium additions also promote the corrosion resistance of iron alloys. As a metal, niobium has applications in tool steels, wear- and abrasion-resistant and stainless steels, and various superalloys (Eggert et al., 1982).

Niobium and iron have complete mutual solubility in the liquid state (Fig. 14.1). In the solid state, several intermetallic compounds form, such as $\text{Nb}_{19}\text{Fe}_{21}$ (also reported as Nb_6Fe_7 ; decomposition $> 1500^\circ\text{C}$) and NbFe_2 (1655°C). The existence of η -phase Nb_3Fe_2 has also been mentioned. Alloys such as standard ferroniobium ($\sim 50\%$ to 70% Nb + Ta) have liquidus points in the range 1580° to 1620°C .

With carbon niobium forms two stable carbides (Fig. 14.2): Nb_2C (5.43% to 5.83% wt. C) and NbC (stoichiometric compositions 11.45% wt. C, melting point 3613°C , density of 7.82 g/cm^3). Carbides have a wide range of homogeneity. The existence of metastable carbide Nb_3C_2 has not yet been confirmed. Carbide Nb_2C has three modifications: α -phase (rhombohedral $< 1200^\circ$ to 1230°C), β -phase (hexagonal, 1200° to 2500°C), and γ -phase (disordered hexagonal, $> 2500^\circ\text{C}$). Maximal solubility of carbon in solid niobium is up to 1% wt. C at eutectic temperature.

Niobium has a high affinity for phosphorus, forming the thermodynamically strong phosphides NbP (with a wide homogeneity range $\text{NbP}_{0.8-1.2}$) and NbP_2 . The latter phosphide decomposes upon melting ($\sim 1730^\circ\text{C}$).

In the system Nb-Si (Fig. 14.3), three stable silicides have been identified: Nb_3Si , Nb_5Si_3 , and NbSi_2 , among which Nb_5Si_3 has different structures in high-temperature (β) and low-temperature (α) ranges. This intermetallide usually

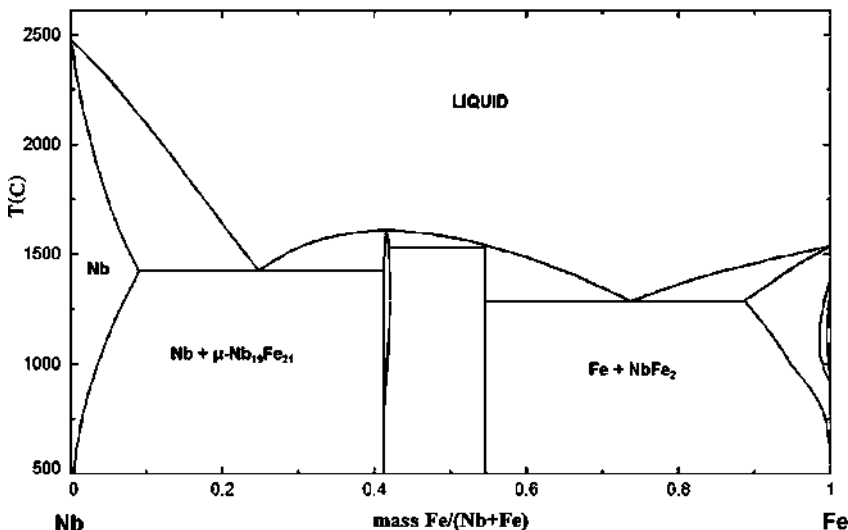


FIGURE 14.1 Equilibrium state diagram of the system Nb-Fe.

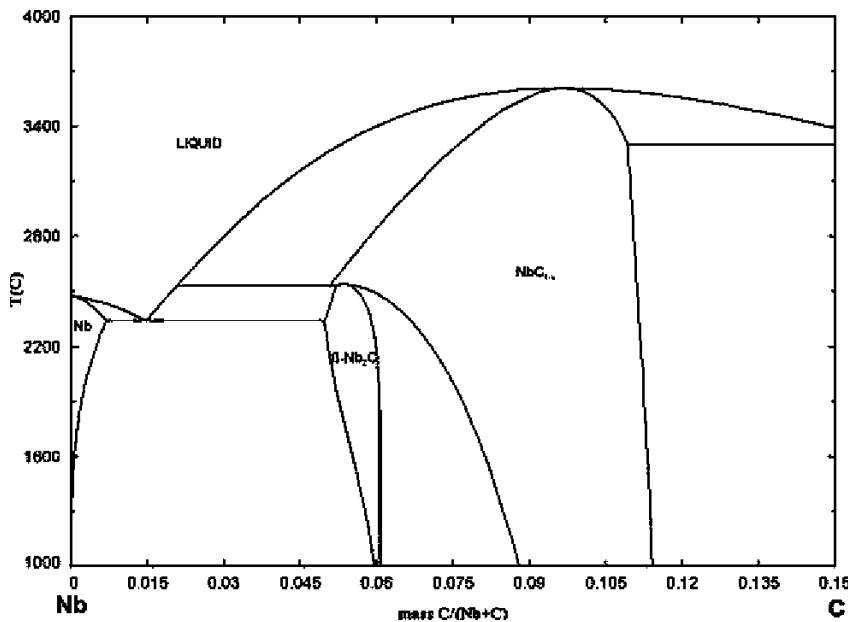


FIGURE 14.2 Equilibrium diagram of the system Nb-C.

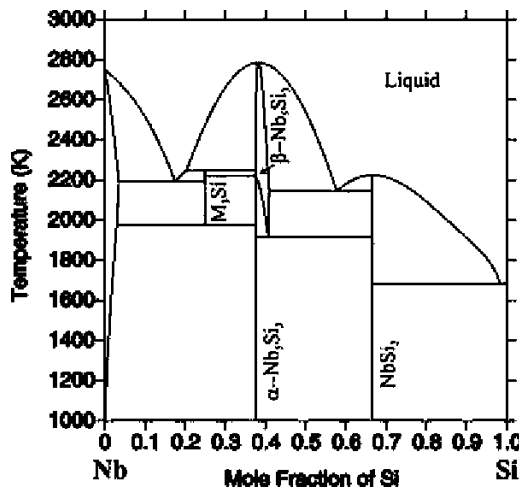


FIGURE 14.3 Equilibrium diagram of the system Nb-Si.

forms in the standard FeNb alloy and increases the melting temperature of the alloy. Silicon dissolves in Nb < 0.5 at. % at 1170°C and < 1.2 at. % at 1920°C, but niobium is practically insoluble in silicon. The silicon percentage in FeNb actually determines its liquidus temperature, phase constitution, and density.

With aluminum niobium forms a number of niobium aluminides—NbAl₃, Nb₂Al, and Nb₃Al (Fig. 14.4)—all having rather high melting points: 1694, 1933, and \sim 2050°C, respectively. The eutectic temperature in the NbAl₃–Nb₂Al range is 1598°C. The solubility of Al in niobium at peritectic temperature is 21% to 23% at. Al, and niobium in aluminum is below 0.3% at. Nb.

With oxygen, niobium forms three stable oxides (Fig. 14.5), namely NbO (melting point 1945°C), NbO₂ (melting point 1915°C), and Nb₂O₅ (melting point 1510°C). The latter oxide is a commonly appearing form in niobium-containing minerals and is a base for many niobate systems. It has three known modifications, of which the monoclinic β -phase is the most stable for metallurgical conditions. The other two phases eventually appear during the oxidation of niobium at low (α -phase) or high (γ -phase) temperatures.

Another oxide phase, Nb₄O₅ (not shown in Fig. 14.5; tetragonal lattice type), was found in the residuals of electrolysis of Nb-O-F melts, and its formation mechanism has not yet been studied.

Three niobates are formed with calcium oxide (Fig. 14.6) as CaO·Nb₂O₅, 2CaO·Nb₂O₅, and 3CaO·Nb₂O₅, all of them with rather high melting points.

Contrary to CaO, there are no chemical compounds in the Nb₂O₅–SiO₂ system, which is of a eutectic type. Both oxides Nb₂O₅ and SiO₂ have an acidic nature. Above 1695°C there is a wide region of two immiscible liquids. With alumina, Nb₂O₅ does form three stable compounds: Al₂O₃·Nb₂O₅, Al₂O₃·9Nb₂O₅, and Al₂O₃·25Nb₂O₅.

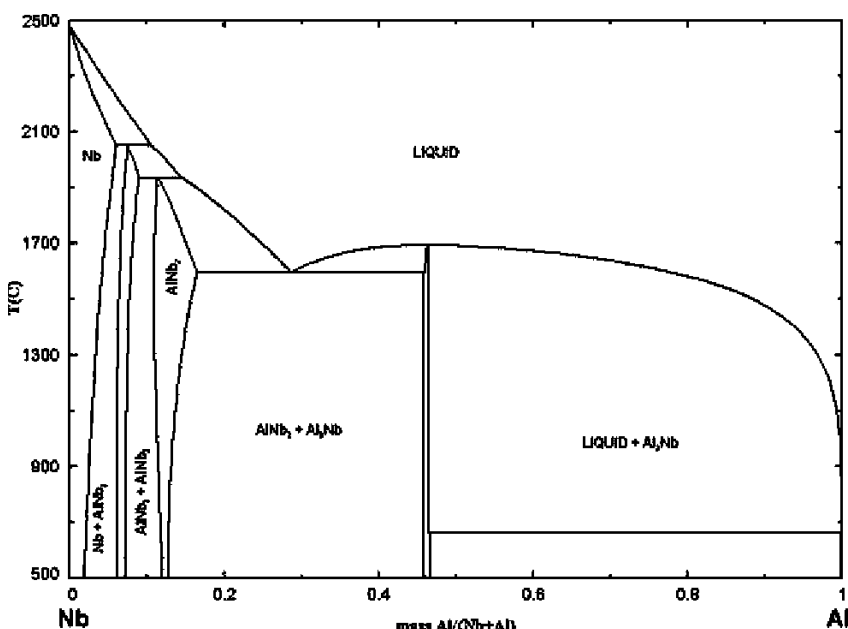


FIGURE 14.4 Equilibrium state diagram of the system Nb-Al.

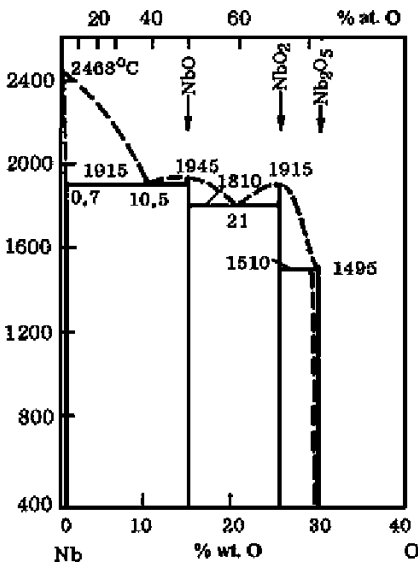


FIGURE 14.5 Phase diagram of the system Nb-O.

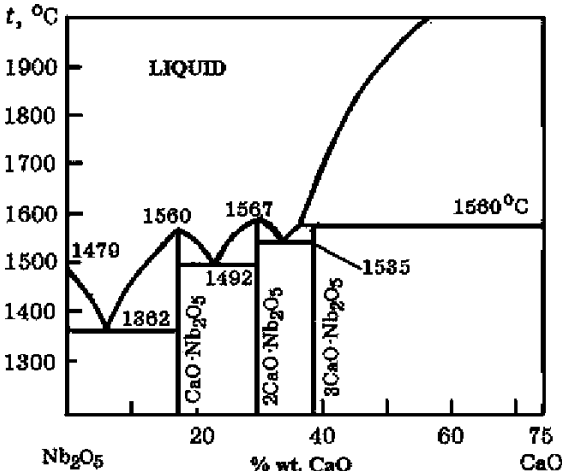


FIGURE 14.6 Equilibrium state diagram of the system Nb₂O₅-CaO.

14.2 SOURCES OF NIOBIUM AND ITS REDUCTION

14.2.1 Minerals of Niobium

Niobium, together with tantalum, appears in a large group of minerals (tantalum-niobates). A generalized formula of these minerals might be written as $A_nB_mX_p$, where “A” represents cations of large size (Ca^{2+} , REM^{3+} , U^{4+} ,

Th^{4+} , Na^+ , and possibly Pb^{2+} , Sb^{2+} , Bi^{3+}) and medium size (Fe^{2+} , Mn^{2+} , Mg^{2+}); “B” sites are Nb^{5+} , Ta^{5+} , replacing Ti^{4+} , Sn^{4+} , Fe^{3+} ; and anions “X” are O^{2-} , OH^- , F^- . Of the more than 130 known minerals that contain niobium (tantalum), six minerals are of a direct industrial relevance (Gasik et al., 2009). The most important niobium minerals that compose the niobium ores are columbite ($\text{Fe}, \text{Mn}(\text{Nb}, \text{Ta})_2\text{O}_6$ (~50% to 67% Nb_2O_5) and pyrochlore ($\text{Ca}, \text{Na}_2(\text{Nb}, \text{Ta}, \text{Ti})_2\text{O}_6(\text{OH}, \text{F})$ with ~40% to 70% Nb_2O_5). If tantalum is dominating in columbite instead of niobium, the mineral is called tantalite. In some deposits, equally important is loparite ($\text{Ca}, \text{Na}, \text{Ce}(\text{Ti}, \text{Nb}, \text{Ta})\text{O}_3$ (~7–20% Nb_2O_5)). It falls in the class of niobium and rare earth perovskites (CaTiO_3), where calcium is partially replaced by REM, and titanium by niobium and tantalum. Besides loparite, other similar minerals of this type are knopite (CeTiO_3) and dizanalite ($\text{Ca}, \text{Na}, \text{Ce}(\text{Ti}, \text{Nb}, \text{Fe})\text{O}_3$).

Industrially suitable niobium ore, from which it is cost-effective to obtain niobium concentrates, contains at least 0.15% to 0.20% wt. Nb_2O_5 . In the richest niobium ores known in the world, the Nb_2O_5 content may reach up to 1% to 4%. The leading mineral resources of niobium at the moment are in Brazil (84.2% of total), Canada (9.8%), and Zaire (4.2%). The primary Brazilian ore is the pyrochlore type, which is easier to enrich than the columbite/tantalite ores (Gupta et al., 1994).

14.2.2 Reduction of Niobium

A reduction reaction of Nb_2O_5 by carbon is possible, but it will ultimately lead to the formation of niobium carbide (NbC). This practically excludes carbon from potential reductant lists, as niobium ferroalloys are limited in carbon content because of their intended applications.

Practically, niobium might be reduced either by silicon or aluminum. With silicon, the reaction $\text{Nb}_2\text{O}_5 + \text{Si} = \text{Nb} + \text{SiO}_2$ does not proceed to a great extent, and the extraction degree of niobium in such a process is usually small. The alloy with 50% to 60% Nb in this case is obtained with a high content of silicon (5% to 8% Si).

The best extraction of niobium is achieved via the reduction by aluminum, which has favorable thermodynamics for the reaction between Nb_2O_5 and aluminum $3\text{Nb}_2\text{O}_5 + 10\text{Al} = 6\text{Nb} + 5\text{Al}_2\text{O}_3$ (~1000 kJ/mol oxide Nb_2O_5) but less favorable for the reaction $3\text{NbO} + 2\text{Al} = 3\text{Nb} + \text{Al}_2\text{O}_3$ (~165 kJ/mol oxide NbO). The temperatures of the aluminothermic process reach 1800° to 2000°C and the extraction of niobium into the alloy approaches 99.8%.

14.3 TECHNOLOGY OF NIOBIUM FERROALLOYS

The content of niobium in standard ferroniobium is normally from 55% to 65% wt. The alloy also contains <2 Si, <5 Al, <2 Ti, <0.3 C, <0.03 S, <0.05 to 0.10 P, balance – Fe. The highest premium grades with 62% to 70% wt. Nb +

Ta are additionally limited in aluminum (<1% Al) and other components content (<0.2 Si, <0.1 C, 0.3 Ta, <0.5 Mn, <0.5 Cr, <0.02 S, <0.02 P). Because the concentration of niobium in most low-alloy and HSLA steels is less than 0.1% and in the highly alloyed steels <~1%, such impurities in the niobium ferroalloys do not usually present a problem, with the possible exception of phosphorus. On the other hand, as shown later, lower-grade FeNb alloys (50% to 60% Nb) with higher silicon (<15%) might also be produced from specific ores. However, this FeSiNb grade is more difficult to dissolve in steels than FeNb with low silicon, and thus the alloy is first crushed down to sizes below 20 mm. Most FeNb lumps might have relatively high gas concentrations (<0.05% to 0.2% wt. N, <0.2 O, <0.01 H). To improve the addition of niobium to steels, Nb-lean alloys and different master alloys have been designed and produced, among which Fe-25Nb, Fe-25Mn-40Nb, and Fe-30Ti-16Nb-10Al compositions could be mentioned (Gasik et al., 2009).

All smelting processes use niobium pentoxide Nb_2O_5 and niobium concentrates. The pentoxide should have more than 95% Nb_2O_5 and a limited amount of other impurities. The range of the variation of impurities (depending on the source) is (% wt.) 0.1 to 1.2 Ta_2O_5 , 0.02 to 1.8 SiO_2 , 0.06 to 0.9 TiO_2 , 0.09 to 4 Fe_2O_3 , 0.05 to 0.4 P, 0.03 to 0.1 C, 0.01 to 0.2 S, <0.02 As, <0.0006 Pb, and <0.03 Sn.

The methods for ferroniobium processing by aluminum reduction include (1) off-furnace smelting “on the block” (ingot), (2) smelting in the ladle with the release of metal and slag, and (3) smelting in an electric arc furnace.

The first method is no longer widely used because it has certain drawbacks, among which are the nonoptimal combination of smelting and crystallization of the metal and slag in one unit, the increased amounts of the charge and refractory materials required, higher labor costs for lining and disassembly of the reactor furnaces, and cleaning of metal and refractory slag. A single use of a reactor and the necessity to move each furnace with the liquid products from the melting chamber to the site for cooling add to the complexity of the process.

The second method includes the release of ferroalloy slag. In exothermic reactions, heat release is sufficient to self-sustain the process. The charge for this method consists of 100 kg of niobium pentoxide, 52 to 60 kg of aluminum, 38 to 40 kg of iron ore pellets, 20 kg of iron scale, 30 kg of lime, and ~0.1 kg of sodium nitrate (NaNO_3) to initiate the reaction. The melting rate after initiation of the reaction proceeds with rates of 160 to 180 $\text{kg}/(\text{m}^2\text{min})$. The furnace is lined with magnesite (MgO) bricks. For a batch run, the mass of pentoxide used is typically 1000 to 1200 kg Nb_2O_5 . Tapping of metal and slag is made into a cast-iron mold by tilting of the melting furnace. The melt is cooled in the mold for ~2.5 h, removed, and after an additional exposure for ~2 h, the metal and slag are delivered to a crusher.

The average consumption of the materials of 1 ton of Fe-50%Nb alloy is 758 kg of niobium pentoxide (base 100% Nb_2O_5), 385 kg of aluminum powder, 275 kg of iron ore (pellets), 86 kg of lime, and 31 kg of magnesite powder.

Respective composition of the slag is 70% to 75% Al_2O_3 , 9% to 12% CaO , 3% to 6% MgO , and 0.3% to 0.5% Nb_2O_5 , and during the solidification of the slag the mineral phases formed are, respectively, $\text{MgO}\cdot\text{Al}_2\text{O}_3$ (10% to 15%), $\text{CaO}\cdot 2\text{Al}_2\text{O}_3$ (75% to 85%), and $(\text{Ca},\text{K},\text{Na})\text{O}\cdot\text{Nb}_2\text{O}_5(\text{O},\text{F}) < 0.5\%$ to 3%. The properties of the slag after the grinding of the properties correspond to high-alumina refractory cements, and this slag is a valuable raw material for the production of high-alumina refractories.

The third method (melting in an arc furnace) is especially suitable for processing niobium-lean concentrates. It may have different versions, specifically the following:

1. Subsequent loading of the ore, aluminum, and flux mixture
2. Melting of the ore and flux of the mixture, followed by the addition of aluminum powder
3. Melting of the ore and flux mixture components with the subsequent addition of the remainder of the ore mixed with aluminum powder when the furnace power is off
4. Single-stage melting of a mixed charge together in an electric furnace to compensate for missing heat in the thermal balance.

The first method is characterized by low productivity of the furnace. Here, especially in the initial period, the interaction of the oxide with aluminum cannot be regulated. The degree of extraction of niobium does not exceed 70% to 80%, and the loss of aluminum as a result of oxidation reaches 30% to 40%.

The two-stage process is used for niobium ores containing high concentrations of tin (2% SnO_2) and phosphorus (0.15% P_2O_5). In the first melting stage, the slag is obtained with 47% ($\text{Nb}_2\text{O}_5 + \text{Ta}_2\text{O}_5$), 0.03% Sn, 0.04% P_2O_5 , and the metal containing 2.3% Sn, 0.06% P, and 3.3% ($\text{Nb} + \text{Ta} + \text{Zr} + \text{Ti}$). This option most completely utilizes the advantages of aluminothermic reduction by using electric power for the process and intensifying melting of the mixture with the required amount of flux (lime) to improve the extraction of niobium. In the second melting, a niobium-rich slag is mixed with lime and melted in an arc furnace, which also contains the molten iron scrap. Product FeNb alloy contains as average 66.2% Nb, 4.9% Ta, 0.02% Sn, 0.03% P, 0.2% Al, 1.0% Si, 2.3% Mn, and 0.004% S, and the final slag has 4.6% ($\text{Nb} + \text{Ta}$). The extraction of niobium in the alloy in the second stage is 95.2%, and the total extraction efficiency at these two stages is about 85%.

It is also possible to carry out one-step smelting of FeNb from pyrochlore concentrate, which is made in an electric arc furnace with a 3-ton capacity and lined with magnesite (MgO) bricks. After the furnace bath has been warmed, the mixture of 1000 kg of iron ore, 350 kg of recycled aluminum, and 200 kg of lime is arc-melted. The charge is composed of 100 kg of pyrochlore concentrate, 28 to 33 kg of recycled (secondary) aluminum powder, 3 to 10 kg of iron ore, and 5 to 12 kg of iron scrap. The first melting is carried out at 140 V. It takes 50 minutes to melt the 1200 kg concentrate charge; the second part with 1500

kg of concentrate takes 70 minutes, and the period with the subsequent charge of 1700 kg of concentrate takes 90 minutes. The cast-iron mold lined with MgO bricks for receiving the metal and slag is prepared during the previous smelting. The slag is partially tapped into the mold and cooled to form an autogenic lining layer, which is necessary to increase the durability of the mold and to obtain a clean surface of the ingot. After metal tapping, the mold is held for 2.5 h and after 2 more hours it is delivered for crushing and alloy extraction.

This method allows the production of FeSiNb with the composition of 56% to 62% (Nb + Ta), 10.7% to 12.5% Si, 2% to 6% Al, 3% to 8% Ti, 0.10% to 0.25% P, 0.05% to 0.15% C, and 0.004% to 0.5% S, and it can be applied in cases where high silicon content is not a limitation. However, as mentioned previously, excess silicon leads to the formation of high-temperature silicides (Nb_5Si_3), which delay dissolution of the alloy in the molten steel. To reduce the silicon percentage, FeSiNb can be purged with oxygen in the furnace, after tapping the process slag and setting new oxidation slag (niobium concentrate and lime), but this also reduces the extraction of niobium and part of it oxidizes and transfers back to slag.

REFERENCES

- Eggert, P., Priem, J., Wettig, E., 1982. Niobium: a steel additive with a future. Economic Bulletin 19, 8–11.
- Gasik, M.I., Lyakishev, N.P., Gasik, M.M., 2009. Physical Chemistry and Technology of Ferroalloys [in Ukrainian]. Sistemnye Tehnologii, Dnipropetrovsk, 494 pp.
- Gupta, C.K., Suri, A.K., Gupta, K.G., 1994. Extractive Metallurgy of Niobium. CRC Press, 272 pp.

Technology of Titanium Ferroalloys

Michael Gasik

Aalto University Foundation, Espoo, Finland

Chapter Outline

15.1 Properties of Titanium and Its Compounds	421	15.2.2 Reduction of Titanium from Oxides	428
15.2 Sources of Titanium and Methods of Its Reduction	428	15.3 Technology of Titanium Ferroalloys	429
15.2.1 Titanium Raw Materials	428	References	432

15.1 PROPERTIES OF TITANIUM AND ITS COMPOUNDS

Titanium (atomic number 22) belongs to the transition metals of the first period of the periodic table. Its atomic mass is 47.88, the external electron shell configuration is $3d^24s^2$, its melting temperature is 1671°C, and its boiling temperature is 3260°C. The density of titanium is 4.5 g/cm³, and its typical valencies are 2, 3, and 4. Titanium exists in two allotropic modifications: α -Ti with a hexagonal close-packed (HCP) lattice ($a = 0.2951$ nm, $c = 0.4697$ nm) and β -Ti with a body-centered cubic (BCC) lattice (A2 type), $a = 0.3269$ nm. Titanium's phase transition temperature is 883°C. In some titanium alloys (such as Ti-Al), the high-temperature BCC phase may undergo ordering into BCC (B2) type (Gasik et al., 2009).

The high affinity of titanium for oxygen, carbon, nitrogen, and sulfur is utilized in steelmaking to bind these elements and to decrease their harmful effects (Demos and Kremin, 1981). Titanium also acts as a grain refiner in many steels and alloys, much like niobium. In stainless steels, titanium is an important addition to control carbide and nitride precipitates (e.g., at mass ratio

Ti/C ~5, it prevents the precipitation of chromium carbides on grain boundaries, which greatly improves the corrosion resistance of stainless steels). In low-alloyed steels, titanium with excess carbon and nitrogen forms carbonitride (TiCN), which is known to remain in the structure during welding and thereby helps to retard austenite grain growth.

In the liquid state, titanium and iron form solutions with unlimited mutual solubility, but in the solid state they form intermetallic compounds such as TiFe_2 (Laves phase) and TiFe (Fig. 15.1). The system has two eutectics, one is iron-rich and the other titanium-rich. From the point of view of iron-based alloys, titanium belongs to a ferrite-forming group of elements and thus greatly reduces the austenitic γ -region.

With carbon, titanium forms thermodynamically strong titanium carbide (TiC) (density of 4.4 g/cm³). Carbide has a cubic structure and a wide-ranging stoichiometry (Fig. 15.2). The formation of carbide is preferential over the metallic phase when titanium oxides are reduced by carbon.

Titanium forms several compounds with silicon (Fig. 15.3). Silicides TiSi_2 and Ti_5Si_3 melt congruently, whereas monosilicide TiSi melts incongruently. Silicide Ti_3Si is known to require a rather long equilibration time to form, so in many cases its existence in solid Ti-Si alloys is kinetically suppressed.

The system Ti-Al is very complex and has been a subject of many investigations. One of the most recent versions is shown in Figure 15.4 (Witusiewicz et al., 2008). Titanium and aluminum form solid solutions and a number of

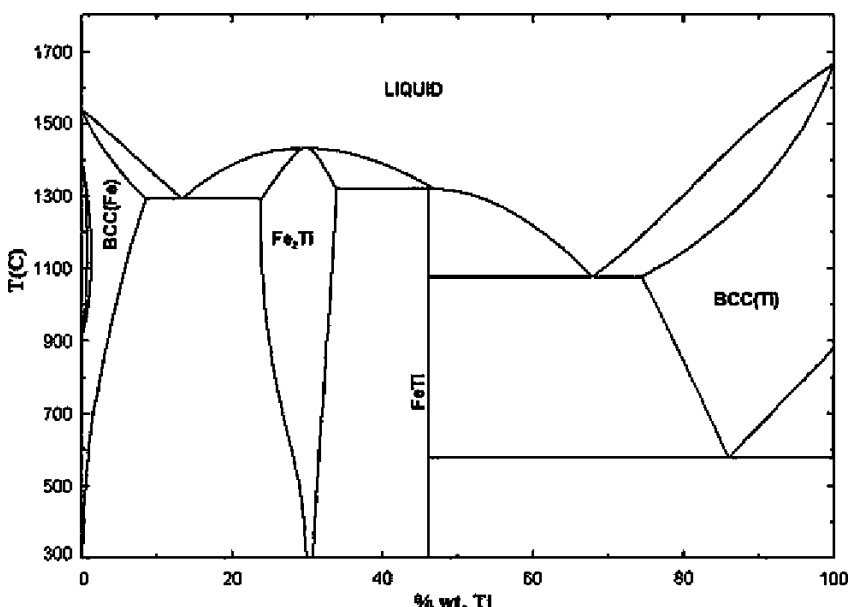


FIGURE 15.1 Diagram of the equilibrium state of the system Ti-Fe.

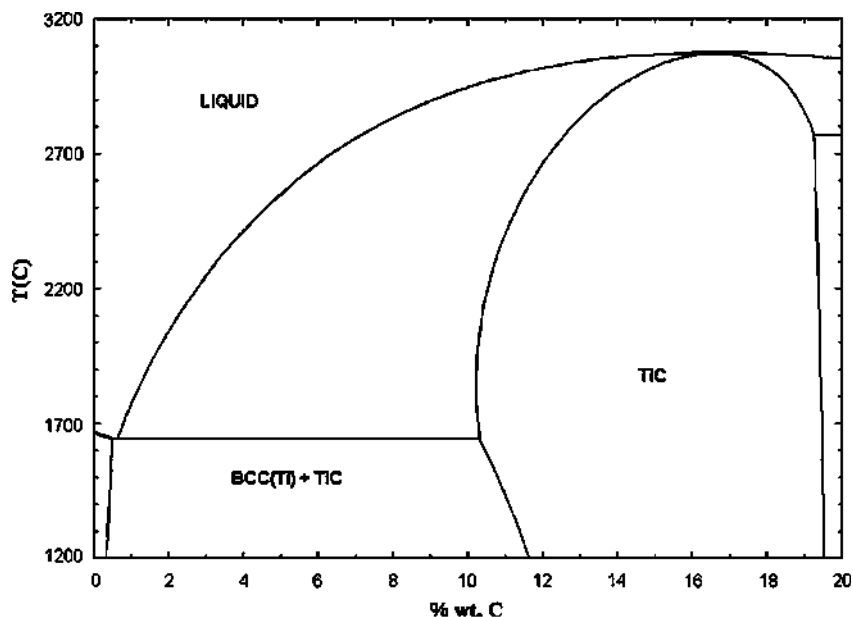


FIGURE 15.2 Diagram of the equilibrium state of the Ti-C system.

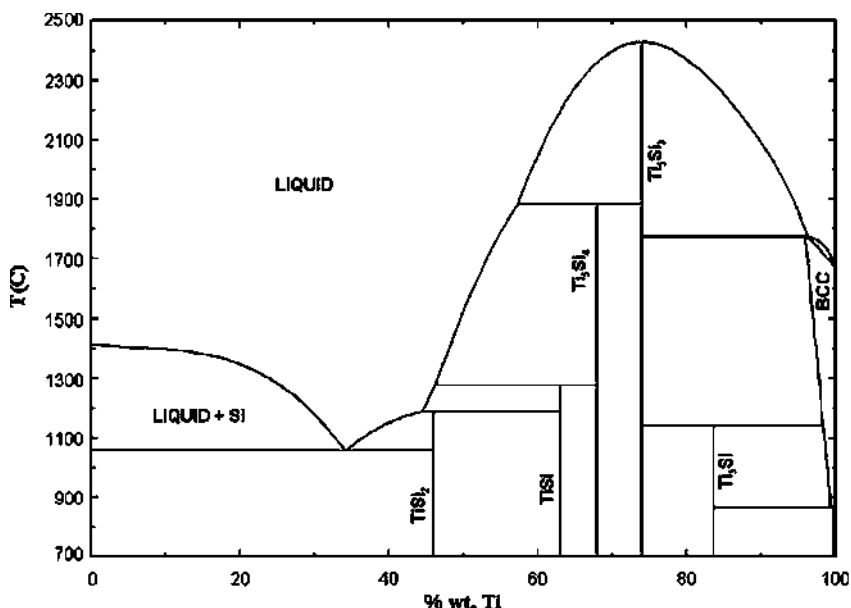


FIGURE 15.3 Diagram of the equilibrium state of the system Ti-Si.

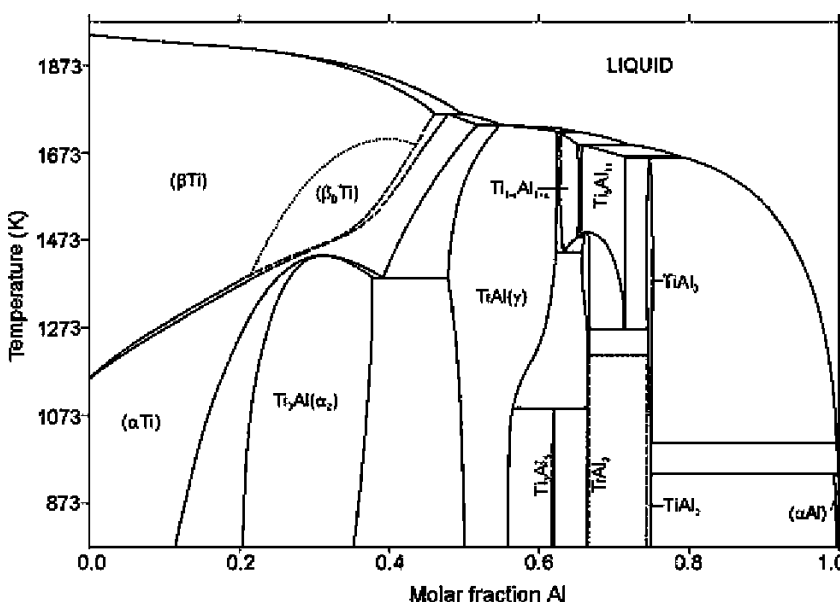


FIGURE 15.4 Diagram of the equilibrium state of the system Ti-Al.

aluminides: $\alpha_2\text{-Ti}_3\text{Al}$ (hexagonal DO_{19} structure), $\gamma\text{-TiAl}$ ($\text{L}1_0$ tetragonal structure), TiAl_2 , and TiAl_3 . Aluminides Ti_3Al and TiAl have a wide homogeneity range.

Titanium is a highly active element, which oxidizes at room temperature, forming a stable protective oxide coating on its surface. With oxygen, titanium forms several stable oxides (Fig. 15.5): TiO_2 , Ti_3O_5 , Ti_2O_3 , and TiO_x , but also a number of intermediate oxides, known as oxygen-deficit Magneli phases $\text{Ti}_n\text{O}_{2n-1}$ (Ti_2O_5 , Ti_4O_7 , etc.). As HCP $\alpha\text{-Ti}$ dissolves significant amounts of oxygen at all temperatures, this phase sometimes is referred to as $\alpha\text{-}(\text{TiO})$ or $\alpha\text{-TiO}_{0+x}$ (to show that the homogeneity range extends toward pure HCP titanium). Titania (TiO_2) exists in three modifications, of which rutile is the most stable; anatase and brookite are less stable (Gasik et al., 2009).

For the practice of ferrotitanium processing, oxide systems with iron, aluminum, and silicon, and calcium oxides, are important. In the system $\text{FeO}\text{-TiO}_2$, three compounds are known: ulvöspinel ($2\text{FeO}\cdot\text{TiO}_2$), ilmenite ($\text{FeO}\cdot\text{TiO}_2$), and pseudobrookite ($\text{FeO}\cdot 2\text{TiO}_2$) (Fig. 15.6).

Oxide TiO_2 has acidic properties, so basic oxides such as CaO readily form the corresponding compounds (Fig. 15.7), but acidic oxides (SiO_2) do not form compounds with TiO_2 (Fig. 15.8). In the system $\text{TiO}_2\text{-Al}_2\text{O}_3$, two compounds are known (Fig. 15.9).

In the ternary system $\text{CaO-SiO}_2\text{-TiO}_2$ (Fig. 15.10) sphene CaTiSiO_4 is the only ternary compound, but there are wide ranges of solid solutions (based on sphene, perovskite, rutile, and silica).

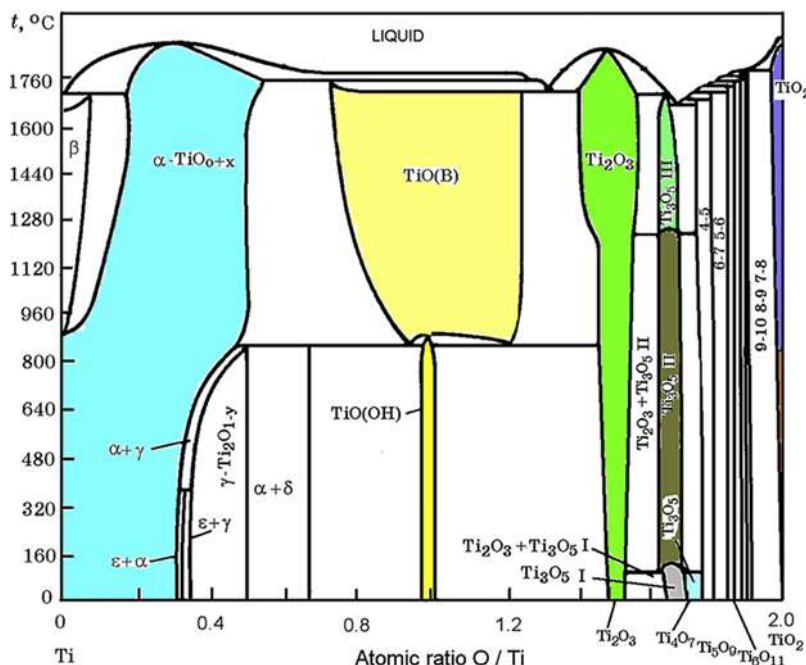


FIGURE 15.5 The phase diagram of the system Ti-O, built on aggregated data (α - TiO_{0+x} , solid solution of oxygen in titanium; TiO , high- and low-temperature modification of titanium monoxide; Ti_3O_5 , different phase modifications (I, II, III), and Magneli phases Ti_nO_{2n-1} ($n = 4$, Ti_4O_7 ; $n = 5$, Ti_5O_9 ; $n = 6$, Ti_6O_{11} ; etc.).

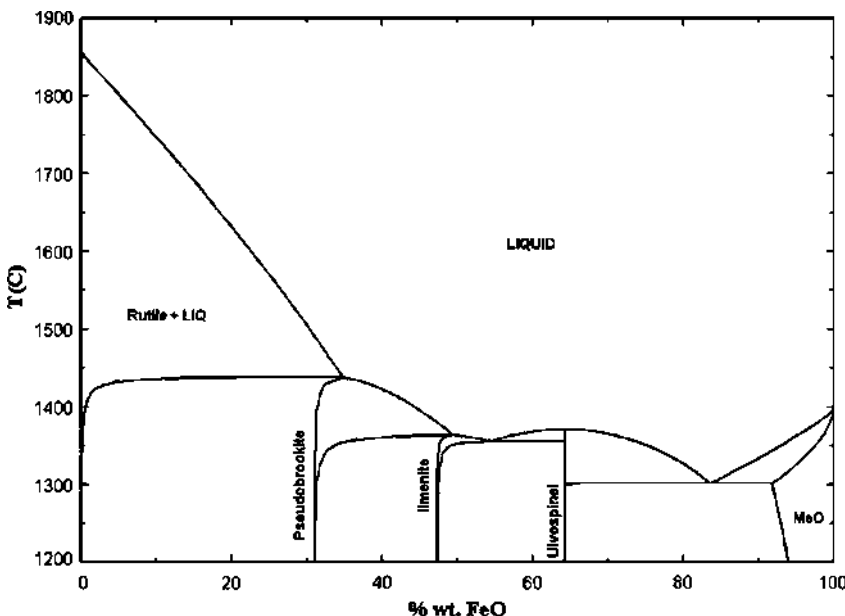


FIGURE 15.6 Diagram of the equilibrium state of the system FeO-TiO₂.

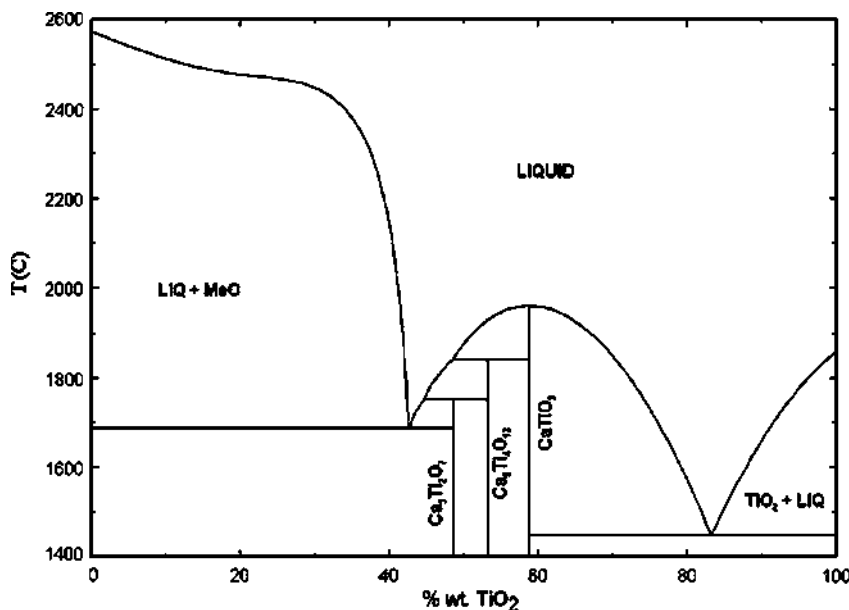


FIGURE 15.7 Diagram of the equilibrium state of the system CaO-TiO₂.

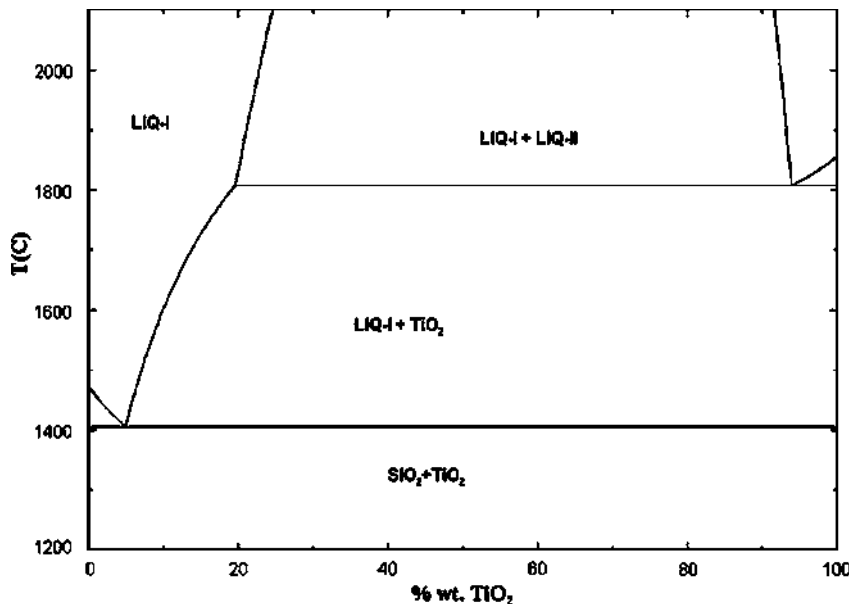


FIGURE 15.8 Diagram of the equilibrium state of the system SiO₂-TiO₂.

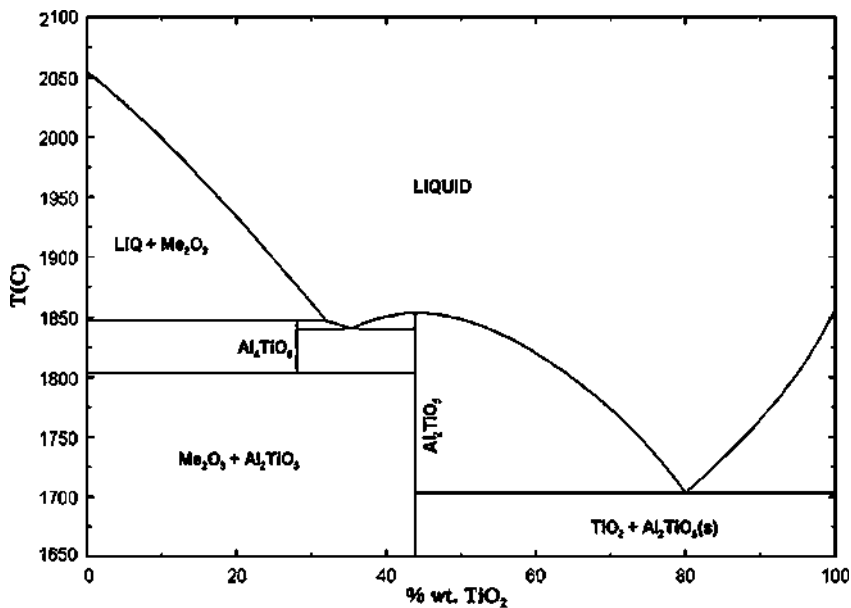


FIGURE 15.9 Diagram of the equilibrium state of the system $\text{Al}_2\text{O}_3\text{-TiO}_2$.

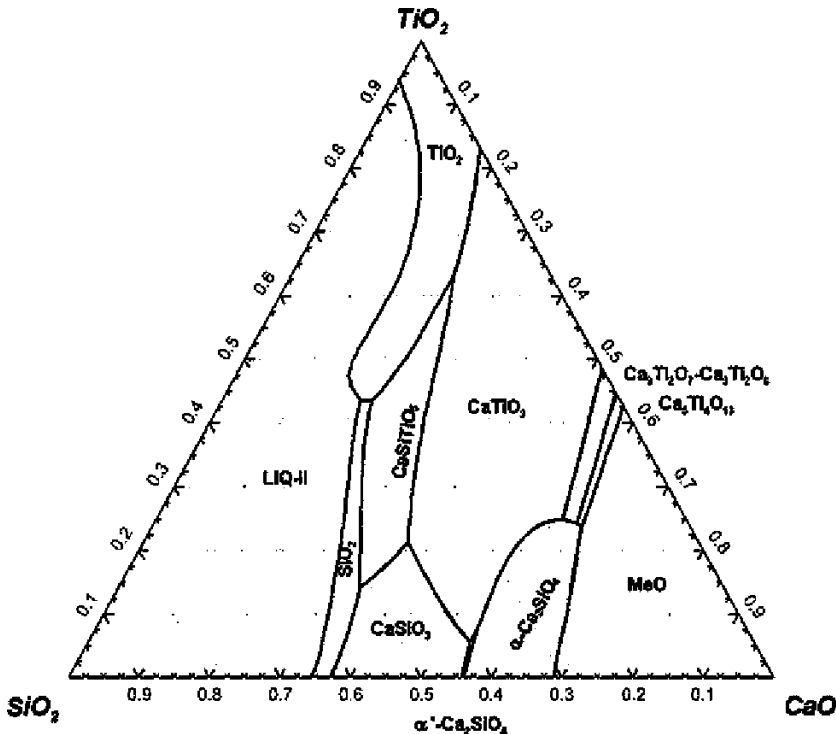


FIGURE 15.10 Diagram of the equilibrium state (liquidus projection, composition in weight fractions) of the system $\text{CaO}\text{-TiO}_2\text{-SiO}_2$.

15.2 SOURCES OF TITANIUM AND METHODS OF ITS REDUCTION

15.2.1 Titanium Raw Materials

There are many known titanium minerals, which might be combined into five groups: rutile (TiO_2), ilmenite ($\text{FeO} \cdot \text{TiO}_2$), perovskite ($\text{CaO} \cdot \text{TiO}_2$), pyrochlore ($\text{Na,Ca,..}(Nb,\text{Ti})_2\text{O}_6(\text{F},\text{OH})$), and sphene $\text{CaTiSiO}_4 \cdot (\text{O},\text{OH},\text{F})$. The rutile-type minerals in the first group (anatase TiO_2 , brookite TiO_2 , leukocene $\text{TiO}_2 \cdot \text{nH}_2\text{O}$, etc.) are often observed together due to the proximity of the titanium ionic radii making it possible to substitute isomorphically with other metals. The most important and most common titanium mineral is, however, ilmenite, which forms continuous solid solutions with geikilit (MgO· TiO_2) and hematite (Fe_2O_3). Ilmenite, titanomagnetite, and titanium-zirconium ore are of great importance to the ferrotitanium industry (Gasik et al., 2009). They are usually subjected to gravitational enrichment (separation), and magnetic and flotation methods. The chemical composition of titanium concentrates used for the smelting of ferrotitanium is given in Table 15.1.

Ilmenite concentrates normally have 96% to 98% ilmenite (corresponding to 50% to 65% TiO_2) and up to 0.20% to 0.25% S. This is too much for making standard ferrotitanium, so concentrates are roasted in a rotary kiln at 600° to 800°C. The roasting process leads also to the oxidation of FeO and the formation of Fe_2O_3 . This breaks down the ilmenite structure and improves the recovery of titanium. In some cases, titanium oxide lean materials are also used (e.g., “red mud” containing <20% TiO_2) (Puri et al., 2004).

15.2.2 Reduction of Titanium from Oxides

Reduction of titanium from ilmenite and rutile by carbon proceeds first with the reduction of iron oxides and later with the reduction of titanium, which partially dissolves in ion melt and partially transforms into carbide (TiC). Smelting of ilmenite with carbon usually leads to the formation of Fe-Ti-C alloy with a high

TABLE 15.1 Chemical Composition of Major Titanium Concentrates, % wt.

Ore		TiO_2	Fe_2O_3	Fe_{tot}	SiO_2	Al_2O_3	MgO	MnO	V_2O_5	S
Concentrate										
Ilmenite										
		52–63	~26.5	~33.5	1–3	1.5–3	0.6–1.6	0.5–1	0.1–0.3	0.04–0.05
Ilmenite from										
titanomagnetite		44.3	—	36.5	2.16	2.55	2.52	0.68	0.22	0.4
Iron-titanate		59.8	—	20.4	2.6	6.12	0.6	0.77	0.2	—

carbon content (35% to 40% Ti; 5% to 8% C; 1% to 3% Si). Such alloys with high carbon content may be used for deoxidation and alloying of carbon steels.

Using silicon as a reductant for titanium is more problematic, as silicon has a lower affinity for oxygen than does titanium, and thus recovery of TiO_2 is only possible with a high content of silicon in the ferroalloy. Also, the presence of iron is needed as it decreases titanium activity and promotes reduction. The resulting Fe-Si-Ti alloy has a composition of 20% to 25% Ti, 20% to 25% Si, and ~1% C, which has limited application in steelmaking.

The aluminothermic method for ferrotitanium processing is the most common (Gous, 2006). Reduction of titanium by aluminum from ilmenite and rutile proceeds via the formation of intermediate monoxide TiO (TiO_x), which, as basic oxide, is able to form titanium aluminate. This decreases the activity of TiO and makes titanium recovery more difficult. To suppress the process of binding TiO with alumina, lime is injected to the charge: CaO replaces TiO , forming $\text{CaO} \cdot \text{Al}_2\text{O}_3$. However, the balance must be kept, as an excess of CaO in the charge is not desirable: it decreases the activity of titanium dioxide by forming perovskite $\text{CaO} \cdot \text{TiO}_2$. Lime also has a great influence on the viscosity and fluidity of the slag. The optimum amount of it in the charge is about 20% by weight of aluminum (Gasik et al., 2009). This method has been greatly improved and applied in several ways, both by using a conventional furnace and by using an electric furnace with preheating of the charge and the use of iron-thermal (exothermic) mixtures (Kotzé et al., 2006). Slag of ferrotitanium is then postprocessed in an electric furnace to recover the rest of titanium and to produce high-alumina (68% to 78% Al_2O_3 , 14% to 17% CaO) slag, which is used as a high-alumina cement addition (Pourabdoli et al., 2007). Although different alternative methods of ferrotitanium processing are being studied (e.g., by electrolysis in molten salts as shown by Shi et al., 2011), these methods still mostly take place in the laboratory.

15.3 TECHNOLOGY OF TITANIUM FERROALLOYS

The composition of standard ferrotitanium is shown in Table 15.2 (Gasik et al., 2009). Depending on its composition, it may also have <0.8% Mn, <0.8% Cr, 0.2% to 1.5% Zr, and 0.05% to 0.3% Sn. Different alloy manufacturers also produce other compositions on demand.

For titanium reduction by aluminum, the main critical parameter is the specific exothermal heat release of the process, referred to 1 kg or mole of smelting products (metal and slag). Assuming some heat losses (~11%), it provides the required temperature of the melt after the end of the process:

$$\Delta H_{req} = \frac{T_{process} + C}{K \cdot 0.89}$$

where for ferrotitanium smelting $K = 32.6$ and $C = 170$ (Gasik et al., 2009). To provide the necessary conditions for the smelting process, the temperature

TABLE 15.2 Composition of Ferrotitanium, % wt.

Alloy	Ti	AI	Si	C	P	S	V	Mo	Cu
		Max.							
FeTi70Si05	68–75	5	0.5	0.2	0.05	0.05	0.6	0.6	0.2
FeTi70Si08	68–75	4	0.8	0.3	0.03	0.03	1.8	2	0.3
FeTi70Si05V	65–75	5	0.5	0.3	0.03	0.03	2.5	2.5	0.3
FeTi70Si1	68–75	5	1	0.4	0.05	0.05	3	2.5	0.4
FeTi35Si5	28–40	8	5	0.2	0.04	0.04	0.4	0.2	2
FeTi35Si7	28–40	9	7	0.2	0.07	0.05	0.8	0.5	2
FeTi35Si8	28–40	14	8	0.2	0.07	0.07	1	1	3
FeTi30	28–37	8	4	0.12	0.04	0.03	0.8	0.4	0.4
FeTi20	20–30	5–25	5–30	1	0.08	0.03			—

should be at least 2260 K, so the equation leads to a required exothermic heat supply of 83.6 kJ/mol. The whole heat supply comes from reactions of the reduction of iron and titanium oxides by aluminum, and it is believed that the best conditions correspond to the ratio of $\text{Fe}_2\text{O}_3:\text{TiO}_2$ in ilmenite concentrates close to unity.

The most common technology of this process is realized as follows. The cast-iron hearth is mounted on a movable platform, lined with a refractory brick. The hearth walls are coated with a mixture of magnesite (95%), fired clay (4.3%), and sodium silicate (“liquid glass”) as a binder up to the thickness of the lining of 10 to 15 mm. The hearth is moved into the melting chamber space, equipped with feeding hoppers and ventilation hoods.

The composition of the charge for the smelting of ferrotitanium is shown in Table 15.3. About 200 kg of the charge is loaded into the hearth, and the ignition mixture is placed on top of it (sodium nitrate and magnesium turnings or chips). The mixture is initiated with a spark or magnesium, and the exothermic process starts. Upon the progress of the melting, small portions of charge are regularly added into the hearth. One typical heat consists of smelting of 4 to 4.5 tons of ilmenite concentrate in 15 to 20 min leading to an ingot that is 3 to 4.5 m in length (Gasik et al., 2009).

To produce 1 t of ferrotitanium, the requirement is about 940 kg ilmenite concentrate, 400 kg aluminum powder, 100 kg lime, 24 kg ferrosilicon FeSi75, and 130 kg iron ore. Up to 9 to 10 kg of titanium scrap might also be added. The phase composition the alloy depends on the content of titanium and impurities in

**TABLE 15.3 Charge Composition for Smelting of Ferrotitanium
(kg by 100 kg of ilmenite concentrate)**

	Ignition Mixture	Main Charge	Reducant Mix
Ilmenite concentrate		100	
Iron ore	100	15–30	100
Aluminum powder	30–40	45–60	35–40
FeSi	12–20	<6	
Lime	15–25	8–12	10–25
NaCl		<2	

ferrotitanium. In the microstructure of FeTi alloy eutectics and intermetallics, FeTi, Fe₂Ti are usually present. Excess phases in ferrotitanium are nitride (TiN), aluminide (AlTi), and sulfide (TiS). Oxide inclusions consist mainly of corundum (α -Al₂O₃), alumina with a mixture of TiO₂ and Cr₂O₃, mullite (3Al₂O₃·2SiO₂), gehlenite (2CaO·Al₂O₃·SiO₂), sphene (CaTi(SiO₄)(O,OH,F)), and the ilmenite (FeO·TiO₂).

The process could be carried out with either top or bottom primer (ignition). In the first case, all charge is loaded in the hearth and the ignition is started from the top, so the melting front and the liquid phase go down. The final liquid products' volume in the hearth is only 30% to 35% of the hearth's total volume, so the productivity of this method is not high. Additionally, it is not possible to control the melting rate once the process has been started. The benefit, however, is that the process is straightforward and easily executed. The bottom primer in general is more efficient, as additional charge might be loaded later and the hearth volume could be fully utilized.

Besides ilmenites, perovskite (CaO·TiO₂) is also a valuable raw material for smelting ferrotitanium. It may substitute for up to ~ 25% of the ilmenite concentrate in the charge, thus eliminating the need to add extra lime to the charge. However, the heat of exothermic reduction reactions in this case is not enough, so the perovskite must be preheated up to 600° to 700°C, reaching the temperature of the mixture ~300°C. The recovery degree of titanium in the process is approximately 75% to 80%. Figure 15.11 shows a flow sheet schematic of melting ferrotitanium with its postreduction from liquid slag.

Although reduction by aluminum is feasible due to high reaction heat, it is not economical to consume extra aluminum just for the reduction of iron (to provide necessary heat). Thus, an alternative method includes heating the melt

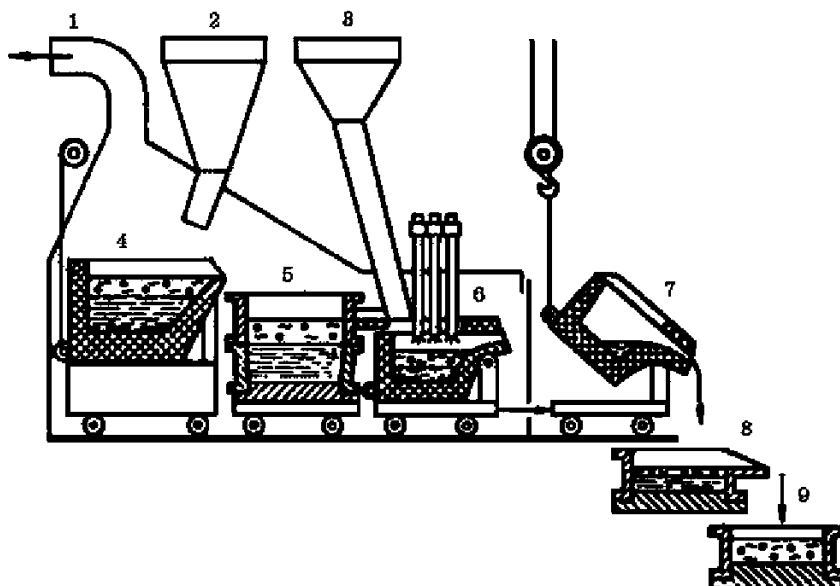


FIGURE 15.11 Scheme of ferrotitanium production from liquid slag: 1, gas extraction hood; 2, charge feeder for the smelting of ferrotitanium; 3, charge feeder for titanium recovery from the slag; 4, hearth for smelting ferrotitanium; 5, molds for metal and slag; 6, electric furnace to reduce the slag; 7, removable furnace hearth; 8, skimmer; 9, mold.

in an electric furnace to add the energy needed to finalize reactions and to ensure metal and slag conditioning.

REFERENCES

- Demos, A.C., Kremin, D.W., 1981. Titanium and its alloys for use in iron and steelmaking. In: Lampman, J.R., Peters, A.T. (Editors), *Ferroalloys and Other Additives to Liquid Iron and Steel*. ASTM, Baltimore, pp. 144–150.
- Gasik, M.I., Lyakishev, N.P., Gasik, M.M., 2009. Physical Chemistry and Technology of Ferroalloys [in Ukrainian]. Sistemnye Tehnologii, Dnipropetrovsk, 494 pp.
- Gous, M., 2006. An overview of the Namakwa Sands ilmenite smelting operations, Proceedings of Southern African Pyromet. In: Jones, R.T. (Ed.) South African Institute of Mining and Metallurgy, Johannesburg, pp. 189–201.
- Kotzé, H., Bessinger, D., Beukes, J., 2006. Ilmenite smelting at Ticor SA, Proceedings of Southern African Pyromet. In: Jones, R.T. (Ed.) South African Institute of Mining and Metallurgy, Johannesburg, pp. 203–214.
- Pourabdoli, M., Raygan, S., Abdizadeh, H., Hanaei, K., 2007. A new process for the production of ferrotitanium from titania slag. *Canadian Metallurgical Quarterly* 46 (1), 17–23.
- Puri, D., Tewari, V.K., Prakash, S., 2004. Some observations on the role of charge particle size in aluminothermic processing of red mud. *Transactions of the Indian Institute of Metals* 57, 195–199.

- Shi, R., Bai, C., Hu, M., Liu, X., Du, J., 2011. Experimental investigation on the formation mechanism of the Ti-Fe alloy by the molten-salt electrolytic titanium concentrate. *Journal of Mining and Metallurgy* 47B (2), 99–104.
- Witusiewicz, V.T., Bondar, A.A., Hecht, U., Rex, S., Velikanova, T.Ya., 2008. The Al-B-Nb-Ti system III. Thermodynamic re-evaluation of the constituent binary system Al-Ti. *Journal of Alloys and Compounds* 465 (1–2), 64–77.

Technology of Zirconium Ferroalloys

Michael Gasik

Aalto University Foundation, Espoo, Finland

Chapter Outline

16.1 Properties of Zirconium and Its Main Compounds	435	16.3.1 Ferrosilicozirconium	443
16.2 Sources of Zirconium and Its Reduction	441	16.3.2 Technology for Producing Ferro-aluminum-zirconium	446
16.3 Technology of Zirconium Ferroalloys	443	References	447

16.1 PROPERTIES OF ZIRCONIUM AND ITS MAIN COMPOUNDS

Zirconium is an element of group IV of the second great period of transition elements of the periodic system. It has serial number 40, atomic weight 91.22, and an atomic outer electronic configuration of $4d^25s^2$, thus mostly leading to valencies +2 and +4.

Zirconium density at room temperature is 6.49 g/cm^3 , its melting point is 1855°C , and its boiling point is 4350°C (there are also other data estimating that the melting point is $\sim 1860^\circ\text{C}$ and the boiling point is between 4377° and 4409°C). Elementary zirconium exists in two modifications: $\beta\text{-Zr}$ has a body-centered cubic (BCC) lattice with lattice period $a = 0.361 \text{ nm}$ and a density 6.5107 g/cm^3 , and $\alpha\text{-Zr}$ has a hexagonal lattice ($a = 0.3231 \text{ nm}$, $c = 0.5146 \text{ nm}$), which is stable at room temperature. The phase transition $\alpha\text{-Zr} \leftrightarrow \beta\text{-Zr}$ occurs at 863°C . The molar heat capacity of zirconium is shown in Figure 16.1.

Pure zirconium is a highly reactive metal (analogous to titanium). Its high affinity for oxygen, sulfur, and nitrogen dictates its principal uses in steel-making for the control of nonmetallic inclusions and the fixation of nitrogen

(into ZrN) and to some extent sulfur as well (into ZrS₂). Zirconium also reacts with carbon, forming rather strong carbides (ZrC). In some steels and alloys, zirconium is known to inhibit grain growth and prevent strain aging, giving better isotropy of mechanical properties. As an alloying element (<0.5% Zr) in steels, it improves ductility, strength, wear, and corrosion resistance (Chokkalingam et al., 2011).

The manufacturing of pure zirconium requires a combination of complex extractive metallurgical processes, and this makes the pure metal very expensive and supports its application in steelmaking in the form of a ferroalloy (Gasik et al., 2009). The phase equilibria diagrams, which have a practical interest with respect to zirconium alloys, are shown here with iron, carbon, silicon, aluminum, and oxygen.

The system Zr-Fe has a variety of intermetallic compounds: Fe₄Zr (possibly a metastable phase), Zr₃Fe, Zr₂Fe, ZrFe₂, and ZrFe₃, and two eutectic temperatures of ~1337 and 928°C. The most refractory compound is ZrFe₂ (melting point ~1673°C) (Fig. 16.2). It is noteworthy, however, that the exact phase equilibria diagram of this system is not yet well studied and there are some contradictory data in phases existence, composition, and transition temperatures. The presence of metallic and nonmetallic (O, N) impurities may significantly affect the constitution of observed phases.

With carbon, zirconium forms one single stable compound—carbide ZrC (structure of NaCl type) with a melting point of ~3540°C, a density of 6.66 g/cm³, and a wide composition range (36% to 49% at. C). In this system, two eutectic temperatures are 1805 (Zr-ZrC) and 2927°C (ZrC-C) (Fig. 16.3).

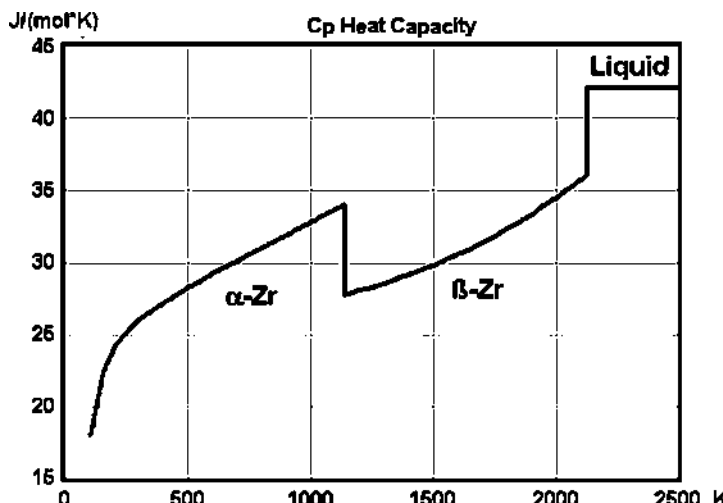


FIGURE 16.1 Molar heat capacity of zirconium versus temperature.

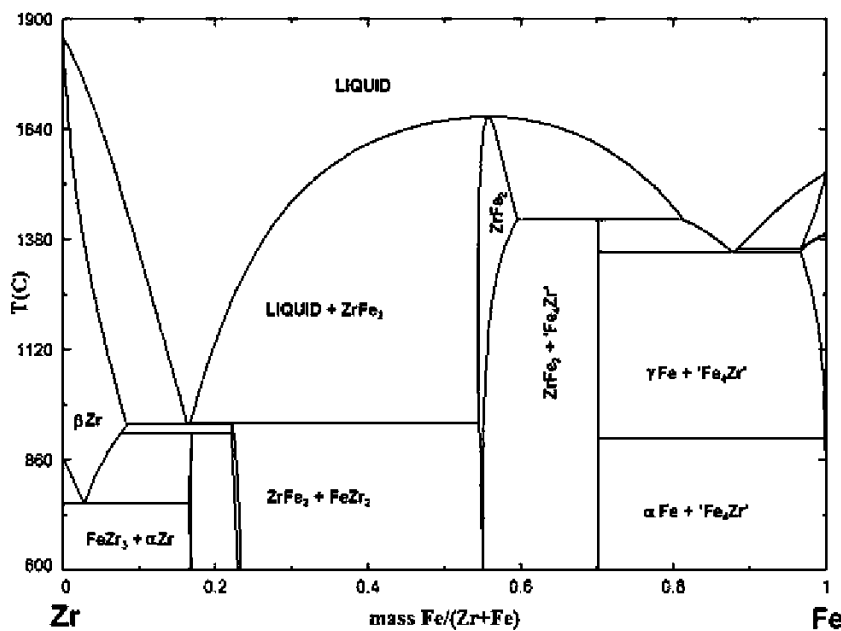


FIGURE 16.2 Zr-Fe phase equilibrium diagram.

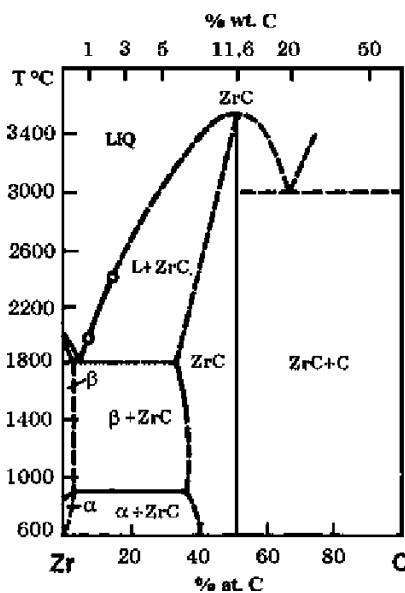


FIGURE 16.3 Zr-C phase equilibrium diagram.

For the Zr-Si system, there are seven known zirconium silicides, and they are commonly considered to be stoichiometric compounds. The most refractory is Zr_5Si_4 , with a melting point of $\sim 2250^\circ\text{C}$. Zirconium dissolves up to 0.2% wt. Si, whereas the solubility of zirconium in silicon is negligible (Fig. 16.4). In this version of the calculated phase diagram, some compounds are not shown (Zr_5Si_4 , Zr_3Si_2) as there are not enough reliable thermodynamic data yet to predict their phase boundaries. Other compounds' existence (like Zr_4Si) is still questionable, as the experimental data might differ depending on the sample preparation method and the purity of materials. For example, impurities stabilize Zr_5Si_3 , which is not stable at room temperature, and which formation suppresses all other silicides. This does not yet allow for the determination of more precise phase reaction temperatures.

Like iron and silicon, there are also many intermetallic compounds that zirconium forms with aluminum (at least 10 compounds have been identified). The maximal solubility of aluminum in α -Zr is 3.7% wt. at 940°C ; in β -Zr it is 9.3% wt. at the eutectic temperature 1350°C (Fig. 16.5). The solubility of zirconium in solid aluminum is negligible. The most refractory compounds in this system are $ZrAl_3$, $ZrAl_2$, and Zr_3Al_2 with melting points of 1580° , 1645° , and 1595°C , respectively.

In the Zr-O system, the stable oxide of zirconium is ZrO_2 , often referred to as zirconia. It has a well-expressed polymorphism: at room temperature the stable phase α - ZrO_2 has a monocline structure, which transforms into the

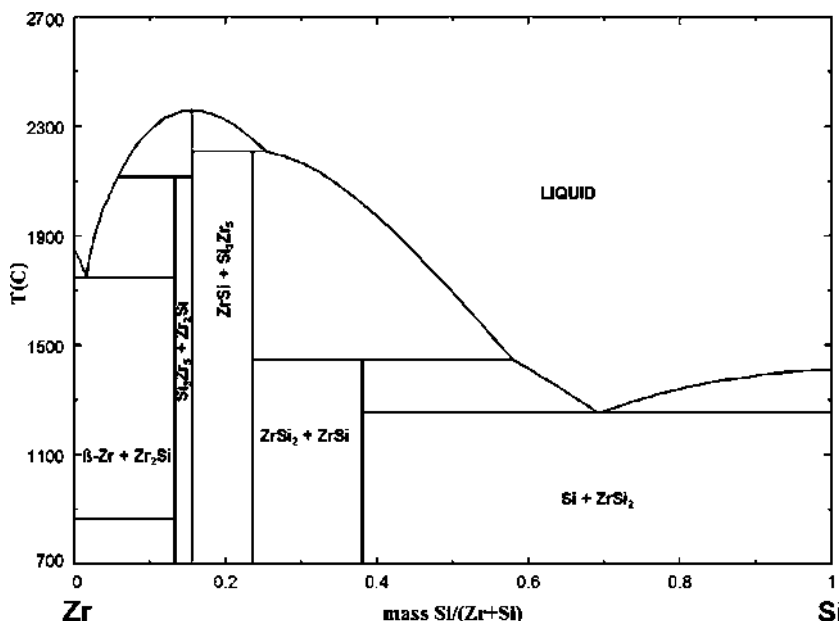


FIGURE 16.4 Zr-Si phase equilibrium diagram.

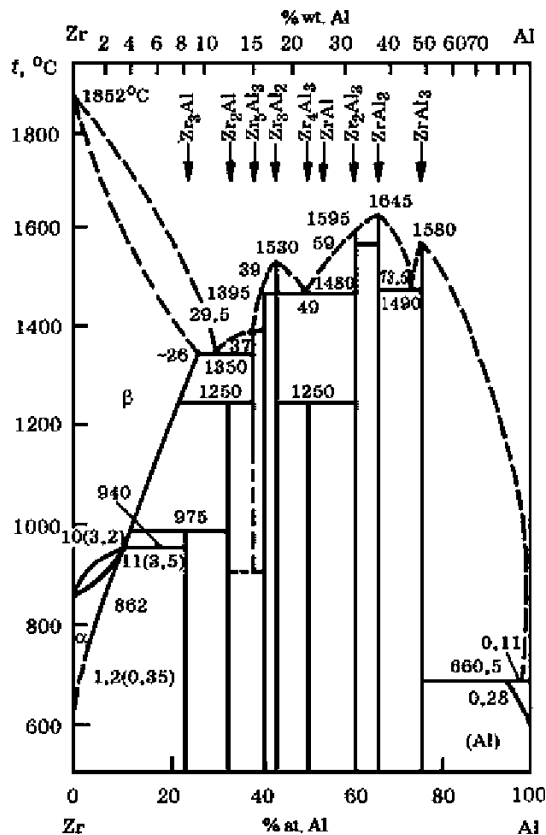


FIGURE 16.5 Zr-Al phase equilibrium diagram.

tetragonal $\beta\text{-ZrO}_2$ (HgI_2 type) above 1205°C , remaining stable up to 2330°C (Turova, 2011). The phase $\beta\text{-ZrO}_2$ transforms to the cubic modification $\gamma\text{-ZrO}_2$ (CaF_2 type) above 2330°C . For the $\alpha \leftrightarrow \beta$ transformation of zirconia, the phenomenon of temperature hysteresis is typical, where the $\alpha \rightarrow \beta$ transition temperature may vary between 1160° and 1190°C (purity-dependent), and the reverse transformation $\beta \rightarrow \alpha$, respectively, between 1070° and 1100°C . The high-temperature reversible transformation $\beta \leftrightarrow \gamma$ at 2330°C has a minimal hysteresis of $\sim 30^\circ\text{C}$. Impurities such as CaO , MgO , and transition metal oxides may stabilize β and γ phases down to room temperature, which is widely used in the application of zirconia in engineering ceramics. The molar heat capacity of ZrO_2 is shown in Figure 16.6, and the Zr-O phase equilibria are shown in Figure 16.7.

Like titanium, $\alpha\text{-Zr}$ may dissolve a substantial amount of oxygen (up to 8.5% wt.) in the solid state, and at low temperatures ($<700^\circ\text{C}$) it tends to form suboxide phases (solutions) of variable compositions (see Fig. 16.7). As noted

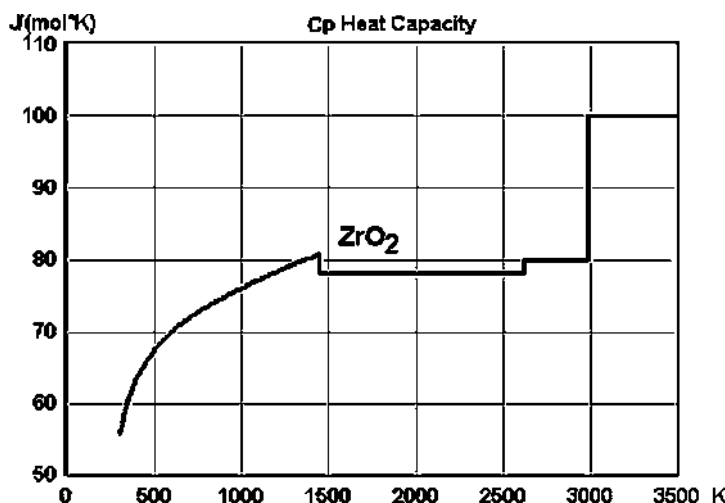


FIGURE 16.6 Molar heat capacity of zirconia.

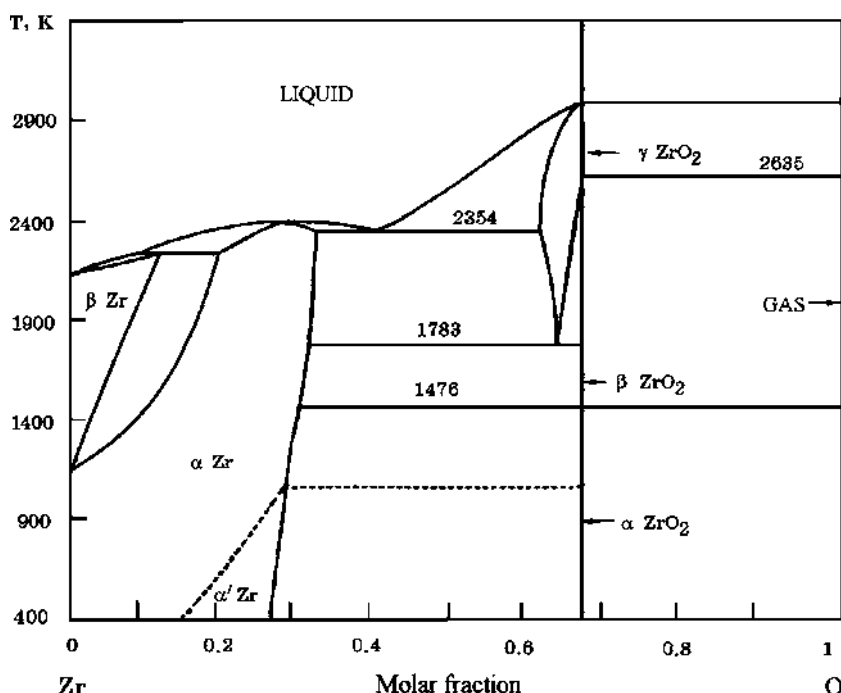


FIGURE 16.7 Zr-O phase equilibrium diagram.

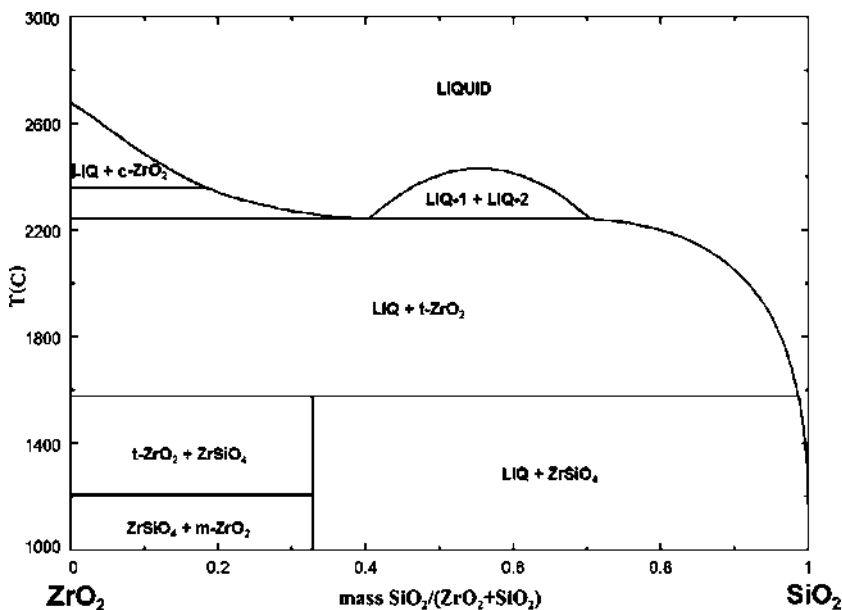


FIGURE 16.8 $\text{ZrO}_2\text{-SiO}_2$ phase equilibrium diagram.

previously, zirconium's high affinity to non-metallic elements restricts the direct application of metallic zirconium in steelmaking or generally at high temperatures in the presence of oxygen, carbon, or nitrogen.

In the system $\text{ZrO}_2\text{-SiO}_2$, one stable compound $\text{ZrO}_2\cdot\text{SiO}_2$ (ZrSiO_4) is formed (Fig. 16.8). Zirconium silicate is also the base of the mineral zircon, appearing in nature, in which lattice a number of zirconium sites might be replaced by hafnium and thorium. Zircon usually appears in alluvial deposits, where it associates with other stable minerals. Zirconia and silica practically have no mutual solubility in the solid state, and there is a miscibility gap in the liquid state (42% to 62% wt. SiO_2) over 2250°C.

The phase diagram of the $\text{ZrO}_2\text{-Al}_2\text{O}_3$ compound is of a simple eutectic type with an eutectic temperature of 1887°C. This system is important for the manufacturing of alumina-zirconia refractory and abrasive materials.

In the system $\text{ZrO}_2\text{-CaO}$, compounds CaZrO_3 and CaZr_4O_9 , as well as solid solutions of CaO in monoclinic, tetragonal, and cubic ZrO_2 crystal structures are known (Fig. 16.9). CaO , along with yttria and magnesia, is commonly applied to stabilize the cubic phase.

16.2 SOURCES OF ZIRCONIUM AND ITS REDUCTION

Zirconium is a rare element, despite its presence in many minerals, although in small amounts (Hedrick, 2004). The most common minerals of industrial

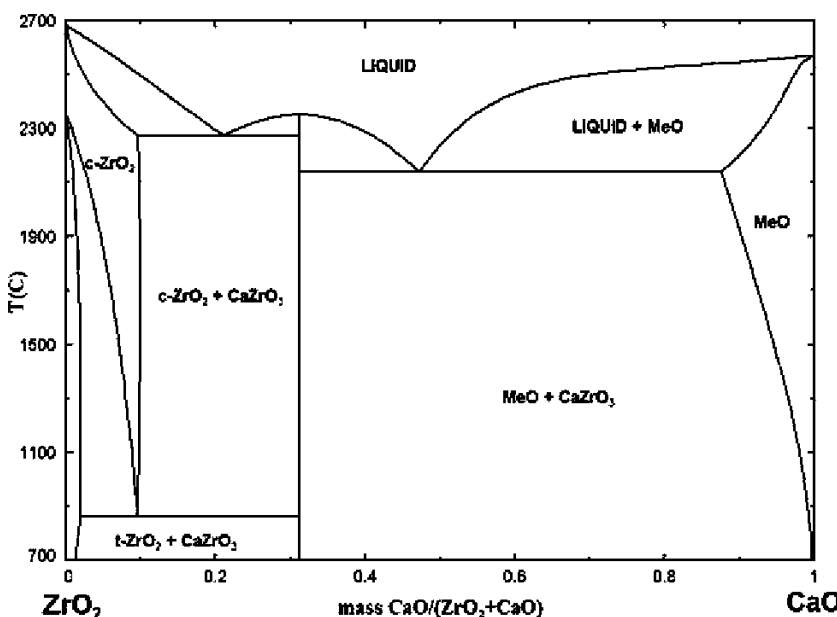


FIGURE 16.9 $\text{ZrO}_2\text{-CaO}$ phase equilibrium diagram.

relevance are zircon ($\text{ZrO}_2 \cdot \text{SiO}_2$) and baddeleite (ZrO_2). Zirconium also forms eudialyte $[\text{Na}_4(\text{Ca},\text{Ce},\text{Fe}_2)_2\text{ZrSi}_6\text{O}_{17}](\text{OH},\text{Cl}_2)$, which is much less common. Most zircon is mined from placer deposits. Typical zircon concentrates contain 60% to 65% wt. ZrO_2 , <0.1 Fe_2O_3 , <0.4 TiO_2 , <2 Al_2O_3 , <0.1 CaO , <0.1 MgO , <0.15 P_2O_5 , and a balance made up of SiO_2 .

Zirconium can be practically reduced from the concentrates by carbon, silicon, or aluminum. For carbon reduction, as for many other metals, the carbide ZrC is always a reaction product at conventional metallurgical conditions. Figure 16.10 shows the phase dominance (stability) diagram for 1600°C. As the figure shows, the ternary equilibrium point is located at rather low oxygen ($\sim 10^{-21}$ atm O_2) and CO ($\sim 10^{-8}$ atm) potentials, which makes it impossible to reduce ZrO_2 to metallic zirconium here at normal pressure.

Reduction by silicon eventually leads to the formation of zirconium silicides, zirconium intermetallides, and respective melts, forming ferrosilico-zirconium (FeSiZr). As silica is present in zircon concentrates and also is the product of the reactions, the thermodynamics of the reduction process are generally not favorable for getting a high-zirconium-percentage alloy. It would require high temperatures, the addition of basic flux, and an increase of silicon activity, which limits zirconium content to 40% to 45% wt. Therefore, to enhance the process and limit silicon content in the alloy, the reduction is realized by aluminum.

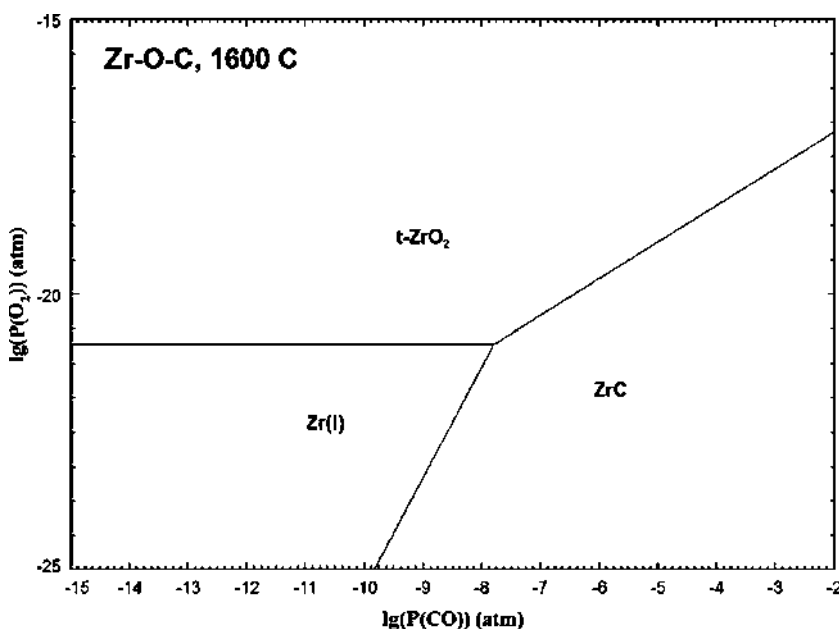


FIGURE 16.10 Zr-O-C phase stability diagram at 1600°C.

Reduction of zirconium by aluminum in the presence of an iron source (exothermic) is used for the production of ferro-alumin-zirconium (FeAlZr) alloy with a low silicon content.

16.3 TECHNOLOGY OF ZIRCONIUM FERROALLOYS

Among the more common zirconium ferroalloys are FeSiZr (average 35% to 40% Zr, 46% to 52% Si), NiZr (67% to 74% Zr, 24% to 30% Ni), FeZr (75% min. Zr), and FeAlZr (15% to 21% Zr, 20% to 26% Al, <4% Si, <0.15% C).

Ferrozirconium, produced by remelting zirconium (zircalloy grades) and steel scrap, may contain between 40% and 90% Zr, depending on the grade, but also low amounts of silicon and aluminum. Nickel-zirconium master alloy is sometimes used as an addition agent in nickel-based superalloys. The technology of FeZr and NiZr relying on scrap remelting, without the reduction of primary materials, is not considered here. The choice of the zirconium alloy depends on the intended application, and for silicon-containing alloys the level of silicon allowed in the steel composition is usually important.

16.3.1 Ferrosilicozirconium

The composition of FeSiZr typically spans from 20% to 45% Zr, with 5% to 9% wt. Al, <0.2% to 0.5% C, <0.15% to 0.20% P, and <3% to Cu. The mass ratio

Si/Zr varies according to the Zr content from 0.5 for high-zirconium grades ($>35\%$ Zr) to ~ 1.7 for the lowest grades (20% to 30% Zr).

The main method used to produce FeSiZr is the reduction of raw materials by aluminum, but it is also possible to use silicon and carbon as reductants. This can be realized in two ways: a flux process and a flux-less process (Gasik et al., 2009). The first option foresees the use of flux (additions of lime and fluorspar) and its main product is the ferroalloy only. The second option involves simultaneously making two products (FeSiZr and zirconium-corundum slag) without fluxing additions. For a proper thermal balance, the charge includes magnetite ore (iron ore with $>60\%$ Fe and low phosphorus, preferably also with $<7\%$ of silica; grain size up to 3 mm). Either primary or secondary aluminum powder is used as a reductant, and it mainly determines the amount of impurities in the final alloy. The one-stage flux process of FeSiZr smelting could be realized either for a tapping of a liquid alloy or for the manufacture of a solid alloy ingot ("block" type). Figure 16.11 shows a schematic of the production of FeSiZr by the flux process with melt tapping. The arc furnace used is typical in steelmaking, of power 1 MVA and carbon-based lining, overlaid with carbon paste. The lining is first fixed and cured by coking it for 8 to 10 h under a normal current and periodically switching off the furnace power.

The charge is calculated for the concentration of zirconium in the alloy as 50% to 54% Zr. The average consumption of charge materials for smelting of 1 ton of FeSiZr using secondary aluminum and with the melt tapping method is 1094 kg of zircon concentrate (60% ZrO_2), 543 kg of secondary aluminum

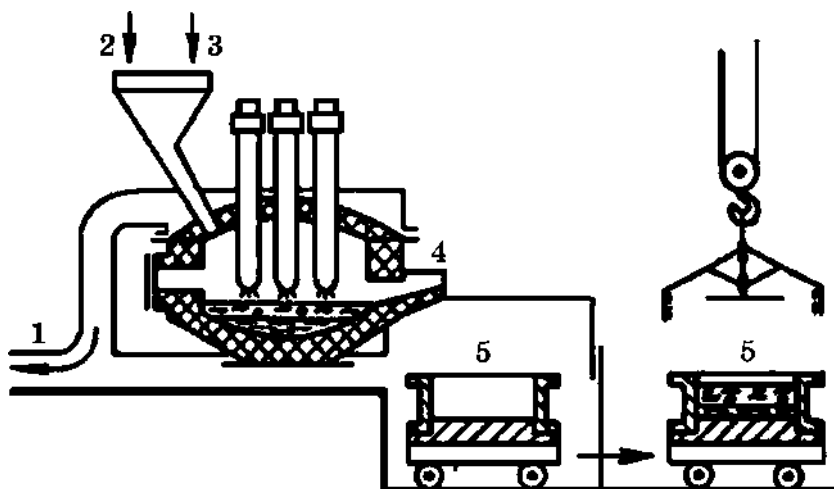


FIGURE 16.11 Schematic of FeSiZr smelting by the flux process: 1, gas exhaust; 2, zircon concentrate feeding; 3, flux and reductant feeding; 4, arc furnace; 5, cast alloy.

powder, 424 kg of lime, 65 kg of ferrosilicon Fe-75%Si, 114 kg of iron ore, and 24 kg of sodium nitrate (used as a reaction initiator). For this kind of smelting, the electricity consumption for 1 ton of the alloy is up to 1500 to 1510 kWh and the zirconium extraction level is 80% to 85%.

The alloy made with this charge typically has 50% to 51% Zr, 26% to 27% Si, 5% to 8% Al, and 0.1% to 0.13% S. The slag composition includes 7% to 9% ZrO_2 , 54% to 56% Al_2O_3 , 28% to 30% CaO, 0.5% to 2.5% SiO_2 , 1.3% to 1.6% MgO, and 0.2% to 0.5% FeO. This method (see Fig. 16.11) allows production of FeSiZr with more than 50% Zr by the simultaneous reduction of Zr and Si by aluminum, but its drawback is that it does not extract zirconium from the oxide melt to a better extent (Gasik et al., 2009).

To improve the zirconium utilization, the simultaneous smelting of FeSiZr and zirconia–corundum (ZrO_2 – Al_2O_3 material used in abrasive and refractory products) is also used. Flux (lime) is not used in this case, whereas the zirconium-rich slag becomes a commercial by-product (20% to 35% ZrO_2 , <3% SiO_2 , <2% CaO, <2% MgO, and the balance made up of Al_2O_3). The smelting batch of this flux-less process of total weight 2100 to 2400 kg includes zircon concentrate (~1250 kg), secondary aluminum powder (~500 to 630 kg), ferrosilicon (<150 kg), and iron ore (~250 kg). Charge materials must contain a minimum amount of calcium and magnesium oxides, as they represent a decreasing quality of fused zirconia–corundum abrasive products (reducing hardness and cutting ability). The composition of the charge is determined by the fused zirconia–corundum grade required: by decreasing the amount of aluminum powder, the degree of zirconium reduction is decreased and zirconium content increases in the oxide melt.

Melting is performed in an electric furnace of the steelmaking type with a carbon lining. After melting of approximately two thirds of the charge, the fused oxide mixture (slag) is poured into a metal mold. When the melting stage has completed, the rest of the slag is tapped at the bottom of another mold and after it cools down (~3 min), the metal is tapped onto the slag. Per such batch composition, 500 to 600 kg of FeSiZr alloy (40% to 50% wt. Zr, 25% to 35% Si) and 1300 to 1400 kg of zirconium–corundum (25% to 40% ZrO_2) are typically obtained.

The technology for producing zirconium–corundum together with FeSiZr is more effective than for the flux process because here there are practically no zirconium losses. However, the total economic efficiency of the process also depends in this case on the market situation for both the metal and the ceramic materials (by-products), and they may not always be simultaneously correlated.

In the case of the silicon reduction method, the charge consists of zircon concentrate, FeSi75, and lime. This FeSiZr alloy naturally has a higher silicon content (47% to 50% Si) and a lower zirconium content (33% to 37% Zr). The advantages of this alloy are a better utilization of zirconium in steelmaking and the simultaneous addition of silicon to molten steel, decreasing the need for extra additions of FeSi.

In the case of the carbon reduction method, charcoal is also added to the charge and the resulting alloy has 15% to 18% Zr, 36% to 40% Si, <1% Al, and <0.5% C. It is possible to produce FeSiZr with higher zirconium content, but it comes at the expense of the increased silicon percentage. The selection of the reduction method in that case is based on the whole set of technical and economic conditions.

16.3.2 Technology for Producing Ferro-aluminum-zirconium

The composition of ferro-aluminum-zirconium usually includes 15% to 20% Zr, 15% to 30% Al, and balance – Fe; the main impurity is silicon (<3%). Due to the limitation of silicon content, zircon ZrSiO_4 cannot be used as a raw material and the zirconium source is mainly zirconia concentrate (baddeleite). Iron is added in the form of iron ore pellets and iron scale. The reductant is aluminum powder in the presence of lime as flux. For ignition of the charge, sodium nitrate is also added. **Table 16.1** gives an example of the charge: it consists of three types: for ignition, for zirconium reduction, and for exothermal generation.

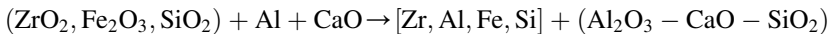
This process has a complex set of physicochemical interactions. First, the ignition charge gives a necessary thermal impulse for the whole process of initiation. It is based on the very exothermic reaction (-1250 kJ/mol of sodium nitrate):



TABLE 16.1 Composition of Charge for Making Fe-18% Al to 22% Zr Alloy

Charge Components	Amount, kg			
	For Ignition	For Ore Reduction	For Exothermal Part	Total
Zirconia ZrO_2	—	480	—	480
Zircon ZrSiO_4	150	—	—	150
Iron scale	20	400	180	600
Iron pellets	—	200	—	200
NaNO_3	35	—	—	35
Lime	40	350	100	490
Al powder	90	590	80	760
Total, kg	335	2050	360	2715

The main reduction process involves the formation of the metallic melt, and it is a summary product of many reactions that might be presented schematically as follows:



At the final stage, the process is accelerated by feeding the exothermic mixture (iron oxide, lime, and aluminum powder) into the bath of the furnace. This is supposed to cause extra local heating and finalization of the reduction and the slag formation. Zirconium extraction in this process is nevertheless only 45% to 50%.

Different kinds of more complex master alloys with zirconium are also being produced. They may also contain manganese, aluminum, silicon, and titanium, with less zirconium (10% to 15%)—for example, the FeSiZrMn alloy may have 4% to 22% Zr, 4% to 15% Mn, and 45% to 67% Si, which could be complemented by 3% to 9% REM and <15% Ti on request.

REFERENCES

- Chokkalingam, B., Mohamed Nazirudeen, S.S., Ramakrishnan, S.S., 2011. Investigation into the mechanical properties of micro-alloyed as-cast steel. Materials and Technology 45, 159–162.
- Gasik, M.I., Lyakishev, N.P., Gasik, M.M., 2009. Physical Chemistry and Technology of Ferroalloys [in Ukrainian]. Sistemnye Tehnologii, Dnipropetrovsk, 494 pp.
- Hedrick, J.B., 2004. Zirconium and hafnium. U.S. Geological Survey Minerals Yearbook, 85, 1–11.
- Turova, N., 2011. Titanium, zirconium, hafnium. In: Inorganic chemistry in tables. Springer, Berlin-Heidelberg, pp. 66–67.

Boron Ferroalloys

Oleg Polyakov

National Metallurgical Academy of Ukraine, Dnipropetrovsk, Ukraine

Chapter Outline

17.1 Properties of Boron and Its Compounds	449	17.3.1 Boron Alloys Types	453
17.2 Boron Sources and Its Reduction	452	17.3.2 Ferroboron Technology	453
17.3 Technology of Boron Alloys	453	17.3.3 Technology of Other Boron Alloys	456
		References	457

17.1 PROPERTIES OF BORON AND ITS COMPOUNDS

Boron is the lightest nonmetallic element on the periodic table after hydrogen and helium. Its serial number is 5, its atomic weight is 10.811, its melting point is 2074°C, and its boiling point is ~3658°C. This makes boron at the same time one of the most refractory elements, compatible with carbon. Boron belongs to group III of the period table (its outer electronic shell configuration is $2s^22p^1$), normally appearing in the oxidation state +3. Several allotropic modifications of boron are known, of which α -B and β -B (the most stable) are rhombohedral, γ -B is orthorhombic, and T-phase is tetragonal. The last two modifications are formed at high pressures and temperatures but remain stable after release into ambient conditions.

Natural boron consists of two stable isotopes of ^{10}B (19.57%) and ^{11}B (80.43%). The cross section of the thermal neutron capture for ^{10}B is very high ($3 \cdot 10^{-25} \text{ m}^2$) in comparison with ^{11}B ($4 \cdot 10^{-32} \text{ m}^2$).

Boron is a typical microalloying element—even small additions in steel have a great influence on the mechanical properties (Davis, 2001). This in many cases saves expensive and scarce alloying elements as well as mineral and energy resources. Boron is added to steels for its unique ability to increase hardenability when present in concentrations of around 0.001% to 0.004%, so very small amounts of boron in combination with carbon and manganese might be an effective substitute for more traditional alloying elements. In stainless steels,

boron is used to improve their creep properties or for the nuclear industry, where enhanced neutron absorption is required (a very high neutron capturing cross section has already been achieved for steels <1% B). It is also used for high-strength low-alloy (HSLA) and other structural steels. Ferroboron may be added also to avoid the interstitial nitrogen effect and to improve the steel's formability. It is normally added in preliminarily deoxidized (by aluminum) steel, which provides a high uptake of boron (70%) with its stable content (0.002% to 0.0025% B).

With iron, boron forms thermodynamically stable borides Fe_2B , FeB , and FeB_2 (Fig. 17.1). Dissolution of boron in liquid iron is highly exothermic.

In the system B-C, the stable carbide is B_4C , which has a wide concentration homogeneity range and a high melting point $\sim 2450^\circ\text{C}$ (Fig. 17.2).

Boron and silicon form stable boron silicides SiB_3 , SiB_6 , and SiB_{14} . Silicide SiB_6 melts incongruently at 1850°C (Fig. 17.3).

Boron also forms stable borides with many metals. In the system B-Al, known borides are AlB_2 , AlB_{10} , and AlB_{12} . Aluminide AlB_2 melts incongruently at $\sim 960^\circ\text{C}$, and AlB_{12} melts congruently at $\sim 2150^\circ\text{C}$. Compound AlB_{10} exists in a narrow temperature range of 1660° to 1850°C (Fig. 17.4).

With oxygen, boron produces a number of oxides with different boron/oxygen ratios: B_7O , B_6O , B_2O , B_4O_3 , BO_2 , B_4O_5 , and B_2O_3 , the last one being the most stable. The melting point of B_2O_3 is 450°C , and it is well known to form glassy phases upon cooling, which is used for the production of borosilicate glasses. Boron oxide reacts with water, generating weak boric acid H_3BO_3 .

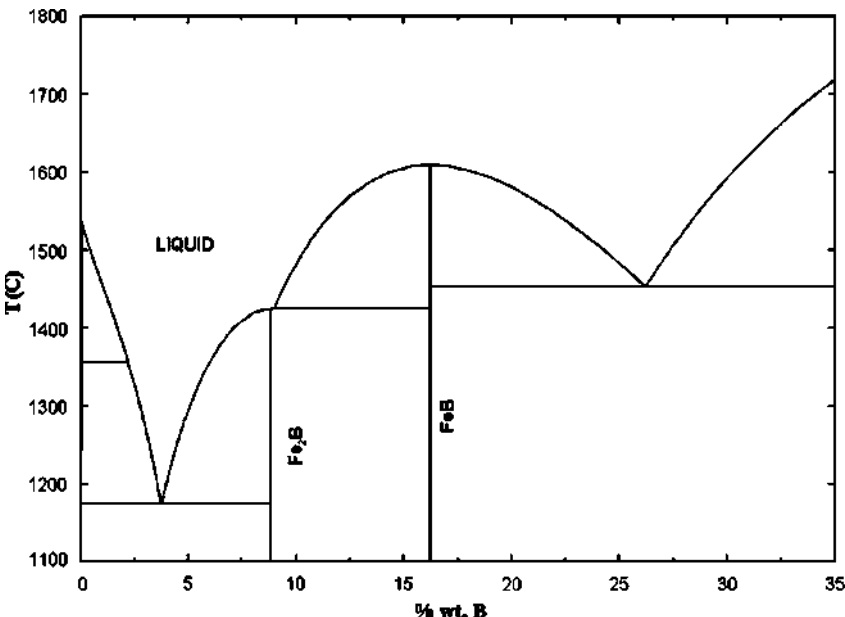


FIGURE 17.1 Equilibrium diagram of the system Fe-B (FeB_2 compound not shown).

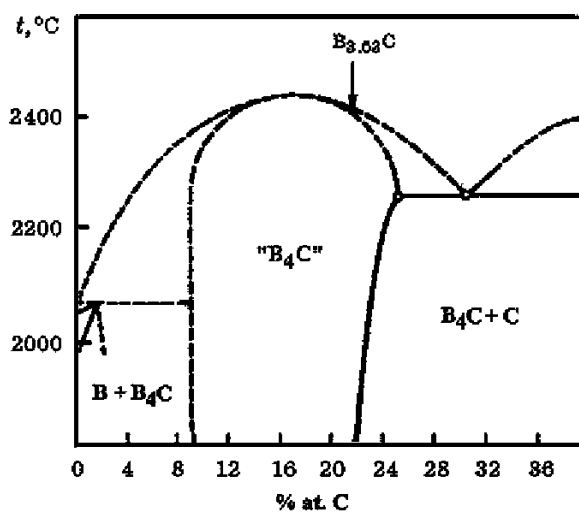


FIGURE 17.2 Diagram of the equilibrium state of the system B-C.

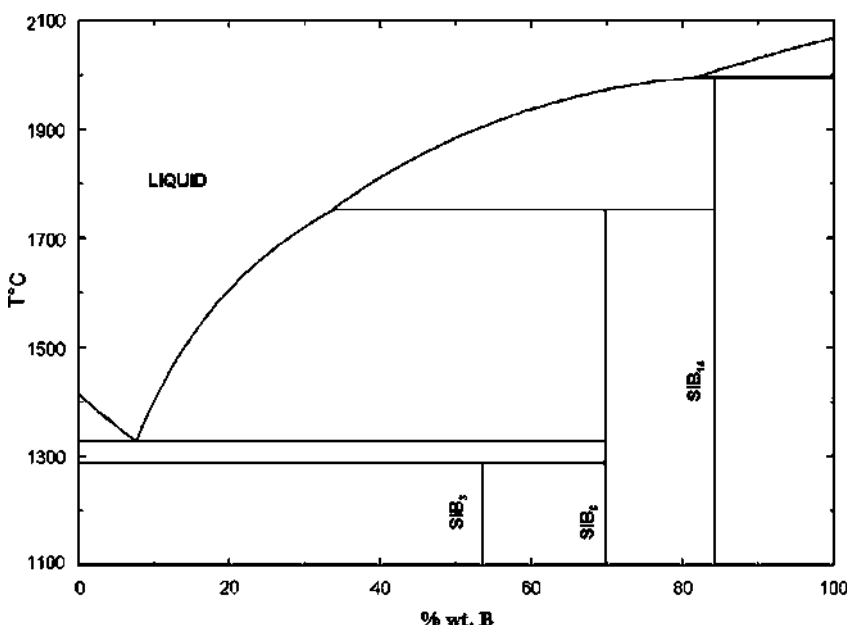


FIGURE 17.3 Diagram of the equilibrium state of the system B-Si.

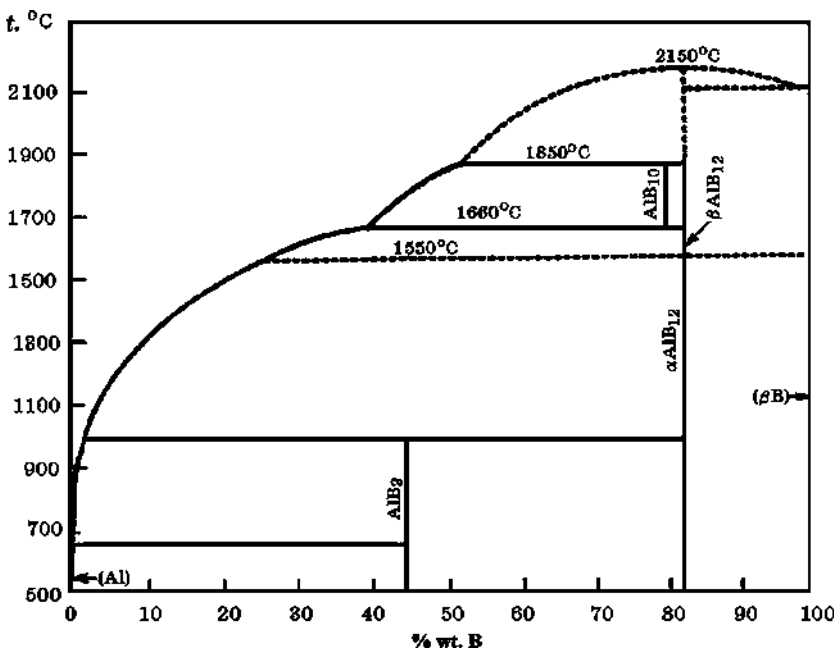


FIGURE 17.4 Diagram of the equilibrium state of the system B-Al.

17.2 BORON SOURCES AND ITS REDUCTION

The main minerals of boron are boracite $(\text{Mg}, \text{Fe}, \text{Mn})_3[\text{ClB}_2\text{O}_3]$, ascharite $\text{Mg}_2[\text{B}_2\text{O}_5] \cdot \text{H}_2\text{O}$, colemanite $\text{Ca}[\text{B}_3\text{O}_4(\text{OH})_3]$, kernite $\text{Na}_2[\text{B}_4\text{O}_6(\text{OH})_2] \cdot 3\text{H}_2\text{O}$, ulexite $\text{NaCa}[\text{B}_5\text{O}_6(\text{OH})_6] \cdot 5\text{H}_2\text{O}$, and probably the most well-known, borax $\text{Na}_2[\text{B}_4\text{O}_7(\text{OH})_4] \cdot 8\text{H}_2\text{O}$. More than a hundred minerals with boron are known, but not all have commercial potential (Garrett, 1998). As an example, borate ore has the following composition (Gasik et al., 2009), % wt.: 8 to 8.5 B_2O_3 , <13 SiO_2 , 15 to 25 CaO , 10 to 30 MgO , 2 to 5 FeO , 2 to 6 Na_2O , 2 to 3 C, 5 to 10 S, and ≤ 0.01 P. From such ores several grades of concentrates are recovered (Table 17.1).

These concentrates are suitable for the smelting of some boron ferroalloys such as ferroboral (FeBAI) and ferrosilicoboral (FeSiBAI). For more boron-rich master alloys, technical quality grade boron anhydrite or more pure raw materials are used (Gasik et al., 2009).

Boron might be reduced from its oxide form by carbon, silicon or aluminum. In the case of carbon reduction, the formation of boron carbide (B_4C) is preferred thermodynamically, so in the presence of iron this FeB alloy has <10% to 20% B and <2% to 4% C.

Silicon reduction is not thermodynamically favorable and not used in practice, as the maximum boron content in the alloy does not exceed 4% B.

TABLE 17.1 Chemical Composition, max. % wt., of Boron Concentrates

Concentrate Type	B ₂ O ₃	CaO	MgO	SiO ₂	Fe ₂ O ₃	Na ₂ O	H ₂ O
Boric anhydrite (B ₂ O ₃)	>95	—	—	—	0.0065	—	3–5
Calcium diborate (CaO·B ₂ O ₃ ·2H ₂ O)	>38	35.6	1	2	0.04	0.1	22
Boric acid (H ₃ BO ₃)	>99.5	—	—	0.8	0.0065	—	—
Sodium octaborate (Na ₂ B ₈ O ₁₃)	>74	—	—	1	—	23	—

Thus, aluminum is the only choice for the processing of boron ferroalloys and master alloys where carbon content should be minimized.

17.3 TECHNOLOGY OF BORON ALLOYS

17.3.1 Boron Alloys Types

The composition of commercial boron alloys is shown in Table 17.2 (Gasik et al., 2009). Ferroboron is the most common addition agent in steelmaking. However, as ferroboron does not have protective elements (with a higher affinity to oxygen and nitrogen than boron), it might only be added to deoxidized steel.

Boron master alloys (see Table 17.2) are more efficient in terms of application and results stability, but with the drawback of higher costs.

17.3.2 Ferroboron Technology

Ferroboron is processed in electric furnaces by reduction of either aluminum or carbon. For the aluminum reduction process, the main part of the charge is composed of borate ore (see Table 17.1) and secondary aluminum chips. Iron-termite mix (exothermic mixture) has secondary iron oxides and aluminum chips, and the ignition mix consists of all three components (calcined borate ore, iron oxides, and aluminum) (Table 17.3). Ignition mix for the initiation of the process is about 6% to 7% of the total charge, whereas the iron-rich mixture is 20% to 27% of the total charge depending on the ferroboron grade required.

The furnace with a power of ~1 MVA is lined with magnesite bricks and the hearth is movable (installed on the truck), which means it can roll in and out under the electrodes. The melting process can be divided into three periods: the formation of a melt, oxides reduction, and processing of the slag with iron-rich

TABLE 17.2 Chemical Composition, % wt. of Ferroboron and Special Boron Master Alloys (maximal allowable, except for boron)*

Grade	B	Si	Al	C	S	P	Cu	Other
Ferroboron								
FeB20	20	2	3	0.05	0.01	0.015	0.05	
FeB17	17	3–4	5	0.2	0.02	0.03	0.1	
FeB17A	17	4	0.5	4				
FeB10	10	5–15	8–12					
FeB6	6	5–12	6–12					
Master Alloys								
Ferroboral (FeBAI)	6	10	10					
Ferrosilicoboral (FeSiBAI)	10	15	15					
Nickelboron (NiB)	11	2	9	0.1	0.01		Ni	
Chromeboron (CrB)	8	2	2	0.1	0.01		Cr	
Ferrochromeboron (FeCrB)	15	3	5	0.4	0.02		Cr	
Greynal	1	6	15	0.2	0.06	0.06	Ti 10, Zr 1.5	

*The balance elements are Fe, Ni, or Fe + Cr depending on the alloy type. Empty cells: content not specially regulated.

TABLE 17.3 Composition of the Charge for Ferroboron Smelting with Aluminum Reduction (% wt.)

Component of the Charge	Ignition	Main	Iron-Rich Precipitant
Borate ore	11.6	81.9	13.3
Iron oxide	58.1	—	64
Aluminum powder	18.6	18.1	22.7
Iron chips	11.6	—	—

TABLE 17.4 Material Balance of FeB Smelting with Reduction of Boric Anhydride by Aluminum

Input Stream	kg	Output Stream	kg
Boric anhydride (93% B ₂ O ₃)	1200	FeB (21.8% B)	1095
Iron ore (90% Fe ₂ O ₃)	1400	Tapped slag (9.4% B ₂ O ₃)	1200
Aluminum (99.2% Al)	1167	Furnace slag (10.6% B ₂ O ₃)	1858
Lime (88% CaO)	340	Bottom slag (12.7% B ₂ O ₃)	167
Magnesite bricks use	265	Dust in gas ducts (28% B ₂ O ₃)	30
Total	4372	Total	4350

precipitant. The ignition mix is loaded first and heated with an electric arc. Upon reaction and melting of the ignition mix, half of the main charge is loaded and melted; after that half of the iron-rich precipitant is added and the furnace is switched off until the slag is tapped out. Then the second half of the main charge is added with the second part of the precipitant mixture (Gasik et al., 2009). The temperature of the melt is supported at about 1750° to 1780°C. After the smelting has been completed, the rest of the slag is tapped but the metal is left in the hearth to cool down. Tapped slag has (% wt.) 6 to 10 B₂O₃, <2 SiO₂, 10 to 14 CaO, 3 to 7 MgO, 2 to 4 FeO, and 65 to 73 Al₂O₃. The boron extraction yield in this process is 60% to 65%. The material and heat balances of ferroboron smelting by aluminum reduction are shown in Tables 17.4 and 17.5, respectively.

TABLE 17.5 Heat and Energy Balance of FeB Smelting

Energy Input	%	Energy Output	%
Chemical exothermic reactions	60	Slag latent heat	49.2
Electric energy	21.3	FeB latent heat	16.7
Metal and slag formation reactions	9.7	Anhydride dehydration	0.5
		Furnace accumulated heat	24.2
		Heat radiative losses	8.4
Total	100	Total	100

It is also possible to smelt FeB with both slag and alloy tapping, which enables better utilization of latent and accumulated heat and reduces the consumption of refractories.

Reduction by carbon might be used when there are no high restrictions to carbon content in ferroboron (Gasik et al., 1995). With this method, 10% to 20% B and 4% to 6% C alloy could be produced. The technology is based on the use of recycled, secondary, and lower-grade boron materials such as captured B_2O_3 dust, recycled boron carbide, iron mill scale (Fe_3O_4), and petroleum coke as reductant. Here carbon from petcoke and carbon from B_4C reduce iron and form iron borides in parallel with carbon reduction of B_2O_3 . A lower temperature of reduction is ensured by the exothermic effect of iron borides formation.

17.3.3 Technology of Other Boron Alloys

Among the master alloys (see Table 17.2), ferroboral (FeBAI) is produced in a manner similar to that used to produce ferroboron utilizing aluminum reduction. The process attains better performance if fused borate ore is used instead of raw B_2O_3 sources, also achieving a complete breakdown of sulfates and carbonates.

Nickelboron (NiB) contains 11% to 18% B, but the base metal is nickel, not iron. NiB alloy could be made either in a smelting hearth or in an electric furnace. In the first case, the charge for NiB smelting is shown in Table 17.6. The main difference from FeB technology is that the precipitant in this case is based on NiO and aluminum.

Nickelboron is smelted in a hearth with MgO lining, starting from a partial melting of boric acid and aluminum under the electrodes. Upon melting of the ore part of the charge, and after 5 to 10 min of soaking, the reduction part of the charge is loaded. The duration of the melting of ore charge and the reducing part of the charge at 600 kW power is 45 to 60 min. After that, the precipitant

TABLE 17.6 Composition of the Charge for Nickelboron Smelting with Aluminum Reduction (% wt.)

Component of the Charge	Reduction Charge	Main Charge	Precipitant
Calcined borate ore (<3% SiO_2)	8.8	83.6	—
Boric acid (52%–55% B_2O_3)	44.7	—	—
Nickel oxide (NiO)	28.2	—	74.1
Aluminum powder	18.3	16.4	18.5
Lime	—	—	7.4

part is loaded; the furnace is kept on for the next 20 min and then switched off. The alloy is extracted from the furnace after about 20 h.

Chromium–boron (CrB) alloys are processed with the same technology, where NiO is replaced by chromium oxide. The boron extraction yield is ~70%, and the chromium yield is ~86% (Gasik et al., 2009).

In special steels and alloy, boron is often added in other master alloys such as the “greynal” type (see Table 17.2). For the smelting process, the metal part of the charge is composed of FeBAI, FeSi, and titanium scrap. The exothermic part of the charge is composed of iron ore, lime, and aluminum powder, of which about half goes toward reduction and the other half is used for greynal alloying.

Smelting of greynal is carried out in a melting hearth lined with MgO bricks. The metal part of the charge is preheated to 400°C and loaded on the hearth. Then the whole exothermic mixture is loaded and the charge is ignited from the top. The rate reaction propagation through the charge is very high—it takes only 4 minutes to produce 1 ton of the alloy. The resulting liquid melt settles down on the hearth, where it reacts and dissolves the metal part of the charge. Limiting the thickness of greynal ingot to <100 mm is recommended in order to avoid elements liquation.

The production of 1 t of greynal requires about 440 kg FeB (calculated as for 5% B), 150 kg FeSiZr (with ~40% Zr), 150 kg of titanium scrap, 630 kg of aluminum powder, 1000 kg iron ore, and 150 kg of lime. The yield of boron in this process is ~88%, titanium ~99.5%, zirconium 100%, and aluminum 92%. Such high yield numbers are due to a minimal reduction of these elements, as most are added to the charge in the form of already reduced ferroalloys.

REFERENCES

- Davis, J.R., 2001. Alloying: Understanding the Basics. ASM International. Materials Park, OH, 647 pp.
- Garrett, D.E., 1998. Borates: Handbook of Deposits, Processing, Properties, and Use. Academic Press, 483 pp.
- Gasik, M.I., Porada, A.N., Kiselogof, O.L., 1995. Development and industrial implementation of high-boron content ferroboron by carbon reduction method. Stahl 3, 31–34.
- Gasik, M.I., Lyakishev, N.P., Gasik, M.M., 2009. Physical Chemistry and Technology of Ferroalloys [in Ukrainian]. Dnipropetrovsk: Sistemnye Tehnologii, 494 pp.

Technology of Ferroalloys with Rare-Earth Metals

Oleg Polyakov

National Metallurgical Academy of Ukraine, Dnipropetrovsk, Ukraine

Chapter Outline

18.1 Properties of Rare-Earth Metals and Their Compounds	459	18.3 Technology for Producing Ferroalloys with REM	466
18.1.1 Yttrium	461	18.3.1 Reduction by Carbon	467
18.1.2 Lanthanum	462	18.3.2 Reduction by Aluminum	468
18.1.3 Cerium	464	References	469
18.2 Minerals, Ores, and Concentrates of Rare-Earth Metals	465		

18.1 PROPERTIES OF RARE-EARTH METALS AND THEIR COMPOUNDS

Traditional classifications of rare-earth metals (REM) include lanthanum ($z = 57$) and lanthanides (elements from cerium, $z = 58$, to lutetium, $z = 71$), with the addition of scandium ($z = 21$) and yttrium ($z = 39$) to this list (Table 18.1). Of these rare-earth elements, steelmaking technology mainly uses three of them, namely yttrium, lanthanum, and cerium, although in steels and ferrous alloys of this type all other REM might be present in various amounts. These three elements are considered in more detail in this section.

The main function of REM in steels is to control the shape of nonmetallic inclusions (sulfides, silicates, oxides) remaining in killed and desulfurized steel (Trethewey and Jackman, 1981). REM have very high affinity for oxygen and sulfur, and thus may reduce other silicates and oxides (including Al_2O_3),

TABLE 18.1 Summary of the Properties of Rare-Earth Metals (Gasik et al., 2009)

Element	Atomic Mass	Valency (oxidation states)	Density, g/cm ³	Melting Temperature, K
Sc	44.96	3	3	1832
Y	88.9	3	4.47	1782
La	138.91	3	6.19	1193
Ce	140.12	3, 4	6.75	1077
Pr	140.91	3, 4	6.77	1208
Nd	144.24	3	7.01	1297
Pm	[147]	3	7.14	[1300]
Sm	150.35	2, 3	7.54	1325
Eu	151.96	3	5.24	1100
Gd	157.23	3, 5	7.87	1600
Tb	158.92	3	8.25	1700
Dy	162.3	3	8.56	1733
Ho	164.93	3	8.8	1773
Er	167.26	3	9.06	1800
Tm	168.93	3	9.32	1900
Yb	173.04	2, 3	9.96	1097
Lu	174.97	3	9.85	2000

forming rather hard globular inclusions (oxysulfides such as REM₂O₂S). The vapor pressure of REM at steelmaking temperatures is very small compared, for example, to calcium or magnesium, which have similar affinity for oxygen, and thus REM are much more efficient (yet more expensive) additions for steel deoxidation. Excess REM might also reduce refractory oxides from furnace and ladle lining, so their content must be controlled to achieve the desired effect. REM are generally very beneficial in hot-rolled steels as their presence decreases the anisotropy of properties due to the tendency to form globular inclusions. REM ferroalloys are also used in cast iron modification for the spheroidization of graphite (Cornell et al., 1981). Metallurgical applications account for about one third of the worldwide consumption of REM.

18.1.1 Yttrium

The element yttrium belongs to group III of the periodic table, as do all other REM. Natural yttrium is composed of one stable isotope. The configuration of the outer electron shell of yttrium is $4d^15s^2$, and its typical oxidation state is 3+. Yttrium has two allotropic forms: up to 1482°C the stable modification is α -Y (hexagonal lattice, $a = 0.3647 \text{ nm}$) and it has a density of 4.45 g/cm^3 . Above 1482°C , the stable modification is β -Y (cubic lattice of α -Fe type, $a = 0.408 \text{ nm}$). The melting point of yttrium is 1528°C , and the boiling point is $\sim 3320^\circ\text{C}$. The vapor pressure at 1450°C is $6.5 \cdot 10^{-2} \text{ Pa}$.

Yttrium forms a very stable oxide Y_2O_3 (Fig. 18.1), which melts at 2430°C and boils at $\sim 4300^\circ\text{C}$. It has a phase transformation at 2277°C , with lattice type change from cubic to hexagonal.

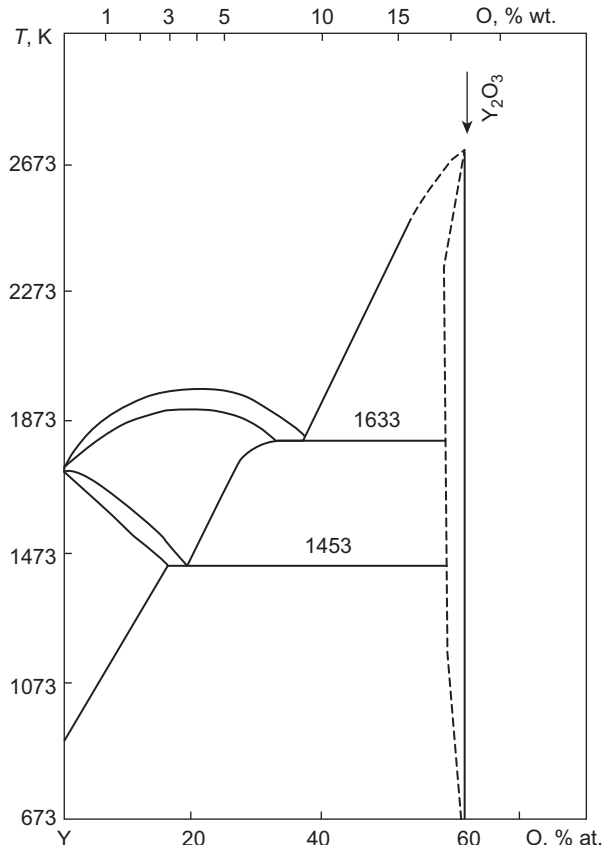


FIGURE 18.1 Diagram of the equilibrium state of the system Y-O.

With iron, yttrium forms several chemical compounds: YFe₉, also referred to as Y₂Fe₁₇ (melting point ~1400°C); YFe₄, also referred to as Y₆Fe₂₃ (melting point ~1300°C); and YFe₃ (melting point ~1400°C)—these all melt congruently. The YFe₂ compound melts incongruently at 1125°C. In yttrium-rich alloy eutectic is formed at 65.3% (at.) yttrium at 900°C. In the liquid state yttrium and iron form continuous solutions.

In the system Y-C, three carbides have been found (Fig. 18.2): YC, Y₂C₃, and YC₂. Y₂C₃ carbide is formed by the peritectoid reaction YC + YC₂ → Y₂C₃ at ~1500°C. The eutectic contains ~15% (at.) C. Carbide YC (~40% at. C) has a small inhomogeneity range. Carbide YC₂ forms congruently at 2300°C.

The system Y-Si (Fig. 18.3) has four compounds (yttrium silicides): Y₅Si₃ (melting at 1850°C), Y₅Si₄ (melting at 1840°C), YS (melting at 1835°C), and Y₃Si₅ (incongruent melting temperature of 1635°C). The silicide YSi has an orthorhombic crystal lattice system with a density of 4.33 g/cm³. In the system Y-Si eutectic, there are three eutectics: two with relatively low temperatures of 1260° and 1215°C, and one with a high temperature of 1710°C in the Y₅Si₃–Y₅Si₄ range. The solubility of yttrium in solid silicon is negligible.

18.1.2 Lanthanum

Lanthanum is a chemical element of group III, of the yttrium subgroup. Natural lanthanum is composed of two isotopes: stable La-139 (99.911%) and radioactive La-138 (0.089%) with a half-life period of $2 \cdot 10^{11}$ years. The electron

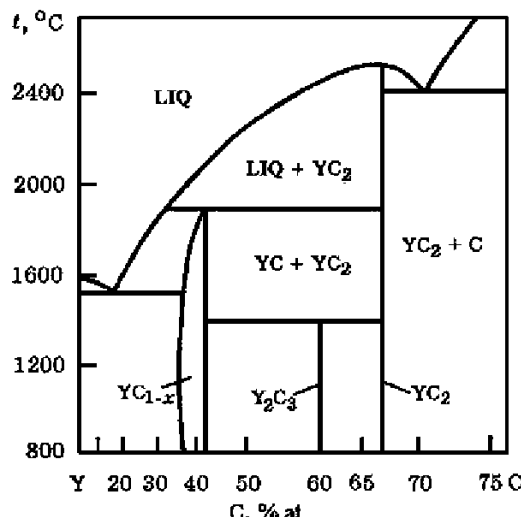


FIGURE 18.2 Diagram of the equilibrium state of the system Y-C.

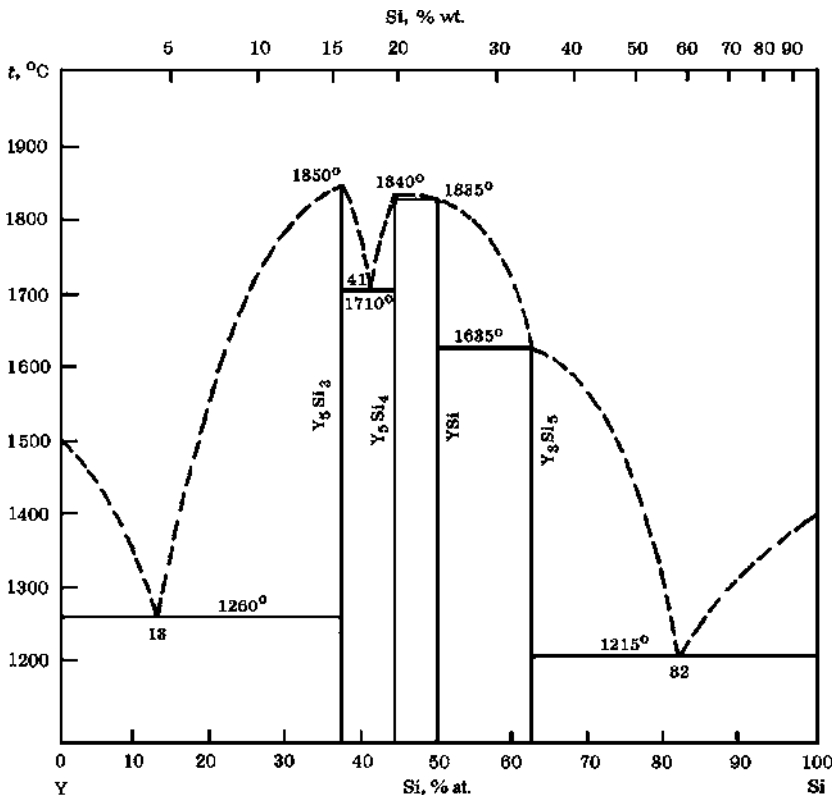


FIGURE 18.3 Diagram of the equilibrium state of the system Y-Si.

shell configuration of lanthanum is $5d^16s^2$, and its main oxidation state is $3+$. At low temperatures ($<277^\circ\text{C}$) the stable modification of lanthanum is α -La (hexagonal with $a = 0.3772 \text{ nm}$, $c = 1.2144 \text{ nm}$). In the range 277° to 861°C , β -La with cubic lattice ($a = 0.5296 \text{ nm}$) becomes more stable with a density of 6.19 g/cm^3 . Within the 861° to 920°C range, the most stable modification is γ -La with an FCC lattice of α -Fe type ($a = 0.426 \text{ nm}$) and a density of 5.97 g/cm^3 . The melting point of lanthanum is 920°C , and the boiling point is 3454°C . With oxygen, lanthanum forms the stable oxide La_2O_3 with a melting point of $\sim 2313^\circ\text{C}$.

Contrary to yttrium, lanthanum does not form compounds with iron and it has unlimited solubility in the liquid state. The solubility of lanthanum in the solid iron does not, however, exceed 0.1% (at.). The eutectic in this system forms at 785°C at 91.5% (at.) La.

With carbon, lanthanum forms carbides La_2C_3 and LaC_2 (Fig. 18.4), but not LaC (unlike in the Y-C system; see Fig. 18.2). LaC_2 carbide has a tetragonal crystal structure, a density of 5.35 g/cm^3 , and a melting point of 2360°C .

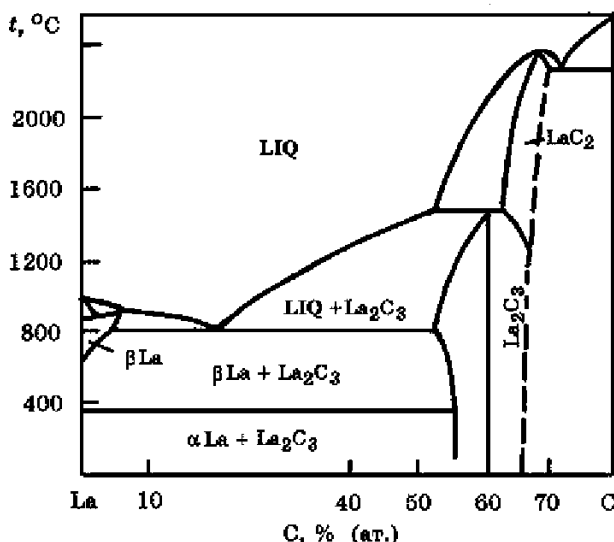


FIGURE 18.4 Diagram of the equilibrium state of the system La-C.

In the system La-Si, known compounds are LaSi, La₃Si₂, and LaSi₂. The melting point is assumed to be, for LaSi₂, 1520°C. This silicide crystallizes in the tetragonal crystal system and has a density of 5.05 g/cm³.

18.1.3 Cerium

Cerium is also a chemical element in group III of the periodic table. Cerium starts the row of lanthanides (4f elements), as the configuration of the outer electron shells of the cerium atom is 4f²6s². There are several known crystalline modifications of cerium. At room temperature \$\alpha\$-Ce with a lattice of \$\alpha\$-La type is stable. Between 61° and 727°C, \$\beta\$-Ce is stable (FCC lattice of Cu type), and above this temperature \$\gamma\$-Ce (BCC lattice of W type) is stable.

Cerium forms two stable oxides, Ce₂O₃ and dioxide CeO₂ (Fig. 18.5). Oxide Ce₂O₃ is less stable (contrary to many other lanthanides and REM), and in the presence of O₂ is rapidly oxidized to CeO₂ with a large exothermic effect. Several intermediate phases with various oxygen contents have also been observed in this system, which makes cerium somewhat different from other lanthanides, with the exception of praseodymium.

The system Ce-Fe has two compounds, CeFe₂ and CeFe₅, which melt incongruently at 925° and 1060°C, respectively. There is also a eutectic with the coordinates of 14% (at.) cerium at 592°C. The formula of the CeFe₅ compound might be better described as Ce₂Fe₁₇ (similar to Y₂Fe₁₇) with low- and high-temperature modifications.

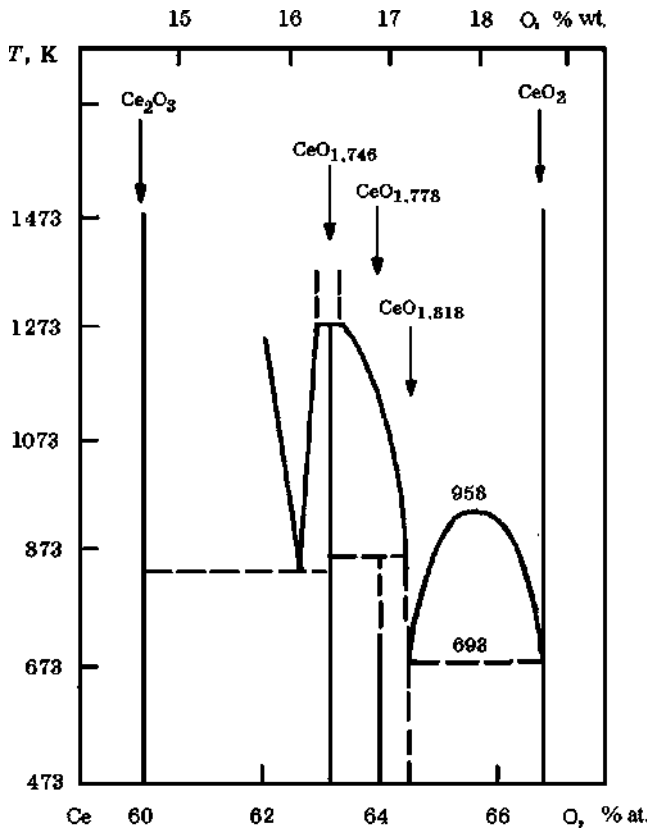


FIGURE 18.5 Diagram of the equilibrium state of the system Ce-O.

With carbon, cerium forms two stable carbides, similarly to lanthanum, namely CeC_2 and Ce_2C_3 . The latter has a cubic lattice ($a = 0.844 \text{ nm}$), and CeC_2 carbide has a tetragonal lattice and a density of 5.6 g/cm^3 , melting at 2290°C . Ce_2C_3 carbide is formed by a peritectic reaction at temperatures above 1700°C .

With silicon, cerium forms several silicides, such as CeSi , Ce_5Si_3 , and CeSi_2 .

18.2 MINERALS, ORES, AND CONCENTRATES OF RARE-EARTH METALS

Contrary to their name, REM are relatively widespread in nature. For example, if the aluminum content in Earth's crust is taken as 100 units, the relative amount of REM would be 0.18, which is much greater than that for copper and cobalt (0.12), uranium (0.1), tungsten (0.060), or molybdenum (0.001). Rare-earth metals exist in the form of oxides, phosphates, carbonates,

fluorcarbonates, and other compounds. The main minerals containing rare-earth metals are bastnaesite ($\text{Ce}, \text{La}[\text{FCO}_3]$, with a density of 4.2 to 5.2 g/cm³, and monazite ($\text{Ce}, \text{La}, \text{Nd}, \text{Th}[\text{PO}_4]$, which also contains impurities such as ThO_2 (10%), UO_2 (6,6%), and ZrO_2 .

Monazite is most common in pegmatite rocks and it is used as a raw material for cerium and thorium extraction. Loparite is a mineral of the fluorcarbonate group with the formula $\text{Ca}(\text{Ce},\text{La})_2[\text{CO}_3]\text{F}_2$ and it contains 30.5% Ce_2O_3 , 10.44% CaO , and 24.58% CO_2 . Minerals of pyrochlore groups have the general formula $(\text{Ca}, \text{Na}, \text{U}, \text{Ce}, \text{Y})_{2-\text{m}} \cdot (\text{Nb}, \text{Ta}, \text{Ti})_2\text{O}_6(\text{OF})_{1-\text{m}} \cdot \text{H}_2\text{O}$ and usually are associated with other similar minerals, rich in REM, tantalum, uranium, titanium, and other elements (Gasik et al., 2009).

The main industrial sources of rare-earth metals are bastnaesite, monazite, and xenotime. The first of these forms its own deposits; the other two usually present as minor components with ilmenite, rutile, zircon, and other minerals. Additionally, some REM might be extracted from specific sources (e.g., about 16% of yttrium comes from uranium ore waste). The leading REM producers are China, the United States, Brazil, and India.

Ores with minerals containing rare-earth metals are usually subjected first to a gravity separation step to isolate heavy minerals—monazite, xenotime, and so on. Monazite is further extracted from a mixture with a combination of gravitational, electromagnetic, and electrostatic methods. Chemical methods of processing concentrates include leaching and separation of radioactive impurities and the REM themselves, ensuring at the end the attainment of pure RE metals. Bastnezeite concentrate is leached with hydrochloric acid, which allows the isolation of cerium concentrate from the nondissolved precipitate. Loparite concentrates are processed via chlorination. Recent monazite and bastnezeite concentrates contain, respectively, about 60% and 70% wt. of rare-earth oxides. The mass fraction of each element of the rare earth in those concentrates is typically as shown in Table 18.2.

18.3 TECHNOLOGY FOR PRODUCING FERROALLOYS WITH REM

Some REM are produced in their pure form, usually by a reduction of extracted and purified fluoride salt by aluminum, but sometimes by calcium, magnesium,

TABLE 18.2 Typical Breakdown of REM in Different Mineral Concentrates, % wt.

REM Type	La	Ce	Pr	Nd	Sm	Eu
Monazite concentrate	22	45	5.6	17.8	3.2	0.1
Bastnaesite concentrate	34	50	4	11	0.5	0.1

or sodium. The obtained ingot is refined by vacuum remelting, but such production is not on a large scale.

The mixed alloy (“mischmetal,” >98% wt. REM) and in some cases ferrocerium (>85% REM; mainly of the Ce group) are commonly produced by electrolysis of molten REM chloride and fluoride salts. Alkali chlorides are added to the melt and the composition of reduced metal at the cathode is roughly proportional to the composition of the chloride melt. The electrolysis is carried out in steel reactors (walls serve as the cathode) with graphite rods (the anode) at 800° to 900°C. The resulting mischmetal alloy contains usually (wt. %): >45 Ce, 23–26 La, <20 Nd, and <10 other REM and impurities such as iron and aluminum. The electrolysis process has, however, a high energy consumption and limited applicability.

For steelmaking applications, ferroalloys with REM are the most common product (Oprea et al., 1989). As mentioned previously, these ferroalloys are mostly used to modify the structure of nonmetallic inclusions. The nominal grades of Fe-REM alloys commonly produced are shown in Table 18.3 (all of these alloys have 30% to 50% wt. Si and a balance made up of Fe). These alloys have been recommended to be used in the lump form with size below 20 to 30 mm to ensure their better utilization in steelmaking (Vichlevscuk et al., 1990).

18.3.1 Reduction by Carbon

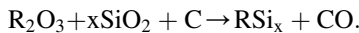
Lean REM ferroalloys (<15% REM) can be produced by carbon reduction. These REM ferroalloys with a high percentage of silicon are normally produced in ore-reduction ovens using a continuous smelting method. The charge contains a concentrate with REM, quartzite, carbon reductant, and steel chips. The exact dosing of carbon is of particular importance for the reduction of silicon and rare earths (R), as deviations of the carbon amount in the charge

TABLE 18.3 Approximate Composition of Fe-Si-REM Alloys

Fe-REM	% wt. REM	% Al	
		For Reduction by C	For Reduction by Al
FeSi-30REM	30-40	2-4	4-8
FeSi-20REM	20-30	2-3	3-6
FeSi-15REM	15-20	2-6	6-10
FeSi-10REM	10-15	2-3	3-6
FeSi-5REM	5-10	2-8	6-15

would cause an undesirable formation of accretions at the bottom of the furnace (SiC, RC, RC₂, unreduced R₂O₃, and SiO₂) and a decrease of REM recovery.

The general reaction of REM reduction by carbon might be presented as follows:

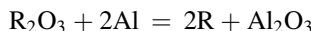


This reaction usually develops over 2000 K. REM recovery is facilitated by reducing their thermodynamic activity due to the formation of their solution with silicon and iron. In the ferroalloy with 30% to 40% REM, the rare-earth metals are in the silicide form. Reduction processes are accompanied by the formation of oxycarbides and carbides.

The increase of REM content in the ferroalloy leads to a drop of the extraction degree of these metals due to the formation of gaseous oxides (RO) and to an increase in the amount of slag. The density of the slag with increasing silicon content in the alloy is close to the density of the metal melt, and this may lead to difficulties in slag/metal separation. It is advisable to keep REM content in the molten alloys at 35% to 45% wt. REM, as in this case an REM utilization of 75% to 85% could theoretically be reached. It also leads to better utilization of REM in steelmaking and processing of modified cast iron.

18.3.2 Reduction by Aluminum

To obtain a significant number of REM-containing ferroalloys with low carbon content and without the risk of accumulating carbide accretions, the reduction of REM oxides by aluminum has been developed. In this case, the general reaction might be written as



and the Gibbs energy change (ΔG) for this process is usually positive in the standard state for practically achievable process temperatures (only cerium might be theoretically reduced to a pure metallic state by aluminum). Therefore, to achieve a sufficient degree of REM reduction, an excess amount of aluminum in the charge is required. Commonly >100% of the theoretically necessary aluminum is added to the charge, and this will lead to formation of master alloys with 3% to 7% Al and a significant amount of silicon. Altogether this creates favorable conditions for the reduction of REM activity during their dissolution in the melt.

The process is carried out in an electric arc furnace (power rating 1.8 MVA) with a hearth and walls lining made of carbon. The charge includes a concentrate of REM (yttrium or cerium subgroup) and a lanthanum oxide concentrate containing 40% to 47% CeO₂ and 41% to 48% (La₂O₃ + Nd₂O₃ + Pr₂O₃). Reductant is a primary or secondary aluminum powder (depending on the required chemical composition of the alloy). Additionally the charge contains ferrosilicon FeSi75, low-phosphorus iron ore concentrate (>63% Fe), and

fluxes (fresh lime and fluorspar). Per 100 kg of REM concentrate, 32 to 41 kg of aluminum powder are consumed, plus 110 to 125 kg of ferrosilicon, 30 to 37 kg of lime, and 0 to 5 kg of iron concentrate and fluorspar.

The charge is loaded after setting up the electric load. The charge is divided into two parts; the first has 55% to 75% concentrate, 60% to 65% lime, 60% ferrosilicon, and 42% aluminum powder (of their total amounts per batch). After this first part is melted and soaked for 5 to 7 min under constant current, the second part of the charge is loaded. Upon the completion of the melting process, slag is tapped into a lined ladle and the metal into a cast iron mold.

The metal (see Table 18.3) contains 11% to 40% rare-earth metals, 33% to 52% Si, 7% to 9% Al, 5% to 6.3% Ca, 0.01% to 0.03% C, and 12% to 20% Fe, and it has a density in the range 3.3 to 3.9 g/cm³. Because the slag density is 3 to 3.6 g/cm³, such small differences can cause extra losses of REM with the slag. An injection of fluorspar and sodium chloride is used to improve the separation of metal and slag—this decreases the density of the slag.

To produce 1 ton of the Fe-Si-REM ferroalloy, the following consumption of raw materials is observed: 520 to 565 kg of REM oxides concentrate, 203 to 210 kg of aluminum powder, 225 kg of lime, 630 to 695 kg of Fe-Si75, and 30 to 35 kg of iron ore. The energy consumption is 2100 to 2200 kWh/t of the alloy.

It is also possible to produce REM alloys in two stages, where the first reduction is carried out by silicon and the second is carried out by aluminum. The studies have shown a high degree of extraction of rare-earth elements in the metal (92% to 97%) and the possibility of obtaining lime–alumina slag with a low content of oxides of REM (1.6% to 4.8%). The development of the technology of melting alloys with rare earths offers the possibility of reducing the cost of 1 ton of alloy (30% REM). The lime–alumina slag (50% to 60% Al₂O₃, 35% to 40% CaO, and up to 5% rare-earth oxides) can be effectively used for secondary treatments.

REFERENCES

- Cornell, H.H., Loper, C.R., Pan, E.N., 1981. Rare-earth additions to blast furnace iron for the production of large castings. In: Lampman, J.R., Peters, A.T. (Editors), Ferroalloys and Other Additives to Liquid Iron and Steel. ASTM, Baltimore, pp. 110–124.
- Gasik, M.I., Lyakishev, N.P., Gasik, M.M., 2009. Physical Chemistry and Technology of Ferroalloys [in Ukrainian]. Sistemnye Tehnologii, Dnipropetrovsk, 494 pp.
- Oprea, F., Ciocan, A., Ciocan, N., 1989. Ferroalloys based on reactive elements. Metalurgia (Bucharest) 41, 270–272.
- Trethewey, W.H., Jackman, J.R., 1981. Trends in rare-earth metal consumption for steel applications in 1980's. In: Lampman, J.R., Peters, A.T. (Editors), Ferroalloys and Other Additives to Liquid Iron and Steel. ASTM, Baltimore, pp. 99–109.
- Vichlevsuk, V.A., Pipijuk, V.P., Kondraskin, V.A., Badogin, J.G., 1990. Experimental investigations on ferroalloys and prealloys for steel microalloying. Metallurgie Werkstofftechnik, Freiberger Forschungs. B;269, 91–95.

Technology of Ferroalloys with Alkaline-Earth Metals

Mihail I. Gasik

National Metallurgical Academy of Ukraine, Dnipropetrovsk, Ukraine

Chapter Outline

19.1 Calcium and Its Alloys	472	19.3 Strontium	485
19.1.1 Properties of Calcium and Its Systems	472	19.3.1 Properties of Strontium and Its Systems	485
19.1.2 Technology Used for Smelting Calcium Carbide	475	19.3.2 Smelting Technology of Strontium Alloys	487
19.1.3 Smelting Technology Used for Calcium–Silicon Alloy	477	19.4 Barium	488
		19.4.1 Properties of Barium and Its Systems	488
19.2 Magnesium	480	19.4.2 Smelting Technology of Ferrosilicobarium	490
19.2.1 Properties of Magnesium and Its Systems	480	19.4.3 Smelting Technology of Al–Ba Alloys	491
19.2.2 Technology for Producing Magnesium and Ferroalloys	483	19.5 Metallurgical Lime References	491
			494

19.1 CALCIUM AND ITS ALLOYS

19.1.1 Properties of Calcium and Its Systems

Calcium is a typical representative of the group of alkaline-earth metals of the periodic table (serial number 20 and atomic weight 40.08). The configuration of the outer electron shell of the Ca atom is $2s^2$, the melting temperature is 839°C, and the boiling temperature is 1495°C. Calcium is allotropic: α -Ca with an FCC lattice ($a = 0.558$ nm) that is stable below 443°C, and β -Ca with a BCC lattice ($a = 0.448$ nm) that is stable in the 443° to 842°C range. The density of calcium is 1.54 g/cm³.

Even though calcium is practically insoluble in iron and steels, it is extensively used to control the composition and shape of oxygen, sulfur, and nonmetallic inclusions. Pure calcium is too reactive and vaporizes easily, so it is not easy to apply it directly. Therefore, calcium is used in steelmaking in the form of calcium silicon (SiCa), calcium manganese silicon (SiMnCa), and more complex master alloys (CaSiBa, CaSiBaAl), as well as calcium carbide (CaC₂).

In the Ca-Si system, calcium forms several silicides: Ca₂Si (25.95% Si), probably Ca₅Si₃ (28.31% Si), CaSi (41.20% Si), Ca₃Si₄ (48.3% Si), and CaSi₂ (58.36% Si) (Fig. 19.1a). Not all silicides have reliable thermodynamic functions, and this calculated phase diagram may show only the most stable and well-studied phases (Fig. 19.1b).

With carbon, calcium forms one stable carbide, CaC₂ (62.54% Ca), which has a melting point of ~2430 K and a density of 2.204 g/cm³. Calcium carbide is also widely used in the chemical industry, in the organic synthesis used to produce synthetic rubber, and to produce calcium cyanamide (CaCN₂). The phase diagram Ca-C has not been put together yet, and it is assumed there is very little mutual solubility of Ca and C. The carbide CaC₂ is known to exist in four modifications: I, in the range 450°C; triclinic II, below 25°C and above 250°C; III, in the 350° to 435°C range; and IV, above 435° to 500°C (temperatures of these phase transitions are overlaid due to different levels of purity in the materials).

The system Ca-O has several compounds: CaO (calcia), CaO₂ (peroxide), CaO₄ (hyperoxide), and CaO₆ (ozonide). All but CaO (71.42% Ca) are usually unstable. Calcia (lime) has a melting point of 2613°C, a boiling point of ~3000°C, and a density of 3.37 g/cm³. Solubility of oxygen in solid calcium is negligible (Fig. 19.2). The high-temperature part of the diagram is not yet well defined, and there are opinions that CaO-Ca liquid might have a miscibility gap near the CaO-rich corner.

The equilibria in the CaO-SiO₂ system (Fig. 19.3) are very important in steelmaking and ferroalloys processing. As follows from the phase diagram of this system, the interaction of CaO with SiO₂ leads to a number of silicates—3CaO·SiO₂, 2CaO·SiO₂, 3CaO·2SiO₂, and CaO·SiO₂—which are characterized by relatively high thermodynamic stability. Orthosilicate 2CaO·SiO₂ melts congruently at 2130°C, and monosilicate CaO·SiO₂ melts congruently at 1544°C.

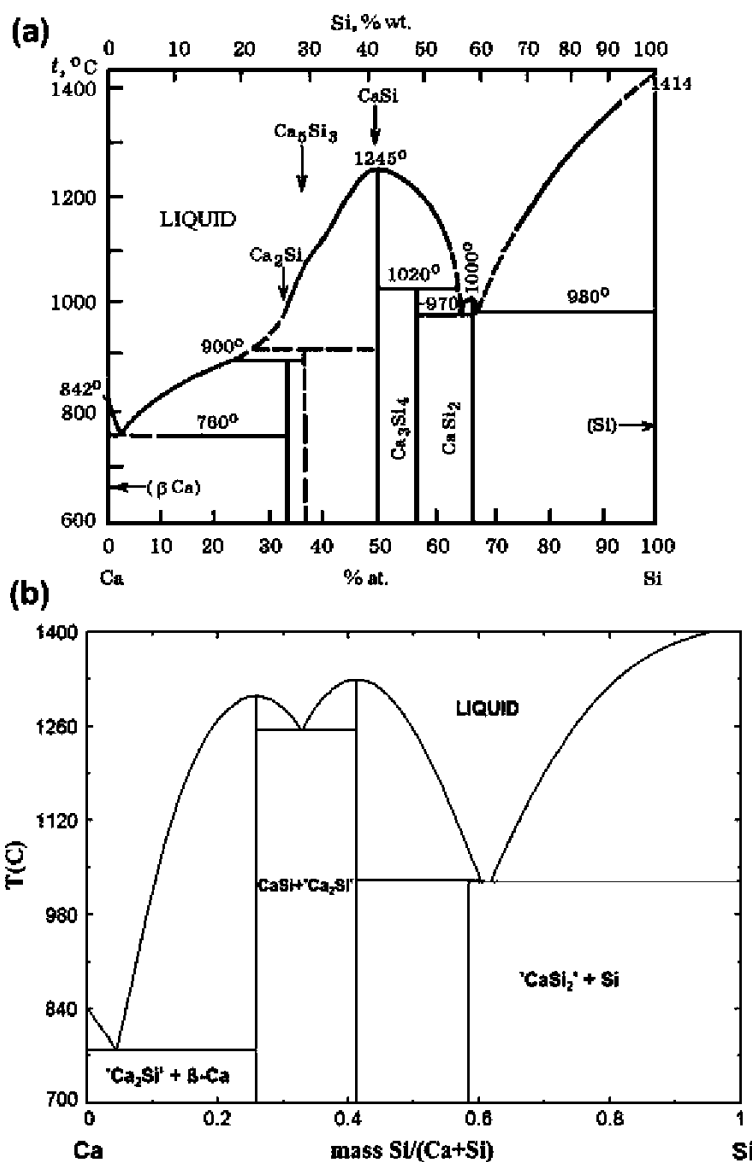


FIGURE 19.1 The system Ca-Si by different sources: based on experiments (a) and calculated from known thermodynamic data (b).

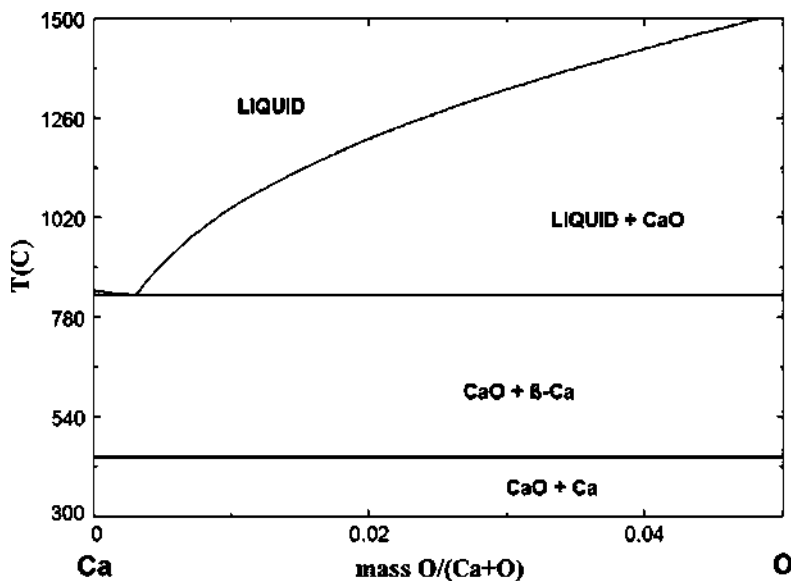
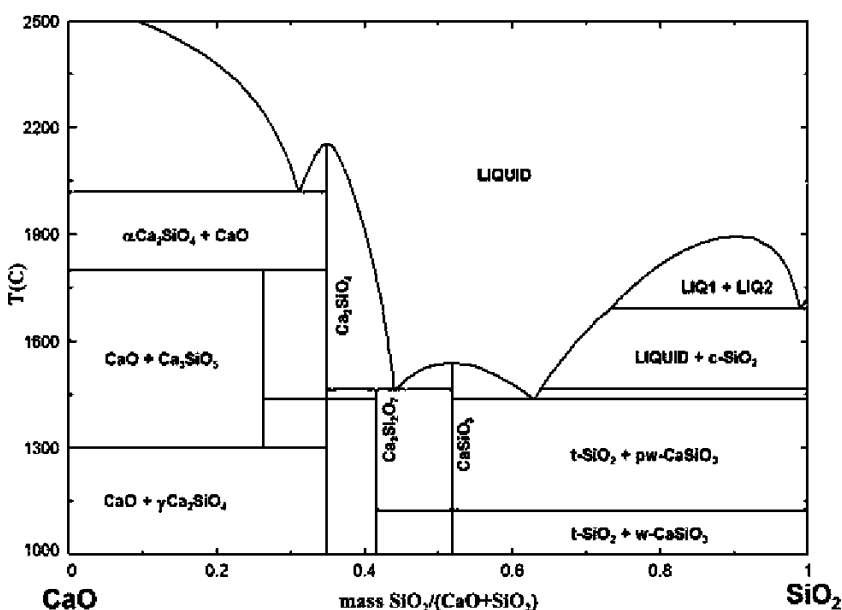
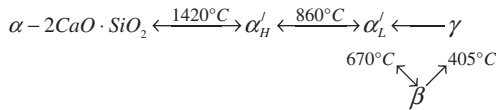


FIGURE 19.2 The system Ca-O.

FIGURE 19.3 The system CaO-SiO₂.

Orthosilicate $2\text{CaO} \cdot \text{SiO}_2$ has a complex polymorphism, which is of a high metallurgical relevancy:



The transformations $\alpha \rightarrow \alpha'_H$ and $\alpha'_L \rightarrow \beta$ are reversible, whereas $\beta \rightarrow \gamma$ and $\gamma \rightarrow \alpha'_L$ are not. The $\beta \rightarrow \gamma$ transformation is accompanied by a volume increase of 12%, leading to excess stresses and cracking of the material. This causes excess dusting and difficulties in handling highly basic orthosilicate-rich slag from the production of metallic manganese and low carbon ferrochromium.

19.1.2 Technology Used for Smelting Calcium Carbide

The equipment used for the smelting of calcium carbide is similar to that employed in electric furnaces used for other forms of ferroalloys processing, where carbon is used as a reductant. Calcium carbide is also an intermediate product in the smelting of calcium–silicon alloy. Technical grade calcium carbide is crystallized from the melt and contains ~80% CaC_2 and 10% to 15% CaO (Fig. 19.4). Commercial calcium carbide is a gray-black material due to the presence of residual carbon. The reaction of CaC_2 with water is known to generate acetylene gas (C_2H_2), and therefore the product must be kept in dry storage.

The modern technology used for the production of calcium carbide is based on the reduction of calcium oxide (lime) to CaC_2 by carbon for the overall reaction $\text{CaO} + 3\text{C} = \text{CaC}_2 + \text{CO}$. During this process, impurities such as sulfur

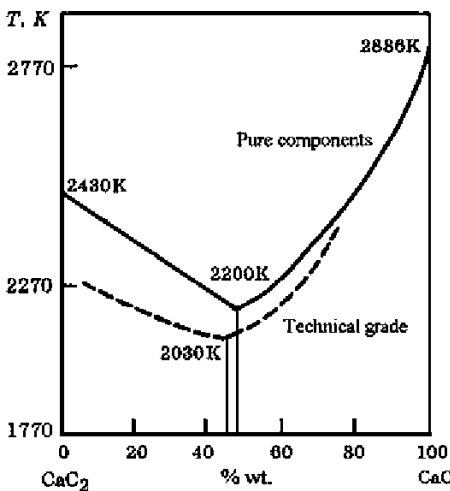


FIGURE 19.4 The liquidus in the system $\text{CaC}_2\text{-CaO}$.

and phosphorus, contained in the charge components, are also reduced and dissolved in molten calcium carbide. Calcium and sulfur form a sufficiently strong compound, CaS (which decreases the quality of the carbide product). Calcium and phosphorus also form the phosphide Ca_3P_2 , which is easily decomposed by moisture resulting in hydrogen phosphide (phosphine, PH_3), a very poisonous gas. The PH_3 content in acetylene is usually limited <0.08% vol.

Other undesirable impurities in CaC_2 come from lime and coke ash (Al_2O_3 , SiO_2). Therefore, the lime should contain at least 92% to 95% CaO and less than 1% to 2% CO_2 . The content of solid carbon in the coke should be 85% to 89%, and it should be dried to a moisture level <1%. The particle size of the lime used is 8 to 10 mm, and the particle size of the coke is 8 to 25 mm. The quality of technical grade calcium carbide (aside its acetylene-generating ability and PH_3) is determined by the sulfide phase (<0.5% to 1%) and free carbon (<1%).

Calcium carbide is produced in ore-reduction electric furnaces with a round or rectangular bath and a capacity of 60 to 80 MVA (Fig. 19.5). Rectangular bath dimensions are about $10.9 \times 8.9 \times 5.6$ m with rectangular self-backed electrodes of 3200×850 mm cross-section. The furnace is covered with water-cooled elements. The charge-feeding funnel (~300 mm) is placed around each

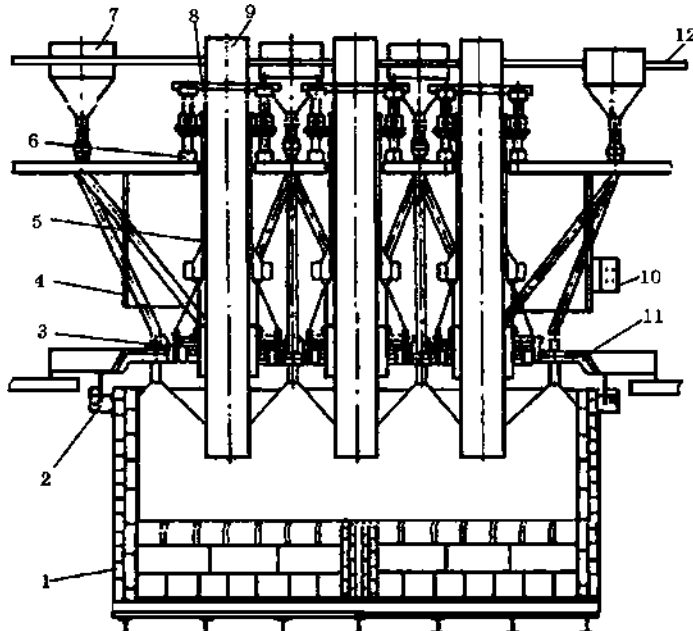


FIGURE 19.5 Closed electric furnace for calcium carbide production with rectangular bath type: 1, furnace lining; 2, sand seal; 3, dry seal; 4, hood; 5, electrode guide; 6, mechanism for moving the electrode; 7, charge feeder; 8, displacement mechanism (bypass) of electrodes; 9, electrodes; 10, power feeder; 11, furnace cover; 12, top level of the electrodes.

electrode. The main gas collectors are located between electrodes (catching up to 80% of the top gas). For a furnace power capacity of 60 MVA, the voltage is between 87 and 167 V and the average current range is 80 to 120 kA. For a furnace capacity of 80 to 85 MVA, the maximum voltage is 202 V. These values may vary for different furnace designs and electrical supply system versions.

For every ton of calcium carbide, about 250 to 330 m³ of gas is released (72% vol. CO, 5 CO₂, 7 to 8 H₂, <0.1 CH₄, balance N₂). Dust content in the gas is 100 to 150 mg/m³ and it is removed by scrubbers (cleaning of 1000 m³ of gas consumes 2.7 to 3.5 m³ water). The calcium carbide melt is tapped through a tap hole into the water-cooled drums.

19.1.3 Smelting Technology Used for Calcium–Silicon Alloy

Calcium–silicon (also referred to as ferro–silicon–calcium, FeSiCa)—which contains 10% to 35% Ca, 5% to 25% Fe, and the balance made up of Si—is the most commonly used calcium ferroalloy. It may contain 0.2% to 1% C, up to 1% to 2% Al, and below 0.02% to 0.03% P. There are also other alloys, such as calcium–manganese–silicon (16% to 20% Ca, 14% to 18% Mn, 53% to 60% Si, and the balance made up of Fe [<10%]) plus other residuals as noted earlier, although they are less commonly used. In industrial practice, there are three different ways to melt calcium–silicon alloy, of which reduction by carbon is the most common (Berdnikov et al., 2008). It utilizes a combined simultaneous reduction of calcium and silicon from their oxides. In the second method, the reduction of CaO is realized by silicon contained in the added ferrosilicon alloy. The third method utilizes a reduction of silicon from quartzite by carbon coming from CaC₂.

19.1.3.1 The Method of Reduction by Carbon

In this process, the charge consists of metallurgical lime (>87% CaO, <0.01% P) with a lump size of 40 to 100 mm, quartzite (95% SiO₂) of 25 to 200 mm size, coke (<11% to 13% ash) of 5 to 20 mm size, and black coal. A strict requirement on sulfur content in the components is imposed, as calcium and sulfur form a thermodynamically stable sulfide, CaS. The sulfur content in CaSi alloy may reach 0.2%. The main sources of sulfur are quartzite (50% to 55%), coke (20% to 30%), and coal (10% to 15%). The high-calcium grades (20% to 35% Ca) are obtained by reducing the lime and quartzite with coke in open electric furnaces of 16.5 MVA. The process can be represented by the scheme CaO + 3SiO₂ + 7C → [CaSi₂ + Si]_{Fe} + 7CO. The reduction process is facilitated due to the formation of thermodynamically stable associates close to CaSi₂, which lowers the activity of calcium and silicon and improves the recovery of these elements from their oxides. Intermediate products are formed (SiC and CaC₂) in this process, and therefore excess carbon in the charge has to be avoided to eliminate the overgrowth of carbides in the furnace bath.

A sample charge load consists of 85 kg lime, 200 kg quartzite, 30 kg coal, 50 kg charcoal, and 85 to 95 kg coke. When melting alloys of low-calcium grades (10% to 15% Ca), ~40 kg of iron chips are added to the charge. The exact composition of the charge is calculated taking into account the practical efficiency of recovery use for each element. For example, for the charge for alloy with 30% Ca the extraction efficiency of calcium is normally taken as 67% and of silicon, 75%.

Special attention has to be paid to control the slag formation processes, because the slag has a higher density than metal and it is deposited on the bottom of the bath. Its excessive accumulation leads to disorders in the operation of the furnace. The composition of the slag varies according to the grade of the alloy. The low-grade alloys (~15% Ca) have preferentially basic slags (60% to 70% CaO, 25% to 30% SiO₂), whereas high-grade alloys (~30% Ca) have acidic slags (15% to 20% CaO, 40% to 55% SiO₂) with extra carbide content (<10% SiC, <10% to 15% CaC₂). Slags with a high content of calcium carbide have higher fluidity and reduced sulfur concentration, but the drawbacks are poor separation of the slag from the metal and thus more difficult tapping.

An electric furnace with 14 MVA of power operates at a 50 to 60 kA current. Even if the process is within its optimal parameters limits, the bath accumulates autogenic (“frozen”) lining over time, consisting of a half-reduced charge (oxides and carbides). This requires periodic stops and relining of the furnace. In industrial practice, to avoid delays, the problem is partly solved by periodically changing the furnace operation for smelting of 45% ferrosilicon. The tapping of the alloy and slag in the normal course of melting is performed (every 2 h) into a carbon-lined walled and fireclay bottom ladle. The approximate composition of the CaSi alloy obtained by this carbon reduction process is 28% to 31% Ca, 60% to 68% Si, 3% to 4% Fe, 1% to 2% Al, 1% to 1.5% C, <0.1% S, and <0.02% P.

The sulfur and aluminum presence in the CaSi alloy is the result of the use of carbon reductants with high sulfur and ash (Al₂O₃) contents. At high temperatures, alumina is reduced by carbon and forms carbide Al₄C₃, which dissolves into the alloy. Therefore, the use of components with a high content of impurities (such as Al₂O₃) in the smelting of calcium–silicon is limited to keep a permissible level (<2% wt. Al).

19.1.3.2 The Method of Reduction by Silicon

This method is based on the use of ferrosilicon as a reductant, giving the overall reaction $(\text{CaO}) + [\text{Si}]_{\text{FeSi}} \rightarrow [\text{CaSi}_2 + \text{Si} + \text{FeSi}_2] + (2\text{CaO} \cdot \text{SiO}_2)$. Because the chemical affinity of silicon for oxygen is lower than that of calcium, the reaction can proceed in the direction of obtaining calcium–silicon only in the case of a substantial reduction of the activity of calcium. This specifies high silicon and lower calcium content in the final alloy. Reaction equilibrium is achieved at relatively low concentrations of calcium, so the method can be used

to obtain lower grades of calcium–silicon (referred to as FeSiCa) with calcium at less than 20%.

The calcium–silicon smelting is carried out in open furnaces as a batch process. The typical composition of the charge has 200 kg lime, 196 kg ferrosilicon (Fe-75% Si), and 30 kg fluorspar (CaF_2). The use of fluorspar is necessary to reduce viscosity of the highly basic slag and to improve conditions for the separation of melt products from the slag. The recovery of calcium is only 20% to 30% (calcium also partially vaporizes) and the utilization of silicon from the ferrosilicon is about 75% to 85%. From the charge materials, into the alloy are transferring approximately 25% to 35% Al, 15% to 30% S, 15% to 35% P, and 25% to 30% Mg. The actual chemical composition of FeSiCa is (% wt.) 15 to 19 Ca, 55 to 65 Si, 18 to 22 Fe, <1 Al, <0.01 S, <0.02 P, and <0.07 C.

The quality of FeSiCa made by silicon reduction is higher than that resulting from carbon reduction, especially in respect of sulfur and carbon contents. Comparative technical and economic indicators of the smelting of calcium–silicon alloy is normally supplied to steel mills in different sizes (<2, 2 to 5, 5 to 20, and 20 to 200 mm lumps). Fine sizes of the alloy are not very efficient for steel deoxidation due to significant losses of calcium (low density and high activity with respect to atmospheric oxygen and oxides of the ladle slags). Better use of calcium–silicon is achieved when it is applied in the form of cored wire.

TABLE 19.1 Comparison of Charge Materials per 1 Ton of the CaSi Alloy (15% and 30% wt. Ca) for Different Methods of Smelting

Category	15% Ca	30% Ca	15% Ca	30% Ca
	Carbon Reduction		Silicon Reduction	
Materials, kg				
Quartz	1436	1875	—	—
Lime	456	748	960	940
Coal	281	265	—	—
Charcoal	244	370	—	—
Dry coke	388	600	—	—
Ferrosilicon 65% Si	—	—	917	805
Iron chips	318	—	—	—
Electrode paste	107	134	—	—
Graphitized electrodes	—	—	12.5	10.5

19.1.3.3 The Method of Reduction by Calcium Carbide

The first method for smelting CaSi by carbon reduction described earlier relies on the simultaneous reduction of Si and Ca from quartzite and limestone, but despite its apparent simplicity, this method has some significant drawbacks. It is difficult to apply it to the smelting of calcium–silicon with more than 30% Ca due to the autogenic lining accumulation in the furnace bath. Fused products resulting from the interaction of SiO_2 and CaC_2 form deposits on the bottom and on the walls. Because CaSi alloy has a lower density than these deposits, it collects under the electrodes and over the bottom deposits, disturbing the electrical conditions (also causing shortcuts) and furnace operation. As noted previously, for these reasons the furnace is periodically switched to the smelting of ferrosilicon (Fe-45% Si) to bring the bath back to the desired state for the subsequent smelting of calcium silicon.

These disadvantages are largely eliminated upon implementation of the two-step calcium–silicon smelting process. The first stage of this process consists of manufacturing technical grade calcium carbide, which is smelted from lime and coke charge (as described in Section 19.1.2). The second step is the smelting of the charge composted of calcium carbide and quartzite, where the reduction follows the scheme $\text{CaC}_2 + \text{SiO}_2 \rightarrow [\text{Ca-Si}] + 2\text{CO}$.

To produce calcium–silicon with 30% to 35% Ca using this method, the charge materials required for 1 ton of the alloy are (kg) 1700 to 2000 quartz, 600 to 1000 calcium carbide, 560 to 580 coke, and 170 to 200 charcoal. A typical furnace of 2.5 MVA makes 3500 tpa of calcium–silicon, which is enough to deoxidize ~1 million ton of steel. Smaller furnaces can be also used, and a comparison of these furnaces using this production method is shown in Table 19.2.

19.2 MAGNESIUM

19.2.1 Properties of Magnesium and Its Systems

Magnesium is an element of group II of the periodic table of elements; its atomic number is 12, its atomic weight is 24.305, and it belongs to the group of alkaline earth metals (AEMs: Be, Mg, Ca, Sr, Ba, Ra). The configuration of the outer electron shell is $3s^2$, and the typical oxidation degree is +2, rarely +1. Magnesium has a hexagonal crystal lattice ($a = 0.321$ nm, $c = 0.520$ nm). Its melting point is 650°C, and its density is 1.74 g/cm³ (20°C), 1.54 g/cm³ (700°C). The equation of the temperature dependence of vapor pressure (in mm Hg) above liquid Mg has the form $\lg P_{\text{Mg}} = 16.7974 - 7844.2/T + 2.548 \cdot 10^{-4} \cdot T - 2.728 \cdot \lg T$ (407–1390 K). Like calcium, magnesium is practically insoluble in iron and steels. It might be used for deoxidation and sulfur removal (Zhuchkov et al., 1977), but its main metallurgical use is for the inoculation of cast irons.

In the Mg–O system, the stable oxide formed is MgO with a melting temperature of 2827°C, a boiling temperature of 3600°C, and a density

TABLE 19.2 Technical Parameters Comparison for Small-Scale Calcium–Silicon Smelting Using the Two-Step Technology

Furnace Transformer, MVA (x phases)	0.63	1.2	1.5	2.5	2.5 (x 3)
Maximal current, kA	6.7	11.4	11.7	17.5	35.2
Graphitized electrodes, diameter in mm	300	400	400	500	610
Self-baked electrodes, diameter in mm	—	—	—	—	850
Average production capacity, tpa	800– 900	1200– 1500	1800– 2000	3000– 4000	10,000– 12,500
Hearth length, m	11.6	12	12	13.5	16.7
Hearth width, m	6.1	7.2	7.2	7.85	10.8
Hearth height, m	8.5	12.6	12.6	12.6	14.1
					15.8

of 3.58 g/cm^3 . Oxide MgO has a substantial vapor pressure at high temperatures. Other oxides reported to exist are MgO_2 , MgO_4 , and Mg_2O , but they are not stable in the typical conditions required for ferroalloys processing.

In the system Mg-C, two stable carbides are known: MgC_2 and Mg_2C_3 . The density of MgC_2 is 2.204 g/cm^3 . The interaction of magnesium carbide with water or water vapor proceeds similarly to that for CaC_2 , leading to the formation of C_2H_2 and the mixture of hydrocarbons. Monocarbide MgC has been observed, but only at high pressures (a few GPa). The phase dominant diagram of the Mg-O-C system is shown in Figure 19.6 at 1 atm total pressure and 1600°C . As the figure shows, pure magnesium can only be reduced to carbides or to magnesium gas, which requires low oxygen partial pressures and low CO pressures.

The system Mg-Si has one stable silicide, Mg_2Si (36.56% Si), which congruently melts at 1102°C (Fig. 19.7). There is practically no solubility of Mg in Si or otherwise. Two metastable silicides of MgSi and MgSi_4 compositions have been mentioned but without enough detailed data to allow a reassessment of the phase equilibria.

With sulfur, magnesium forms a stable sulfide, MgS , with a melting temperature of about 2200° and a density of 2.86 g/cm^3 . With CO_2 , magnesium oxide forms carbonate, MgCO_3 , which dissociates back to MgO and CO_2 at high temperatures. With silica, magnesium oxide (Fig. 19.8) forms two stable silicates: $2\text{MgO}\cdot\text{SiO}_2$ and $\text{MgO}\cdot\text{SiO}_2$.

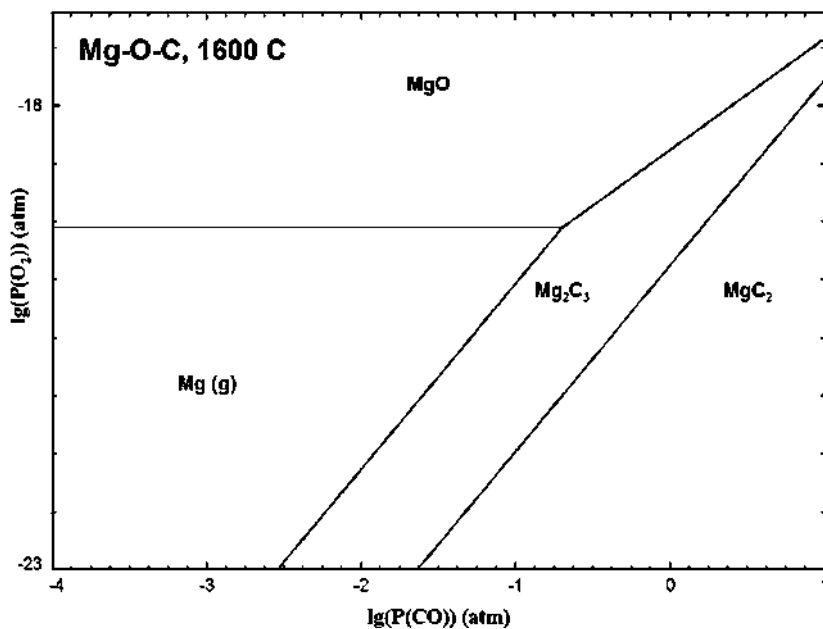


FIGURE 19.6 Mg-O-C dominant phases diagram at 1600°C.

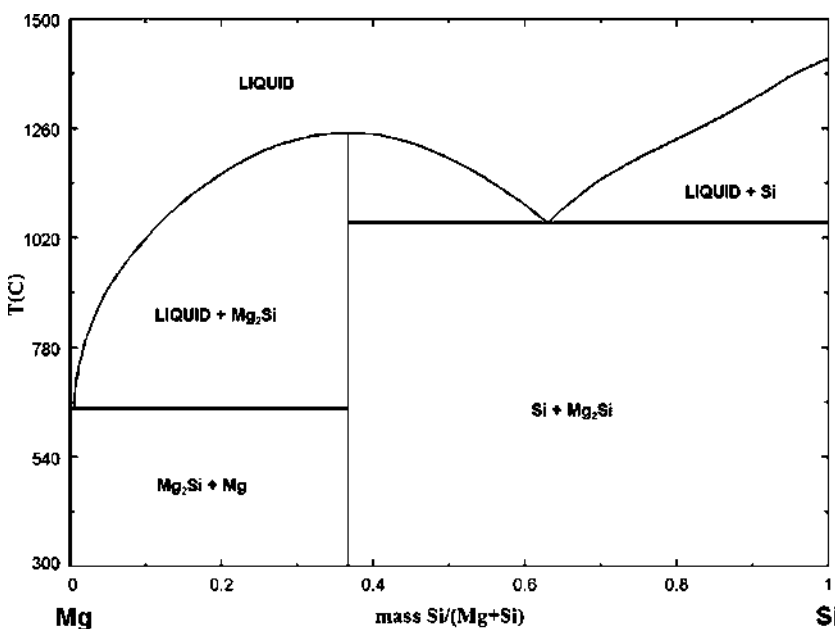


FIGURE 19.7 Mg-Si system diagram.

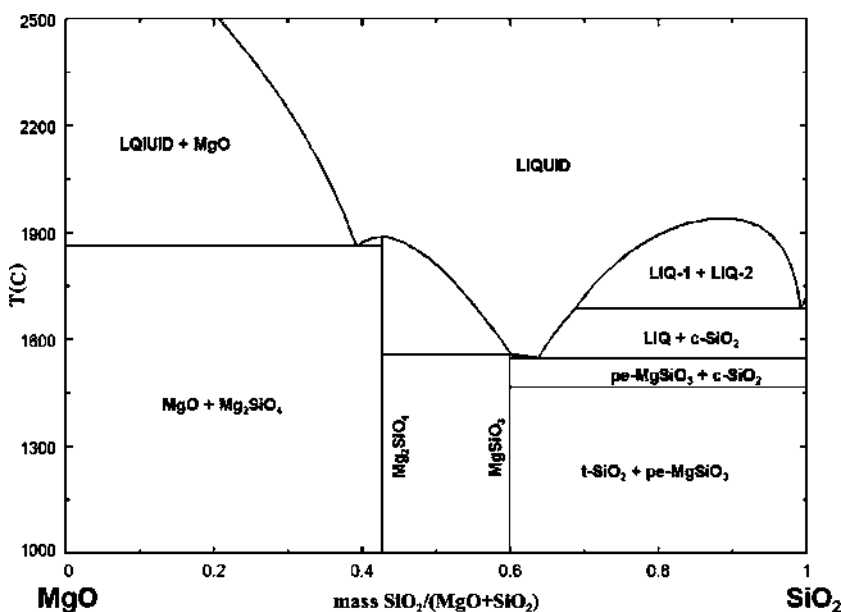


FIGURE 19.8 MgO-SiO₂ system phase diagram. Pe, pseudoenstatite; c, cristoballite; t, tridymite.

Magnesium exists in nature in various minerals: carbonates MgCO₃, (Ca, Mg) CO₃, chlorides (MgCl₂·6H₂O), sulfate (MgSO₄·H₂O), silicates (3MgO·2SiO₂·2H₂O), magnesium oxide (periclase, MgO), hydroxide Mg(OH)₂, and so on. Worldwide magnesium production is based on the firing of MgCO₃ and on extraction from seawater or brines. The product from firing contains 75% to 96% MgO total, and from seawater and brines it usually contains more than 97%.

19.2.2 Technology for Producing Magnesium and Ferroalloys

The major type of magnesium ferroalloy is in the form of magnesium–ferrosilicon (FeSiMg) with 5% to 10% Mg and calcium–silicon–magnesium (25% to 30% Ca, 50% to 55% Si, and 10% to 15% Mg). Minor types are also different master alloys such as Ni-15% Mg, with (<30% Si) or without silicon. Pure magnesium is manufactured by electrolysis of the chloride compounds.

There are several ways to make magnesium alloys by the reduction of magnesium from MgO or calcined dolomite in a vacuum smelting process using silicon (from FeSi) as a reductant. The vacuum–thermal process in general is described by the overall reaction



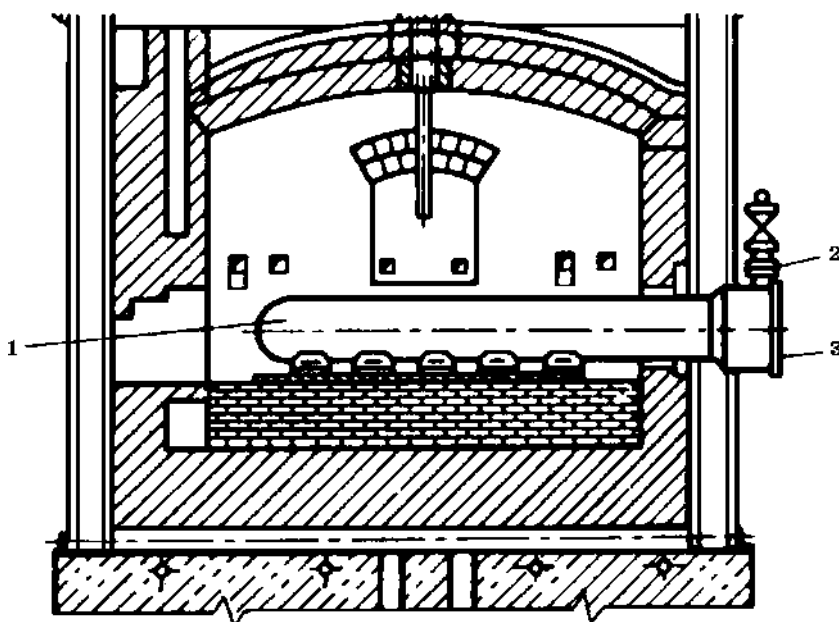
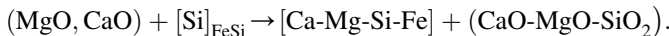


FIGURE 19.9 Production of magnesium by silicon reduction in a vacuum retort: 1, retort; 2, valve; 3, cover.

In the reaction zone, Mg evaporates, passes, and cools down in a metal retort area (Fig. 19.9) where it is condensed. Besides the use of silicon (ferrosilicon) as a reducing agent, aluminum can be used. Due to the evaporation-condensation route, this method can be used to obtain magnesium of technical purity.

To process FeSiMg alloy, the reduction by silicon from FeSi is used at normal pressure in an arc furnace. The charge is composed of magnesite (MgO), limestone, dolomite, ferrosilicon (Fe-75% Si), and fluorspar (CaF_2). The process in general can be represented by the following scheme:



The maximum Mg content in the alloy (2.3% to 2.6%) is obtained when the ratio in the mixture $\text{MgO}:\text{CaO} = 0.3$ and the ratio $\text{CaF}_2/(\text{CaO}+\text{MgO}) = 0.1$ to 0.15. Excess of fluorspar in the charge leads to a loss of silicon due to the reaction $2\text{CaF}_2 + \text{Si} = \text{SiF}_4(\text{g}) + 2\text{Ca}$.

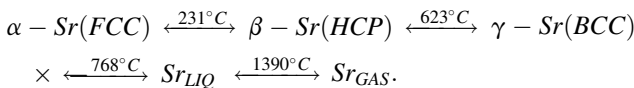
There is also the technique of processing Ca-Mg-Si-Fe alloys by dissolution of magnesium ingots (produced by the electrolytic method) in the liquid ferrosilicon. According to industrial experience, in the first stage the charge composed of Fe-65% Si, Fe-75% Si, CaO, and magnesite is melted to obtain an alloy with 2% to 3% Mg (using the process described earlier). In the second

stage, magnesium content is adjusted to 6% to 7% by dissolving extra magnesium ingots in this alloy. This FeSiMg alloy contains 5% to 7% Mg, 53% to 65% Si, and a balance made up of iron. The disadvantages of this method, however, are substantial losses of magnesium and the generation of intense smoke and sparks.

19.3 STRONTIUM

19.3.1 Properties of Strontium and Its Systems

Strontium is an element of group II of the periodic table of elements. Its atomic number is 38, its atomic weight is 87.62, the configuration of the outer electron shell of an atom is $5s^2$, and it belongs to the alkaline-earth metals (AEMs) group. The typical oxidation of strontium is +2, rarely +1. Strontium metal exists in three allotropic modifications, the transformation of which takes place at the following temperatures:



In the system Sr-O the stable oxide formed is strontium oxide (SrO), colorless crystals with a density of 4.7 g/cm^3 and a melting point of $2660^\circ C$. Under the high pressure of oxygen, SrO may ignite to form peroxide (SrO_2). Strontium and strontium oxide react with water, forming hydroxide $Sr(OH)_2$, colorless hygroscopic crystals with a melting point of $535^\circ C$ and a density of 3.632 g/cm^3 . In the system Sr-C, the most stable solid carbide is SrC_2 .

In the system Sr-Si, several silicides are formed: $SrSi$ (24.23% Si) and $SrSi_2$ (38.99% Si) (Fig. 19.10). Silicides $SrSi$ and $SrSi_2$ melt congruently at 1140° and $1150^\circ C$, respectively. The system has three eutectic temperatures of 700° , 1044° , and $1000^\circ C$. The existence of Sr_2Si and Sr_5Si_3 has also been reported.

Strontium oxide with CO_2 forms strontium carbonate ($SrCO_3$), which exists in several polymorphic modifications. The low-temperature stable phase (α) with a rhombohedral structure is stable below $925^\circ C$, and the high-temperature hexagonal phase (β) is stable within the 925° to $1416^\circ C$ range. The third cubic phase (γ) forms under higher pressure of CO_2 ($> 2\text{ MPa}$).

With silica, strontium oxide forms several silicates (e.g., $2SrO \cdot SiO_2$, $SrO \cdot SiO_2$). The melting point of $2SrO \cdot SiO_2$ has not been exactly determined, but it is above $1700^\circ C$ (Fig. 19.11). The compound $SrO \cdot SiO_2$ melts congruently at $1580^\circ C$, and the lowest eutectic temperature in this system is $1358^\circ C$.

With alumina- SrO , several compounds exist, namely $4SrO \cdot Al_2O_3$, $3SrO \cdot Al_2O_3$ (melting point $1660^\circ C$), $SrO \cdot Al_2O_3$ (melting point $1790^\circ C$), $SrO \cdot 2Al_2O_3$ (melting point $1820^\circ C$), and $SrO \cdot 6Al_2O_3$ (melting point $1900^\circ C$), Fig. 19.12. Aluminate $4SrO \cdot Al_2O_3$ has two modifications: a high-temperature

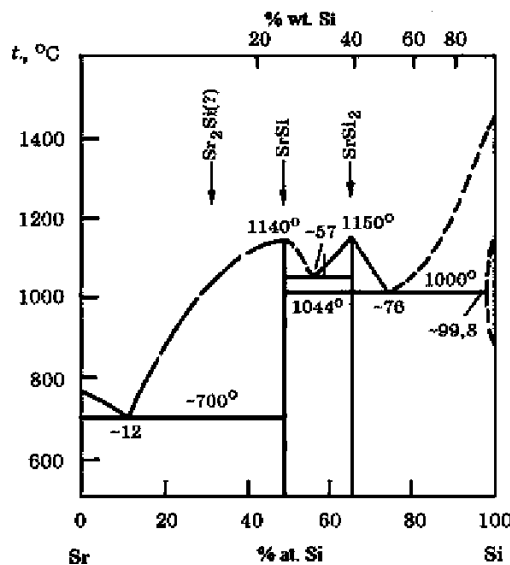
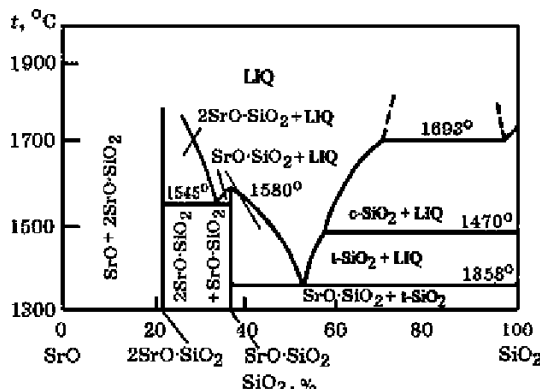
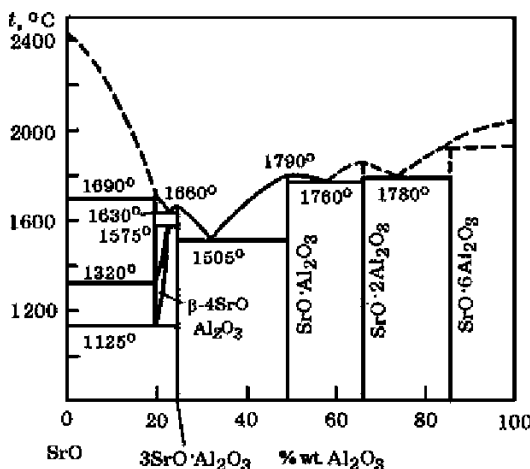


FIGURE 19.10 Sr-Si phase diagram.

phase ($\beta\text{-}4\text{SrO}\cdot\text{Al}_2\text{O}_3$), stable in the 1320\$^{\circ}\text{C}\$ to 1690\$^{\circ}\text{C}\$ range, and a low-temperature phase ($\alpha\text{-}4\text{SrO}\cdot\text{Al}_2\text{O}_3$), stable in the 1125\$^{\circ}\text{C}\$ to 1320\$^{\circ}\text{C}\$ range. The lowest eutectic temperature in this system is 1505\$^{\circ}\text{C}.

The total content of strontium in Earth's crust is estimated as $3.4 \cdot 10^{-2}\%$ (by weight). Strontium is known to form about 40 minerals, of which only two are of practical relevance, namely celestine (SrSO_4) and strontianite (SrCO_3). Strontium is present as an isomorphous impurity in a variety of magnesium, calcium, and barium minerals, such as $(\text{Sr,Ca})_2\text{B}_{14}\text{O}_{23}\cdot 8\text{H}_2\text{O}$, and it is also

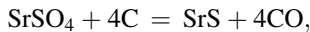
FIGURE 19.11 SrO-SiO₂ phase diagram.

FIGURE 19.12 SrO-Al₂O₃ phase diagram.

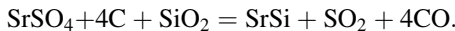
found in different natural mineral species. Part of the strontium in the oceans is concentrated in ferromanganese nodules (Gasik et al., 2009).

19.3.2 Smelting Technology of Strontium Alloys

Strontium raw materials are used mainly in the form of celestine (SrSO₄). Celestine concentrate contains about 86% SrSO₄. At high temperatures strontium sulfate interacts with carbon to form strontium sulfide (SrS):



but in the presence of SiO₂ this reduction proceeds to strontium silicide:



In areas of carbon deficiency, silicates of strontium can additionally form into the slag: SrSO₄ + SiO₂ + C = (2SrO·SiO₂) + CO + SO₂.

For a complex ferroalloy containing strontium and barium, concentrates of strontianite (SrCO₃) and BaCO₃ are used. A typical concentrate grade has a lump size of up to 10 mm and a chemical composition (% wt.) of 5 to 6 SrO, 15 to 17 BaO, 20 to 22 CaO, and 23 to 25 SiO₂; the rest of the components are mainly MgO, Na₂O+K₂O, and FeO.

Ferrosilicostrontium alloy is processed in small electric arc furnaces with a capacity of 160 kVA at 30 V and a nominal current of 1500 A. The charge consists of celestine ore, quartzite, coke, and iron chips. The resulting FeSiSr alloy contains 8% to 10% Sr, 48% to 59% Si, and a balance made up of iron. The slag/metal ration in this process is ~1.5. Industrial experience shows that specific energy consumption is high and strontium extraction is low, so there is a need to improve the technology (Liu and Yang, 1998).

19.4 BARIUM

19.4.1 Properties of Barium and Its Systems

Barium is an element found in Group II of the periodic table of the elements. Its atomic number is 56, its atomic weight is 137.33, it belongs to the group of alkaline-earth metals, and it has a density of 3.78 g/cm^3 . The configuration of the outer electron shell of an atom of barium is $6s^2$, and its main oxidation state is +2, rarely +1. Barium exists in two allotropic modifications: α -Ba below 375°C and β -Ba between 375° and 727°C .

In the Ba-O system, the most stable oxide is barium oxide (BaO) (89.57% Ba), which is made up of colorless crystals with a cubic lattice ($a = 0.5542 \text{ nm}$) and a density of 5.7 g/cm^3 . When heated in an oxygen environment, BaO forms barium peroxide (BaO_2) at about 500°C , with a hexagonal lattice ($a = 0.534 \text{ nm}$, $c = 0.677 \text{ nm}$) and a density of 4.96 g/cm^3 . At higher temperatures, BaO_2 thermally dissociates to form BaO and O_2 . The peroxide BaO_2 is the main component of the charge for manufacturing Al-Ba master alloys. The melting point of BaO is 2017°C , but it sublimates before reaching melting temperature. Barium oxide (BaO) forms during the dissociation of barium carbonate (BaCO_3) at 700° to 900°C .

Barium carbonate (77.69% BaO), like strontium carbonate, exists in three modifications: up to 840°C α - BaCO_3 with orthorhombic lattice ($a = 0.639 \text{ nm}$, $b = 0.883 \text{ nm}$, $c = 0.528 \text{ nm}$); in the range 840° to 960°C , β -phase with a hexagonal lattice; and 982°C , γ - BaCO_3 with a cubic lattice. BaCO_3 forms solid solutions with SrCO_3 , CaCO_3 , and BaO .

Barium hydroxide Ba(OH)_2 exists in two modifications; the low-temperature modification transforms into the high-temperature form at 246°C . Hydroxide decomposes to BaO and H_2O when heated above 800°C . Barium peroxide, carbonate, and hydroxide are considered to be toxic materials and regulations limit their allowable concentration in the air.

With carbon, barium forms stable carbide phase BaC_2 (14.88% C), with properties similar to those of calcium carbide. Carbide crystallizes in a tetragonal lattice type of CaC_2 , has a density of 3.895 g/cm^3 , and melts above 2000°C with decomposition.

The system Ba-Si contains barium silicides BaSi (83.07% Ba) and BaSi_2 (71.03% Ba). The compound BaSi_2 melts congruently at 1180°C , and BaSi melts incongruently at 840°C (peritectic reaction). Two eutectic temperatures in this system are 630°C and 1020°C . The solubility of silicon in solid barium is very small and does not exceed 0.14% (at.).

Barium and sulfur form several sulfides, of which the most studied is barium sulfide (BaS) (81.07% Ba), which melts at 2200°C . Other sulfides of barium are Ba_2S , BaS_2 , and BaS_3 . The sulfide BaS crystallizes in a cubic lattice of the type NaCl ($a = 0.6381 \text{ nm}$), which has a density of 4.252 g/cm^3 . When stored in air, BaS absorbs CO_2 to form BaCO_3 and H_2S . Upon heating in air BaS oxidizes to

sulfate BaSO_4 . Due to the high thermodynamic stability of barium sulfide, barium can be used for the desulfurization of iron and steel (Grigorovich et al., 2011; Han et al., 1992). In nature, barium is present in mineral barite (BaSO_4), which is used for the smelting of barium-containing ferroalloys. BaSO_4 dissociates upon heating to BaO , SO_2 , and oxygen.

With aluminum, barium forms one stable compound, BaAl_4 , melting congruently at 1097°C . On both sides of the aluminide line there are eutectics: at 1% (at.), Ba at 651°C ; and at 70% (at.), Ba at 528°C (Fig. 19.13).

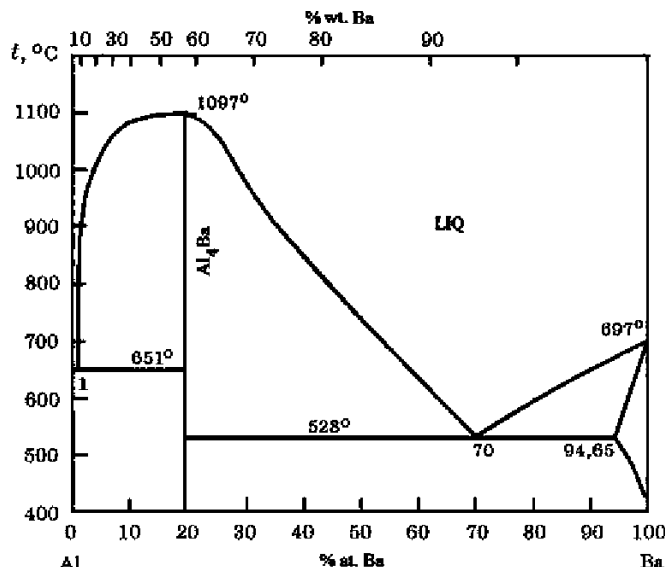


FIGURE 19.13 Al-Ba system.

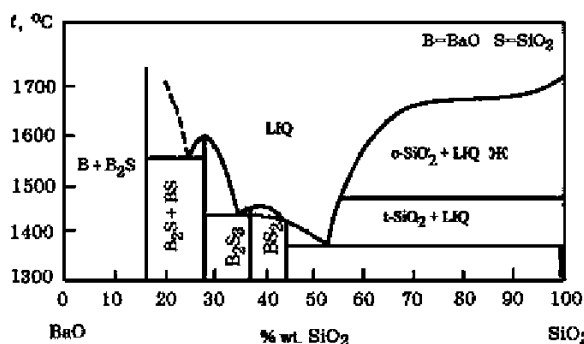


FIGURE 19.14 Equilibrium phase diagram of the system $\text{BaO}-\text{SiO}_2$.

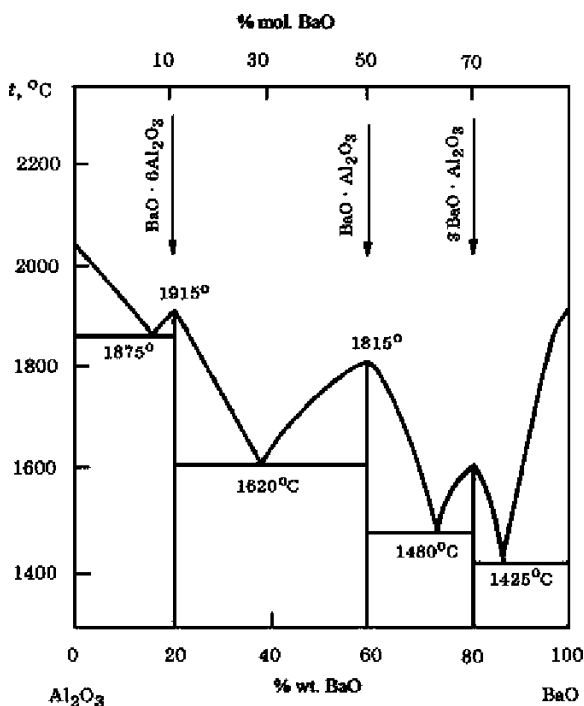


FIGURE 19.15 Equilibrium phase diagram of the system BaO-Al₂O₃.

The system BaO-SiO₂ is shown in Figure 19.14. In this system, several barium silicates are formed. Barium silicate 2BaO·SiO₂ has two phase modifications, the temperature of the transformation $\beta \longleftrightarrow \alpha$ is 1350°C, and the melting point is 1760°C. The system BaO-Al₂O₃ incorporates several aluminates of barium (Fig. 19.15).

19.4.2 Smelting Technology of Ferrosilicobarium

Ferroalloys with barium can be obtained by using carbon, silicon, and aluminum as reducing agents. The most economical method of smelting is the carbon reduction process with the use of barite concentrate (65.7% BaO), quartzite, and coke. The co-reduction of Ba and Si from this charge can be represented by the reaction $\text{BaSO}_4 + \text{SiO}_2 + 4\text{C} \rightarrow [\text{BaSi}] + 4\text{CO} + \text{SO}_2$.

Melting is performed in the electric arc furnace as a continuous process. The FeSiBa alloy obtained in this way has the following chemical composition (wt. %): 27 to 35 Ba, 46 to 52 Si, 0.15 to 0.3 C, 3 to 5 S, and the balance made up of Fe. The furnace slag contains 19% to 26% Ba, 25% to 37% SiO₂, 3% to 7% C, and 3% to 5% S.

The reduction of barium by silicon from Fe-75% Si could be described as $2\text{BaO} + [\text{Si}]_{\text{FeSi}} = [\text{BaSi}] + (2\text{BaO} \cdot \text{SiO}_2)$. This process produces FeSiBa alloy with up to 25% barium, and it is also possible to make a complex alloy containing both Ba and Ca. Melting is carried out in a batch process in an electric arc furnace. The charge load normally consists of 100 to 120 kg BaO, 190 kg Fe-75% Si alloy, 200 kg lime, and 50 kg fluorspar. The resulting complex has a ferroalloy chemical composition of (wt. %) 5 Ba, 15 Ca, 27 Fe; 1,5 Al; and the balance is made up of Si.

Ma et al. (1992) reported on the application of Fe-20% Si-40% Al-8% Ba alloy as a steel deoxidizer in a converter. Besides saving aluminum, improvements in shape of nonmetallic inclusions and in steel mechanical properties were obtained (the share of nonmetallic inclusions was decreased by 29% versus deoxidation with Fe-20% Si-50% Al alloy).

Kulinski and Gladala (1981) studied the production and application of complex ferroalloys with barium and calcium, using reduction of barium sulfate concentrate with lime with Fe-75% Si ferrosilicon. This results in high-silicon alloys (60 ± 5 % Si) with 8% to 10% of both calcium and barium. The addition of manganese (<10%) was also found to be beneficial to the storage and use of alloys in steelmaking.

19.4.3 Smelting Technology of Al-Ba Alloys

Alloys of Al-Ba have a highly deoxidizing potential, as each component separately has a high affinity for oxygen dissolved in the molten metal (Mukai and Han, 1999). These master alloys can be used as structure modifiers for engineering steels and iron-based alloys. The basis of the process of smelting Al-Ba alloys is the reaction of oxides of barium with aluminum. Typical master alloys contain 40% to 45% Ba, <1% Si and Fe, and a balance composed of Al.

The charge is composed of barium peroxide ($\text{BaO}_2 > 93\%$), aluminum powder (fractions 0 to 0.1 mm ~20%, 0.1 to 1 mm ~70%, and 1 to 3 mm ~15%), and fluorspar ($\text{CaF}_2 > 95\%$). For 100 kg of barium peroxide, the load of aluminum is 56 kg and that of fluorspar is 11 kg.

The reduction of BaO_2 by aluminum is an exothermic process that is carried out in a cast iron mold with a diameter of ~1 m and a height of ~0.6 m with an extension sheet metal cover of 5 to 10 mm. The batch dose of the charge is 200 to 250 kg of barium peroxide. The charge is ignited and the process proceeds forming the liquid alloy, which is collected above the slag because of its lower density. The alloy block is cooled, crushed, and packaged.

19.5 METALLURGICAL LIME

Lime (CaO) is a very important component of many ferroalloys processes to form and adjust proper slag formation. The lime charge for the smelting of ferroalloys with reduction by silicon (metallic manganese, medium carbon

ferromanganese, low-carbon ferrochrome) as well as by carbon (ferrosilicon) must have the proper chemical composition: <1.5% to 2% SiO₂, <0.03% to 0.08% S, and <0.02% to 0.03 % P, depending on the quality grade of the lime (Gasik et al., 2009). A strict limit on phosphorus content in lime is due to almost complete phosphorus reduction by either carbon or silicon and its transfer into ferroalloys. Allowable sulfur content in lime is higher than that of phosphorus, because sulfur is assimilated in basic slag, especially better with the higher the basicity of the slag.

The source for lime production is natural limestone. It is composed of mineral calcite—CaCO₃ (56% CaO, 44% CO₂)—and impurity oxides (MgO, SiO₂, Fe₂O₃). When heated to 900° to 1100°C, it thermally dissociates by the reaction CaCO₃ → CaO + CO₂ (gas). The most important feature of the crystal-chemical transformations during the thermal dissociation of calcite is the process of forming crystalline phases CaCO₃ and CaO. The dissociation reaction of calcite is localized at the interface of CaCO₃-CaO. As heating and isothermal holding of the reaction boundary move deeper into a piece of limestone, the CaCO₃ crystal lattice is transformed into the crystal lattice of CaO.

The size of the crystallites (grains) of obtained lime determines its chemical activity when lime is dissolved in slags. With the increasing firing temperature of limestone, lime crystal size increases, which leads to a decrease of its chemical reactivity. It is known that for cases in which lime should be more resistant to moisture, the firing temperatures must be high enough. The most stable lime is obtained by remelting it in electric arc furnaces to produce fused lime with rather large crystals.

Often limestone also contains magnesium carbonate MgCO₃, which also thermally dissociates upon heating with the formation of magnesia (MgO) and CO₂. The complex carbonate of calcium and magnesium is considered an equimolar mixture of CaCO₃ isomorphic with MgCO₃, or as a double compound, dolomite (Ca, Mg)(CO₃)₂. The thermal dissociation of dolomite proceeds in two stages: (1) the decomposition of dolomite into CaCO₃, MgO, and CO₂, and (2) the dissociation of CaCO₃.

There are different technologies of lime production. In the following two examples, lime is made in shaft-slit furnaces or in kiln furnaces.

The shaft-slit furnace example (Fig. 19.16) has a height of 22.5 up to the charging devices level and has three main zones from the top down: preheating (6.18 m), firing (6.5 m), and cooling (4.32 m). The length of the slit is 6 m but the width is not uniform: 1.7 m in the firing zone, 1.35 m in the heating zone, and 2.4 m in the cooling zone. The lining has a base of chromia-magnesia bricks.

The furnace is equipped with two tiers (rows) of burners. The lower tier in this case has 10 burners on each side of the shaft furnace, and the top (at the “square” oven) has 4 burners on each side. As furnaces are often build inside the ferroalloy plant, it is a common practice to mix the exhaust gas from ferroalloys (FeSi, FeSiMn) production (80% to 85% CO, 3% to 5% H₂) as fuel to

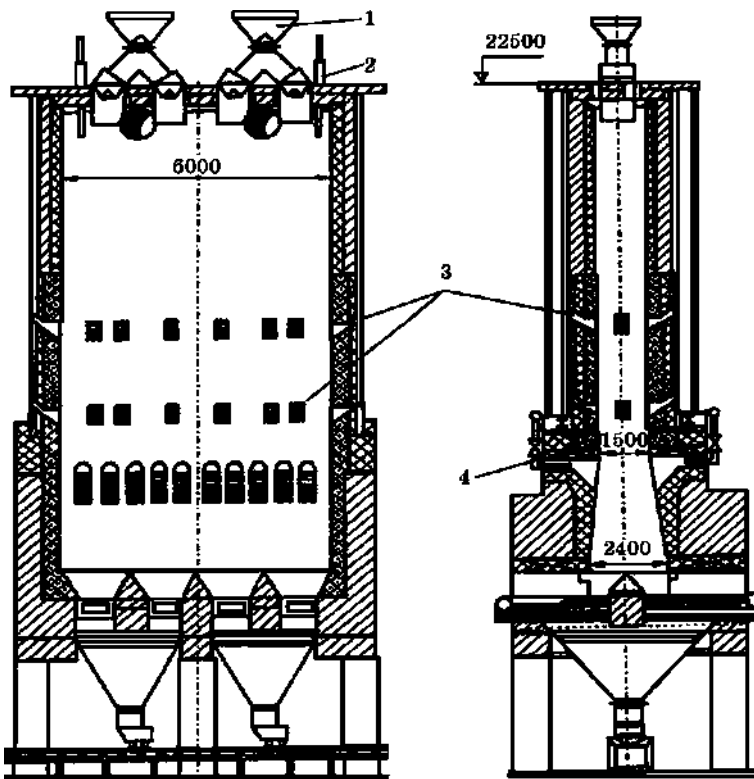


FIGURE 19.16 Shaft-slit furnace design: 1, tapered charging device; 2, limestone level indicator; 3, viewing window; 4, burner.

decrease the consumption of natural gas. For example, for a gas with 80% CO, its calorific value is about 6.6 Gcal/h for a $3000 \text{ m}^3/\text{h}$ flow rate. The addition of $200 \text{ m}^3/\text{h}$ of natural gas will complement the fuel calorific value with an extra 1.64 Gcal/h, which is similar to the value for a $1000 \text{ m}^3/\text{h}$ flow rate of natural gas, if it were used alone. The exhaust gases from the shaft-slit furnace have a composition of 27% to 30% CO₂, 0.6% to 1.2% O₂, 3% to 6% CO, and the balance made up of nitrogen.

Temperatures in the shaft-slit furnace are kept in the firing zone of 900° to 1100°C and in the heating zone of limestone 600° to 680°C. The temperature of the flue gases from the shaft furnace should not exceed 250°C. The productivity rate of the furnace much depends on the flow of gas. At the gas flow rate of 416 to 480 Nm³/h, a furnace similar to the one shown in Figure 19.16 produces 50 to 60 tons of lime a day, consuming 105 t/day of limestone. Increasing the gas flow rate up to 1024 to 1056 Nm³/h might raise the productivity level to 140 to 150 t/day with a daily limestone consumption of 250 t (Gasik et al., 2009).

Another method of making metallurgical lime is the use of rotary kiln furnaces. They have some advantages over shaft-slit furnaces in that they offer a higher level of process mechanization, easier operation, and a higher and more continuous performance of the limestone firing process. However, they also require higher investment and more fuel consumption per 1 ton of lime produced. The kiln is commonly 2.4 to 3.6 m diameter and 63 to 70 m length, heated by natural gas, with or without the additions of ferroalloy gas, resulting in a burner temperature of 1400° to 1500°C. The kiln has three main zones: preheating, firing (refractory lining temperature of 1200° to 1300°C), and cooling. Limestone with a lump size of 10 to 50 mm is almost completely dissociated at 1200° to 1250°C for 1.5 to 3 h kiln residence time.

To improve heat recovery, rotary kiln feeders are equipped with tubular heaters that utilize the waste heat of flue gases. They preheat limestone up to 150° to 200°C, which improves the kiln's thermal performance by 30% to 50%.

Lime can also be produced in fluidized bed process furnaces, but shaft-slit and kiln furnaces are more widespread for ferroalloy applications.

REFERENCES

- Berdnikov, V.I., Gudim, Yu.A., Karteleva, M.I., 2008. Thermodynamic modeling of silicocalcium production based on reduction by carbon. *Steel in Translation* 38, 275–280.
- Gasik, M.I., Lyakishev, N.P., Gasik, M.M., 2009. Physical Chemistry and Technology of Ferroalloys [in Ukrainian]. Sistemnye Tehnologii, Dnipropetrovsk, 494 pp.
- Grigorovich, K.V., Demin, K.Yu., Arsenkin, A.M., Garber, A.K., 2011. Prospects of the application of barium-bearing master alloys for the deoxidation and modification of a railroad metal. *Steel in Translation* 9, 912–920.
- Han, Q., Tang, L., Wang, Q., 1992. Application of barium-containing alloys in steelmaking. *Journal of Iron & Steel Research (China)* 4, 22–26.
- Kulinski, Z., Gladala, K., 1981. Production of multicomponent ferroalloys containing barium. *Pr. Inst. Met. Zelaza* 33, 125–134.
- Liu, J., Yang, Z., 1998. The production and application of Sr-containing alloy. *Journal of Iron & Steel Research (China)* 2, 11–16.
- Ma, C., Song, M., Yuan, Y., Jiang, G., 1992. Application of silicon-aluminum-barium ferroalloy in deoxidation and alloying for converter steelmaking. *Iron and Steel (China)* 27, 15–19.
- Mukai, K., Han, Q., 1999. Application of barium-bearing alloys in steelmaking. *ISIJ International* 39, 625–636.
- Zhuchkov, V.I., Lukin, S.V., Shilina, I.V., 1977. Deoxidation of steel by calcium-magnesium-silicon ferroalloys. *Steel USSR* 7, 689–690.

Complex Ferroalloys and Other Master Alloys

Oleg Polyakov

National Metallurgical Academy of Ukraine, Dnipropetrovsk, Ukraine

Chapter Outline

20.1 Complex Ferroalloys	495	20.1.3 Ferroalloys with Other Elements	498
20.1.1 Relevancy of Complex Ferroalloys Development	495	20.2 Ferroalloys with Nonmetallic Elements	500
20.1.2 Ferroalloys and Master Alloys with Aluminum	496	20.3 Exothermic Ferroalloys References	503
			504

20.1 COMPLEX FERROALLOYS

20.1.1 Relevancy of Complex Ferroalloys Development

Complex ferroalloys and master alloys are used in steel and special alloys manufacturing for alloying (and composition adjustment) and refining (oxygen, sulfur, etc. removal) purposes. Historically, complex ferroalloys have been made by fusing (smelting) several ferroalloys and then tapping and casting, and classifying them into relevant sizes. However, this method is not very economic—once produced, ferroalloys must be again heated, melted, and processed. This leads to substantial energy and material losses and possibly more environmental pollution. Therefore, it has been suggested that complex alloys might be co-reduced and co-smelted directly from raw materials, similarly to the process used to separate ferroalloys (Gasik et al., 2009). A good example of this processing is the smelting of silicomanganese (SiMn), discussed in Chapter 7, where both silicon and manganese are co-reduced into a joint alloy.

The complex alloys presented in this chapter are essentially alloys (1) with more than two alloying elements, (2) produced from raw materials (i.e., usually not just by co-melting already made ferroalloys), and (3) aimed at the synergistic utilization of materials and energy. The last factor means that the co-reduction of several elements usually is based on a substantial decrease of their activity (better extraction of elements) and melting temperature (formation of eutectics, etc.), which is particularly important in the case of rare and expensive metals, as well as refractory metals (W, Mo, Nb, Ta). For example, the melting temperature of ferrotungsten (FeW) might be too high for its fast dissolution in liquid steel. With the creation of complex ferroalloys, this feature might be substantially improved. Another example of advantages of complex alloys is more controlled nonmetallic inclusions formation in steels. The use of silicon, manganese, and aluminum together allows more efficient deoxidation and delivery of the elements in situ, which is impossible if FeSi, FeMn, and Al are added separately (Vikhlevshchuk et al., 1987).

As requirements from the steelmakers differ depending on the steel grades produced, this stipulates a variety of different complex ferroalloys. This chapter lists the most common compositions and their applications, although some producers might have their own recipes. Some integrated steel plants may also employ in-house production of specific complex ferroalloys.

20.1.2 Ferroalloys and Master Alloys with Aluminum

Typical compositions of complex ferroalloys with aluminum are shown in Table 20.1 (Gasik et al., 1975, 1988).

Ferroaluminum is produced in large, closed, submerged arc furnaces. The raw materials normally include electrocorundum (fused Al_2O_3 from refining smelting of bauxites or similar materials), steel chips, and coke. The process is flux-less with a low slag formation (<3% of metal mass). Smelting is continuous, and metal and slag are tapped periodically (~2 h). Slag contains 4% to 8% SiO_2 , 2% to 3% FeO , 10% to 15% CaO , <1% MgO , and a balance that consists of Al_2O_3 , and it usually has no tapping problems. However, for higher-grade FeAl (>30% Al), there is a possibility of aluminum carbide formation, so care must be taken to ensure carbides are eliminated during formation of the alloy (Gasik et al., 1988).

It is also possible to produce nitrided ferroaluminum (FeAlN) containing 4% to 10% N by solid-state nitriding of the alloy lumps in nitrogen or ammonia at 1200° to 1250°C, using a process similar to the one used to produce nitrided manganese and ferrochromium.

Ferromanganese–aluminum (FMA) alloy is used especially for deoxidation and alloying of high-quality tube steel and improves its properties at low (subzero) temperatures. Earlier technology of FMA alloys required dissolving aluminum in liquid medium carbon ferromanganese (MC FeMn), but since then the technology of smelting with carbon reduction has been developed. One

feature of this process is the use of the charge as fused alumina material (electrocörundum), as in the FeAl production process. The presence of liquid FeMn supports easier reduction of aluminum from the oxide, which lowers the temperature of alloy formation. Joint deoxidation of steel with FMA has shown an increased utilization of manganese and aluminum in comparison with their separate additives. The charge for FeMnAl smelting is composed of fused alumina, HC FeMn, steel chips, and coke. Slag formation here is also minimal, 1% to 2% of the metal mass. Smelting is continuous and tapping usually occurs every 2 h, as in FeAl smelting (Gasik et al., 1988).

Ferrosilicon-aluminum, also known as feralsit, alsimin, or FSA, is a complex steel deoxidizer as well as reductant used to process other ferroalloys that utilize reduction by silicon and aluminum (FeMo, FeV, etc.). The smelting process is carried continuously in submerged arc furnaces of 16 to 33 MVA power capacity. Charge materials include fused alumina, as in FeAl and FeMnAl processing, but here lower-grade aluminum and silicon sources also can be used, such as coal beneficiation wastes (ash, coal-dressing residuals, etc.) if their Al/Si ratio is suitable. This ratio should be selected according to the requirements in final steel composition, but also taking into account the stability of the FSA alloy during storage (Gasik et al., 1975). Thus, most FSA composition has Al:Si = 1:(4 to 6), although higher is also possible for a higher aluminum percentage (see Table 20.1). Additional charge materials are iron (steel) chips, FeSi, and coke. The ratio and the presence of FeSi are dictated by the composition of mineral charge components (FeSi is added if the SiO₂ concentration there is too low).

The technology of FMA and FSA alloys is also suitable for the production of ferrosiliconmanganese-aluminum alloys (FAMS). This alloy is a well-known efficient deoxidizer in comparison to separate additions of aluminum, ferrosilicon, and ferromanganese. The reduction of ferroalloy consumption in this case might be 15% to 30%, increasing the share of deoxidation in the ladle by 30% to 70%. Alumina-silica raw materials (basically, any suitable mineral combination might be used) are briquetted with carbon reductant and smelted with silicomanganese (20% Si), coke, and possibly extra steel chips. Although manganese ore or high-MnO slag could be used as a manganese source, in practice it is not recommended due to a much lower melting temperature of the charge and premature slag formation. Using stavrolite mineral concentrates (46% to 50% Al₂O₃, 36% to 38% SiO₂, 13% to 15% Fe₂O₃) the resulting FAMS alloy contains 10% to 14% Al, 22% to 24% Mn, 10% to 15% Si, about 0.3% to 0.5% Zr, and 1% to 2% C. A low phosphorus content is essential (see Table 20.1) to prevent this alloy from decomposition upon storage. It was found that phosphides (AlP) in the alloy react with moisture to form poisonous phosphine (PH₃), which transforms alloy into a dust form (Gasik et al., 1988).

The addition of components with higher CaO content allows the reduction of some calcium and the formation of the more complex Fe-Al-Mn-Si-Ca alloy (see Table 20.1). This alloy has a special application in nonmetallic inclusion control

in steels: calcium promotes dispersed and globular forms of the inclusions, which is important, for example, in ball-bearings steels (Gasik et al., 1975).

Chromium and ferrochromium have a relatively low deoxidizing ability compared to aluminum and silicon, so the Fe Cr Al complex ferroalloy is a good option for the combination of deoxidizing and alloying properties. Upon addition to the liquid steel, these alloys quickly dissolve, which reduces the duration of their contact with the air (lower oxidation and nitridation). FeCrAl alloys are produced by reducing chromium oxide raw materials with aluminum in the presence of a large excess of aluminum in the charge mixture.

Some plants produce ferrochrome–aluminum prepared by dissolving aluminum in liquid ferrochrome, but as mentioned this route is not very economic. Additionally, production of FeCrAl by the aluminothermic method allows lower phosphorus content in the alloy in comparison with the method whereby FeCr and Al are fused. Ferro-chrome-aluminum is produced in a single step in ferroalloy furnaces by carbon reduction of fused alumina (or a similar alumina source, such as kyanite) in the presence of charge ferrochrome or ferrosilicochrome (Gasik et al., 1988).

Among other master alloys with aluminum, which are produced mainly by aluminum reduction, those with molybdenum, tungsten, and chromium might be mentioned (see Table 20.2). These master alloys have a limited amount of iron in comparison with those shown in Table 20.1, as their main application is the production of nonferrous alloys (nickel superalloys, aluminum alloys, etc.).

20.1.3 Ferroalloys with Other Elements

The common complex ferroalloys, which are not based on the reduction of aluminum, are usually of the Fe-Cr-Mn-Si system. These alloys (Table 20.3) are used, for example, to manufacture special Cr-Mn stainless steels where low carbon (LC) FeCr or FeSiCr and manganese metal have been traditionally used, but separately (Gasik et al., 2009).

Complex ferrochrome–manganese alloys (FeCrMn) are a useful option to reduce manganese evaporative losses and to decrease the FeCr melting temperature. Standard LC FeCr (~70% Cr) has a melting temperature of 1640° to 1680°C, but the addition of 30% to 35% Mn decreases it to 1400° to 1500°C, which is a positive factor for faster dissolution of the alloy in liquid steel. The advantage of FeCrMn alloy smelting is that lower-grade ores ($\text{Cr}/\text{Fe} < 3$) might be used together with MnO-rich slag, using crude SiMn or FeSiCr as reductants. Chromium dissolves up to 70% Mn in the solid state, which assists in the decrease of manganese activity and improves the reduction process (Gasik et al., 1988).

This alloy with additional silicon (FeMnCrSi) could be produced by various methods. Besides the evident process of smelting different ferroalloys (fusion), reduction of MnO-rich slag and lime–chromite melt by FeSiCr or joint co-reduction of Mn, Cr, and Si sources by carbon might be applied. One method is to reduce dumped slag of manganese metal production (10% to 14% MnO;

TABLE 20.1 Ferroalloys with Aluminum, wt. %, Balance: Iron*

Alloy	Al	Mn	Si	Ca	Cr	C	S	P
FeAl10	8–12		<4			<3	<0.03	<0.04
FeAl15	12–17		<3.5			<3	<0.03	<0.04
FeAl20	17–22		<3.5			<2	<0.03	<0.04
FeAl25	22–30		<2			<1	<0.03	<0.04
FeAl35	33–37	<0.7	<0.5			<0.02		
FeAl40	~40	<0.7	<0.5			<0.02		
FeAl50	~50	<0.7	<0.5			<0.02		
FeMn45Al	12–16	40–50	<2.5			<1.5	<0.03	<0.3
FeMn55Al	12–16	50–60	<2.5			<1.5	<0.03	<0.3
FeMn65Al	12–16	60–80	<2.5			<1.5	<0.03	<0.3
FeSiAl [†]	18–22		40–45					<0.07
FeSiAl [‡]	48–50		35–37					
FeMnAlSi [§]	10–14	22–24	10–15			1–2		<0.06
FeMnAlSiCa	4–10	17–22	45–50	7–12				
FeCrAl	18–22		0.5–1			48–52		

*Empty cells mean no data specified.

[†]Feralosit alloy.

[‡]Alsimin alloy.

[§]FAMS alloy

which already has a low phosphorus content) by FeSiCr. If the FeMnCrSi alloy smelting is organized cooperatively with manganese production, the liquid slag latent heat might be additionally utilized. Industrial practice shows a possibility of such FeCrMnSi alloy production with 0.01% to 0.013% P. Such an alloy is stable during storage.

A special category of complex ferroalloys is made up of niobium master alloys (Table 20.4). Although ferroniobium (FeNb) is suitable for many applications, in many cases its dissolution rate and melting temperature are too high for economic steelmaking (Patel and Khul'ka, 2001). This also concerns master alloys for no-ferrous applications (superalloys). The melting point of these alloys is less than 1400°C, and the rate of dissolution is two times higher than for the standard FeNb.

TABLE 20.2 Composition of Aluminum Master Alloys, wt. % (Gasik et al., 1988; Gasik and Mazur, 2003)

Master Alloy	Al	Mo	W	Cr	Fe	Si	Ti
Al-Cr	15–40			60–85	<1	<0.5	
Al-Cr-Mo	30–40	30–36	1–8	23–27	4–7	2–5.5	
Al-Cr-Mo-W	28–33	24–28	12–19	18–21	5–8	<3	
Al-Cr-Ti	9–12	18–23		64–70	<1.8	<0.6	4–7
Al-Mo-Ti	38–48	48–52	1.5–5.5		<1.5		6.5–8
Al-Mo-W-Ti	46–52	26–32	11–15		<1	<2.5	7–9
Al-W-Mo-Ti	40–42	15–18	30–36		<0.8	<3.5	6–7
Al-W-Ti	48–58	5–6	40–43		<1	<2.5	4–6
Al-W-Cr-Mo	<2	2.5–4	30–40	50–60	<2	<0.8	

TABLE 20.3 Composition of the Complex Fe-Cr-Mn-Si Alloys, wt. %

Ferroalloy	Mn	Si	Cr	C	P	S
FeMnSiCr	15–20	35–40	20–30	<0.03	<0.02	<0.05
	20–30	30–35	20–25	<0.04	<0.02	<0.05
	30–35	20–30	20–25	<0.05	<0.02	<0.05
FeMnCr	16–25	<1	45–54	<0.05		
	26–35	<1.5	39–49	<0.05		
	36–44	<1.6	31–39	<0.05		
	~45	<2	~30	<0.05		

20.2 FERROALLOYS WITH NONMETALLIC ELEMENTS

There are few ferroalloys with nonmetallic elements especially produced for steelmaking applications. Besides ferroalloys with boron (Chapter 17), those of industrial relevance are alloys with phosphorus, sulfur, and probably selenium, although some plants might have other forms of ferroalloys production.

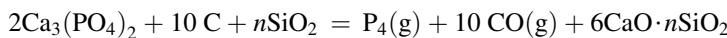
TABLE 20.4 Some Niobium-Contained Complex Master Alloys

Ferroalloy	Nb	Mn	Al	Cr	Fe	Ni	Ti	Si	C
FeNb	20–30				Bal.				
FeNbMn	30–50	20–30			Bal.				
CrNb	60–88		<1	Bal.	<1		<1		<0.1
NiTiNb	7–12		4–8		<2	Bal.	15–23	<2	<0.1
FeNbTi	15–18		8–12		Bal.		27–38	<3	<0.2

Ferrophosphorus might contain up to 24% to 28% P, and it is used in both lumpy and powder form. Powdered FeP is mainly intended for ferrous powder metallurgy applications as phosphorus is beneficial for liquid phase sintering and better “soft” magnetic properties (Antsiferov et al., 1999). In steels, phosphorus is usually an undesired impurity, but in some applications reasonable phosphorus content is beneficial. For example, phosphorus gray cast iron (0.5% to 0.8% P) is applied for the centrifugal casting of pipes and fittings, and some phosphorus in steel improves its machining feasibility. Cast iron with an even higher phosphorus content (2% to 5% P) is used for metallurgical equipment (cast iron molds for slag and metal, etc.). An increase of phosphorus up to 0.2% P in austenitic stainless steel (20% Cr, 10% Ni, 2% Mo) allows formation of a more fine dispersion of precipitates during heat treatment, increasing hardness and creep resistance (Gasik et al., 1975).

Ferrophosphorus could be produced in electric furnaces and in blast furnaces, but most FeP is produced by using by-product alloy of phosphorus production by carbon reduction of calcium phosphates. The process is implemented in closed (hermetic) submerged arc furnaces, as all reduced phosphorus vapor must be properly collected (Scheepers et al., 2010). The furnace power is 10 to 80 MVA, but there is a tendency to build and exploit larger power furnaces (60 to 80 MVA) with self-baking electrodes of 1700 mm diameter (Fig. 20.1).

Phosphorus is reduced from calcium phosphate melt by carbon from coke in the presence of silica flux (quartzite):



At the same time, iron and manganese oxides from phosphate charge are also reduced and form molten metal, which is periodically tapped and delivered as ferrophosphorus. Its exact composition depends on the quality and composition of phosphorite ore, but usually the alloy contains 15% to 30% P, 2% to 12% Si, and 2% to 4% Mn, the balance being made up of iron and other impurities (Gasik et al., 1975). Gaseous phosphorus is trapped from the gases by cooling

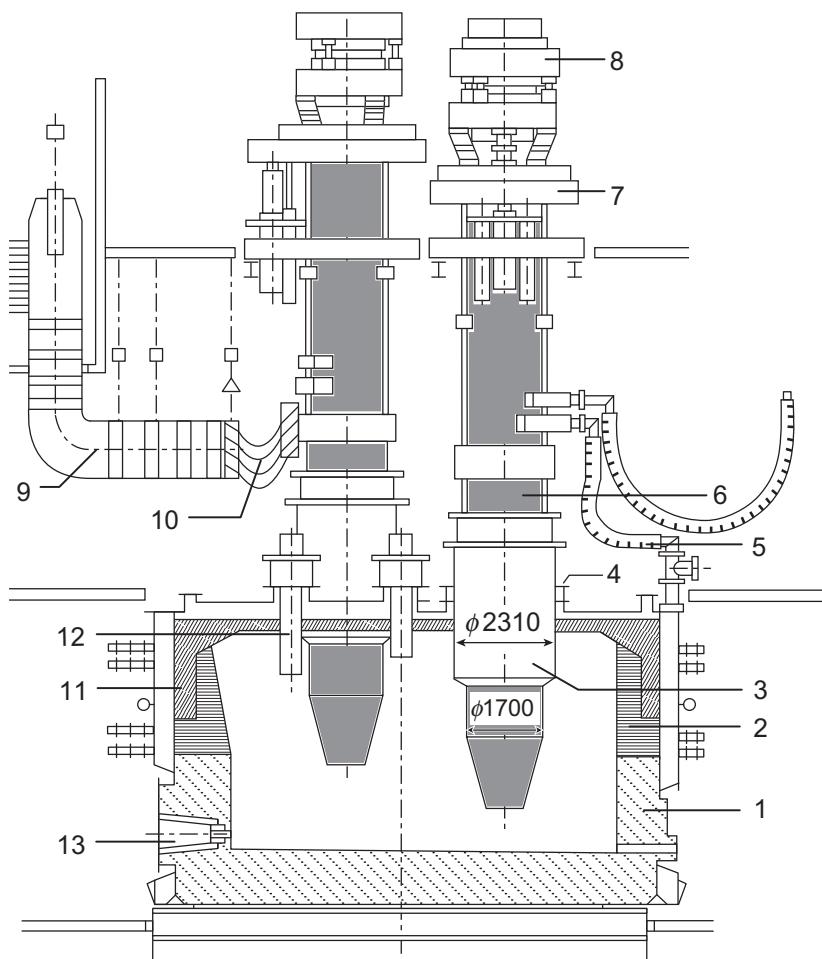


FIGURE 20.1 Submerged arc furnace of 72 MVA with hermetic cover for phosphorus reduction: 1, shell; 2, lining; 3, electrode cylinder; 4, gasket; 5, furnace water cooling system; 6, electrode holder; 7, hydraulic lift; 8, electrode shifting mechanism; 9, short net; 10, flexible current bus bars; 11, cover; 12, charge feeders; 13, tap hole.

below 50°C under water, leading to a condensation of white phosphorus. The amount of ferrophosphorus is about 1.8% to 2.2% of the charged phosphorus mass.

As with phosphorus, sulfur is often regarded as an impurity in steels. However, steels that undergo machining operations are required to have a certain amount of sulfur content for proper chip formation (chip breakup upon turning, drilling, etc.). Sulfur is often added to steels and alloys in the form of ferrosulfur (28% to 32% S), if the use of other sulfur-containing compounds is not feasible for any reason (Zhukov et al., 1998).

Other chalcogenides—especially in the form of ferroselenium with 25% to 50% Se and ferrotellurium (<50% Te)—are also used for the same purpose (Gol'dshtein et al., 1979). Selenium and tellurium improve the machinability of steels (up to 0.05% to 0.30%). Their addition requires more care, as proper ratios of Mn/(S + Se + Te) and S/(Se + Te) have to be maintained for optimal effect (Zaslavskii et al., 1969). When selenium is absent, sulfur in steel is usually combined into MnS, which forms elongated nonmetallic inclusions at hot rolling, causing less corrosion resistance toward H₂S. The addition of selenium (Se/S ~0.8) decreases this phenomenon two- to three-fold, leading to smaller globular inclusions. In comparison with sulfur's effect on machining, even minor selenium addition leads to the formation of complex compounds (Mn, Me)(S, Se), improving significantly the lifetime of cutting tools at very high machining rates (Alferov and Belov, 1975). It was reported that microalloying with selenium reduces the loss of metal (scrap and rejects) due to metallurgical defects and also the tendency to form quench cracks. In terms of improved machinability with high-speed machining utilizing hard-alloy cutters, the addition of selenium is much superior to microalloying with lead, especially in machining that uses high-speed steels (Gol'dshtein et al., 1979).

20.3 EXOTHERMIC FERROALLOYS

These types of special ferroalloys (or, more precisely, mixtures of ferroalloys with exothermic compounds) are not widespread but are used from time to time to process special steels and alloys, especially in-house. The quality of exothermic ferroalloys is measured by several indicators: minimal temperature of the beginning of the reaction, temperature of the reaction of ferroalloys with liquid metal, and the optimum reaction rate considering particular steel grades. However, the basis is that the alloying should be done under a spontaneous metallothermic process.

The main components of the exothermic charge are a mixture of ferroalloys, oxidant, and possibly reductant (aluminum powder) and fluxes (calcium fluoride). Previously sodium nitrate was used as an oxidant, but it is not recommended because there is a risk that it will lead to an increase of nitrogen content in steel. Thus, traditional oxidants used now are potassium chlorate, oxides of chromium, manganese, and the like, which exclude nitrogen (Gasik et al., 1975).

Some typical compositions of exothermic ferroalloys and their properties are shown in [Table 20.5](#).

As follows from the data in [Table 20.5](#), most of these exothermic ferroalloys have been designed for implementation of alloying by Cr, Mn, W, Ni, and Nb, but this list can be greatly expanded.

Optimal grain size for the metal part of the exothermic charge is 1.5 to 2 mm. The other components (oxides, flux) should have a grain size of 0.2 to 0.5 mm. The calorific value of briquettes is usually within 33 to 84 kJ/g·atom, and

TABLE 20.5 Some Properties of Exothermic Ferroalloys

Compounds	% wt.	Grain Size, mm	Heat effect, kJ/mol	Density, g/cm ³
LC-FeCr or HC-FeCr	81	1.6	33.5	4.2
NaNO ₃	8.2	0.5		
FeSiCr	10.8	0.2		
LC-FeCr	87.2	1.6	33.5	4.1
KClO ₃	6.3	0.5		
FeSiCr	6.5	0.2		
LC-FeCr	61.6	1.6	5.44	4
Mn ore (55% Mn)	24	0.4		
Al powder	7.2	—		
FeSiCr	5.1	0.2		
CaF ₂	2.1	0.2		
FeMn	70	2	33.5	4.2
FeSiMn	19	0.25		
NaNO ₃	8	0.5		
CaF ₂	3	0.2		
W concentrate	67.8	0.5	62.8–79.5	4
Scheelite (CaWO ₄) concentrate	17	—		
Al powder	15.2	—		
W concentrate	84	0.5	54.4	4.1
FeSi65	16	0.2		
NiO	71.2	0.5	73.5	3.5
FeSiMn	18.4	0.2		
FeSi75	6.5	0.2		
Al powder	3.8	0.2		

the recommended density is 3.5 to 4.2 g/cm³. Briquettes can weigh up to 20 kg, although smaller briquettes weighing up to 2 kg are also used. The strength of the raw briquettes is about 6 MPa, and their dry-state strength is 25 to 50 MPa (after drying at 90° to 120°C to remove 40% to 50% moisture, and then at 300° to 350°C to a moisture content of <0.1%).

REFERENCES

- Alferov, V.P., Belov, A.D., 1975. Effect of chalcogens on mechanical properties of cast carbon steels. Metal Science and Heat Treatment 17, 672–674.
- Antsiferov, V.N., Shatsov, A.A., Oglezneva, S.A., 1999. Structure and properties of powder metallurgy phosphorous steels. Powder Metallurgy and Metal Ceramics 38, 162–165.

- Gasik, L.N., Ignatiev, V.S., Gasik, M.I., 1975. Structure and quality of commercial ferroalloys and master alloys. *Tekhnika*, Kyiv, 152 p.
- Gasik, M., Mazur, V., 2003. Creation of master alloys for aluminum. In: Totten, G.E., MacKenzie, D.S. (Eds.), *Handbook of Aluminum*, second ed. Marcel Dekker Publ, New York, pp. 81–114.
- Gasik, M.I., Lyakishev, N.P., Emlin, B.I., 1988. Theory and technology of ferroalloys production. *Metallurgy*, Moscow, 784 pp.
- Gasik, M.I., Lyakishev, N.P., Gasik, M.M., 2009. Physical chemistry and technology of ferroalloys: a university handbook [in Ukrainian]. System Technologies Publ., Dnipropetrovsk. 494 pp.
- Gol'dshtein, Ya.E., Mushtakova, T.L., Komissarova, T.A., 1979. Effect of selenium on the structure and properties of structural steel. *Metal Science and Heat Treatment* 21, 741–746.
- Patel, Zh., Khul'ka, K., 2001. Niobium for steelmaking. *Metallurgist* 45, 477–480.
- Scheepers, E., Yang, Y., Adema, A.T., Boom, R., Reuter, M.A., 2010. Process modeling and optimization of a submerged arc furnace for phosphorus production. *Metallurgical and Materials Transactions* 41B, 990–1005.
- Vikhlevshchuk, V.A., Storozhenko, A.S., Kulikov, I.V., Levin, D.Yu., Zhilinskii, V.V., Ob'edkov, A.P., Pliskanovskii, A.S., Nosochenko, O.V., Mel'nik, S.G., 1987. Microalloying and finishing steel with regard to chemical composition in the ladle. *Metallurgist* 31, 200–203.
- Zaslavskii, A.Ya., Gorokh, A.V., Gol'dshtein, Ya.E., Shenk, R.I., 1969. Reaction of selenium and tellurium with iron and carbon steel. *Soviet Materials Science* 5, 187–189.
- Zhukov, A.A., Savulyak, V.I., Pakhnyushchii, I.O., 1998. High-sulfur and sulfur-copper antifriction cast irons with improved machinability. *Metal Science and Heat Treatment* 40, 119–121.

Handbook of Ferroalloys

Theory and Technology

Edited by

Michael Gasik



ELSEVIER

AMSTERDAM • BOSTON • HEIDELBERG • LONDON • NEW YORK • OXFORD • PARIS
SAN DIEGO • SAN FRANCISCO • SINGAPORE • SYDNEY • TOKYO



Butterworth-Heinemann is an Imprint of Elsevier

Contributors

Johan Basson, Outotec South Africa, Centurion, South Africa

Jorma Daavittila, Outotec Finland, Espoo, Finland

Michael Gasik, Aalto University Foundation, Espoo, Finland

Mihail I. Gasik, National Metallurgical Academy of Ukraine, Dnipropetrovsk, Ukraine

Lauri Holappa, Aalto University School of Chemical Technology, Espoo, Finland

Heikki Jalkanen, Aalto University Foundation, Espoo, Finland

Isobel Mc Dougall, Tenova Minerals Ltd. Tenova Pyromet, Johannesburg,
South Africa

Oleg Polyakov, National Metallurgical Academy of Ukraine, Dnipropetrovsk, Ukraine

Gudrun Saevarsdottir, Reykjavik University, Reykjavik, Iceland

Merete Tangstad, Norwegian University of Science and Technology, Trondheim,
Norway

Butterworth-Heinemann is an imprint of Elsevier
The Boulevard, Langford Lane, Kidlington, Oxford, OX5 1GB
225 Wyman Street, Waltham, MA 02451, USA

First published 2013

Copyright © 2013 Elsevier Ltd. All rights reserved.

No part of this publication may be reproduced or transmitted in any form or by any means, electronic or mechanical, including photocopying, recording, or any information storage and retrieval system, without permission in writing from the publisher. Details on how to seek permission, further information about the Publisher's permissions policies and our arrangement with organizations such as the Copyright Clearance Center and the Copyright Licensing Agency, can be found at our website: www.elsevier.com/permissions

This book and the individual contributions contained in it are protected under copyright by the Publisher (other than as may be noted herein).

Notices

Knowledge and best practice in this field are constantly changing. As new research and experience broaden our understanding, changes in research methods, professional practices, or medical treatment may become necessary.

Practitioners and researchers must always rely on their own experience and knowledge in evaluating and using any information, methods, compounds, or experiments described herein. In using such information or methods they should be mindful of their own safety and the safety of others, including parties for whom they have a professional responsibility.

To the fullest extent of the law, neither the Publisher nor the authors, contributors, or editors, assume any liability for any injury and/or damage to persons or property as a matter of products liability, negligence or otherwise, or from any use or operation of any methods, products, instructions, or ideas contained in the material herein.

British Library Cataloguing in Publication Data

A catalogue record for this book is available from the British Library

Library of Congress Cataloging-in-Publication Data

A catalog record for this book is available from the Library of Congress

ISBN: 978-0-08-097753-9

For information on all Butterworth-Heinemann publications visit our website at store.elsevier.com

Printed and bound in the United Kingdom

13 14 15 16 10 9 8 7 6 5 4 3 2 1



Working together
to grow libraries in
developing countries

www.elsevier.com • www.bookaid.org

Preface

Ferroalloys development and production have been boosted together with the rapid increase in steel and alloys processing. It soon became very clear that ferroalloys require new techniques as the then existing blast furnace or steel-making converter technologies were not capable of fulfilling the demanding needs of industry. As the requisite electrical technology was developed in parallel, at the beginning of 20th century ferroalloys had caught up with electrometallurgy—and this has continued until today. In 1907 two pioneering books, “Electrometallurgy” by John Kershaw and “The Electric Furnace: Its Construction, Operation and Uses” by Alfred Stanfield, were published. Already by then the authors had recognized the need to give a brief and clear account of industrial developments in electrometallurgy, although the theoretical basics and engineering background had only just started to be thought about and were not explicitly treated in those publications. The dynamics of the subsequent developments were noted by John Kershaw, who stated “The patent literature of electrometallurgy [is] unusually extensive and voluminous.” Only six years after Alfred Stanfield published the second, twice as large, edition of his book, he noted that “the development of the electric furnace and its uses has been so rapid.”

It took, however, many more years to develop the theory and technology of ferroalloys smelting, taking into account the variety of raw materials, furnaces, and alloys, and environmental and economic constraints. Whereas several books on ferroalloys were published in the 1900s in different languages, it became evident that there existed a need for a new publication aiming at providing a holistic, integrated overview of all practically relevant ferroalloys processes and equipment, and other pertinent aspects. This was the reason behind the preparation of this text.

This handbook is a combined product of many contributors, who tried their best to collate, process, outline, and present the most comprehensive information on the subject as was available at the time of writing. The authors aim to provide scientific and technological knowledge that will be of use worldwide, and with sufficient detail for practical application. The material in this book is also intended to help students, plant engineers, and managers as well as researchers in the relevant fields, to understand the theory and technology of different ferroalloys in accordance with modern-day practice and current scientific developments.

As the Editor of this volume, I gratefully acknowledge all contributions and also my colleagues who assisted in the preparation of the book. I hope the reader will find it practical and effective, whether for processes theory development or industrial implementation.

Prof. Michael M. Gasik

*Aalto University Foundation,
School of Chemistry Technology,
Espoo, Finland*

General References

- Akbiev, M.A., Medvedev, G.V., Basaev, I.P., Volkov, S.S., Spirin, V.B., Tsymbal, V.P., 1985. Use of complex AMS and FASK deoxidizers in steel production. *Metallurgist* 29, 305–307.
- Bodyanski, E.V., Kucherenko, E.I., Mihalyov, O.I., Filatov, V.S., Gasik, M.M., Kutsyn, V.S., 2011. Artificial intellect methods in the management of ferroalloys processing technology. National Metallurgical Academy of Ukraine, Dnipropetrovsk, 420 pp.
- Coudurier, L., Hopkins, D.W., Wilkomirsky, I., 1978. *Fundamentals of Metallurgical Processes*. Pergamon Press, Oxford, 382 pp.
- Davis, J.R., 2001. *Alloying: Understanding the Basics*. ASM International, Materials Park, OH, 647 pp.
- Downing, J.H., 1984. Production of Ferroalloys. 41st Electric Furnace Conference Proceedings, 41, AIME, Detroit, 273–278.
- Fine, H.A., Geiger, G.H., 1979. *Handbook on Material and Energy Balance Calculations in Metallurgical Processes*. Metallurgical Society of AIME, 572 pp.
- Gasik, L.N., Ignatiev, V.S., Gasik, M.I., 1975. Structure and Quality of Commercial Ferroalloys and Master Alloys. *Tekhnika*, Kyiv, 152 pp.
- Gasik, M.I., 1985. *Electrodes of Ore-reduction Furnaces*. Metallurgia, Moscow, 284 pp.
- Gasik, M.I., Lyakishev, N.P., Gasik, M.M., 2009. *Physical Chemistry and Technology of Ferroalloys [in Ukrainian]*. Sistemnye Tehnologii, Dnipropetrovsk, 494 pp.
- Habashi, F., 1997. *Handbook of Extractive Metallurgy*, volumes 1–4. WILEY-VCH, Heidelberg.
- Habashi, F., 1999. *Kinetics of Metallurgical Processes*. Metallurgie Extractive Quebec, Quebec, 376 pp.
- Lampman, J.R., Peters, A.T., 1981. *Ferroalloys and Other Additives to Liquid Iron and Steel*. ASTM, Baltimore MA, 208 pp.
- Leont'ev, L.I., Zhuchkov, V.I., Smirnov, V.A., Dashevskii, V., Ya, 2007. Global and Russian ferroalloy production. *Steel in Translation* 37, 283–287.
- Pistorius, P.C., 2002. Reductant selection in ferro-alloy production: The case for the importance of dissolution in the metal. *Journal of the South African Institute of Mining and Metallurgy* 1/2, 33–36.
- Rankin, W.J., 2011. *Minerals, Metals and Sustainability: Meeting Future Material Needs*. CSIRO Publishing, Collingwood, 440 pp.
- Rosenqvist, T., 2004. *Principles of Extractive Metallurgy*. Tapir Academic Press, Trondheim, 508 pp.
- Serov, G.V., 2010. A century of Russian electroferroalloy production. *Steel in Translation* 40, 647–654.
- Woldman, N.E., Frick, J.P., 2000. *Woldman's Engineering Alloys*, ninth edition. ASM International, 1363 pp.
- Young, L.E., 2001. Ferroalloys: production and use in steelmaking. In: *Encyclopedia of Materials: Science and Technology*. Elsevier, pp. 3039–3044.

Index

Note: Page numbers followed by "f" denote figures; "t" tables.

A

- Acting masses law, 45
- Activation energy, 60–61, 75–76, 78
- Active power, 146
- Activity, 42–45
- Activity coefficient, 42–45
- Agglomeration, 127–129
 - briquetting. *See* Briquetting
 - of manganese, 234–238
 - pelletizing. *See* Pelletizing
 - sintered pellets production, 128–129
 - sintering. *See* Sintering
- Alabandine, 233t
- Al-Ba alloys, smelting of, 491
- Alkali-earth metals (AEM), 471–494
 - barium, 488–491
 - Al-Ba alloys, smelting of, 491
 - ferrosilicobarium, smelting of, 490–491
 - properties of, 488–490
 - calcium, 472–480
 - properties of, 472–475
 - calcium carbide, smelting of, 475–477, 476f
 - calcium-silicon alloy, smelting of, 477–480
 - reduction by calcium carbide, method of, 480
 - reduction by carbon, method of, 477–478
 - reduction by silicon, method of, 478–479
 - magnesium, 480–485
 - production of, 483–485
 - properties of, 480–483
 - metallurgical lime, 491–494
 - strontium, 485–487
 - alloys, smelting of, 487
 - properties of, 485–487
- Alloying, 9–10
- Alloy tapping, 350–351
- Al₂O₃, 459–460
- Alsimin. *See* Ferrosilicon-aluminum
- Alternating current (AC), 140–143
 - circuits, impedance and power in, 145–146
 - furnaces. *See* Alternating current furnaces
 - sinusoidal, 141–142

- Alternating current (AC) furnaces, 87, 140, 148–153, 320
 - electrical supply to, 108–109
 - one-phase circuit, 149–150, 149f
 - submerged arc
 - closed, 335–340, 336f, 337f, 338f
 - open, 331–333, 333f, 334f
 - semiclosed, 331–333, 333f
 - smelting, 340–344
 - three-phase circuit, 151–153, 151f, 153f
- Aluminothermal processes, 32–33
- Aluminum, 195, 198, 214–215
 - ferrotungsten reduction by, 385
 - ferrovanadium reduction by, 407
 - master alloys, composition of, 500t
 - reduction, smelting with
 - boric anhydrite, 455t
 - ferroboron, 454t
 - ferrotitanium, 429–432, 431t
 - nickelboron, 456t
- Anorthite, 205–206, 214–215
- Apparent power, for real circuit, 146, 147f
- Argon oxygen decarburization (AOD), 14–15, 318, 326
- Arrhenius equation, 60–61, 62t
- Ascharite, 452
- Ash, 194–195, 205, 214
- Atomizing, of silicon, 213t
- Automatic furnace control, 121–122

B

- Baddeleite, 441–442, 446
- Bag filter plant, 96–97, 100–101, 104, 128–129, 357–358
- Barite, 488–490
- Barium, 488–491
 - Al-Ba alloys, smelting of, 491
 - ferrosilicobarium, smelting of, 490–491
 - properties of, 488–490
- Bastnesite, 466, 466t
- Batch ferroalloy process, 33–35
- Bessemer process, 10

- Best available technology (BAT), 24–25
 Bixbyite, 229–231, 233t
 Black-box models, 158
 Böckmann compensation, 168–169, 169f
 Boracite, 452
 Borax, 452
 Boric acid, 453t
 Boric anhydrite, 453t
 smelting with aluminum reduction
 heat and energy balance of, 455t
 material balance of, 455t
 Boron carbide, 452, 456
 Boron ferroalloys, 449–458
 properties of, 449–451
 reduction of, 452–453
 sources of, 452–453
 types of, 453, 453t
 Braunit, 229–231
 Bravoiite, 402t
 Briquetting, 34, 128
 chromites, 228–289
 of manganese, 236
 Brown condensate, 203–204
 Bulat steel, 12
 Bulk ferroalloys, 31t
 Bus bar, 85, 88, 100, 107, 109, 125
- C**
- Calcia (CaO), 472, 474f
 Calcining, 372–373
 Calcium, 179–180, 472–480
 properties of, 472–475
 Calcium carbide (CaC_2), 472
 smelting of, 475–477, 476f
 Calcium cyanamide (CaCN_2), 472
 Calcium diborate, 453t
 Calcium manganese silicon (SiMnCa), 472
 Calcium silicon (SiCa), 472
 smelting of, 477–480
 reduction by calcium carbide, method of, 480
 reduction by carbon, method of, 477–478
 reduction by silicon, method of, 478–479
 CALPHAD (CALculation of PHAses
 Diagrams) method, 54
 $\text{CaO}\text{-SiO}_2$, 474f
 Capacitance, electric, 144
 Capital investment, for high carbon
 ferrochrome production, 330–331
 Carbon
 ferrotungsten reduction by, 382–385
 interaction with manganese, 222–229
 monoxide, 122–123
 reductants, 191–195
 for ferroalloys processing, 79–81, 80t
 Carbothermal processes, 30–32
 Carnotite, 401–402, 402t, 404
 Casting, 4, 133–135
 of ferronickel, 373–374
 of high-carbon ferrochrome, 348, 352
 of manganese ferroalloys, 259–260
 net shape, 260
 of silicon, 211–212, 213t
 Cavity, 202–207, 210
 Celestine (SrSO_4), 486–487
 Cerium, 464–465
 Chalcopyrite, 392
 Channel arc models (CAM), 158–159, 159f
 Charcoal, 193–194
 Charge (electrical), 78
 Charge chrome, 320
 defined, 318
 specification of, 319t
 Chemical potentials, 39, 42–43, 45
 Chemical reactions, thermodynamics of, 45–53
 Chromeboron, 457
 Chrome direct reduction (CDR) process, 341
 Chromite, production of, 323t
 Chromite ores
 briquetting of, 228–289
 classification of, 283t
 pelletizing of, 287–288, 288t
 processing of, 285–289
 general requirements for, 286t
 sintering of, 287, 287t
 Chromium, 11, 267–316
 -containing systems, phase equilibria with, 268–276, 372t
 environmental issues of, 312–314
 dust and wastewaters treatment, 313–314
 fire and explosion hazards, 314
 human health hazards, 312–313
 ferroalloys technology, 289–307
 low-carbon ferrochrome, 289–297
 hexavalent, 360–362, 313–314
 minerals, 280–283
 processing of, 285–289
 properties of, 268–280
 resources of, 283–285
 spinel, 278, 280–281, 287–288, 303
 spinelides, 280–282, 282t, 283–285
 composition of, 282t
 Chromium carbide, 367–368
 Chromium oxide, 368
 phase equilibria with, 276–280

- Circuit(s)
AC
 impedance and power in, 145–146
 one-phase, 149–150, 149f
 three-phase, 151–153, 151f, 153f
reactance, 143–145
resistive, 143
- Clausius-Clapeyron equation, 43–44
- Clinopyroxene, 236–237
- Closed roof, 94, 94f
- Closed submerged arc AC furnaces, 335–340, 336f, 337f, 338f
- Coal, 193
- Coal tar pitch volatiles (CTPVs), 363
- Cobalt, 367, 371
- CO₂ emissions, from ferroalloys production, 22–25, 23t, 24t
- CO gas reticulation and utilization, 358–360, 359f, 361f
- Coke, 320, 335–336, 338–339, 341–344, 287–288, 299–300
 bed, 242–245, 249
 metallurgical, 193
 petroleum, 194
- Colemanite, 452
- Columbite, 415–416
- Columbium, 411
- Complex ferroalloys, 495–499
 development, relevancy of, 495–496
- Composite electrode, 118–119
- Conduction, 37
 heat transfer by, 65–66
- Continuous ferroalloy process, 33–35
- Convection, 37
 heat transfer by, 66–67
- Convective mass transfer, 71–72
- Convective momentum transfer, 71–72
- Converting, 372, 374
- Crater, 201, 204, 206–207
- Creusot-Loire Uddeholm (CLU) refining process, 326
- Cristobalite, 181, 189–190, 189t, 207
- Cr-O-C Systems, Equilibria in, 372t
- Crushing, of manganese ferroalloys, 260
- Cryptomelane, 233t
- Culsonite, 402t
- Cuprodescloizite, 402t
- D**
- Damascus steel, 12
- Davidite, 402t
- Dead-band regulation, 166–168, 168f
- Decarburization, of high-carbon ferromanganese, 257–258, 258t
- Dephosphoration, 240, 374
- Descloizite, 402t
- Desulfuration, 372–373
- Differential scanning calorimetry (DSC), 61–62
- Differential thermal analysis (DTA), 61–62
- Diffusion, 59–60
- Diffusive emissions, 219t
- Diffusive mass transfer, 70–71
- Direct current (DC), 140–143
 furnaces, 104–107, 140, 147–148, 148f, 320
 electrical supply to, 109
 open arc, 344–348, 346f, 349f
- Disintegrators, 355–357, 356f
- Doloma, 10
- Dolomite, 483–484, 492
- Donpeacorite, 236–237
- Dust, 162, 170–172, 190, 200–201, 217–219
 chemical composition, 173, 173t
 from chromium ferroalloys processing, 313–314
 hexavalent chromium, 362–363
- E**
- Electrical energy efficiency, of high carbon ferrochrome, 329–330
- Electric arc, 153–155, 154f, 156f, 157f
 models, 156–160
 black-box models, 158
 channel arc models, 158–159, 159f
 magneto-hydrodynamic model, 159–160, 160f
 momentum source models, 158
- Electric capacitance, 144
- Electric circuit theory, 140–146
 AC circuits, impedance and power in, 145–146
 alternating current, 140–143
 direct current, 140–143
 reactance circuits, 143–145
 resistive circuits, 143
 voltage, 140–143
- Electric conductivity, of slags, 76–78
- Electric current, 141
- Electric resistance, 143
- Electrodes, 109–119
 composite, 118–119
 control of, 166–169
 graphite, 116–118, 118f
 prebaked, 116–118, 117t
 regulating, 109–110

- E**
- Electrodes (*Continued*)
 - self-baking, 110f, 111–116
 - slipping, 110–111, 113–114
 - Söderberg, 109, 110f, 111–116, 112f, 113t, 115f
 - Electrometallurgy, 6
 - Electrostatic precipitators, 358
 - Ellingham diagram, 30, 45–46
 - Emissions, 4, 66, 67t
 - control, 168–169
 - gaseous, 173–174
 - heat, 174
 - particulate, 170–173
 - in silicon production plant, 219t
 - control of, 217–219
 - Energy, 4
 - demand, for ferroalloys making, 22, 23t
 - recovery, in silicon production plant, 215–217
 - Enthalpy, 38–40
 - Entropy, 37–39
 - Environmental control, 217–219
 - Environmental impact, of high carbon ferrochrome production, 354–360
 - Environmental issues
 - associated with chromium, 312–314
 - dust and wastewaters treatment, 313–314
 - fire and explosion hazards, 314
 - human health hazards, 312–313
 - associated with furnaces, 170–174
 - gaseous emissions, 173–174
 - particulate emissions, 170–173
 - associated with silicon production, 215–219
 - emissions control, 217–219
 - energy recovery, 215–217
 - Equilibrium phase diagrams, 53–58
 - eutectoid system, 55, 56t
 - peritectic system, 56t, 57
 - Equipment
 - ferroalloy processing, 83–138
 - for furnace feed processing, 127–133
 - agglomeration, 127–129
 - manganese ore, sintering of, 129–130
 - preheating, 131–132
 - prereduction, 132–133
 - Excess free energy, 41–42
 - Exhaust gas, 85, 94, 96–97, 100, 103–104, 120, 128–129, 131–133
 - Exothermic ferroalloys, 503–504, 273f
 - Explosions, 93–94, 123, 125, 134–135
 - hazards, of chromium ferroalloys, 314
- F**
- FactSage, 53
 - FactSage 6.2, 6, 52
 - Fans, 115–116, 128–130
 - Faraday number, 71
 - Fe-Cr-Mn-Si Alloys, composition of, 500t
 - FeCr₂O₄ spinel structure, 281f
 - Feed bins, 84, 95–96, 104, 129
 - Feralsit. *See* Ferrosilicon-aluminum
 - Ferroalloys, 3–4
 - basics of, 9–28
 - classification of, 4, 31t
 - defined, 29–30
 - development and production of, 9–12
 - major, 4
 - minor, 4
 - processing, theory of, 29–82
 - smelter, 84f
 - types of, 31t
 - Ferroaluminum (FeAlN), 496, 499t
 - Ferro-alumino-zirconium (FeAlZr), 443, 446–447, 446t
 - Ferroboral (FeBAI), 452, 456
 - Ferroboron, 453–456
 - chemical composition of, 454t
 - smelting with aluminum reduction, charge composition of, 454t
 - Ferrocerium, 467
 - Ferrochrome-aluminum (Fe-Cr-Al), 498
 - Ferrochrome (FeCr) furnaces, 92–98, 92f, 94f, 95f, 98f
 - tapping of, 134f
 - Ferrochrome-manganese (FeCrMn), 498
 - Ferrochrome preheating system, 131f
 - Ferrochromium
 - high-carbon, 287–297, 290t, 291t
 - low carbon, 294t
 - medium-carbon, 287, 291t, 297–299
 - nitrated, 305–312, 305t
 - ultra-low carbon, 303–305, 304f
 - Ferromanganese (FeMn)
 - furnaces, 92–98, 127
 - high-carbon, 246–250, 249t, 257–258, 258t
 - post-tap hole processing for, 252–253
 - Ferromanganese-aluminum (FMA), 496–497, 499t
 - Ferromanganese-vanadium, composition of, 408t
 - Ferromolybdenum, 387–388
 - production of, 393–395, 394t
 - smelting of, 137, 137f
 - Ferronickel, 367–376
 - alloys, composition of, 372t

- calcining, 372–373
casting of, 373–374
converting, 372, 374
furnaces, 101–104
oxidative roasting of, 372–373
refining of, 373–374
smelting of, 371–373
- Ferroniobium (FeNb), 412, 416–419, 499
- Ferrophosphorus, 501–502, 502f
- Ferroselementum, 503
- Ferrosilicobarium, smelting of, 490–491
- Ferrosilicoboral (FeSiBAI), 452
- Ferrosilicochrome (FeSiCr)
charge materials for, 302t
chemical composition of, 299t
technology of, 299–303
- Ferrosilicon (FeSi)
compositions of, 195–198, 197t
equilibrium diagram, 188f
furnaces, 92–98
smelting technology, 198–210
basic principles of, 198–201
costs of, 209–210
energy demand for, 207t, 209–210
materials of, 207t
parameters of, 207t
peculiarities of, 205–207
reactions in furnace, 201–205
- Ferrosilicon-aluminum (FSA), 497
- Ferro-silicon-calcium (FeSiCa).
See Calcium-silicon alloy
- Ferrosiliconniobium, 416–417, 419
- Ferro-silicon-magnesium (FeSiMg), 483–485
- Ferrosiliconmanganese (FeSiMn),
production of, 250–252
- Ferrosiliconmanganese-aluminum alloys
(FAMS), 497
- Ferrosilicostromium, 487
- Ferrosilicovanadium, composition of, 408t
- Ferrosilicozirconium (FeSiZr), 442–446
- Fersulfur, 502
- Ferrotellurium, 503
- Ferrotitanium
composition of, 430t
smelting of, charge composition of, 431t
- Ferrotungsten, production of, 382–385
reduction by aluminum, 385
reduction by carbon, 382–385
reduction by silicon, 382–385
- Ferrovanadium, 405–407
composition of, 406t
nitrided, 408–409
reduction by aluminium, 407
reduction by silicon, 405–407, 406t
- FeSiREM alloys, composition of, 467t
- Fick's law of diffusion, 70–71
- Fines, 189–190, 200–201, 211–212, 217
- Fire hazards, of chromium ferroalloys, 314
- Flotation method, 286
- Flux, 444–445
- Flux ferroalloy process, 33–35, 243, 248
- Flux-less ferroalloy process, 33–35, 243, 248, 252, 256
- Fourier's law, 65–66
- Fourier transform infrared spectrometry
(FTIR), 61–63
- Free energy
excess, 41–42
Gibbs, 45
- Freeze lining, 102–103
- Friability index, 190
- Fumes, 200, 202, 217–218, 219t
hexavalent chromium, 362–363
- Furnace(s)
alternating current, 87, 140, 320
closed submerged arc, 335–340, 336f, 337f, 338f
one-phase circuit, 149–150, 149f
open submerged arc, 331–333, 333f, 334f
semiclosed submerged arc, 331–333, 333f
smelting submerged arc, 340–344
three-phase circuit, 151–153, 151f, 153f
control, 121–122, 165–169
crucible, 93–94
design of, 85–92
parameters for, 90t
direct current, 104–107, 140, 147–148, 148f, 320
open arc, 344–348, 346f, 349f
downstream processing, 133–135
casting, 133–135
refining, 133
- electrical supply to, 107–119
AC furnaces, 108–109
DC furnaces, 109
electrodes, 109–119
- environmental issues of, 170–174
gaseous emissions, 173–174
particulate emissions, 170–173
- feed processing, equipment for,
127–133
agglomeration, 127–129
manganese ore, sintering of, 129–130
preheating, 131–132
prereduction, 132–133
- ferrochrome, 92–98
- ferromanganese, 92–98
- ferronickel, 101–104

- Furnace(s) (*Continued*)
 ferrosilicon, 92–98
 heat dissipation in, modes of, 153–165
 current paths of, 162–163
 distribution of, 163–165
 electric arc, 153–155, 154f, 156f, 157f
 electric arc models, 156–160
 resistive heating, 160–161, 161t
 linings, 119–120
 operations, for ferroalloys processing, 85–92, 139–140
 parameters, 87t
 principal operating stages of, 120–121
 processing hazards and risk management of, 122–126
 hazardous gases, 122–124
 high current, 125
 high voltage, 125
 molten metal, 124–125
 repairs and maintenance, 125–126
 slag, 124–125
 water, 125
 refractory lining, 92–93, 93f
 resistance and electrode parameter, relationship between, 87–88
 roof, 94, 94f, 95f
 silicomanganese, 92–98
 silicon metal, 98–101
 silicon reactions in, 201–205
 slag cleaning, 237–238
 submerged arc, 234, 242–243, 245–247, 250, 256
 tensioning springs on, 120f
 Future outlook, for ferroalloys industry, 26–27
- G**
 Gas cleaning plant, 96–97, 104
 Gas cleaning systems, 354–358
 bag filter plants, 357–358
 disintegrators, 355–357, 356f
 electrostatic precipitators, 358
 Venturi-type scrubbers, 354–355, 355f
 Gaseous emissions, 173–174
 Gauerite, 233t
 Gehlenite, 205–206
 Gibbs-Duhem equation, 41, 44
 Gibbs energy, 30, 37–40, 45–52
 Gibbs minimization method, 6
 Gladkikh *et al.* method, 89–92
 Granshot granulation, 353
 Granulation
 Granshot, 353
- of high carbon ferrochrome, 352–353
 of manganese ferroalloys, 260
 Showa Denko, 352
 Graphite electrode, 116–118
 column, 118f
 Grashof number, 68t
 Gravity concentration method, 286
 Greynal, 457
- H**
 Hausmannite, 229–231, 233t
 Hazards, in smelting manganese ferroalloys, 263–265
 Hazards management of furnaces, 122–126
 hazardous gases, 122–124
 high current, 125
 high voltage, 125
 molten metal, 124–125
 repairs and maintenance, 125–126
 slag, 124–125
 water, 125
 Heat capacity, 38–39
 Heat dissipation in furnaces, modes of, 153–165
 current paths of, 162–163
 distribution of, 163–165
 electric arc, 153–155, 154f, 156f, 157f
 electric arc models, 156–160
 Heat emissions, 174
 Heat generation, 69–70
 Heat losses, 174
 Heat recovery systems, 174
 Heat transfer, in ferroalloys processing
 by conduction, 65–66
 by convection, 66–67
 by equation, 67–69
 heat generation, 69–70
 by radiation, 66
 Helmholtz energy, 37–39
 Henrian reference state, 43
 Hexavalent chromium, 360–362, 313–314
 High-carbon ferrochrome (HGFeCr), 317–364
 applications of, 326
 mass and energy balance of, 327t
 nominal composition of, 289, 290t
 production of, 318–326, 321t, 323t
 alloy tapping, 350–351
 environmental impact of, 354–360
 occupational health hazards of, 360–363
 product types, 351–353
 slag handling and utilization, 353
 slag tapping, 350–351

production of, technology routes for, 328–350, 332t
 capital investment, 330–331
 closed submerged arc AC furnaces, 335–340, 336f, 337f, 338f
 economy of scale, 330
 electrical energy efficiency, 329–330
 metallurgical efficiency, 328–329
 occupational health, 331
 open arc DC furnaces, 344–348, 346f, 349f
 open submerged arc AC furnaces, 331–333, 333f, 334f
 prereduction, 340–344
 semiclosed submerged arc AC furnaces, 331–333, 333f
 submerged arc AC furnaces smelting, 340–344
 Tecnored process, 348–350
 specification of, 318, 319t
 uses of, 326

High-carbon ferromanganese
 decarburization of, 257–258, 258t
 production, 246–250, 249t
 High current, risk management of, 125
 High voltage, risk management of, 125
 History of ferroalloys, 9–12
 Hollandite, 233t
 HSC Chemistry, 53
 HSC Chemistry 7.1, 6
 Human health hazards, of chromium, 312–313
 Hyperoxide (CaO_4), 472

I

Ilmenite, 424–425, 428–432, 428t, 431t
 Impedance, of AC circuits, 145–146
 Inductance, 143
 Internal energy, 37–38
 Iron-titanate, 428t

J

Jacobsite, 233t

K

Kanoite, 236–237
 Katana swords, 12
 Kelly factor, 87–88, 88t, 91
 Kelly's method, 87–88
 Kernite, 452
 Kinetics, of pyrometallurgical processes, 58–65

L

Ladle, 97–100, 104, 121, 124–125, 133–135
 Lanthanum, 462–464
 Laterite, 371–373
 Lime, 491–494
 Limestone, 480, 484, 492–494
 Loparite, 415–416, 466
 Low-carbon ferrochrome
 nominal composition of, 294t
 production, by aluminum reduction, 311t
 slag compositions, 312t
 technology of, 298–297
 furnace method, 294t
 off-furnace technology, 294–295
 Low-carbon silicomanganese, production of, 258–259
 Lump size distribution, 189–190

M

Magneli phases, 424
 Magnesium, 480–485
 production of, 483–485
 properties of, 480–483
 Magnesium-ferrosilicon (FeSiMg), 483–484
 Magnetic concentration method, 286
 Magnetite, titaniferous, 401–405, 402t
 Magneto-hydrodynamic (MHD) model, 159–160, 160f
 Manganese, 10–11, 221–266
 agglomeration of, 234–238
 background of, 222
 history of, 222
 interaction with carbon, 223–225
 interaction with other elements, 225–228
 interaction with oxygen, 223–225
 metal, production of, 253–256
 minerals, 233t
 ores, 229–234
 compositions of, 235t, 237t
 particle size distribution of, 236t
 in oxide systems, 228–229
 properties of, 222–223
 in slags, 228–229
 Manganese ferroalloys, 238–240
 casting of, 259–260
 composition of, 239t
 crushing of, 260
 high-carbon, 227
 impurities in, 240, 241t
 low-carbon, 227, 238–240, 246–247, 256–259
 medium-carbon, 227, 238–240, 246–247
 nitrided, 261–262

- Manganese ferroalloys (*Continued*)
 processing
 energy use in, 262–263
 operational hazards of, 263–265
 sieving of, 261–262
 smelting technologies for, 240–246
 industrial practice, 242–246
 reduction processes, 240–242
 specifications of, 238–240. *See also*
 Ferromanganese
 Manganese ore, sintering of, 129–130
 Manganese oxide, 222–223, 237, 242–244,
 250–253, 262
 Manganese oxygen refining (MOR), 257–258
 Manganite, 233t
 Manganocalcite, 233t
 Markets of ferroalloys, 17–22
 Mass spectrometry (MS), 61–62
 Mass transfer
 convective, 71–72
 diffusive, 70–71
 Master alloys, 447
 with aluminum, 496–498
 composition of, 500t
 boron, 454t
 niobium-contained complex, 501t
 tungsten, 377–378, 385
 MatCalc, 53
 Materials production, ferroalloy processes in,
 35, 36f, 36t
 Maxwell-Ampere law, 69–70
 Maxwell-Stefan equation, 70–71
 Medium-carbon ferrochrome
 nominal composition of, 289, 291t
 technology of, 297–299
 Metallic chromium
 nominal composition of, 308t
 production, by aluminum reduction,
 307–312
 Metallic manganese, smelting of, 136,
 136f
 Metallic melts, 72–74
 Metallurgical coke, 193
 Metallurgical efficiency, of high carbon
 ferrochrome, 328–329
 Metallurgical lime, 491–494
 Metal tapping, 97–98
 Meyer-Neldel rule, 76
 Micro-alloying, 13
 Minerals, 465–466
 Minor ferroalloys, 31t
 Mischmetal, 467
 Mixing method, 294–295
 Molten metal, hazardous and risk
 management of, 124–125
 Molybdenite, 388–390, 392
 concentrates, oxidative roasting of, 392–393
 Molybdenum
 concentrates of, 392
 oxidative roasting, 392–393
 ferromolybdenum, production of, 393–395,
 394t
 minerals of, 392
 ores of, 392
 properties of, 387–390
 Molybdenum carbide, 388
 Molybdenum oxide, 390
 Molybdite, 392
 Momentum source models, 158
 Momentum transfer, convective, 71–72
 Monazite, 466, 466t
- N**
- Navier-Stokes equation, 71–72, 75
 Nernst-Planck equation, 71–72
 Net shape casting, 260
 Nickel
 ferronickel, 367–376
 alloys, composition of, 372t
 calcining, 372–373
 casting of, 373–374
 converting, 372, 374
 oxidative roasting of, 372–373
 refining of, 373–374
 smelting of, 371–373
 properties of, 367–369
 raw materials, 371
 Nickelboron, 456–457
 smelting with aluminum reduction, charge
 composition of, 456t
 Niobium, 499
 -contained complex master alloys, 501t
 ferroalloys, 416–419
 minerals of, 415–416
 properties of, 411–414
 reduction of, 416
 sources of, 415–416
 Niobium oxide, 414, 416
 Nitrided ferrochromium, 305
 nominal composition of, 305t
 Nitrided ferrovaniadium, 408–409
 Nitrided manganese ferroalloys, 261–262
 Nodules, 371
 Nondimensional numbers, 68t
 Nonmetallic elements, ferroalloys with,
 500–503

Nontronite, 371
Nusselt number, 68–69, 68t

O

Occupational health hazards, of high carbon ferrochrome, 331, 360–363
dust, 362–363
fumes, 362–363
hexavalent chromium, 360–362
Ohm's law, 69–70, 166–167
Ohmic (joule) heating, 69–70
Oligonite, 233t
One-phase AC furnace circuit, 149–150, 149f
Open arc DC furnaces, 344–348, 346f, 349f
Open furnace, 92, 96
Open submerged arc AC furnaces, 331–333, 333f, 334f
Ores, 465–466
Orthosilicate, 475
Oxidation, 60–61, 69–70, 73
Oxide melts, 74–78
Oxide systems, manganese in, 228–229
Oxygen interaction with manganese, 222–229
Ozonide (CaO_6), 472

P

Pandat, 53
Particulate emissions, 170–173
Patronite, 402t
Pelletizing, 34, 84, 127–128, 132–133
chromites, 287, 288t
of manganese, 234–237
Perovskite, 425, 429, 432
Peroxide (CaO_2), 472
Petroleum coke, 194
Phase coupling, 168
Phase diagrams, equilibrium, 53–58
Phase reactance, 152
Phase resistance, 152
Phase shift, 140, 142, 144–146, 149
Phosphorus, 497–499, 501–502, 502f
Polycrystalline, 392
Polytypes, of silicon carbide, 184f, 193f
Post-tap hole processing, for FeMn/SiMn, 252–253
Povellite, 392
Power, of AC circuits, 145–146
Power control, 166
Power factor, 145–146, 148, 150, 153, 167–168
Prandtl number, 68t
Prebaked electrode, 116–118, 117t
properties of, 117t

Preexponential factor, 75–76, 78
Preheating, of furnace feed materials, 131–132
Prereduction, 132–133
of high carbon ferrochrome, 340–344
Production of ferroalloys, 9–12, 17–22
Programmable logic controller (PLC), 121–122, 123f
Pseudobrookite, 424
Psilomelane, 233t
Pyrochlore, 415–416, 418–419, 466
Pyrolusite, 222, 229–231, 233t, 235f
Pyrometallurgical (high-temperature chemical) processes
kinetics of, 58–65
thermodynamics of, 37–58
chemical reactions, 45–53
equilibrium phase diagrams, 53–58
general considerations and definitions, 37–40
solutions, 41–45
Pyroxene, 236–237

Q

Quartz, 186–191
phase transformations, schematic of, 189t
Quartzite, 186–191
materials, compositions of, 192t

R

Rabbling, 98–99
Radiation, 37
heat transfer by, 66
Raoult reference state, 42–43
Rare-earth metals (REM), 459–470
cerium, 464–465
concentrates of, 465–466
ferroalloys with, production of, 466–469
reduction by aluminum, 468–469
reduction by carbon, 467–468
lanthanum, 462–464
minerals, 465–466
ores, 465–466
properties of, 460t
yttrium, 461–462
Raw materials, 6
Rayleigh number, 68t
Reactance
circuits, 143–145
phase, 152
Reaction mechanism, 59–60
Reaction rate, 60–61

- Reactive losses, 30, 62–65, 69–70
 Reactivity of silicon monoxide, 191,
 194–195, 205, 210
 Redlich-Kister-Muggianu polynomial, 54–55
 Reductants, 320–326, 341
 Reduction
 by aluminum, 32–33. *See also* Aluminum
 by carbon, 30–32. *See also* Carbon
 by silicon, 32. *See also* Silicon
 Refining
 Creusot-Loire Uddeholm, 326
 of ferronickel, 373–374
 furnaces, 133, 136–137
 manganese oxygen, 257–258
 of medium-carbon ferrochrome alloys, 299
 operations, for low-carbon manganese
 ferroalloys, 256–259
 silicothalmic reduction, 256–257, 257f
 of silicon, 200–201, 212–215
 trace elements distribution, 212–214
 Refractory lining, 92–93, 93f
 $\text{REM}_2\text{O}_2\text{S}$, 459–460
 Resistance, phase, 152
 Resistance-heating furnaces (RHF),
 139–140, 162
 Resistive circuits, 143
 Resistive heating, 160–161, 161t
 Reynolds number, 68–69, 68t
 Rhodochrosite, 229–231, 233t
 Rhodonite, 228, 233t, 252
 Risk management of furnaces, 122–126
 hazardous gases, 122–124
 high current, 125
 high voltage, 125
 molten metal, 124–125
 repairs and maintenance, 125–126
 slag, 124–125
 water, 125
 Roasting, oxidative
 of chromium ferroalloys, 287–288, 314
 of ferromolybdenum, 392–393
 of ferronickel, 372–373
 Root mean square (RMS) value, 142–143
 Roscoelite, 402t
 Rutile, 424–425, 429
- S**
- Scheelite, 380–381, 381t, 383, 385, 392
 Scrubber, 96
 Segregation coefficient, 211–212, 212t
 Selenium, 500, 503
 Self-baking electrode, 110f, 111–116
 Semiclosed submerged arc AC furnaces,
 331–333, 333f
 Sensitization phenomenon, 14–15
 Shell cooling
 copper coolers, 103
 forced convection, 84–85, 93–94, 99,
 102–103, 105
 natural convection, 84–85, 99
 water film, 84–85, 93–94
 water spray, 84–85, 93–94
 Showa Denko (SDK) granulation, 352
 Sieving of manganese ferroalloys, 261–262
 Silica
 fume, 200, 202, 217–218, 219t
 sources of, 186–191
 Silicate, 180–181, 205, 215, 217
 network structure, 75t
 Silicides, 186, 212
 Silicomanganese (SiMn), 250–252
 crude, 238–240, 250, 253–254, 256
 furnaces, 92–98, 127
 low-carbon, 258–259
 nitride, 261–262
 post-tap hole processing for, 252–253
 Silicon, 11–12, 179–186
 atomizing of, 213t
 casting of, 211–212, 213t
 compositions of, 195–198, 197t
 equilibrium phase diagram of, 182f
 ferrotungsten reduction by, 382–385
 ferovanadium reduction by, 405–407, 406t
 interaction with other elements, 181–186
 production, environmental issues associated
 with, 215–219
 emissions control, 217–219
 energy recovery, 215–217
 properties of, 180–181
 refining of, 200–201, 212–215
 trace elements distribution, 212–214
 smelting technology, 198–210
 basic principles of, 198–201
 costs of, 209–210
 energy demand for, 209–210
 parameters of, 207t
 reactions in furnace, 201–205
 solubility of impurities in, 184, 185f
 world production of, 196, 196t
 yield, 209–210
 Silicon carbide (SiC), 181, 258–259
 equilibrium phase diagram of, 183f
 polytypes, 184f, 193f
 Silicon dioxide (SiO_2), 181
 Silicon metal furnaces, 98–101

- Silicon monoxide (SiO), 181
Silicothermal processes, 30, 32
Simultaneous thermal analysis (STA), 61–62
SINTEF reactivity test, 194
Sintered pellets production, 128–129
Sintering, 34
 chromites, 287, 287t
 of manganese, 129–130, 236–237
Slags, 74–78, 394–395
 electric conductivity of, 76–78
 ferroalloy process, 33
 granulation, 135
 handling of, 353
 hazardous and risk management of, 124–125
 -less ferroalloy process, 33
 manganese in, 228–229
 process, charge materials for, 302t
 silicate network structure formation in, 75t
 tapping, 97–98, 350–351
 utilization of, 353
 viscous properties of, 75–76
Smelting, 4, 12, 20–22, 34–35, 37, 74–75,
 84–86
 of calcium carbide, 475–477
 of calcium-silicon alloy, 477–480
 reduction by calcium carbide, method of,
 480
 reduction by carbon, method of, 477–478
 reduction by silicon, method of, 478–479
 electric, 11
 of ferromolybdenum, 393–395, 394t
 of ferronickel, 371–373
 of ferrosilicobarium, 490–491
 ferrosilicon, 198–210
 basic principles of, 198–201
 costs of, 209–210
 energy demand for, 207t, 209–210
 materials of, 207t
 parameters of, 207t
 peculiarities of, 205–207
 reactions in furnace, 201–205
 of low-carbon ferrocchrome, 294t
 of manganese ferroalloys, 240–246
 industrial practice, 242–246
 reduction processes, 240–242
 silicon, 194, 198–210
 basic principles of, 198–201
 costs of, 209–210
 energy demand for, 209–210
 parameters of, 207t
 reactions in furnace, 201–205
 of strontium alloys, 487
 submerged arc AC furnaces, 340–344
Soda, 404
 treatment, 373
Söderberg electrode, 109, 110f, 111–116,
 115f
 column, 115f
 paste, properties of, 113t
 zonal structure of, 112f
Sodium octaborate, 453t
Solid state reduction with carbon (SRC)
 process, 341
Specific heat, 66–68
Spheine, 424–425, 431
Spiegeleisen, 10–11
Steel development, ferroalloys in, 12–17
Steelmaking, 3–4, 6, 10
Stefan-Boltzmann law, 66
Stoking, 98–99
Strontianite (SrCO_3), 486–487
Strontium, 485–487
 alloys, smelting of, 487
 properties of, 485–487
Submerged arc, 86
 AC furnaces smelting, 340–344
 furnace (SAF), 12, 18, 22, 25, 139–140, 149,
 152, 154–155, 160–162, 234, 242–243,
 245–247, 250, 256
 operations, Kelly factors for, 88t
Sulfur, 502
Sulanite, 402t
Supervisory control and data acquisition
 (SCADA) system, 121–122
- T**
- Tantalum, 415–416
Tapping, 4
 alloy, 350–351
 of ferromolybdenum, 395
 of manganese ferroalloys, 252–253
 of silicon, 181–184, 201, 205, 218–219
 slag, 350–351
Tecnored process, 348–350
Tellurium, 503
Tephroite, 228, 233t
Theisen disintegrator, 355–356
Thermal analysis, 61–62
 differential, 61–62
Thermal conductivity, 65–66, 68–69
ThermoCalc, 53
 ThermoCalc R, 6
Thermodynamics, of pyrometallurgical
 (high-temperature chemical)
 processes, 37–58
 chemical reactions, 45–53

Thermodynamics, of pyrometallurgical (high-temperature chemical) processes
(Continued)

equilibrium phase diagrams, 53–58
 general considerations and definitions, 37–40
 solutions, 41–45

Thermogravimetry (TG), 61–62

Thermo-mechanical controlled rolling process, 12

Three-phase AC furnace circuit, 151–153, 151f, 153f

Titaniferous magnetite, 401–405, 402t

Titanium

concentrates, chemical composition of, 428t
 ferroalloys, 429–432
 from oxides, reduction of, 429
 properties of, 421–424
 raw materials, 425–429
 sources of, 425–429

Titanium carbide, 422, 429

Titanium oxide, 422, 428–430

Titanomagnetite, 425, 428t

Todorokite, 233t

Trace elements distribution, 212–214

Transformer power, 89, 91–92

Transformer-rectifier, 104–105, 107

Traveling grate technology, 237

Tridymite, 181, 189, 189t

Tungsten

concentrates of, 380–381
 ferrotungsten, production of, 382–385
 reduction by aluminum, 385
 reduction by carbon, 382–385
 reduction by silicon, 382–385
 minerals of, 380–381
 ores of, 380–381
 properties of, 377–380

Tungsten carbide, 378–381, 383–384

U

Ulexite, 452

Ultra-low carbon ferrochrome, technology of, 303–305, 304f

Ulvospinel, 424

V

Vacuum argon decarburization (VOD), 326

Vacuum treatment, 296, 307

Vanadates, 400

Vanadiferous phosphate rock, 402t

Vanadinite, 402t

Vanadium

ferrovanadium, 405–407
 composition of, 406t
 nitrided, 408–409
 reduction by aluminum, 407
 reduction by silicon, 405–407, 406t
 minerals of, 402t
 properties of, 397–400
 raw materials, treatment of, 402–405
 chemical treatment, 404
 metallurgical processing, 404–405
 reduction from oxides, 405
 sources of, 401–402

Vanadium pentoxide, 400, 404–407

Venturi-type scrubbers, 354–355, 355f

Vernadite, 233t

Viscosity, of slags, 75–76

Voltage, 140–143

W

Wastewater treatment, from chromium ferroalloys processing, 313–314

Water, hazardous and risk management of, 125

Westly's heat distribution coefficient, 165

Westly's method, 88–89

White condensate, 204

Wolframite, 380–381, 381t, 383, 392

Wulfenite, 392

X

Xenotime, 466

Xstrata Premus process, 341–344, 343f

Y

Yttrium, 461–462

Z

Zircon, 441–442, 444–446

Zirconia, 438–439, 441, 446

Zirconium

ferroalloys, 443–447
 ferro-alumo-zirconium, 446–447, 446t
 ferrosilicozirconium, 443–446
 properties of, 435–441
 reduction of, 441–443
 sources of, 441–443

Zirconium carbide, 435–436, 442